Order Number 9409265

Studies on soil-foundation interaction in the sabkha environment of eastern province of Saudi Arabia

Al-Amoudi, Omar Saeed Baghabra, Ph.D.

King Fahd University of Petroleum and Minerals (Saudi Arabia), 1992

U·M·I
300 N. Zeeb Rd.
Ann Arbor, MI 48106

STUDIES ON SOIL-FOUNDATION INTERACTION IN THE SABKHA ENVIRONMENT OF EASTERN PROVINCE OF SAUDI ARABIA

BY

OMAR SAEED BAGHABRA AL-AMOUDI

A Thesis Presented to the

FACULTY OF THE COLLEGE OF GRADUATE STUDIES

KING FAHD UNIVERSITY OF PETROLEUM & MINERALS

DHAHRAN, SAUDI ARABIA

In Partial Fulfillment of the
Requirements for the Degree of

DOCTOR OF PHILOSOPHY

In

CIVIL ENGINEERING

SEPTEMBER, 1992

KING FAHD UNIVERSITY OF PETROLEUM AND MINERALS
DHAHRAN 31261, SAUDI ARABIA

COLLEGE OF GRADUATE STUDIES

This dissertation, written by *OMAR SAEED BAGHABRA AL-AMOUDI* under the direction of his Dissertation Advisor and approved by his Dissertation Committee, has been presented to and accepted by the Dean of the College of Graduate Studies, in partial fulfillment of the requirements for the degree of *DOCTOR OF PHILOSOPHY*.

Dissertation Committee

15/9/92

Dr. S. N. Abduljauwad
Dissertation Advisor

Prof. Rasheeduzzafar
Dissertation Co-advisor

Prof. M. M. Safar
Member

Prof. Z. R. El-Naggar
Member

Department Chairman

Dean, College of Graduate Studies

١٤١٣/٣/١٨

Date

DEDICATION

It has been vexing my head since the day I started this work: To whom should I dedicate this work? To **my parents** for the great sacrifices they have been offering to me, or to **my lovely wife and children** for their patience and ecouragement, or to **my faithful instructors** who taught me morality, or to **the friends** who help for no return, or to **the modest managers** who are assisting all persons with a smile.

This humble work is dedicated to:

THOSE,

MEN AND WOMEN,

WHO DO GOOD DEEDS

FOR THE SAKE OF

ALLAH

ACKNOWLEDGEMENTS

I wish to express my sincere appreciation to ***King Fahd University of Petroleum and Minerals*** for providing facilities and financial assistance to me during the course of this investigation. I am would like to thank ***Dr. Sahel N. Abduljauwad*** and ***Prof. Rasheeduzzafar***, the major advisor and the coadvisor of my dissertation committee, for their sincere advice and guidance. The constructve comments of ***Prof. Mahmoud M. Safar*** and ***Prof. Zaghloul R. El-Naggar***, the other two members of the committee, are also greatly appreciated. The cooperation of ***Mr. Mohammed Maslehuddin*** in the materials portion of this investigation and of ***Mr. Hassan Zakaria Saleh*** in the soil portion is greatly acknowledged.

The encouragement of ***Dr. Bakr Abdulla Bin Bakr***, the Rector of KFUPM, ***Dr. Saleh A. Bakhrebah***, the Dean of Engineering, as well as ***all faculty members of the Department of Civil Engineering*** is greatly appreciated.

I am thankful to ***Mr. Mumtaz Khan***, ***Mr. Essam El-Deeb***, ***Eng. Yaser A. Barakah***, ***Eng. Mahmoud M. Saadi***, ***Mr. Taha Okasha***, ***Mr. Abdul-Hafeez*** and ***many others***, for their assistance.

Lastly, but not the least, I am also obliged to ***my parents***, ***my wife*** and ***my children***, whose moral support, prayers, encouragement and patience, provided me the much needed initiatives towards presenting this humble work.

TABLE OF CONTENTS

Chapter		*Page*
	List of Tables	**xiii**
	List of Figures	**xvi**
	List of Plates	**xxvii**
	Dissertation Abstract	**xxix**
1	**INTRODUCTION**	1
	1.1 Geotechnical and Constructional Problems in Sabkha	1
	1.2 Objectives of This Study	3
	1.3 Research Program	6
	1.3.1 Site Selection	*6*
	1.3.2 Sabkha Field Tests	*6*
	1.3.3 Sabkha Laboratory Tests	*7*
	1.3.4 Correlations of Field and Laboratory Test Results	*7*
	1.3.5 Sabkha-Foundation Materials Interaction	*8*
2	**LITERATURE REVIEW ON SABKHA**	13
	2.1 Definition of Sabkha-Related Terms	13
	2.1.1 Coastal Sabkhas	*14*
	2.1.2 Continental Sabkhas	*15*
	2.1.3 Other Sabkha-Related Terms	*16*
	2.2 Distribution of Sabkhas	23

2.3 Geology of Sabkha 24

2.4 Factors That Control Sabkha Formation 34

2.4.1 Climatic Factors *36*

2.4.2 Geochemical Factors *39*

2.4.3 Geomorphological Factors *50*

2.4.4 Hydrological Factors *50*

2.4.5 Biological Factors *54*

2.5 Geotechnical Properties of Sabkha Soils 55

2.6 Foundation Problems in Sabkha Soils 62

3 LITERATURE REVIEW ON DURABILITY OF CONCRETE IN SULFATE-CHLORIDE ENVIRONMENTS 66

3.1 Introduction 66

3.2 Durability of Concrete in the Arabian Gulf 67

3.2.1 Corrosion of Reinforcement *71*

3.2.2 Sulfate Attack *77*

3.3 Durability of Concrete in Chloride-Sulfate Environments 83

3.3.1 Durability of Concrete in Sea Water *83*

3.3.2 Performance of Concrete in $SO_4^{--} - Cl^-$ *Environments* *88*

3.3.2.1 Effect of Primary (Internal) Chlorides on Sulfate Attack *88*

3.3.2.2 Effect of Secondary (External) Chlorides on Sulfate Attack *90*

3.3.2.3 Effect of Sulfate on Chloride-Induced Reinforcement

Corrosion 95

3.3.3 Performance of Plain and Blended Cements in $SO_4^{--} - Cl^-$ *Environments* 97

3.3.3.1 Role of Blended Cements 98

3.4 Aggressiveness of Sabkha Environment 103

4 METHODOLOGY OF RESEARCH 105

4.1 Site Selection 105

4.2 Field Tests on Sabkha Soil 106

4.2.1 Standard Penetration Test (SPT) *108*

4.2.2 Static Cone Penetration Test (CPT) *109*

4.2.3 Pressuremeter Test (PMT) *111*

4.2.4 Plate Load Test (PLT) *117*

4.2.5 Field California-Bearing Ratio (CBR) Tests *119*

4.3 Laboratory Tests on Sabkha Soil 120

4.3.1 Specific Gravity Tests *124*

4.3.2 Grain-Size Distribution Tests *124*

4.3.3 Atterberg Limits Tests *125*

4.3.4 Classification Tests *126*

4.3.5 Permeability Tests *127*

4.3.6 Moisture-Density Relationship (Compaction) Tests *128*

4.3.7 Field Density Measurements *129*

4.3.8 Consolidation Tests *130*

4.3.8.1 Conventional Consolidation

Tests 130

4.3.8.2 Development of a Modified Oedometer 131

4.3.9 Unconfined Compression Tests 138

4.3.10 Direct Shear Tests 139

4.3.11 Triaxial Tests 139

4.3.12 California-Bearing Ratio (CBR) Tests 141

4.4 Foundation Materials-Sabkha Interaction in Laboratory 143

4.4.1 Test Solutions 144

4.4.2 Mixes and Materials Used 149

4.4.2.1 Specimens 149

4.4.2.1.1 Cement Paste Specimens 149

4.4.2.1.2 Cement Mortar Specimens 150

4.4.2.1.3 Concrete Specimens 151

4.4.2.2 Materials Used 155

4.4.3 Experimental Techniques 155

4.4.3.1 X-Ray Diffraction (XRD) 155

4.4.3.2 Scanning Electron Microscopy (SEM) 158

4.4.3.3 Pore Solution Expression Analysis 161

4.4.3.4 Reduction in Compressive Strength 162

4.4.3.5 Visual Observation 164

4.4.3.6 Corrosion Monitoring 165

4.4.3.6.1 Time to Initiation of Reinforcement Corrosion 166

4.4.3.6.2 Corrosion Current Density Measurements *166*

4.5 Foundation Materials-Sabkha Interaction in the Field 171

4.5.1 Specimens and Materials Used *171*

4.5.2 Reduction in Compressive Strength *173*

4.5.3 Chemical Analysis Tests *173*

4.5.3.1 Alkalinity and Water-Soluble Chlorides *175*

4.5.4 Metal Weight Loss *177*

5 RESULT PRESENTATION AND DISCUSSION ON SABKHA SOIL CHARACTERIZATION 179

5.1 Introduction 179

5.2 Site Selection 179

5.3 Field Tests Results on Sabkha 185

5.3.1 SPT Results *185*

5.3.2 Thin-Walled (Shelby) Tube Results *193*

5.3.3 CPT Results *195*

5.3.4 PMT Results *197*

5.3.5 PLT Results *203*

5.3.6 Field CBR Test Results *208*

5.4 Results of Laboratory Tests on Sabkha *208*

5.4.1 Specific Gravity Test Results *212*

5.4.2 Grain-Size Distribution Test Results *212*

5.4.2.1 Mechanical (Sieve) Analysis Test Results *212*

5.4.2.2 Hydrometer Testing

Interpretation 223

5.4.3 *Classification Test Results* 226

5.4.4 *Permeability Tests Results* 227

5.4.5 *Compaction Tests Results* 237

5.4.6 *Field Density Measurement Results* 240

5.4.7 *Consolidation Tests Results* 242

5.4.7.1 *Conventional Oedometer Test Results* 243

5.4.7.2 *Modified Oedometer Results* ... 249

5.4.7.2.1 *Preliminary Test Results* 249

5.4.7.2.2 *Systematic Test Results* 262

5.4.7.2.3 *Effect of Sabkha Brine on Collapse Potential* 280

5.4.8 *Unconfined Compression Test Results* 296

5.4.9 *Direct Shear Test Results* 300

5.4.10 *Triaxial Test Results* 303

5.4.11 *Laboratory CBR Test Results* 322

6 DURABILITY PERFORMANCE OF FOUNDATION MATERIALS IN SULFATE-CHLORIDE ENVIRONMENTS 326

6.1 Performance of Plain and Blended Cement Mortars in Sulfate-Chloride Environments 327

6.1.1 *Visual Inspection* 327

6.1.2 *Characterization of Deterioration* 333

6.1.3 *Reduction in Compressive Strength* 333

6.2 Mineralogical Composition of Hydrated Cements 350

6.2.1 *Plain and Blended Cements in Potable Water* 351

6.2.2 *Plain and Blended Cements in Pure Sulfate Solution* 358

6.3 **Sulfate Attack Mechanisms** 359

6.3.1 *Mechanism of Gypsum-Oriented Sulfate Attack* 370

6.3.1.1 *SEM Micrographs for Plain and Blended Cements in Potable Water* 377

6.3.1.2 *SEM Micrographs for Plain and Blended Cements in Pure Magnesium-Sodium Sulfate Environments* 377

6.3.2 *Magnesium-Gypsum Attack* 397

6.3.3 *Performance of Plain and Blended Cements in Sodium Sulfate Environment Compared to Magnesium-Sodium Sulfate Environments* 408

6.4 **Effect of Chlorides on Sulfate Attack** 414

6.5 **Corrosion of Reinforcement in Plain and Blended Cements** 453

6.5.1 *Time to Corrosion Initiation* 454

6.5.2 *Corrosion Current Density* 462

6.5.3 *Pore Solution Expresstion Analysis* 474

6.6 **Mechanisms of Reinforcement Corrosion in Chloride-Sulfate Environments** 476

6.7 **Strength Reduction and Reinforcement Corrosion in Specimens Placed in the Field** 489

6.7.1 *Strength Development* 489

6.7.2 *Chlorides and Hydroxyl Ion Concentration* 492

6.7.3 *Reinforcement Corrosion* 493

6.7.4 *Discussion of the Field Results* 496

7 CONCLUSION 499

8 REFERENCES 508

9 APPENDICES 546

LIST OF TABLES

Table		*Page*
2.1	Regional sabkha/playa nomenclature (Ellis, 1973)	20
2.2	Definition and characterization of some evaporitic basins (Fookes and Collis, 1975)	21
2.3	Major cation and anion concentrations in sabkhas of eastern Saudi Arabia in g/l (Johnson et al., 1978)	45
2.4	Physical and mechanical properties of an Eastern Saudi sabkha (Abu-Taleb and Egeli, 1981)	58
3.1	Average composition of ocean waters (Eglinton, 1987)	86
4.1	Range of cation and anion concentrations in Wadi As-Sirhan sabkha brine (Smith, 1980)	147
4.2	Degree of Severity and Recommendations for Normal Weight Concrete Subject to Sulfate Attack	148
4.3	Grain-size analysis for coarse and fine aggregates	153
4.4	Summary of type and number of paste, mortar and concrete specimens tested	154
4.5	Chemical composition of cements and blending materials	156
4.6	Pertinent XRD cement phases in terms of 2θ	160
5.1	Chemical analysis of sabkha brine and sea water in g/l (i.e., parts per thousand)	184
5.2	Relative density classification of sands based on SPT and CPT	188
5.3	Chemical analysis results of the rock salt layer	191
5.4	Summary of pressuremeter test results	198
5.5	Bulk specific gravity of rock salt	202
5.6	Bulk specific gravity of a soil sample from 8.2 meter depth	202

5.7	Summary of field and laboratory CBR test results.....	211
5.8	Specific gravity test results	213
5.9	Summary of sieve analysis test results	217
5.10	Semi-quantitative XRD analysis results (surficial and deep sabkha samples).....	222
5.11	Classification test results of sabkha soil	228
5.12	In-situ density test results using the sand-cone method.	241
5.13	Summary of consolidation test results (series #1 and #2)	247
5.14	Summary of modified oedometer test results (series #3, #4 and #5)	293
5.15	Summary of various triaxial test results.....	320
6.1	Durability performance of plain and blended cements in pure sulfate solution.....	329
6.2	Durability performance of plain and blended cements in high sulfate-chloride solution	331
6.3	Durability performance of plain and blended cements in low sulfate-chloride solution	334
6.4	Durability performance of plain and blended cements in pure chloride solution	335
6.5	Summary of strength development in plain and blended cement mortar specimens.....	340
6.6	Summary of chloride beneficiation in plain and blended cements after 720 days of exposure	426
6.7	Summary of time to corrosion initiation for plain and blended cements exposed to various environments	461
6.8	Summary of corrosion current densities on steel in plain and blended cements exposed to various environments...	472
6.9	Performance rating of plain and blended cements in terms of corrosion current density.....	473
6.10	Summary of pore solution results expressed from	

hardened plain and blended cement paste specimens..... 475

6.11 Summary of chemical analysis results of field mortar specimens after 540 days of exposure..... 494

6.12 Corroded surface area of reinforcing steel in field mortar specimens..... 494

6.13 Loss in weight in reinforcing steel and performance rating in field mortar specimens after 540 days of exposure 495

LIST OF FIGURES

Figure		*Page*
1.1	Details of research program	5
1.2	Research program for evaluation of sabkha characteristics in field	9
1.3	Research program for evaluation of sabkha characteristics in laboratory	10
1.4	Research program for evaluation of sabkha-foundation materials interaction	11
1.5	Research program for evaluation of sulfate resistance	12
2.1	Diagrammatic cross-sections illustrating the difference between (a) a coastal evaporite pan, and (b) a coastal sabkha (Renfro, 1974)	18
2.2	Generalized cross-section across a typical coastal sabkha (Akili and Torrence, 1981)	19
2.3	Naturally-existing sabkha cross-section in Jizan (Erol, 1989)	19
2.4	Idealized cross-section of sabkha, playa, salt playa and salina (Fookes, 1976)	22
2.5	Sabkha terrains in the coastal region of Eastern Saudi Arabia (Johnson et al., 1978)	25
2.6	Simplified geology of the Arabian Gulf countries (Fookes and Higginbottom, 1980)	26
2.7	World map showing locations of active coastal sabkhas (Renfro, 1974)	27
2.8	World map showing locations for potentially favorable strata for sabkha (Renfro, 1974)	28
2.9	Summary of the factors controlling the sabkha formation	35
2.10	Consecutive precipitation of the different minerals from evaporation of sea water	46
4.1	Idealized in-situ stress-deformation relationshiP	115

4.2	Actual stress-deformation relationship using elastmeter 100 pressuremeter	116
4.3	The fixed-ring oedometer	132
4.4	The floating-ring oedometer	132
4.5	The KFUPM-Modified oedometer	135
4.6	Swan's oedometer	135
4.7	A typical diffraction pattern from crystal planes according to Bragg's law	159
4.8	Idealized Tafel plot	168
4.9	Schematic representation of set-up used to measure corrosion current density	172
5.1	Vicinity map showing potential sabkha locations and the selected Ras Al-Ghar sabkha	183
5.2	Locations of individual borings	186
5.3	Standard penetration test (SPT) results	187
5.4	Thin-walled (Shelby) tube results	194
5.5	Cone penetration test (CPT) results	196
5.6	Typical pressuremeter test (PMT) raw data conducted at a depth of 0.5 meter	199
5.7	A summary of the boring test results	204
5.8	Plate-load test results (natural condition)	206
5.9	Plate-load test results (flooded condition)	207
5.10	Field CBR test results (natural condition)	209
5.11	Field CBR test results (flooded condition)	210
5.12	Grain-size analysis results using "standard" techniques	215
5.13	Summary of the grain-size analysis results	216
5.14	X-ray diffraction pattern for surficial sabkha	220

5.15 X-ray diffraction pattern for deeper sabkha strata (8.2 meter depth) 221

5.16 Combined grain-size analysis results for the wet sieving with distilled water 225

5.17 Constant head permeability test results using sabkha brine (specimen #1) 231

5.18 Constant head permeability test results using sabkha brine (specimen #2) 232

5.19 Variable head permeability test results using sabkha brine (specimen #3) 233

5.20 Constant head permeability test results using distilled water (specimen #4) 234

5.21 Constant head permeability test results using distilled water (specimen #5) 235

5.22 Variable head permeability test results using distilled water (specimen #6) 236

5.23 Effect of distilled water and oven temperature on compaction test results 238

5.24 Effect of sabkha brine and oven temperature on compaction test results 239

5.25 Results of the conventional oedometer tests (series #1).. 245

5.26 Results of the conventional oedometer tests (series #2).. 246

5.27 Typical time-settlement data from a conventional consolidation test (before flooding) 250

5.28 Typical time-settlement data from a conventional consolidation test (after flooding) 251

5.29 Consolidation test results (series #3) 253

5.30 Initial time-flow data for the modified oedometer (series #3) 256

5.31 Time-Flow data for the modified oedometer (series #3)... 257

5.32 Flow-Pressure test results (series #3) 258

5.33 Chemical analysis of the percolating water (series #3) ... 261

5.34 Conductivity test results of percolating water (series #3) ... 263

5.35 Consolidation test results (series #4) ... 265

5.36 Time-Flow data for the loading cycles (series #4) ... 268

5.37 Time-Flow data for the unloading cycles (series #4) ... 272

5.38 Time-Flow data for the reloading cycles (series #4) ... 273

5.39 Flow-Pressure results (series #4) ... 274

5.40 Chemical analysis of percolating water (series #4) ... 277

5.41 Conductivity test results of percolating water (series #4) ... 278

5.42 Chemical analysis-pressure test results (series #4) ... 279

5.43 Consolidation test results (series #5) ... 281

5.44 Time-Flow data for the loading cycles (series #5) ... 286

5.45 Time-Flow data for the unloading cycles (series #5) ... 287

5.46 Time-Flow data for the reloading cycles (series #5) ... 288

5.47 Flow-Pressure results (series #5) ... 289

5.48 Effect of distilled water percolation on the rate of flow (series #5) ... 291

5.49 Unconfined compressive strength test results for the undisturbed sabkha samples ... 297

5.50 Effect of moisture content on unconfined compressive strength of compacted sabkha ... 299

5.51 Shear stress-horizontal displacement data for the direct shear test results ... 301

5.52 Mohr-Coulomb envelope for the direct shear test results 302

5.53 Stress-strain data for the CD triaxial tests without volume change measurement ... 304

5.54 Mohr-Coulomb envelope for the CD triaxial tests without volume change measurement 305

5.55 Stress-strain data for the CD triaxial test saturated with distilled water 308

5.56 Volume change measurement for the CD triaxial test saturated with distilled water 309

5.57 Mohr-Coloumb failure envelope for the CD triaxial test saturated with distilled water 310

5.58 Stress-strain data for the CD triaxial test saturated with sabkha brine 311

5.59 Volume change measurement for CD triaxial test saturated with sabkha brine 312

5.60 Mohr-Coulomb failure envelope for the CD triaxial test saturated with sabkha brine 313

5.61 Stress-strain data for the CU triaxial test saturated with distilled water 314

5.62 Pore-water pressure measurement for the CU triaxial test saturated with distilled water 315

5.63 Mohr-Coloumb failure envelope for the CU triaxial test saturated with distilled water 316

5.64 Stress-strain data for the CU triaxial test saturated with sabkha brine 317

5.65 Pore-water pressure measurement for the CU triaxial test saturated with sabkha brine..... 318

5.66 Mohr-Coloumb failure envelope for the CU triaxial test saturated with sabkha brine 319

5.67 Laboratory CBR test results (unsoaked condition)..... 323

5.68 Laboratory CBR test results (soaked condition) 324

6.1(a) Schematic representation of deterioration rating in pure sulfate and high sulfate-chloride solutions 330

6.1(b) Schematic representation of deterioration rating in low sulfate-chloride and pure chloride solutions 336

6.2 Strength development in plain cement mortar specimens . 341

6.3 Strength development in blended cement mortar specimens 342

6.4 Reduction in compressive strength with time (Type I cement mortar specimens) 343

6.5 Reduction in compressive strength with time (Type V cement mortar specimens) 344

6.6 Reduction in compressive strength with time (fly ash cement mortar specimens) 345

6.7 Reduction in compressive strength with time (silica fume cement mortar specimens) 346

6.8 Reduction in compressive strength with time (blast furnace slag cement mortar specimens) 347

6.9 X-ray diffractogram for Type I cement in potable water after 720 days of immersion 353

6.10 X-ray diffractogram for Type V cement in potable water after 720 days of immersion 354

6.11 X-ray diffractogram for fly ash cement in potable water after 720 days of immersion 355

6.12 X-ray diffractogram for silica fume cement in potable water after 720 days of immersion 356

6.13 X-ray diffractogram for blast furnace slag cement in potable water after 720 days of immersion 357

6.14 X-ray diffractogram for Type I cement in pure sulfate solution after 720 days of immersion 360

6.15 X-ray diffractogram for Type V cement in pure sulfate solution after 720 days of immersion 361

6.16 X-ray diffractogram for fly ash cement in pure sulfate solution after 720 days of immersion 362

6.17 X-ray diffractogram for silica fume cement in pure sulfate solution after 720 days of immersion 363

6.18 X-ray diffractogram for blast furnace slag cement in pure sulfate solution after 720 days of immersion 364

6.19 Effect of $\bar{S}/S$ ratio on C/S ratio of C_3S paste (Bentur, 1976) 375

6.20 Effect of C/S ratio on the intrinsic strength of C_3S paste (Bentur, 1976) 376

6.21 EDX analysis for BFS cement in potable water 378

6.22 EDX analysis for spot A in Plate 6.8 379

6.23 EDX analysis for spot B1 in Plate 6.9 380

6.24 EDX analysis for spot B2 in Plate 6.8 380

6.25 EDX analysis for Type V cement exposed to pure sulfate solution 382

6.26 EDX analysis for Type I cement exposed to pure sulfate solution 383

6.27 EDX analysis for spot A in Plate 6.10 384

6.28 EDX analysis for spot B in Plate 6.10 385

6.29 EDX analysis for spot A in Plate 6.11 386

6.30 EDX analysis for spot B in Plate 6.11 387

6.31 EDX analysis for spot C in Plate 6.11 388

6.32 EDX analysis for silica fume cement exposed to pure sulfate solution 390

6.33 EDX analysis for BFS cement exposed to pure sulfate solution 391

6.34 EDX analysis for spot C in Plate 6.17 392

6.35 EDX analysis for spot B in Plate 6.17 393

6.36 EDX analysis for spot A in Plate 6.17 394

6.37 EDX analysis for spot C in Plate 6.16 394

6.38 EDX analysis for spot B in Plate 6.16 395

6.39 EDX analysis for gypsum crystal growth in silica fume cement exposed to pure sulfate solution 396

6.40 X-ray diffraction of the deteriorated block material in Plate 6.20 400

6.41 Performance of 20% fly ash cement in 5% $N\bar{S}$ solution (Rasheeduzzafar et al. 1992) 409

6.42 Performance of 10% silica fume cement in 5% $N\bar{S}$ solution (Rasheeduzzafar et al. 1992) 410

6.43 Performance of 60% BFS cement in 5% $N\bar{S}$ solution (Rasheeduzzafar et al. 1992) 411

6.44 Performance of 70% BFS cement in 5% $N\bar{S}$ solution (Rasheeduzzafar et al., 1992) 412

6.45 X-ray pattern for the 20% silica fume blended with Type I (C_3A = 14%) exposed to 5% $N\bar{S}$ solution (Rasheeduzzafar et al., 1990) 413

6.46 Effect of chloride on sulfate attack in Type I cement (360 days) 415

6.47 Effect of chloride on sulfate attack in Type I cement (720 days) 416

6.48 Effect of chloride on sulfate attack in Type V cement (360 days) 417

6.49 Effect of chloride on sulfate attack in Type V cement (720 days) 418

6.50 Effect of chloride on sulfate attack in fly ash cement (360 days) 419

6.51 Effect of chloride on sulfate attack in fly ash cement (720 days) 420

6.52 Effect of chloride on sulfate attack in silica fume cement (360 days) 421

6.53 Effect of chloride on sulfate attack in silica fume cement (720 days) 422

6.54 Effect of chloride on sulfate attack in blast furnace slag cement (360 days) 423

6.55 Effect of chloride on sulfate attach in blast furnace slag cement (720 days) 424

6.56 X-ray diffractogram for Type I cement in pure chloride solution after 720 days 429

6.57 X-ray diffractogram for Type V cement in pure chloride solution after 720 days 430

6.58 X-ray diffractogram for fly ash cement in pure chloride solution after 720 days 431

6.59 X-ray diffractogram for silica fume cement in pure chloride solution after 720 days..... 432

6.60 X-ray diffractogram for blast furnace slag cement in pure chloride solution after 720 days 433

6.61 X-ray diffractogram for Type I cement in low sulfate-chloride solution after 720 days..... 434

6.62 X-ray diffractogram for Type V cement in low sulfate-chloride solution after 720 days..... 435

6.63 X-ray diffractogram for fly ash cement in low sulfate-chloride solution after 720 days..... 436

6.64 X-ray diffractogram for silica fume cement in low sulfate-chloride solution after 720 days 437

6.65 X-ray diffractogram for blast furnace slag cement in low sulfate-chloride solution after 720 days 438

6.66 X-ray diffractogram for Type I cement in high sulfate-chloride solution after 720 days..... 439

6.67 X-ray diffractogram for Type V cement in high sulfate-chloride solution after 720 days..... 440

6.68 X-ray diffractogram for fly ash cement in high sulfate-chloride solution after 720 days..... 441

6.69 X-ray diffractogram for silica fume cement in high

sulfate-chloride solution after 720 days 442

6.70 X-ray diffractogram for blast furnace slag cement in high sulfate-chloride solution after 720 days 443

6.71 EDX analysis for Type V cement exposed to high sulfate-chloride solution 445

6.72 EDX analysis for spot A in Plate 6.23..... 446

6.73 EDX analysis for silica fume cement exposed to high sulfate-chloride solution 447

6.74 EDX analysis for BFS cement exposed to high sulfate-chloride solution..... 448

6.75 EDX analysis for spot A in Plate 6.26..... 449

6.76 Half-cell potential-time record in high sulfate-chloride solution 455

6.77 Half-cell potential-time record in low sulfate-chloride solution 458

6.78 Half-cell potential-time record in pure chloride solution . 459

6.79 Half-cell potential-time record in pure sulfate solution... 460

6.80 Corrosion current density on steel in Type I cement concrete specimens 463

6.81 Corrosion current density on steel in Type V cement concrete specimens 465

6.82 Corrosion current density on steel in fly ash cement concrete specimens 469

6.83 Corrosion current density on steel in silica fume cement concrete specimens 470

6.84 Corrosion current density on steel in blast furnace slag cement concrete specimens 471

6.85 Effect of sulfate ions on chloride-induced corrosion rates in plain cements (425 days)..... 481

6.86 Effect of sulfate ions on chloride-induced corrosion rates in plain cements (500 days)..... 482

6.87	Effect of sulfate ions on chloride-induced corrosion rates in plain cements (650 days)	483
6.88	Effect of sulfate ions on chloride-induced corrosion rates in blended cements (425 days)	484
6.89	Effect of sulfate ions on chloride-induced corrosion rates in blended cements (500 days)	485
6.90	Effect of sulfate ions on chloride-induced corrosion rates in blended cements (650 days)	486
6.91	Compressive strength reduction in field mortar specimens (plain cements)	490
6.92	Compressive strength reduction in field mortar specimens (blended cements)	491
A1	Pressuremeter test data conducted at a depth of 1.3 m.	547
A2	Pressuremeter test data conducted at a depth of 5.0 m.	548
A3	Pressuremeter test data conducted at a depth of 6.5 m.	549
A4	Pressuremeter test data conducted at a depth of 7.6 m.	550
A5	Pressuremeter test data conducted at a depth of 8.6 m.	551
A6	Pressuremeter test data conducted at a depth of 10.6 m.	552
A7	Pressuremeter test data conducted at a depth of 11.6 m.	553
A8	Pressuremeter test data conducted at a depth of 12.6 m.	554

LIST OF PLATES

Plate		*Page*
4.1	PVC tubes used to retrieve undisturbed surficial sabkha samples	121
4.2	Measurement of flow using the modified oedometer	136
4.3	Reservoir used to maintain a constant head in the modified oedometer	136
4.4	Reinforcing steel and cylindrical moulds used in casting reinforced concrete specimens	153
5.1	Presence of soft gypsum intercalated with halite crystals	190
6.1	Visual documentation of the different cements in the pure sulfate solution after 360 days	337
6.2	Visual documentation of the different cements in the high sulfate-chloride solution after 360 days	337
6.3	Visual documentation of the different cements in the pure sulfate solution after 720 days	338
6.4	Visual documentation of the different cements in the high sulfate-chloride solution after 720 days	338
6.5	A conceptual model showing the essential mechanism of gypsum-oriented sulfate attack	372
6.6	Backscattered electron image (BEI) of 10% silica fume paste exposed to 4.2% magnesium sulfate solution (Bonen and Cohen, 1992)	373
6.7	SEM micrograph indicating intrusion of gypsum crystal into CSH gel	373
6.8	SEM micrograph for BFS cement cured in potable water	378
6.9	A blow up of spot A in Plate 6.8	379
6.10	SEM micrograph for Type V cement exposed to pure sulfate solution	382

6.11	SEM micrograph for Type I cement exposed to pure sulfate solution	383
6.12	A blow up of spot A in Plate 6.10	384
6.13	A blow up of spot B in Plate 6.10	385
6.14	A blow up of spot A in Plate 6.11	386
6.15	A blow up of spot B in Plate 6.11	387
6.16	SEM micrograph for silica fume cement exposed to pure sulfate solution	390
6.17	SEM micrograph for BFS cement exposed to pure sulfate solution	391
6.18	A blow up of spot B in Plate 6.17	393
6.19	A blow up of spot B in Plate 6.16	395
6.20	A typical mode of gypsum-oriented sulfate attack in the Arabian Gulf region	399
6.21	Another documentation of the gypsum-oriented sulfate attack in the Arabian Gulf region	399
6.22	Presence of dense, protective brucite layer on surface of silica fume specimen (Bonen and Cohen, 1992)	406
6.23	SEM micrograph for Type V cement exposed to high sulfate-chloride solution	445
6.24	SEM micrograph for spot A in Plate 6.23	446
6.25	SEM micrograph for silica fume cement exposed to high sulfate-chloride solution	447
6.26	SEM micrograph for blast furnace slag cement exposed to high sulfate-chloride solution	448

Dissertation Abstract

Full Name : **Omar Saeed Baghabra Al-Amoudi**

Title of Study : **Studies on Soil-Foundation Interaction in the Sabkha Environment of Eastern Province of Saudi Arabia**

Major Field : **Civil Engineering**

Date of Degree : **September 1992**

The large, extremely flat, saline, evaporative areas situated either along the coasts or farther inland of many arid, semi-tropical countries are known by the word "sabkha". The main distinguishing features of sabkha are its heterogeneous matrix and its highly concentrated groundwater. These characteristics of sabkhas contribute to many unresolved geotechnical problems which could hamper the performance of foundations.

In an attempt to assess the safety and serviceability of foundations in eastern Saudi sabkha environments, a full-scale research was conducted to: (i) study the sabkha, its load-bearing and compressibility characteristics as well as other relevant geotechnical properties to assess the safety of foundations; and (ii) investigate the interaction between foundation materials and chloride and/or sulfate salts in the sabkha to evaluate the performance of plain and blended cements in resisting reinforcement corrosion and sulfate attack to assess the durability of foundations.

Results of this research indicate that the surficial sabkha soil is very loose and possess low strength. Some standard techniques, such as sieve and hydrometer, permeability and consolidation, are shown to be inappropriate. The collapse potential of sabkha, as determined by a modified oedometer, rather than its compressibility, is classified as "very severe trouble". Silica fume and BFS blended cements exhibited deterioration to a higher degree than other cements in both pure sulfate and high sulfate-chloride environments. The chloride beneficiation for these two cements is only marginal because of the excessive magnesium decomposition of C-S-H due to the lower CH content, which is shown to be unhampered by the presence of chloride ions. However, reinforcement corrosion, as determined by time to initiation of corrosion and corrosion current density, is much lesser in silica fume and BFS cements due to their denser structure. The concomitant presence of sulfate ions aggravated the chloride-induced corrosion. Field results indicated that reinforcement corrosion in these two cements was 32 to 21 times lower than that in plain cements. These results indicated that the high performance blended cements such as silica fume and BFS blended cements can be used in sabkha environment. However, water-resistant epoxy coatings should be applied on these structures if the magnesium sulfate concentration is high.

دراسات عن تداخلات التربة والأساسات في البيئة السبخية للمنطقة الشرقية في المملكة العربية السعودية

الملخص

يُطلق لفظ « سبخة » على المساحات المسطحة المالحة والبخرية الواقعة على الشواطئ أو في القارات وذلك في المناطق الجافة والمدارية . تتميز السبخة ببيئتها غير المتجانسة وبمياهها الأرضية شديدة الملوحة . ولقد أدت هذه الخواص إلى مشاكل جيوتقنية عديدة مما يؤدي إلى عرقلة الاداء السليم للأساسات .

في محاولة لتقويم سلامة ونفعية الأساسات في البيئات السبخية ، تم في هذه الدراسة الموسعة مايلي : (أ) دراسة التربة وقوتها ومدى إنضغاطيتها بالإضافة للخواص الجيوتقنية الأخرى لها وذلك لتقويم سلامة الأساسات ، و (ب) دراسة تأثير أملاح الكلور والكبريتات الموجودة في السبخة على مواد الأساسات لتقدير أداء أنواع الإسمنت العادية والمضافة لمقاومة صدأ حديد التسليح والتلف الكبريتاتي وذلك لتقويم تحمّليّة ونفعيّة الأساسات .

توضح نتائج هذه الدراسة أن التربة السبخية ضعيفة جداً وأن بعض الإختبارات القياسية ، كإختبارات تحديد حجم الحُبيبات ، النفاذية ، والانضغاطية ، لا تصلُح لتقويم خواص السبخة . وأن الأنهيار الكامن للسبخة - وليس إنضغاطيتها - يُعتبر « عالي جداً ومزعج » . ودلت النتائج أن إسمنت دخان السيليكون وخبث الفُرن العالي قد تعرضا إلى درجة عالية من التدهور مقارنة بأنواع الإسمنت الأخرى وذلك في محلول الكبريتات ومحلول الكبريتات مع الكلور ، ولذلك فإن درجة " الإنتفاع بالكلور " لهذين النوعين من الإسمنت كانت هامشية . كما أن صدأ حديد التسليح ، والذي تم تحديده بالزمن اللازم لظهور الصدأ وكثافة تيار الصدأ ، لهاذين النوعين من الإسمنت كان قليلاً جداً نظراً لبنيتها الكثيفة . وقد إزداد مُعدل صدأ الحديد بوجود أيونات الكبريتات المصاحبة لأيونات الكلور . ودلت نتائج الدراسات الحقلية أن صدأ حديد التسليح في هاذين النوعين من الإسمنت أقل بـ ٣٢ و ٢١ ضعفاً من الإسمنت العادي . لذلك فإن الأداء المتفوق لإسمنت المواد المضافة (مثل دخان السيلكون وخبث الفرن العالي) يجعلها الأمثل للإستخدام في البيئات السبخية . ولكن يجب وضع طبقة عازلة (كالأبوكسي) على هذه المنشآت عند تعرضها لتركيز عالٍ من كبريتات المغنيسيوم .

Chapter 1

INTRODUCTION

1.1 GEOTECHNICAL AND CONSTRUCTIONAL PROBLEMS IN SABKHA

The large, extremely flat, saline, evaporative areas situated either along the coasts or farther inland of many arid, semi-tropical countries are known by the Arabic word "sabkha". These soils are generally viewed as unconsolidated, heterogeneous, layered or unlayered sedimentological framework, bathed in highly concentrated, subsurface brines. These features of sabkha soils have given them hazardous geotechnical properties that need thorough investigation. The determination of these properties has to be dealt with careful attention due to the presence of soluble and insoluble salts that exist in the sabkha matrix and its brine.

In the past two decades, the Arabian Gulf countries including the Kingdom of Saudi Arabia have gone through a spectacular era of industrialization and establishment of the infrastructure. Some of the construction activity, particularly in Eastern and Western Provinces such as Jubail, Ras Tanura, Jau'aimah, Jeddah, Yanbu'a, etc., was inevitably located in sabkha flats. Also, future urban development in these areas is expected to be located in this highly aggressive environment, where the salinity of

groundwater ranges between four to six times that of typical sea water. As a consequence, serious technical consideration must be given to these unusual deposits.

Previous experience with sabkha in Saudi Arabia and elsewhere has shown that the main geotechnical problems could be grouped into four categories:

i) Problems due to periodic changes in moisture content

ii) Problems due to excessive differential settlements

iii) Problems due to the proximity of groundwater table

iv) Problems due to the presence of highly corrosive brines.

The last category seems to be the most prominent in eastern Saudi Arabia. SCECO has recently conducted a comprehensive evaluation of manholes and handholes in and around the vicinity of Jubail. It was found that the majority of these manholes will have to be either repaired or completely replaced. The cost of restoration of these manholes is estimated to be more than 1.5 billion Saudi Riyals. In another recent investigation, many substructures which included piers, foundations, columns, etc., that were buried in sabkha, were reported to exhibit considerable degree of deterioration. Excessive differential settlements of some structures in Jizan, although not exclusively due to sabkha, were reported. Feedback data on the performance of foundations in sabkha is exi-

gently needed so that measures could be taken to mitigate the consequences of this hostile environment.

This research is aimed at investigating the practical aspects of the four potential problems listed above. The choice was made on the basis of thorough literature review as well as experimental and financial limitations. In this study, the sabkha will be characterized from geotechnical viewpoint, and the interaction of sabkha with foundation materials will be investigated. The data developed in this study will be useful in better understanding the criteria for the design of foundations that are safe and serviceable from load and settlement points of view, as well as durable from the standpoint of materials in such unparalleled hostile environment.

The former requirements necessitate a full-scale research to study the sabkha, its load-bearing characteristics as well as an assessment of its other relevant geotechnical properties; whereas the latter necessitates that materials should be developed which do not deteriorate quickly in sabkha environment.

1.2 OBJECTIVES OF THIS STUDY

The broad objectives of this research are to characterize sabkha in terms of physico-chemical and geotechnical properties and to investigate the interaction between the foundation materials and the chloride and sulfate ions in sabkha. The specific objectives

of this study are:

(i) to characterize a typical eastern Saudi sabkha in terms of its stratigraphy,

(ii) to evaluate the physical and chemical properties of sabkha,

(iii) to evaluate the geotechnical properties of sabkha, namely, its load-bearing and compressibility characteristics, both in the field and in the laboratory,

(iv) to elucidate the sulfate attack mechanisms in sulfate-chloride environments for plain and blended cements,

(v) to evaluate the role of chlorides on sulfate attack,

(vi) to study the mechanisms of reinforcement corrosion in plain and blended cements in sulfate-chloride environments, and

(vii) to elucidate the performance of plain and blended cements in resisting reinforcement corrosion and sulfate attack in actual sabkha environment.

The above research objectives are schematically shown in Fig. 1.1

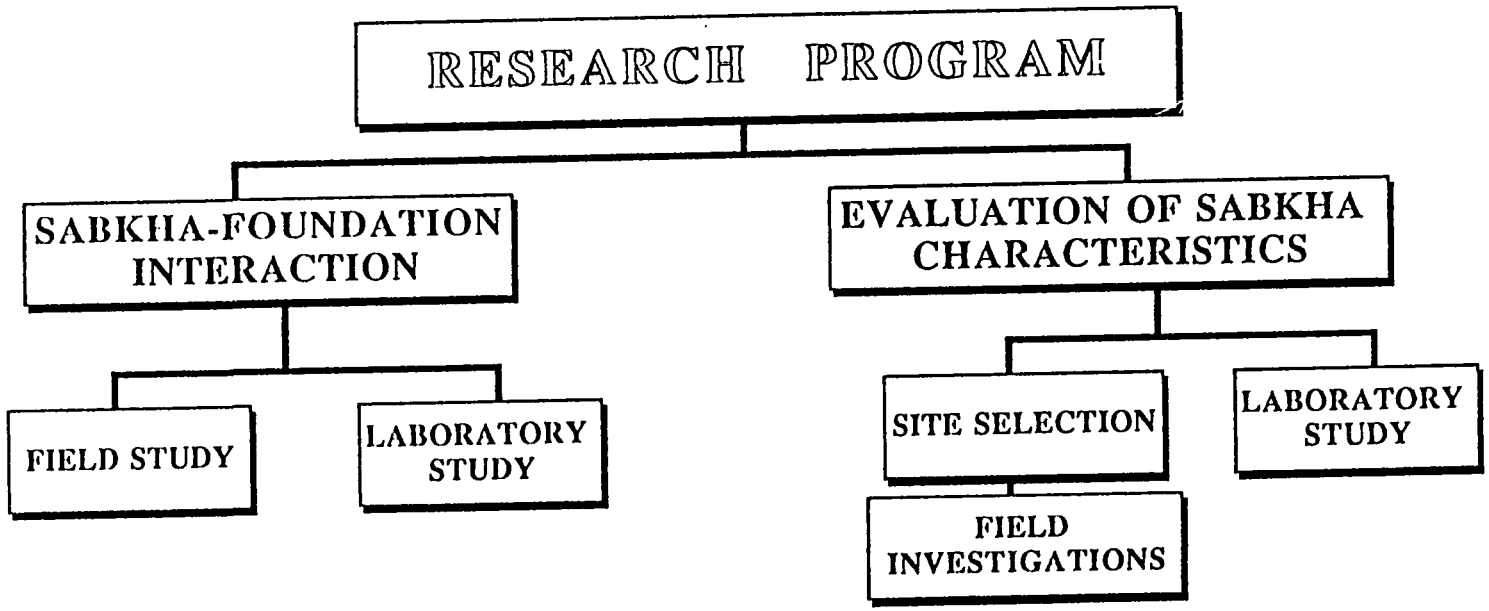

Fig. 1.1 : Details of Research Program.

1.3 RESEARCH PROGRAM

To fulfill the objectives of this research study, extensive field and laboratory investigations were carried out. The salient features of the research program are discussed in the following paragraphs, while the experimental techniques used are discussed in Chapter 4.

1.3.1 Site Selection

Site selection was based on surveying several locations of potential sabkha environments. Published literature and geotechnical reports were reviewed for the selection of a potential sabkha site. Test pits were excavated down to the watertable in some selected sites, and samples of sabkha brine were collected for chemical analysis.

1.3.2 Sabkha Field Tests

Several field tests were conducted, including standard penetration test (SPT), cone penetration test (CPT) and pressuremeter test. These tests were performed in individual boreholes to avoid disturbance. The depth of penetration was 10 m minimum, which is reasonably enough for shallow or even deep foundation. The reason for running several tests at the same location is that each of these tests has inherently some advantages and drawbacks, specially in such a highly variable material, which may reflect sev-

eral subsoils through the proposed depth. Plate-load and CBR tests were conducted under natural and inundated condition. Natural condition would reflect the existing (dry) condition, while the inundated condition would reflect the degree of cementation of the surficial stratum.

1.3.3 Sabkha Laboratory Tests

Laboratory investigations were carried out on disturbed and undisturbed samples. Undisturbed samples were obtained using PVC tubes for the surficial (above groundwater table) layer and thin-walled tubes (Shelby tubes) for deeper stratum. Due to the salty nature of sabkha, emphasis was placed on the effect of water and/or sabkha brine on the properties of sabkha. Additionally, standard techniques (ASTM or BS) were evaluated for their suitability. Further, samples were tested to determine specific gravity, classification, activity, compaction and mineralogy of sabkha.

1.3.4 Correlation of Field and Laboratory Test Results:

Results of the field and laboratory tests were analyzed to establish any correlation between these tests. Additionally, field and laboratory test results were correlated in terms of strength parameters (i.e. angle of internal friction and cohesion), stiffness (i.e. elastic modulus) and compressibility.

1.3.5 Sabkha-Foundation Materials Interaction

The effect of the aggressive sabkha environment on the durability of foundation materials will be evaluated using two methodologies : exposure-site investigations and laboratory testing. Mortar specimens were buried in sabkha environment and deterioration was monitored. Laboratory investigation was carried out in sabkha-simulated environments to evaluate the effect of chlorides and sulfates on sulfate attack and reinforcement corrosion.

X-ray diffraction, scanning electron microscopy and pore solution analysis and expression techniques were used to characterize the products of reaction and to develop a comprehension of the operative mechanisms.

The aforesaid research approach is summarized in Figs. 1.2 through 1.5.

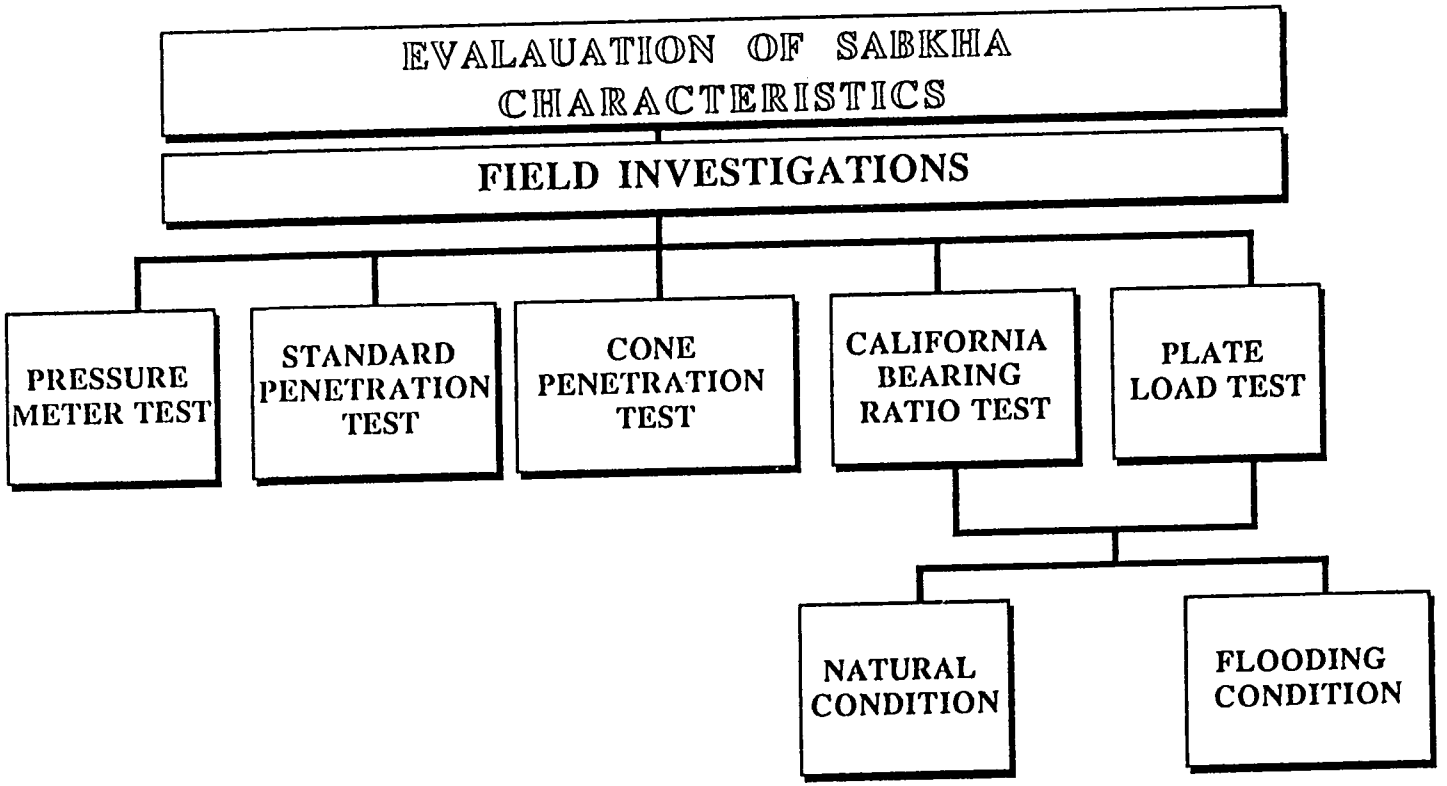

Fig. 1.2 : Research Program for Evaluation of Sabkha Characteristics in Field.

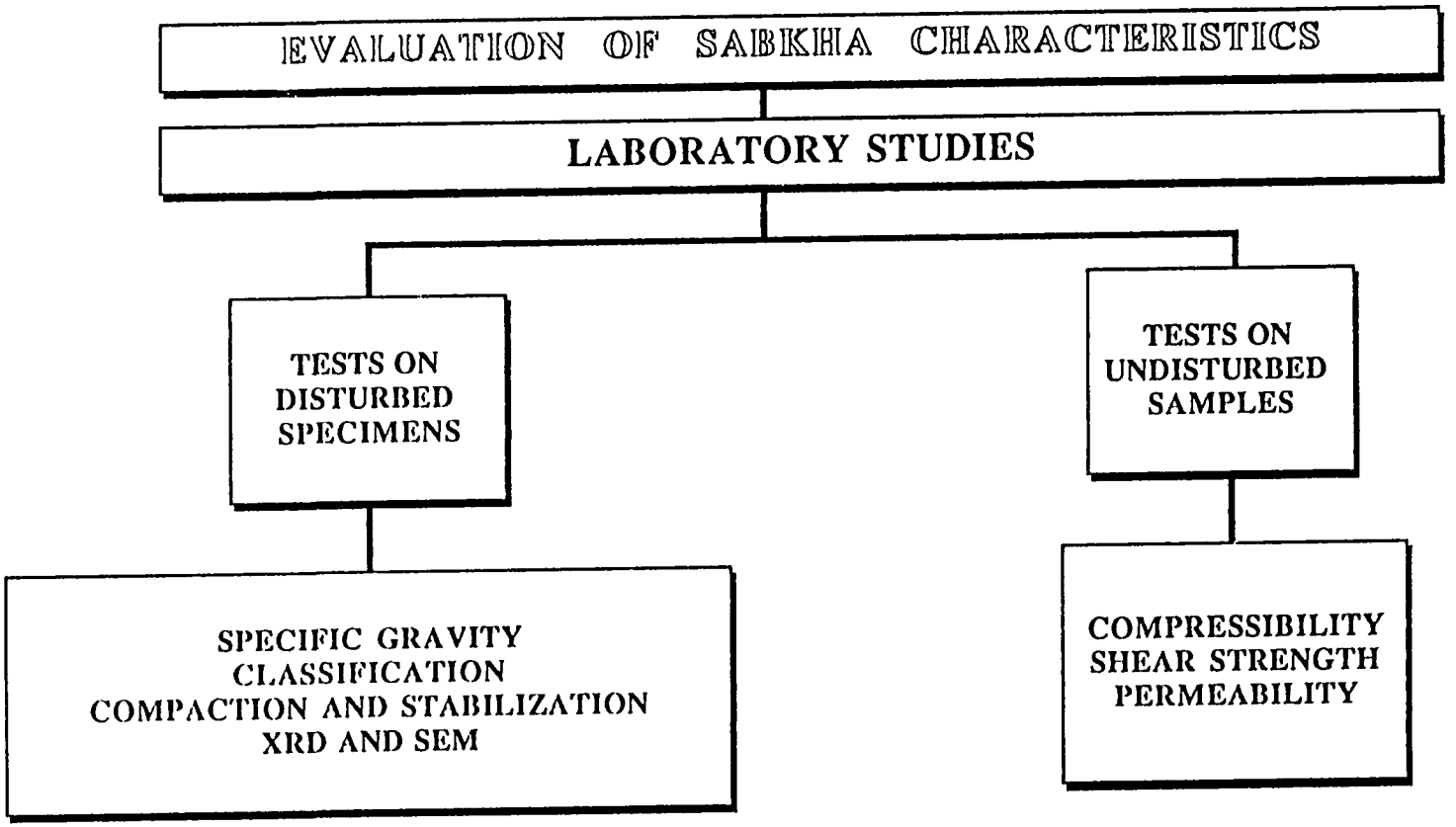

Fig. 1.3 : Research Program for Evaluation of Sabkha Characteristics in Laboratory.

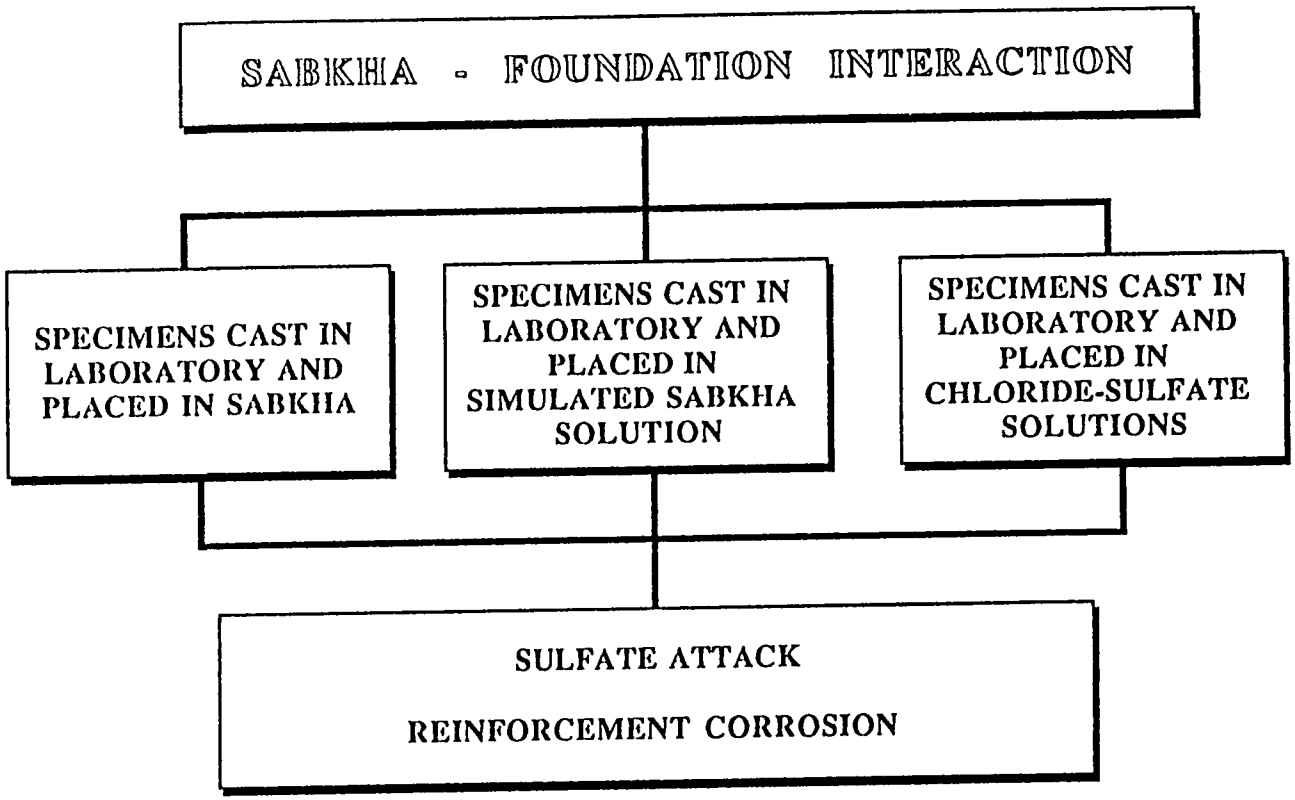

Fig. 1.4 : Research Program for Evaluation of Sabkha-Foundation Materials Interaction.

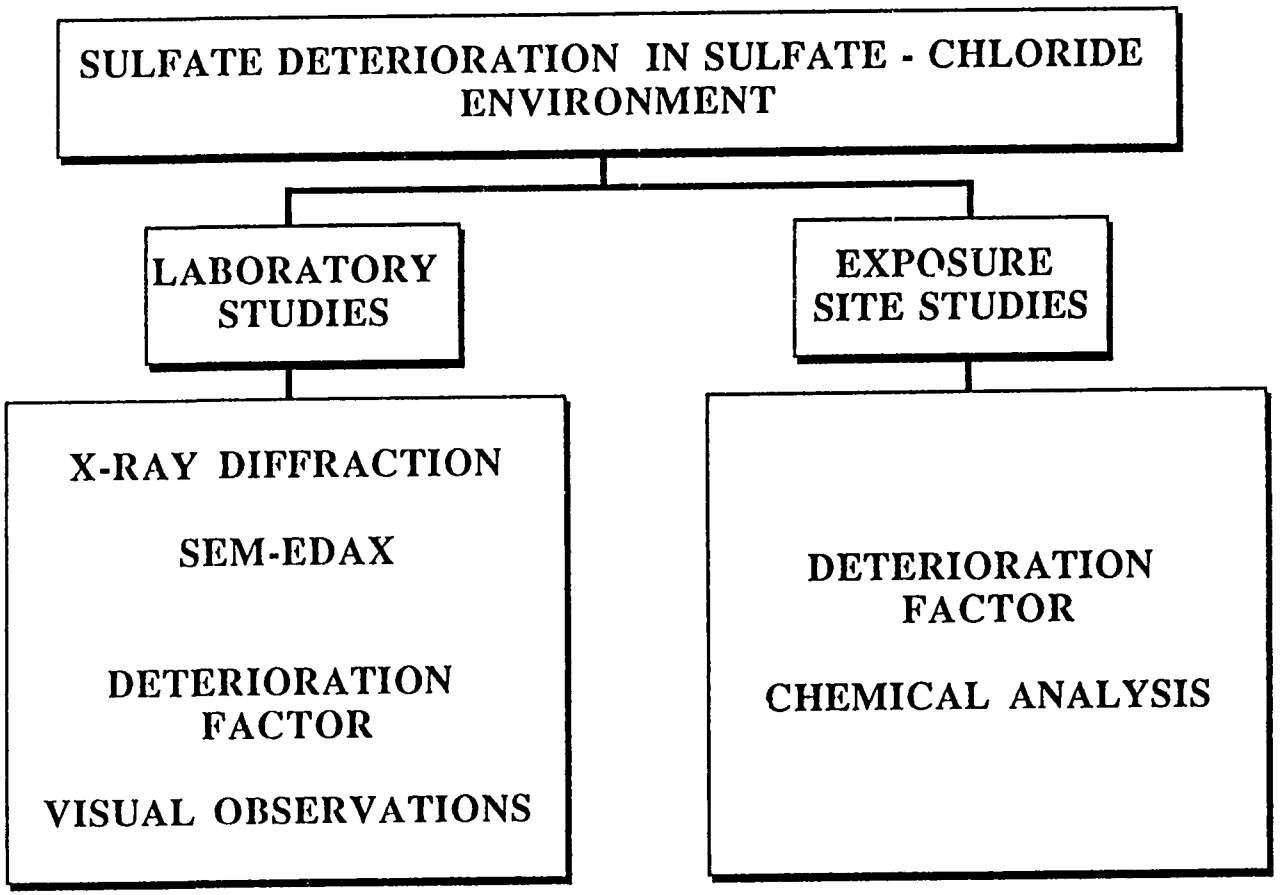

Fig. 1.5 : Research Program for Evaluation of Sulfate Resistance.

Chapter 2

LITERATURE REVIEW ON SABKHA

2.1 DEFINITION OF SABKHA-RELATED TERMS

There is no consensus among geologists, sedimentologists and geotechnical engineers on the "precise" definition of the term "sabkha", due to the considerable ramification of names for various high watertable situations in the Middle East (1). The expression "sabkha" (spelled in some publications sabkhah, subkha, sebkha, etc.) is an Arabic name for saline flats that are underlain by sand, silt and clay, and often encrusted with salt. It is an equilibrium surface whose level is largely controlled by hydrological and climatic conditions (2). Sabkha soils are defined as the subaerial evaporite flats that border partially landlocked seas (coastal sabkha), or cover a number of continental depressions (continental or inland sabkha) that usually form under hot, arid climates; and associated with high groundwater table (3,4,5). Sabkhas' surfaces are usually hard enough to support a medium-weight vehicle, and become impassable when wet that a person would sink in nearly to knee depth. A sabkha differs from a salt pan (or an evaporitic basin) in that its depositional interface is subareal, whereas that of a salt pan is subaqueous. Also, the water that nourishes a sabkha has a major, lateral component of

interstitial flow, while being concentrated by evaporation, as shown in Figs. 2.1 (a and b). This causes numerous diagenetic changes that probably can not be duplicated in any other single environment (5).

2.1.1 Coastal Sabkha

Coastal sabkhas can be the result of depositional offlap, at least in their seaward parts. A shoreline regression rate of about 1 to 2 m/year has prevailed in many areas during the past 4000-5000 years, especially in subtidal, intertidal and supratidal environments (4,6,7). A coastal sabkha is typically bordered on the seaward side by a semi-restricted lagoon, and on the landward side by a desert or rock outcrops. It is usually stark, salt-encrusted, and virtually flat, except for possible, scattered storm tide channels and small isolated sand dunes. Its surface dips very gently seaward at imperceptible rates, and does not normally exceed a few centimeters to one or two meters in elevation above the mean high-water level (4,7,8). Fig. 2.2 shows a generalized cross-section across a typical coastal sabkha and Fig. 2.3 shows a naturally-existing sabkha cross-section in Jizan, southwestern Saudi Arabia. Both figures show that a barrier is required for the development of coastal sabkhas, the rather flat characteristics of sabkha and the shallowness of groundwater tables. Since virtually the whole spectrum of sedimentation in the Arabian Gulf is carbonates, the major constituents of these types of sabkhas are

aragonite and calcite (9,10); and by virtue of their proximity to the coasts, the carbonate content decreases as sabkhas grade landward. An extremely hot and arid climate with much more evaporation than precipitation is most conducive to sabkha development (5). An active sabkha is usually characterized by brine-saturated, porous and permeable sediments that are capable of supplying sufficient volumes of water to keep pace with, but not exceed, water volumes being lost to the atmosphere by evaporation. If the water influx exceeds the evaporation loss, an evaporite pan, rather than a sabkha, will form (5). Conversely, an evaporite pan can evolve into a sabkha by either the increase in evaporation or the decline in recharge, or by both. Because of this evaporative discharge of water through the sabkha, a subsurface hydraulic gradient toward the sabkha is generated by the induced flow of both the subsurface marine waters and terrestrial groundwaters. Thus, the former flow is induced landward towards the sabkha, while the latter is induced seaward towards the same target. Marine waters can also recharge the sabkha during intermittent tide- and storm-induced flooding of the sabkha margin (7,11), or through the floor of the lagoon that normally separates it from open sea (4,5,12,13).

2.1.2 Continental Sabkhas

The other type of sabkha is the continental or inland sabkha which develops without marine sedimentological association; although Illing and Taylor (14), Fookes, et al. (1985) and Smith

(16) suggested that the term "sabkha" be restricted to only coastal salt flats, because the continental salt flats are "covered by the well-established term "playa". However, these two types of salt flats share more similarities than differences, and it might be inaccurate to distinguish between them by calling one a sabkha while the other a playa (4). Inland sabkhas are often interpreted as deflation surfaces, from which the wind removes dry small particles, parallel to the watertable at a level controlled by the dampness of the sediments (15). The groundwater table has to be higher than the bedrock surface and the base level of deflation has to lie just above the capillary fringe in the sediments (2). Evaporation through the surface causes both the formation of brines and the precipitation of evaporite minerals. Consequently, the groundwater table plays a substantial role in the development of inland sabkhas which are usually less-developed than coastal sabkha flats and are predominantly tectonically and/or topographically controlled (3). The sediments of these sabkhas are dominantly composed of gypsum (desert roses), quartz and calcite, with halite always existing at the crust (16).

2.1.3 Other Sabkha-Related Terms

The term "megasabkha" was used in the literature to indicate such gigantic types of sabkhas with an order of magnitude several times of an ordinary sabkha, and with a full evaporite

succession, which an ordinary sabkha usually lacks (4). However, this term has not been in use anymore, due to the fact that all sabkhas; whether very large or small, have almost the same evaporite succession. Variation in such succession depends on many controlling factors which will be discussed later, including the sabkha environment and the rate of sabkha development (4).

Terms such as arenaceous (i.e. sandy) and argillaceous (i.e. clayey) sabkhas (17) have almost disappeared, because of the simple fact that the composition of sabkha is highly variable. Nevertheless, if distinct layers can be recognized in the sabkha profile, such terms as arenaceous, argillaceous, etc. can be used (see for example Ref. 18)

Again, as sabkha is associated with brine evaporation, many types of evaporite minerals are expected. Local names for these evaporite associations are many and are indeed highly bewildering (19). Ellis (10) presented some local names in many countries (Table 2.1). At the risk of gross over-simplification, Fookes and Collis (20) have reduced these names, for engineering purposes, to: sabkha (coastal salt "marsh"), playa (an ephemeral lake flat), salt playa (as playa but with salty surface due to evaporation of salty lake waters) and salina (local depression with high salt watertable and capillary rise reaching the surface with the formation of a salt crust), as illustrated in Table 2.2 and Fig. 2.4.

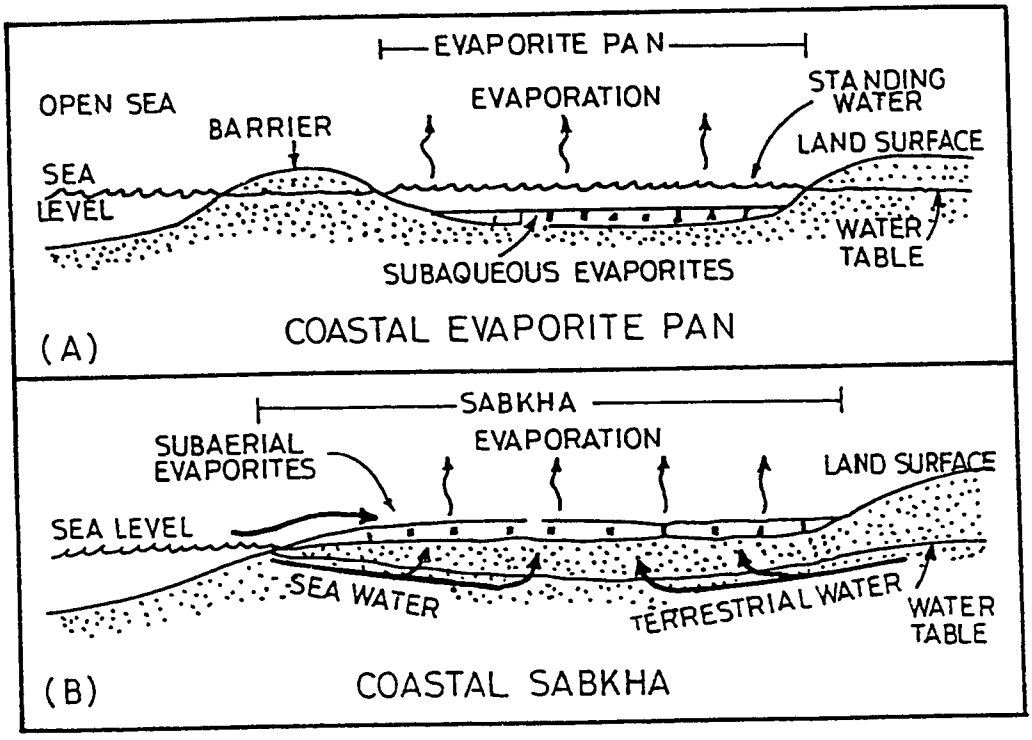

Fig. 2.1 : Diagrammatic Cross-Sections Illustrating the Difference between (a) a Coastal Evaporite Pan, and (b) a Coastal Sabkha (Renfro, 1974).

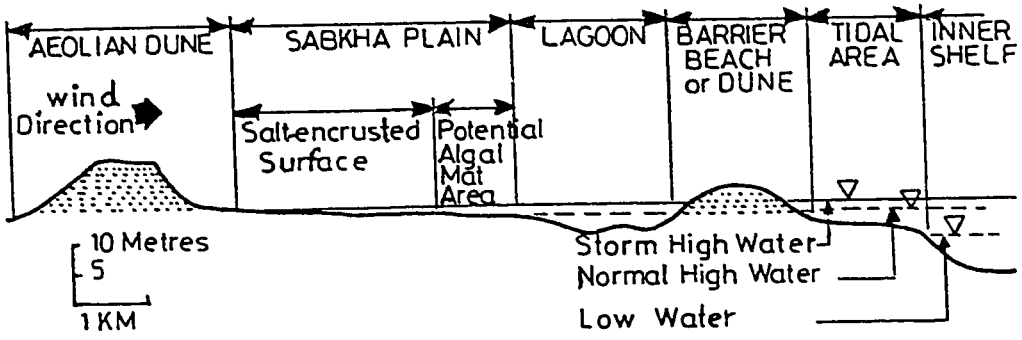

Fig. 2.2 : Generalized Cross-Section across a Typical Coastal Sabkha (Akili and Torrence, 1981).

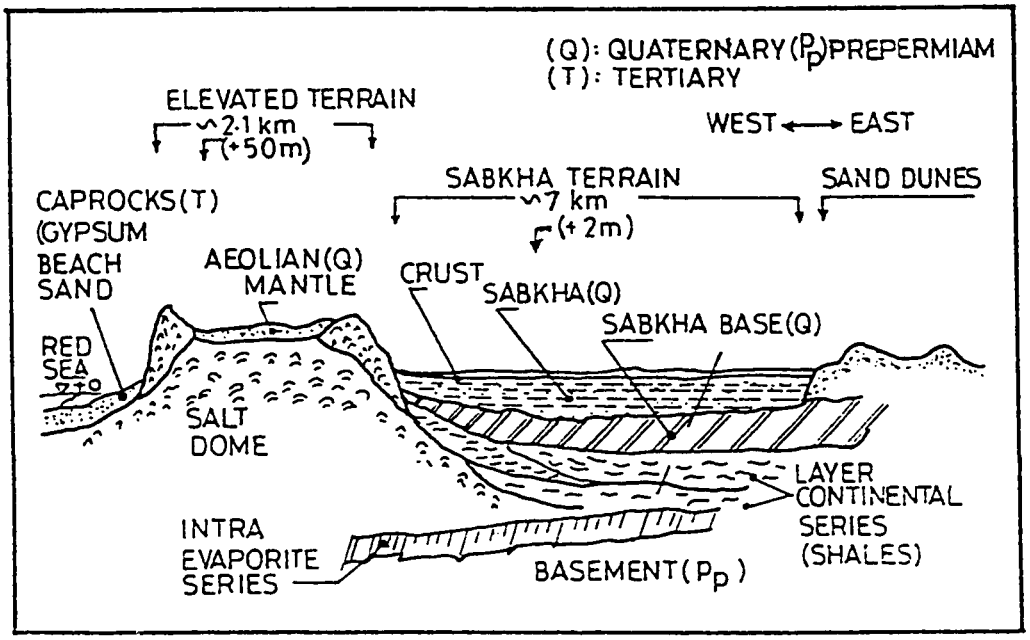

Fig. 2.3 : Naturally-Existing Sabkha Cross-Section in Jizan (Erol, 1989).

Table 2.1 : Regional Sabkha/Playa Nomenclature (Ellis, 1973)

Location	General Terms	Clay-Silt Playas	Saline Playas
United States	Playa,dry,lake alkali flat	Dry playa, clay playa	Salt flat, salt marsh, salina
Mexico	Laguna, salina	Laguna, Salina	
Chile	-	-	Salina (moderate salt) salar(much salt)
Australia	Playa, lake	Clay Pan	Salt pan, salina
Russia	Pliazh	Takir	Tsidam
Mongolia	Gobi, nor	Takyr	Tsaka, nor
Iran	Daryacheh	Dayq	Kavir
South Africa	Pan, vloer mbuga	Clay pay	Salt pan, kalahari ulpfannen (lime)
North Africa	Sebkha	Garoet, qavat	Sebkha, chott
Arabia	-	Khabra	Mamlahah (salt flat) sabkah (coastal salt flat)
Jordan	Ghor	Qa	-
Iraq	Hawr	Foydat	Sabkhat
India	Rei	-	-
Pakistan	Hamun	-	-

Table 2.2 : Definition and Characterization of Some Evaporitic Basins (Fookes and Collis, 1975)

Name	Terrian	Groundwater Table	Salts	Special Significance	Construction Notes
Sabkha	Coastal flat, inundated by sea water during exceptional floods	Very near the surface	Thick surface salt crusts from evaporating brines. Salts usually include carbonates, chlorides and others.	Generally aggressive to all types of foundations by salt weathering of stone and concrete and/or sulphate attack on cement bound materials. Evaluate bearing capacity	Carefully investigate consider tanking concrete foundations; use dense concrete. For surface roads consider using inert aggregate raised embankment or positive cut-off below sub-bases. Use as fill may be suspect. May not be deleterious to unsurfaced roads.
Playa	Inland, shallow centrally-draining basin of any size	Too deep for the capillary moisture zone to reach the ground surface, but area will be a temporary lake during floods	None if temporary lake is of salt-free water	Non-special. Ground surface may be silt/clay or covered by windblown sands. Evaluate bearing capability	Non-special
Salt playa	As playa, but sometimes smaller	As above, but lake of salty water	Surface salt deposits from evaporating temporary salty lake water. Salts usually includes chlorides and sometimes sulphates and carbonates	Can be slightly to moderately aggressive to all types of foundations by salt weathering and sulphate attack. More severe near watertable.	As sabkha
Salina	Inland basin of any size	Near surface, capillary moisture zone from salty ground can reach the surface	Surface crust from evaporating salty groundwater. Salts includes sulphates and others	Can be slightly to exceptionally aggressive to all types of foundations by salt weathering and sulphate attack	As sabkha

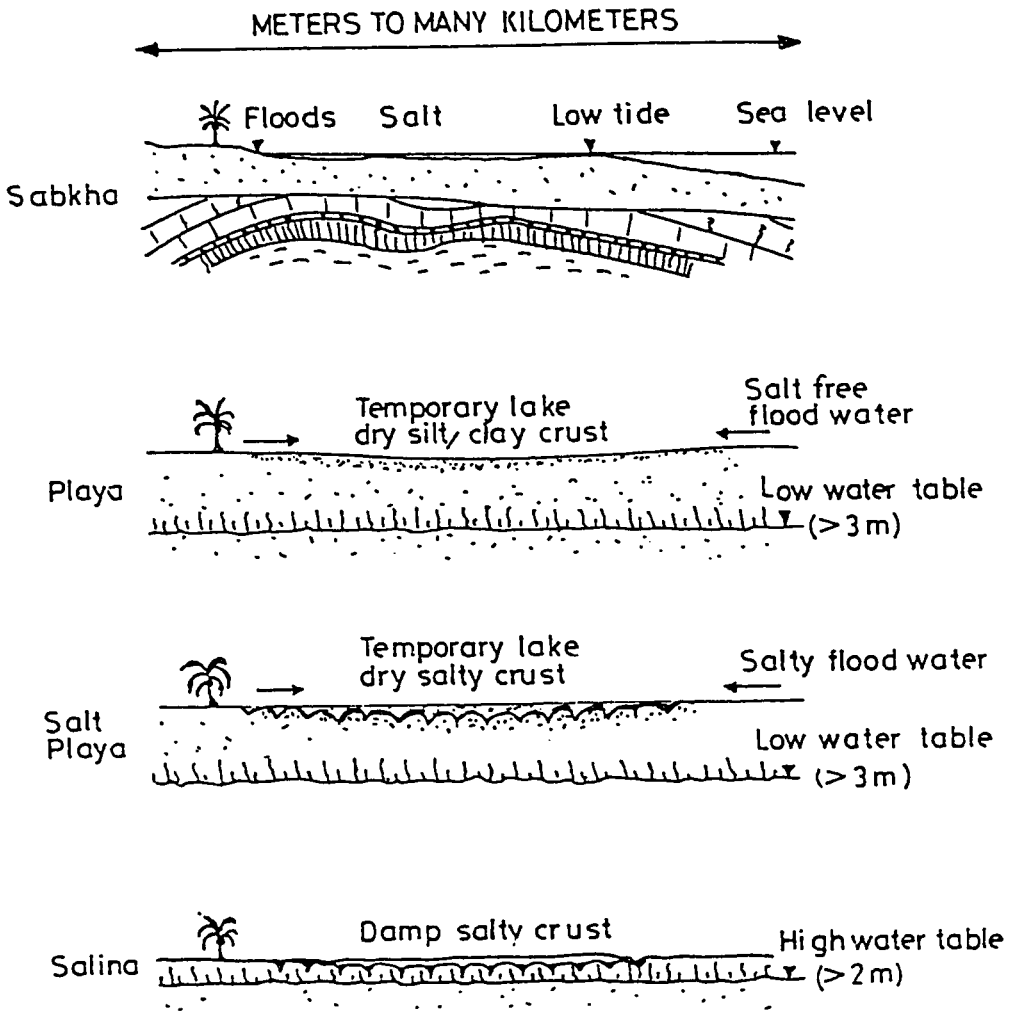

Fig. 2.4 : Idealized Cross-Section of Sabkha, Playa, Salt Playa and Salina (Fookes, 1976).

2.2 DISTRIBUTION OF SABKHAS

Saudi Arabia has a large number of sabkhas, both coastal and inland. A summary of these sabkhas in the coastal plains of the Eastern Province - based mainly on reconnaissance visits - is shown in Fig. 2.5. These sabkhas are, as described by Johnson et al. (2), either coastal (close to the sea) or continental (further inland). Along the western shores of Saudi Arabia, coastal sabkhas also exist at Obhor (21,22), Al-Lith (250 km south of Jeddah) (23), and Yanbu (24). In Southwestern Saudi Arabia, near the town of Jizan, coastal sabkha is shown to exist surrounding a salt dome (25,26). In the North, continental sabkhas are reported to exist in Wadi As Sirhan (16).

Sabkha distribution in Saudi Arabia is shown to be quite extensive specially in the well-populated cities along both the Red Sea and the Arabian Gulf coasts.

The sabkha distribution along the southern and southwestern shores of the Arabian Gulf is well documented. Fig. 2.6 (27) gives a good presentation of the prevalence of sabkha along the Arabian Gulf.

It has been reported that sabkhas are present in Mexico, Utah and Texas in U.S.A. and Ethiopia as well as other locations (28). Active coastal sabkhas are also reported to exist in Australia, Sudan and North Africa (10) and Libya (29,30). Sabkhas

typically exist in semi-arid, arid or extremely arid climatic regions (excluding the polar arid), and cover about 30% of the total land area of the earth, principally within latitudes 10° 50' N and 20° 30' S, where most of the Arab and Muslim countries lie (31). The active and potentially favorable locations of sabkhas are depicted in Fig. 2.7 and 2.8 respectively.

2.3 GEOLOGY OF SABKHA

A sabkha soil is generally viewed as an unconsolidated, heterogeneous, layered or unlayered sedimentological framework, bathed in highly concentrated subsurface brines. It normally has a loose, rather porous and permeable, gritty structure, with an obviously high rate of infiltration. Its outer surface is usually composed of hygroscopic salts, and thus, when damp can render the normally stable surface crust impassable (2,3,10,19).

The continuous interaction of the brines with the sediment framework leads to steady production of new - or at least modified - sedimentary features and new minerals to the sabkha. Consequently, both primary and later (secondary, tertiary,etc.) sedimentary features and minerals are among the numerous characteristics of sabkha deposits. The primary features are related to the original framework of deposition, while the later are the consequence of the continuous reaction of the interstitial brines in the system during the processes of deposition and diagenesis (3).

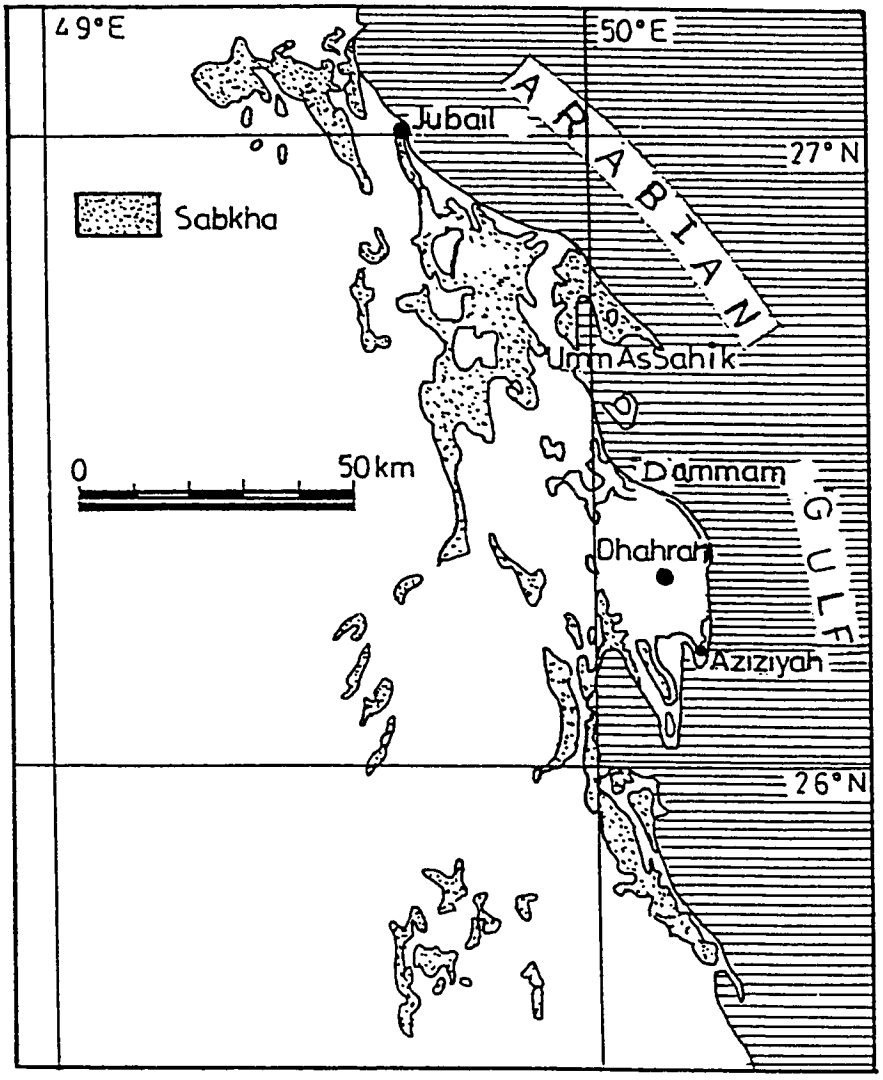

Fig. 2.5 : Sabkha Terrains in the Coastal Region of Eastern Saudi Arabia (Johnson et al., 1978).

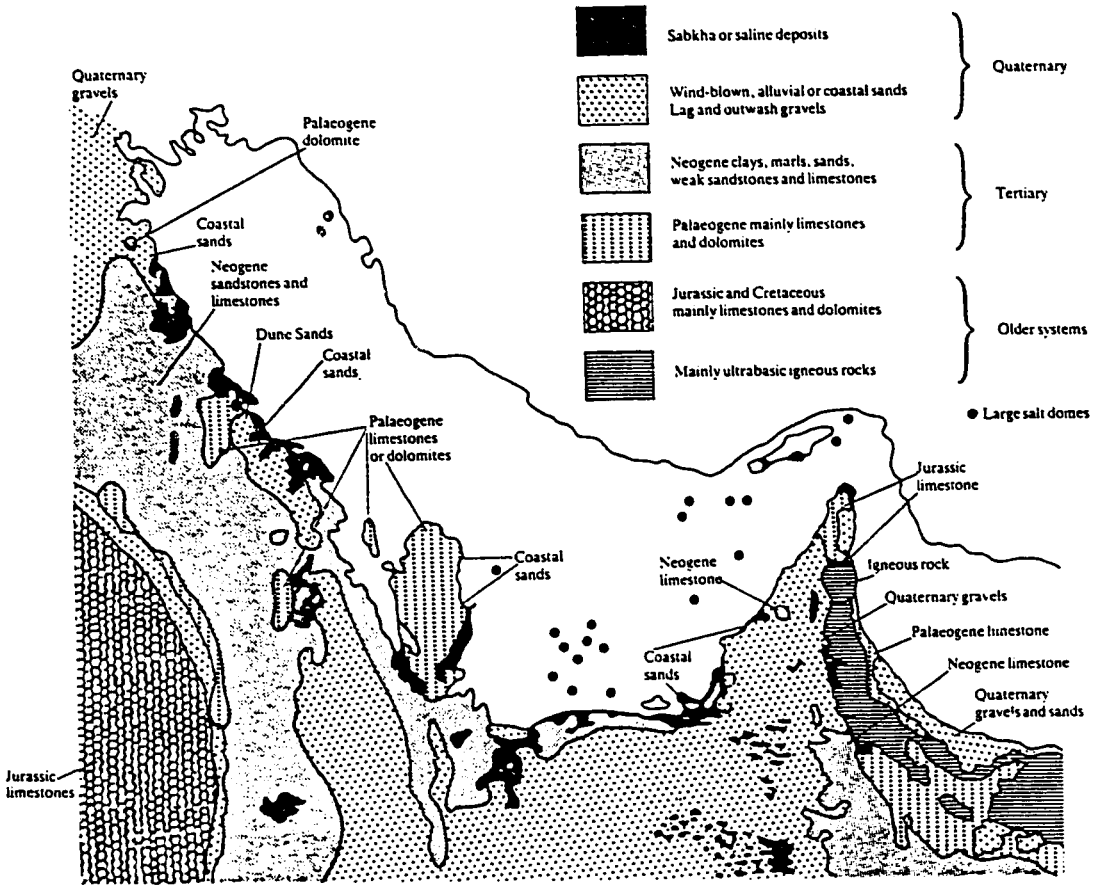

Fig. 2.6 : Simplified Geology of the Arabian Gulf Countries (Fookes and Higginbottom, 1980).

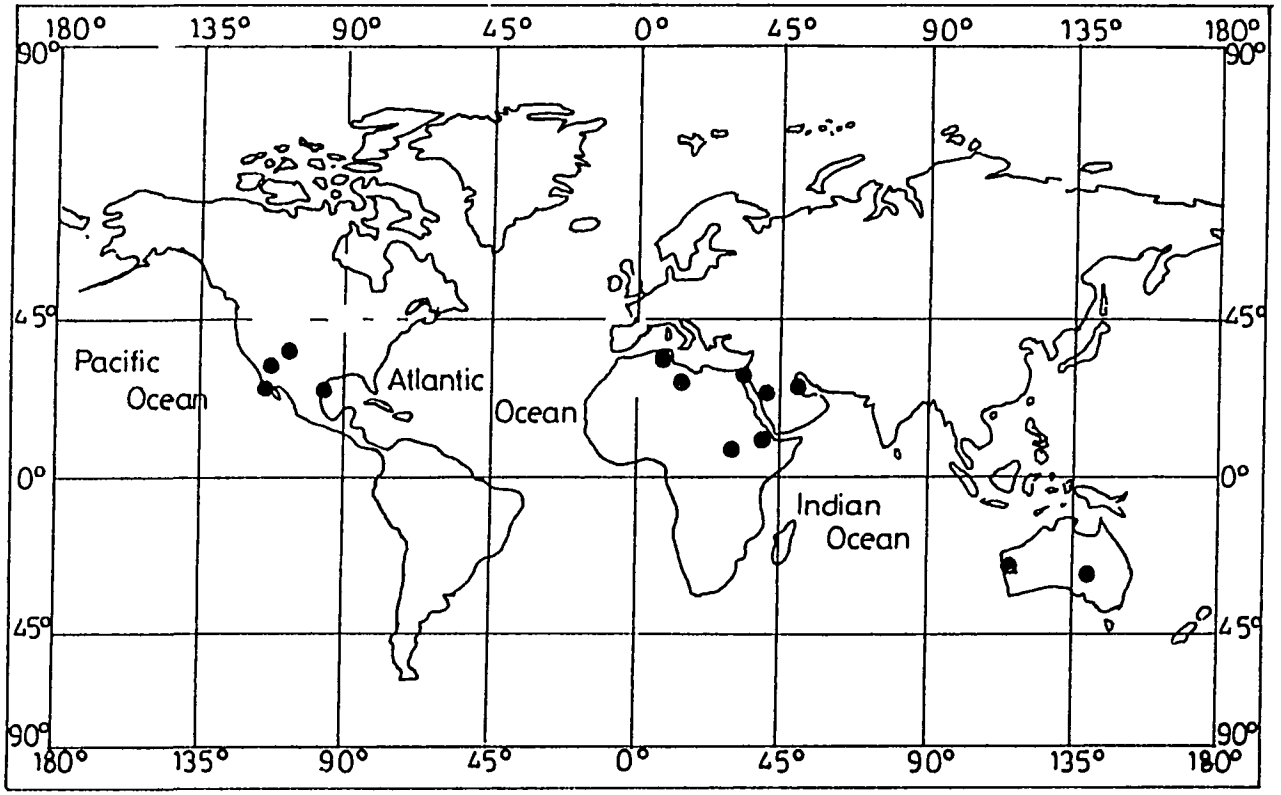

Fig. 2.7 : World Map Showing Locations of Active Coastal Sabkhas (Renfro, 1974).

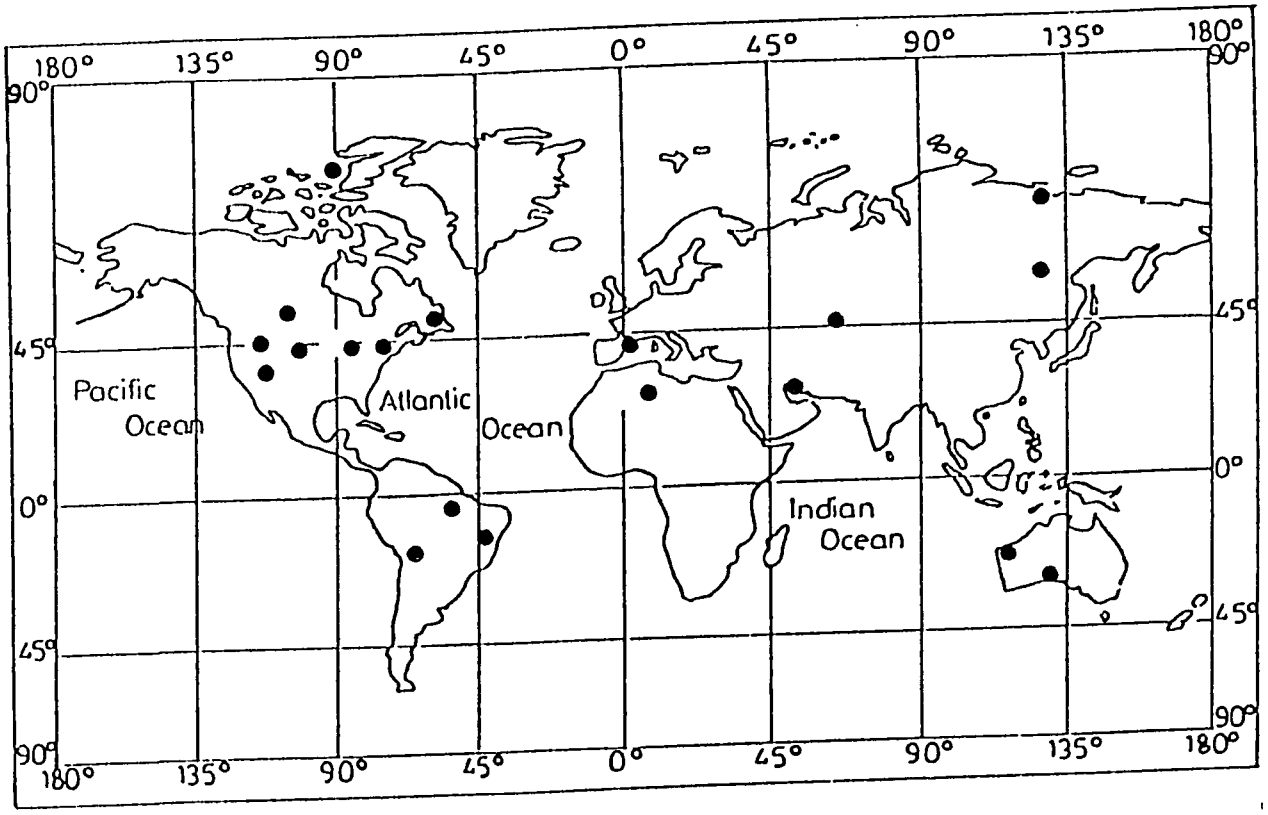

Fig. 2.8 : World Map Showing Locations for Potentially Favorable Strata for Sabkha (Renfro, 1974).

Despite the fact that these processes are slow, commonly being of geological rather than engineering significance, however, the understanding of the old sabkha developments can help enormously in the understanding of the recent sabkha evolution. This is because it is well documented that sabkhas keep repeating themselves by what is known as "sabkha cycles" (32). An extensive sedimentologically-based research on sabkha soil was carried out by the Imperial College of London, Shell Research B.V. and Kiel University on the sabkhas of both the United Arab Emirates (mainly Abu Dhabi and Dubai) and Qatar during the sixties and early seventies. Part of this work is documented by Purser (33) and Bathurst (34).

The sequence of major palaeogeographic events in the formation of these sabkhas can be summarized as follows (3):

i) In the Late Pleistocene (about 400,000 Y.B.P.), the Arabian Gulf waters stood at a level of 150 m higher than its present-day mean (17,35). Most of the present-day coastal areas were submerged by the Gulf waters, and the sabkhas around the +150 m level were formed along the Gulf's ancient coasts in - more or less - the same way present-day coastal sabkhas are being formed.

ii) In the Latest Pleistocene (shortly before 100,000

Y.B.P.), glaciation led to a worldwide lowering of the sea level, which caused the Arabian Gulf waters to drop down to a level 120 m below its present-day mean (33,36). Consequently; the Arabian Gulf basin dried up completely, except for a small arm at the Hormuz Strait. This phase reached its climax at about 20,000 Y.B.P., and was followed by:

iii) A gradual rising of the sea level and the re-infilling of the Arabian Gulf basin with waters from the Indian Ocean during the (latest Pleistocene - earliest Holocene) post-glacial transgression, between 20,000 and about 7,000 Y.B.P. (35,37).

iv) In the early and middle Holocene (7,000-4,000 Y.B.P.), oscillations in the eustatic sea level brought in local marine transgressions, during which the water level was slightly higher than today. From investigations in sabkha areas at Abu Dhabi (7,38,39,40) it is concluded that the early-middle Holocene transgression began about 7,000 Y.B.P. and continued until about 4,000 Y.B.P., when the sea level reached the position of a new, free-lying strand bank; with minor oscillations to the present-day mean level.

v) From about 4,000 till around 1,000 Y.B.P., the sea

level was still oscillating in minor transgressions and regressions that left their marks in the form of abraded, raised terraces (2 to 3 m above the sea level) in many coastal areas (35). These oscillations were accompanied by a relatively quick fall in the sea level of about 1 m at about 3,750 Y.B.P., and another drop of about 0.6 m to the present-day level during the period from 3,750 to 1,000 Y.B.P.

vi) If this information is applied to the whole Gulf area, the water level up to 3,750 Y.B.P. would have been between 2.7 to 2.9 m above the present-day level. This means that during that period, the present-day sabkha area would have been lain under a free-water surface, which extended for more than 1 km west of the present-day shoreline, with strand coastal banks and barriers that represent series of transgressions, vertical build-ups or regressions (41).

As related to the geologic history and the development of the sabkhas themselves, radiocarbon dating of the sabkha sediments has made it possible to trace the sequence of events which led to their formation (8). Bush (40) has summarized these events as follows:

Approximately 7,000 Y.B.P., the Gulf waters transgressed

over the site of the present sabkha plain, which at that time was covered by sub-aerial dunes composed of quartzose carbonate sand. The extent of this transgression varied from place to place. In the area of the southwest of Abu Dhabi Island, the maximum transgression reached a point between 5 and 6 km landward of the present low water mark by approximately 4,000 Y.B.P., and a beach ridge developed at the margin of the lagoon so formed. Landward of the ridge, the dunes were deflated to the level of the watertable, as their source of sediment had been submerged beneath the waters of the lagoon.

Seawards of the beach ridge, the original, aeolian, quartzose carbonate sand was reworked during transgression, and then gradually buried under newly formed skeletal carbonate sand which contained considerable amounts of re-worked aeolian sand in its lower parts. It was finally covered with grey, muddy carbonate sand as the lagoonal environment became established. Deposition continued until the lagoon became very shallow and further accumulation of sediment was prevented by the action of waves and currents.

A lithified crust, cemented with high magnesium calcite, formed on the surface of the sediments in the area of non-deposition (a similar crust is found on the lagoon floor at the present time). Sediments were transported by waves and currents to be deposited at the margins of the lagoons to form intertidal flats.

This resulted in the lateral filling of the lagoon and the progradation of the coastline.

An apparent fall of sea level by approximately 1 m occurred between 4,000 Y.B.P. and 3,750 Y.B.P. This resulted in some of the sediments of the inner lagoon becoming intertidal instead of subtidal. The new intertidal area was colonized by an algal mat. At first, the algal mat grew out over the lithified crust, but later it continued to grow over the sediments pushed to the margins of the lagoons by the waves and currents. As this algal mat grew seawards it was slowly covered by sediments carried onto its surface by winds and the occasional storms. About 1,000 Y.B.P., this algal mat ceased to grow and was buried by intertidal sediments, but the plain continued to prograde seaward and finally a new algal mat developed and has continued to grow until the present day.

Sabkhas situated at different levels, further inland (e.g. north of Jubail, 80 km inland and as far west as Wadi Al-Miyah, or between the Gulf coast and Al-Hofuf/Abqaiq area, etc.) are not authentic inland sabkhas formed in deflation basins, but are remnants of older coastal sabkhas formed during the early-middle Pleistocene high sea stands (17,42). This is also the same case for the numerous sabkhas on the eastern margin of Al-Rub'a Al-Khali (i.e., the Empty Quarter).

The same processes of sabkha formation were also recorded in much older rock units. Core samples from the Jurassic-Cretaceous boundary in the Umm Shaif oil field (offshore the U.A.E.) have revealed 9 successive sabkha cycles (32), and numerous other fossil sabkha cycles have been penetrated during drilling for oil down to depths that exceed 176 ft. (53.7 m).

2.4 FACTORS THAT CONTROL SABKHA FORMATION

Numerous factors play different roles in the genesis of the sabkha system. These factors can be grouped under five categories (Fig. 2.9):

1) Climatic: which include rainfall, temperature, humidity and prevailing wind.
2) Geochemical: including both brine chemistry and diagenetic minerals.
3) Geomorphological: which include surface gradient, groundwater table, etc.
4) Hydrological: these are, by one way or another, considered as the resultant of the above-mentioned three factors.
5) Biological: which include algal mats and burrowers.

The interaction of these factors, or of any combinations of them, will result in the processes and reactions which characterize the sabkha environment. Should any of these factors change, then

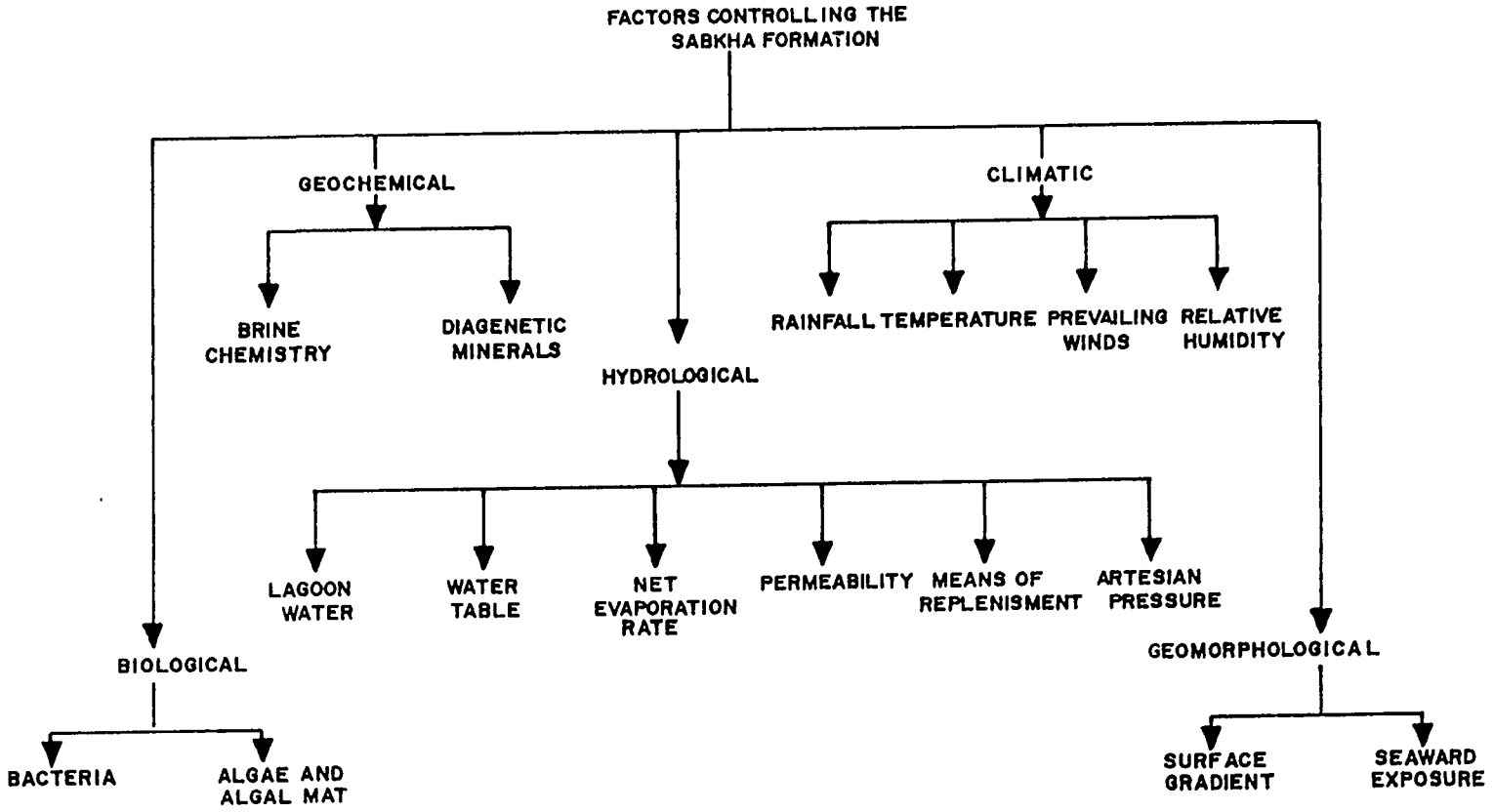

Fig. 2.9 : Summary of the Factors Controlling the Sabkha Formation.

the end results would be affected. For example, if over a period of years, climatic changes bring in generous rainfall, this will probably be reflected in the sabkha profile by strata lacking in halite deposits. Therefore, to better understand the sabkha environment, it is crucial to study the factors of genesis of the sabkha and determine their values and boundary ranges. These factors can be briefly summarized as follows:

2.4.1 Climatic Factors

The Arabian Gulf sabkhas lie in the northern sub-tropical zone, and are surrounded, mostly, by vast deserts and have a general arid climate. As aridity is a measure of dryness, the best index is, therefore, the one based on water balance of the area (i.e. the difference between the moisture received by the area and the moisture lost) (43).

1) Rainfall: is one of the three main water sources to the sabkha system, but is by far the least important of the three (at least volumetrically) (3). Butler (7) quotes an average annual rainfall for the Arabian Gulf sabkhas of less than 5 cm; however, it is probably mainly between 3 to 4 cm (44); compared to an average annual evaporation rate of approximately 125 cm (45). Although rainfall is scanty and sporadic, it is mostly thinly spread over a

period between October and March, but it is not unusual for the region to go for several successive months without any rain. The region averages 360 days per year of sunshine.

The only major effect of rainfall on the sabkha system is that it tends to dissolve the precipitated salts on or near surface strata (especially the ephemeral halite), but this is only effective when it occurs at night, or in torrential downpours. Rainfall might also temporarily dilute the sabkha brine and might raise the watertable level (44).

2) Temperature: is one of the chief driving factors for the evaporative mechanism of the sabkhas. The climate of the Arabian littoral area is hot and arid, with a daily average temperature range of 15°C to 44°C (20°C to 25°C in winter), and a summer average of 40°C. The range can be much wider in the inland margins of the sabkha, where the temperature can reach up to 50°C during summerdays and drop down to almost 0°C during winternights (28). The Arabian Gulf itself is the warmest sea in the world, averaging 20°C at the surface in February and 34°C in August. The average temperature of the sabkha watertable surface is 34°C, while just below the sediment surface of the sabkha, the daily temperature

ranges from 18°C to 53°C (7).

3) Relative Humidity: is proposed as a constraint on the final salinity of a brine, and hence, the ultimate evaporite mineral facies (46). It is shown that different evaporite minerals will be precipitated at different activities of water, as follows (46):

at H_2O = 0.93 - 0.76 Sulfate minerals will precipitate

at H_2O = 0.76 - 0.67 Halite will precipitate

at H_2O < 0.67 Potash minerals will precipitate

For arid coastal evaporite areas, Kinsman (46) gives mean relative humidities ranging from 70 to 80%, mainly suitable for sulfate minerals precipitation.

The variation in relative humidity is great, reaching 20% in day time and almost 100% at night and early mornings (44).

4) Prevailing Winds: Their persistence, seasonability and direction all play important roles in the genesis of sabkha in the Arabian Gulf. On the other hand, strong onshore winds, called Shamal winds, are north to northwest winds that do not generally bring rain, but are accompanied by

hazy conditions, as a result of suspended dust. These Shamal winds can transport huge quantities of aeolian sands onto and across the sabkha flats. The sand adheres to both the damp surfaces and the algal mats. Often, entire sand dune fields can migrate across the sabkha in an offshore direction, and this is the main reason for producing arenaceous (i.e., siliciclastic) sabkhas and for calling the sabkhas "deflation basins".

On the other hand, seasonal, strong offshore winds, called Monsoon, are south to southeast in direction and can cause flooding of sabkha surfaces, providing critical replenishment of its water. The variable extent of this flooding has led Evans, et al. (38) to distinguish a number of flood recharge zones, each characterized by its own mineral suite and water chemistry values. Such wave-driven sabkhas are mostly calcareous in composition with minor amounts of quartzose sand if any.

2.4.2 Geochemical Factors

The chemistry of the sabkha brines is, naturally, the most crucial factor in determining the nature of the evaporite minerals' suite. The extremely high salinities of the Arabian Gulf waters, as compared with other open seas, and its sabkhas are dictated by

the excessive rate of evaporation and the restrictive nature of the Gulf waters and of its sabkhas. Such high salinity has been advised to be exploited economically, as suggested by Johnson, et al. (2) and Smith (16), and it is being utilized for this purpose in the Ras Al-Ghar Salt Plane by SADAF.

1) Lagoon and Sabkha Brine Chemistry: Due to the low precipitation and high evaporation rates that are coupled with the restricted nature of the Gulf, the salinities are, consequently, high. Values ranging from 37 - 38 ‰ in the outer shelf areas, to 42 - 43 ‰ in the inner shelf areas, to over 60 ‰ in very restricted lagoons have been reported (47); compared with an average of about 3 to 4.2 ‰ for the Gulf waters (33). Ellis and Russell (48) quoted a range of groundwater salinities from 70 to about 400 parts per thousand, compared with salinities of 55 to 75 parts per thousand in the adjacent lagoon waters (8). Such unbelievable variation is expected in the sabkha systems, which are exemplarily highly variable environments, even within short distances (2,7,8). The lower salinities occur close to the lagoon; where lagoonal waters keep diluting the sabkha brine, and also adjacent to the rocky upland; because of the terrestrial groundwater influx. This is why Patterson and Kinsman (44) call this central region the "chloride plateau".

Lagoon waters are recorded as having pH values of about 8.3, interstitial algal flat waters of 7.5, while in mid and inner sabkha pH values fall to 6.0 to 6.4 (47). It is shown by Butler (7) that pH values generally decrease inland from the lagoon and then rise again towards the inland margin of the sabkha. The overall acidity of the brines in the sabkha sediments, as reflected by pH measurements, has probably been caused by the decomposition of organic matter releasing carbon dioxide and hydrogen sulfide. Variation in the pH values is not only in the transverse profile of the sabkha, but also in the vertical direction (7).

By virtue of its chemical nature, analysis of the sabkha's brine is considered as the pre-requisite test to understand the spontaneously perpetual interaction between the sabkha sediments and its groundwaters; and, ultimately, the behavior and characterization of this system. Table 2.3 presents some typical data for the major cations and anions concentrations for a typical sabkha brine of Eastern Saudi Arabia. Johnson, et al. (2) observed that the chloride and sodium concentrations are approximately 6 times the concentrations present in a typical sea water; although Taylor and Illing (49) have reported that 8-fold concentration of the interstitial sab-

kha brine is not unusual. Additionally, it was found (2) that the ratios of the various ions, except for Ca^{++} and SO_4^{--}, are almost similar to those normally found in seawater. The same authors concluded that the sabkha brines may be considered as a "concentrated sea water" (50). This clue can provide a further evidence for the sea water depositional offlap hypothesis; as discussed before. The reduction in the calcium and sulfate ions is mainly attributed to the formation of gypsum.

Solubility of the different salts should be well recognized, because only soluble salts are more likely to migrate and crystallize at the surface. Sodium chloride, sodium sulfate and magnesium sulfate are all soluble and potentially more deleterious than the relatively insoluble calcium sulfate (51). However, the solubility of a single salt is not invariant but is affected by other factors; such as other phases existing in the solution, presence of dissolved gases, pH and Eh of the solution, temperature, etc.

2) Diagenetic Minerals: The sediments of the coastal sabkha can consist mainly of either carbonate muds or calcareous sands carried up by high tides and onshore winds in the first place (9,47), or by offshore winds in the second

case. However, the characteristic feature of the sabkha sediments is the continuous development of diagenetic minerals. Sabkha diagenesis involves interstitial emplacement of evaporite minerals within the host sediments and the continuous interaction between these interstitial minerals and the host sediments. However, the replacement mechanism (i.e. whether solid-state dehydration or dissolution-reprecipitation) is not known (4). What is known is that these new minerals are formed in response to the chemical and physical milieu of the sabkha environment (6). The time when diagenetic minerals began to form can not be precisely determined (8).

Experimental studies on the sequence of salt precipitation from the direct evaporation of sea water (Fig. 2.10) leads to the deposition of calcium carbonate (aragonite) first when sea water is evaporated to about half of its original volume, followed by calcium sulfate (gypsum) at 19% of the original volume. Next in succession comes sodium chloride (halite), and at about 4% of the original volume, the highly soluble salts of potassium and magnesium - the so-called "bitterns" or polyhalites - start to develop as a co-precipitate with halite (52,53). The majority of sabkha deposits; however, show major discrepancies. Commonly, there is a much greater propor-

tion of carbonate and calcium sulfate than would be expected. The anomaly of the sabkha, with regard to sea, is attributed to diurnal variations in temperature, pressure and relative humidity of the system, and on the availability of trace elements in it. Moreover, incomplete evaporative concentration, and the difficulty of achieving equilibrium precipitation in a system as large as a sabkha, added to complex diagenetic changes may lead to sharp deviation from the results of evaporating sea water (3).

Bush (40) divided the diagenetic mineral suite of sabkha deposits into the following two groups:

a) Diagenetic Minerals Produced by Evaporation:

i) Aragonite: which is precipitated in the lagoon, and even more during the early stages of concentration of the brine both within the sabkha sediments, and also on its surface. It is the primary cement of the quartzose sabkha (54,55), especially in its uppermost parts (47). Its frequency decreases inland until, in places, it disappears completely, probably as a result of dolomitization.

ii) Gypsum: is the most common evaporite mineral

Table 2.3 : Major Cation and Anion Concentrations in Sabkhas of Eastern Saudi Arabia in g/l (i.e. parts per thousand) (Johnson et al., 1978)

Station No.	Na^{+}	Mg^{++}	K^{+}	Ca^{++}	Cl^{-}	$(SO_4)^{--}$	$(HCO_3)^{-}$	pH*
1	46.7	5.25	2.81	2.25	99.3	5.58	0.095	7.1
4	93.3	9.17	3.22	1.50	209.2	4.45	0.082	6.0
7	88.3	6.83	2.28	1.63	163.1	5.87	0.054	7.0
10	95.0	8.00	2.90	1.60	184.4	5.46	0.037	6.5
13	76.7	7.17	2.50	1.48	148.9	7.12	0.048	6.6
16	83.3	8.33	3.08	1.99	162.9	4.66	0.044	6.4
19	75.0	6.58	2.06	2.54	139.6	3.55	0.032	5.7
Average	79.8	7.33	2.69	1.86	158.2	5.24	0.056	6.7
Salt Mine	85.0	12.50	5.53	1.74	189.7	5.10	0.089	6.8
Gulf Water	15.3	2.30	1.00	0.81	34.5	4.71	0.110	8.1
Ras Al-Ghar	78.8	10.3	3.1	1.5	157.2	5.45	0.087	6.9

*Non-arithmetic Average

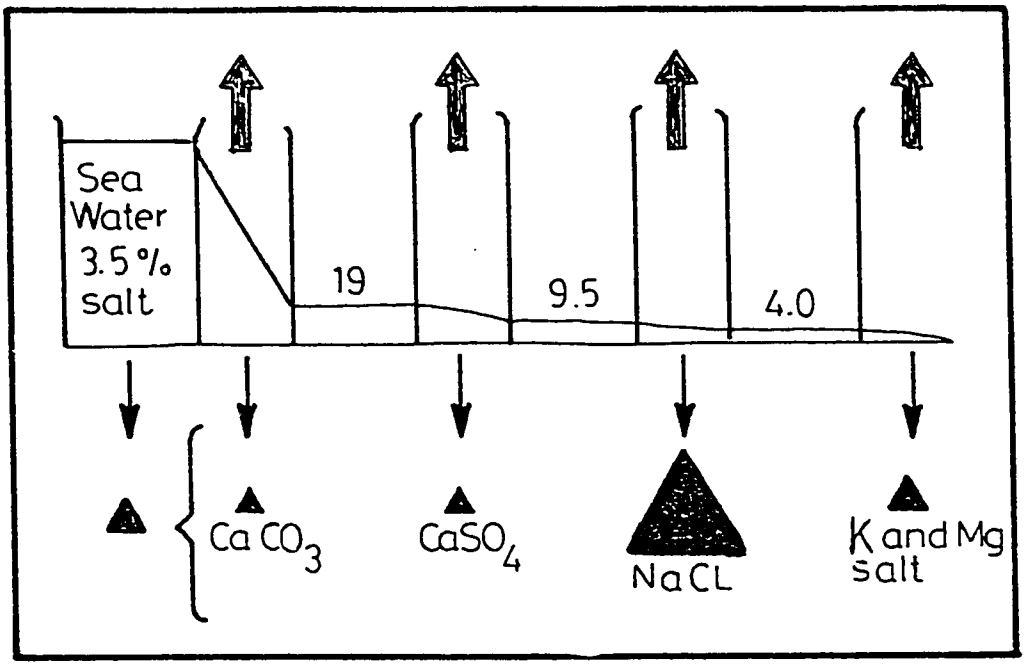

Fig. 2.10 : Consecutive Precipitation of the Different Minerals from Evaporation of Sea Water.

in sabkhas, constituting, in some places, more than 50% of the top meter of the sabkha sediments (47). It occurs as well-developed crystals of varying sizes and shapes (8), and locally as poikilitic cement. The crystals are rarely free from fine-grained carbonate inclusions (47). This mineral always develops in the interstitial spaces, but never as precipitate upon the upper sediment surface.

iii) Anhydrite: is developed just below the sediment surface in the capillary zone, where the host sediment is displaced as the anhydrite nodules grow in size (32). It is formed as a primary precipitate and not by the dehydration of gypsum (47). It occurs in the form of crystals of varying sizes and shapes (8) as well as in amorphous nodules. Although some sabkhas may contain up to 50% of this mineral, (9); it can form only a very minor proportion of the minerals present in others (13).

iv) Halite: is precipitated as the dominant salt on the top surface layer. Brines, if present on sabkha surfaces, evaporate readily leaving halite crusts of several centimeters thick. It is

also precipitated at lower levels, which are governed by the upper limits of the capillary movement (3). The halite is ephemeral, as it is promptly dissolved, unless in cases when the halite crust is buried. Halite will probably only be preserved in ultra-dry and restricted sabkhas further inland, provided the terrestrial groundwater table is too low to dissolve it.

v) Celestite: is a minor accessory mineral associated with gypsum and forms in sheep-like bundles (47). The celestite ($SrSO_4$) could form as a primary mineral with the sea water as the source of strontium, or as an early diagenetic mineral with the strontium acquired during the dolomitization of aragonite (56).

vi) Other Accessory Minerals: discovered in sabkha environments include: polyhalite, sylvite, huntite and epsomite (7,50,etc.).

b) Diagenetic Minerals Produced by the Reaction Between Brines and Sediments:

i) Dolomite: occurs in the stiff muds that bear the large gypsum crystals. The precipitation of diagenetic aragonite, gypsum and anhydrite

raises the magnesium to calcium ratio of the pore fluid brines, and values of over 12 have been recorded, compared with only 5 for the sea water. When this ratio reaches 10, dolomitization of fine-grained aragonite occurs to produce fine-grained dolomite (6,40). The calcium released is combined with sulfate from the brines to precipitate as gypsum. The intimate association of this penecontemporaneous dolomite is a special characteristic of the sabkha (32). Dolomite [$CaMg(CO_3)_2$] increases in content landward, where it may become the most abundant mineral in the top half meter.

ii) Magnesite: occurs in areas of high magnesium concentration in the brines. Although it is considered volumetrically as an unimportant member of the diagenetic mineral suite (47), it may constitute up to 50% of the material finer than 0.0625 mm (40). Magnesite [$Mg(CO_3)_2$] is formed by further dolomitizing the dolomite, according to the following reaction (40):

$$Mg^{++} + CaMg(CO_3)_2 \rightarrow 2Mg(CO_3)_2 + Ca^{++}$$

2.4.3 Geomorphological Factors

1) Surface Gradient: is a primary condition in the development of sabkhas. Gradients usually control the shape (as low gradient means a larger evaporation surface area), the recharge ability and the general morphology of a sabkha (3). A most unusual feature of the Arabian Gulf sabkhas is their almost planar surfaces, which rise inland from the lagoon with slopes ranging from 0.4 m/km (8) to 1 m/km (7). Patterson and Kinsman (44) found the gradient to be higher in the coastal regions and lower inland, being 1:4,000 in the former and about 1:20,000 to 1: 40,000 in the latter.

2) Seaward Exposure of Sabkha: It has been observed that northern Sinai sabkhas in contact with lagoonal water exhibit arid zone diagenetic dolomite, while in sabkhas cut off from the lagoon by sand dunes, the hydrologic influence is primarily that of saline terrestrial groundwater, and only gypsum and halite occur (57,58).

2.4.4 Hydrological Factors

These factors are considered the most cumbersome to investigate, because they involve a thorough study of the sabkha site as a whole, either laterally or vertically. Additionally, they

are directly affected by the above factors. Butler (7), Kamal, et al. (50), Johnson, et al. (2), and Patterson and Kinsman (44), amongst others, have studied the hydrology of the sabkha. Needless to mention that sabkha sediments have good porosity and permeability; despite the fact that these properties have not yet been well documented in the literature. Both porosity and permeability play an extremely important role in the diagenesis of the sabkha; as the whole processes of brine seepage and evaporative rise depend on good permeability (3).

1) Lagoon and Terrestrial Waters: The hydrology of coastal sabkhas is the resultant of interaction between lagoon and terrestrial waters. Based on this concept and on the nature of the diagenetic minerals developed as well as on the nature of the host sediments, Butler (7) has divided the coastal sabkha into five zones:

   i) Intertidal Zone: which is largely flooded by tide waters.

   ii) Inner Flood Recharge Zone: which is subject to monthly or more frequent flooding.

   iii) Intermediate Flood Recharge Zone: which is flooded at intervals longer than one month.

   iv) Outer Flood Recharge Zone: which is flooded at

four to five years' interval.

v) High Supratidal Zone: which is not flooded by sea water and the groundwaters are in part terrestrial.

2) Watertable: is found to be always above the high-tide level and slopes gently, but consistently, seaward, indicating that the direction of groundwater flow is towards the sea. Even in the seaward region that is periodically flooded, the watertable is never found to slope inland (44). The depth to watertable increases gradually with the distance from the present high-tide strandline, but never deeper than 1.5 m; however, this depth is affected by the refluxing phenomena, such as rain, floods, etc.

3) Net Evaporation Rate: of about 6 cm/year of groundwater is relatively low compared to the 124 cm/year for the Arabian Gulf waters. However, some factors, such as the sediment section above the watertable, high ionic strength, high relative humidity, and vertical stratification of the air mass above the sabkha, significantly reduce the rate of evaporation from the sabkha (44). With the average porosity of about 40% for the marine sediments, the net average upward groundwater table flow velocity across most of the coastal sabkhas is in the order of 15 cm/year.

4) Permeability of Sabkhas: is influenced by the percentage of silt sizes, degree of cementation, crystal growth, etc.; and since the topography of the sabkha is flat, the true velocity of groundwater flow is unlikely to exceed 10^{-6}m/sec (15). James and Little (59) reported an in-situ permeability of $6x10^{-5}$m/sec which is likely to represent mainly the horizontal permeability, and the corresponding vertical permeability could be as little as one hundred times less (59).

5) Means of Replenishment: in the coastal sabkhas are (40,60):

   i) The horizontal movement of water from the lagoon in the sabkha sediments, mainly when the tidal level sufficiently exceeds the level of groundwater.

   ii) The horizontal movement from the sabkha to the lagoon, as discussed above, and

   iii) The vertical downward movement of water which inundates the sabkha surface during the exceptionally high tides, flash floods or infrequent rains. These waters, whether fresh or marine, cause dissolution of precipitated salts on the crustal layer and transport them down. Additionally, these

waters tend to dilute the sabkha brine.

6) Upward Flow: is the result of the aridity of the sabkha region which stimulates the upward movement of moisture, which is known by evaporative pumping (61). This upward "Darcy-flow", which is necessary for dolomitization, is not due to the capillary action in the vadose zone but to reduction in pore pressure due to the evaporation of interstitial vapor (61).

7) Artesian Pressures: is reported to exist in sabkha areas at Jubail (59); although their origins are uncertain.

2.4.5 Biological Factors

Despite the existence of highly saline, or sometimes hypersaline, brines, biological activity does exist in the sabkha matrix, but their influence is limited. The most important biologic factors within the sabkha environment can be listed as follows (3):

1) Algae and Algal Mats: These represent an integral part of the sabkha system (extending from the lagoons into the lower reaches of the intertidal zones) and affect it in two ways:

   i) by incorporating adhered sediment particles in their growth cycles; thus directly contributing to both the

upward and outward growth of the sabkha by forming an impervious base for the sediments; and

ii) by releasing gas vents of H_2S and CH_4 from their decaying dead bodies, that escape upwardly through the sediments and serve to increase both their porosity and permeability.

2) Sulfate-reducing Bacteria: These produce both sulfur and hydrogen sulfide, and the reducing environment can help to precipitate trace metals.

3) Burrowers: These are not common, due to intense heat and salinities, but they are not totally lacking, and where present, their burrowing activities enhance sediment porosities.

2.5 GEOTECHNICAL PROPERTIES OF SABKHA SOILS

Along the Arabian Gulf coasts, sabkha soils extend intermittently for more than 1,700 km with varying inland extensions that average 20 km. These are generally viewed as unconsolidated, heterogeneous, layered or unlayered sediments bathed in highly concentrated brines. The sedimentary features, mineralogical composition and the chemistry of the interstitial brines in such coastal sabkhas vary greatly in both the horizontal and vertical

directions. Horizontal variations are expected to be related to proximity from the shoreline (62); while vertical variations represent successive stages in the development of the sabkha cycle, including the depositional environment at a specific depth, diagenesis and other factors.

Problems posed by significant variations in sabkha characteristics are greatly accentuated by the fact that local people are still unaware of the whole spectrum of their hostile nature, and even engineers and researchers are still calling sabkha a "special soil" (24). Geotechnically, sabkha soils are considered to be highly variable in terms of grain size and shape (63), texture, degree of cementation, diagenetic minerals, layering, compaction, etc. (62). Such variations arise from the factors discussed before. Sabkhas generally exist in the form of alternating uncemented and cemented layers, as well as in the form of lumps of quartz sand. In the cemented layers, the main cementing materials vary according to the location; however, common cementing materials in sabkhas are aragonite and calcite ($CaCO_3$), gypsum ($CaSO_4.2H_2O$) and sometimes anhydrite ($CaSO_4$) as well as halite (NaCl) (2,54,55,63,etc.).

Taylor and Illing (49) spelled out that sabkhas in Qatar display cementation that tends to decrease with depth, and the cemented layers vary in thicknesses from 5 to 100 cm. These

cemented layers are often separated by layers of uncemented quartz sands or weakly bonded lumps of carbonate sands that can extend down to 10 m or more. Thus, it was postulated that each cemented layer is most likely the consequence of early diagenetic changes at the top or close to the top of the prograding sediments prior to their burial under newer sediments. Shinn (55) reported that the principal cementing materials filling the intergranular spaces and locally replacing grains are aragonite (in several growth forms) and microcrystalline magnesium calcite. It is further added that the aragonite cement seems to be unstable and inverts locally to the more stable calcite within the marine environment. Based on several boreholes, it was reported that the sabkha deposits appear to be cemented with depth, and the process of cementation "appears to be selective". The coarser, more porous layers tend to be more readily cemented, while the finer more silty layers frequently remain uncemented (64).

The variability of characteristics, as well as the presence of saturated brines, are the distinguishing features of sabkha material. The physical and mechanical properties of sabkha samples from a petrochemical site near Jubail (65) is shown in Table 2.4, which clearly reflects this nature. Such a highly variable nature of the sabkha soils has given them hazardous geotechnical properties that need thorough investigation prior to any major engineering construction on such soils. Nevertheless, very little

Table 2.4 : Physical and Mechanical Properties of an Eastern Saudi Sabkha (Abu-Taleb and Egeli, 1981)

Description	Maximum	Minimum
Passing Sieve No.75, %	97	18
Natural Water Content, %	84.6	10
Liquid Limit, %	84	30
Plasticity Index, %	39	NP*
Bulk Density, g/cm^3	1.89	1.34
Specific Gravity	2.82	2.51
SPT, blows/300 mm	6	0
Cohesion, kg/cm^2	0.54	0
Angle of Friction, φ^o	22	0
Initial Void Ratio	2.16	1.08
Compression Index, C_c	0.95	0.39

*NP = Non-plastic

Note: 55 samples were tested.

has, so far, been published on the geotechnical properties of sabkha soils, except for some information on their utilization in highway engineering (e.g., 10,19,48,51,63,66,67), or for sewerage project construction (e.g., 29), or for housing construction (e.g., 30,41,68), or for ground condition (15,60,64,69,70). Such publications do present thoroughly the potential geotechnical properties of the sabkha, based on field tests. The findings of these publications have recently been summarized as follows (71):

1) Accurate determination of the geotechnical properties of sabkha has not as yet been fulfilled. The presence of soluble salt makes the use of distilled water, as recommended by ASTM and BS standards, inappropriate. This is because the distilled water tends to dissolve the salts that are considered part of the soil.

2) Decrease in strength of the surface crust of sabkha as a result of rainfall, flash floods, storm tides, or merely due to absorption of water from a humid environment. This decrease in strength can render the normally stable surface crust impassable. Since these soils derive their strength from the soluble chemical cementation which is often due to the presence of chlorides, sulfates or carbonate salts, they are being characterized as chemically unstable. The degree of cementation will vary reasonably and may be subject to leaching and dissolution or

softening leading to strength loss in wet conditions.

3) Potential variation of compressibility characteristics of sabkha sediments, particularly in the uncemented layers, could lead to excessive differential settlement. Sabkha deposits, in general, are known to vary from very loose or loose to dense conditions within a relatively short distance of five to ten meters.

4) Gypsum is known to undergo alternate hydration and dehydration under the hot and humid conditions that characterize the sabkha environment. This conversion of phases can be enhanced in the presence of certain soluble salts (72). Where this mineral is abundant, the associated volume changes may cause serious problems.

5) The high concentrations of chlorides and sulfates in the sabkha sediments and its brines are highly corrosive to both concrete and steel. The effect of soluble salts on the suitability of soil for construction is dependent on the quantity and type of salts as well as their solubilities, the coefficient of permeability of the soil, temperature regime, chemical characteristics of groundwater and rate of flow.

6) The evaporative pumping mechanism moves soluble salts from the watertable towards the surface where they

precipitate. The salt crystals thus formed may form salt blisters and initiate surface cracking particularly in pavements. Counter measures to deal with this problem have been suggested by Blight (73).

7) Attempts to densify the upper portion of sabkha material by conventional means, in order to improve its bearing capacity and reduce its settlement characteristics, could break up cementation bonds in underlying layers and consequently lower its bearing capacity. Replacement of sabkha soil by structural fill (74), even though effective, would involve massive dewatering, as well as the induction of a considerable amount of imported material for fill. Dynamic compaction, densification piles, stone columns, use of geotextiles and preloading are reported to be the most suitable solution for large-scale construction (74-77). Recent investigations based on simulated and naturally-existing sabkha soils indicate that both portland cement and lime in quantities as little as 5% by weight, can improve the behavior of these soils (24,77).

8) With the presence of certain readily soluble salts in the sabkha, which may contribute to its strength, and of some less soluble salts, such as gypsum, one should be careful in the handling of waste fresh water, since movement of this water into the sabkha could have the effect

of dissolving some of the cementing agents and decreasing the strength of the sabkha. Needless to mention that the change of salinity in the soil profile can influence the stability of the profile (78) due to the chemically unstable nature of the sabkha.

9) Inaccessibility of a large number of sabkha sites for part of the year, as they become impassable upon saturation, and weakening or loss of the crust, has hampered construction activities. Consequently, provision of temporary roads, constructed by filling and compacting over sabkha surfaces to facilitate movement of materials and equipment to selected sites, has been an expensive solution (68).

This list of problems and other potential problems should by no means be considered complete, since the utilization of the sabkha as an engineering material has only just begun and long term aspects of sabkha performance have not yet been fully studied.

2.6 FOUNDATION PROBLEMS IN SABKHA SOILS

It is a well-known fact that sabkha soils are extremely hostile to foundations. This is mainly due to their high moisture content, their proximity to the groundwater table, the general

loose nature of their soil profile, their susceptibility to severe settlements and/or swellings and their highly corrosive salts, amongst many other factors.

Foundation problems in sabkha soils can be briefly listed (30,68,71, 79, etc.) as follows:

1) Problems due to periodic changes in moisture content:

The periodic changes in the high moisture content of sabkhas leads to large changes in density, consistency and strength, as well as to significant effects on the volume change characteristics of the soil. Such changes can lead to periodic swelling and shrinkage in the soil that can cause serious damages to foundations as well as to constructions, particularly to lightweight structures 2-3 stories high. In these cases, swelling pressures may lead to excessive foundation pressures which can cause damages in the form of wide cracks which increase in size from the foundation right up to the full height of the building. Also, the air pressure in the pore space of the sabkha soil helps the development of swell potentials under cyclic wetting and drying conditions which are very common in the arid and semi-arid climates under which sabkhas usually develop. An internal swell pressure can reduce the effective stress, and hence, the shearing strength of soils.

2) Problems due to excessive differential settlements:

Excessive differential settlements can take place in constructions built on top of a sabkha soil by virtue of the inhomogeneity of its profile, the looseness of certain layers within the profile and the highly variable compressibility of its various components. The physical composition of sabkhas can vary in classification from sand to clay within the same site. Sand layers in the sabkha soil, with their high void ratios and intercalating clay lenses or pockets (of high compressibility), can cause severe differential settlements and lead to serious cracks and tilting in constructions on such soils.

3) Problems due to the presence of highly corrosive salts and brines:

The restoration of the capillary rise after excavation and refilling brings with it the addition of soluble salts to the new foundations (15). The high concentration of chloride and sulfate salts in the sabkha brine are well known to be highly corrosive to both concrete and steel reinforcement; however, the conjoint prevalence of these salts poses several unresolved questions on their concomitant interaction with the reinforced concrete foundations. The problem is significantly intensified by the co-existence of intermiftent, but regularly occurring, moisture with this high salt content that is liable to

produce the worst conditions and the most severe deterioration. Also, the crystallization of salts in the concrete pores often leads to its slow disintegration due to pressures caused by the crystallization power of salts. This form of crystallization disintegration in the concrete foundation usually occurs above the watertable, where crystallization is enhanced by evaporation. The various forms of brine attacks present severe conditions for ordinary "Portland cement" and warrants for strict precautionary measures.

4) Problems due to the proximity of the groundwater table:

The groundwater table usually lies within a short distance from the sabkha surface, and fluctuations in its level, although infrequent, can cause serious problems of settlement during the life time of any structure built on a sabkha soil. A sudden rise or fall in the level of the groundwater table can cause excessive settlement due to the wetting of dry, loose sands or due to the compressibility of dewatered, loose, sandy soils.

These problems are in addition to the susceptibility of sabkha terrain to flooding because of the low elevation of the sabkha surface, to the difficulties of excavation below the watertable and the associated problems of dewatering.

Chapter 3

LITERATURE REVIEW ON DURABILITY OF CONCRETE IN SULFATE-CHLORIDE ENVIRONMENTS

3.1 INTRODUCTION

Portland cement concrete is foremost among the construction materials used in civil engineering construction around the world. The reasons for it's pre-eminence are relatively many and varied, but among the more important ones are: the widespread availability of its constituents, the economic superiority compared with any other structural materials, its versatility and adaptability, and the minimal maintenance requirements during service (80). With all these advantages, there are still some limitations associated with concrete. Examples include the low ductility that is typically evidenced by the brittle nature of concrete; its very low tensile strength, the considerable irreversible shrinkage which concrete undergoes due to moisture loss and ambient temperatures; the spontaneous creep that occurs under applied loads even under normal service conditions. Awareness of these problems, nevertheless, coupled with suitable design and construction practices can ameliorate the performance of concrete in any service environment. Ignorance of these facts may lead and has led to to serious problems worldwide. Among the problems that are related to concrete

are its low durability performance in aggressive environments, such as bridge decks in U.S.A. and reinforced structures in the Arabian Gulf coast.

3.2 DETERIORATION OF CONCRETE IN THE ARABIAN GULF

Since mid-seventies, there has been an unprecedented demand for concrete construction of all kinds in the Arabian Gulf countries to accommodate the rapidly growing social and industrial infrastructure. The construction has been particularly concentrated along the coastal areas. The local construction industry, beset by an inadequate infrastructure, shortage of suitable materials, equipment, skilled manpower and inadequate specifications and construction practices has succeeded only in producing structures which are showing an alarming degree of deterioration within a short span of about 10 to 15 years (81). The deterioration is accentuated by the aggressive service environment which is characterized by adverse climatic and geomorphic conditions (33).

The climatic factors that affect concrete durability in the Arabian Gulf countries are the large fluctuations in daily and seasonal temperature and humidity conditions. The temperature can vary by as much as 30°C during a typical summer day, and the relative humidity ranges from 40 to 100% over a period of 24 hours. These sudden and continuous variations in temperature and humidity initiate ever present cycles of expansion/contraction and hydra-

tion/dehydration which cause damage due to thermal and mechanical stresses. This damage, reflected by microcracking and enhanced permeability of concrete, is accentuated by the differential thermal expansion and contraction movements of aggregate material and the hardened cement paste, which may set up tensile stresses far beyond the tensile strength of concrete. The microcracking is significantly magnified if the coefficient of thermal expansion of the aggregates used in concrete construction is widely different from that of hardened cement paste (82,83). The climatic factors at the early stages of concrete mixing, also influence the properties of hardened concrete, in that concrete cast and cured under hot weather conditions and not cured sufficiently thereafter may show as much as 30 to 40% reduction in strength (84). Corrosion initiation and other electrochemical/chemical reactions are known to be accelerated with higher temperatures. In the Arabian Gulf, the surface temperature of concrete may be as high as 70°C due to the direct solar radiation effect on a typical summer day.

Climatic and geomorphic factors may combine to accelerate the deterioration process. In the coastal flats, the groundwater table is relatively high and close to the ground surface and evaporation is intense. The capillary rise of moisture and frequent flooding followed by high evaporation rates leaves a heavy crust of salt in the upper few feet of the soil. This leaves the ground, groundwater, atmosphere, and the aggregates heavily contaminated

with chloride and sulfate salts (85). The concrete structures situated in coastal areas are also continuously exposed to the frequent and persistent "Monsoon" winds which are charged with sea water and sea salts that can attack concrete chemically and physically. To these factors must be added the geomorphic conditions resulting in reactive minerals and marginal aggregates. Most of the coarse aggregate available in the region is crushed limestone which is known to be rich in magnesium and some varieties are true dolomite (20,27,86). The limestone aggregate is weak, highly absorptive, and dusty on crushing. It has been observed that chlorides and sulfates tend to become concentrated in the fine fraction and dust in the coarse aggregates. Furthermore, these fine fractions and dust create a high water demand resulting in enhanced shrinkage and associated problems. The fine aggregates, mostly beach sand and to some extent dune sand, usually have smooth rounded grains. The specific gravity of the fines is around 2.7, and absorption is 0.227% and the fineness modulus is in the range of 0.83 to 1.82 (87). Nearly all the material passes Sieve #30 and appreciable portion, 10 to 20%, passes Sieve #100 leading to the large surface area effect. The excessive fineness of sand and its narrow grading lead to gap-graded particle size distribution in the combined aggregate grading for nearly all the mixes made using local materials.

The surprisingly low durability performance of concrete in

the Arabian Gulf has attracted the attention of concrete technologists since the early eighties. Research initiated at King Fahd University of Petroleum and Minerals was directed towards evaluating the causal factors for deterioration (88), optimizing mix design for the local materials to design durable concrete mix (87), assessing the durability performance of concrete and reinforcement when exposed to the Gulf environment (82), studying the performance of pozzolanic concrete when exposed to high chloride or sulfate environment (89), and finally evaluating the permeability and corrosion-resisting characteristics of pozzolanic concrete (90). These investigations, which were based on laboratory and field studies, have culminated in substantial data to formulate preventive measures to mitigate deterioration of reinforced concrete structures.

Condition surveys of concrete structures located in the Eastern Province (86) have shown that the main causal factors for concrete deterioration, in decreasing order of importance, are:

(i) corrosion of reinforcement;

(ii) sulfate attack and salt weathering, and

(iii) cracking due to environmental factors and potential aggregate-cement reactivity.

Thus, corrosion of reinforcement, which is by far the most effectively operative causal factor resulting in concrete deterioration, and sulfate attack, are the visible manifestations of internal and

external salt inclusions. The chloride and sulfate salts are inadvertently included in the concrete mix through the concrete ingredients and the external environment. The results of the above-mentioned investigations have persistently emphasized that concrete in this region must be designed for durability rather than strength alone (84).

The preceding paragraph entails that concrete in the Arabian Gulf region contains seeds for potential deterioration due to the presence of chloride and sulfate salts. Therefore, the mechanisms of reinforcement corrosion and sulfate attack need to be clarified.

3.2.1 Corrosion of Reinforcement

It is a known fact that well-made and salt-free concrete provides immunity against corrosion of reinforcing steel. This is because steel is passivated against corrosion if embedded in an alkaline environment corresponding to a pH in the range of 11 to 13. The hydrated cement medium around rebars in concrete provides exactly such an environment. The high-alkaline conditions present within concrete (pH of about 12 to 12.5) cause a passive oxide film, known as gamma ferric oxide, to form on the surface of the rebars, effectively inhibiting the corrosion process. This is analogous to the passive layer of alumina that prevents aluminum from corroding under normal conditions of use. This protective

film, however, may be disrupted or destroyed by mainly two specific circumstances. First, when atmospheric carbon dioxide (CO_2) makes a possible ingress through the concrete matrix and its penetrating front advances so deeply that it intercepts the steel reinforcement. Carbon dioxide reacts with calcium hydroxide and neutralizes it by forming calcium carbonate thereby damaging the quality of protective environment or even rendering it ineffective. It should be pointed out that both CO_2 and moisture are necessary for the process of carbonation to occur, as gaseous CO_2 does not react directly with hydrated cement (91). With good quality concrete, however, the process of carbonation is known to be slow and the prevention of carbonation is one of the main functions of the concrete cover. Moreover, the products of carbonation block some of the pores in the concrete and thereby impeding further ingress of CO_2 and moisture. The process of carbonation slows down, ultimately reaching a negligible rate. Reduction in alkalinity could also occur due to leaching out of portlandite (i.e. calcium hydroxide), particularly if the concrete is to be placed in acidic or neutral solutions. Second, and more important, the chloride ion, being a "specific and unique destroyer" (92) of the passivating film, is especially effective in breaking the passive film. Its presence in concrete, therefore, is uniquely effective in promoting rebar corrosion. This has been confirmed by field data developed as a result of chloride and corrosion analysis of 108 cores

retrieved from 20 structures located in Eastern Saudi Arabia (93). Although chloride present in concrete usually reacts with certain products of cement hydration to form insoluble compounds, a part of it remains in solution; and it is this free chloride in the pore fluid which causes the depassivation of steel in concrete. It is believed that there is a threshold concentration of the chloride ion which must be exceeded before corrosion occurs; nevertheless, it is extremely difficult to quantify this threshold value even approximately (93). There are at least three reasons for this uncertainty. First, the amount of chloride ion which can be tolerated increases with an increase in the alkalinity (pH) of the cement paste (94). Second, it is only soluble chlorides, and not all the chlorides, that are relevant to the process of corrosion. It is noteworthy to mention that chlorides are usually present in hydrated cement concrete in essentially three different forms:

a) free chloride ions, literally known as water-soluble chlorides,

b) chlorides bound with calcium silicate hydrates (CSH), and

c) chlorides chemically combined with hydrated calcium aluminate (C_3A) phase of cement as an insoluble compound, calcium chloro-aluminate hydrate ($C_3A.CaCl_2.10\ H_2O$), known as Friedel's salt.

Free chloride ions (item a) promote corrosion while bound chlorides (item b) may or may not cause corrosion depending on the strength of the bonds and some other factors (95). Chlorides which are combined with the cement hydration product, calcium chloro-aluminate hydrate, (item c), are mostly insoluble and do not release significant amount of corrosion inducing chloride ions into the concrete. It has been shown that when the total chloride content is near the corrosion threshold level, from 50 to 85 percent of it may be soluble (96,97). Third, there are other possible sources of variations (98) such as: chlorides associated with different cations, chlorides introduced at or after the time of mixing, and presence of other contaminant anions such as sulfates. Other possible reasons may include type of cement used and whether blending materials are incorporated in the concrete matrix. Due to the different kinetics these materials may affect the chloride binding and the pH of the hydrate cement paste.

The mechanism of chloride-induced corrosion is primarily an electro-chemical process in which corrosion cells incorporating anodic and cathodic regions may be formed on the steel surface owing to either nonuniformities in metallurgical structure of steel, or concentration gradients in the pore electrolyte solution in hardened cement paste surrounding the reinforcement, or even due to differences in environment between the upper and lower surfaces of the rebar due to bleeding, segregation or unequal compaction,

or just because of different exposure conditions of the concrete (91). The overall corrosion process is a complex one. However, it can be virtually simplified as follows: owing to the difference in potential between anodic and cathodic regions, positively charged metal ions at the anode pass into solution as Fe^{++} and the free electrons (e^-) pass along the steel into the cathode. These electrons are absorbed by the constituents of the electrolyte and combine with water and oxygen to form hydroxyl ions. The hydroxyl ions complete the electric circuit by flowing back to the anodic site where they combine with the ferrous ions (Fe^{++}) to form ferric hydroxide; i.e. the rust product. These consecutive reactions can schematically be explained as follows:

Anodic reactions: $Fe \rightarrow Fe^{++} + 2e^-$ (3.1)

Cathodic Reaction: $4e^- + O_2 + 2H_2 \rightarrow 4\ (OH)^-$ (3.2)

$Fe^{++} + 2(OH)^- \rightarrow Fe(OH)_2$ (ferrous hydroxide) (3.3)

$2Fe^{+++} + 6(OH)^- \rightarrow 2Fe(OH)_3$ (ferric hydroxide) (3.4)

$2Fe(OH)_3 \ldots \rightarrow Fe_2O_3 + 3H_2O$ (ferric hydroxide) (3.5)

In the presence of chloride ions, the passivating film can be destroyed, even in uncarbonated concrete, and the surface of

the steel thus becomes activated locally and a small anode is formed. The remaining passivated surface of the steel becomes the cathode, which is much larger than the anode. Consequently, the dissolution of the iron in the anode extends in depth, rather than over the surface of the steel bars, unlike the previous case, and a pit is formed. It is postulated that the chloride ion releases hydroxyl ions and combines with water to form hydrochloric acid (91) which produces an acidic environment in the pit (pH $\approx$ 5). The pit is protected by the rust products, so that the acidic conditions continue and so does the rusting. It is because of this protection in the pit, once it has formed, that pit remains active and increases in depth. These reactions can possibly be explained schematically as follows:

$$Fe^{+++} + 3Cl^{-} + 3H_2O \rightarrow Fe(OH)_3 + 3HCl \qquad (3.6)$$

$$HCl \rightarrow H^{+} + Cl^{-} \qquad (3.7)$$

It can be seen that the chloride ion is regenerated, and the rust contains no chloride although ferric chloride is formed at an intermediate stage.

The above description entails that there are basically two electrochemical cells, depending on the prevailing conditions. The first type, commonly known as the macrocell, operates when the anodic and cathodic sites are remote from each other but in metallic

contact. The other type, often called microcell, is characterized by microscopic distance separating the anodic and cathodic regions. In the presence of chloride, it is anticipated that the latter cell will form and the so-called "microenvironment" is no longer inhibitive of corrosion action and thereby numerous microcells will operate. Summarizing the above discussion, oxygen and moisture are required to promote corrosion; that is why there is no corrosion in dry or totally submerged concrete, even in the presence of large quantities of chlorides. Moreover, once corrosion is promoted, it is the electrical conductance of the concrete, i.e. concrete resistivity, that controls the rate of corrosion.

The above discussion outlines the effect of chloride ions as a corrosion igniter; however, direct chemical damage of the concrete constituents by extraneous chlorides, although unusual (99), has been reported in the literature (100-104). What seems more significant is that those chloride ions are capable of diffusing rapidly into concrete, thereby exacerbating other deleterious reactions, as will be discussed later.

3.2.2 Sulfate Attack

This type of deterioration has received much earlier attention as compared to corrosion of reinforcement. According to Lerch et al. (105), Candlot appears to have been the first to establish the formation of a definite compound by the interaction of

aqueous solutions of calcium aluminates and calcium sulfate in 1890. According to Aroni et al. (106), Michaelis in 1892, was the first to attribute the disruption of concrete, when attacked by sulfate waters, to the reaction between C_3A and sulfates to form ettringite.

Concrete is invariably attacked by sulfate salts only when they are in solution. Moreover, an attack implies the combination of the sulfates with the products of cement hydration resulting in their removal from solutions. This renders the rate of replenishment important for a continued deterioration. Two types of manifestations are usually associated with sulfate attack (81): First, a deterioration akin to eating away of the hydrated cement paste and progressively reducing it to a noncohesive granular mass leaving the aggregate proud and exposed and associated with loss of strength. This type of sulfate attack is attributed mainly to the formation of gypsum. The second type, which is normally characterized by expansion and cracking, takes place when the reactive hydrated aluminate phases present in sufficient quantities is attacked by sulfate ions, thereby forming tricalciumsulfo-aluminate hydrate, also called ettringite or Candlot salt. It has been hypothesized that ettringite formed in the presence of $Ca(OH)_2$ is colloidal and the formation of this type of product leads to disruptive expansion (107). The mechanism through which sulfate attack takes place depends on the presence of certain phases that are

formed by the hydration of cement. At the grinding stage of cement, gypsum is added at a dosage of 3 to 5% by weight of cement to delay the time of set, due to the instantaneous reaction of C_3A with water. As soon as cement starts to hydrate, the C_3A reacts with sulfate in gypsum ($CaSO_4$). The product of this reaction depends exclusively on the content of C_3A phase. If C_3A content is less than 5% (i.e. typical type V cement), then ettringite is formed and there will be no excess C_3A left for further reaction. However, if C_3A is greater than 8%, the balance of C_3A will react with the ettringite formed earlier, to produce calcium monosulfate. The ettringite formed at the initial stages is stable while the monosulfate is unstable. The latter will be transformed to ettringite if the conditions allow, as will be later explained schematically. This secondary expansive ettringite is formed after the cement has hardened and that is why it causes cracking. The cation associated with sulfate plays a considerable role on the degree of sulfate attack. For example, magnesium sulfate is known to attack most, if not all, the constituents of hydrated cement paste, and its action is well-documented (108). This salt (known as Epsom salt) reacts with portlandite, $Ca(OH)_2$, to form ettringite, magnesium hydroxide, and aluminum hydroxide, as indicated by the following reaction:

$$3MgSO_4.7H_2O + 2C_3AH_{12} \rightarrow C_3A.3CaSO_4.H_{31}$$

$$+ 3Mg(OH)_2 + 2Al(OH)_2 + 8H_2O \quad (3.8)$$

Also, magnesium sulfate reacts with calcium hydroxide to form calcium sulfate (gypsum), which in turn, reacts with calcium aluminate hydrate to form additional ettringite:

$$MgSO_4.7H_2O + Ca(OH)_2 \rightarrow CaSO_4.2H_2O$$

$$+ Mg(OH)_2 + 5H_2O \quad (3.9)$$

$$3(CASO_4.2H_2O) + C_3AH_{12} + 13H_2 \rightarrow C_3A.3CaSO_4.H_{31} \quad (3.10)$$

Unlike other sulfates, magnesium sulfate reacts also with calcium silicate hydrate to form calcium sulfate, magnesium hydroxide, and silica gel. The latter does not have any cementitious properties.

$$MgSO_4.7H_2O + C_3S_2H_X \rightarrow CaSO_4.2H_2O$$

$$+ Mg(OH)_2 + SiO_2.aq \quad (3.11)$$

The gypsum thus produced may then react with tricalcium aluminate hydrate according to Equation 3.10. Finally $Mg(OH)_2$ produced in reactions 1 and 4 will react slowly with silica to form magnesium silicate hydrate. This magnesium silicate hydrate is known to lack any binding capacity.

$$4Mg(OH)_2 + SiO_2.aq \rightarrow 4MgO.SiO_2.8.5H_2O + aq \qquad (3.12)$$

The attack due to gypsum is rather limited due to its low solubility in water at normal temperatures (approximately 1,400 mg/l SO_4^{--}). Higher concentrations of sulfate in groundwaters, therefore, are generally due to the presence of magnesium and sodium. Therefore, sodium sulfate may follow the above three reactions (Equations 3.8 to 3.10); the formation of sodium hydroxide as a by-product of the reactions ensures the continuation of high alkalinity in the cement system, which is essential for stability of the calcium silicate hydrate (C-S-H). On the other hand, because of the low solubility of magnesium hydroxide and its relatively poorly alkaline nature (pH of about 10.4), the decomposition of C-S-H can proceed to completion and all the calcium content of the binder may be finally replaced by magnesium. Therefore, the magnesium sulfate attack is significantly more severe on concrete. It is noteworthy to mention that the ettringite produced in Equation 3.8 is 2.27 times greater in volume than the volume of the original calcium aluminate hydrate it has replaced (109). The volume of gypsum produced in Equation 3.9 is, likewise, more than two times greater than the volume of calcium hydroxide. It is anticipated, therefore, that these solid-liquid reactions also lead to destructive pressure of significant magnitudes.

It should be noted that increased concentrations of sodium

and magnesium sulfates alter the character of the sulfate attack qualitatively. An increase in sodium sulfate concentration causes the ettringite formation to change into gypsum-ettringite formation and finally into pure gypsum formation (110). Increased magnesium sulfate concentration causes even more severe qualitative modification in the physiochemical characteristics of sulfate attack. According to Kind (110), when the magnesium sulfate concentration is smaller than 1000 mg/l, only ettringite-type sulfate attack takes place (Equation 3.8 above); at higher concentrations of sulfate, the attack is a combined ettringite-gypsum type (Equations 3.9 and 3.10), similar to sodium sulfate attack; with a very high sulfate concentration (4,000 to 6,000 mg/l SO_4^{--}) gypsum and magnesium sulfate attacks take place (Equations 3.11 and 3.12) at which ettringite crystallizes in a non-harmful manner. Figg (99) has observed that there are generally three modes of failure:

i) **Acidic type** that is characterized by eating away or softening of the cement matrix to leave the aggregate standing proud from the eroded concrete; this form occurs due to formation of gypsum and tends to predominate with very strong solutions with cements containing low C_3A content, with relatively impermeable concrete and with the presence of magnesium ions in the solution.

ii) **Expansive type** which is associated with high C_3A cements and relatively high concentration of $Ca(OH)_2$ this form occurs due to formation of a colloidal form of ettringite by the reaction of monosulfate phase in the solution in the presence of $Ca(OH)_2$.

iii) **Onion-peeling type** which is characterized by scaling or shelling of the concrete surface in successive layers in a form of "onion-skinning" delamination; this form appears to be an intermediate form of reaction due to the use of a moderately permeable concrete and a fairly high C_3A content.

3.3 DURABILITY OF CONCRETE IN CHLORIDE-SULFATE ENVIRONMENTS

3.3.1 Durability of Concrete in Sea Water

Due to their extensive spread all over the world, seas and oceans constitute about 80 percent of the earth surface. One-fifth of the world's oil and gas production comes from off-shore facilities and it is believed (111) that piers, foundations, retaining walls, breakwaters for sea structures and off-shore oil facilities will grow and will continue to be made from concrete. This is because in the context of the aggressive medium of seawater, concrete is not

only the most economical structural material for construction of such structures, but also is the most durable.

Durability of concrete structures in seawater is the most complicated system to investigate; where deterioration operates by freezing and thawing, by corrosion of reinforcement, and by chemical constituents of the sea. There are other possible causes of deterioration such as erosion and wave action, crystallization of salts due to concentration being increased by capillary action and evaporation, particularly in and above the tidal zone (112). In the Arabian Gulf seawater, more operating factors are there and they have been enlisted and discussed before. The interaction of all of these chemical and physical agents will lead to a maze of interwoven factors causing deterioration. The situation will be worse if immature cracking or microcracking by any means, does exist.

Sea water may convey the impression of a constant chemical composition, and it is true that the relative proportions of dissolved salts are generally invariant; but the total concentration varies with geographical and geomorphological locations. For example, it is known that the Arabian Gulf water is about 25% or more saline than the Atlantic, while the Mediterranean is about 20% more saline than the latter (113). It is shown, consequently, that even the air in the vicinity of Dhahran contains more chloride than some other cities because of the salt-spray carried by winds (81). However, typical concentrations in the surface waters of deep

oceans correspond to about 3.5 percent soluble salts by weight; the relative ionic concentrations of major ions in ocean waters are shown in Table 3.1. If these ions are to be presented as salts (i.e. compounds), the accepted method is based on the solubilities of these salts in water; that is on the order in which they precipitate from solution on evaporation. This procedure, although looks simple, is extremely hypothetical; the theoretical combinations as salts of ocean water is also presented in Table 3.1. Whereas the effect of chloride in sea water has considerable influence on corrosion of steel in concrete, it is the magnesium salts, particularly those of sulfate and chloride, which exercise the most deleterious effect on the hydration products of portland cement.

Thus, there are mainly two deteriorating actions; chloride-induced corrosion and sulfate attack. It is noteworthy to mention that relevant cement phase which locks chloride ions into insoluble compound of calcium chloro-aluminate hydrate (Friedel's salt), thereby causing its removal from its hazardous role of corrosion promotion, is tricalcium aluminate (C_3A). This is the same phase of cement, which in excess of a certain critical level, reacts with sulfate ions to form ettringite and gypsum thereby leading to degradation of concrete into a noncohesive granular mass and to disruptive expansion (107). It is obvious that whereas a higher proportion of (C_3A) would reduce the level of rebar corrosion by

Table 3.1 : Average Composition of Ocean Waters (Eglinton, 1987).

Constituent	Concentration (g/l)
Ions (determined):	
Chloride, Cl^-	18.6
Sulfate, SO_4^{--}	2.6
Sodium, Na^+	10.6
Calcium, Ca^{++}	0.4
Magnesium, Mg^{++}	1.4
Salt Compounds (theoretical):	
Calcium Sulfate, $CaSO_4$	1.0
Magnesium Sulfate, $MgSO_4$	1.4
Magnesium Chloride, $MgCl_2$	3.2
Sodium Chloride, NaCl	26.8

removing or lowering corrosion-inducing free chlorides from the pore electrolyte solution, would pose a serious concrete durability problem in terms of sulfate attack. It is very important to consider that when chlorides and sulfates concomitantly exist, such as in sea water, both of them would react with (C_3A) to form insoluble compounds. However, it has been found (114) that sulfate ions react preferentially with (C_3A) to form two insoluble compounds of calcium sulfo-aluminate hydrates, namely trisulfo-aluminate hydrate ($C_3A.3CaSO_4$.Aqueous) and the monosulfo-aluminate hydrate ($C_3A.CaSO_4$.Aqueous). Lerch et al. (105) have studied these formations and report that both of these sulfo-aluminate hydrates remained unchanged in the presence of chlorides. If this is so, it means that C_3A, once converted to the sulfo-aluminate hydrates, would no longer be available for chloride removal. Stoichiometric calculations indicate that about 8% C_3A is needed to completely consume the gypsum added to regulate the time of set (115) and to convert it into the monosulfo-aluminate hydrate. If this is so, and because type V portland cements are limited to a maximum of 5 percent C_3A, then it is clear that there will not be adequate C_3A in these cements to complex with the chlorides of sea water to reduce the corrosion risk. This approach satisfactorily explains the well known results of Verbeck (116) where significant reduction in concrete cracking due to corrosion of reinforcements was

pozzolanic cement concrete when calcium chloride was used. Likewise, Thorvaldson (119) reported that the rate of expansion of cement mortars was only slightly affected by the addition of up to 3% sodium chloride; but at higher chloride concentrations the rate of expansion in solutions of sodium, magnesium or calcium sulfate was significantly and progressively decreased. Brown (120) reported, in a published discussion on a paper by Locher (121), that the addition of 2% sodium chloride by weight of cement imparted considerable sulfate resistance to ordinary portland cement (OPC) mortar and little improvement was observed for sulfate-resisting portland cement (SRPC) mortar. Yeginobali (122) and Dalq (123) reported no significant effect on the sulfate resistance due to the use of sea water of various chloride concentrations and the incorporation of 2% calcium chloride; respectively. According to Ikezr, quoted by Alsamarai and Raouf (124), the addition of calcium chloride up to 1% to a concrete containing high sulfate content in sand (1 to 2%) increased expansion and drying shrinkage. It was suggested that the presence of chlorides intensified the aggressive action of sulfates by increasing both the porosity and the early drying shrinkage cracks due to increased heat of hydration. Harrison (118) studied the effect of sodium and calcium chloride additions in the range of of 0 to 4.5% in mortar and concrete cubes using OPC and SRPC over a period of one year for mortar and over seven years for concrete. The results of the mortar cubes have shown that the chloride has either a negligible

or a generally beneficial effect on the sulfate resistance in both OPC and SRPC mortars. A similar overall trend has been observed in the concrete cubes; with the apparent exception of some concretes containing calcium chloride, particularly those containing below 0.5% chloride by weight of cement, and immersed in strong sulfate solutions (1.5% SO_3, magnesium and sodium sulfates), for which the sulfate resistance was considerably reduced.

3.3.2.2 Effect of Secondary (External) Chlorides on Sulfate Attack

The conjoint action of chloride and sulfate ions on concrete exposed to salina soil or maritime environment is of great practical significance; particularly for the durability of concrete substructures in the Arabian Gulf States. Under these conditions, the chloride ions can not influence the early hydration reactions, and the effect of its subsequent ingress on sulfate ions will be quite different to those of primary chlorides. Thorvaldson (119) reported that high concentrations of sodium chloride in sulfate solutions tended somewhat to reduce the rate of expansion of lean mortars. Out of 51 different commercial cements investigated by Cook (125), only 8 cements containing C_3A content in excess of 12% had failed after 9 years of exposure to sea water; the remainder had not. Batta and Baivellin (126) found out that the expansion was reduced in sea water by the presence of chloride. Kind (127), through his extensive research on chloride-sulfate

interaction, evaluated small prisms by a coefficient of resistance after 6 months of exposure to these $Cl^- - SO_4^{--}$ solutions. His conclusions show that the increased resistance of the different cements in sulfate solutions occur mainly when chloride exists at high concentrations. He attributed the increased sulfate resistance in high chloride solutions to three factors (127):

i) the increased solubility of calcium hydro-aluminate phase leading to calcium sulfo-aluminate crystallization in the liquid phase, i.e. ettringite is formed in the non-expansive form;

ii) decrease in lime concentration in the pore solution leading to the conversion of the insoluble highly basic hydro-aluminate phases to soluble, low-basic forms; forming ettringite in the liquid phase in the non-expansive form;

iii) transformation of hydro-aluminate phases into chloro-aluminates, thereby reducing the quantity of ettringite formed.

Based on microscopic examination, Kind (110) reported that the calcium sulfo-aluminate occurred in smaller quantities and was formed as weakly-developed crystals in the presence of sodium and magnesium chlorides. This is the main reason behind specify-

ing higher sulfate limits in the presence of higher chloride concentrations for the Russian Standards. The maximum allowable sulfate concentration in water in which portland cement is to be placed is 250 mg/l, regardless of the type of associated cation. This allowable sulfate concentration may be increased to 500 mg/l at a chloride concentration greater than 3,000 mg/l, and to 1,000 mg/l at a chloride concentration greater than 5,000 mg/l (110).

The above literature indicates that sulfate attack will be mitigated by the presence of chloride ions. However, other opinions contradicting this position also exist. Smith (128) reported that the addition of 1% calcium chloride at the mixing stage had generally reduced the sulfate resistance of concrete, particularly of concrete made with type II cement. Moreover, the temperature seemed to play a significant role; concretes made of Type II or Type V cement were more sulfate resistant when mixed and cured at 40°F than similar concretes mixed and cured at normal room temperatures (70°F). van Aardt (104) showed that no improvement in sulfate resistance could be obtained due to the presence of chlorides in sulfate solutions. This work was based on dimensional change (expansion) and measurement of dynamic modulus of elasticity and the chloride was obtained using sodium chloride. Locher (121) concluded that "sulfate attack is generally increased by the addition of chloride to the sulfate solution" based on bending strength and expansion of small prisms that were placed in 2,500

mg/l sodium or magnesium sulfate with 18,200 mg/l chloride solution. This increased sulfate attack due to the presence of chlorides was attributed to (121):

i) formation of the ettringite was not hindered by the addition of chlorides,

ii) the presence of monochloride was attributed to the consumption of monosulfate and tetracalcium aluminate hydrate by part of chloride reacting with the nonhydrated C_3A phase in the cements,

iii) this monochloride was unstable in the presence of sulfate ions; therefore, it was converted to ettringite when sulfate attack commenced with time, and

iv) at higher concentrations of chloride, both monochloride and trichloride hydrates were found; the former reacts with the penetrating sulfate ions to form ettringite without generation of crystallization pressure {i.e. dissimilar to statement (iii)}, and the latter hydrate is resistant against sulfate attack.

The formation of trichloride hydrate ($3CaO.Al_2O_3.3CaCl_2.32H_2O$) was reported to be favorable at high chloride concentration by Schwiete, et al. as quoted by Hjorth (129). Heller and Ben-Yair (130) and Ben-Yair (131) have

confirmed that the presence of chlorides intensified the sulfate attack, and the presence of calcium chloro-aluminate crystals enhanced the growth of ettringite crystals. It was found that the addition of 3.5% sodium chloride to 0.4% sulfate solution caused more expansion of the 0.3 w/c paste bars than the higher 0.5 w/c paste bars (131); however, in solutions of 3.5% of either sulfate or chloride solutions, the expansion of the lower w/c bars were found to be less than the higher w/c bars in the sulfate solutions; the opposite was found in chloride solutions.

It is thus seen that there are mainly three schools of thoughts: (i) the effect of chlorides on the sulfate attack seems to be insignificant (104), (ii) chlorides tend to intensify the sulfate attack (121,131) and (iii) chlorides tend to mitigate sulfate attack (Kind and Others). Lea (132), based on Batta's work, confirmed that the expansion of concrete by sulfate attack in sea water is definitely retarded. Biczok (109), based on Kind's work, also confirmed this fact. Both attributed this retardation to the increased solubility of ettringite and gypsum by sodium and calcium chloride solutions. Cornor and Rippstain, quoted by Harrison (118), found that the solubility of ettringite was three times greater in chloride solutions than in water. The variation of these results could be attributed to any one of the many possible reasons, such as: the general heterogeneity of concrete, methods and experimental conditions (104), variations in the concentrations of

both chloride and sulfate (a pessimum concentration of chloride could probably exist for each sulfate concentration at which the sulfate attack is maximum, as is evident from the work of Harrison, 1990), duration of experimental work, and finally workability, w/c ratio and cement type used in the mix.

3.3.2.3 Effect of Sulfate on Chloride-Induced Reinforcement Corrosion

Another important point to be investigated is the effect of sulfates on chloride-induced reinforcement corrosion. Stratful (133) has investigated the individual effect of sodium sulfate or sodium chloride on reinforcement corrosion and has also studied the effect of subjecting reinforced concrete specimens to alternate and partial immersion in saturated solutions of these two salts. He found that corrosion of reinforcing steel in concrete was observed only in sodium chloride solution, while no corrosion developed in sodium sulfate solution within the duration of tests (214 days). The effect of sodium chloride as well as sodium chloride plus sodium sulfate inducted at the mixing stage on the chemistry of hardened plain and blended cement pastes was investigated by Holden, et al. (134). Based on pore solution extraction, they reported that sulfate ions tended to result in substantial decrease in chloride binding capacity of the different types of cement pastes investigated. This effect is attributed to the preferential reaction of the C_3A of the cement with the sulfate ions, thus inhibiting the

binding of chlorides with C_3A and formation of calcium chloro-aluminate (Friedel's Salt). An increase in the hydroxyl ion concentration is also observed with sulfate addition because the hydroxyl ions tend to enter pore solution to balance the anions removed in the form of insoluble complex salts. However, the net effect of sulfate addition to chloride was found to be an increase the in (Cl^-/OH^-) ratio compared to the effect when chlorides existed alone in cement for the five types of cement pastes investigated.

For the case of secondary (external) sulfate and chloride ions, i.e. those which penetrate the hardened cement matrix from external sources during the service life, the data seem to be sparse and scanty; although it is well-known that the chloride ions penetrate concrete at a much faster rate than sulfate ions (135). Therefore, the formation of Friedel's Salt is the first step in the mechanisms of $Cl^- - SO_4^{--}$ attack. This salt may, later on, when the sulfate ions penetrate, be transformed into ettringite, as suggested by Locher. Whether this reaction causes expansive pressure is still a debated question. It is anticipated that this reaction between Friedel's Salt and sulfate ions leads to the liberation of the chlorides, thereby, increasing the concentration of free chloride ions in the pore solution of the hardened cement paste (129). This hypothesis seems to be rational, but data confirming this hypothesis are still lacking.

3.3.3 Performance of Plain and Blended Cements in $SO_4^{--}-Cl^-$ Environments

The classification of ASTM cement types is primarily based on the C_3A content of cement. It was pointed out in Section 3.2.1 that a low C_3A cement is more sulfate-resistant in pure sulfate solution. For the case of chlorides, Hjorth (129) presented data from various sources on chloride diffusion coefficient through cement paste and found out that these data fall within two areas and concluded that:

i) the data for low C_3A cements do not vary significantly from those for ordinary portland cement,

ii) the diffusion coefficient is strongly affected by the w/c ratio, and

iii) the presence of slag or pozzolanic materials decreases the diffusion coefficient considerably.

Page, et al. (136) reported that the effective diffusivity of chloride ions in pastes made with w/c ratio of 0.5 and C_3A contents of 7.7% and 14.3% does not vary significantly; however, if the C_3A content is reduced to 1.9%, the diffusivity increases. The diffusivity in blended cements was observed to be lower than in high C_3A plain cements.

For the case of sulfate attack, the use of SRPC complying with BS 4027 (C_3A < 3.5%) or ASTM C 150 Type V ($C_3A \leq 5\%$) may provide good sulfate resistance; however, these types of cements may contain large amounts of calcium hydroxide and are thus not immune to the acidic type of sulfate attack (99).

In $SO_4^{--}-Cl^-$ environments, the use of low C_3A content cement is required to avoid deterioration due to sulfate attack and the use of high C_3A content cement is a pre-requisite for a high chloride binding capacity so as not to endanger the reinforcement. Therefore, it has been suggested to recommend a cement with a C_3A content of 5 to 8% (129), i.e. a cement similar to ASTM C 150 Type II.

3.3.3.1 Role of Blended Cements

In recent years, the use of mineral admixtures such as natural pozzolans, fly ash and industrial by-products like blast furnace slag and silica fume are being strongly recommended to improve the properties of concrete in general and durability in particular. The use of these materials is reported to reduce the water demand and bleeding in fresh concrete, improve workability resulting in better placement and compaction characteristics, decrease the size and number of large voids in hydrated cement paste, lower the amount and degree of orientation of crystalline

calcium hydroxide as well as microcracking in the transition zone and improve the impermeability of portland cement concrete (137). In addition to these attributes, pozzolanic concretes generate less heat of hydration, show significantly high resistance to sulfate attack and alkali-aggregate expansion and cracking, and provide better protection against rebar corrosion (138).

It is generally accepted currently that the cementitious and pozzolanic properties of mineral admixtures, used as a replacement for portland cement (90) or as cement additive, depend on their particle size and shape as well as their mineralogical composition, and not purely on their chemical composition and source of origin as it was thought before (139). These admixtures are classified as cementitious (e.g. blast furnace slag), cementitious and pozzolanic (e.g. high calcium fly ash, natural pozzolans and low calcium fly ash) and highly pozzolanic (e.g. silica fume and rice husk ash) (139). The hydration of these materials is based on the well-established "pozzolanic reaction" which takes place by the reaction between the calcium hydroxide that is released from the hydration of the cement and the silica present in the mineral admixtures. This pozzolanic reaction generates secondary calcium silicate hydrates similar to those developed by cement hydration. This reaction is associated with pore-size refinement and results in a structure that is likely to be dense with a refined discontinuous pore matrix (140).

There are both potentially detrimental and potentially beneficial effects resulting from the use of these materials. On the detrimental side, there are three major concerns. First, pozzolanic reaction characterized by the consumption of alkaline calcium hydroxide may proceed to a degree at which the pH level of the pore solution may be reduced to below the level necessary to passivate the steel. Second, even if the pozzolanic reaction is not complete, the reduced hydroxyl ion concentration in the pore fluid of cement paste may result in more rapid and deeper levels of carbonation than in normal cements (141) which, again will cause depassivation of the steel. Third, the pozzolanic reaction of most of these mineral admixtures requires longer curing periods for ensuring superior properties over normal cement concretes. The beneficial influences of these materials, from durability point of view, generally include the reduced pore-size leading to significantly impermeable concretes, increased resistivity leading to reduced corrosion current and reduced quantities of leachable $Ca(OH)_2$ which may be considered more deleterious than beneficial from durability consideration.

The above argument entails that while cements blended with mineral admixtures are physically stable and durable; they are, however, chemically more vulnerable, because of the reduced alkalinity due to the pozzolanic reaction. Some of these fears are, however, negated by many researchers. Studies carried out at

KFUPM (141) have shown that pozzolanic portland cement concretes contaminated with various levels of chlorides and exposed to the Arabian Gulf environment gave approximately the same degree of pH as companion plain cement concretes; although the carbonation depth was slightly more for the case of pozzolanic cement concrete. Increased carbonation of pozzolanic concrete is also confirmed by the data developed by Tsukayama et al. (142) based on outdoor and indoor exposure of concrete. Their results show that even for equal compressive strength in the range of 200 to 500 kg/cm^2, 30% fly ash concretes had an average of about 2 mm more carbonation depth than corresponding plain cement concretes after an exposure of 2 years. It should be mentioned that carbonation of concrete tends to level out with time (91) because the product of carbonation, i.e. calcium carbonate, blocks the pores and, consequently, reduces the rate of carbonation. Moreover, it is anticipated that for substructures, such as foundations, carbonation will not be a problem. Regarding the prolonged curing period, the problem can be resolved by mix design adjustments; examples include the use of lower w/c ratio; or the use of highly pozzolanic materials, such as silica fume, that can develop better properties within the minimum achievable curing period. The last point to be explained is the reduction in OH^- ions and the deleterious role of $Ca(OH)_2$. It has been shown by Haque and Kayyali (143), based on pore solution extraction technique, that although marginal reduction in OH^-

content was attained by the use of 30% fly ash blended with Types I, II and V cement pastes; the pH of the pore solution was still higher than that of saturated $Ca(OH)_2$ solution (i.e. pH = 12.4), which does not signify corrosion risk. The deleterious action of the extra, unnecessary calcium hydroxide is that it is highly leachable, thereby leading to either increased permeability or to be exchanged with aggressive ions. The deleterious action of the excessive $Ca(OH)_2$ also emerges from the vulnerability of the cements to sulfate attack. Figg (99) pointed out that the increased sulfate resistance of pozzolanic concretes appears to be the results of the following three factors:

i) the solubility of calcium aluminate hydrate (CAH_6) increases with reduced $Ca(OH)_2$ and this encourages a "through-solution" reaction with sulfate ions to form crystalline ettringite with the expansion associated with the "topotactic" or the colloidal mechanisms;

ii) the concentration of sulfate ions required to form ettringite increases as the $Ca(OH)_2$ concentration in the cement paste decreases, and

iii) the pozzolanic reaction reduces the concrete permeability, thereby impeding the penetration of sulfate ions.

From corrosion point of view, blended cements are known to reduce the chloride diffusion by as much as 10 to 100 times compared to diffusion in normal plain cements (135), thereby leading to effective protection against rebar corrosion.

The above review indicates that blended cements have a high potential in mitigating the durability problems in aggressive environments.

3.4 AGGRESSIVENESS OF SABKHA ENVIRONMENT

The sabkha is a highly aggressive environment to both concrete and reinforcing steel; its deleterious action emerges from the fact that the chloride concentration in the sabkha brine amounts to four to six times that in sea water (Table 2.3). What makes the problem worse is that geotechnical engineers usually investigate the load-bearing and compressibility characteristics of sabkhas and are rarely concerned with the durability performance of concrete substructures in such hostile environments (144). This unintentional ignorance of the aggressive service-environment has led to a substantial reduction in the useful service-life of concrete structures. Furthermore, the normal practice of using Type V sulfate resisting cement, although provides adequate protection against sulfate attack, fails to remove the excessive free chlorides from the concrete matrix thereby increasing the corrosion risk. A significant amount of the tricalcium aluminate (C_3A) phase in cement

is preferentially consumed by gypsum that is typically added to regulate the time of set of concrete (115). To inhibit reinforcement corrosion, a high (C_3A) cement is required, particularly in chloride environment (145).

Several feedback reports have recently been made available on the durability performance of substructures in sabkha environment. SCECO (146) performed a comprehensive evaluation of their manholes and handholes in an around Jubail. It was found that the majority of these substructures had to be rebuilt or repaired (147). The cost of restoration is estimated to be more than 1.5 billion Saudi Riyals (146). Another recent investigation has indicated that many substructures which included piers, foundations, etc. buried in sabkha have shown considerable degree of deterioration (148). A further recent investigation has reported serious deterioration of reinforced concrete structures exposed to sabkha and seawater conditions within less than ten years of construction (149).

These investigations emphasize the fact that corrosion of reinforcement is the main durability problem in sabkha environment and concrete should not be merely designed for strength, but also for durability.

Chapter 4

METHODOLOGY OF RESEARCH

This chapter outlines test methods implemented to achieve the objectives of this investigation. Whenever possible, standard ASTM or BS test methods have been adopted; otherwise, usage of any other method or modification to standard methods will be referred to and highlighted. The following main stages have been thoroughly explained: site selection, field tests on sabkha soil, laboratory tests on sabkha, foundation materials-sabkha interaction in the laboratory, foundation materials-sabkha interaction in the field.

4.1 SITE SELECTION

The first phase of this research program was to select a site in the Eastern Province that represents a typical sabkha. Published literature and geotechnical reports were reviewed for selecting this potential site. Sites located at Ju'aymah, Jubail, Ras Tanura and Ras Al-Ghar were surveyed. Reconnaissance visits to each of these four sites were based on visual observation of the surficial layers above groundwater table. Salt-encrusted surface, sandy nature of the layers, presence of pockets of diagenetic materials and depth of groundwater table were the symptoms considered. If the groundwater table was close to the surface, a

sample of sabkha brine was taken for chemical analysis in order to compare the ionic phases at the site with those quoted in literature. Brine was collected in a clean plastic bottle that was rinsed with brine before taking the sample. Ionic phases determined were: chloride, sulfate, bicarbonate, sodium, magnesium, calcium and the pH of the brine.

4.2 FIELD TESTS ON SABKHA SOIL

In an attempt to study the stratigraphy and subsurface conditions of the sabkha soil at the selected site, boreholes and other field tests were conducted. These tests included standard penetration test (SPT), cone penetration test (CPT) and pressuremeter test (PMT). Each of these tests was performed in an individual boring in order to avoid interference and/or disturbance. The depth of penetration was at least 10 meters, which is reasonable enough for shallow or even deep foundations. The reason behind running several tests at the same site was because each of these tests has inherently some advantages and drawbacks (150), particularly in sabkha which is a highly heterogeneous soil. The other field tests comprised of surficial field tests such as plate-load test and California-bearing ratio (CBR) test, which were conducted under natural and flooding conditions to assess the collapse potential of sabkha in the field.

All borings were drilled with a truck-mounted, drilling

rig. The boreholes were advanced using the mud rotary drilling technique; wherein a prepared solution of bentonite and water was recirculated to perform the following functions: (i) to cool and lubricate the tools thereby enhancing the drilling process, (ii) to remove the cuttings from the hole, and (iii) to maintain and support the borehole stability. Bentonite drilling mud has been developed as an economic option for all the above functions. In addition, the requirements of geotechnical drilling is to obtain representative samples. It is, therefore, necessary to maintain a hydraulic head in the open borehole in excess of the groundwater level. Failure to maintain an excess hydraulic head results in disturbance of the in-situ soil by boiling up into the open borehole. Bentonite has another advantage in that it does not penetrate into the pore space of subsurface formations. The advantages of bentonite drilling mud are recognized in ASTM D 1586 which specifies sampling in a fluid-filled borehole. In some circumstances, different drilling fluids are used. For example, clean water may be used for rock coring where support is not required and where there is no problem of rock solubility. In cases where there is a solubility problem such as for the rock salt layer, a drilling fluid (such as sabkha brine) is selected to minimize solution of the core drilling mud used to recover salt cover.

The following paragraphs are devoted to detail the field tests conducted in this research program.

4.2.1 Standard Penetration Test (SPT)

In principle, SPT is based on the idea of forcing a rod through the soil and measuring its resistance to penetration. Variation in this resistance indicates dissimilar soil layers and the numerical values of the resistance, therefore, permit an estimate of some of the physical properties of the strata (151). This test was initially developed in 1927 and is presently practiced worldwide to a great extent compared to any other soil field test (152).

In this investigation, SPT was conducted by driving a 50-mm-OD split-barrel sampler in general accordance with the "Standard Penetration Test (SPT)" procedure as described in ASTM D 1586. The test was made by dropping a "free" hammer weighing 63.5 kg (140 lb) onto the drill rod from a height of 0.76 m (30 in.) The number of blows, N, required to drive the sampler the final 0.3 m (1 ft.) of the 0.45 m (1½ ft.) is usually referred to as the SPT N value (the first 0.15 m of the total 0.45 m penetration is not considered in N values because these blows are usually not considered as representative of in-situ densities due to the possible presence of loose materials or cuttings from the drilling operation during the seating drive). SPT N values were recorded on the boring log. Where very dense material was encountered, the actual penetration after the initial 0.15 m seating of the sampler was recorded for a total of 50 blows. Where the sampler could not attain the initial 0.15 m sampler penetration

within 50 blows, it was considered as refusal and was shown on the boring log as "Ref".

Salt encountered at the site was cored continuously as the borehole was advanced using a size NW double-tube rock core barrel. Sampling with this NW core barrel generally followed the procedures outlined by ASTM D 2113. The diameter of the core samples obtained was about 54 mm. The cumulative sample length recovered from each core run was measured and tabulated on the boring logs as a percentage of the length of core run (*i.e. % recovery*). The Rock Quality Designation, *RQD*, was also determined. It is the ratio, in percent, of the cumulative length of intact salt (generally rock) specimens of 100 mm (4 in.) length or longer to the total length of the core run. The RQD values were also included in the boring logs.

4.2.2 Static Cone Penetrometer Test (CPT)

The cone penetrometer test is a static, or more accurately quasi-static, field penetration test. Many of the CPT penetration devices were developed and initially used in Europe and have gained widespread popularity in the United States and worldwide. Various options have been added to the originally simple CPT to produce piezo, thermal, conductivity, nuclear, seismic, acoustic and permeability cones (153-155). The main features for the increasing interest in CPT are the simplicity of testing, the low

cost, continuous in-situ profiling, reproducibility of the results and the test data are more amenable to rational analysis (152) as well as the CPT results are relatively operator-independent.

In this investigation, a 20-ton rated capacity Gouda Dutch cone penetrometer was used to perform static cone probing. The penetrometer was fitted with a mechanical type friction sleeve cone. The cone was truck-mounted and capable of applying 90 kN force before practical refusal was encountered. The sounding was performed by hydraulically pushing the 10 cm^2 area end cone, that has a 60° apex angle, into the ground at a constant rate of 20 mm per second in accordance with ASTM D 3441. The salt stratum, when encountered, was drilled and the cone test was thereafter continued. Readings of the total cone resistance and cone plus friction-sleeve resistance were obtained at about 200 mm intervals. The total cone resistance, usually called cone resistance and abbreviated as q_c, is obtained by dividing the total force acting on the cone, Q_c, by the area of the base of the cone A_c (10 cm^2):

$$q_c = \frac{Q_c}{A_c} \tag{4.1}$$

This resistance is usually expressed in kPa or MPa (psi or tsf). The local side friction is obtained by dividing the force needed to push down the friction sleeve, Q_s, by the sleeve's surface area

A_s:

$$f_s = \frac{Q_s}{A_s} \tag{4.2}$$

which is also expressed in the same units as q_c. The ratio of the local side friction f_s to the cone tip resistance q_c, at the same depth, and expressed as percentage, is defined as the cone friction ratio, R_f. This ratio is usually used to indicate the frictional tendency of soils. Although there is a tendency to use the friction index, I_f, (the reciprocal of R_f), that gives directly a figure larger than one (156), the results of the CPT were presented in terms of q_c and R_f.

4.2.3 Pressuremeter Test (PMT)

The pressuremeter was originally proposed by Franz Keegler and subsequently brought to a state of practical development by Menard in 1957 (157). It is an in-situ stress-strain test that is performed on the walls of a pre-drilled borehole using a cylindrical probe that can be inflated radially (158). There are many types of self-boring pressuremeters that do not require a pre-drilled borehole in order to minimize the effects of drilling disturbance and relaxation, and are able to measure the porewater pressure. PMT is almost the single-most test that can measure the in-place

deformation characteristics, at-rest (K_o) conditions, and volume change at various depths of both soils and rocks.

The PMT was conducted at about 1 to 2 m depth intervals using OYO Elasmeter 100 which consists of a probe, a pump with pressure gage and an electronic readout unit, together with umbilical hoses and electrical cables. The probe (i.e., flexible bladder) was lowered into the borehole and then inflated with incompressible fluid (water) under pressure that was provided by the pump at the ground surface. This probe applied stresses to the borehole walls, and a caliper monitored the change in radius of the stressed part of the borehole. The water pressure was read directly from the pressure gage on the pump. The caliper operated a transducer which was read by a digital electronic unit at the surface. The readings were taken at equal increments of applied pressure. An idealized stress-deformation relationship is shown in Fig. 4.1, which depicts the following seven conditions:

(1) The probe does not touch the wall and stress is not yet transmitted to the ground. The rubber tube expands freely and the relationship is definitely non-linear.

(2) The probe touches the borehole wall. At this point the relationship is also non-linear.

(3) The boreholes wall is recompressed back to its initial

in-situ conditions. In this stage, ground reaction force gradually increases and deformation rate goes down.

(4) This point is considered as the static soil pressure p_{oh}, which has regained the initial soil strength (before drilling) after which the deformation rate begins to show minimum value.

(5) The initial linear stage, where passive soil pressure is produced in the ground, is called a quasi-elastic deformation area of the ground at which the stress-deformation curve forms almost a straight line and the deformation rate maintains an almost fixed value.

(6) The yield point of the ground stress-deformation curve at which the deformation rate starts increasing.

(7) Fluidity (i.e. extensive plastic deformation) of the ground gradually advances and begins to enter the process leading to failure.

In practice, however, conditions (2) and (3) will not appear per se, but rather they will be combined with condition (4) as shown in Fig. 4.2 (159).

Some very important in-situ parameters can be obtained from PMT data. From Fig. 4.2, the modulus of subgrade reaction,

K_s, can be computed as the slope of the linear portion of the curve (159). The modulus of elasticity can also be computed from PMT data using the following equation:

$$E = R_m * K_s * (1 + \mu) \qquad (4.3)$$

where:

E = modulus of elasticity, kg/cm^2,

K_s = modulus of subgrade reaction, kg/cm^3, and

μ = Poisson's ratio

PMT data can also be used to determine the soil at-rest state (K_o condition). The pressure at the beginning of the linear portion of the curve is the stress required to bring the soil back to its initial field condition. This pressure is considered as the total horizontal stress, p_{oh}. The effective vertical pressure p_{ov} can easily be calculated from the knowledge of the unit weight (γ_t) and the depth (h) of soil stratum as well as porewater pressure. The following example demonstrates the procedure for obtaining K_o value from PMT (reference is made to Fig. 4.2, from which the total horizontal pressure at-rest, p_{oh}, was evaluated):

$p_{oh} = p_1 = 5\ kg/cm^2 = 500\ kPa$

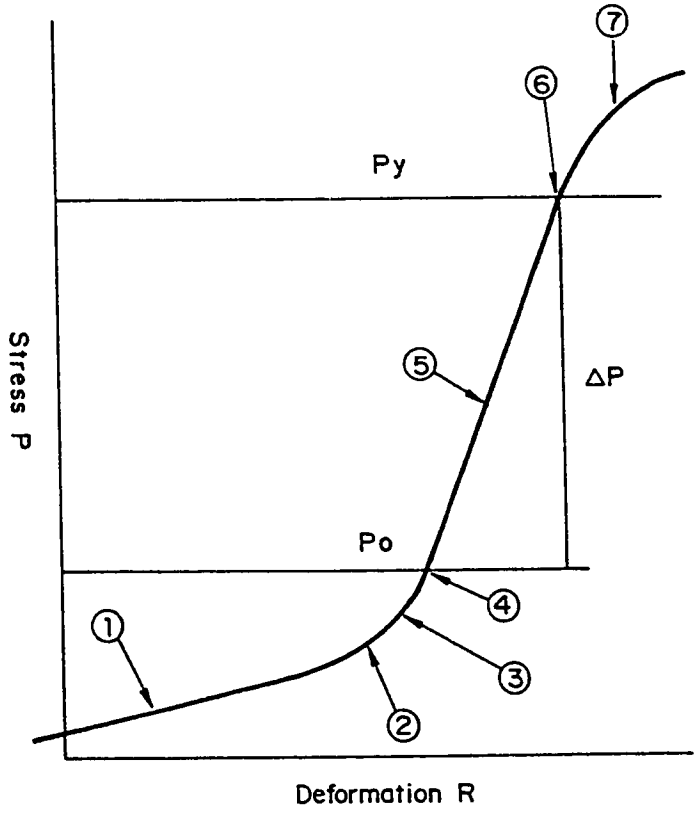

Fig. 4.1 : Pressuremeter Idealized Stress-Deformation Relationship.

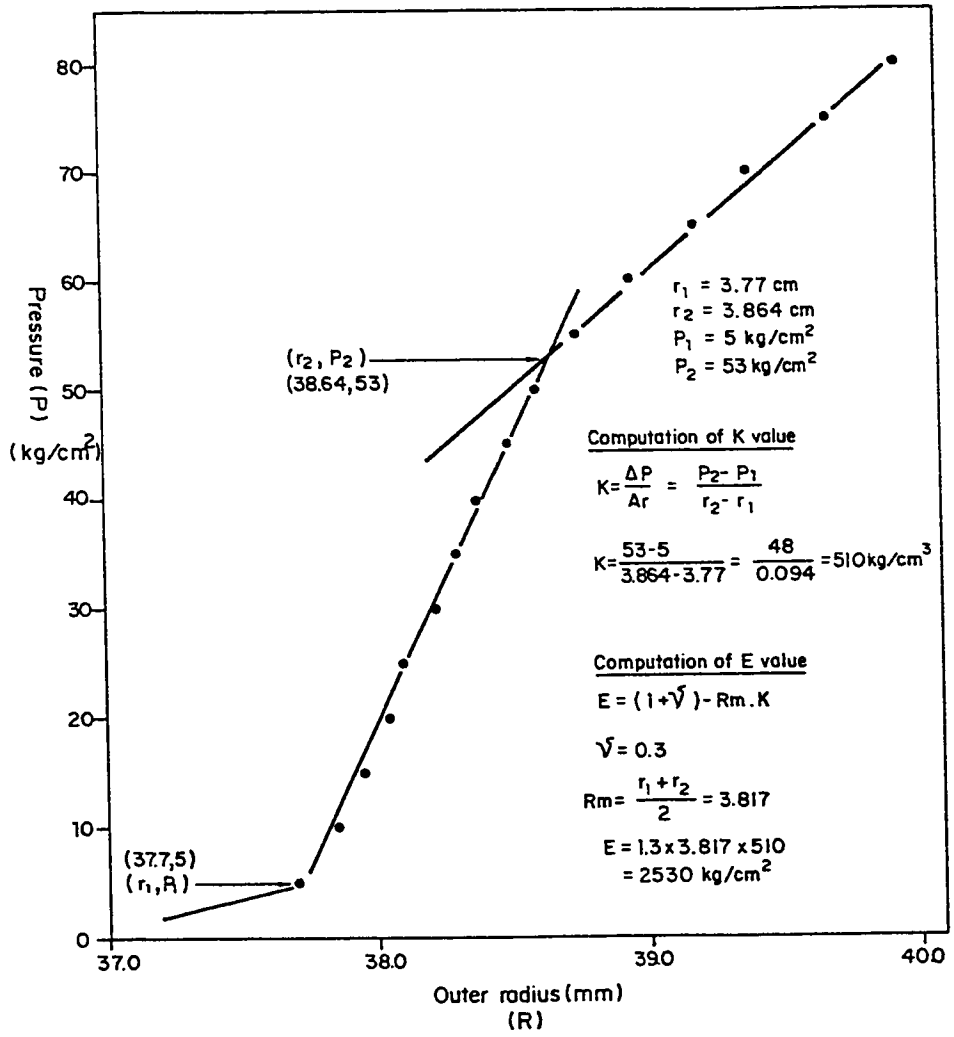

Fig. 4.2 : Actual Stress-Deformation Relationship Using Elastmeter 100 Pressuremeter.

If the depth of testing is at 30 m and γ_t is 20 kN/m³ and the water table is at 20 m from the ground surface, then:

$$u_o = (30 - 20) \times 9.8 = 98 \text{ kN/m}^2 = 98 \text{ kPa}.$$

$$p_{ov} = 30 * 20 = 600 \text{ kPa}$$

$$p'_{ov} = 600 - 98 = 502 \text{ kPa}$$

$$p'_{oh} = 500 - 98 = 402 \text{ kPa}$$

$$K_o = \frac{p'_{oh}}{p'_{ov}} = \frac{402}{502} = 0.80 \qquad (4.4)$$

The accuracy of the K_o values obtained from PMT is subject to controversy and debate, however, in summary, these K_o values should be used with great caution (160) and, consequently, should be complemented by other tests.

4.2.4 Plate Load Test (PLT)

PLT, sometimes called load-bearing test, represents the first known application of in-situ testing to investigate soil and rock strength and compressibility, and has been traditionally incorporated in pavement and building codes to justify the evaluation of the greatest pressure that can be applied to soil beneath foundations, thereby causing either failure of the loaded soil or excessive settlement. Although Terzaghi and Peck (161) criticize

PLT for the determination of the coefficient of subgrade reaction, K_s, on the basis of the constant pressure between the soil and plate, and in spite of the fact that other types of in-situ tests have now emerged and gained more popularity, primarily because of the cost and time required for testing; the PLT remains a valuable test method. It is best suited to investigate the compressibility and strength of miscellaneous fills, stony and bouldery soils and other materials which contain large particles or are too heterogeneous to be represented by smaller scale tests, or are not amenable to the recovery of good undisturbed samples (157).

Two PLTs were conducted in general accordance with ASTM D 1194 at which a test pit was excavated with an approximate diameter of more than four times the diameter of the steel-bearing plate (46 cm, 1.5 ft diameter plate). The plate was placed at the center of the pit (at a depth of 40 cm from the ground surface) and the loads were applied with a hydraulic jack and were measured with a load cell. The load readings were displayed on an electronic digitizer. The reaction load for the test was provided through a loaded truck. Loads were applied in fourteen increments to a maximum of 3.2 tonnes followed by three unloading decrements. Displacements were measured with three dial gages mounted on a rigid reference frame. The equipment was set up so that the reference frame supports were not affected by movements of the soil being tested or by movements of the reaction load

supports.

The first PLT was devoted for testing the sabkha soil at its natural condition. The second test was, however, designed to test the sabkha when inundated with water in order to evaluate the collapse potential due to flooding, in a manner, more or less, similar to that conducted by Erol (25) on a salt dome. However, the contractor did not agree to use water to avoid the possibility of collapse, which might be dangerous to his crew and damaging to his machinery; therefore, sabkha brine was used in the inundated condition.

4.2.5 Field California-Bearing Ratio (CBR) Tests

It is not very frequent to conduct CBR in the field to test the natural conditions of a soil, nevertheless, many times it is desirable to check the laboratory CBR values with those actually obtained during construction. The field CBR test is basically the same as the laboratory tests, in that the standard 3-inch square piston is used and surcharge weights are used (detailed description of the laboratory CBR will be given in Sec. 4.3.12).

In order to evaluate the collapse potential of sabkha, and therefore compensate the failure of performing the PLT under flooding condition with water, six field CBR tests were conducted. Three of these were conducted at natural conditions and the remaining three under flooding conditions with water. Although

the standard procedure (ASTM D 1882) necessitates that the tested materials be flooded for four days, flooding in the field was lasted for only three hours, due to time limitation.

4.3 LABORATORY TESTS ON SABKHA SOIL

In an attempt to characterize the sabkha in-depth and evaluate its response to standard tests, full laboratory investigation was conducted on disturbed and/or undisturbed samples. Undisturbed samples from deep strata were obtained using thin-walled (Shelby) tubes, while those from the surficial layer were obtained using thin walls PVC tubes which had been sharpened from their penetrating ends in order to reduce disturbance, as shown in Plate 4.1. These tubes were made with two different sizes, 2 x 4 inch (5 x 10 cm), and 4 by 8 inch (10 x 20 cm), in order to suit the different types of tests. The first type was primarily used in unconfined compression and triaxial tests while the latter type was used in consolidation and direct shear tests. The classical moulds, usually made of steel or brass, were not recommended to be used in retrieving undisturbed sabkha soils due to the susceptibility of rusting of the moulds because of the high salt content in sabkha. However, typical CBR moulds were inevitably used, because these specimens were tested once they were retrieved.

It has been reported in literature that sabkha soils display

Plate 4.1 : PVC Tubes Used to Retrieve Undisturbed Surficial Sabkha Samples.

alternate layering and cementation (2,62,63), and, therefore, may lead to different properties. For the sabkha at our selected site, it was found that about five different layers did exist above the groundwater table. These layers might change from one place to another; the thickest layer being at a depth from 22 to 42 cm, from which all the undisturbed samples were brought, nevertheless, diagenetic soft materials, probably gypsum and anhydrite as well as halite crystals were also present. The PVC tubes used to retrieve undisturbed samples were inserted up to this depth, and through the use of a shovel and a knife, the tubes were released and retrieved. Each specimen was, thereafter, placed in a double nylon sheet along with a label indicating the date of sampling. As soon as the samples were brought to the laboratory, they were uncovered from the nylon and their top and bottom ends were sealed by wax. They were, therefore, preserved until they were tested and, only at testing, their natural moisture content, density, dimensions, etc. were determined. These samples did conform to those described by Hvorslev (151) as "samples in which the material has been subjected to so little disturbance that it is suitable for all laboratory tests and thereby for approximate determination of the strength, consolidation and permeability characteristics and other physical properties of the material in-situ. The term is to some extent misleading, since it is impossible to obtain a truly undisturbed sample, but it is firmly established in the engineering terminology and therefore being retained".

Large volume of disturbed sabkha was brought to the laboratory and spread over large area for drying for about one month. Oven drying was not preferred owing to the fact that these soils usually contain large proportions of soluble and insoluble salts. Particularly important is the presence of gypsum ($CaSO_4.2H_2O$) which is transformed into anhydrite under temperature. The temperature at which this phase transformation occurs is a subject of considerable debate (162); however, Fookes et al. (15) recommend the temperature not to exceed 80°C. Thereafter, the soil was crushed gently in general accordance with ASTM D 421 using plastic hammers to break down aggregated particles that were cemented together, allowing the soil to pass ASTM sieve No. 10 (2 mm). The soil was then thoroughly homogenized and kept in plastic drums until testing. These samples are to be considered "remolded", yet they were exactly similar to those defined by Hvorslev (151) as "representative samples that contain all the mineral constituents of the strata from which they are taken and they have not been contaminated by material from other strata or by chemical changes, but the soil structure is seriously disturbed and the water content may be changed. These samples are suitable for general classification tests and positive identification of the materials, but are not suitable for major laboratory tests and determination of the structural properties of the material in-situ", and, hence, were considered as disturbed.

These disturbed samples were used in grain-size distribution, plasticity determination, compaction, stabilization, etc., where the original structure of sabkha is not of great importance.

4.3.1 Specific Gravity Tests

This test was conducted on three representative disturbed samples. The test was performed in general accordance with ASTM D 854 using only vacuum. Oven drying, however, was carried out at 70°C until constant weights were attained.

4.3.2 Grain-Size Distribution Tests

This test is a basic test in any soil investigation. It is essential in almost all classification soil systems and filter design analysis. Knowledge of the sizes of soil grains may give preliminary ideas on permeability, strength characteristics (i.e. friction and cohesion), swelling-shrinkage properties, etc. The importance of grain-size determination therefore is well-recognized and its correct determination should reflect the nature of the soil.

Due to the high salt content of the sabkha and its brine (Table 2.3), standard ASTM or BS procedure for grain-size analysis is expected not to be suitable for such a soil. Consequently, four types of mechanical (sieve) analysis tests were conducted in an attempt to determine the correct grain-size distribution as well as to develop a comparative evaluation of the different techniques

implemented.

Sample preparation of grain-size analysis was conducted in compliance with ASTM D 421. Mechanical analysis was carried out using ASTM sieves No. 20, 40, 60, 100, 140 and 200. Dry sieving was conducted according to ASTM D 422; the wet sieving was carried out using: (i) distilled water, (ii) methylene chloride (according to Ref. (63)), (iii) sabkha brine. In the case of wet sieving, the fluid was allowed to flow into the top sieve from a plexiglas reservoir which was placed at a height of about 130 cm. Based on preliminary trials, about one cubic foot (0.283 m^3) fluid was used during each wet sieving test, which was enough to make the passing fluid clear. Materials passing the No. 200 sieve were collected in a plexiglas container with the passing fluid left in the container to settle down and precipitate for about one to two days, until the fluid was clear. The fluid was poured off the container and the material was collected in a dish and allowed to be air-dry. Thereafter, the dry material, passing Sieve No. 200, was kept in plastic bags until it was tested by the hydrometer.

The hydrometer test was conducted through exactly similar procedure to that reported by Wray (163) using type 152 H hydrometer. The sieve analysis and the hydrometer test was combined as described by Lambe (164).

4.3.3 Atterberg Limits Tests

These types of limits (i.e. liquid limit, plastic limit and shrinkage limit) are essential parameters for cohesive soils. For the case of Ras Al-Ghar sabkha, these limits were not determined because the soil was invariably cohesionless and, therefore, non-plastic.

4.3.4 Classification Tests

Although soils can be classified in a variety of ways, i.e. by colour, texture, odor, etc., these ways are not sufficiently specific to reflect the engineering properties of the soil. Therefore, a classification system should give the impression of the suitability of a soil for specific construction projects and be able to communicate this information to concerned people.

There are many classification systems worldwide; some of these are invariably used in their own countries. The AASHTO (American Association of State Highway and Transportation Officials) (165), and the USCS (Unified Soil Classification System) (166), are the most widely used. The former is primarily used in highway construction and the latter is used by most of the geotechnical engineers. Both, the AASHTO and USCS, are solely based on the grain-size distribution and the Atterberg limits. Since sabkha is virtually non-plastic; the grain-size analysis was the only data to be considered.

The steps followed in AASHTO and USCS are

well-explained in all geotechnical books and soil laboratory manuals (167).

4.3.5 Permeability Tests

Six 9.7 cm diameter undisturbed samples were tested under constant (ASTM D 2434) and variable head permeability conditions. The head was 177 cm for the former while the head differential was 150 cm for the latter (i.e. H_1 = 150 cm and H_2 = 50 cm), both of which were kept constant during all tests. Distilled water was used first for testing three samples. For the remaining three samples, sabkha brine was used. This is because it is noticed that after the sporadic and scanty rainy days, water does not seep through sabkha easily and it remains standstill for long periods (44,168). This water becomes concentrated under the extremely high rates of evaporation in sabkha terrain. Moreover, the use of sabkha brine to measure the permeability simulates actual groundwater flow, irrespective of the rather well-established low accuracy of laboratory-permeability determination. The aim here is to study the trend rather than define quantitative output.

A pre-requisite parameter to be evaluated for the case of permeability test is the viscosity of the fluid to be used (i.e. whether kinematic or dynamic one), in order to calculate the standardized permeability coefficient at 20°C. For the case of distilled water, it is easy to obtain this value from laboratory manuals,

while for the sabkha brine, this was determined according to ASTM D 455 and the density was determined by the use of a hydrometer.

4.3.6 Moisture-Density Relationship (Compaction) Tests

The purpose of any moisture-density test, commonly called the compaction test, is to determine the optimum moisture content at which the density of soil (more specifically the dry density) is maximum. It is generally desirable to increase the density in the field in order to increase the shear strength of the soil and to decrease soil permeability and future settlement.

In this investigation, standard Proctor test (ASTM D 698) of 24.5 N hammer weight and 0.305 m drop height (i.e. 2.2 lb and 1.0 ft., respectively) was conducted on disturbed samples to identify the maximum dry density and optimum moisture content.

In addition to mixing the sabkha with distilled water, as recommended in standard compaction tests, sabkha brine was also used as a lubricating fluid in another series. The use of sabkha brine may sometimes be a unique choice since sabkha terrains are usually remote from urban areas; the use of distilled or sweet water may therefore be economically unfeasible. Further, the moisture contents were determined first at the oven-drying temperature of 70°C until constant weight, were obtained; thereafter, the temperature was raised to 110°C and again the constant dry weight, were recorded. The use of 70°C and 110°C temperatures

was intended to study the role of temperature increase on the shape of compaction curves due the presence of diagenetic minerals in sabkha.

4.3.7 Field Density Measurements

This test is an essential criterion to verify whether a particular site is within an acceptable density for construction. If not, the soil has to be compacted, and it has to be checked again until a satisfactory density is achieved. This satisfactory density is typically related to the maximum dry density of a standard compaction test. The term "relative compaction" is normally used to denote this satisfactory density, and it is defined as follows:

$$R.C. = \frac{(\gamma_d)_f}{(\gamma_d)_{max}} \times 100 \qquad (4.5)$$

where R.C. = relative compaction (90, 95, 105,...etc.), %

$(\gamma_d)_f$ = dry field density, gm/cm^3

$(\gamma_d)_{max}$ = max dry density obtained from a standard compaction test.

For the selected sabkha site, three field density measurements were conducted using the classical sand-cone method (ASTM D 1556, AASHTO T-191). The locations of the tests were so chosen to represent the area from which disturbed and undisturbed

samples were retrieved. Therefore, the tests were conducted at the apices of equal-sided triangle that surrounded this area. The depth at which the holes were made was about 25 cm from the ground surface.

4.3.8 Consolidation Tests

Consolidation tests are the most cumbersome and time consuming to perform and, for the case of difficult soils such as sabkhas, they are very difficult to interpret. Nevertheless, these tests are very instrumental to predict the compressibility and swell potential and sometimes, collapse potential. The most important parameters to be determined from these tests are the compression index C_c, and the coefficient of consolidation, C_v. The first parameter is usually used to estimate the total amount of consolidation while the latter is used to estimate the rate of consolidation.

4.3.8.1 Conventional Consolidation Tests

Prediction of the settlements of structures in the field is primarily based on a method of extrapolating laboratory test results. The laboratory tests commonly used are solely based on the one-dimensional Terzaghi theory of consolidation, irrespective of the validity of the assumptions that this theory is based on (164).

There are typically two types of oedometer: the fixed-ring

oedometer and the floating-ring oedometers. In the first (Fig. 4.3), the compression is downward, while in the latter (Fig. 4.4), the compression takes place from both faces of the soil sample. Also, the effect of friction between the soil and the ring is more in the fixed-ring than the floating ring. However, the main advantage of the fixed-ring is that it can be adapted for permeability measurements from the bottom porous stone or otherwise drainage may be controlled (164).

In this research program, consolidation tests were conducted on undisturbed samples in general accordance with ASTM D 2435 using the fixed-ring oedometer. The samples were initially loaded with the overburden pressure of 9 kPa. Some of the samples were then flooded with distilled water while others were flooded with sabkha brine. This was essential to study the collapse potential of sabkha soil. Load increments were applied until a maximum pressure of 1,810 kPa was reached after which unloading was started. Reloading was then continued until test termination at a pressure of 1,810 kPa. Unloading-reloading curves were instrumental to evaluate the swelling index (C'_s).

4.3.8.2 Development of a Modified Oedometer

It was suggested by Lambe (164) that the fixed-ring oedometer could be modified to measure permeability (both constant head and variable head). Even earlier, Taylor (169) had discussed

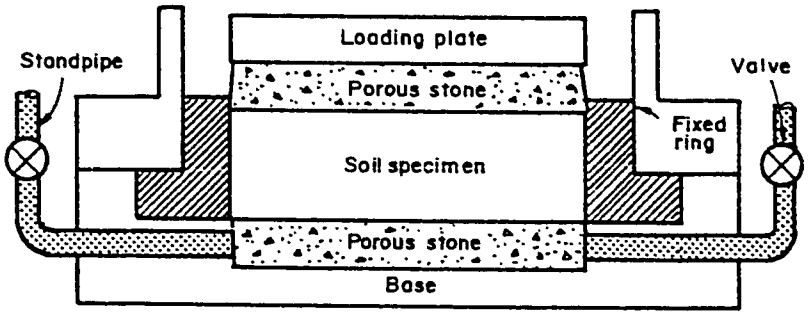

Fig. 4.3 : The Fixed-Ring Oedometer.

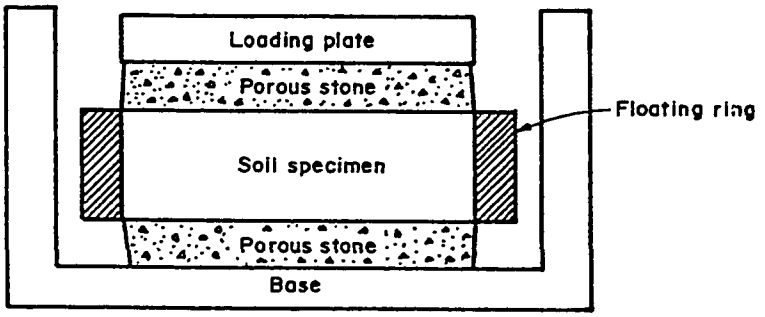

Fig. 4.4 : The Floating-Ring Oedometer.

the use of a standpipe and pressure line attached to the bottom drainage connection to allow the use of the consolidometer as an upward flow permeameter and, consequently, permits direct determinations of the sample permeability. However, no such modification has been implemented in the literature. In this investigation, this idea was adapted in a way that constant head permeability could be measured without the application of an external pressure. This was accomplished by making two holes below the consolidating specimen and an inlet for water supply and an outlet for the overflow of excess water from a reservoir, in order to keep the head constant, as shown in Fig. 4.5. From the two holes, the percolating water can be collected using a graduated cylinder, as shown in Plates 4.2 and 4.3. The volume of this water could be measured over regular intervals, thereby measuring the rate of flow with respect to both time and pressure during the loading, unloading and reloading cycles.

One of the two main features of the modified oedometer, compared to the one proposed by Lambe and Taylor, is the use of a ring, rather than a container, as shown in Fig. 4.3. The ring can be inserted into the undisturbed soil to obtain high quality undisturbed samples; unlike the container for which the undisturbed sample would have to be first prepared and then inserted into the container, thereby leading to more disturbance. Moreover, the sample might not exactly fit the container. The second

feature is that the flow of water is mainly due to difference in head of water, while for the one proposed by Lambe and Taylor, air pressure was used to induce the flow. The reason for the use of air pressure might be attributed to the fact that soils with very low permeability were considered. For sabkhas, no air pressure is actually required to induce flow because of its cohesionless nature.

Recently, Swan (179) reported the development of a large scale consolidometer, (Fig. 4.6), that had a diameter to height ratio of 1.4 (the minimum diameter to height ratio is 2.5 as specified by ASTM D 2435), to accommodate loads up to 320 kN/m^2 (i.e. 320 kPa) applied through a compression testing machine, as no arm was used. Water was allowed to percolate by applying a 0.75 meter head of water. No further details on the set-up and procedural methodology, particularly the measurement of flow, were reported.

The basic reason for designing this modified oedometer was the inability of the conventional oedometer to measure the potential collapse of sabkha due to flooding with distilled water. Therefore, the relevance of this development to sabkha soil is not to measure the permeability per se, but rather to allow distilled water to flow through sabkha samples. The percolation of distilled water induces salt dissolution which can be established by chemical analysis of the passing fluid and, consequently, the collapse potential can be estimated.

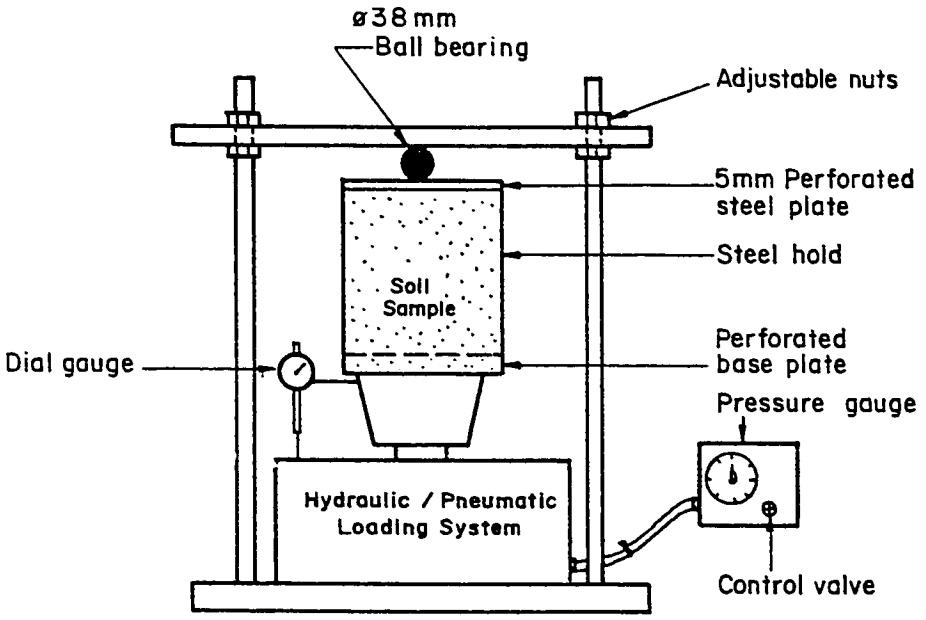

Fig. 4.5 : Swan's Oedometer.

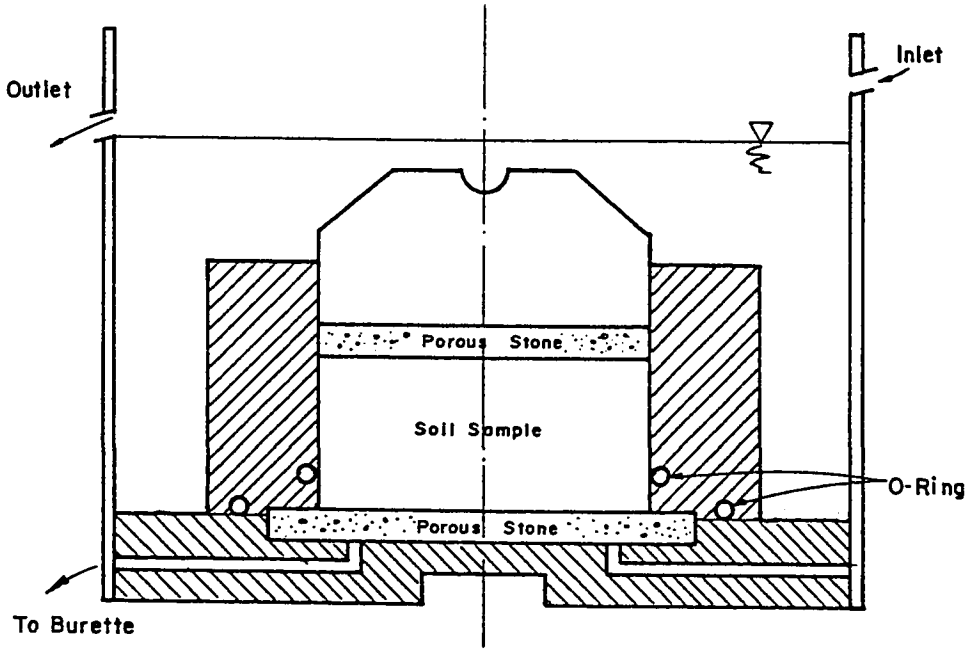

Fig. 4.6 : The KFUPM-Modified Oedometer.

Plate 4.2 : Measurement of Flow Using the Modified Oedometer.

Plate 4.3 : Reservoir Used to Maintain a Constant Head in the Modified Oedometer.

The procedure followed was exactly similar to that of the conventional oedometer with allowance for flow of liquid through the soil sample. This first test was devoted as a preliminary trial to verify the ability of this apparatus to predict collapse potential at a relatively high pressure and whether flow of fluid could pass through the tested specimen at this high pressure. In this test, normal consolidation behavior of sabkha was evaluated until a pressure of 234 kPa was sustained for about 48 hours, thereby achieving full consolidation. Flow was thereafter started and allowed for a period of 5 to 8 days, until the rate of change of settlement was nearly constant. The loads were thus increased in a manner similar to that in the conventional consolidation tests. It is noteworthy to mention that some selective samples of water passing through the consolidating soil sample were taken for chemical analysis in order to assess if there was leaching and/or dissolution of some ions. Further, instantaneous measurement of flow rate were taken at different intervals for each of the pressures applied during loading, unloading and reloading cycles.

The second phase was intended to develop a systematic procedure that could generate as much relevant and conclusive data as possible. Therefore, flow was allowed to commence just after the flooding condition under the overburden pressure in an attempt to compare the flooding condition (i.e. same as conventional oedometer) and percolating condition and, consequently, to

estimate the collapse potential if any. The measurements of instantaneous flow were also taken at regularly consecutive periods for each loading cycles. Again, water samples representing each loading cycles were taken; particularly at the initiation of flow when it was anticipated that leaching of soluble salts would occur most.

In the last phase, sabkha brine was used in place of distilled water; and the entire procedure was repeated. At the end of this test, distilled water was also allowed to percolate through the specimen for relative comparison.

4.3.9 Unconfined Compression Tests

Six undisturbed sabkha samples were retrieved, however, only three were tested under unconfined compression (q_u) test. The other three were not intact and therefore they were discarded. Two more series of specimens were tested to study the effect of moisture content on the strength of sabkha. The first series was prepared using distilled water; while the second was prepared using sabkha brine. In both series, the moisture content was changed from around the optimum moisture content down to the minimum attainable moisture. The specimens were compacted using 1.08 kg hammer at approximately three equal layers.

All the unconfined compression tests were performed on 5x10 cm samples using Wykeham-Farrance machine at a constant

loading rate of 0.5 mm/min and in general accordance with ASTM D 2166.

4.3.10 Direct Shear Tests

These tests were conducted on undisturbed samples that were brought in PVC tubes, similar to those used in the consolidation tests. The metallic square ring was then inserted into the specimen; the samples were retrieved and then trimmed after fitting in the shear box. The normal stresses were 1.11, 2.22 and 4.44 kg/cm^2 (109, 218 and 435 kPa) and the loading rate was kept invariant at 0.75 mm/min, and the test was conducted according to ASTM D 3080.

4.3.11 Triaxial Tests

These tests were conducted on undisturbed samples which were similar in size to those used in the unconfined compression test. Six undisturbed specimens were tested under six different confining pressures, namely 2, 5, 10, 15, 20 and 30 psi (i.e. 13.8, 34.5, 68.9, 103.4, 137.9 and 206.8 kPa). The reason for testing many samples is that undisturbed sabkha is virtually weak and cohesionless, and therefore sample disturbance may have significant influence on the results. Moreover, the presence of a white, soft diagenetic material, probably gypsum and/or anhydrite (see Plate 5.1) was also another factor. These specimens, at their natural moisture content, were tested under consolidated-drained

(CD) triaxial test conditions in which each of the specimen was consolidated under a confining pressure (isotropic consolidation) until no change in volume was observed, thereafter, the deviatoric stress was applied until failure. The failure criterion adopted in these tests was either the displacement (at testing) reached about 20% of specimen's length or there was clear reduction in deviatoric load. The tests were in general accordance with ASTM D 2850, however, volume change was not recorded.

Since there is a variety of triaxial tests and each of them has its own applications in geotechnical engineering, several triaxial tests were conducted in this investigation in order to access accurately the shear strength parameters as well as to study the influence of distilled water and sabkha brine on these parameters. Two more triaxial test series were therefore conducted on undisturbed sabkha samples. In the first series, consolidated-undrained (CU) tests were conducted on saturated samples. Saturation was achieved through the application of carbon dioxide (CO_2) gas in an attempt to expel gas in the pores, thereafter back pressure was applied. Due to the high solubility of CO_2 in water, higher degrees of saturation were achieved. It should be mentioned that the least amount of water was allowed to drain out during the saturation stage in order to minimize salt dissolution. After saturation, confining pressure was applied and maintained until no further change in volume was observed. The deviatoric stress was

then applied and continuous measurements of displacement, deviatoric stress and pore-water pressure were taken. For the second series, consolidated-drain (CD) tests with volume change measurements were conducted on saturated sabkha samples. Saturation was applied in the same way as for the first series. After the application of confining pressure, deviatoric stress was applied and continuous measurements of axial displacement, deviatoric pressure, pore-water pressure and volume change were recorded. The first three parameters were recorded using LVDT's that were attached with a data logger which was also connected with a personal computer; while the fourth parameter (i.e. volume change) was measured manually through a burette. The reason behind pore-water pressure measurement was to insure that it was within minimal limits (± 0.5 psi).

These two series were further repeated to evaluate the effect of saturation with sabkha brine, in comparison with distilled water, on sabkha strength. The procedure was exactly the same as that for distilled water. A special reservoir container was fabricated to saturate the samples with sabkha brine.

4.3.12 California-Bearing Ratio (CBR) Tests

This test was originally developed as a means to evaluate the suitability of a soil to be used as a subgrade material in highway construction (171) and, thereafter, adapted by engineering

communities as a test to measure the shear strength of a soil under controlled moisture and density conditions.

In this investigation, CBR tests were conducted in compliance with ASTM D 1883. Eight undisturbed specimens were retrieved from the field in the special CBR moulds and covered with two layers of nylon sheets to prevent any loss in moisture. Four of these specimens were tested at their natural state on the same day they were obtained. The other four were soaked in distilled water for four days under a surcharge of 5 kg, with a gage attached to the specimens to measure any expansion due to water flooding. Surprisingly, settlements were observed without dilatational change. An average of 0.025 inch (0.64 mm) compressive settlement was attained at the fourth day. Thereafter, these specimens were tested at a penetration rate of 0.05 inch/min (1.27 mm/min) and the readings of load and penetration were taken until a little more than 0.50 inch (about 13 mm) was attained.

It is to be mentioned that all data generated from unconfined compression, direct shear, triaxial, and laboratory CBR tests were recorded using a portable TDS-301 Tokyo Sokki data logger, which were, thereafter, analyzed and interpreted. Computer programs were merely developed for this investigation and used in calculation of grain-size analysis, permeability, consolidation, direct shear, triaxial and CBR tests.

4.4 LABORATORY STUDIES ON FOUNDATION MATERIALS-SABKHA INTERACTION

Chemical analysis of the sabkha brine obtained from the selected sabkha site at Ras Al-Ghar (Table 5.1) shows that the chloride and sulfate concentrations were 15.7% and 0.55%, respectively, and the sodium and magnesium concentrations were 7.9% and 1.0% respectively. In order to simulate the sabkha environment, it was decided to incorporate only these four ions (Cl^-, SO_4^{--}, Na^+ and Mg^{++}) for the following four reasons: (i) these are the major ions existing in the Ras Al-Ghar sabkha and they conform very well to other sabkhas in the Eastern Province (2) as well as those in the United Arab Emirates (7), (ii) it is the sulfate and chloride ions which play a major reaction role on the cement hydration products and the reinforcing steel (Chapter 3). Since these ions cannot exist independently, they must be combined with Na^+ and Mg^{++}, the two major cations, (iii) it is not feasible to use all the species in the sabkha brine to make an exactly simulated solution with the same constituents and the same concentrations, and (iv) it is advantageous to reduce the number of species in the solutions to study the mechanisms by which the concomitant presence of chloride-sulfate ions would affect the durability of concrete so that the research would yield fruitful results.

4.4.1 Test Solutions

In order to study the effect of chlorides on sulfate attack in plain and blended cements and the effect of sulfates on chloride-induced corrosion, three other chloride-sulfate solutions were prepared in addition to the sabkha-simulated brine. The concentration of these solutions is as follows:

(i) Solution #1: potable water.

(ii) Solution #23: chloride concentration was the same as that existing in the selected site at Ras Al-Ghar (Cl^- = 15.7%), while the sulfate concentration was similar to those existing in a typical continental sabkha in Wadi As-Sirhan (i.e. SO_4^{--} = 2.1%) (16) (See Table 4.1). This solution is designated as "high sulfate-chloride environment".

(iii) Solution #4: this is the simulated Ras Al-Ghar sabkha brine (Cl^- = 15.7% and SO_4^{--} = 0.55%) and is designated as "low sulfate-chloride environment".

(iv) Solution #5: this is the pure sulfate solution without any chloride addition (Cl^- = 0% and SO_4^{--} = 2.1%).

(v) Solution #6: this is the pure chloride solution without

any sulfate addition (Cl^- = 15.7% and SO_4^{--} = 0%).

The last two solutions (solution #5 and #6) were chosen to represent the maximum sulfate and chloride concentrations in the above two sabkhas. The pure sulfate and pure chloride solutions were chosen to provide reference solutions in order to elucidate the effect of concomitant presence of SO_4^{--} and Cl^- on chloride-induced reinforcement corrosion and sulfate attack mechanisms. It may be noted that the sulfate concentration used in the low sulfate-chloride solution may be classified as "severe" sulfate environment according to Table 4.2 as well as according to the Canadian Standards CAN-A23.1-M77 (80). The sulfate concentration in both pure sulfate and high sulfate-chloride solutions may be classified as "very severe".

Sodium chloride was used to provide the chloride ions while sodium and magnesium sulfates were used to provide the sulfate ions. The latter two salts were so proportioned to provide 50% of the sulfate concentration from each of them. The use of mixed sodium and magnesium sulfate salts to study the durability performance of plain and blended cements is well-documented and standardized (172,173). This kind of mixed solution is recommended if the magnesium ion concentration in groundwater is high as it is the case for sabkha soils in general and for those in eastern Saudi Arabia in particular (Table 2.3).

The specimens were placed in fiber-glass tanks filled with test solutions with ample space between them. The tanks were covered with polyethylene sheets to minimize evaporation. The solutions were agitated gently using plastic water pumps, and the concentrations of the solutions were checked every month and adjusted to preserve the designed concentrations.

In order to successfully complete the research program, the following tests were conducted:

(i) visual inspection to characterize the deterioration type and to evaluate the degree of deterioration;

(ii) reduction in strength. This reduction in strength, due to exposure to the sulfate-chloride solutions, was related to the deterioration factor;

(iii) reinforcement corrosion monitoring to evaluate the corrosion activity on steel reinforcement in plain and blended cement concrete. This was carried out by measuring half-cell potential and determining corrosion current density at periodic intervals;

(iv) X-ray diffraction (XRD) and scanning electron microscopy (SEM) equipped with energy dispersive X-ray analysis (EDXA) to elucidate the mechanism of sulfate attack in pure sulfate and sulfate-chloride

Table 4.1 : Range of Cation and Anion Concentrations in Wadi As-Sirhan Sabkha Brine (Smith, 1980)

Constituent	Concentration (ppm)
Minimum chloride	487
Maximum chloride	223,992
Minimum sulfate	66
Maximum sulfate	23,299
Minimum magnesium	487
Maximum magnesium	9,758
Minimum sodium	23,000
Maximum sodium	89,010

Table 4.2 : Degree of Severity and Recommendations for Normal Weight Concrete Subject to Sulfate Attack.

Potential Degree of Sulfate Attack	Water-Soluble Sulfate (as SO_4^{--}) in Soil (%)	Sulfate as (SO_4^{--}) in Water (ppm)	Type of Cement	Maximum Water/Cement Ratio
Mild	0.00-0.10	0-150	---	0.5
Moderate	0.10-0.20	150-1500	Type II IP (MS) IS (MS)	0.50
Severe	0.20-2.00	1500-10,000	Type V	0.45
Very Severe	Over 2.00	Over 10,000	Type V +Pozzolan	0.45

solutions after long-term exposure to various environments, and

(v) pore solution expression to elucidate the role of sulfate ion on the chloride-induced reinforcement corrosion.

4.4.2 Specimens and Materials Used

4.4.2.1 Specimens

Test specimens were made either with cement paste, mortar or reinforced concrete specimens.

4.4.2.1.1 Cement Paste Specimens:

Cement pastes specimens of plain and blended cements, used for X-ray diffraction and scanning electron microscopy (SEM-EDXA) analyses, were made with a water to cementitious material (i.e. cement plus blending materials) ratio of 0.5. When plain cements were used, the cement was thoroughly mixed with water in a kitchen blender until the mix became uniform and homogeneous. The clean, oiled moulds were thereafter filled in two layers, each layer being compacted on a vibrating table at a rate of 3600 vibrations per second. In the case of blended cements, the cement and blending material were first thoroughly mixed in the dry state and then water was added and mixed thoroughly. Pastes specimens, 12.5x12.5x12.5 mm, were used.

Plain and blended cement paste specimens, used for pore fluid extraction and analysis tests, were also made with a water to cementitious material ratio of 0.6 in a manner similar to that for the X-ray diffraction and scanning electron microscopy specimens. However, the salts inducted into the cement pastes (sodium chloride and sodium sulfate) were anhydrous, AR (analar) grade. They were first dissolved in the mixing distilled water before the mixing process. The admixed chloride was 0.6% by weight of cement while the admixed sulfate was 6% as SO_3 by weight of cement. The latter was incorporated as 6% total SO_3 including the SO_3 in cements and/or blending materials. These specimens were filled into special cylindrical PVC vials of 50 mm diameter and 75 mm length. Pore solution was extracted after 75 days of curing in the sealed vials at laboratory temperature (21°C).

4.4.2.1.2 Cement Mortar Specimens:

Cement mortar specimens, 25x25x25 mm, made of plain and blended cements were used to determine the strength development and strength reduction due to exposure to the various sulfate and/or chloride solutions and the natural sabkha at Ras Al-Ghar. The fine aggregate used was dune sand with 2.64 specific gravity, 0.23 percent absorption and 1.3 fineness modulus. The sand was only air dried. All mortar mixes were made with a water to cementitious material ratio of 0.5 by weight and a ratio of sand to cementitious

material of 2.75. The mixing process was similar to that described in Sec. 4.4.2.1.1.

4.4.2.1.3 Concrete Specimens:

Concrete specimens were used to study the corrosion of reinforcement in different chloride-sulfate environments. These specimens were made with a water to cementitious material ratio of 0.5. The coarse aggregate was 19 mm crushed limestone. The aggregate was first sieved and then washed with potable water to remove dust and salt contamination; it was then dried at 120°C for a period of 20 to 24 hours, and, thereafter, was air-cooled and stored. The coarse aggregate had a bulk specific gravity of 2.42 and average absorption of 3.77 percent. The fine aggregate was the same sand as used in the mortar specimens. A coarse to fine aggregate ratio of 2.0 by weight was kept invariant in all concrete specimens. Table 4.3 shows the grading of the coarse and fine aggregates used in this study.

Reinforced concrete specimens were cast by preparing appropriate weights of the mix constituents and fixing the 12 mm steel reinforcement at the center of the 75 x 150 mm cylindrical moulds (75 mm diameter). The bars were coated with an epoxy at the concrete-air interface and the bottom ends, as shown in Plate 4.4. The bars were coated with epoxy to eliminate crevice corrosion at these locations. The steel bars had a concrete cover of 25

mm at the bottom of the specimen. This cover was provided by using a 25 mm aluminum cube and then the bar was centrally fixed as shown in Plate 4.4. All steel bars were thoroughly cleaned using silicon carbide paper and degreased before casting. The mix ingredients were then mixed in a half-bag electrically-operated revolving drum type concrete mixer for about five minutes. Additional mixing time of about five minutes was provided for silica fume concrete to ensure effective and uniform dispersion. The clean moulds were first oiled using WD-40 spray and then filled in accordance with the method outlined in ASTM C 192. The moulds were vibrated on a vibrating table at a rate of 3600 vibrations per second in three layers. In the last layer, vibration was continued till complete consolidation was assumed to have occurred when a thin film of mortar appeared on the concrete surface. After casting, the specimens were covered with wet burlap for 24 hours prior to demoulding. After demoulding, the specimens were cured in potable water for a further period of 14 days; thereafter, they were air-dried for one day, then the specimens were placed in the respective test solutions.

A summary of the type and number of paste, mortar and concrete specimens tested in this research program is presented in Table 4.4.

Table 4.3 : Grain-Size Analysis for Coarse and Fine Aggregates

Coarse Aggregate (Crushed Limestome)		Fine Aggregate (Dune Sand)	
Sieve Opening (mm)	Cumulative % Retained	Sieve Opening (mm)	Cumulative % Retained
19.0	10	4.75	0
13.0	45	2.4	0
9.5	80	1.2	0
4.7	100	0.6	3.8
		0.3	38.6
		0.15	78.1
		0.075	99.0

Plate 4.4 : Reinforcing Steel and Cylindrical Moulds Used in Casting Reinforced Concrete Specimens.

Table 4.4 : Summary of Type and Number of Paste, Mortar and Concrete Specimens Tested

Test Performed	Specimen Type	Specimen Shape	Dimensions (mm)	Specimens Tested
Compression (Laboratory)	Mortar	Cubes	25	780
Compression (Field)	Mortar	Cubes	25	150
Corrosion (Laboratory)	Reinforced Concrete	Cylinders	76 x 152	72
Corrosion and Chemical Analysis (Field)	Reinforced Mortar	Prisms	31x31x152	24
X-Ray Diffraction and Scanning Electron Microscopy	Paste	Cubes	12.5	360
Pore Solution Expression	Paste	Cylinders	50 x 75	36
Total Number of Specimens Tested				1,422

4.4.2.2 Materials Used

ASTM C 150 Type I and Type V cements were used in this investigation. Three blending materials used were: ASTM C 618 Class F fly ash, silica fume, and blast furnace slag. The fly ash was used as 20% replacement by weight of Type I cement to prepare fly ash blended cement. In the silica fume paste, mortar, and concrete specimens, silica fume was used as 10% replacement by weight of Type I cement. Blast furnace slag cement contained 60% granulated blast furnace slag and 40% Type I cement. The chemical compositions of the cements and blending materials used in this investigation are shown in Table 4.5.

4.4.3 Experimental Techniques

4.4.3.1 X-Ray Diffraction (XRD)

Because most of XRD apparatus have wave-lengths of about 1 Å, which are of the same order as the spacings of atomic planes in crystalline materials, X-rays became very useful for analysis of crystal structures. This is because each crystal has inherently planes of atoms that are separated by a specific distance that is pertinent to only that crystal. These distances between the planes, therefore, are characteristics of the crystalline materials. Once these distances between the planes are determined, through the use of XRD, the identification of that crystalline material is only a simple, routine matter.

Table 4.5 : Chemical Composition of Cements and Blending Materials

Constituent (Wt. %)	Fly Ash	BFSC	Silica Fume	Type V Cement	Type I Cement
Silicon Dioxide	52.3	27.7	92.5	22.0	20.5
Aluminum Oxide	25.2	12.8	0.4	4.1	5.6
Ferric Oxide	4.6	1.2	0.4	4.2	3.8
Calcium Oxide	10.0	44.0	0.5	64.1	65.4
Magnesium Oxide	2.2	8.8	0.9	2.2	2.1
Sulfur Trioxide	0.6	3.1	0.5	2.0	2.1
Loss on Ignition	0.4	0.9	2.6	0.8	0.7
Potassium Oxide	----	----	0.4	0.3	0.3
Sodium Oxide	----	----	1.1	0.2	0.2
C_3S	----	----	----	54.6	56.7
C_2S	----	----	----	21.9	16.1
C_3A	----	----	----	3.5	8.5
C_3AF	----	----	----	12.9	11.6

A detailed description of the XRD apparatus is beyond the scope of the present work (132,174-176). Bragg's law states

$$n \lambda = 2 d \sin \theta \qquad (4.6)$$

where:

- n = order of diffraction, i.e. 1, 2, 3, etc.
- λ = wave-length of X-ray used (for the case of copper, $\lambda = 1.5417$ Å)
- d = spacing between atomic planes, Å
- θ = diffraction angle of X-rays, degrees

Equation 4.6 forms the basis for identification of crystals using XRD. When a collimated beam of monochromatic X-rays of wave-length λ strikes a crystal, some rays penetrate while others partially scatter from the many successive planes within the crystals, and the remaining are reflected (see Fig. 4.7). The reflected rays are reinforced together, and when properly positioned with respect to a receiver (Geiger-Muller counting tube), they will indicate the corresponding spacings of the prominent planes, that are unique for each of the crystalline materials.

Once the complete XRD pattern is recorded, it will typically consist of a series of reflections (peaks) of different intensities and values of 2θ. Each peak must be accounted for in terms of some crystalline component of the sample. Therefore, not only the components of a specimen can be identified but a more or less

accurate estimate of the relative proportions of each phase can be made (132). More often qualitative, rather than semi-quantitative or quantitative, approach is performed because trace elements can not be very easily detected.

The XRD analysis herein was performed using Phillips diffractometer with copper radiation generated at a high voltage of 40 kV and at a current of 20 mA. The effect of chloride-sulfate solutions on different types of cements and blending materials was studied by using paste specimens. These specimens were crushed in a porcelain mortar and pestle to pass ASTM No. 200 (0.074 mm) Sieve. The powder was directly washed by acetone to stop the hydration process and thereafter kept in tightly-closed plastic bags. Part of this powder was placed in the special glass plate and used for XRD analysis. Once the XRD record was developed, the peaks were identified at their respective 2θ. values. Phases relevant to this work, at their d-spacing and intensity, were gathered from literature (121,132,177). The d-spacings have been converted to 2θ through the use of Bragg's law and the knowledge of λ. Table 4.6 shows most of these relevant phases, their 2θ values and intensities.

4.4.3.2 Scanning Electron Microscopy (SEM)

The electron microscope is a valuable tool for the study of cement chemistry, because with modern electron microscopy, it is

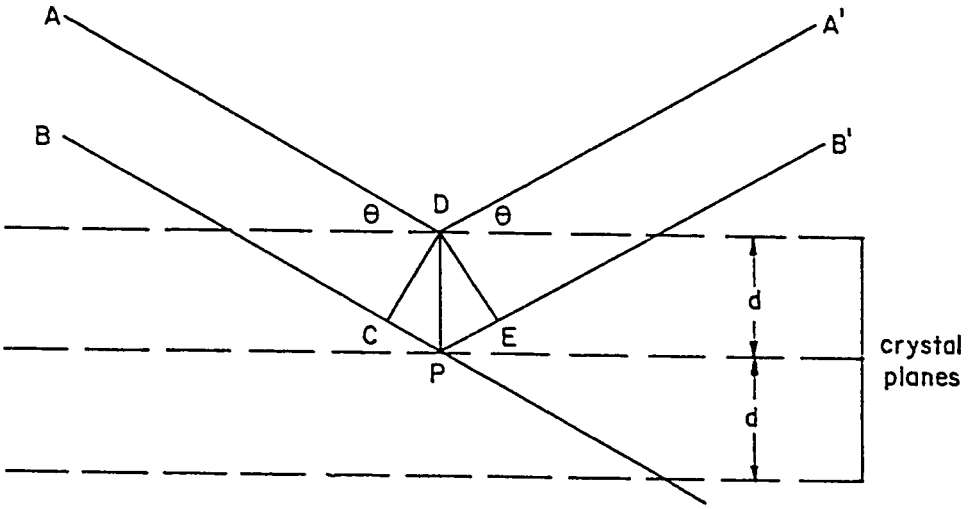

Fig. 4.7 : Typical Diffraction Pattern from Crystal Planes According to Bragg's Law.

Table 4.6 : Pertinent XRD Cement Phases in Terms of 2θ

Phase	Its Chemical Fromula	Major Peaks, 2θ, degrees					R**
		d_1^*	d_2^*	d_3^*	d_4^*	d_5^*	
Portlandite	$Ca(OH)_2$	33.6	17.8 18.0	45.8	49.1	28.41	(1) (2)
Brucite	$Mg(OH)_2$	32.36 26.22	18.53	49.36			(1) (2)
Gypsum	$CaSO_4.2H_2O$	11.7	28.9	20.7	33.0	30.8	(1)
Ettringite	$C_6A\overline{S}H_{32}$	9.1 9.0	15.8 31.7	22.8 15.5	24.8 22.8	40.0 34.4	(1) (2)
Monosulfate	$C_4A\overline{S}H_{12}$ $C_4A\overline{S}H_{13}$	9.9	19.9 15.8	39.6 19.8	22.2 36.1	36.5	(1) (2)
Cl^- - Ettringite	$C_3A(CaCl_3).30\ H_2O$	8.7	24.1	34.4	17.5		(1)
Fe - Ettringite	$C_6F\overline{S}_3H_{32}$	9.0	22.4	15.8	31.6	34.0	(1)
Friedel's Salt	$C_3A.CaCl_2.10\ H_2O$	11.1 11.3	22.4 22.7	23.0 30.8	30.8 38.6	40.9 40.2	(1)+ (1)+
Carbon-Ettringite	$C_3A\overline{C}_3H_{38}$	9.0	22.4	15.8	31.6	34.0	(1)
Thaumasite	$C_3S\overline{C}\overline{S}H_{27}$	9.8	23.3	19.3	16.0	34.0	(1)
C-A-H	C_4AH_{13}	11.2 11.0	22.2 30.9	30.8 32.8	35.9 36.1		(1) (2)
C-S-$\overline{S}$	$Ca_5(SiO_4)_2SO_4$	31.3	31.1	27.7	34.5	33.9	(1)

* d-spacings, where 1, 2,...etc. indicate the most intense peak in decreasing order.

** Reference

\+ Two phases exist

(1) "Guide to Compounds of Interests in Cement and Concrete Research", Highway Research Board, Special Report 127, Washington, D.C., 1972, p. 53.

(2) Lea, F.M., The Chemistry of Cement and Concrete, Edward Arnold Ltd., 3rd Edition, 1970.

possible to resolve distances to less than 10Å, thereby providing excellent studies of hydrated cement phases. The SEM has a magnification range of 20 to 150,000 (176) and a depth of field some 300 times greater than that of the ordinary light microscope.

The SEM used in this investigation was a JEOL Model JSM-840. This equipment is equipped with energy dispersive x-ray analyzer (EDXA) thereby providing elemental analysis of the elements under consideration. These characteristics make the SEM-EDXA a powerful technique for **identifying the morphology** of the different phases in cement as well as providing an analytical evidence of these phases.

SEM provides the additional advantage over the X-ray diffraction technique by identifying the morphology of both the crystalline (same as XRD) as well as the amorphous, noncrystalline phases which could not be detected by the XRD. In this research, some selected paste specimens made of plain and blended cements and exposed to pure sulfate and high sulfate-chloride environments as well as parallel reference specimens exposed to potable water were analyzed using SEM-EDXA technique.

4.4.3.3 Pore Solution Expression Analysis

Description of the pore solution expression device as well as the procedure followed for pore solution expression and analysis at King Fahd University of Petroleum and Minerals has recently

been detailed by Hussain (178).

The extracted pore fluid was used to determine the hydroxyl and chloride ion concentration in order to assess the role of sulfate ions on the internal chemical environment of hardened cement paste. The relevance of these parameters on the corrosion process has been highlighted in Chapter 3. 0.2 to 0.5 ml of the pore solution was diluted with distilled water to 10 ml. The hydroxyl (OH^-) ion concentration was measured by titration against 0.01 M nitric acid using phenolphthalein as an indicator. The pH of the pore solution was calculated from the measured OH^- concentration using the following relationship:

$$pH = 14 + \log_{10} (OH^-) \qquad (4.7)$$

where (OH^-) = Hydroxyl ion concentration in Moles.

Chloride concentration in the pore fluid was determined using a microprocessor-based ion-analyzer in conjunction with a solid-state chloride ion selective electrode and a double junction reference electrode. The values obtained were regularly checked by titration using the Gran plot method (179).

4.4.3.4 Reduction in Compressive Strength

The physical deterioration due to the sulfate salts in different chloride-sulfate environments was evaluated in terms of

reduction in compressive strength of 25 mm (1 in.) mortar cube specimens. The small specimens were used in order to accelerate the sulfate attack by increasing the surface area to volume ratio as it has been used to study the susceptibility of different cements to sulfate attack by Mehta and Gjorv (180). The mortar specimens (25 mm cubes) were tested in compression after 3, 6, 12, 18 and 24 months of immersion in the different chloride-sulfate environments. At the scheduled time of testing, five specimens from each mix were taken out from different solutions and rinsed in distilled water for about 15 minutes to remove any salt deposits and/or loose material. The specimens were then air-dried for a period of 24 hours and tested in compression in accordance with ASTM C 39 using a special 200 kN automatic testing machine specially suited for testing small cubes. Companion specimens of the same mixes, cured in potable water, were also tested along with those placed in different solutions. The reduction in compression strength was evaluated in terms of a "deterioration factor", as used by Rasheeduzzafar et al. (181). The deterioration factor was calculated using the following relationship:

$$R_c = \left(\frac{x - y}{x}\right) * 100 \qquad (4.8)$$

where: R_c = deterioration factor, %

x = average compressive strength of specimens cured in potable water, MPa

y = average compressive strength of specimens immersed in the chloride-sulfate solutions, MPa.

4.4.3.5 Visual Observation

Specimens made of plain and blended cement mortar and exposed to various $SO_4^{--} - Cl^-$ environments were visually inspected to characterize the degree of deterioration. The deterioration was classified on a six-point scale (182) from 0 to 5. A rating of 0 represents perfect condition, indicating no deterioration, while a rating of 5 denotes complete disintegration of the specimen characterized by spalling of the skin caused by either expansion and/or cracking or softening/loss of material.

The relationship between the degree of deterioration and visual rating is shown schematically in Figs. 6.1(a) and 6.1(b) and are described as follows:

Rating of 0: **No deterioration:** Specimen does not show any noticeable deterioration.

Rating of 1: **Deterioration initiation:** Signs of blistering on the four corners or significant salt precipitation on the surfaces of the specimen are observed.

Rating of 2: **Deterioration propagation:** Deterioration extends along the edges of the specimen with enhanced

degree of blistering on the corners.

Rating of 3: **Skin deterioration:** Specimen show signs of deterioration on all the surfaces causing a thin surface film to blister. Specimen is still intact.

Rating of 4: **Delamination propagation:** Extensive deterioration leading to the development of visible cracks along the edges of the specimen. Some increase in volume of the specimen is observed at this stage; however, the deteriorated surfaces are still attached to the specimen's core.

Rating of 5: **Failure stage:** The surface peeled off of the specimen core causing a significant reduction in volume. The sides may be weakly attached to the specimen but collapse is imminent even on touching.

This type of rating provides a relative indication of the performance of various cements in resisting deterioration due to the sulfate or sulfate-chloride solutions. A rating of 5 indicating failure of the tested specimen is comparable to the failure criterion suggested by Mehta (183) based on weight loss of 25%.

4.4.3.6 Corrosion Monitoring

Reinforcement corrosion was monitored by measuring the

time to initiation of corrosion and determining the corrosion current density on steel bars embedded centrally in the 75 x 150 mm concrete specimens made with plain and blended cements.

4.4.3.6.1 Time To Initiation of Reinforcement Corrosion

The half-cell potentials were recorded using a high impedance voltmeter against a saturated calomel electrode (SCE) at periodic intervals. The potential-time record is useful in evaluating the time to initiation of reinforcement corrosion using ASTM C 876 criterion. According to this criterion if the half-cell potentials are in the range of -200 mV to -350 mV against copper copper sulfate electrode (CSE), (i.e., -120 mV to -270 mV SCE), the corrosion activity of the reinforcing steel is uncertain. If the potentials are numerically greater than -350 mV CSE (-270 mV SCE), there is a greater than 90% probability that corrosion of reinforcing steel is occurring. Therefore, the -270 mV SCE is considered as a threshold potential for time to initiation of corrosion.

4.4.3.6.2 Corrosion Current Density:

In order to evaluate the performance of plain and blended cements in resisting reinforcement corrosion in various solutions, quantitative data on the corrosion rate was determined. For this evaluation, there are many electrochemical techniques that can measure the corrosion rates (184,185), amongst which are the Tafel plot, gravimetric weight loss and the linear polarization resistance.

The gravimetric technique is primarily based on the determination of the loss in weight of the metal and, therefore, is considered a destructive method of determining the rate of corrosion. In a corroding system, electrochemically, the corrosion rate measurement is based on the determination of the anodic or the cathodic corrosion current (I_{corr}) at the open circuit potential. The determination of either anodic or cathodic currents separately in the absence of any applied potential, is not possible in practice, because, as discussed in Chapter 3, the production of electrical charges at the anode is exactly equal to its consumption at the cathode to maintain equilibrium of the changes with a zero net current. In the Tafel technique, a potential scan is applied to the specimen starting from E_{corr} and extending to a few hundred millivolts (about 250 mV) either in the cathodic or anodic direction. The applied potential forces the specimen to assume a potential other than E_{corr}. The current measured in this case is the difference between anodic and cathodic currents and is nonzero. The potential is plotted against the measured current, and the resulting potential-current diagram is referred as Tafel plot. Fig. 4.8 shows an idealized Tafel plot. This plot exhibits a linear region, the slope of which is known as Tafel constant (anodic Tafel constant and cathodic Tafel constant). The intersection of the projection of the two linear regions of the plot with E_{corr} gives I_{corr}. Tafel constants are not required for corrosion rate calculation in this technique, but they can be used

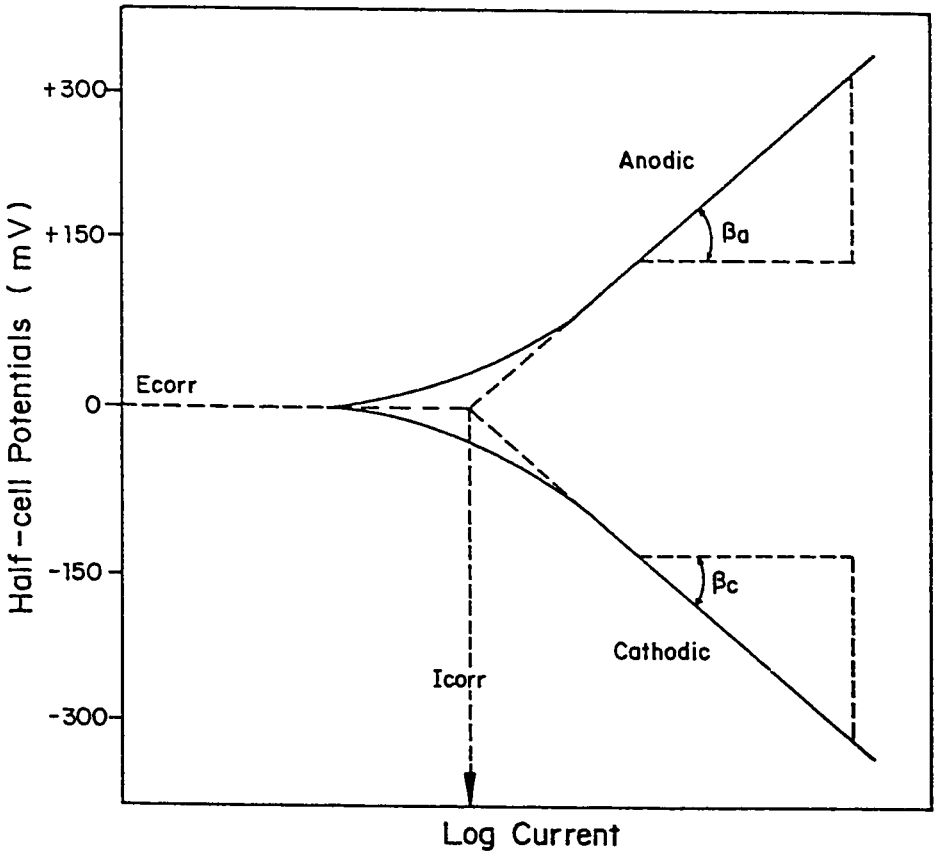

Fig. 4.8 : Idealized Tafel Plot.

in the polarization resistance test as will be described later. Once I_{corr} is determined, the following equation, derived from Faraday's law, can be used for calculating the corrosion rate:

$$\text{Corrosion rate } (\mu m/y) = \frac{3.27 \times I_{corr} \times E.W.}{d} \qquad (4.9)$$

I_{corr} is the corrosion current density in $\mu A/cm^2$, obtained by dividing I_{corr} by the area of the exposed steel. E.W. is the equivalent weight of steel in gm and d is the density of steel in gm/cm^3.

Another technique for determining the corrosion rate is the use of linear polarization resistance technique. In this technique, which was developed by Stern and Geary (186), the steel is polarized to ± 10 mV of the open circuit potential and the resulting current is measured. Since this plot is normally linear, within the range of the small applied voltage, the resistance to polarization, which is the slope of this curve, is calculated. The corrosion current density is then calculated using the Stern-Geary relationship:

$$I_{corr} = \frac{B}{R_p} \qquad (4.10)$$

where: I_{corr} = corrosion current density, $\mu A/cm^2$

R_p = polarization resistance in Ω cm^2

$$B = \frac{\beta_a \times \beta_c}{2.3(\beta_a + \beta_c)} \qquad (4.11)$$

where β_a and β_c are the anodic and cathodic Tafel constants, as defined earlier. For steel in aqueous media, values of β_a and β_c of 120 mV are normally used. However, in the absence of sufficient data on β_a and β_c for steel in concrete, a value of B equal to 52 for steel in passive condition and a value equal to 26 for steel in active condition are normally used. These assumed B values have been deduced so as to produce a better agreement between the gravimetric weight loss and that calculated from the electrochemical results (187,188). Once I_{corr} is determined, it could be inserted in Eqn. 4.9 to estimate the corrosion rate of reinforcement.

In addition to the good correlation between corrosion rates determined by linear polarization resistance technique and weight loss measurements for active and passive steel in concrete, this method offers many features; it is rapid, relatively inexpensive, and simple to perform. The two main drawbacks are that the area of steel under test must be known and, because of the high resistivity of concrete, an electronic compensation for the ohmic drop must be used (184,185,187,188).

In this investigation, linear polarization resistance technique was used to obtain quantitative estimation of corrosion of reinforcement in plain and blended cement concretes after 425, 500 and 650 days of immersion in the various chloride and/or sulfate solutions. The reason behind taking these measurements after 425 days is to allow both chloride and sulfate ions to reach the concrete-steel interface. The polarization resistance (R_p) was determined by conducting a linear polarization scan in the range of ± 10 mV of the half-cell potential (i.e., open circuit potential, OCP). A microprocessor based Potentiostat/Galvanostat was used for polarizing the steel. A stainless steel frame was used as a counter-electrode, while a saturated calomel electrode (SCE) was used as a reference electrode. Fig. 4.9 is a schematic of the test set-up. A scan rate of 0.1 mV/sec was used. Positive feed back technique was employed to compensate for the ohmic drop (IR) between the reference electrode and the reinforcing steel.

4.5 FOUNDATION MATERIALS-SABKHA INTERACTION IN THE FIELD

4.5.1 Specimens and Materials Used

In this part of the investigation the effect of the sabkha environment on the performance of plain and blended cements was investigated. The cements were similar to those used in the laboratory. Mortar specimens, 25 mm cubes, were used to study the effect of sabkha salts on the strength of the various types of

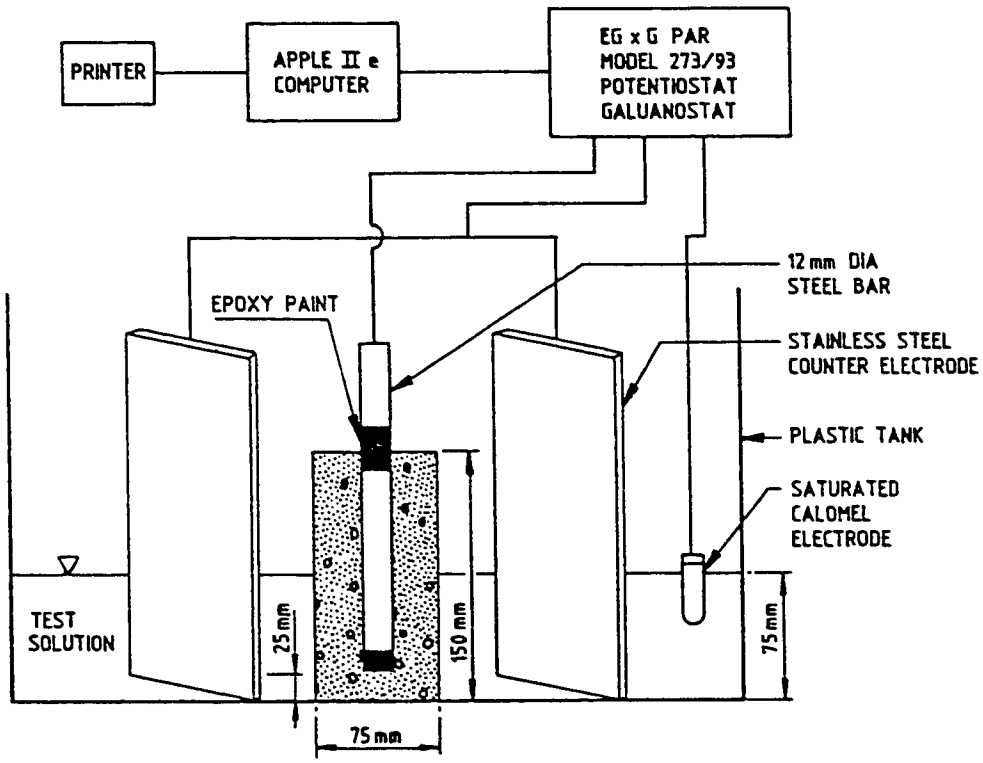

Fig. 4.9 : Schematic Representation of Set-up Used to Measure Corrosion Current Density.

cement. Reinforced mortar prismatic specimens, 32 x 32 x 152 mm, with a 6 mm reinforcing steel bar were used to study reinforcement corrosion. A cover of 12.5 mm was provided on all sides as well as at the top and bottom. The bars were cleaned thoroughly using silicon carbide paper and were degreased with acetone before casting. The ends of the bars were coated with an epoxy coating to prevent crevice corrosion effect. Both types of specimens were cured in water in exactly the same way as for the laboratory investigation. After the curing period, the specimens were stored in the laboratory until they were taken to Ras Al-Ghar, where they were placed in perforated plastic bags and labelled. Labelling was done by engraving the mix numbers on plexiglass sheets which were placed with the specimens in the plastic bags. These bags were placed in a test pit below groundwater table. The pit was refilled with the native soil and the location of the pit was marked.

4.5.2 Reduction in Compressive Strength

The reduction in strength was evaluated in a manner as for the laboratory investigation (Section 4.4.3.4). However, the test periods were 3, 6, 12 and 18 months.

4.5.3 Chemical Analysis Tests

The effect of sabkha and its brine on the performance of the hardened plain and blended cement mortars was chemically evaluated by determining the alkalinity (i.e. hydroxyl ion content)

and the water-soluble chloride contents. In the alkalinity tests, the pH and the hydroxyl ions were measured. The relevance of these parameters to the durability characteristics of different cements has been discussed in Chapter 3. Similarly, the importance of water-soluble chloride from the standpoint of corrosion has been well-documented in the literature as well as building codes (189).

After retrieval from the field, the specimens were cleaned of the salt deposits and were air dried for one day; thereafter, the specimens were cut using a sawing machine. Cutting was done along the bars without using any coolant liquid to avoid dissolution of soluble salt. The mortar, surrounding the reinforcing steel, was taken and then crushed to fine powder. The powder was then flooded with acetone to stop the hydration and to keep the powder dry. Thereafter, the powder was kept in plastic bags which were tightly closed and stored till testing.

The steel bars were visually inspected to determine the percentage corroded area and then were preserved in tightly closed plastic bags which were numbered and kept until testing. Chemical analysis tests of the crushed powder was carried out to determine the alkalinity and the water-soluble chloride concentrations as follows:

4.5.3.1 Alkalinity and Water-Soluble Chlorides:

Ten grams of powdered sample was weighed and placed in a plastic bottle, to which about 400 ml of distilled water was added. The solution was mechanically-stirred for about 4 hours and left undisturbed for about 24 hours. The liquid was first filtered on a coarse Whatman #4 filter paper, and the residue was washed with about 50 ml distilled water and then it was fine-filtered using Whatman #42 filter paper and the residue was again washed with about 50 ml distilled water till the volume of the filtrate became 500 ml. From this filtrate, alkalinity, water-soluble chloride and water-soluble sulfates were determined.

(i) Alkalinity:

25 ml sample of the filtrate was taken into a porcelain dish. The sample was stirred by a magnetic rod. Five drops of phenolphthalein, used as an indicator, was added to the sample and the colour turned pink. 0.01 M sulfuric acid (H_2SO_4) was added by using a mounted burette till the colour disappeared. The volume of 0.01 M H_2SO_4 required for this titration was denoted as P, milliliters. The alkalinity was calculated using the following relationship:

$$Q \times 25 = P \times 0.01 \qquad (4.12)$$

where: Q = alkalinity of the sample in Moles

P = alkalinity of the acid in Moles.

$$\text{Alkalinity } (\%) = 340 \frac{Q}{W} \qquad (4.13)$$

where W = weight of sample in grams.

(ii) Water-Soluble Chloride:

From the 500 ml filtrate, 25 ml was placed in a porcelain dish and stirred using a magnetic bar. About 3 drops (½ ml) of a mixed indicator was added to the sample, a violet colour appeared. 0.1 N nitric acid was added dropwise (normally 2 to 4 drops) till the colour disappeared. The solution was then titrated against mercuric nitrate $\{Hg(NO_3)_2\}$ until the colour reappeared, and the following equation was used to determine the total-chloride concentration:

$$Cl^- = \frac{R * N * 35440}{V * w} \qquad (4.14)$$

where

R = volume of $Hg(NO_3)_2$ used in titration, ml

N = normality of $Hg(NO_3)_2$

V = volume of solution (typically 25 ml)

w = dilution factor of the original concentration of the solution (for 5 gm powder in 100 ml distilled water w = 500).

4.5.4 Metal Weight Loss

To determine the loss in weight of metal, the bars were extracted from the specimens and the products of corrosion were removed by cleaning the bars with Clark's solution, (ASTM G1-81).

Clark's solution was prepared by adding 20 grams of antimony trioxide and 50 grams of stannous chloride in one liter of hydrochloric acid (HCl), and it is known for being inactive in terms of attacking the base material. The bar and pits were scrubbed with a stiff bristle brush and then washed with water and acetone and the bar was thereafter weighed on a precision balance. The loss in weight (W) was determined as follows:

$$W(gm) = \text{pre-exposure weight} - \text{post exposure weight}$$

$$\text{or} \quad W(\%) = \left\{ \frac{\text{pre-exposure weight} - \text{post exposure weight}}{\text{pre-exposure weight}} \right\} \times 100 \qquad (4.15)$$

Once the weight loss was determined, the corrosion rate could be calculated using the following formula:

$$\text{Corrosion Rate } (\mu m/yr) = \frac{8.76 * 10^{7} W}{A * T * D} \qquad (4.16)$$

where W = weight loss in grams

A = exposed surface are of reinforcement, cm^2

T = time for exposure in sabkha, hours

D = density of reinforcement, gm/cm^3.

Chapter 5

RESULTS PRESENTATION AND DISCUSSION ON SABKHA SOIL CHARACTERIZATION

5.1 INTRODUCTION

In this chapter, results and discussion of the investigation on sabkha soil are presented. The data developed in this chapter fall in the following categories:

i) site selection (Section 5.2)

ii) field tests on sabkha (Section 5.3)

iii) laboratory tests on sabkha (Section 5.4)

5.2 SITE SELECTION

The selection of a typical sabkha site that represents the many scattered sabkhas in the Eastern Province of Saudi Arabia constituted the first phase of this investigation. Published literature (2,62,69,74) indicated the presence of sabkhas in Jubail, Safaniya, Ras Tanura, Khobar, Ras Al-Ghar, etc. Previous investigations carried out by a renowned geotechnical company (McClelland Al-Suhaimi) have shown that typical sabkhas do exist in the previous sites. Thus, Ju'aymah, Jubail, Ras Al-Ghar and Ras

Tanura were selected as potential sites for conducting the field tests. These sabkha terrains are fairly large and easily accessible by road.

Reconnaissance visits to the four selected sites (Fig. 5.1) brought about the following observations. The site at Ras Tanura was not suitable due to its proximity from a petroleum factory. For the site at Jubail, which was located in the vicinity of Jubail's sewerage unit, the surface was dry and relatively hard and covered with wind-blown sand of medium size with no signs of salt encrustation. A test pit was dug to about 1.5 meters from the ground surface with no traces of groundwater. The walls of the test pit showed fairly homogenous material which was then recognized as a recent fill. The site at Ju'aymah was characterized by polygonally-patterned surface. The polygons were more or less the same as those described by Johnson, et al. (2) with the presence of relatively very thin salt-encrusted layer. A test pit was dug to about 1.1 m from the ground surface using shovels. The surficial layers seemed to be probably gypsiferrous silt. Groundwater seeped through the hole's walls very slowly indicating the relatively low permeability of the sediments. After about five hours, a sample of groundwater was obtained for chemical analysis. For the site at Ras Al-Ghar, the surface was also characterized by polygonally-patterned ground, however, the polygons were more visible and they were mixed with white coloured salt, most prob-

ably halite. A test pit was dug to about one meter from the ground surface, the walls showed scattered white material that was very soft in texture. This material was described by Johnson, et al. (2) as gypsum. Akili (62) observed the presence of nodular anhydrite in layers from about 30 cm below the ground surface and a few centimeters above the watertable. The sediments at Ras Al-Ghar were lightly to moderately cemented with gypsum, anhydrite and sometimes with carbonates. Water seeped through the pit within about one hour indicating a relatively permeable stratum compared to the site at Ju'aymah; a sample was taken for chemical analysis. About three kilometers west of the Ras Al-Ghar test pit, a shallow pond was observed that was heavily contaminated with halite, as a result of the high rate of evaporation. The source of water was a close-by salt mine belonging to SADAF.

The above reconnaissance observations delineated that both Ju'aymah and Ras Al-Ghar sites were potential sabkhas. The selection of the site was ultimately based on chemical analysis of groundwater (i.e. sabkha brine). Table 5.1 shows results of chemical analysis of brines for these sites. The Table also includes the average values for Sabkhat Ar-Riyas' brines (2) that were reported previously (Table 2.3) as well as those for sea water from KFUPM beach for the sake of relative comparison. These data reveal that Ras Al-Ghar brine has similar ionic concentration to those reported by Johnson, et al. (2). The variation in chloride

and sodium concentration is less than 1% while that of sulfate is less than 4%. It is worth mentioning that all ionic concentrations of Ras Al-Ghar brine fall within those reported in Table 2.3 for Sabkhat Ar-Riyas. The situation was completely different for the case of Ju'aymah brine where, for example, the variation in chloride and sulfate ion concentrations exceeds 100% and 90%, respectively. Therefore, the site at Ras Al-Ghar was chosen to represent an exemplary eastern Saudi sabkha and, consequently, this investigation was devoted to study that particular sabkha site. It is noteworthy to mention that a relative comparison of the concentration of sodium, magnesium, potassium, chlorine, bromide ions and the conductivity indicates that the concentration of these ions is about four to five times that of the Arabian Gulf sea water (Table 5.1). The concentration of calcium in the sabkha brine, on the other hand, is only twice that in sea water while the sulfate concentration is comparable to sea water. This indicates that precipitation of calcium sulfate as a diagenetic mineral, most probably gypsum or anhydrite depending on prevailing condition, is active in the sabkha matrix.

Fig. 5.1 shows the approximate location of the selected site at Ras Al-Ghar which is situated about 15 km southeast of Jubail and about 10 km from the shoreline. A salt mine for SADAF is located at about 3 km from the site.

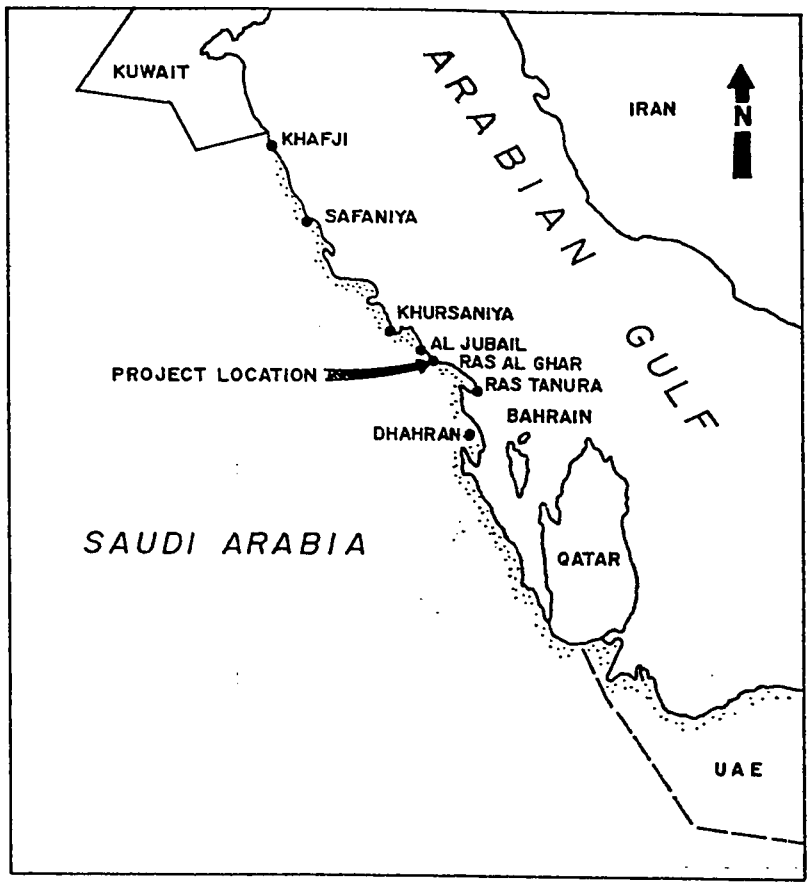

Fig. 5.1 : Vicinity Map Showing Potential Sabkha Locations and the Selected Ras Al-Ghar Sabkha.

Table 5.1 : Chemical Analysis of Sabkha Brines and Sea Water in g/l (i.e., parts per thousand)

Ions	Ju'aymah Brine	Ras Al-Ghar Brine	Averages of Ref.++	KFUPM Beach Sea Water
Na^{+}	41.4	78.8	79.8	20.7
Mg^{++}	4.53	10.32	7.33	2.30
K^{+}	1.40	3.06	2.69	0.73
Ca^{++}	1.34	1.45	1.86	0.76
Fe^{++}	Trace	Trace	----**	----**
Sr^{++}	0.031	0.029	----**	0.013
Cl^{-}	76.8	157.2	158.2	36.9
Br^{-}	0.22	0.49	---**	0.121
$(SO_4)^{--}$	8.43	5.45	5.24	5.12
$(HCO_3)^{-}$	0.114	0.087	0.056	0.128
pH	7.2	6.9	6.7	8.3
Conductivity*	152,000	208,000	----**	46,200

* Microsiemen
** Not reported
++ From Johnson, et al. (1978).

5.3 FIELD TESTS RESULTS

Results of field tests are presented schematically in Figs. 5.2 to 5.11 and quantitatively in Tables 5.2 to 5.7. Standard penetration test (SPT), thin-walled (Shelby) tube sampler, static cone penetration sounding (CPT) and pressuremeter test (PMT) were intended to delineate the stratigraphy and subsurface conditions of the Ras Al-Ghar sabkha. As mentioned in Chapter 4, each of these tests was conducted in an individual boring to avoid disturbance. The location of these borings is depicted in Fig. 5.2. The average distance between borings was about one meter. Moreover, two more field tests, namely CBR and PL tests, were conducted to study the surficial layers and their collapse potential upon flooding with water and sabkha brine respectively.

5.3.1 SPT Results

Fig. 5.3 depicts the subsurface characteristics with SPT values. It can be observed that the Ras Al-Ghar subsurface consists predominantly of the following layers:

i) A surface crust that has a SPT N value of 8. This crust was relatively denser than the underlying layer due to desiccation and the presence of cementation that was enhanced by the high rate of evaporation. The relative density of this layer can be described as loose according to Table 5.2 (161). This layer extends up to

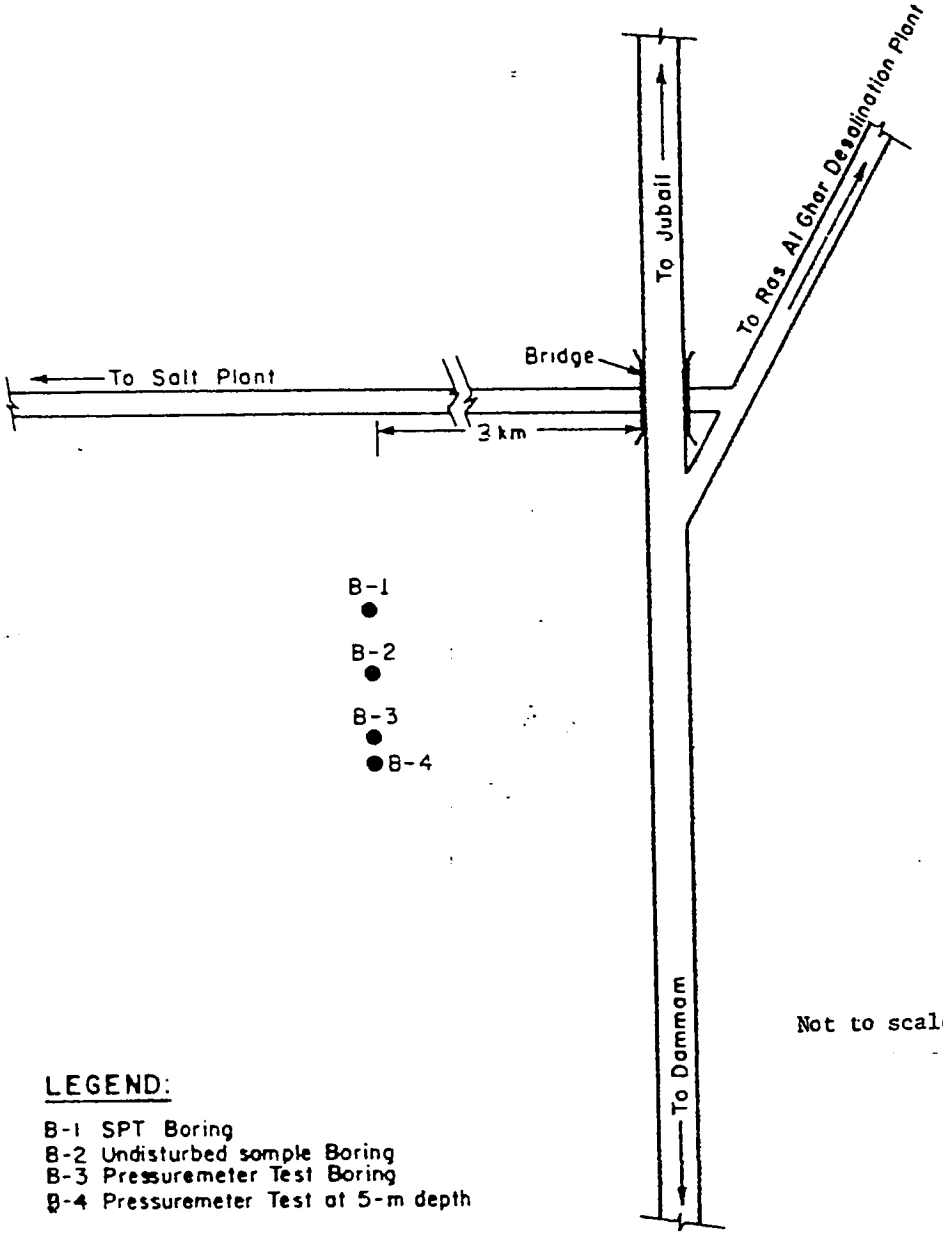

Fig. 5.2 : Locations of Individual Borings.

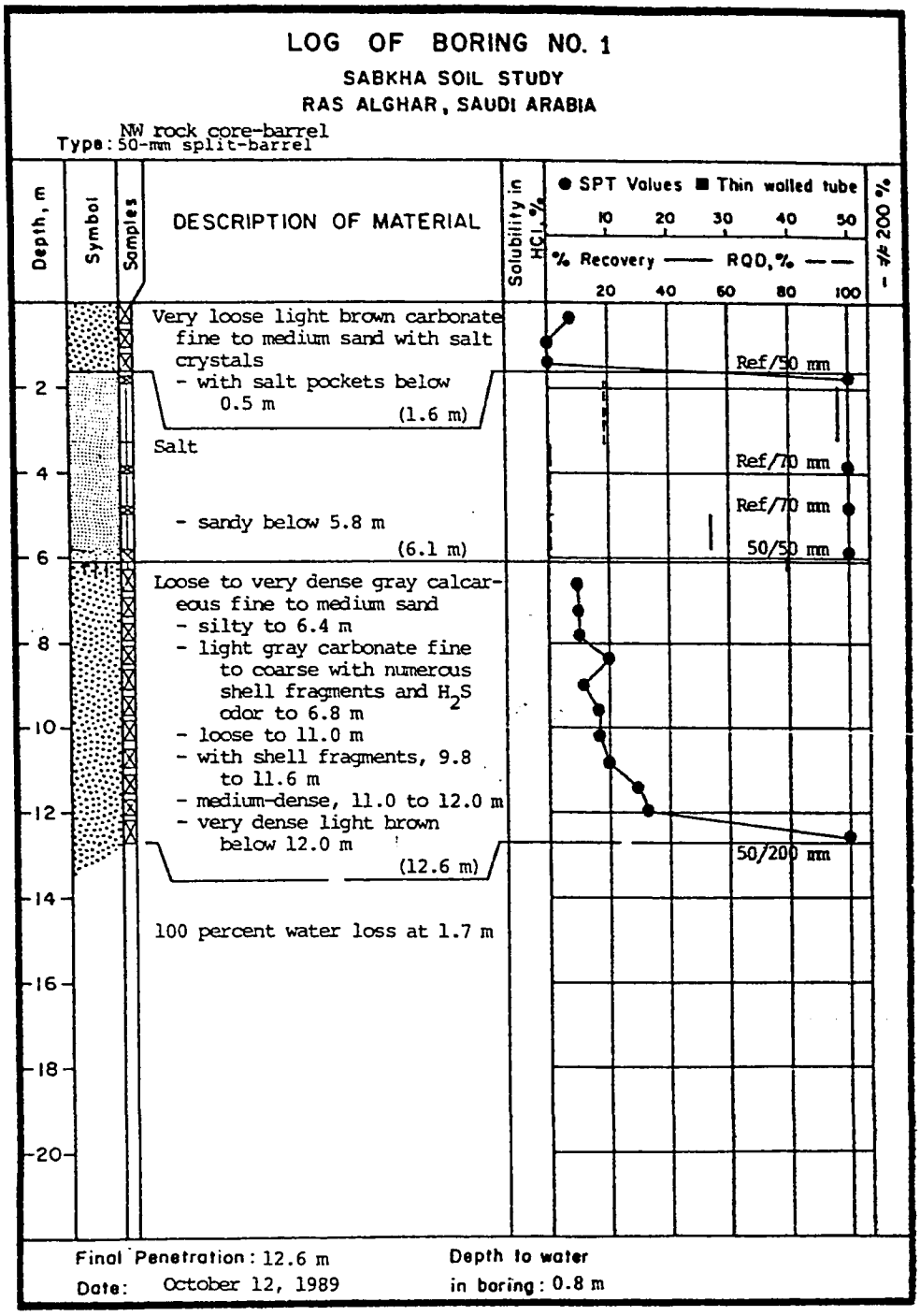

Fig. 5.3 : Standard Penetration Test (SPT) Results.

Table 5.2 : Relative Density Classification of Sands Based on SPT and CPT

Relative Density	SPT, N, Blows*	q_c (Tip Resistance),** MPa
Very Loose	0-4	0-2
Loose	4-10	2-4
Medium	10-30	4-12
Dense	30-50	12-20
Very Dense	Over 50	Over 20

* Terzaghi and Peck (1967)

** Schmertmann (1978).

only 0.3 to 0.5 meter. It was characterized by the presence of profound cemented sands of fine to medium size, which were reworked by deflation of wind-blown dune sand and the saline environment of the sabkha.

ii) The second layer was a very loose light carbonate fine to medium sand with salt crystals. This layer was characterized by very low SPT values (about zero) and within which the watertable existed. It extended from the salt-encrusted layer to about 1.6 m below the ground surface. The presence of high moisture coupled with salt pockets of very soft diagenetic materials (i.e. soft gypsum that was intercalated with halite crystals, as shown in Plate 5.1) could be the contributing factors towards the extremely low SPT values. The watertable was encountered at 0.8 m from the ground surface.

iii) A rock salt layer was the third layer encountered and extended to 4.5 meters (from 1.6 to 6.1 m). It was characterized by very high SPT values that attained refusal all the way during the first 150 mm seating stage. The retrieved salt samples had bright colour and high purity as supported by the chemical analysis. Data shown in Table 5.3 indicate that more than 95% of the salt weight is predominantly sodium chloride

Plate 5.1 : Presence of Soft Gypsum Intercalated with Halite Crystals.

Table 5.3 : Chemical Analysis Results of the Rock Salt Layer

Parameter/Ions	Percentage
Water Content	0.58
Chloride, Cl^-	57.87
Sulfate, SO_4^{--}	1.88
Insoluble Residue	0.22
Carbonate, CO_3^{--}	1.88
Biocarbonate, HCO_3^-	0.08
Sodium, Na^+	37.50
Potassium, K^+	0.06
Calcium, Ca^{++}	0.68
Magnesium, Mg^{++}	0.07

(NaCl). The origin of this and similar rock salt layers in other parts of the world is attributed to evaporation of regressive sea waters entrapped in depressions and subjected to high rates of evaporation (162).

The percentage recovery was quite high within the upper part of this rock salt layer (about 95%) and relatively medium at its base (about 55%), while the RQD was very poor (less than 25%) (190), which indicates that the salt samples were not fully intact. Visual observation of these rock salt samples indicated that they were relatively fractured but coherent. This could be the result of poor sampling by the hammering process of SPT.

iv) The fourth layer was a loose to dense stratum that extended from 6.1 m to about 12.6 m. It was characterized by the presence of various types of sands that varied from loose light gray carbonate sand at the top of the layer to dense gray calcareous sand. In this layer, numerous shell fragments were encountered. The denseness of the layer increased with depth, yielding very high SPT values (50 blows per 200 mm, after seating) at the end of boring at 12.6 meter. Accordingly, this might constitute a rather different layer. This supposition was confirmed by the

thin-walled (Shelby) tube and pressuremeter test results, as will be discussed later.

5.3.2 Thin-walled (Shelby) Tube Results

The bore log for the thin-walled (Shelby) tube is presented in Fig. 5.4. This Figure shows the same trend observed in Fig. 5.3, however, in the salt rock layer, the Shelby tube was not used and the salt layer was drilled in the same way as in the SPT. Also, in the fourth layer, the sampler could not be pushed hydraulically and rather was hammered in the same way as in the SPT. The number of blows for the 600 mm length of the tube was recorded and shown to vary from 14 to 41. At the final penetration, at a depth of 12.4 meter, the stratum was denser as reflected by the 46 blows per 400 mm, in general agreement with SPT results. Again, this is an indication of the presence of a very dense layer of sand.

The Shelby tube was devoted to obtain undisturbed samples throughout the full depth. However, only three samples were retrieved from the layer below the salt rock despite the fact that effort was made to retrieve more samples. Although these samples were preserved in wax, they were not intact and, therefore, could not be considered as "undisturbed". Further, these three samples were considered as few for the seven meters of sounding below the salt layer (from a depth of 6.2 m to 13.2 m, as shown in Fig. 5.4),

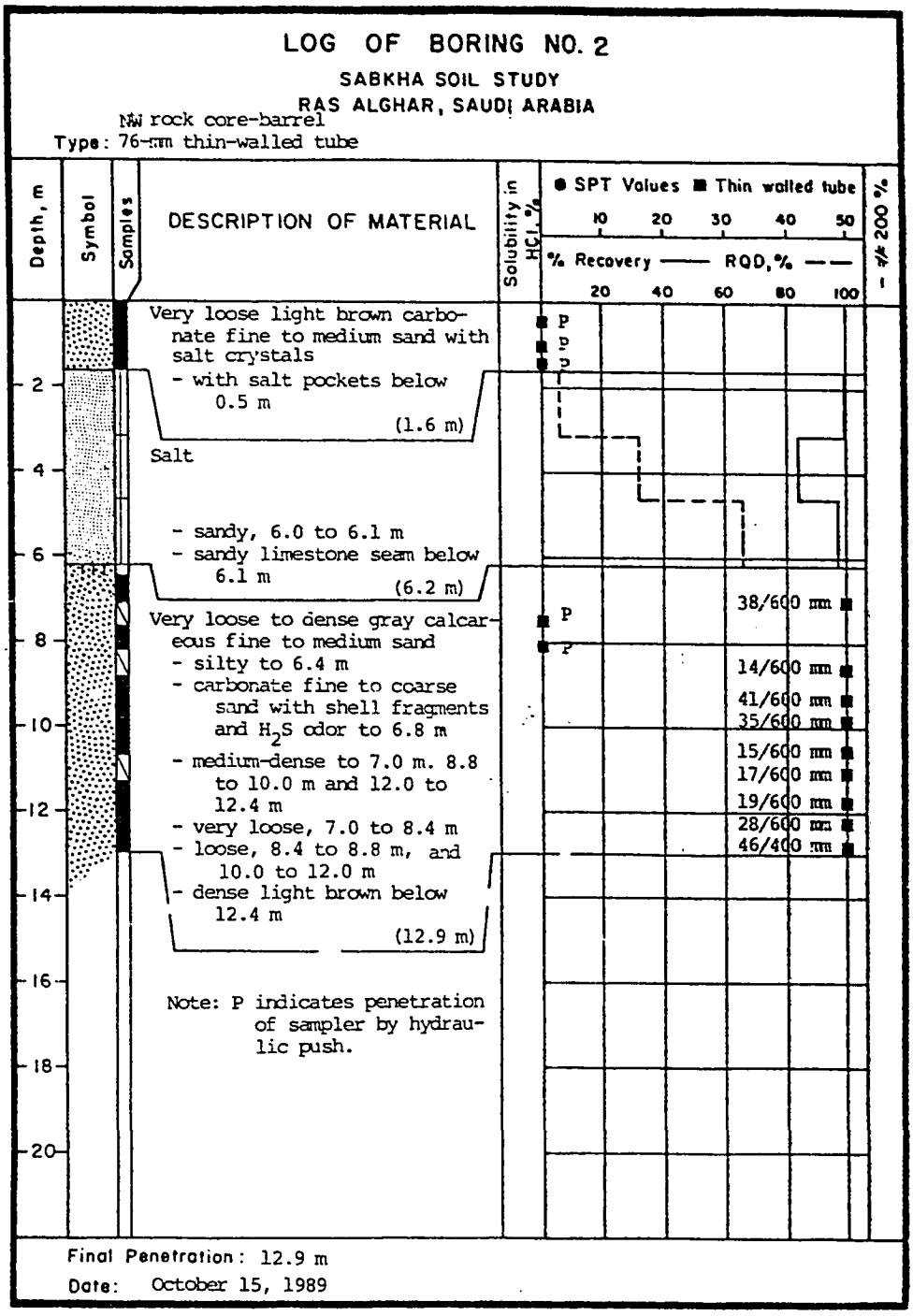

Fig. 5.4 : Thin-Walled (Shelby) Tube Results.

particularly within the heterogeneous nature of the sabkha. This was attributed to the cohesionless nature of these samples rather than poor sampling. Nevertheless, pieces of these samples were used to determine their densities for the pressuremeter test results; and one of these samples was used in X-ray diffraction analysis.

5.3.3 CPT Results

The results of the quasi CPT are presented in Fig. 5.5. The upper layers were very loose and q_c values (cone point resistance) of less than 2 MPa were observed. The rock salt layer was drilled because of the excessively high strength required to penetrate this layer. Therefore, it was decided not to conduct the CPT in this layer to avoid damaging the machinery. The fourth layer, below the salt layer, was much denser than the top layers and q_c generally increased with depth, reaching about 30 MPa at 9 m depth, indicating very dense sand (Fig. 5.5). Another important point is the large fluctuation in CPT results in the fourth layer which was clearly indicative of the high degree of cementation that this layer displayed with increasing strength along the thickness of the layer. The friction ratio was determined for the top layers only and it was very small due to the cohesionless nature of the sabkha. For the fourth layer, the sleeve friction could not be measured in CPT, because salt crystallized inside the

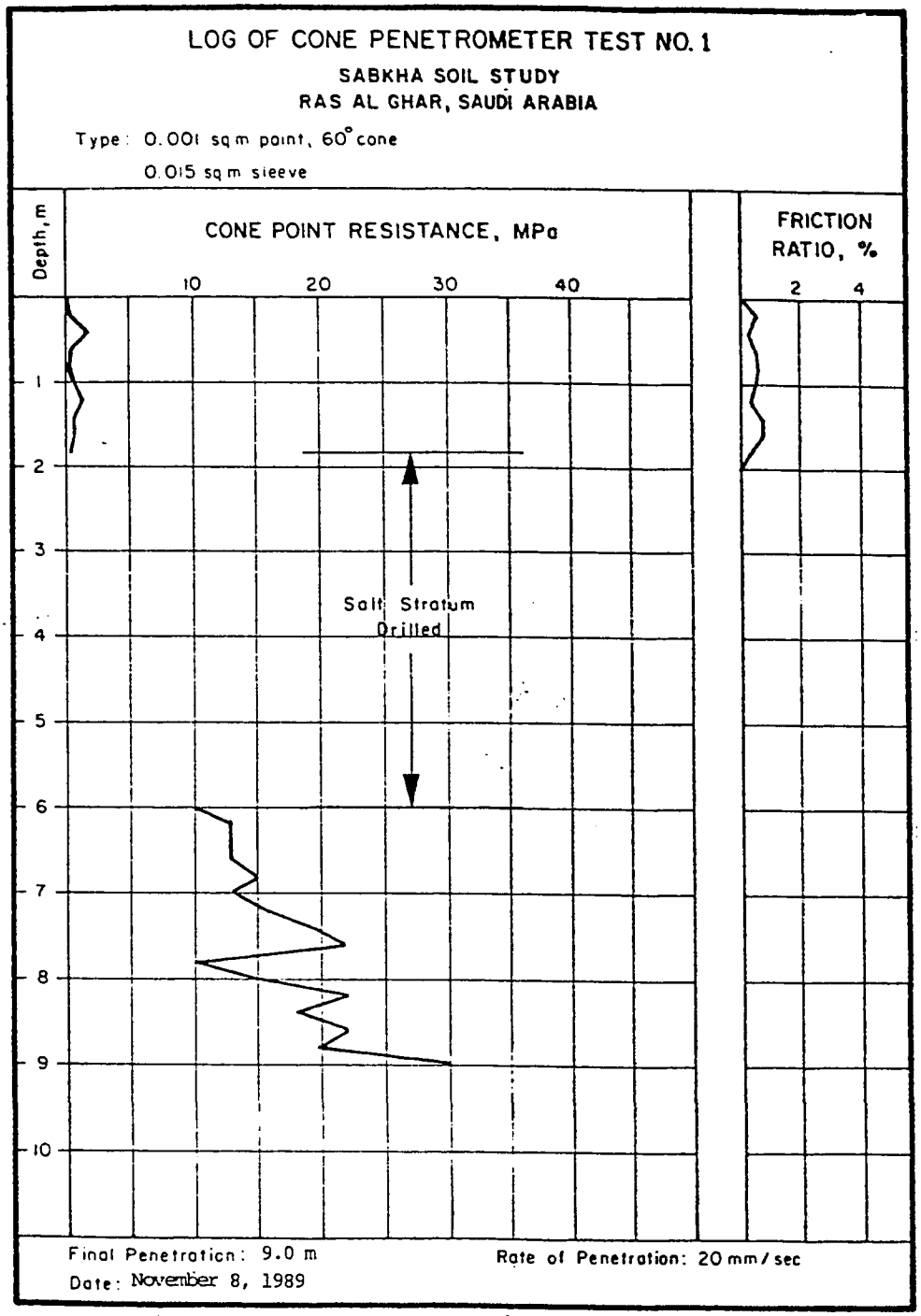

Fig. 5.5 : Cone Penetration Test (CPT) Results.

inner sleeve rod thereby preventing it from functioning properly.

5.3.4 PMT Results

The pressuremeter raw data are shown in the Appendix, while the analyzed test results are presented in Table 5.4. These results show a comprehensive summary of PMT results throughout the full depth of boring and represent the variation in the probe radius with the applied pressure. For the sake of clarification, only typical raw data of pressure vs. radius are presented in Fig. 5.6 for the surficial layer (depth of 0.5 m). The data presented followed the same trend as shown in Fig. 4.2. The value of Poisson's ratio (μ) for typical sandy soils was considered as 0.3 based on published information (150). No reference can be made for the case of rock salt's Poisson's ratio, and, consequently, it was assumed as 0.3. Although this estimation could bring about some error, this error was negligible because only one test was conducted in the rock salt layer and the strength parameters for this layer ($\Delta p, K_s, E, p_L, p'_{oh}$) were so high that any small change in μ could be neglected (see Eqn. 4.3, where μ is to be added, rather than multiplied). The limit pressure (p_L) obtained during PMT is defined as the pressure required to increase the probe volume to twice its intial value (theoretically, p_L is defined as the pressure where infinite expansion of the probe occurs). The limit pressure is not usually obtained by direct measurements during the

Table 5.4 : Summary of Pressuremeter Test Results

Depth, m	Layer, No.	Change in kg/cm²			Change in Radius, mm			R^*_m, cm	K^*, kg/cm³	Σ^{**}, kg/cm²	P_L^{++} kg/cm²	p'_{oh} kg/cm²	p'_{ov} kg/cm²	K_o^{*+}
		p^*_1	p^*_2	ΔP^*	r^*_1	r^*_2	Δr^*							
0.5	First	1.05	3.75	2.70	40.3	42.5	2.2	4.14	12.273	66.05	5.5	1.00	0.092	10.9
1.3	Second	0.40	1.75	1.35	35.9	38.3	2.4	3.71	5.625	27.13	4.3	0.5	0.19	1.8
5.0	Third (salt)	6.50	60.00	63.50	38.8	40.4	1.6	3.96	396.90	2,043	80.0	6.08	0.50	12.2
6.5	Fourth	2.00	6.25	4.25	37.9	40.6	2.7	3.93	15.741	80.42	9.0	1.3	0.63	2.3
7.6	Fourth	2.50	10.00	7.50	38.4	49.2	10.8	4.38	6.94	35.54	11.6	1.8	0.82	2.2
8.6	Fourth	3.50	8.75	5.25	43.2	48.5	5.3	4.59	9.906	59.11	12.7	2.2	1.02	2.7
10.6	Fourth	3.50	11.50	8.00	42.2	48.2	6.0	4.52	13.333	78.34	14.9	2.2	1.23	2.0
11.6	Fourth	3.40	9.75	6.35	42.2	47.0	4.8	4.46	13.229	76.70	16.0	2.2	1.33	1.7
12.6	Fifth	3.90	16.70	12.20	39.2	41.6	2.4	4.04	53.333	280.1	29.2	2.72	1.44	1.9

Note: 1 kg/cm² = 98.07 kPa = 14.223 psi
1 kg/cm³ = 9.807 MN/m³

* Reference is made to Fig. 4.2 for symbolic nomenclature
** Reference is made to Eqn. (4.3)
*+ Reference is made to Eqn. (4.4), assuming normally-consolidated condition
++ Limit pressure, estimated by extrapolation.

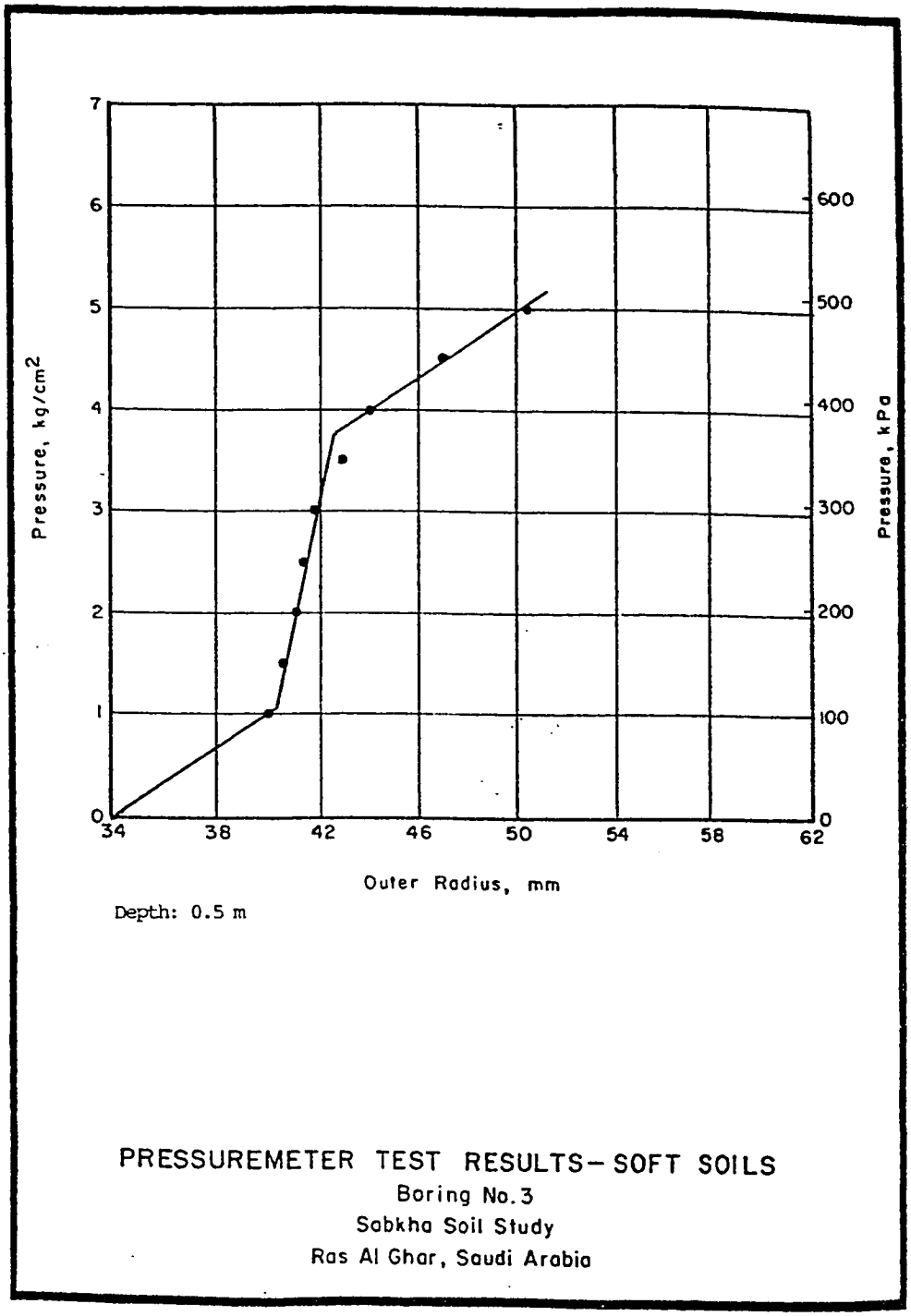

Fig. 5.6 : Typical Pressuremeter Test (PMT) Raw Data Conducted at a Depth of 0.5 Meter.

tests due to limitation in probe expansion and/or excessively high pressure requirements (160). Therefore, PM curves were extrapolated to derive the limit pressure according to the above relationship.

The modulus of subgrade reaction (K_s) was evaluated from the pressure vs. radius curves, as shown in Fig. 4.2, while the elastic modulus (E) was determined as per Eqn. 4.3. The effective horizontal pressure (p'_{oh}) and the effective vertical pressure (p'_{ov}) were determined as explained in the example in Sec. 4.2.3. Since the watertable was encountered at a depth of 0.8 m, p'_{oh} and p'_{ov} were calculated by subtracting the pore-water pressures at the corresponding depth from the total values of p_{oh} and p_{ov}. The values of p_{ov} were determined, based on the density of surficial layer as determined from the sand-cone method (average γ = 1.84 gm/cm^3) and this value was used for the layers above the rock salt. For the rock salt, three samples were used to determine the bulk specific gravity in accordance with ASTM D 1188 using the following equation:

$$G_{s\ bulk} = \frac{A}{\left(D - E - \frac{(D-A)}{F}\right)} \qquad (5.1)$$

where:

$G_{s\ bulk}$ = bulk specific gravity

A = weight of sample in air, gm

D = weight of sample plus paraffin in air, gm

E = weight of sample plus paraffin in water, gm

F = specific gravity of paraffin at 25°C.

Results of these measurements are shown in Table 5.5; the average bulk specific gravity was observed to be 1.83 which is similar to the surficial layers. A value of specific gravity of 1.84 therefore was used. From a depth of 8.2 m, another sample was used in determining $G_{s\ bulk}$ and it was found to be 2.08, as shown in Table 5.6. So, at a depth of 7.6 m, an average value of 1.96 gm/cm³ was used, while at depths of 8.6 m and lower, γ of 2.8 gm/cm³ was used.

Results of PMT indicate a trend similar to SPT and CPT results, with the main difference that the latter two tests measure the potential vertical strength through the full depth, while the former measures the horizontal properties. The strength of the first layer, however, was observed to be pronounced compared to the results of both SPT and CPT. Furthermore, the values of K_s and E for this layer (12.3 kg/cm³ and 66.1 kg/cm², respectively) were more than some of those of the fourth layer, i.e., at depths

Table 5.5 : Bulk Specific Gravity of Rock Salt

Parameter**	Sample #1	Sample #2	Sample #3
A, gm	327.56	442.72	449.13
D, gm	350.14	473.66	530.71
E, gm	159.98	198.89	221.67
$G_{s\ bulk}$	1.86	1.82	1.80

** Refer to Eqn.(5.1)

Table 5.6 : Bulk Specific Gravity of a Soil Sample from 8.2 Meter Depth

Parameter**	Sample #1
A	131.27
D	149.35
E	67.38
$G_{s\ bulk}$	2.08

** Refer to Eqn.(5.1)

of 7.6 and 8.6 meters (Table 5.4). The reason was certainly attributed to the profuse desiccation that this layer was subjected to. This desiccation has probably much more effect on the lateral strength compared to the vertical one. This is the reason behind having very high K_o values (Table 5.4) and excessively high over-consolidation ratios (as outlined in Sec. 5.3.7). For the deeper layers, the soil strength, as reflected by K_s and E, increased with depth, showing the same trend as the other field tests.

A summary of all boring tests is schematically shown in Fig. 5.7 which also includes the estimated relative density based on the correlations presented in Table 5.2. The results seem to be consistent, particularly below the salt layer where more data points were developed. The fluctuations in the CPT results below the salt layer reflects the sensitivity of this test to cementation that was profuse in the Ras Al-Ghar sabkha. If the salt layer were excluded, there will be a general trend that reflects the strength increase with depth throughout the whole profile.

5.3.5 PLT Results

Results of plate-load tests are presented in Figs. 5.8 and 5.9. Fig. 5.8 indicates that the modulus of subgrade reaction (K_s) was 18.3 MN/m³ (i.e. 1.9 kg/cm³) when sabkha was tested under natural conditions. The effect of flooding the sabkha terrain with

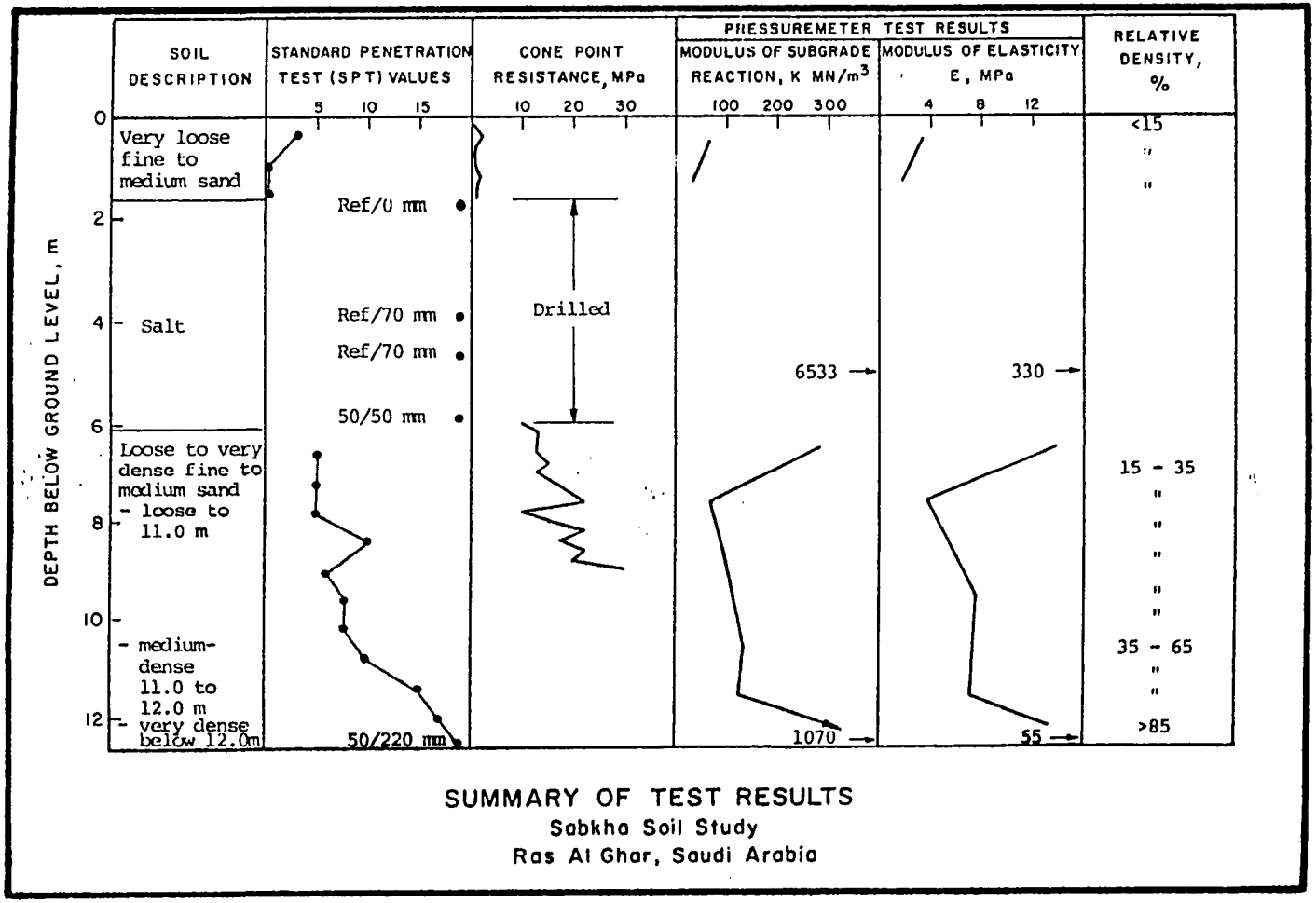

Fig. 5.7 : A Summary of Boring Test Results.

sabkha brine gave 17.8 MN/m³ (i.e. 1.8 kg/cm³) K_s value (Fig. 5.9), which resulted in a reduction of only 3%. This small reduction was anticipated because: Firstly, the duration of flooding was only about four hours, and because of the low permeability to brine (refer to Sec. 5.4.4), this time was probably not enough to fully saturate the influential depth below the plate. It should be mentioned that a similar test was conducted in Jizan (25) and the site was flooded with water for at least 24 hours prior to commencement of loading in order to bring out significant effect. Secondly, and more importantly, sabkha brine is known to be highly concentrated and therefore does not have any affinity towards dissolving the cementing agents in the sabkha, as indicated by the negligible reduction in K_s values; therefore collapse did not take place. This 3% reduction was, however, attributed to wetting the sabkha rather than any sort of salt dissolution.

Comparing the present results with those of PMT at depths of 0.5 and 1.3m (Table 5.4) indicates that the modulus of subgrade reaction as determined by PMT was 6.6 to 3.0 times that determined by PLT, with an average of 4.8 times. This is basically attributed to the characteristics of PMT which measures the horizontal properties. Since surficial sabkha soils are known to be highly desiccated (22); this could only be detected by the PMT which was manifested by the very high strength values.

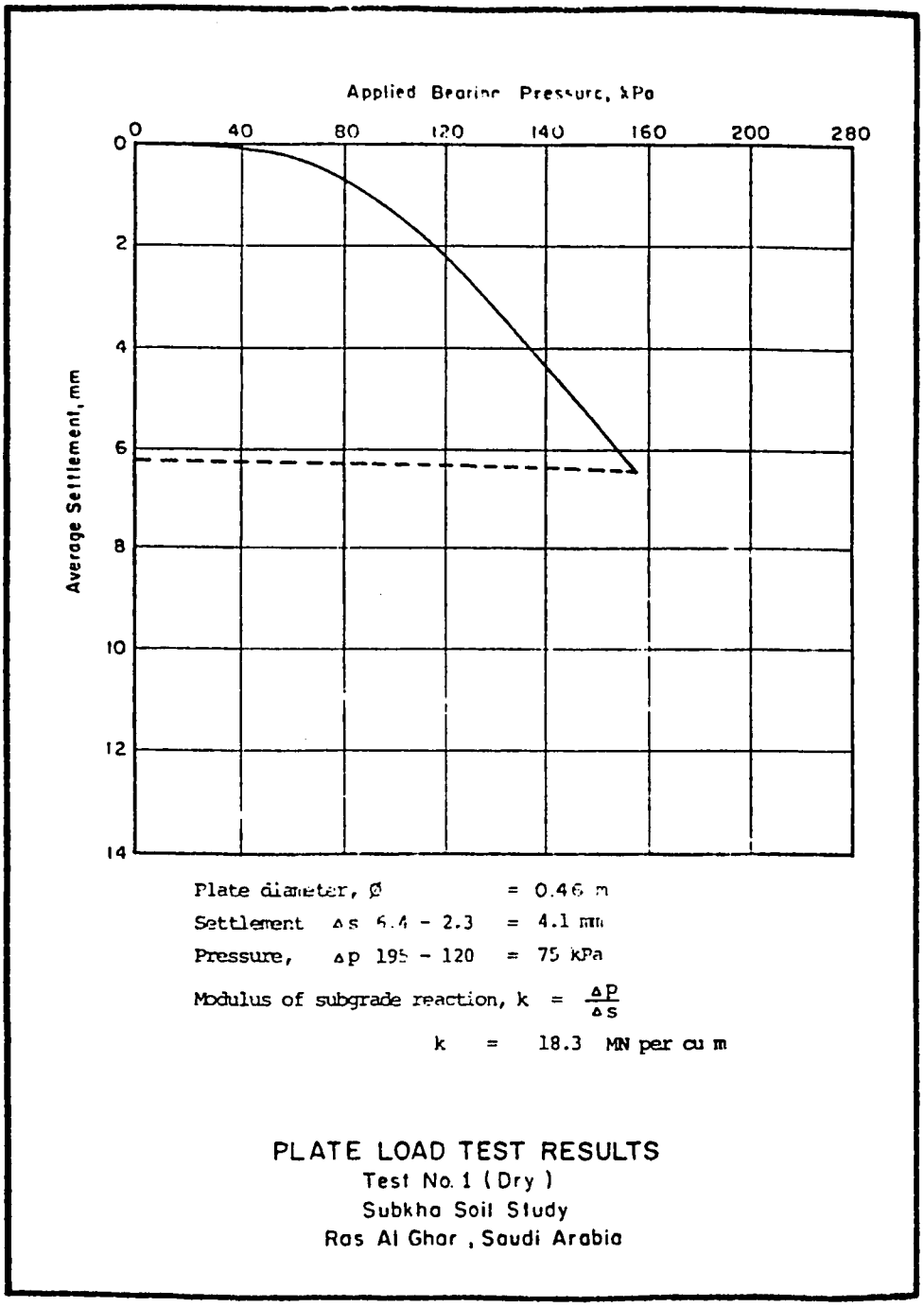

Fig. 5.8 : Plate-Load Test Results (Natural Condition).

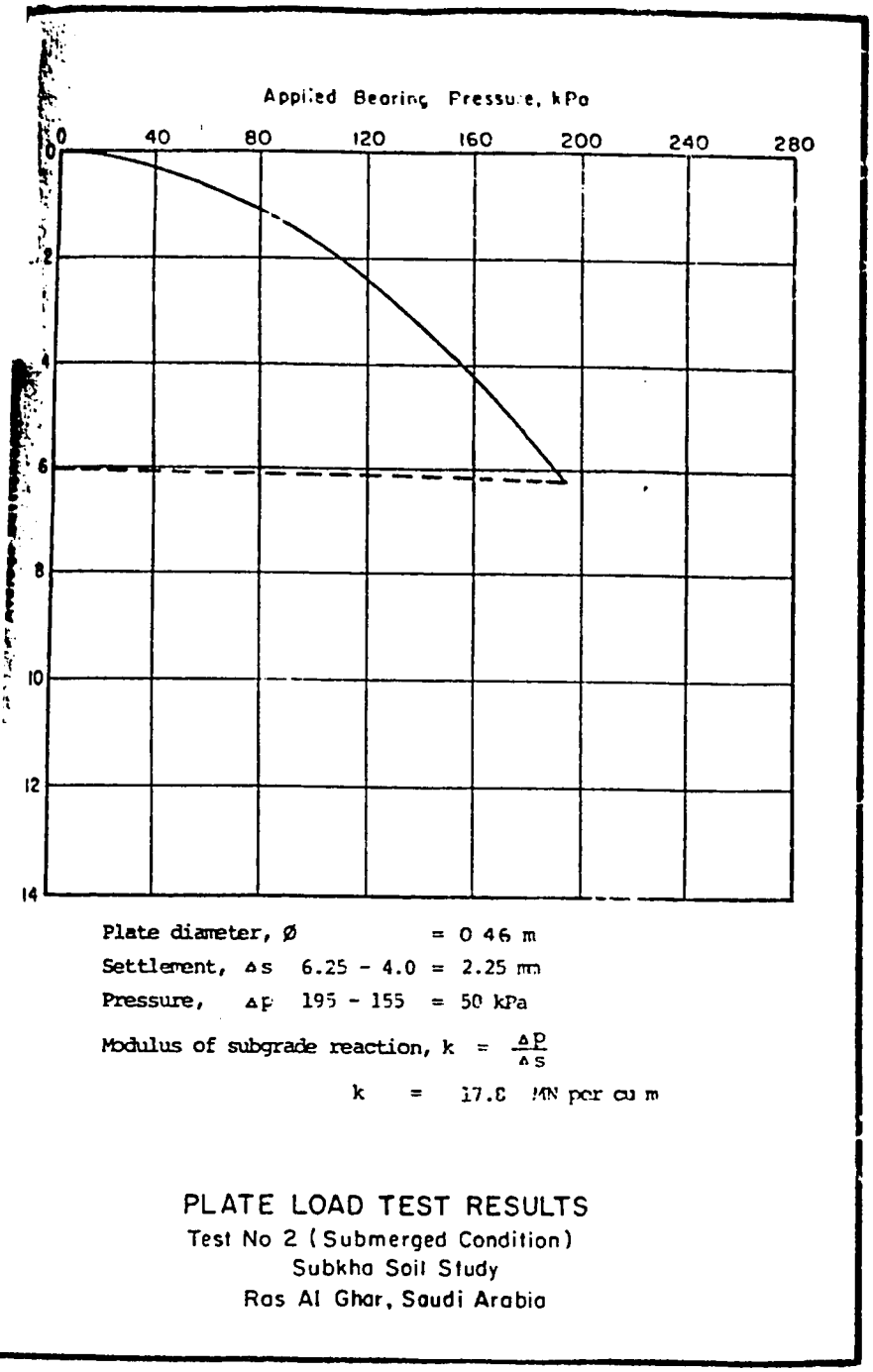

Fig. 5.9 : **Plate-Load Test Results (Flooded Condition).**

5.3.6 Field CBR Test Results

In the case of field CBR tests, the effect of flooding with water was more effective. Fig. 5.10 shows the results of the field CBR tests conducted at the naturally-existing condition, while the soaked test results are shown in Fig. 5.11. These data were reproduced in Table 5.7 where the tests at natural conditions yielded CBR values of 2.1 to 4.3 with an average of 3.2 and the soaked field tests produced CBR values of 0.9 to 2.7 with an average of 1.6. The CBR value of 3.2 for the surficial naturally-existing sabkha soil at Ras Al-Ghar highlights again the very poor to poor conditions of the sabkha soil to perform as a subgrade (171). Even this very low CBR value was reduced by 50% upon flooding by water. This clarifies the susceptibility of sabkha to collapse upon flooding with water. Therefore, these soils have to be protected against such circumstances in order to avoid appreciable settlement.

5.4 RESULTS OF LABORATORY TESTS ON SABKHA

These tests were mostly carried out in accordance with ASTM standards to develop a data base for the sabkha at Ras Al-Ghar. Modifications to standard ASTM techniques, if any, were implemented to suit the unusual properties of sabkha. Data pertinent to these laboratory tests are shown in Tables 5.8 through 5.15 and Figs. 5.12 through 5.68. These tests were conducted on

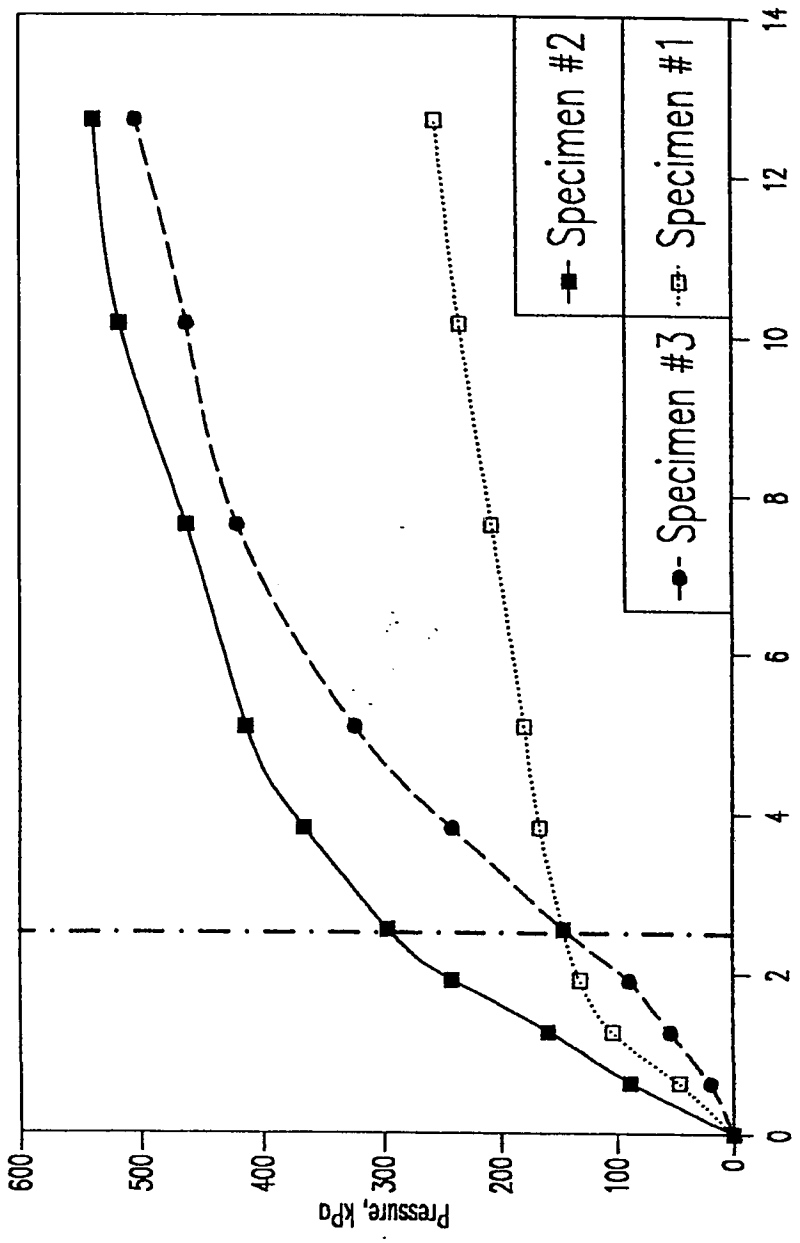

Fig. 5.10 : Field CBR Test Results (Natural Condition)

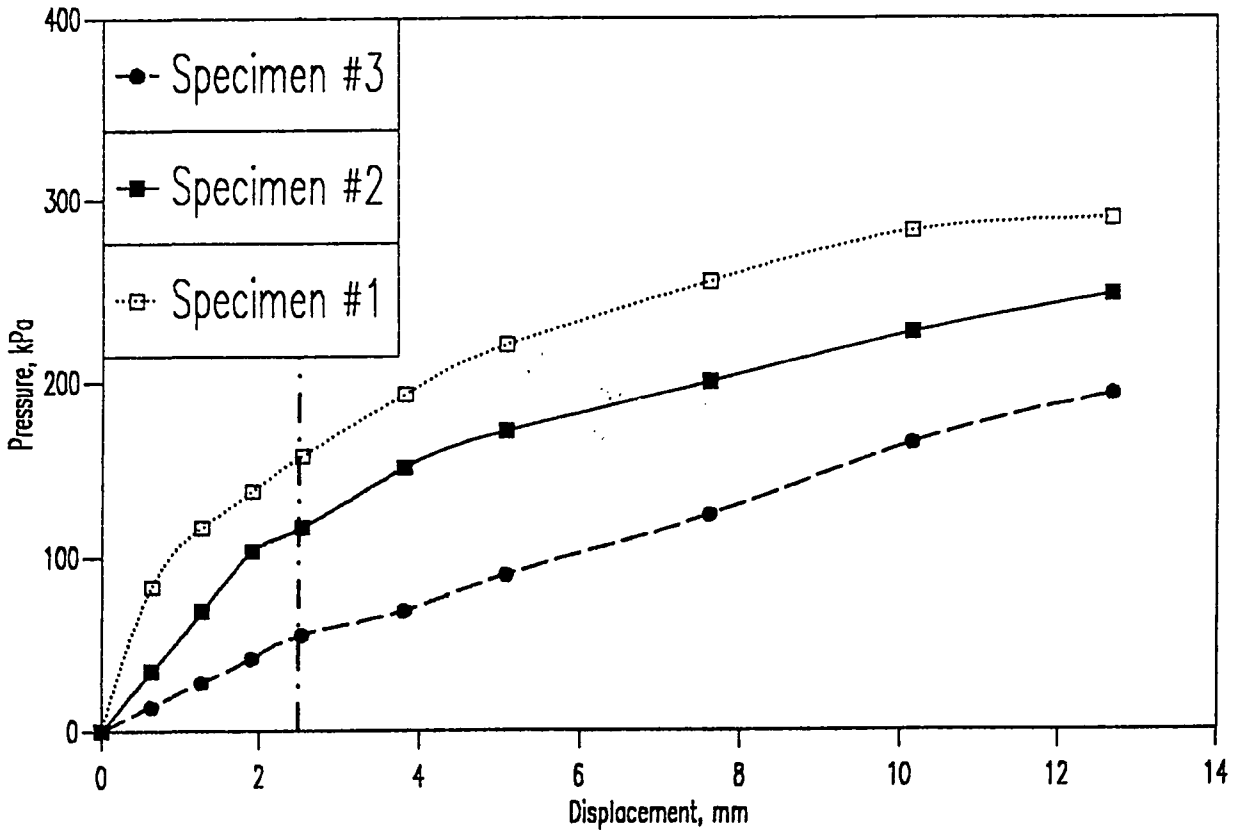

Fig. 5.11 : Field CBR Test Results (Flooded Condtion)

Table 5.7 : Summary of Field and Laboratory CBR Test Results

Type of Test	Sample #	CBR at 0.1 inch		CBR at 0.2 inch		Corrected CBR Value+	Average CBR Value
		Pressure (psi)	CBR*	Pressure (psi)	CBR**		
Field CBR at Natural Condition	1	21	2.1	26	1.7	2.1	3.2
	2	43	4.3	60	4.0	4.3	
	3	21	2.1	47	3.1	3.1	
Field CBR at Soaked Condition	1	23	2.3	32	2.1	2.3	1.6
	2	17	1.7	25	1.7	1.7	
	3	8	0.8	13	0.9	0.9	
Laboratory CBR at Undisturbed Naturl Condition	1	12.79	1.3	20.21	1.3	1.3	3.8
	2	41.96	4.2	65.26	4.4	4.4	
	3	16.24	1.6	23.37	1.6	1.6	
	4	40.12	4.0	50.27	3.4	4.0	
Laboratory CBR at Undisturbed Naturl Soaked-Condition	1	31.30	3.1	42.95	2.9	3.1++	1.7
	2	15.37	1.5	21.61	1.4	1.5	
	3	22.78	2.3	29.07	1.9	2.3	
	4	14.32	1.4	18.21	1.2	1.4	

Note: 1 psi = 6.9 kPa
1 inch = 25.4 mm

* CBR = Pressure/10.0
** CBR = Pressure/15.0
\+ This value equals to the highest of the two CBR values
++ This test was deleted due to disturbance.

disturbed and/or undisturbed sabkha samples.

5.4.1 Specific Gravity Test Results

Data for the three specific gravity tests are presented in Table 5.8. These tests yielded specific gravity of 2.74, 2.72 and 2.72 for Ras Al-Ghar sabkha, with an average value of 2.73. This value was used later in some other tests that included hydrometer and consolidation.

It is noteworthy to mention that these specific gravity values are within the range of those for sabkha soils in the Eastern Province (65), although they are not within the range for typical sands or silty sands as proposed by Bowles (171). The reason could probably be attributed to the conjoint effect of low oven temperature (70°C) at which the specific gravity was determined as well as the high salt content of Ras Al-Ghar sabkha.

5.4.2 Grain-Size Distribution Test Results

The grain-size distribution was determined by mechanical sieving and by using hydrometer.

5.4.2.1 Mechanical (Sieve) Analysis Test Results

Figure 5.12 shows the results of the "standard" mechanical tests. The percentage soil passing sieve No. 200 for the ASTM D 422 dry and the wet (i.e., washed with distilled water) analyses

Table 5.8 : Specific Gravity Test Results

Property	Test #1	Test #2	Test #3
Weight of Flask + Water + Soil, gm	762.46	790.33	748.28
Weight of Flask + Water, gm	683.15	678.60	667.27
Weight of Evaporating* Dish + Dry Soil, gm	609.97	648.09	595.69
Weight of Evaporating Dish, gm	484.67	471.52	468.20
Weight of Dry Soil, gm	125.30	176.57	127.49
Specific Gravity of Water	0.997882	0.997882	0.997882
Specific Gravity of Soil	2.72	2.72	2.74
Average Specific Gravity = 2.73			

* Oven temprature = 70°C (± 2°C)

were 2% and 31%, respectively. This 29% difference between these two "standard" techniques indicates the need for specifying the sieving technique to be adopted. This tremendous difference can perceptibly be the result of salt dissolution in the washed test on the one hand and soil cementation on the other. While the dry sieving is definitively irrelevant because particles tend to be cemented with salt, washing with distilled water tends to dissolve the salts that are considered to be part of this soil. It is cited by Ellis (10) that Curtis et al. have reported water-soluble materials in Abu-Dhabi sabkha as high as 26% by weight of soil. These findings do elucidate the need to use a liquid that does not dissolve any of the sabkha materials.

Russell (63) has stated that water is a dipolar agent and tends to dissolve the salts. He recommends the use of the non-polar and non-aqueous methylene chloride as a solution to the problem. In addition to methylene chloride, a self-environment liquid, sabkha brine was also used. Fig. 5.13 and Table 5.9 summarize the results of using both methylene chloride and sabkha brine (thereafter; abbreviated as MC and SB, respectively) and compare them with the "standard" dry and wet sieve analyses. At a first glance, both MC and SB sieve analysis curves seem to be comparable, although a slight variation is also clear. These two curves fell midway between the two "standard" extremes. The variation between MC and SB could be attributed to the effect of drying

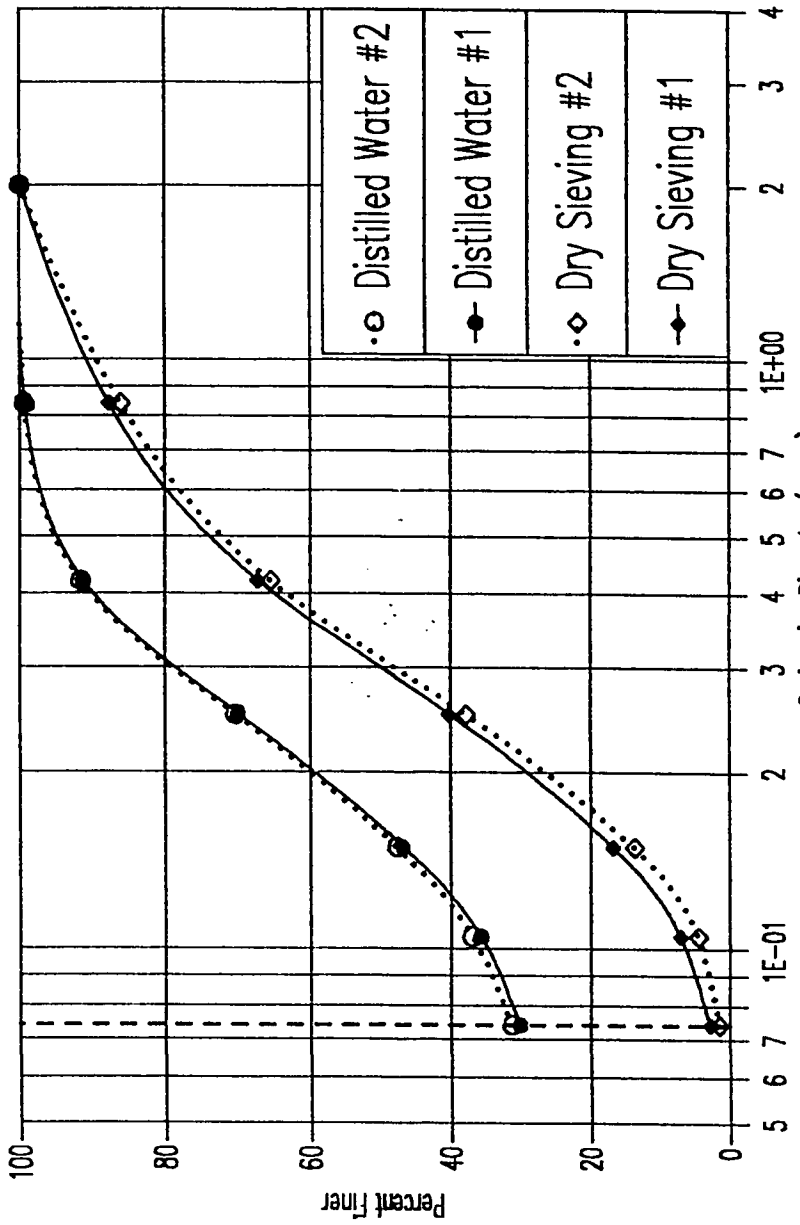

Fig. 5.12 : Grain-Size Analysis Results using "Standard" Techniques

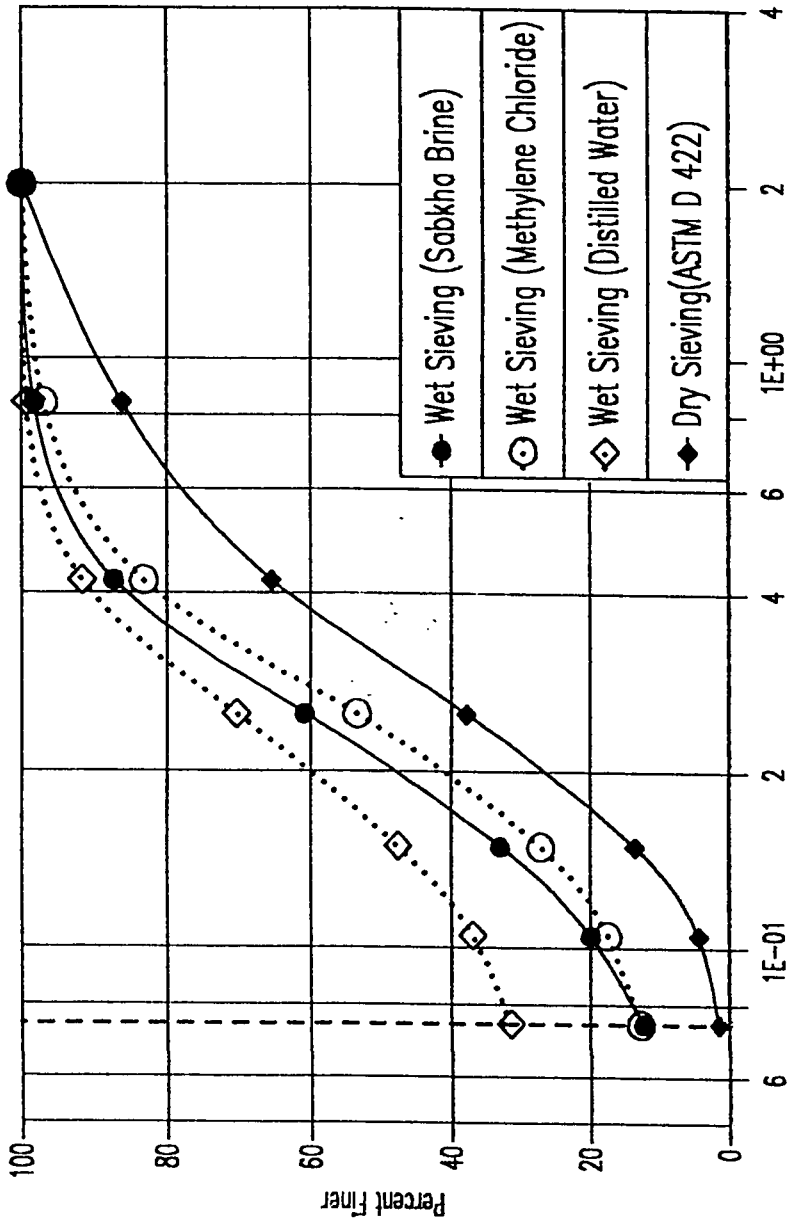

Fig. 5.13 : Summary of Grain-Size Analysis Results

Table 5.9 : Summary of Sieve Analysis Test Results

Sieve No. (mm)	Dry Sieving* (%)	Wet Sieving (%)		
		Distilled* Water	Methylene** Chloride	Sabkha* Brine
10 (2.00)	100	100	100	100
20 (0.84)	86.2	99.4	97.0	98.3
40 (0.42)	65.5	91.7	83.2	87.3
60 (0.25)	37.9	70.4	53.6	60.9
100 (0.149)	13.7	47.8	27.1	33.0
140 (0.105)	4.6	37.0	17.6	20.0
200 (0.074)	1.6	31.5	12.9	12.5

* Average of two tests
** One test only

which was needed to get the combined weight of the sieve and retaining soil, after the sieving test was finished. Drying was achieved by exposing the sieves to air for one day, so that no alteration in phases would occur. Here, since MC is virtually volatile, accurate dry weights could easily be obtained. However, for SB, one day air drying was not sufficient for the moisture to evaporate from sabkha because of the hygroscopic nature of these soils where precipitation of halite as salt-encrustation is frequently observed during dry seasons (191). Therefore, MC seems to be better in this regard, however, many disadvantages are associated with the use of MC. It is irritant, expensive (about 100 Saudi Riyals per 20 liters), volatile and thus it releases unbreathable fumes which might be dangerous, as well as MC is damaging to some of the laboratory apparatus. The damaging effect of MC was observed in melting the plexiglass containers which were used as liquid inlet and outlet for the sieving stack. The main advantage of sabkha brine is that it could be obtained very easily from the site because the groundwater table is never deeper than 0.7 to 1.2 m.

It is anticipated that the performance of the different sieve analysis techniques can be best evaluated by measuring the quantum of soil passing #200 Sieve. This can be explained by the fact that this sieve is the smallest and the particles passing this sieve are the finest in size. These finest particles have the largest specific surface. Since the natural soils are bathed in exces-

sively concentrated brine, smaller particles will, consequently, be more affected than coarser particles. Moreover, ASTM Sieve No. 200 is also very important from classification point of view (Sec. 5.4.3) and it is a boundary line between the fine-grained and coarse-grained soils. For the percentages passing sieve #200 (Table 5.9), there is almost no fundamental difference between methylene chloride and sabkha brine, signalizing their consistency. It can be concluded that sabkha brine obtained from the same vicinity from which the soil is brought, represents a potential solution for the sabkha soil grain-size determination.

X-ray diffraction technique was used to identify the various phases that exist in Ras Al-Ghar sabkha. These phases are (Fig. 5.14) quartz, gypsum, aragonite, calcite, orthoclase and halite. Halite, i.e. sodium chloride, is very soluble and this phase could be the main reason behind the high values of percentage passing when distilled water was used. Table 5.10 shows a semi-quantitative analysis of the X-ray results where it was observed that halite constituted 15.3% of the surficial sabkha. For the sake of relative comparison, another X-ray diffraction test was conducted on a sabkha sample from a deeper stratum (from a depth of 8.2 m), as shown in Fig. 5.15. Table 5.10 shows a comparison of the XRD results of both surficial and deeper layers which indicates that quartz was significantly more profuse in the deeper stratum, while halite was predominant in the surficial layer.

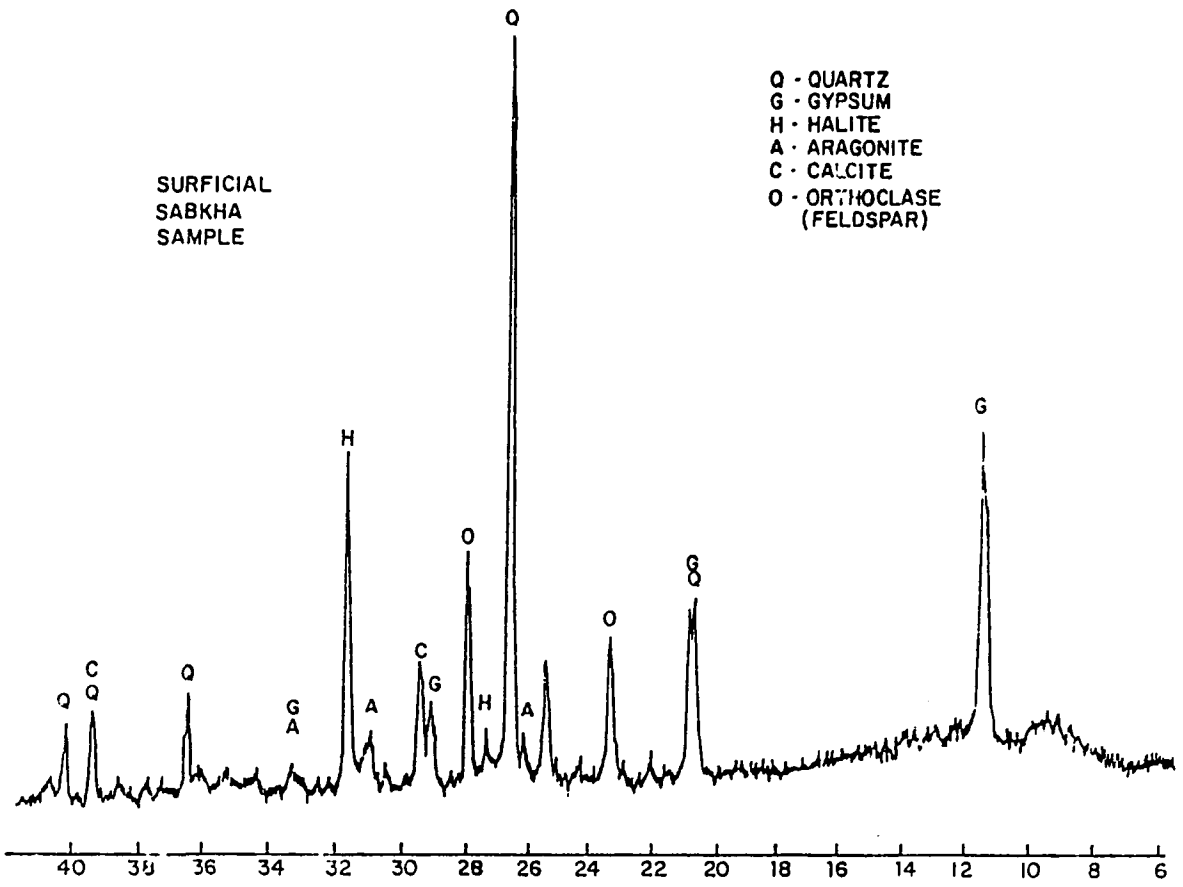

Fig. 5.14 : X-ray Diffraction Pattern for Surficial Sabkha Soil.

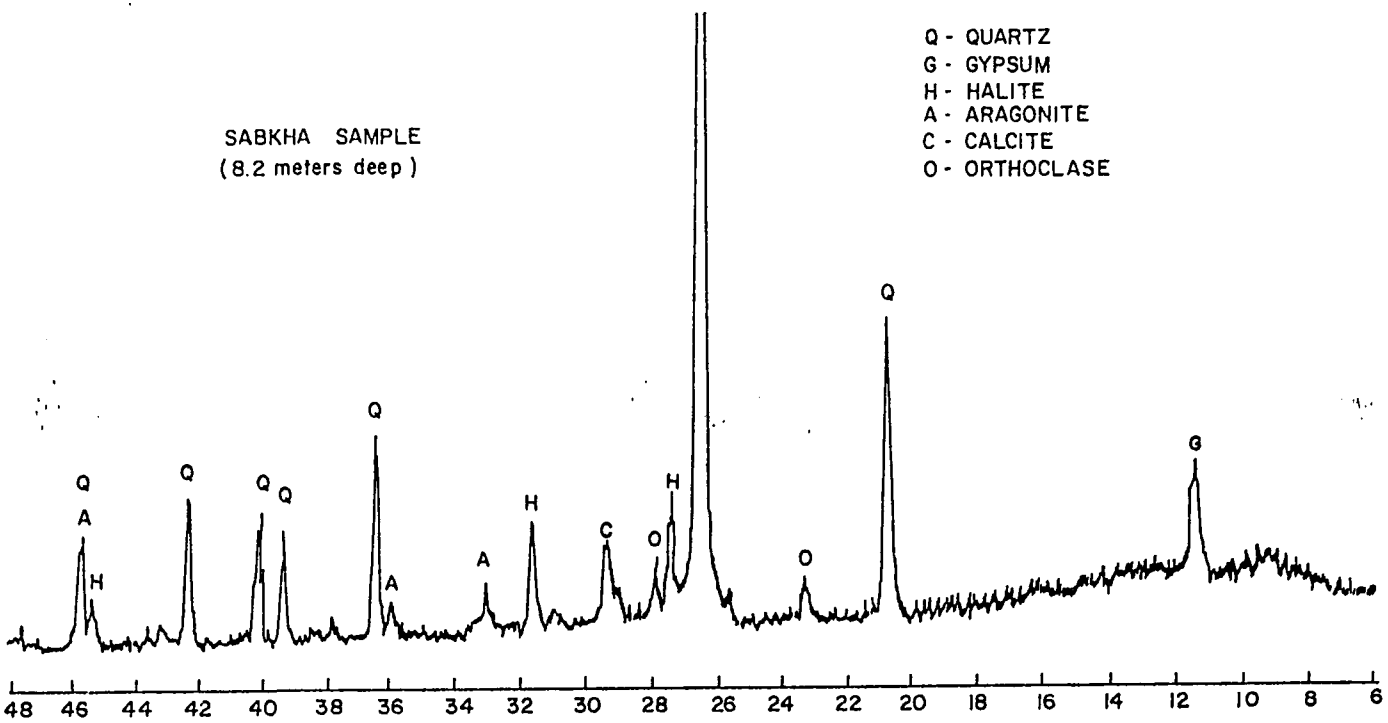

Fig. 5.15 : X-ray Diffraction Pattern for Deeper Sabkha Strata (8.2 Meter Depth).

Table 5.10 : Semi-Quantitative XRD Analysis Results (Surficial and Deep Sabkha Samples)

Minerals	Mineral Presence (%)	
	Surficial Sabkha	Deep Sabkha Sample**
Quartz	44.2	62.0
Halite	15.3	3.1
Aragonite	11.1	25.8
Orthoclase (Feldspar)	11.9	3.3
Gypsum	6.5	1.4
Calcite	9.1	3.5
Total*(%)	98.1	99.1

* The remaining phases comprise trace minerals, most probably anhydrite

** Retrieved from 8.4 m depth.

5.4.2.2 Hydrometer Testing Interpretation

Soil passing the #200 Sieve was allowed to precipitate for one day, thereafter, the liquid was poured off and the passing material was collected for hydrometer testing. This process is very simple for the case of dry sieving. For wet sieving, however, the passing materials are to be left in the outlet container in the liquid, which is normally distilled water, for a period sufficient for the particles to settle down (precipitate). Thereafter, the liquid is poured off, the fine materials collected and dried in preparation for the hydrometer test. For the four different sieving techniques used (Sec. 5.4.2.1), the validity of hydrometer test will be discussed.

(i) Dry sieve analysis

From Table 5.9, the soil passing sieve #200 (0.074 mm) was only 1.6% of the total weight. This is the first aspect that indicates that hydrometer test is not really required. The second aspect is that hydrometer test involves settlement of soil particles of constant weights in distilled water (Stoke's law), which consequently will lead to dissolution of salts. For both reasons, it was concluded that the hydrometer test of dry-sieved soil was invalid, and therefore the hydrometer test was not conducted.

(ii) Wet sieve analysis (distilled water)

As discussed earlier, wet sieve analysis using distilled water

did not reflect an appropriate methodology to evaluate the grain size distribution of sabkha soil. Ignoring this fact, materials passing Sieve #200 were allowed to settle for about 24 hours, after which, the liquid was very clear indicating the precipitation of all soil grains. Water was poured off the container and the soil was collected in a dish and allowed to fully air dry for about 15-20 days and stored in a plastic bag until testing. More than 10 tests were conducted for different sabkha layers and the materials passing sieve #200 were weighed after being dried. Surprisingly, a loss of soil weight of about 9-14% was observed due primarily to salt dissolution. This range of solubility is within the range of those values reported by Ellis (10), in spite of the rather primitive technique implemented here. Now, the soil could be considered as free from soluble salt and thus it could be used in hydrometer testing. This was conducted through a procedure similar to that reported by Wray (163). The sieve analysis and hydrometer tests were combined (164) and the results are shown in Fig. 5.16. It is seen that there is discontinuity in the grain size distribution curve which was attributed to the dissolution of salts in the sieving test.

(iii) Wet sieve analysis (methylene chloride)

Soil passing Sieve #200 could not be preserved for hydrometer testing because, as mentioned previously, the outlet plexiglass container was damaged by MC. Although Russell (63) used this liquid in running his sieve analysis tests; he did not report any-

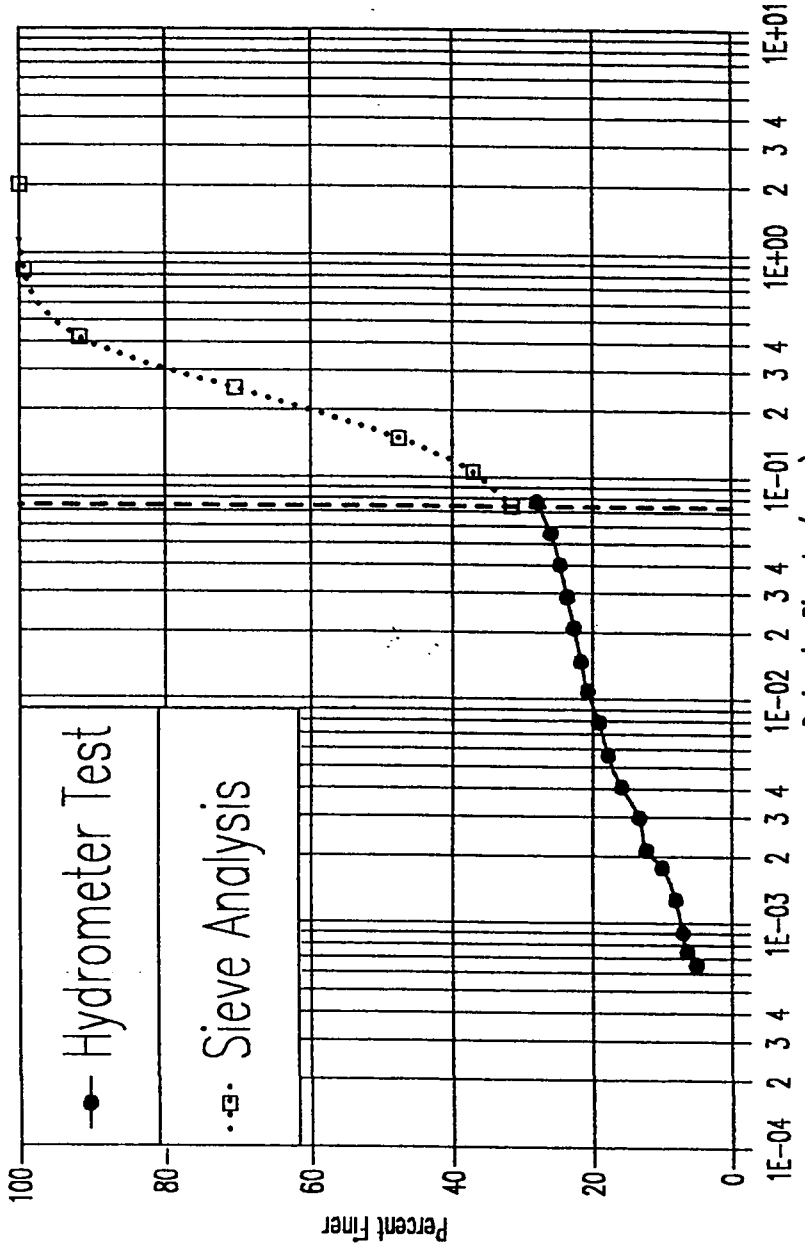

Fig. 5.16 : Combined Grain-Size Analysis Results for the Wet Sieving with Distilled Water

thing about the hydrometer testing or about the problems associated with the usage of this solution. Therefore, hydrometer test could not be conducted. Even if the outlet container was not damaged, materials passing sieve #200 would be in the same condition as those of the dry sieving test and, as a consequence, the hydrometer test would be associated with salt dissolution. For these reasons, the hydrometer tests is considered as inappropriate.

(iv) Wet sieve analysis (sabkha brine)

The 12.5% of soil that passed sieve #200 (0.074 mm) was left in the outlet container, the brine was then poured off and the soil was retrieved and kept in a dish. At this stage, the soil was still wetted by the brine because the brine could not be removed completely. Once the soil was completely dried, salt could easily be seen due to the high concentration of the brine. For this reason, the hydrometer test was decisively not conducted.

These different classes of performance indicate that the hydrometer test could not be applied unless modifications are to be incorporated. Scientifically speaking, there is no exigent need to conduct this test, at least for the Ras Al-Ghar sabkha soil, because only a maximum of about 12% passed sieve # 200 for the case of both SB and MC wet sieving tests.

5.4.3 Classification Test Results

Since Ras Al-Ghar sabkha is virtually non-plastic and

because hydrometer test has proven to be inappropriate, classification tests were, therefore, based solely on mechanical (sieve) analysis. Incorrect determination of the grain sizes will, in effect, lead to misleading interpretation of the classification test results.

Results of AASHTO and USCS are presented in Table 5.11. These results indicate that the AASHTO classification system did differentiate between the dry and wet sieving tests, but it did not differentiate between the different wet sieving techniques implemented here, because these three wet techniques gave surprisingly the same designation "A-2-4". The USCS system, however, showed remarkable difference between the dry and wet sieving tests and between the various wet sieving techniques themselves. The USCS calssification indicates the consistency in results for both methylene chloride and sabkha brine sieving tests. The dual "SW-SP" designation was attributed to the coefficient of uniformity (C_u), which was less than 6. Summarizing the results, the sabkha at Ras Al-Ghar can appropriately be classified as "A-2-4" according to the AASHTO system and as "SW-SP" according to the USCS system.

5.4.4 Permeability Tests Results

Figs. 5.17 through 5.22 depict the constant and variable head permeability results using both distilled water and sabkha brine. Results obtained by the use of sabkha brine in both types

Table 5.11 : Classification Test Results of Sabkha Soil

Classification System	Dry Sieve Analysis	Wet Sieve Analysis Using:		
		Distilled Water	Methylene Chloride	Sabkha Brine
AASHTO*	A-3	A-2-4	A-2-4	A-2-4
USCS:				
D_{60}, mm	0.37	2.0	0.28	0.24
D_{10}, mm	0.18	0.0015**	0.050**	0.058**
D_{30}, mm	0.21	0.07**	0.17	0.15
Cu^{+++}	2.1	1,300	5.6	4.1
C_c^{xx}	0.7	1.5	2.1	1.5
Soil Type	SP	SW	SW-SP	SW-SP

* Based on Sieves #40 and 200
** By extrapolation of the data in Fig. 5.13
+++ Coefficient of Uniformity
xx Coefficient of Curvature

of permeability tests are presented in Figs. 5.17 to 5.19, while those pertinent to distilled water are shown in Figs. 5.20 to 5.22. The use of sabkha brine in the constant and variable permeability tests resulted in reduction in permeability coefficients as the test was repeated. Fig. 5.17 shows that the permeability coefficient was initially 1.07×10^{-2} cm/min and reduced to 8.11×10^{-3} cm/min when the test was repeated twice. The same trend was observed for the second sabkha specimen for which the constant-head permeability coefficient was reduced from 1.20×10^{-2} to 1.02×10^{-2} cm/min, as shown in Fig. 5.18. Variable head test was conducted on specimen #3; results were more or less consistent with the constant head test; the permeability coefficient was reduced from 7.53×10^{-3} to 7.46×10^{-3} cm/min, due to only two repetitions (Fig. 5.19). The change in permeability coefficient with test repetition was, however, very small here. For the case of distilled water, the picture is completely different. The repetition of the test caused the coefficient of permeability to increase from 1.26×10^{-1} cm/min to 1.89×10^{-1} cm/min after four repetitions using the constant head test, as shown in Fig. 5.20. The same trend was observed for the case of the other specimen too (Fig. 5.21). The variable head test was conducted on specimen #6 and the effect of distilled water on permeability was also clear (Fig. 5.22). Again, the change in permeability with test repetition

was very negligible here. It should be mentioned that while the volume of flowing water (and brine) for the constant head permeability test was about 500 cm^3 per test, it was only 35 cm^3 for the variable head test. Comparing the first two specimens for which constant head permeability test when sabkha brine was used, the second one seems to be more pervious, however, the difference between the two was very small. It is also clear that constant head test gave higher values of permeability coefficients than the variable head test. This was mainly attributed to the mechanism of the tests coupled with the higher head for the former test (h = 176.5 cm compared to h_1 = 150 cm for the latter one). For the other case when distilled water was used, specimen #5 seems to be more impervious than specimen #4 with a small difference (compare Figs. 5.20 with 5.21). This difference in k values between constant and variable head tests seems to be negligible although the variable head test yielded relatively lower values. It should be mentioned that the change in k values with test repetitions seems to be more profound for the case of constant head permeability tests. This is in agreement with the observations for sabkha brine results. A final comparison is made between the permeability coefficient values of distilled water and sabkha brine. Permeability coefficient obtained using distilled water was higher than that using sabkha brine by as much as ten times, the same trend could be observed for both constant and variable head tests, although

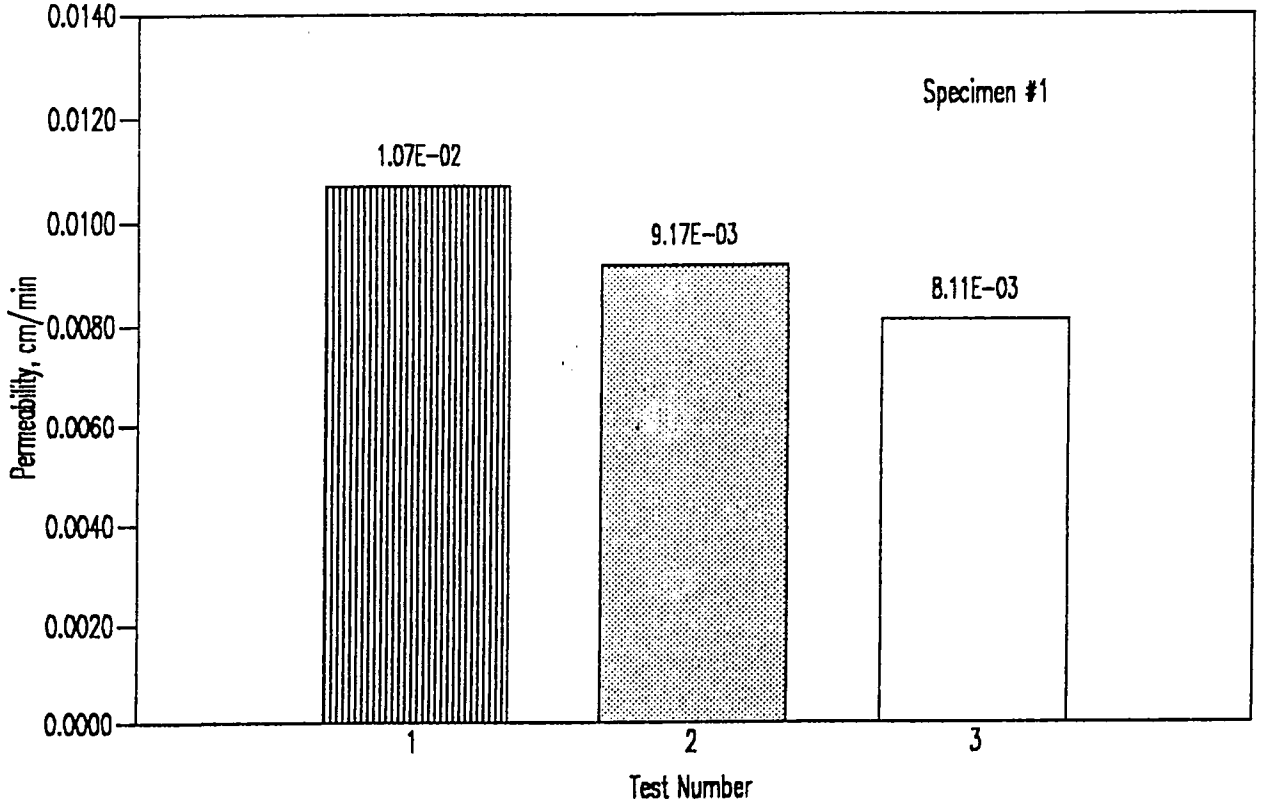

Fig. 5.17 : Constant Head Permeability Test Results using Sabkha Brine (Specimen #1)

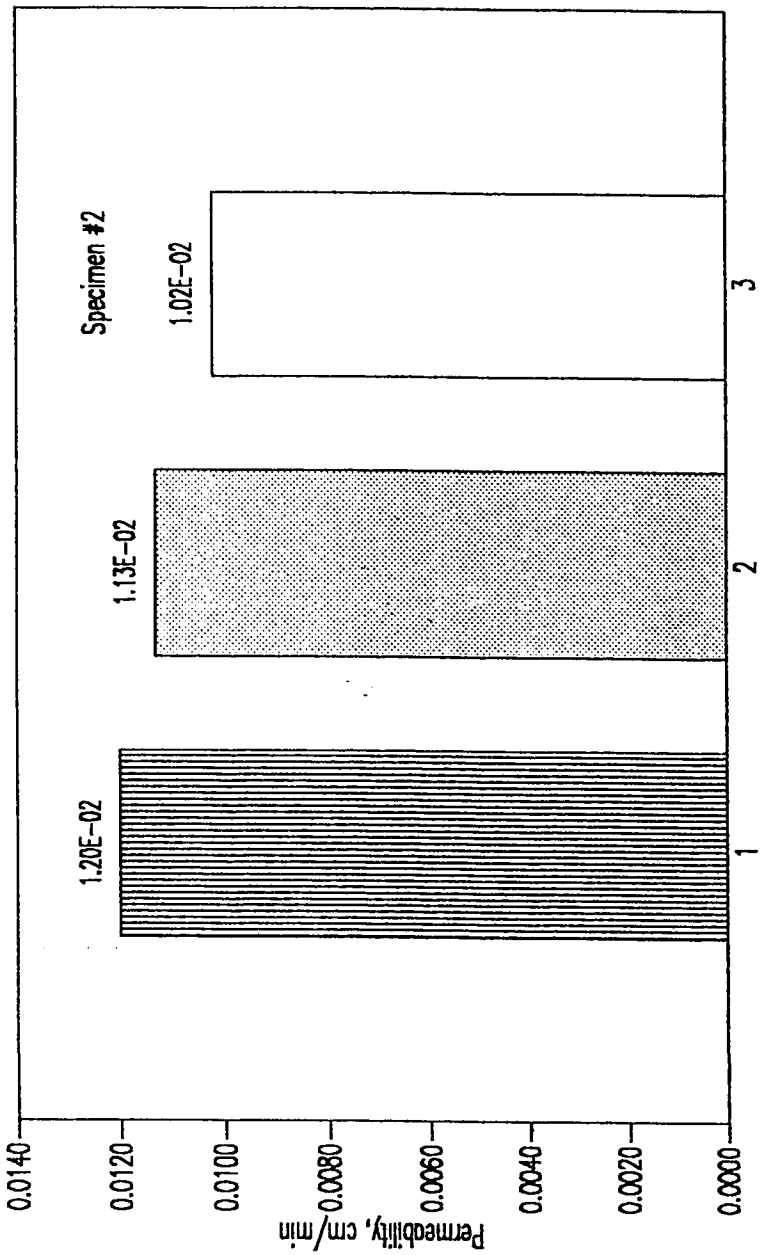

Fig. 5.18 : Constant Head Permeability Test Results using Sabkha Brine (Specimen #2)

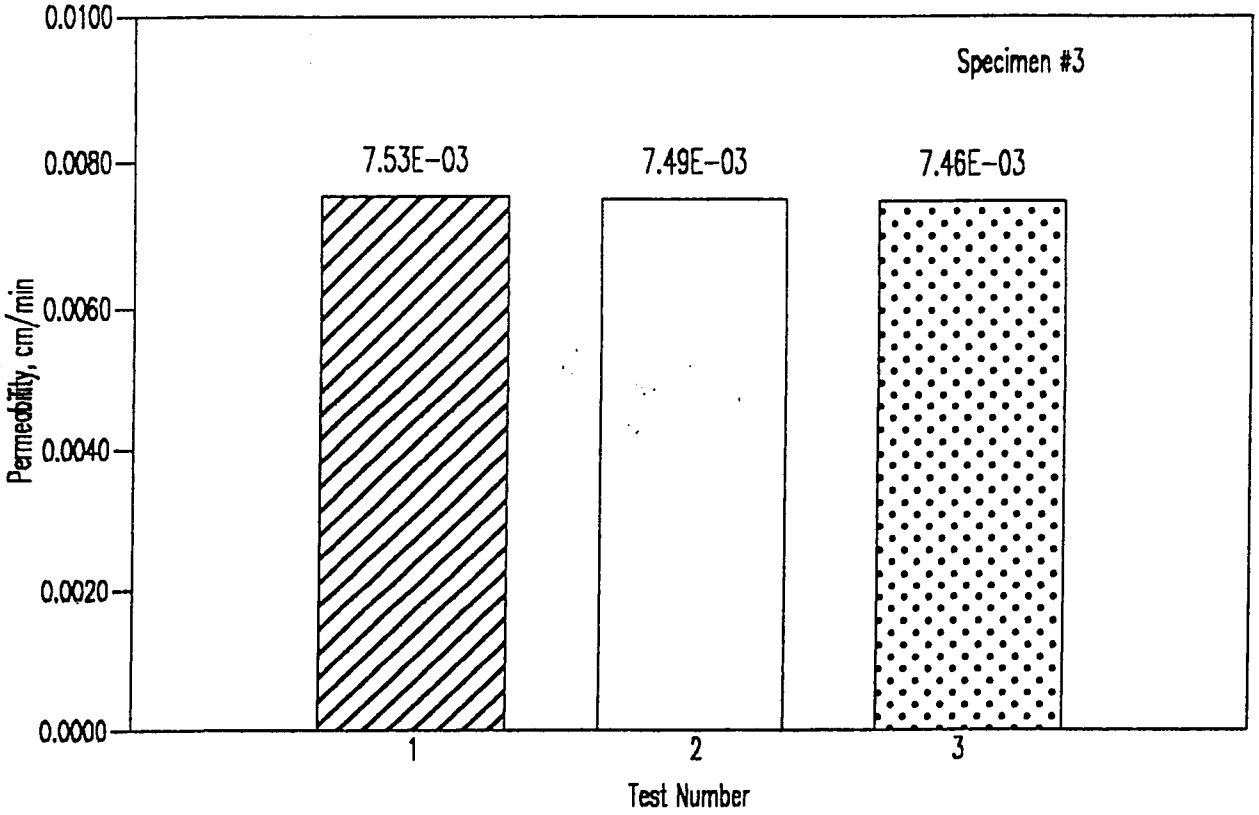

Figure 5.19 : Variable Head Permeability Test Results using Sabkha Brine (Specimen #3)

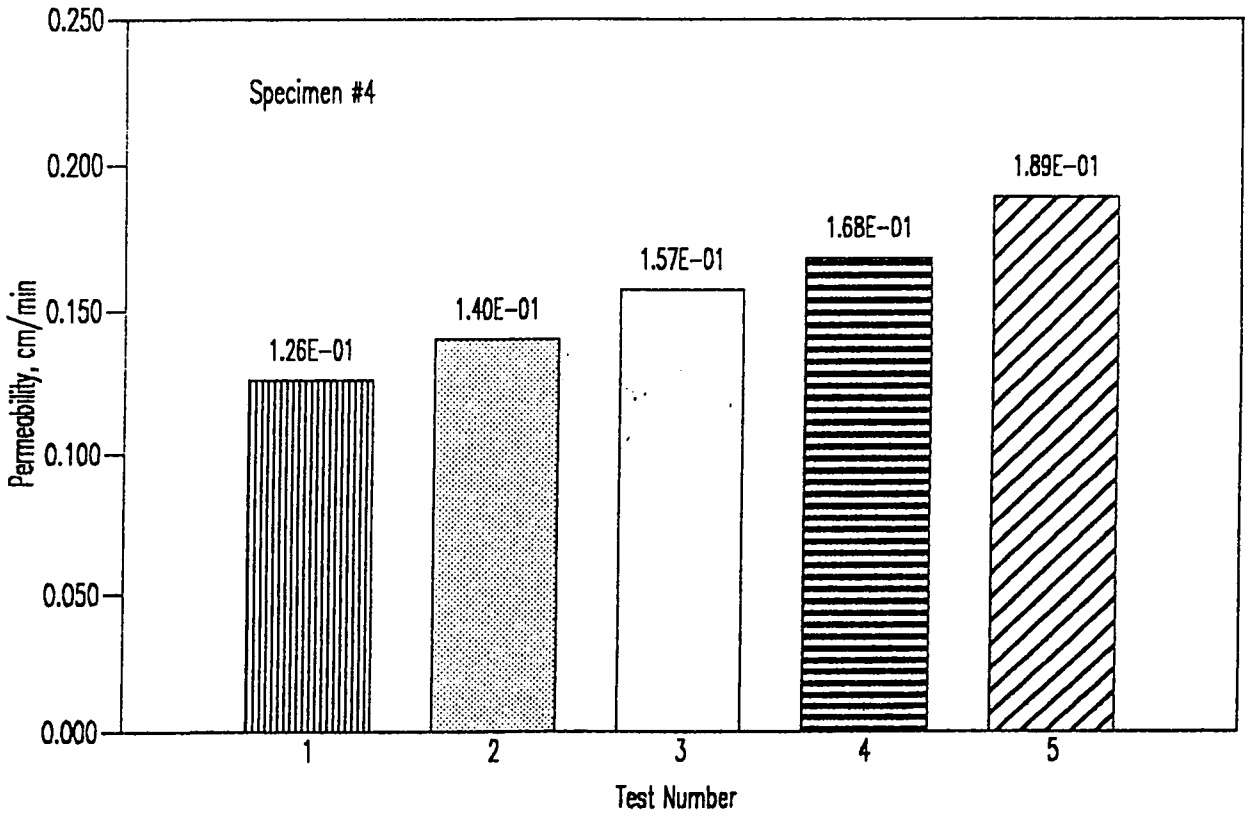

Fig. 5.20 : Constant Head Permeability Test Results using Distilled Water (Specimen #4)

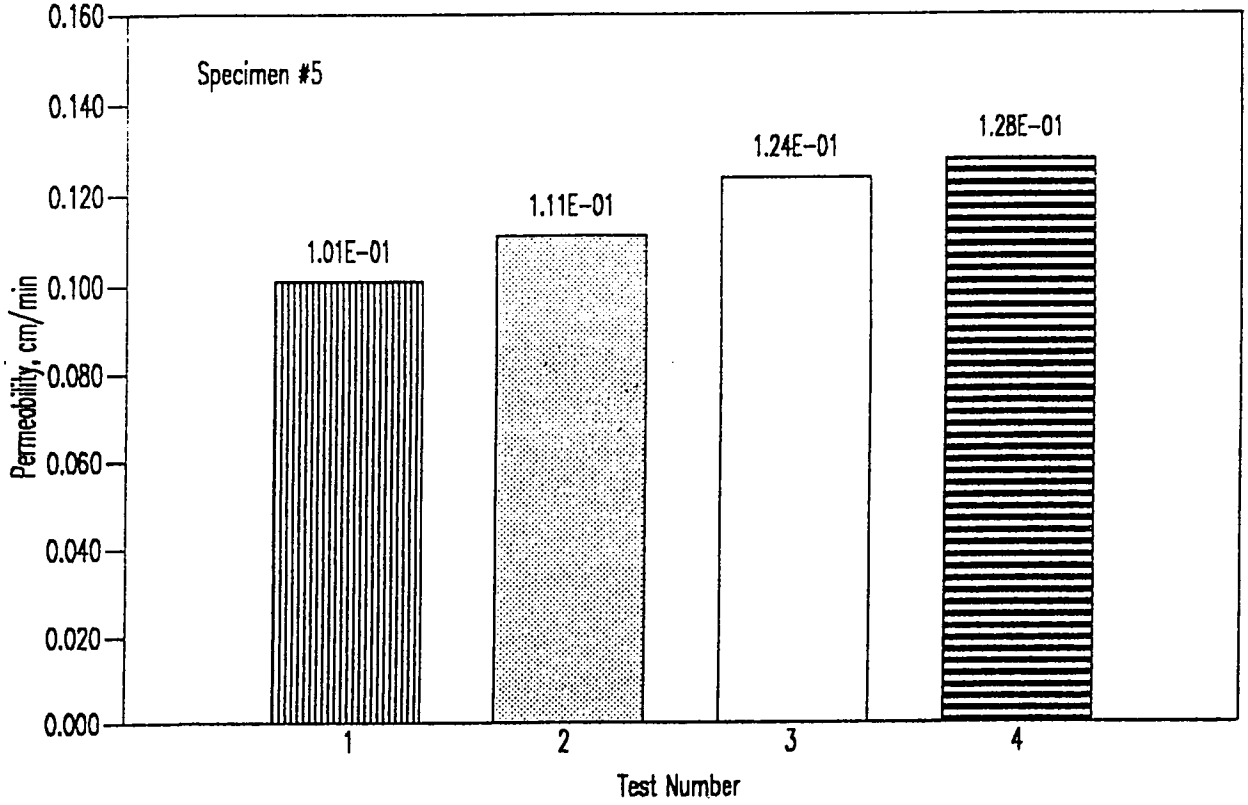

Fig. 5.21 : Constant Head Permeability Test Results using Distilled Water (Specimen #5)

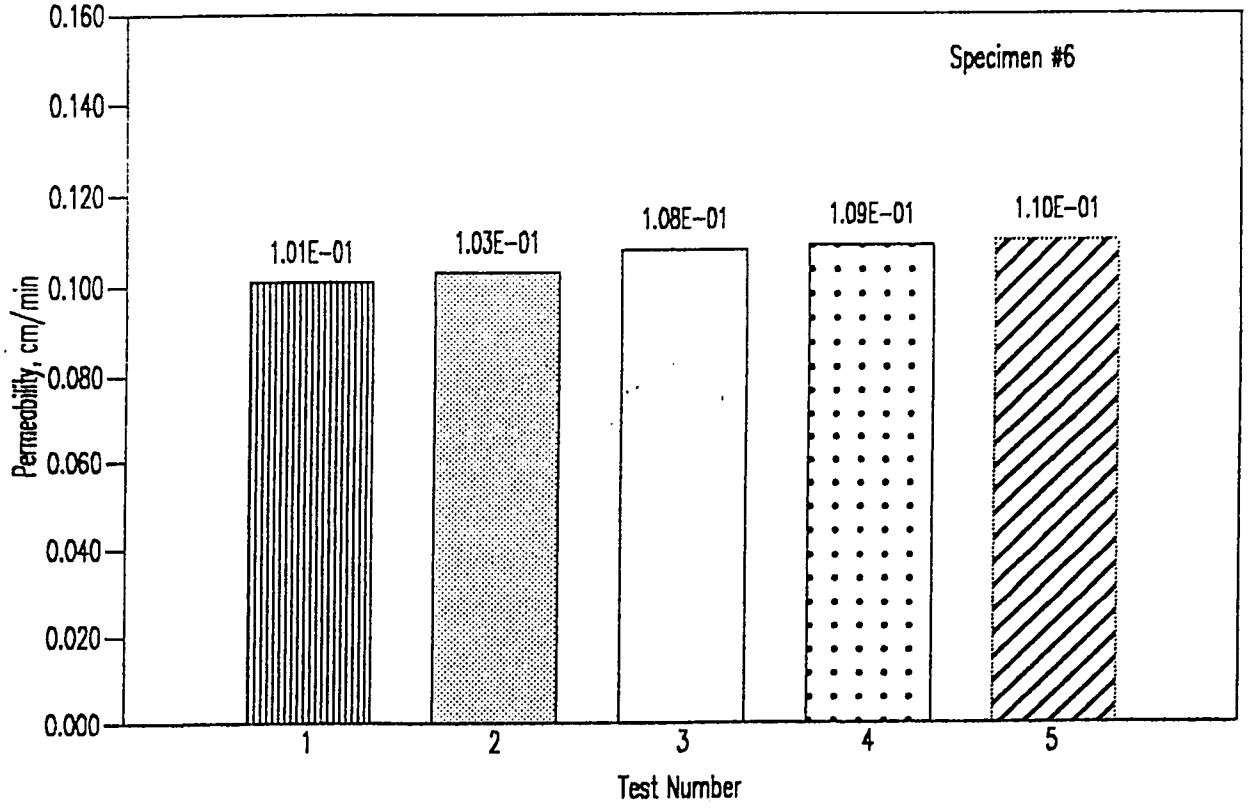

Fig. 5.22 : Variable Head Permeability Test Results using Distilled Water (Specimen #6)

the difference was slightly more pronounced for the case of variable head test. The reason for the higher values of permeability coefficient and its increase with test repetition when distilled water was used was perceptibly attributed to salt dissolution that caused more channels to form and thus increasing the permeability. Salt leaching due to test repetition has recently been observed by Al-Sanad and Al-Bader (192) although they reported negligible changes in permeability coefficient. For the case of sabkha brine, the increase in k values with test repetition was attributed to salt precipitation due to time lag between the test repetitions, rather than salt dissolution, due to the high salt concentration in the brine (Table 5.1).

Irrespective of the accuracy of laboratory permeability testing as a means to evaluate the coefficient of permeability, the present results indicate that the use of distilled water to estimate groundwater (i.e., sabkha brine) flow will be inaccurate. However, if seepage of rain water is to assessed, then the use of distilled water will be appropriate.

5.4.5 Compaction Test Results

Results of the standard Proctor tests are shown in Figs. 5.23 and 5.24. These figures included the effect of using distilled water and sabkha brine as well as the effect of oven temperature. Results indicated that there was no fundamental difference between

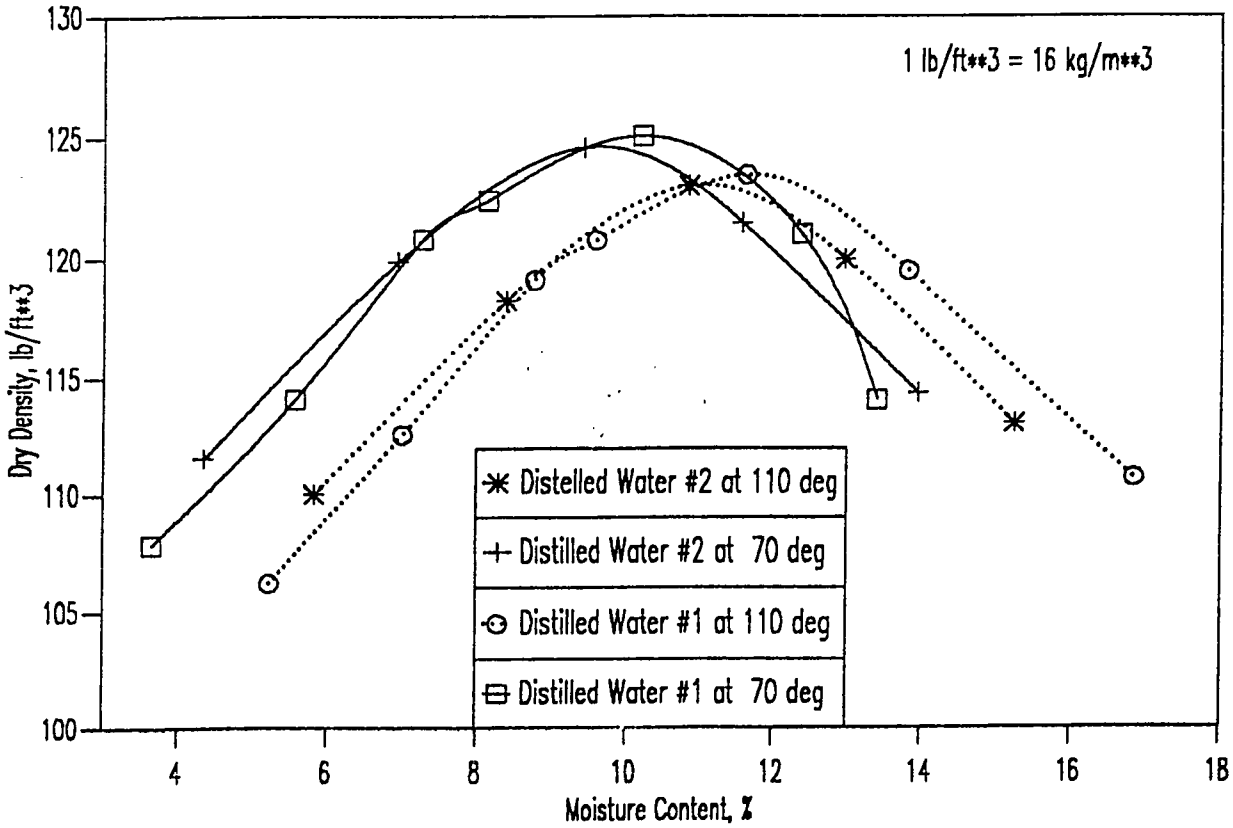

Fig. 5.23 : Effect of Distilled Water and Oven Temperature on Compaction Test Results

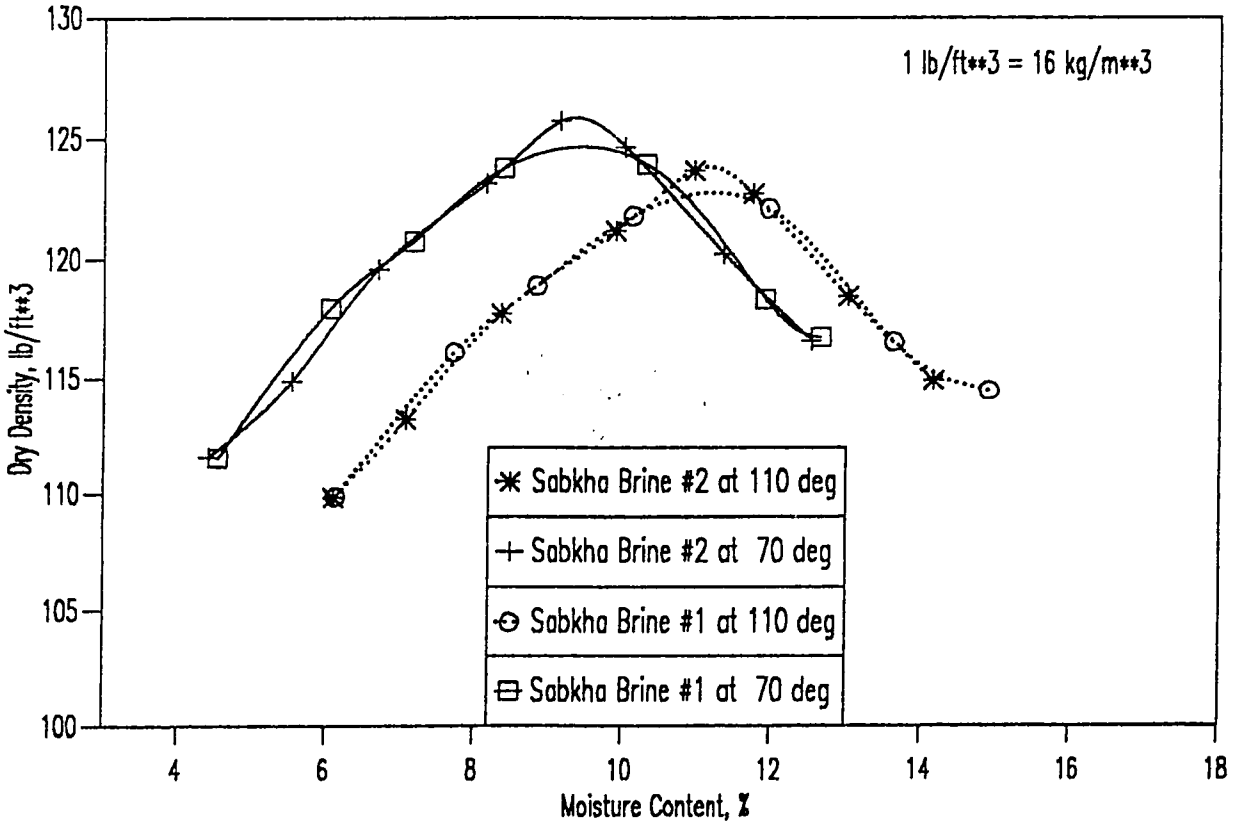

Fig. 5.24 : Effect of Sabkha Brine and Oven Temperature on Compaction Test Results

the moisture-density curves when either distilled water or sabkha brine was used, although minimal reduction in w_{opt} was associated with the latter.

The effect of oven temperature on compaction curves, however, is clear. This was envisaged by the fact that increasing the oven temperature will virtually lead to an increase in the optimum water content thereby leading to lesser dry densities. This difference, nevertheless, was not very significant (not more than 4 lb/ft^3).

The spongy characteristics of sabkha at around the optimum moisture content necessitate that sabkha should not be compacted at the optimum moisture content if and when an increase in strength is desirable.

5.4.6 Field Density Measurement Results

Each of the three in-situ density measurements was performed about 18 meters away from the other, in an attempt to obtain a better representative density of natural soil at Ras Al-Ghar. Results of these tests (using the sand-cone method) gave wet densities of 1.83, 1.77 and 1.91 gm/cm^3, with an average wet field density of 1.84 gm/cm^3 (i.e. 114.5 lb/ft^3) and an average dry density of 1.60 gm/cm^3 (i.e. 99.9 lb/ft^3) (see Table 5.12). Although the wet field densities were relatively scattered, the dry

Table 5.12 : In-Situ Density Test Resuls Using the Sand Cone

Property	Test #1	Test #2	Test #3
Wet Desnity, gm/cm³ (pcf)	1.83 (113.7)	1.77 (110.7)	1.91 (119.1)
Moisture Content, %	15.3	13.8	15.0
Dry Desnity, gm/cm³ (pcf)	1.58 (98.8)	1.56 (97.3)	1.66 (103.6)
Average Wet Density = 1.84 gm/cm³ (114.5 lb/ft³) Average Dry Density = 1.60 gm/cm³ (99.9 lb/ft³)			

According to ASTM D 1556 and AASHTO T-191

densities were a bit narrower. This was attributed to variations in the natural moisture content and heterogeneity of the sabkha soil itself.

Comparison of the dry field density with the laboratory maximum dry density indicates that the relative compaction (R.C.) is about 80%, which is extremely low. Another important point to be highlighted is the fact that the natural moisture contents of the field samples were in the range of 14 to 18%, and sometimes reaching 22%, which were more than the optimum moisture content of 11 to 12%, as determined from Proctor tests. Therefore, the sabkha soil in Ras Al-Ghar lies on the wet side of the compaction curve. If a typical compaction methodology is to be performed in the field, reduction in natural moisture content will be the prerequisite step to start with if and when sabkha strength has to be increased (77,193). Otherwise, other stabilization techniques have to be implemented.

5.4.7 Consolidation Test Results

Consolidation tests were conducted using the conventional (classical) oedometer and modified one. The latter was developed in this research study. Results of these tests are presented in the following paragraphs.

5.4.7.1 Conventional Oedometer Test Results

Consolidation tests are the most cumbersome and time consuming to perform and, for the case of difficult soils such as sabkhas, they are very difficult to interpret. Nevertheless, these tests are very instrumental to predict the compressibility and swell potential and, sometimes, collapse potential. Results of the four consolidation tests are shown in Figs. 5.25 and 5.26 (Series #1 to Series #4, respectively) which indicate that there was unexpectedly insignificant effect of flooding with either distilled water or sabkha brine on the consolidation characteristics of sabkha. This may indicate that the profuse cementation and desiccation of sabkha soils are not destroyed or disrupted in the consolidation test; in contrast to the permeability tests. The increase in permeability coefficient with test repetition in the permeability test is attributed to the head difference which was more than 150 cm compared to few centimeters in these tests. Another important point is that the liquid (whether distilled water or sabkha brine) was not allowed to flow continuously through the specimens and, therefore, the collapse potential could not be accurately detected. Figures 5.25 and 5.26 also show that the response of sabkha to consolidation tests is not unique; different samples showed different total change in void ratio although the samples were retrieved from the same place (i.e. at a depth of 25 cm from the ground surface) at the same time and tested under similar conditions. This could be attributed to the

variability of the sabkha mineralogy due to presence of diagenetic minerals (40). The data pertinent to consolidation tests are quantitatively shown in Table 5.13. These data give rise to the following observations. First, the change in void ratio due to flooding, although not as significant as anticipated, was greater when samples were flooded with distilled water than when flooded with sabkha brine (0.009 for the former compared to 0.002 for the latter). Second, all samples, whether flooded with distilled water or sabkha brine, exhibited an increase in moisture during the test; the increase, however, was generally more when distilled water was used than with sabkha brine (3.8% compared to 1.3%). This probably reflects the ease of wetting the sabkha samples with distilled water than with sabkha brine as shown in permeability tests. Thirdly, the over-consolidation pressure (σ_c') seems to be insensitive to the type of flooding fluid, i.e. flooding with distilled water produced (σ_c') of 130 and 190 kPa while flooding with sabkha brine produced (σ_c') of 185 and 155 kPa. This is in spite of the variation in total change in void ratio that tended to be more in the case of the former. Consequently, different overconsolidation ratios (OCR's) resulted. An average OCR of 19 and 20 were produced when distilled water and sabkha brine were used respectively. These high values of the OCR are not the result of preconsolidation but primarily reflect the desiccation and cementation of sabkhas. Similar behavior has been reported by Hossain and Ali

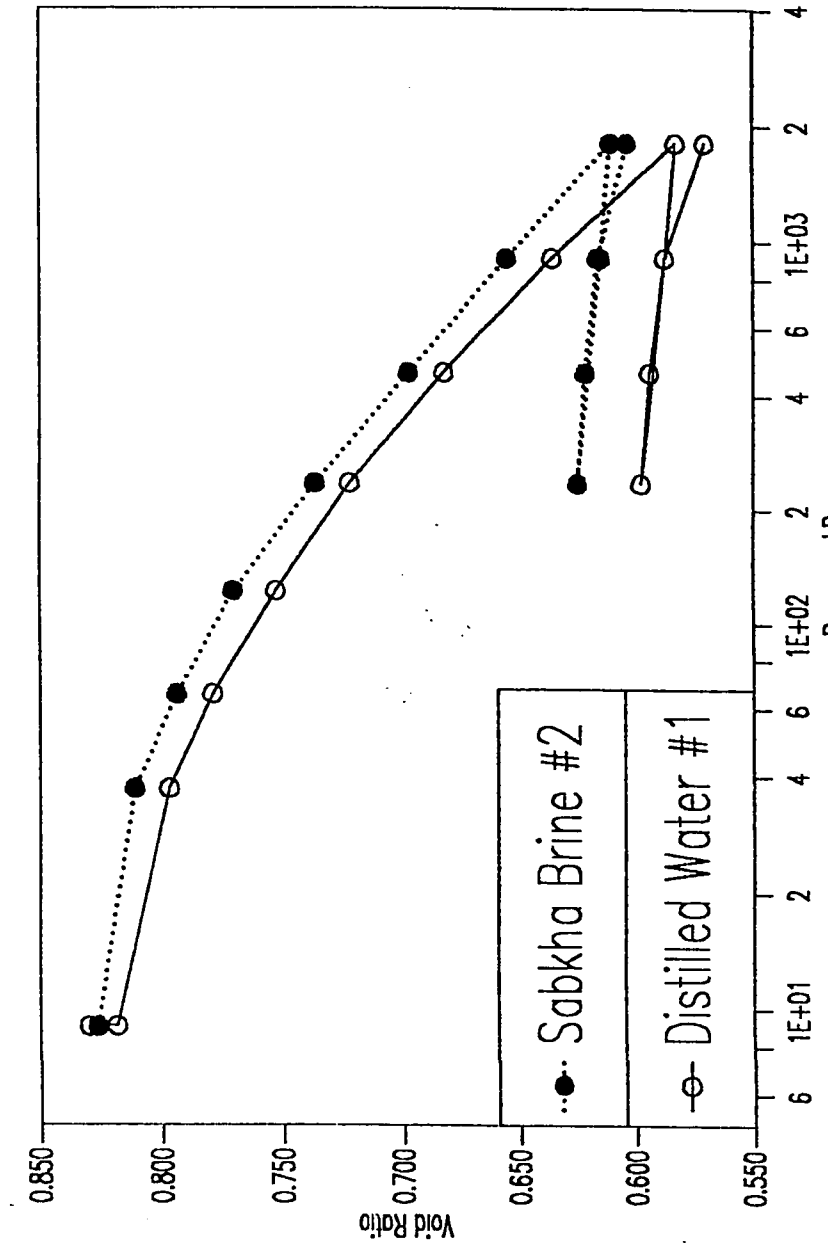

Fig. 5.25 : Results of the Conventional Oedometer Tests (Series #1)

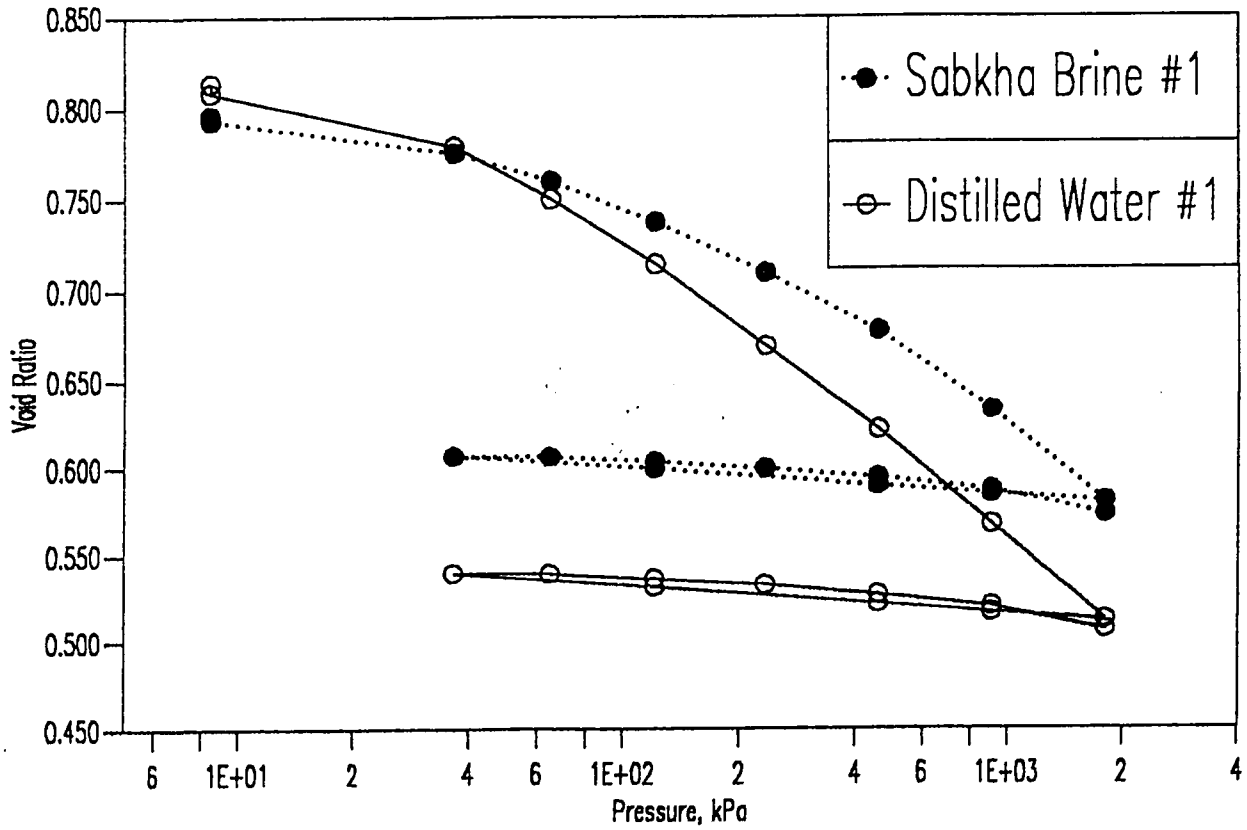

Fig. 5.26 : Results of the Conventional Oedometer Tests (Series #2)

Table 5.13 : Summary of Consolidation Test Results (Series #1 and #2)

Test Characteristics	Series #1		Series #2	
	Distilled Water	Sabkha Brine	Distilled Water	Sabkha Brine
Initial Void Ratio	0.830	0.826	0.814	0.796
Change in Void Ratio due to Flooding	0.012	0.001	0.006	0.003
Final Void Ratio	0.571	0.604	0.507	0.574
Total Change in Void Ratio	0.259	0.222	0.307	0.222
Change in Moisture Content, %	+ 4.0	+ 0.4	+ 3.6	+ 2.1
Overburden Pressure, kPa	8.4	8.4	8.4	8.4
σ'_c, Overconsolidation Pressure, kPa	130	185	190	155
C'_c, Compression Index	0.17	0.15	0.18	0.16
C'_s, Swelling Index	0.017	0.016	0.016	0.015
Overconsolidation Ratio (OCR)	15	22	23	18

(1988) as well as others. The fourth observation is that the compression index (C_c') and the swelling index (C_s') are the same for all the samples, with an average C_c' of 0.16 and C_s' of 0.016, irrespective of the flooding liquids. This indicates that these parameters are also insensitive to changes surrounding the sabkha. C_s' is often assumed to be 5 to 10% of C_c' for typical soils (167), while here it is about 10% of C_c' for both liquids. Typical values of C_s' range from 0.015 to 0.035; the lower values are for clays of low plasticity and low OCR (194). It is thus seen that sabkha falls within the lower limit of this range of values. Furthermore, the ratio C_c'/C_s' for the sabkha under consideration is 10, irrespective of the type of flooding liquid, and according to Saeedy and Mollah (195), if this ratio ranges from 8 to 12 then the soil will possess low to moderate compressibility. Therefore, it can be concluded that Ras Al-Ghar sabkha, a typical of the Arabian Gulf sabkhas, possesses low compressibility.

It should be mentioned that the extensive damage to buildings and other constructional utilities in the southwestern Saudi Arabia as reported by Erol (25), Hudgson et al. (26) and Dhowian (196) was not due to the compressibility of sabkha per se but due to the presence of a salt dome and to the high organic content in that sabkha.

Time-settlement curves are usually used to obtain the coefficient of consolidation (C_v). However, for the case of sabkha, typical curves are shown in Figs. 5.27 and 5.28. These Figures show the time-settlement at the beginning of the test (before flooding) and after flooding; respectively. While the former curve shows a typical shape, i.e. settlement ceased after a certain period that is normally taken to be one day; the latter curve indicates that settlement continued even after more than 10,000 minutes (about seven days of a single loading increment). This could be attributed to the interaction of the fluids and sabkha that caused continued salt dissolution. Creep might have significant influence due to the high salt percentage of the sabkha. For this reason, C_v was not determined.

5.4.7.2 Modified Oedometer Results

As discussed in the experimental program, this oedometer was primarily developed to evaluate the collapse potential of sabkha soils. Therefore, the results are divided into two portions, as follows:

5.4.7.2.1 Preliminary Test Results

The data developed within the context of this preliminary test were based on a single objective, that was to check the reliability of this modified oedometer to detect the collapse potential of

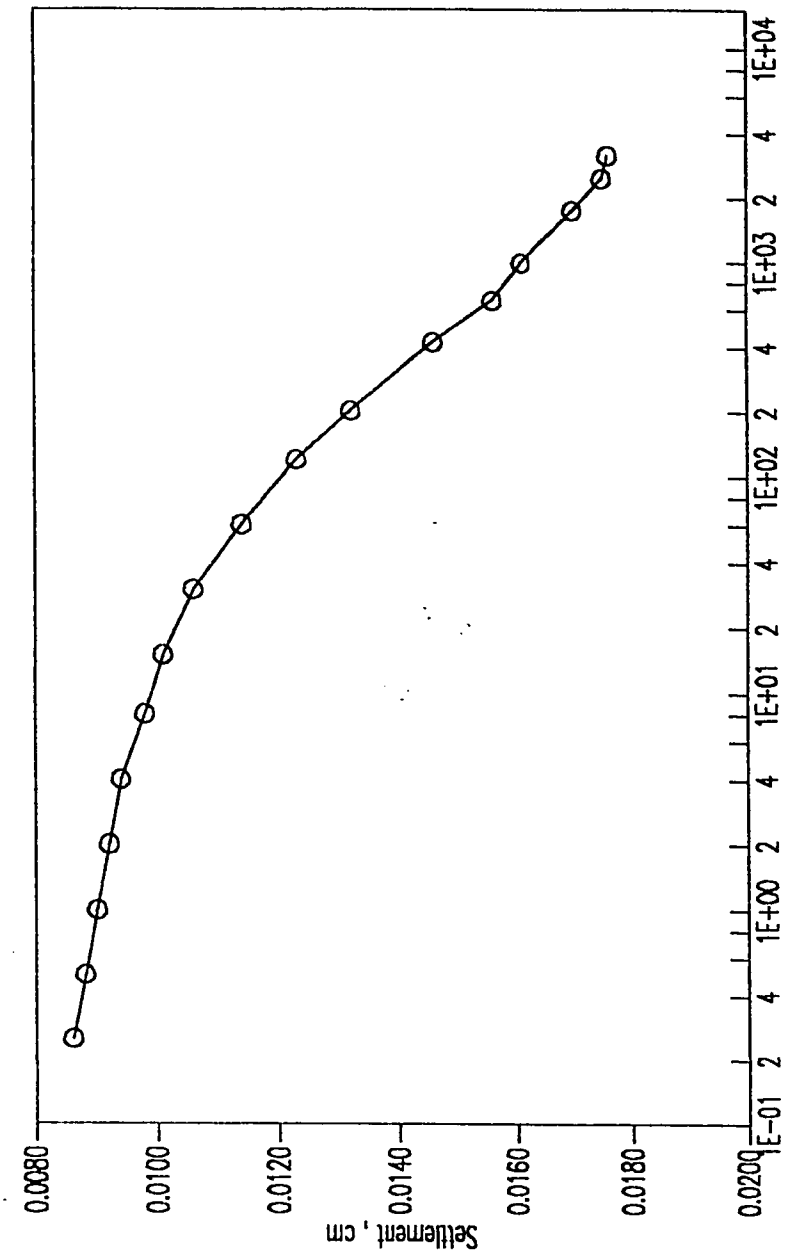

Fig. 5.27 : Typical Time–Settlement Data from a Conventional Consolidation Test (Before Flooding)

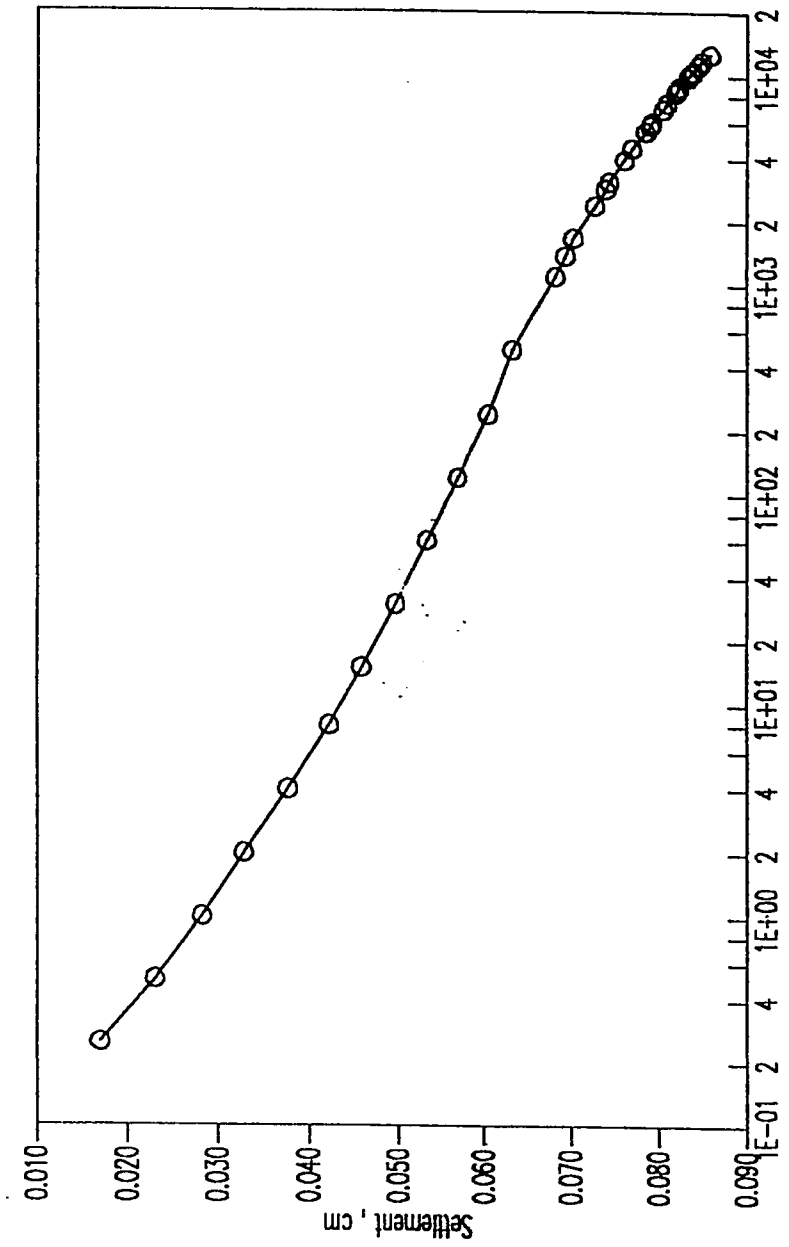

Fig. 5.28 : Typical Time–Settlement Data from a Conventional Consolidation Test (After Flooding)

sabkha under consideration and to establish thereafter a consistent procedure in order to develop more concise and comparative results upon usage of this oedometer. The data developed from this test are presented in Figs. 5.29 through 5.34.

Fig. 5.29 shows the relationship between pressure and void ratio for both modified and conventional oedometers. It is clearly seen that while the effect of initial flooding with distilled water at a pressure of 8.4 kPa did not have any noticeable reduction on void ratio for both oedometers, the effect of flowing water through sabkha at a pressure of 234 kPa did have a significant effect on the void ratio. A reduction in void ratio of 0.09 was primarily attributed to flow of water through sabkha soil. This magnitude of change in void ratio amounts to about 20% and 30% of the total change in void ratio during the whole consolidation tests using the modified and conventional oedometers respectively. This large change in void ratio due to water percolation signifies the very high collapse potential of sabkha. According to Knight (197) and Jennings and Knight (198), the collapse potential can be measured using the double oedometer tests in which two identical specimens are tested, one at the natural water content while the other under saturated condition. The two tests are then compared and the collapse potential of the soil which is defined as the percentage change in volume (i.e. or void ratio) on wetting under a pressure of 200 kPa is determined, and the following correlation is proposed

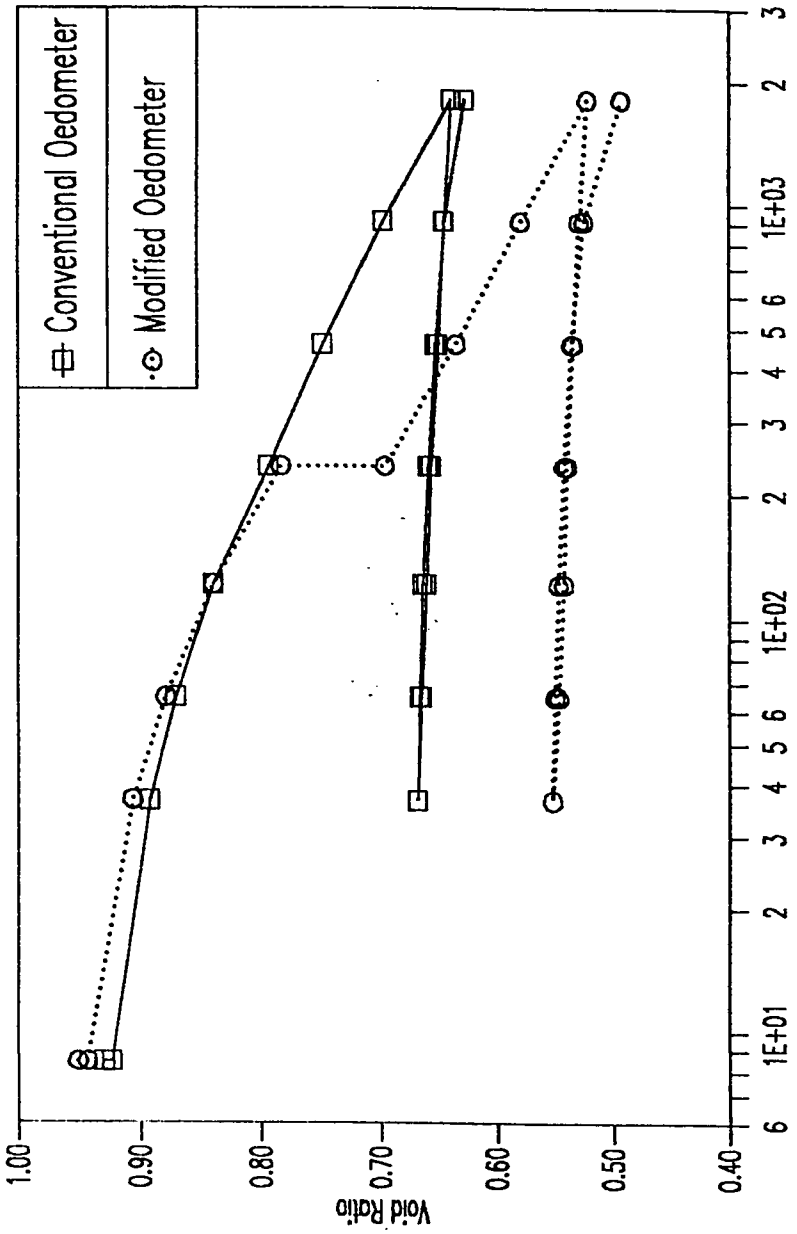

Figure 5.29 : Consolidation Test Results (Series #3)

by Knight:

Collapse Potential (%)	Severity of Problem
0 to 1	No problem
1 to 5	Moderate trouble
5 to 10	Trouble
10 to 20	Severe trouble
above 20	Very severe trouble

Comparison of the double oedometer criterion with the modified oedometer results indicates that both tests share similarities; the collapse potential is due to water sensitivity and the pressure is almost the same. Therefore, Ras Al-Ghar sabkha soil can be classified as having "very severe trouble" collapse potential, and this collapse potential could not be detected by the use of conventional oedometer.

The compression and swelling indices as determined from Fig. 5.29 using both the modified and conventional oedometers are 0.19 and 0.017 for the former and 0.18 and 0.017 for the latter. It is therefore interesting to note that the effect of percolation did not have any effect on the compression and swelling indices.

The results of measurement of flow of water with time under the initially sustained load of 234 kPa are shown in Fig. 5.30. It is obvious that flow of water, and therefore, permeability, tends to decrease with time and, consequently, contrasting the results presented in Section 5.4.4 that showed the permeability coefficient to increase with test repetition when distilled water was

used. This can perceptibly be explained by the fact that the compressed specimen here is under pressure and the passage of water caused salt dissolution that created voids. Due to sustained loading upon the specimen, the void ratio accordingly decreased. This reduction in void ratio outweighed the presence of voids created by salt dissolution and thereby leading to simultaneous reduction in flow. It is noteworthy to mention that the reduction in flow occurred much in the early period of water percolation through the specimen when salts were in their full presence. The rate of reduction in flow, thereafter, was much reduced. Fig. 5.30 shows that about two days of water percolation were required to significantly reduce the permeability and, after which, the reduction was almost negligible. This is manifested in Fig. 5.31 where it is shown that the flow of water for more than an extra 36 days reduced the flow from 0.20 to 0.05 cm^3/minute (a total reduction of 0.15 cm^3/min), while during the first two days the flow was reduced from 0.50 to 0.20 cm^3/min (a total reduction of 0.30 cm^3/min); that is twice the change in flow during the 36 days.

The ups and downs shown in Fig. 5.31 after about 20 days of water flow were attributed to the loading, unloading and reloading cycles during the consolidation test. This point will be discussed in detail in Sec. 5.4.7.2.2.

The effect of pressure on the flow is depicted in Fig. 5.32 (i.e. the amount of flow was based on the average flow during

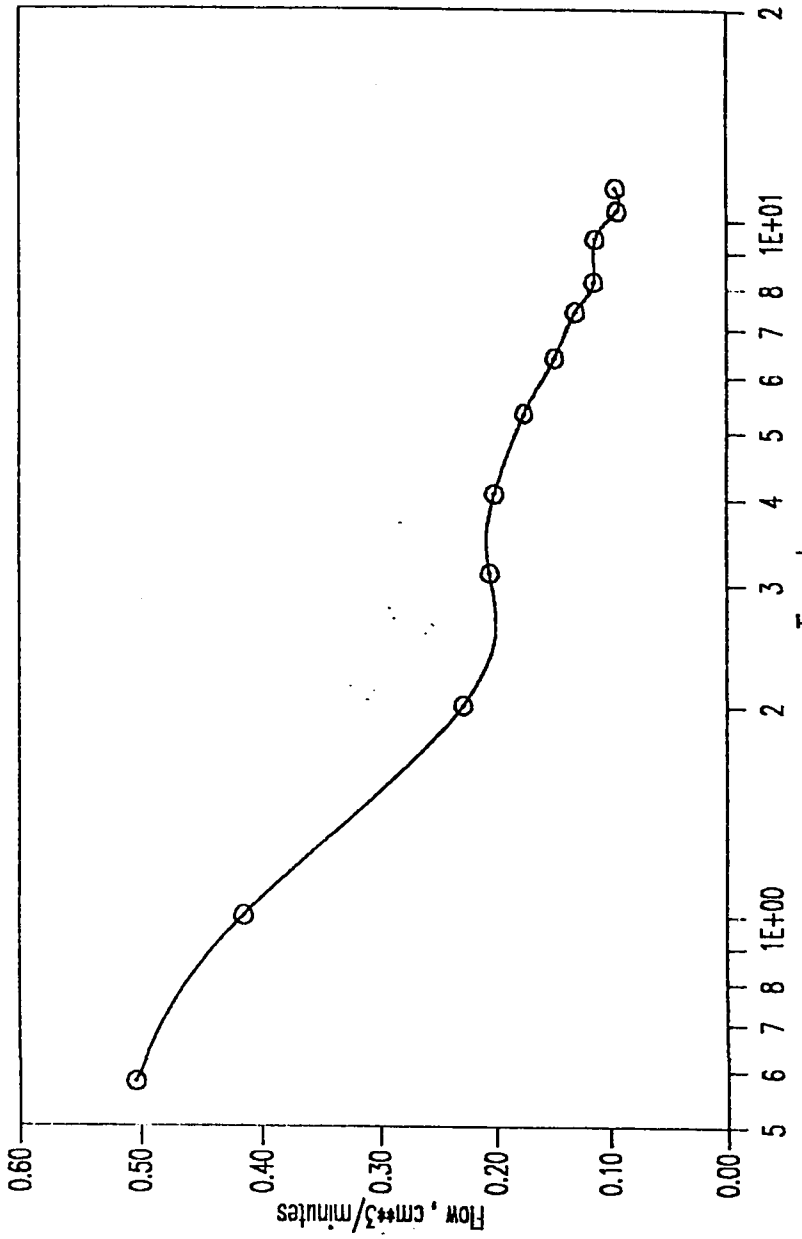

Figure 5.30 : Initial Time–Flow Data for the Modified Oedometer (Series #3)

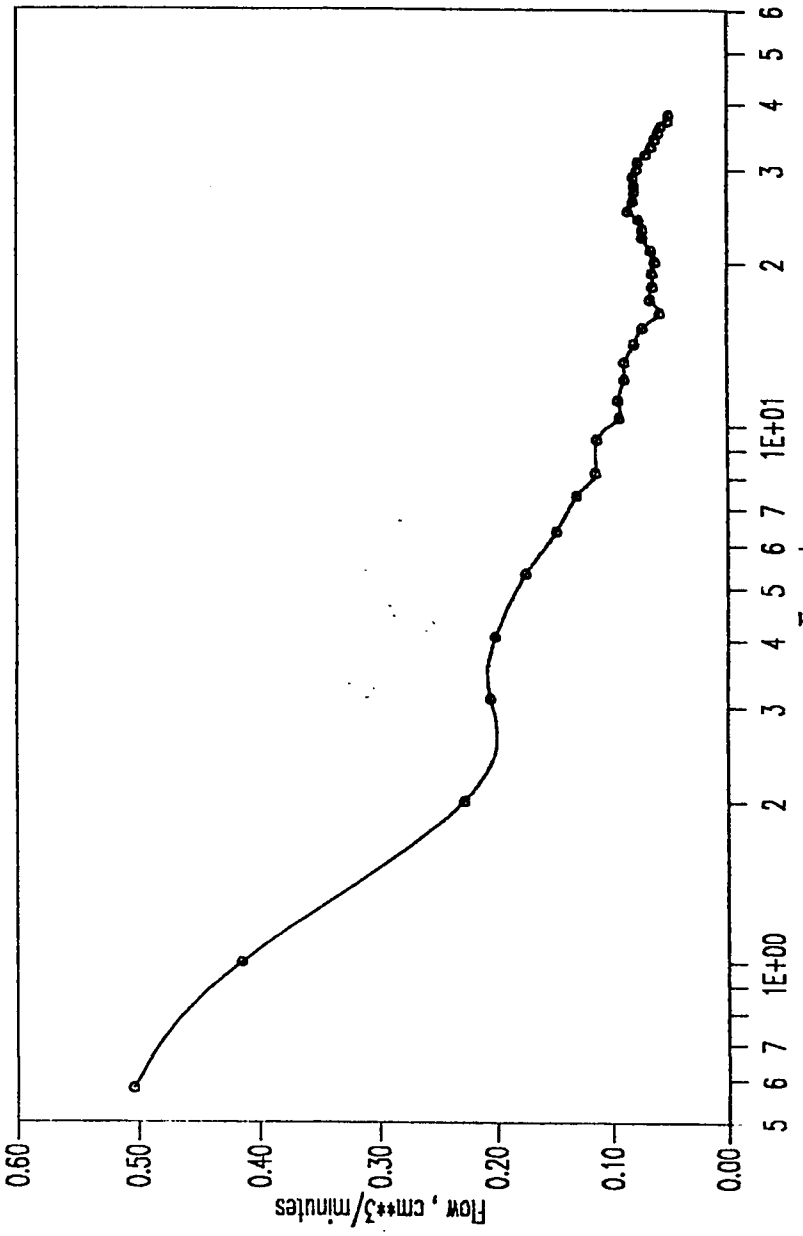

Figure 5.31 : Time–Flow Data for the Modified Oedometer (Series #3)

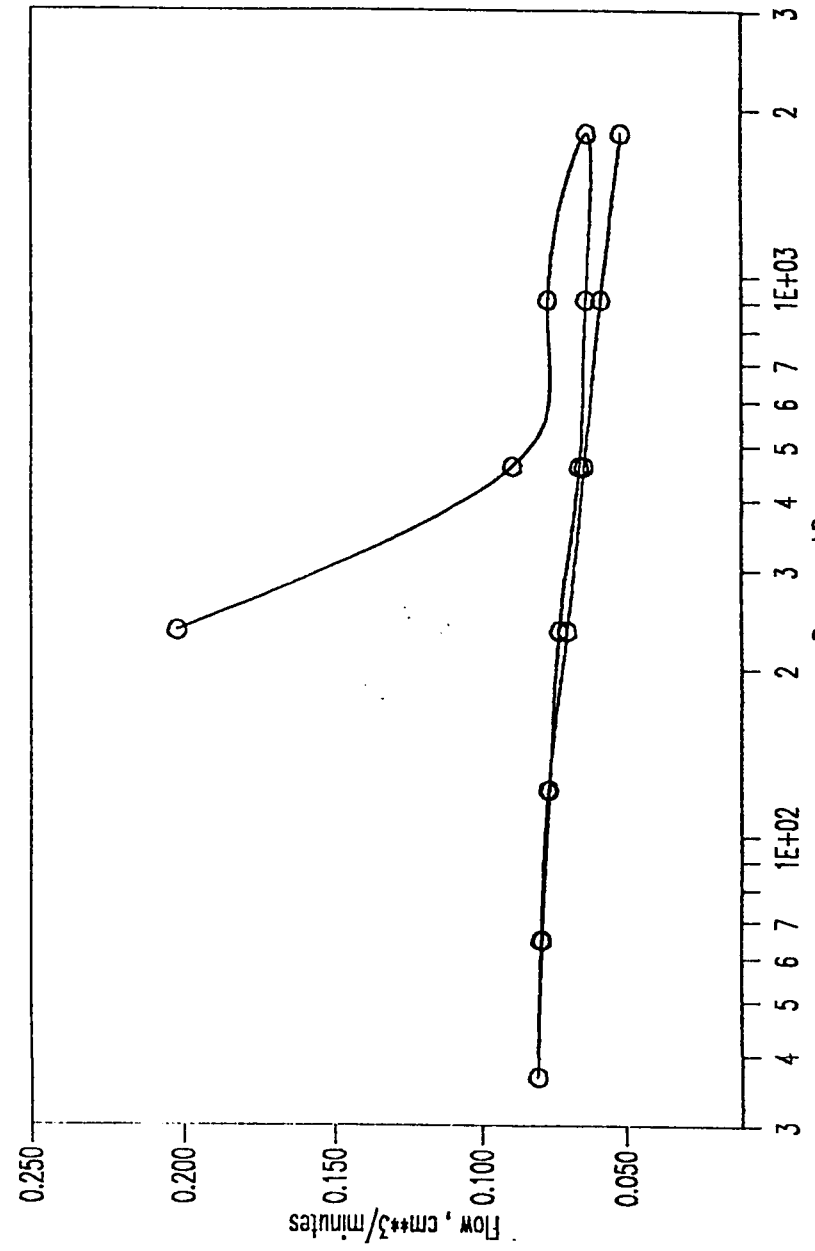

Figure 5.32 : Flow—Pressure Test Results (Series #3)

the full period during which the pressure was acting). It was observed before that the reduction in flow was more significant in the early days of flow; this is also clear in this Figure. Once the effect of initial water percolation was overcome, the flow-pressure relationship followed exactly that of the classical void ratio-pressure pattern during loading, unloading and reloading cycles. The flow was more affected by the loading cycles and, therefore, the increase in flow during unloading was marginal in spite of the large reduction of pressure from 1,810 kPa to 37 kPa.

In order to develop a mechanistic picture for the causes of the high collapse potential of sabkha, chemical analysis tests were conducted on samples obtained from seeping water. Figure 5.33 shows results of these tests where it was observed that variation of magnesium ion (Mg^{++}) during the full consolidation test was insignificant while that of calcium (Ca^{++}) was insensitive at the early age and then reduced after about four days of water percolation and continued to reduce up to the end of test. The variation of sodium (Na^{+}) and chloride (Cl^{-}) ions were more or less similar, and both were reduced significantly during the first two to three days of the test and remained fairly constant thereafter. Comparison of these results with those of flow vs. time presented in Fig. 5.31 reveals the fact that the amount of flow, and consequently permeability of sabkha, is almost proportional to the sodium and chloride ions, and as these ions were reduced after about two days

to very small amounts (about 15 ppm); the flow was accordingly reduced. This can be inferred by the fact that these ions form halite (NaCl, sodium chloride) which is a highly soluble salt and, due to the large amount of water percolation at the first two days, the dissolution of halite was perceptibly very significant. It can therefore be inferred that at this initial stage, it was the dissolution of halite that resulted in the collapse potential of sabkha. This is because once this salt dissolves, it will leave more interfacial voids that will be dissolved by the flowing water. The acting load will reduce the voids and simultaneously will re-arrange the soil grains in a denser, lesser void ratio structure and thereby leading to collapse as discussed before.

Another point to be discussed from Fig. 5.33 is the relatively high concentration of calcium (Ca^{++}) ion in the seeping water, about five to six times those of each of Na^{+}, Mg^{++} and Cl^{-}. This could be attributed to the high content of calcium-based soluble materials in the parent sabkha soil, probably gypsum and calcium (i.e. calcite and aragonite). Although the solubility of each of these phases is relatively very low (the solubility of gypsum, anhydrite, calcite and aragonite is 2,310, 2,090, 14.0 and 15.3 ppm, respectively), their total concentration is greater than the highest concentration of calcium ions (1,123 ppm) in the percolating water. The leaching of Ca^{++} is also a contributing factor to

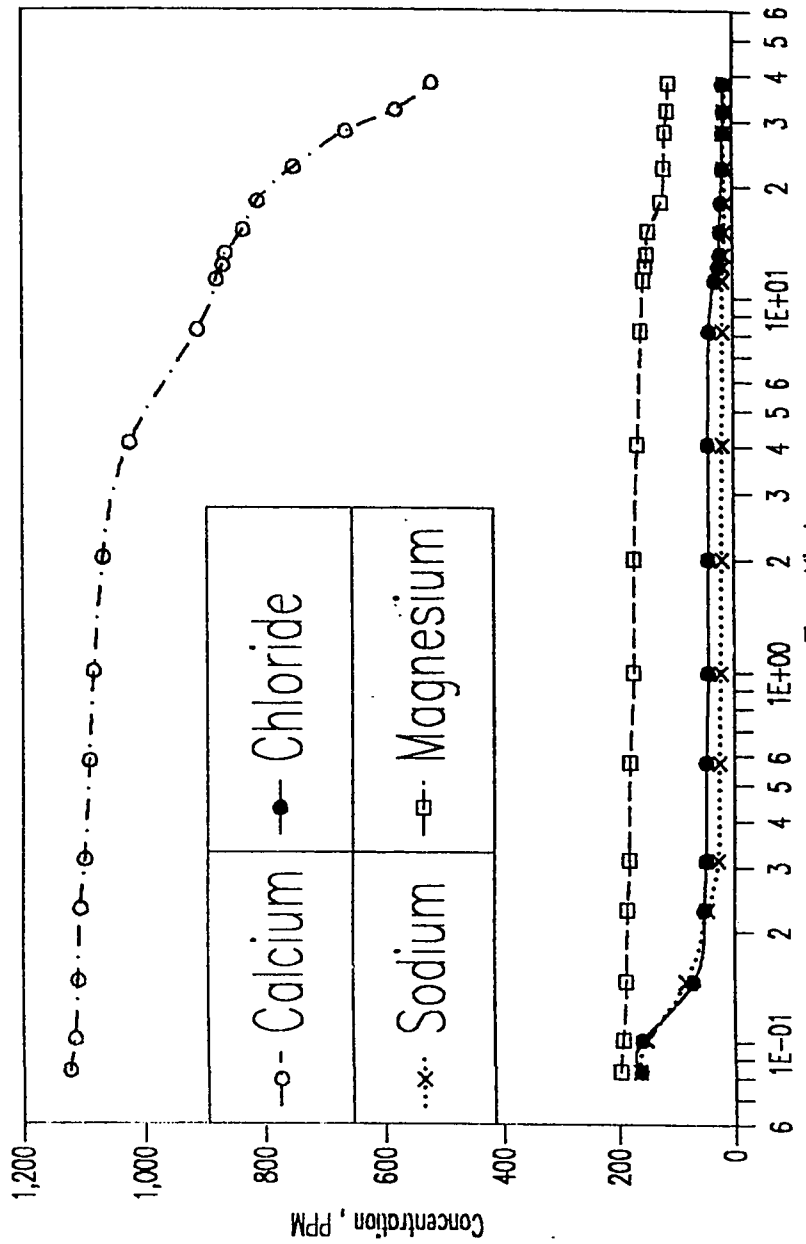

Figure 5.33 : Chemical Analysis of the Percolating Water (Series #3)

the collapse of sabkha.

Fig. 5.34 shows the conductivity of seeping water with time. Conductivity determination is known to reflect the total amount of total dissolved solids (TDS) in any liquid (192), and hence the conductivity data presented in Fig. 5.34 follows more or less the calcium ion concentration presented in the previous Figure. This is because the content of Ca^{++} was the largest in the seeping water and, therefore, forms most of the TDS.

5.4.7.2.2 Systematic Test Results

Once the preliminary results were able to show the collapse potential of the sabkha soil, two series of systematic tests were conducted in order to develop further evidence of the versatility of this modified oedometer to detect the collapse potential as well as to measure permeability and, more-importantly, its variation with time during each loading cycle as well as during the full consolidation test. Moreover, the effect of distilled water and sabkha brine was further investigated to develop a parametric study on the effect of these fluids on flow rate, collapse potential, and other consolidation parameters (C'_c and C'_s).

In the first test, flooding with distilled water took place at the overburden pressure until the specimen ceased to develop further settlement. Percolation was allowed to take place at this

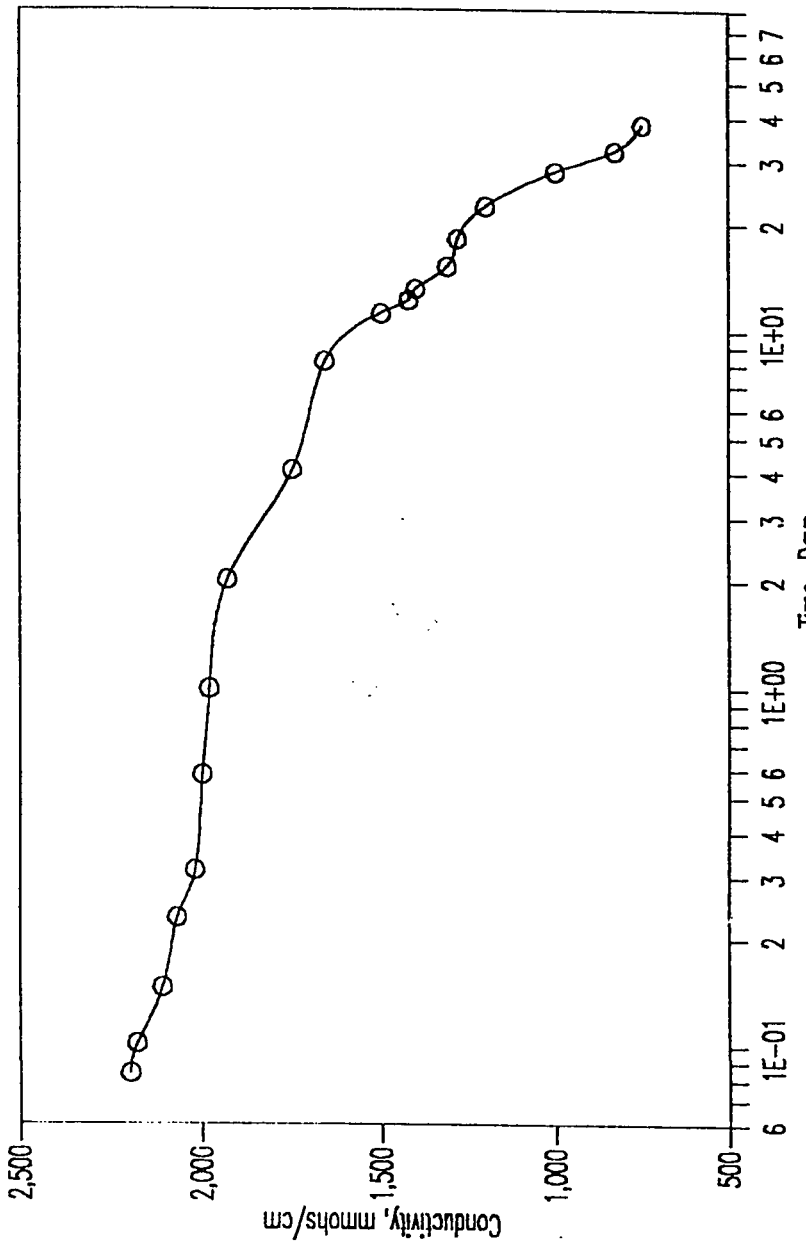

Figure 5.34 : Conductivity Test Results of Percolating Water (Series #3)

pressure until the test termination. The results pertinent to this test are presented in Figs. 5.35 through 5.42. The void ratio-pressure relationship is presented in Fig. 5.35, which again clarified the fact that flooding the sabkha samples with water did not cause any reduction in void ratio in spite of the fact that the present two samples were initially loaded at their overburden pressures. If percolation of water was allowed, this would result in a significant reduction in void ratio. The amount of void ratio reduction due to water percolation amounted to 0.033 during only three days. It was mentioned in the preliminary test that the commencement of percolation took place at a pressure of 234 kPa and that high pressure enhanced the reduction in void ratio due to the concomitant effect of salt dissolution and soil grain adjustment. In the present test, the pressure is only 9.9 kPa (i.e. the overburden pressure) and, accordingly, the reduction in void ratio was anticipated to be primarily to salt dissolution. This is why the reduction in void ratio in the present test is lesser than that in the preliminary one. The effect of sustained pressure has been observed by Kezdi (199) and more recently Lutenegger and Saber (200) who found that the collapse potential increases approximately linearly with increasing pressures up to a limiting stress level. Another important factor is that the duration of water percolation under the same initially-applied pressure during this test and the preliminary one was not the same; here only three days compared to about nine days for the preliminary test. Therefore, both

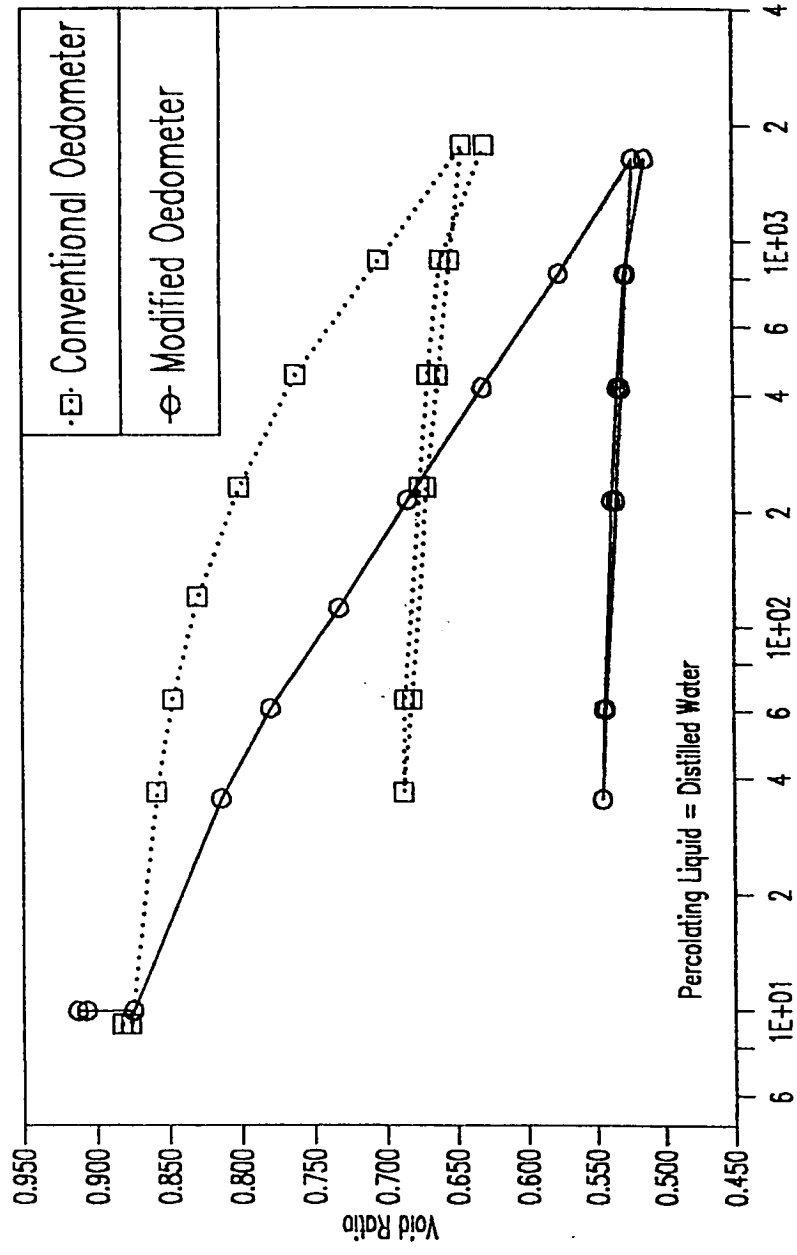

Figure 5.35 : Consolidation Test Results (Series #4)

factors of pressure magnitude and duration of water percolation enhanced the reduction in void ratio more in the preliminary test than the present one.

Another observation can be deduced from Fig. 5.35. While the virgin curve (i.e. the straight line portion) of the consolidation curve obtained using the conventional oedometer test followed the same previous trends (i.e., it starts at about 500 kPa), the straight line portion here started at a much lower pressure (about 60 kPa), thereby enhancing the difference in void ratio between the two types of oedometers at consecutively increasing pressures. For example, the void ratio at about 10 kPa was 0.875 and 0.877 for the modified and conventional oedometers while it was 0.522 and 0.645 for both oedometers at a pressure of about 1700 kPa. This was attributed to the enhanced void ratio reduction with the increase in pressure. This might be the result of both soil grain adjustment and salt dissolution, however, the effect of soil grain adjustment was more significant particularly at higher pressures.

Comparison of the compression and swelling indices indicates again that these parameters are not very much affected by the modified oedometer, as shown in the preliminary test. The values of the compression and swelling indices for the case of the modified oedometer were 0.18 and 0.016, respectively, while they were 0.16 and 0.019, respectively, for the conventional oedometer.

These values are more or less similar to those reported previously in Section 5.4.7.1. Consequently, it can be concluded that these parameters (i.e. C'_c and C'_s) are not very much affected by the percolation of water through sabkha soil.

The change in flow with time during each loading cycle was recorded after about 10, 30, 60,... minutes. This was essential to know how the flow changed with time and with pressure. Fig. 5.36 shows the flow-time data for the eight loading cycles imposed on sabkha during consolidation test using the modified oedometer. This Figure indicates that the flow was decreasing very smoothly upon each loading cycle. This statement holds true for all loading cycles. However, it can be observed that in the case of the first two initial loading cycles (i.e., at loading pressures of 9.9 and 35.3 kPa), the reduction in flow continued to a longer period of time compared to those of later loading cycles. This can be explained by the fact that during the initial loading cycles the pressures were relatively small and therefore the effect of salt dissolution was more operative than soil grain adjustment and because at these low pressures the sample possessed high salt reserves, the dissolution of salt continued for longer periods, thereby leading to more reduction in flow with time. At higher pressures, the situation was different as the sample had already been washed, thereby leading to less salt dissolution and, consequently, the effect of soil grain would be more operative. This is

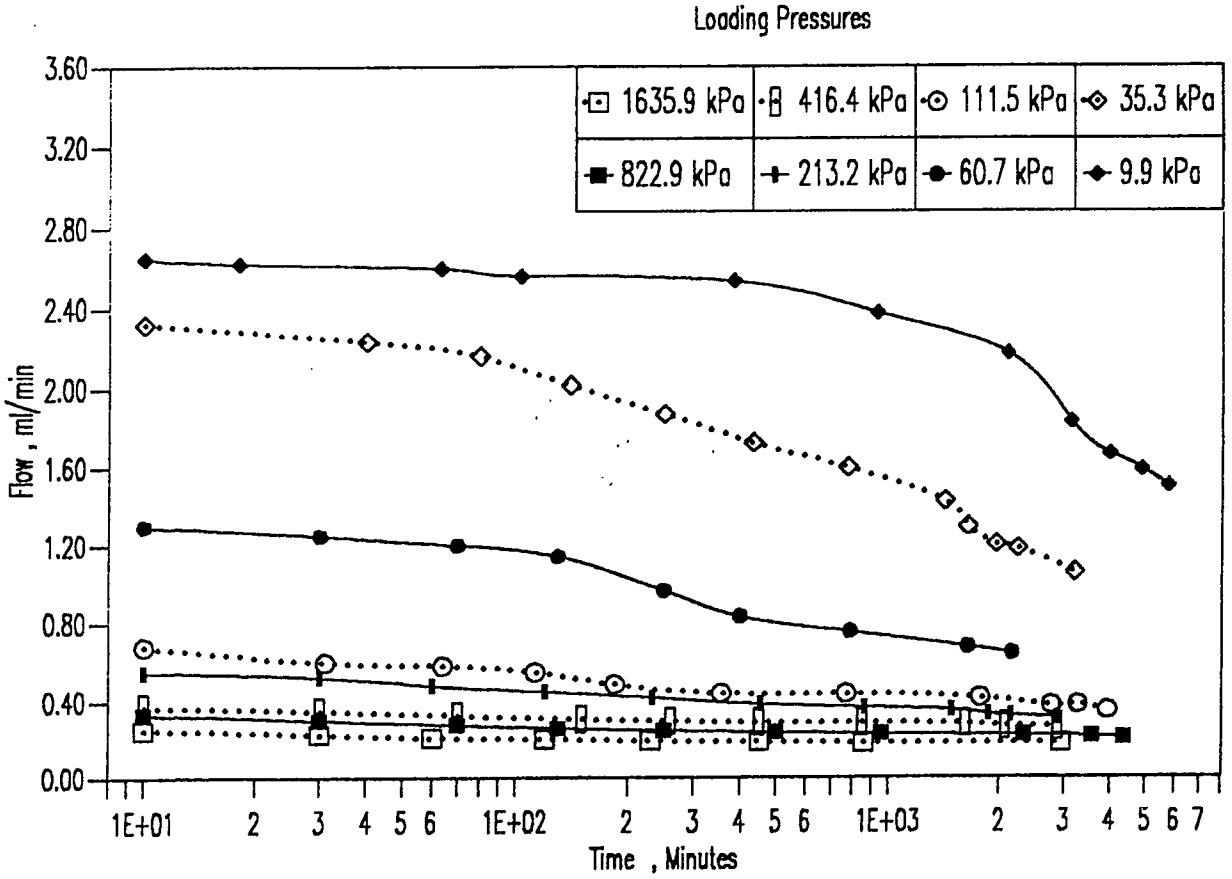

Figure 5.36 : Time–Flow Data for the Loading Cycles (Series #4)

the reason why the change in flow during the initial loading cycles was more than that during the latter loading cycles.

A closer examination of the curves in Fig. 5.36 indicates that the flow at the beginning of each loading cycle was more that at the end of the previous loading cycle. This again holds true for all loading cycles. The main reason behind this behavior could be attributed to the generation of pore-water pressure at the beginning of each loading cycle. This generated pore-water pressure enhanced the flow and, because of the sandy nature of sabkha soil, the dissipation of this pressure was manifested by the increase in flow. It is worth mentioning that each first reading of flow was usually taken after ten minutes of load application which means the true instantaneous flow at the time of loading was not measured due to the rather primitive nature of flow measuring technique used (i.e. using graduated cylinder). However, if a flow-meter was attached to the flow pipe, the instantaneous measurements of flow would be easily and accurately determined.

The flow measurements during unloading cycles are presented in Fig. 5.37, which indicates a completely different trend from loading cycles. The flow tended to increase with unloading (i.e. stress release) up to a period of about 300 minutes for the case of 822.9 kPa unloading pressure and up to a period of only 60 to 80 minutes in the case of lower pressures. The increase in flow could be explained by the fact that unloading results in an

increase in void ratio (refer to Fig. 5.35), thereby leading to an increase in flow. This increase in flow persists for a certain period and thereafter two mutual factors influence the flow. These factors are the void ratio and the sustained pressure. The former factor did not seem to change after a certain period and, consequently, the effect of sustained loading tended to control the flow after that period. This is because the increase in void ratio during unloading cycles was very small, as observed previously for all consolidation curves. The duration of this period in which the flow started to decrease was more for the case of 822.9 kPa pressure compared with all other lower pressures, as discussed before. The reason behind this could be attributed to the significant reduction in pressure (from 1,635.9 kPa to 822.9 kPa), thereby leading to a larger increase in void ratio compared to other lower pressures. Therefore, more time was required for the sustained load effect to dominate. From another perspective, the effective stress is known to increase if the flow is downward (201), i.e. with gravitational forces, and as the effect of void ratio would cease after a certain period, the increased effective stress would certainly reduce the flow.

The flow during the reloading cycles of pressures tends to unexpectedly follow the same trend as that during unloading cycles. This is clearly seen in Fig. 5.38, where flow was observed to increase up to a period of 100 to 200 minutes and

thereafter tended to decrease. The reasoning here is somewhat different from that during unloading cycles. The specimen here was overconsolidated and had experienced all the previous loading cycles and therefore was not significantly affected by reloading pressures. Moreover, the pore-water pressure was generated to high percentages of the applied pressure at the instant of reloading and since the specimen was very well compacted at this stage, the dissipation of pore-water pressures required some more time than the loading cycles. As a consequence of this increase in pore-water pressure, flow tended to increase to a period of about 200 minutes. This period might be enough for most of the pore pressure to dissipate and the decrease in flow was associated with the increase in effective stress.

To obtain a reliable average flow value during each loading cycle, the summation of volume of water passing through the specimen was determined over a period of about 1440 minutes, i.e. one day, (± 40 minutes). From this volume and the time over which this volume was obtained, an average representative flow over a single day period was determined. Fig. 5.39 shows results of this average flow vs. pressure, where it is observed that the reduction in flow was much more pronounced during the first three loading cycles (i.e. 9.9, 35.3 and 60.7 kPa) than the remaining other loading cycles. The flow was reduced from about 3,040 cm^3/day at the overburden pressure to about 1,085 cm^3/day at 60.7 kPa, after

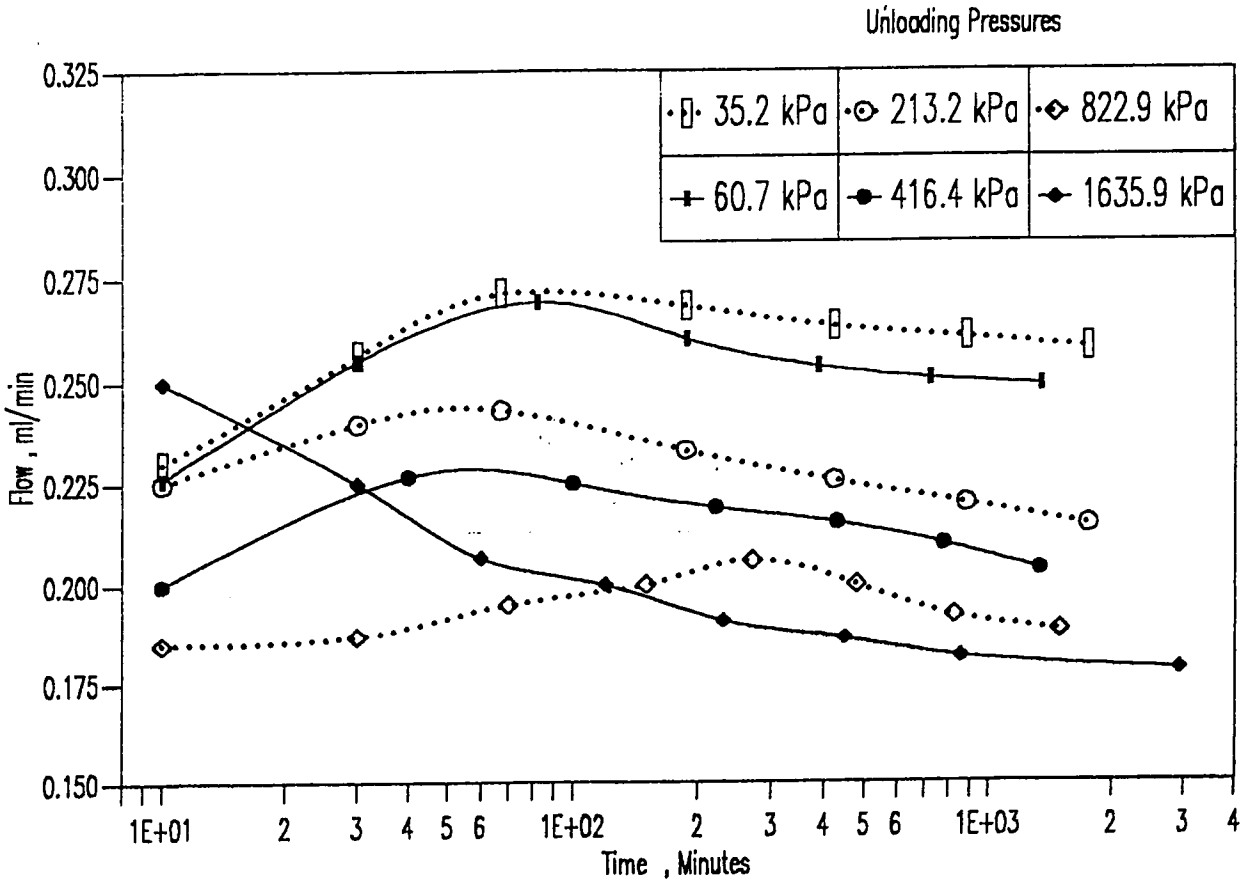

Figure 5.37 : Time–Flow Data for the Unlading Cycles (Series #4)

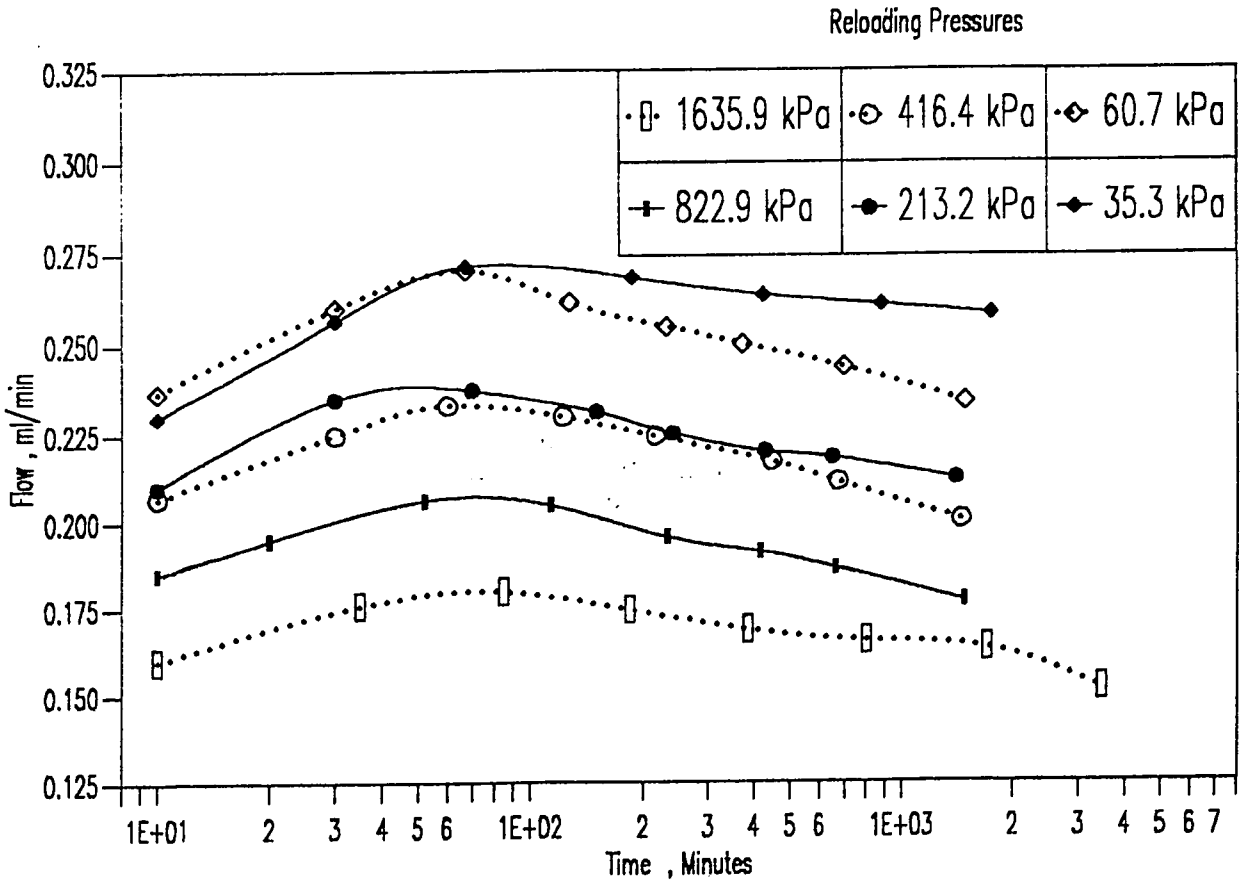

Figure 5.38 : Time–Flow Data for the Reloading Cycles (Sereis #4)

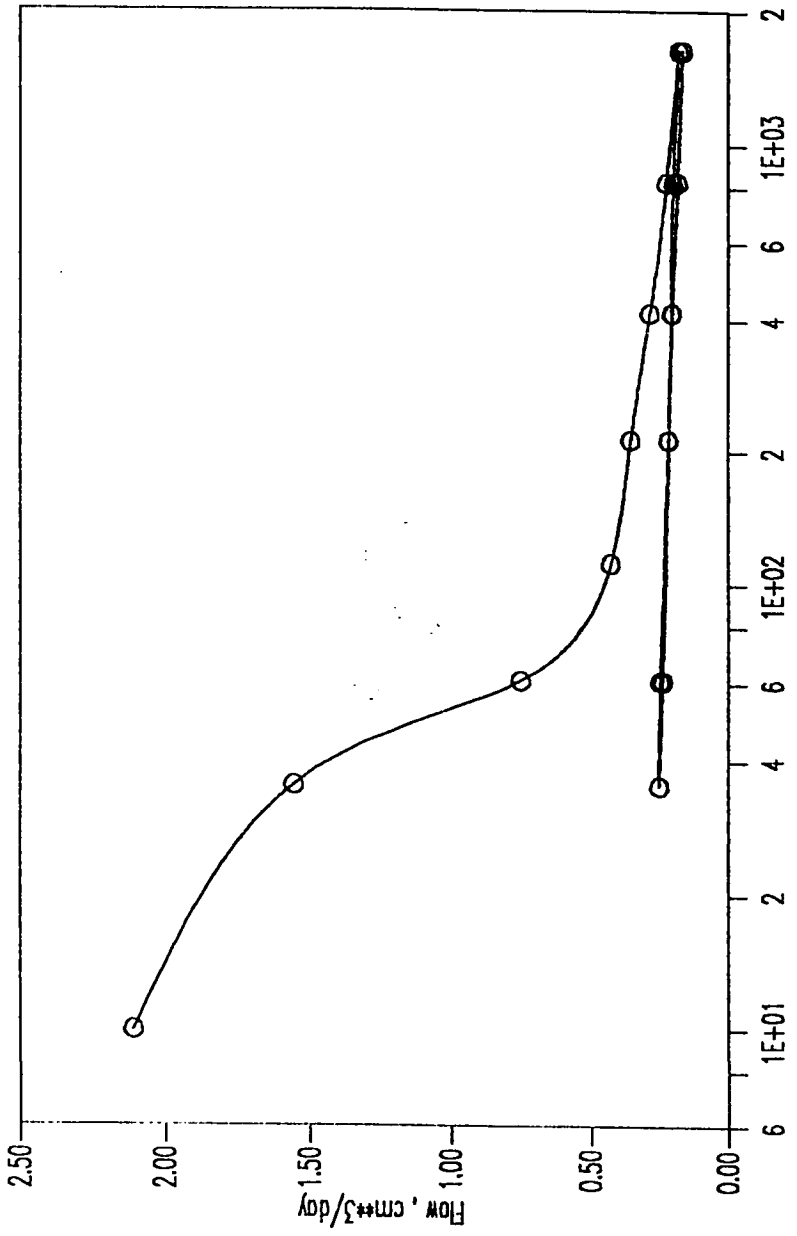

Figure 5.39 : Flow–Pressure Results (Series #4)

which the flow was reduced to 237 cm^3/day at a pressure of 1,635.9 kPa. This trend is very consistent with the preliminary test results reported in Fig. 5.29, in spite of the fact that in the present test only 9.9 kPa was initially applied while in the preliminary test a pressure (at the flow commencement) of 234 kPa was acting. Therefore, it can be concluded that flow was much more reduced during the early stages of water percolation through the specimen when two concomitant phenomena prevail: (i) the relatively high initial void ratio, and (ii) the significantly high salt dissolution. When the effect of these two factors diminished, the change in flow was ceased.

Results of chemical analysis of the percolating water are presented in Figs. 5.40 to 5.42. The concentration of Cl^-, SO_4^{--}, Na^+, Ca^{++} and Mg^{++} is shown in Fig. 5.40 as function of time, while Fig. 5.41 shows the conductivity of percolating water. Fig. 5.42 shows the change in concentration with pressure. Comparison of Figs. 5.40 and 5.33 reveals the following:

a) Calcium ion (Ca^{++}) shows the highest concentration in both Figures. Its concentration is about 3.5 to 5 times those of sodium (Na^+) and magnesium Mg^{++} ions. In Fig. 5.40, however, Ca^{++} reduced very significantly in the first 200 minutes in contrast to Fig. 5.33 where the cal-

cium was almost constant at about 1,500 ppm during the first four days. Also, in the first Figure, the initial concentration of Ca^{++} was 7,500 ppm (i.e. about five times the concentration in the second Figure).

b) The concentration of both Na^{+} and Mg^{++} in each of the two Figures did not vary significantly, although the initial concentration in Fig. 5.40 was 1,800 ppm on the average compared to only 190 ppm in Fig. 5.33. Again, the reduction of Na^{+} and Mg^{++} concentration occurred during the early period of water percolation. This trend was observed in both Figures.

c) The reduction in sulfate (SO_4^{--}) concentration with time (Fig. 5.40) followed exactly the same trend as other ions, i.e. most of the reduction in the concentration of all phases occurred within the first 250 minutes of water percolation.

d) The increased concentration of all phases in Fig. 5.40 reflects again the inhomogeneous nature of the sabkha soil.

It is worth mentioning again that only one day (1,440 minutes) was required to reduce the concentration of almost all phases

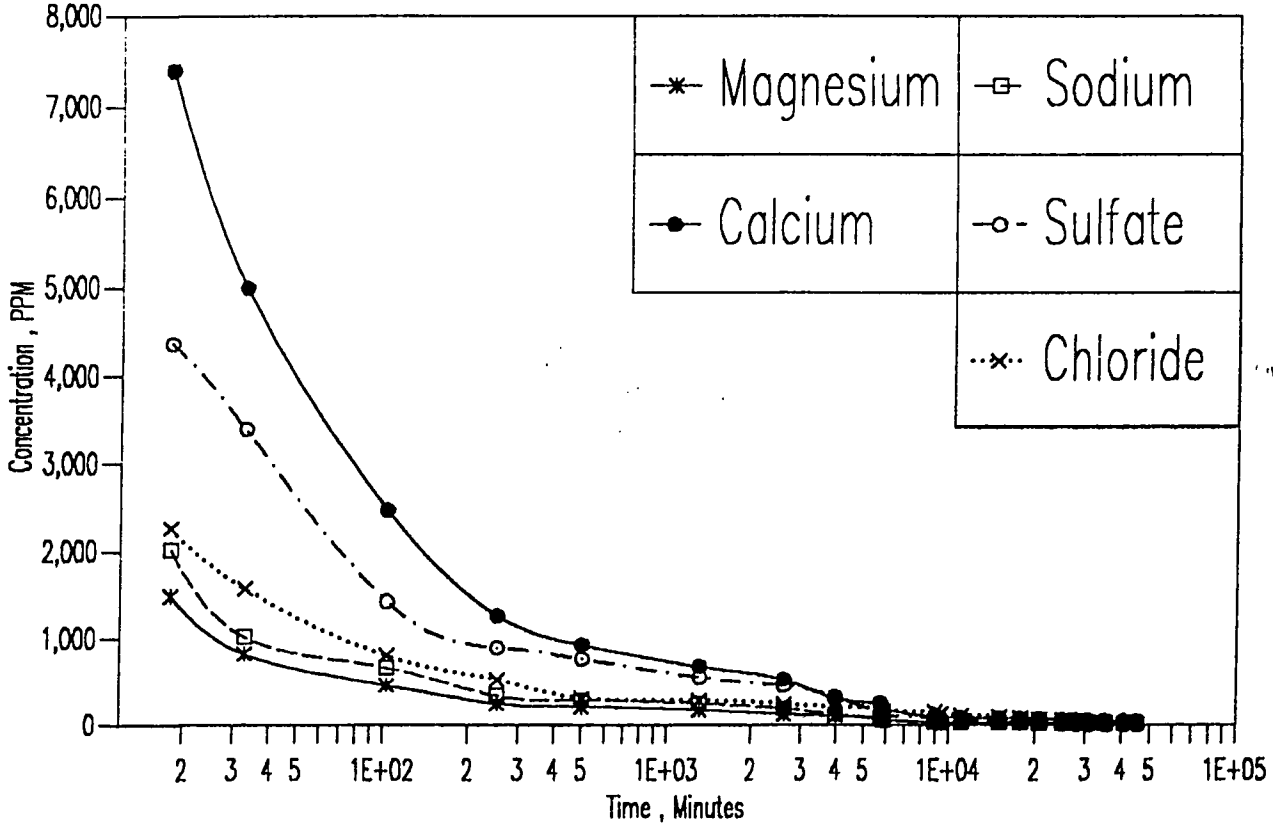

Figure 5.40 : Chemical Analysis of Percolating Water (Series #4)

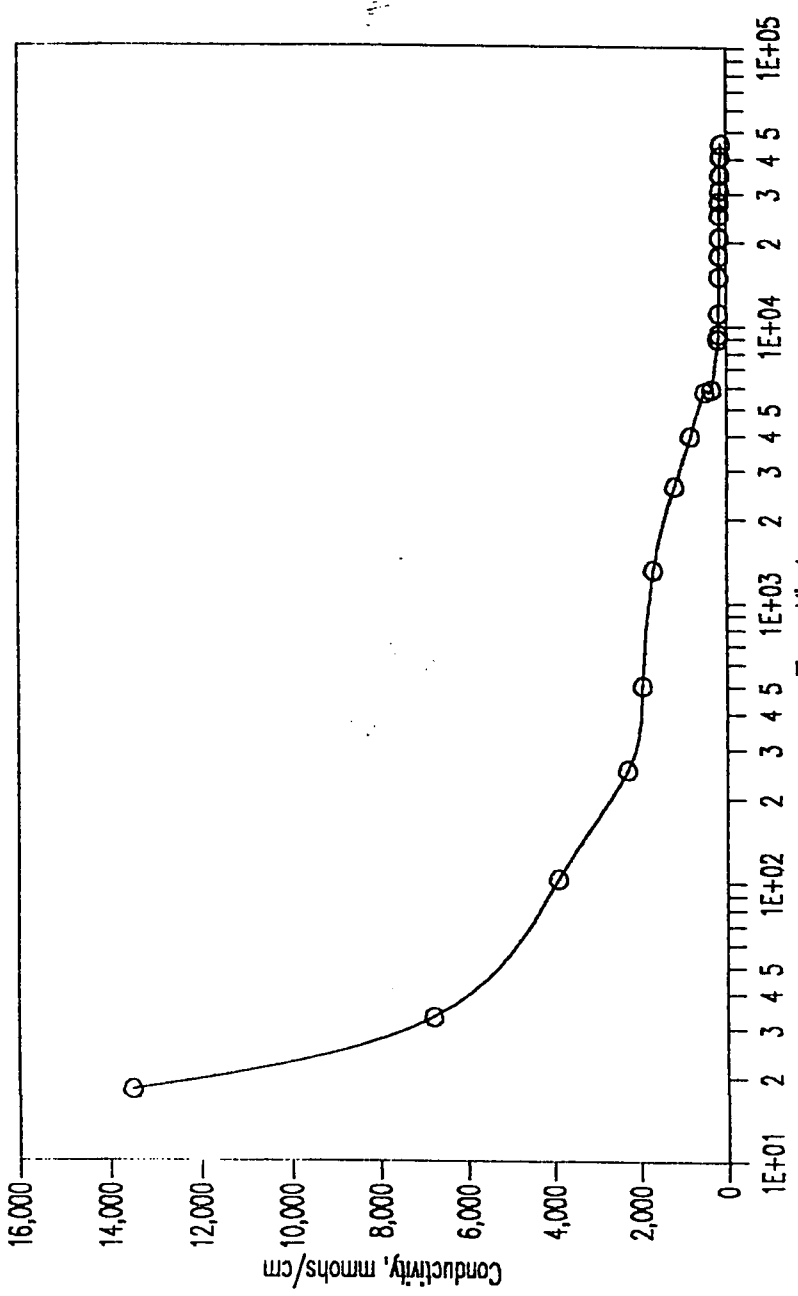

Figure 5.41 : Conductivity Test Results of Percolatig Water (Series #4)

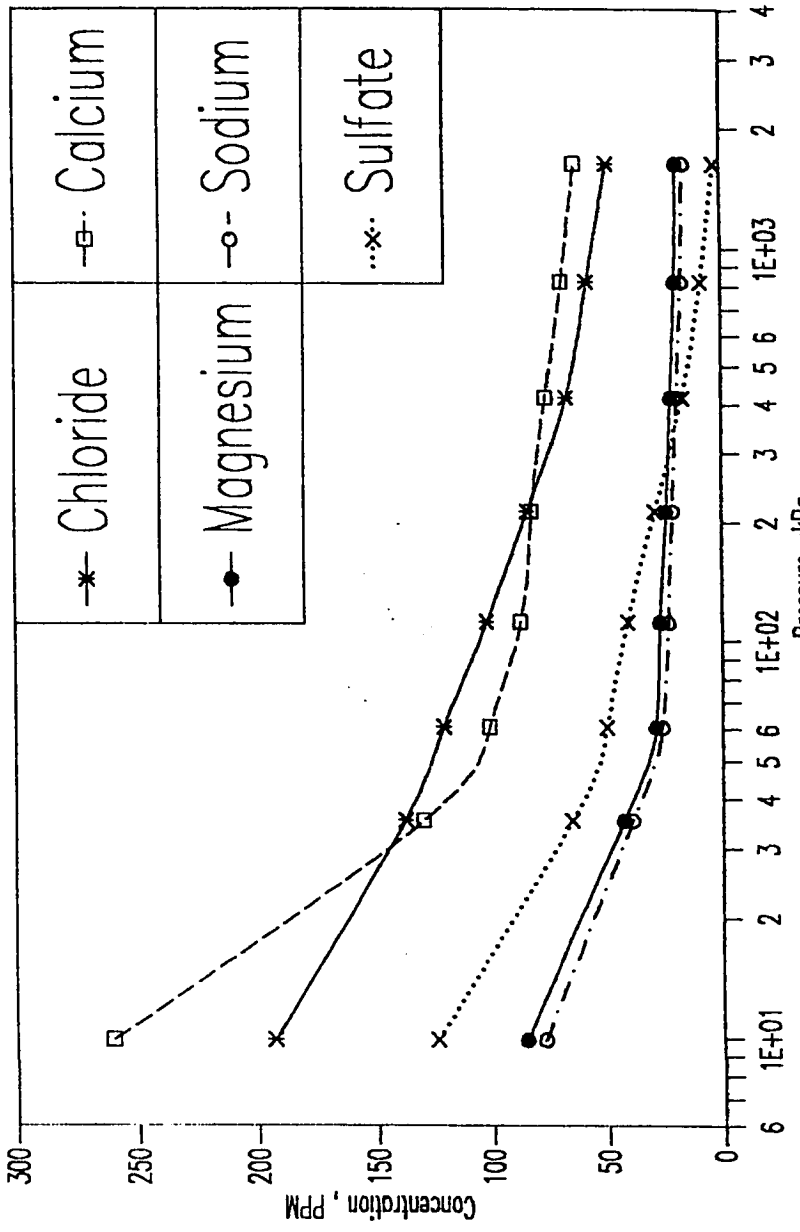

Figure 5.42 : Chemical Analysis–Pressure Test Results (Series #4)

to very small values compared to the initial concentrations. As mentioned previously, the enhanced dissolution of these phases upon commencement of water percolation is a distinct manifestation of the high collapse potential of sabkha.

The change in conductivity of percolating water with time is shown in Fig. 5.41, which is more or less similar to the data of chemical analysis. This behavior is identical to the results of the preliminary test.

Fig. 5.42 shows the change in concentration of the various ions with pressure, where again it could be seen that an increase in pressure from 9.9 kPa (i.e. the overburden pressure) to 35.3 kPa caused a significant reduction (i.e. about 40 to 50%) in the concentration of all ions. This performance validates the previous argument that collapse potential of Ras Al-Ghar sabkha is a consequence of salt dissolution.

5.4.7.2.3 Effect of Sabkha Brine on Collapse Potential

To further assess the collapse potential and its intimate relation to salt dissolution, a third test was conducted. This test was performed in an exactly similar way to the systematic one; however, sabkha brine was allowed to percolate in place of distilled water. The results of this test are presented in Figs. 5.43 through 5.47. In Fig. 5.43, the effect of pressure on void ratio was

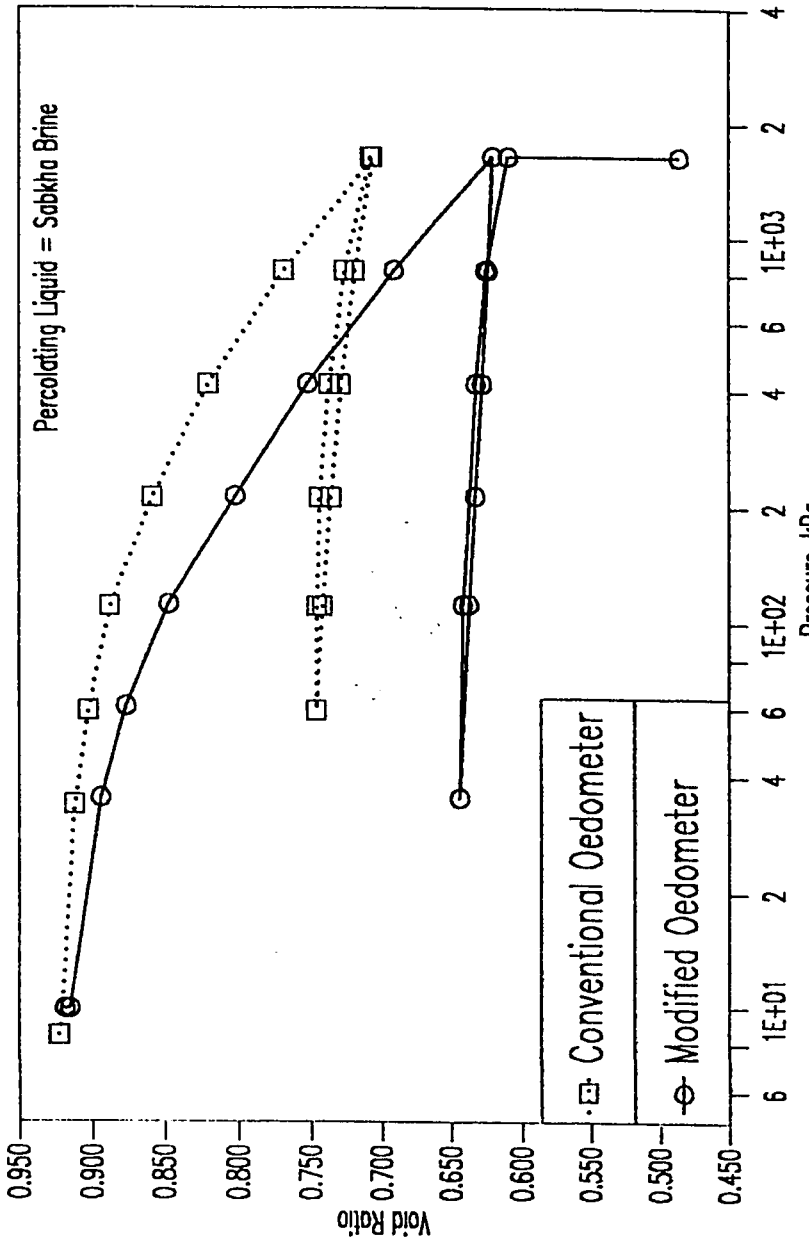

Figure 5.43 : Consolidation Test Results (Series #5)

observed to be similar to those of the conventional oedometers. The change in void ratio due to flooding with sabkha brine was almost negligible, as expected. What seems to be interesting is that percolation of sabkha brine through the specimen under the sustained overburden pressure for a period of about three days (i.e. similar to the previous test) did not almost bring about any reduction in void ratio. Therefore, it can be concluded that collapse potential occurs when water passes through sabkha. This means that it is the dissolution of salts, particularly that of sodium chloride, that causes the collapse potential of sabkha. Another interesting observation can also be inferred from Fig. 5.43. Despite the fact that collapse potential was almost absent in this test, the change of void ratio with pressure was observed to be more in the case of the modified oedometer than the conventional one. This finding confirms the previous deduction that soil grain adjustment was enhanced by the presence of the passing fluid and, therefore, the resultant of this adjustment under the consecutive increase in loading is a mere reduction in void ratio. A comparison of the two consolidation curves in Fig. 5.43 indicates that the total change in void ratio was 0.215 and 0.309 for the conventional and modified oedometers, respectively. It is thus clear that percolation of sabkha brine through the specimen caused soil grain adjustment, and not collapse, thereby resulting in progressive increase in void ratio reduction.

It is further interesting to note that both the compression and the swelling indices are not very much affected by the modified oedometer. The values of these indices are 0.18 and 0.018 for the modified oedometer compared to 0.19 and 0.020 for the conventional one. Again, the ratio of C'_c to C'_s is 10, indicating that these indices are: (i) not affected by either flooding or percolation, and (ii) not affected by the type of liquid, whether distilled water or sabkha brine.

Once the compressibility of the specimen was ceased at the last reloading pressure, sabkha brine was exchanged with distilled water. The latter was allowed to percolate for seven days in order to investigate the effect of distilled water percolation on the collapse potential of sabkha after a long period of brine percolation at a high pressure of 1,635.9 kPa. It is again interesting to note that a significant collapse occurred at this high pressure due to the conjoint effect salt dissolution and soil grain adjustment, as shown in Fig. 5.43. The reduction in void ratio due predominantly to percolation of water amounted to 0.123 which is equivalent to 13.4% and 22.0% of the original void ratio and of the void ratio just before collapse respectively. Again, the commencement of distilled water percolation at a high pressure although had a similar effect of salt dissolution in a similar way to any pressure, the soil grain adjustment was substantially enhanced thereby leading to more reduction in void ratio compared to lower pressures.

The change in flow with time for eight loading cycles is presented in Fig. 5.44. The trend of these curves was indeed exactly similar to those curves for the distilled water (Fig. 5.36), irrespective of absolute values of flow.

Regarding the absolute values of flow, there are many interactive factors that may affect this parameter; the most important is the inhomogeneity of the sabkha. Therefore, ***any comparison between the absolute values of properties of sabkha specimens should pay special consideration to the fact that the variability of sabkha may sometimes outweigh the small variation in the response of a sabkha sample to a test.*** Comparison of Figs. 5.36 and 5.44 indicates that the flow was more when distilled water was used during the first two loading cycles (i.e. 9.9 and 35.3 kPa). Moreover, the decrease in flow with time for each loading was more pronounced when distilled water was used.

The response of flow due to unloading pressures is shown in Fig. 5.45. Again, the trend is more or less similar to that of distilled water except the range of variation here was relatively smaller. This might be attributed to salt precipitation in the tested specimen. This point would be much appreciated if it were known that sabkha brine was percolating through the specimen for more than 15 days before the first unloading pressure was commenced. Salt precipitation was observed over the whole oedometer cell for both the conventional and modified oedometers. For the

latter, this salt could have significant effect on the percolation. This was also the reason for the inconsistency of results during reloading cycles presented in Fig. 5.46.

The change in flow of sabkha brine with pressure is shown in Fig. 5.47. It is clear from this Figure that as the acting pressure increases the flow will decrease. This was attributed to soil grain adjustment, as discussed before. It is also clear that the change in flow during the first loading cycle (from a pressure of 9.9 kPa to 35.3 kPa) was more significant than that during the other loading cycles because the specimen was initially porous and permeable and therefore the passage of sabkha brine enhanced the movement of soil grains to achieve in a rather denser state that led to a significant reduction in flow.

Comparison of Fig. 5.47 with Fig. 5.41 indicates that the response of the consolidating specimen to the percolation of sabkha brine is completely different from that due to the percolation of distilled water, particularly at the early stages of flow. Brine caused only soil grain adjustment, and this is why the change in flow with pressure was almost linear during the loading cycles. Water, on the other hand, signified the conjoint effect of soil grain adjustment and salt dissolution and this is why the reduction in flow was very significant during the first three loading cycles. This again confirms the previous findings that ***the collapse potential is uniquely attributed to salt dissolution, while the reduction***

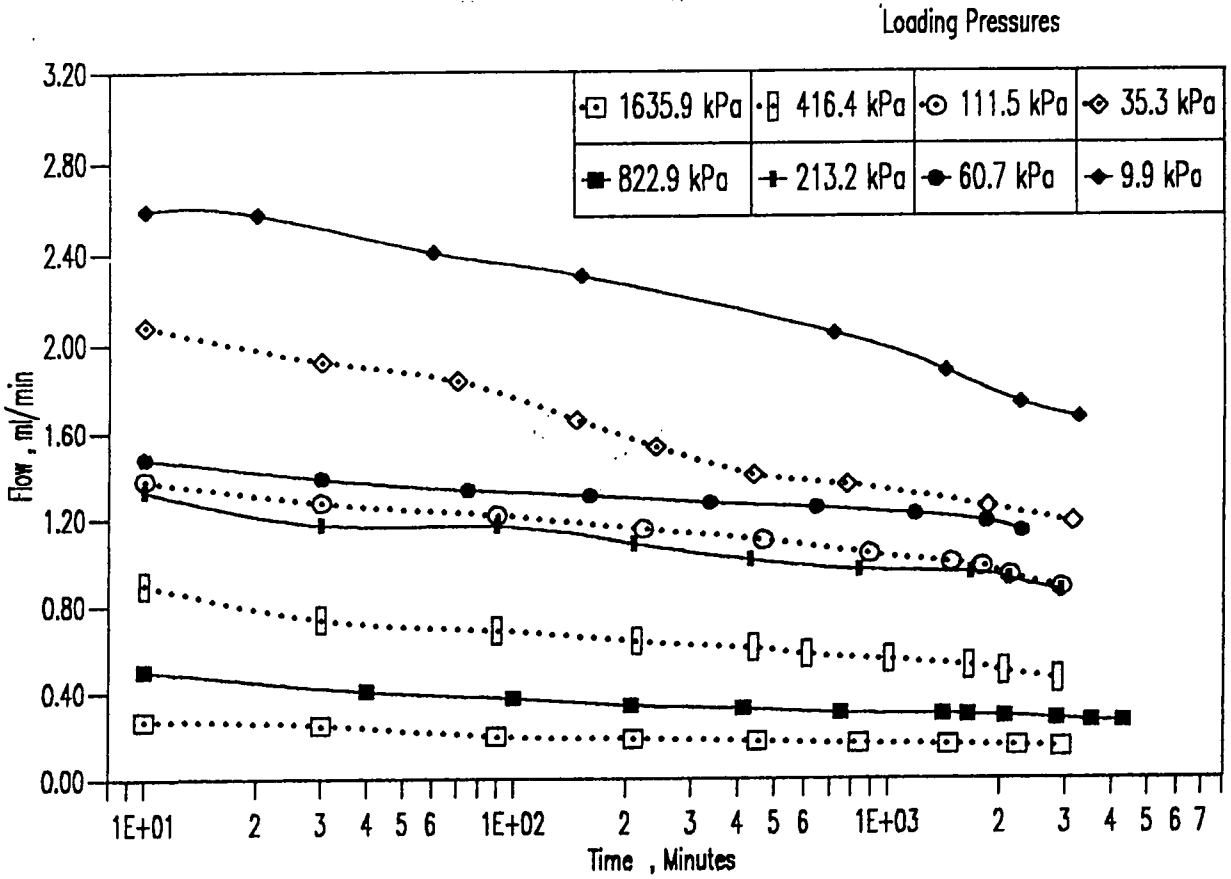

Figure 5.44 : Time–Flow Data for the Loading Cycles (Series #5)

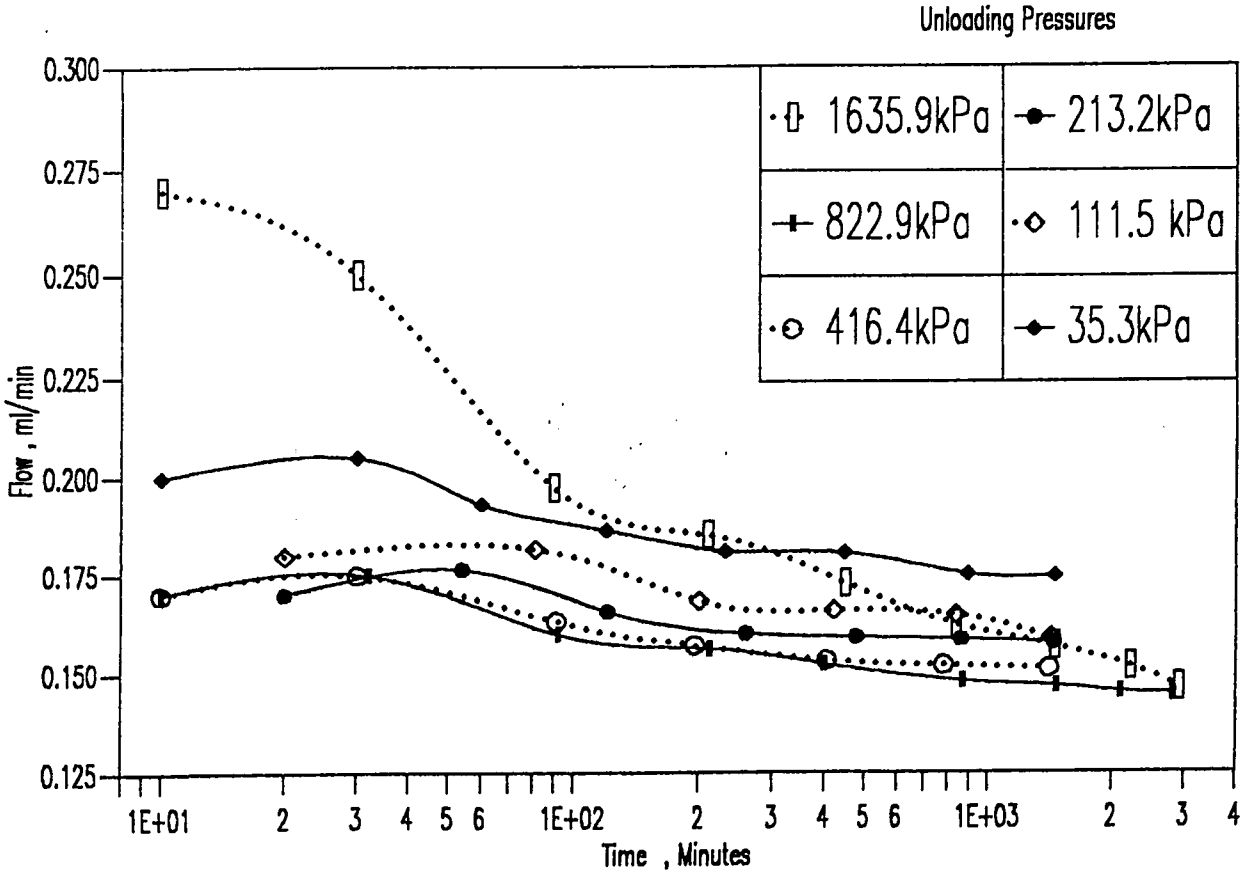

Figure 5.45 : Time–Flow Data for the Unloading Cycles (Series #5)

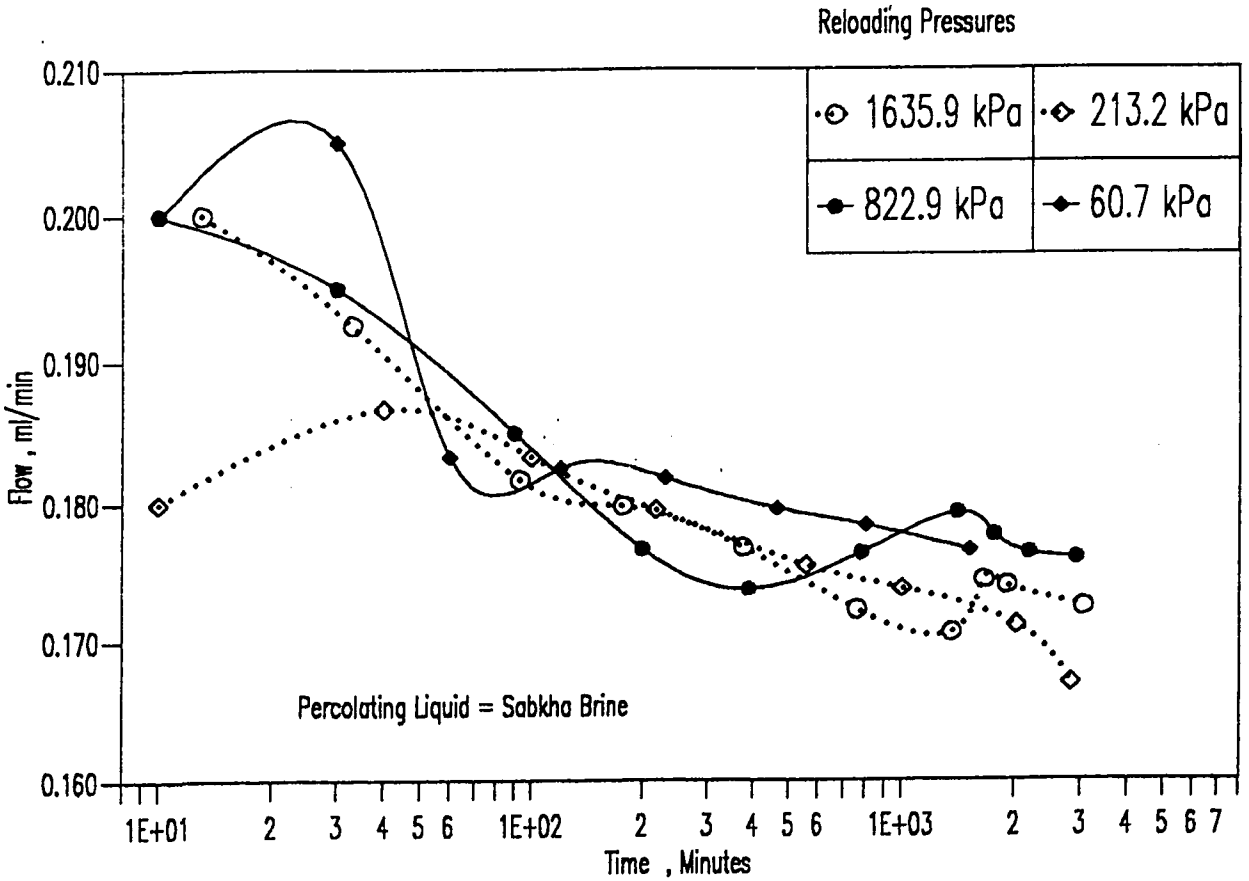

Figure 5.46 : Time–Flow Data for the Reloading Cycle (Series #5)

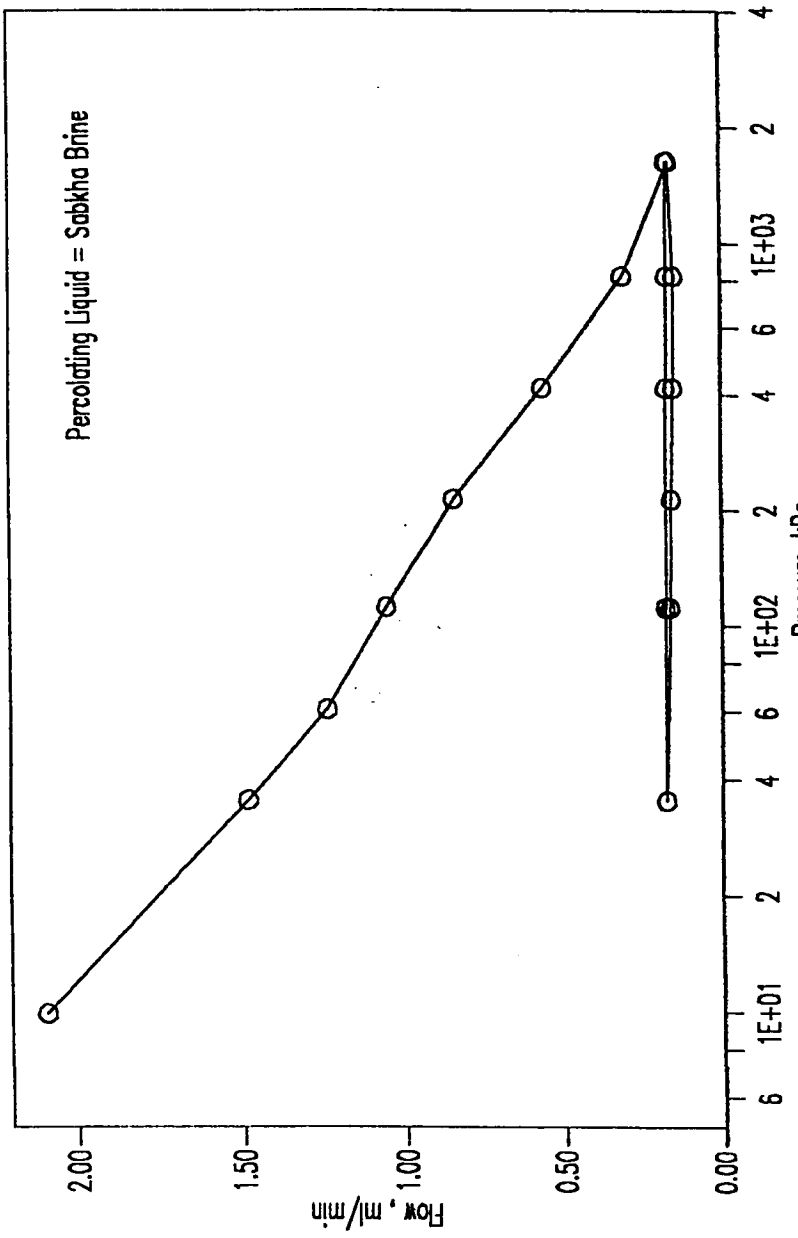

Figure 5.47 : Flow–Pressure Results (Series #5)

in flow and the enhanced reduction in void ratio is attributed to both salt dissolution and soil grain adjustment. As mentioned earlier, the percolation of distilled water after the termination of the present test at a pressure of 1,635.4 kPa resulted in a considerable collapse potential, as shown in Fig. 5.43. The change in flow is presented in Fig. 5.48 where it could be observed that the flow was increased from 0.26 ml/min at the commencement of distilled water percolation to 0.35 ml/min at 156 minutes and to 0.63 ml/min at 971 minutes and continued to increase until the end of the test. Most of the increase in flow took place during the period between 156 and 971 minutes which means that salt dissolution requires sufficient time (i.e. and sufficient volume of distilled water) to make the dissolution process efficient. Again, the reduction in flow after about 3,800 minutes was only marginal. This is because a major portion of the salt had already dissolved.

Collapsible soils are generally characterized by *sudden* and rather large volume decrease at usually constant stress when exposed to water (200). Accordingly, collapse potential can be detected at the flooding stage when the prescribed pressure is sustained in the consolidation test. Regarding the measurement of collapse potential, and apart from the difference in stress level at which flooding of distilled water is commenced, there are basically two criteria to evaluate the collapse potential (200):

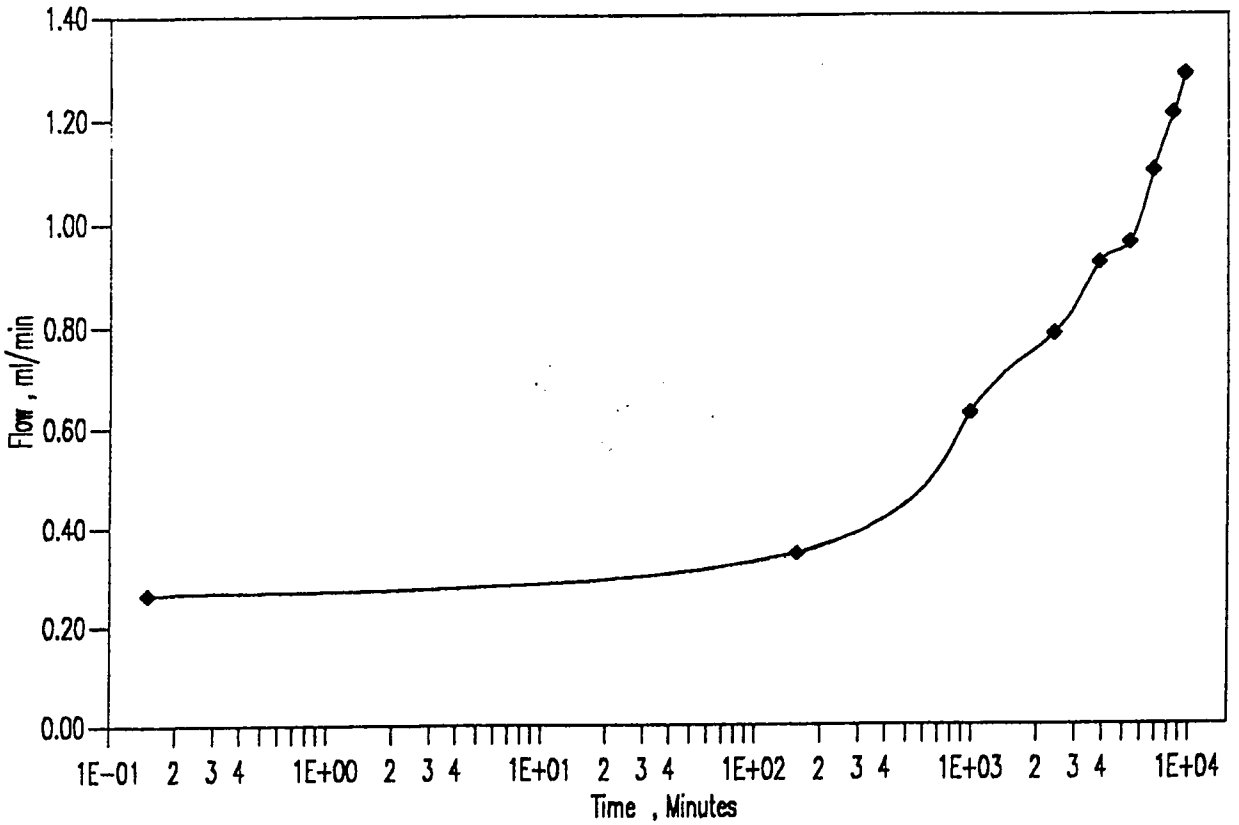

Figure 5.48 : Effect of Distilled Water Percolation on the Rate of Flow (Series #5)

$$i_{c1} = \left(\frac{\Delta e_c}{1 + e_1} \right) \times 100 \qquad (5.2)$$

and

$$i_{c2} = \left(\frac{\Delta e_c}{1 + e_o} \right) \times 100 \qquad (5.3)$$

where: i_{c1} = collapse potential (1),

i_{c2} = collapse potential (2),

Δe_c = reduction in void ratio upon wetting,

e_1 = void ratio at beginning of saturation, and

e_o = initial void ratio.

A summary of the three series of consolidation tests is shown in Table 5.14, where Series 3 represents the preliminary test and Series 4 represents the systematic test in which distilled water was used, while Series 5 represents the test in which sabkha brine was used. All tests were presented with their companion specimens that were tested using the conventional oedometer. In Table 5.14, the change in void ratio due to flooding was observed not to vary very much for both conventional and modified oedometers, a behavior that is similar to the data reported in Table 5.13 using the conventional oedometer. The total change in

Table 5.14 : Summary of Modified Oedometer Test Results (Series #3, #4 and #5)

Test Characteristics	Series #3 (Preliminary)		Series #4 (Systematic)		Series #5	
	Conventional	Modified	Conventional	Modified	Conventional	Modified
Initial Void Ratio	0.930	0.952	0.883	0.913	0.923	0.919
Change in Void Ratio due to Flooding	0.006	0.008	0.006	0.006	0.001	0.001
Void Ratio at Commencement of percolation	--	0.784	--	0.907	--	0.908
Change in Void Ratio due to Percolation	--	0.087	--	0.032	--	0.003
Final Void Ratio	0.628	0.494	0.630	0.514	0.708	0.610
Total Change in Void Ratio	0.302	0.458	0.253	0.399	0.215	0.309
Change in Moisture Content, (%)	0.0	+0.5	+2.1	+2.2	-0.1	+0.4*
Change in Wet Weight of Soil, (%)	-4.2	-13.2	-4.4	-12.8	+5.8	+12.8*
C'_c	0.18	0.19	0.16	0.18	0.19	0.20
C'_s	0.017	0.017	0.019	0.016	0.020	0.016
Collapse Potential(1)	--	4.9%	--	1.7%	--	0.2%
Collapse Potential(2)	--	4.5%	--	1.7%	--	0.2%

* Estimated

void ratio during the full test, which indicates the collapse potential as discussed previously, shows much variation between the two oedometers. The modified oedometer was observed to enhance significantly the reduction in void ratio, even when sabkha brine was used as the percolating liquid. The change in moisture content was not significantly affected by the percolation of water; the reason was primarily attributed to the high natural moisture content of sabkha. Another variation between the two oedometers was the change in wet weight of the sample during the consolidation test, which is defined as:

$$\text{Change in wet weight (\%)} = \left(\frac{x - y}{y}\right) \times 100 \qquad (5.4)$$

where x = final wet weight of sample, gm

y = initial wet weight of sample, gm

An average reduction in wet weight of 13.0% for the modified oedometer samples compared to only 4.3% for the conventional oedometer samples is indicative of the significant salt dissolution that was mainly attributed to distilled water percolation. The situation was different for the case when sabkha brine was used. The increase in weight was perceptibly attributed to salt precipitation. Finally, both the compression and swelling indices (C'_c and C'_s respectively) were not influenced by liquid percolation, as observed previously (Table 5.13). According to the compression

and swelling indices values, it can be concluded therefore that Ras Al-Ghar sabkha has low compressibility.

The data in Table 5.14 pertinent to collapse potential (1) and collapse potential (2) (Eqns. 5.2 and 5.3, respectively) indicate that there is, at least for the Ras Al-Ghar sabkha samples, no noticeable difference between the two criteria and, therefore, any of them can be representative of the other. The sabkha sample tested in Series #3 (the preliminary test) showed a much higher collapse potential compared to the one tested in the systematic series; a collapse potential of 4.7% for the former and only 1.7% for the the sample tested in Series #4, which is solely indicative of the significant effect of the sustained pressure at which percolation of water took place. The collapse potential for the sample tested in Series #5 is only 0.2% which clarifies the significant role of salt dissolution. Comparison of the collapse potential in Series #3 and #4 (Table 5.14) indicates that an appropriate pressure should be chosen in evaluating the collapse potential. A further comment is that a collapse potential of 4.7% might be thought as a quantitatively low value compared to the Knight's correlation reported earlier; despite the fact that both are a measure for the same collapse potential. Therefore, there is an urgent need for the development of such a criterion as that reported by Knight for the case of collapse potential (1) or (2) {i.e. Eqns. 5.2 and 5.3}, as recommended by Lutenegger and Saber (200), in order to assess and

compare the collapse potential of different soils under some specific conditions.

An eventual comment is related to the definition of collapsible soils and its intimate relationship with the sudden and large volume decrease upon saturation. The volume change comes about via a large scale particle re-arrangement in the initial soil structure that consists of bulky-sized particles (sand and silt particles) which are weakly bonded by clays, silts or water in a relatively unstable manner (202,203). For the case of a typical saline soil, such as sabkha, the collapse occurs primarily due to dissolution of soluble salts; mainly sodium chloride. The collapse of sabkha, therefore, does not occur suddenly but requires relatively long time as well as continuous percolation of water to dissolve the salty matrix of sabkha soils. This could be the main reason for the inability of conventional oedometers to detect the collapse potential of such a soil.

5.4.8 Unconfined Compression Test Results

Three unconfined compression tests were conducted on undisturbed sabkha samples. Results are presented in Fig. 5.49 and show that the surficial natural sabkha has very low strength of 14.9, 19.9 and 22.0 kPa with an average of 18.6 kPa (2.7 psi). These results confirm the low relative field density results presented in Section 5.4.6 and the spongy behavior of the sabkha soil

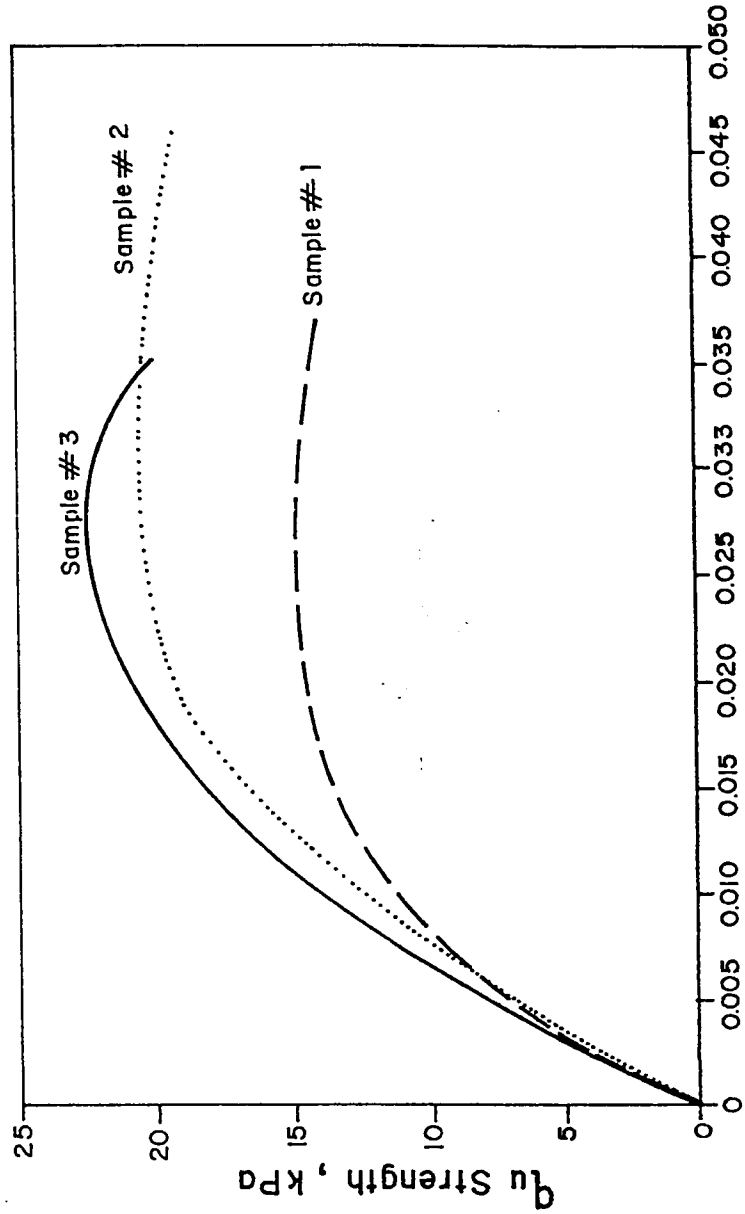

Fig. 5.49 : Unconfined Compressive Strength Test Results for the Undisturbed Sabkha Samples.

on the wet side of the optimum moisture content.

In an attempt to evaluate improvement that could be attained by compacting sabkha, two series of samples were prepared in the laboratory at different moisture contents and subjected to an unconfined compression (q_u) test using both distilled water and sabkha brine as lubricating liquids. Fig. 5.50 shows results of these two series which leads to the fact that compaction of sabkha can increase its strength by as much as 370% if distilled water is used and 550% for the case of sabkha brine. Furthermore, Fig. 5.50 indicates a fundamental difference between water and sabkha brine in terms of the strength achieved and the optimum moisture content at which the strength is maximum. The use of distilled water resulted in a maximum unconfined strength (q_u) of about 70 kPa at a moisture content of 7.1% compared to a maximum q_u of 103 kPa at a moisture of 6.4% for the case of sabkha brine. This difference in performance can be attributed to the excessively high salt content in the brine that enhanced the cementation between the sabkha particles. Another observation can also be deduced from Fig. 5.50 is the difference in optimum moisture content as determined from strength and compaction tests; the latter was evaluated by the standard Proctor test. From strength perspective, the moisture content should be around 7% while it should be around 10-11% from density point of view. This could

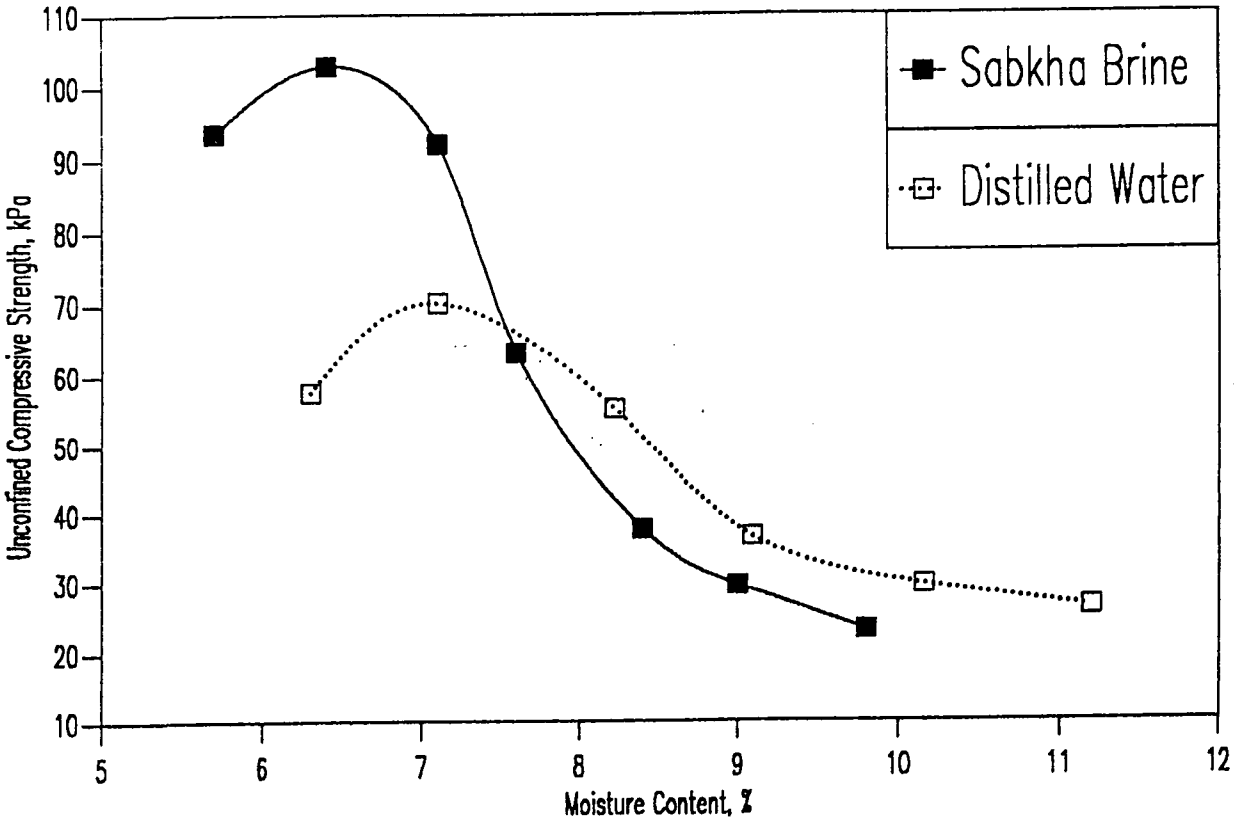

Fig. 5.50 : Effect of Moisture Content on Unconfined Compresssive Strength of Compacted Sabkha

be the reason for the spongy characteristics that sabkha displayed when it was compacted at w_{opt}.

Although the use of sabkha brine has brought about a significant increase in strength, it might cause problematic consequences such as enhanced susceptibility to collapse upon flooding. Therefore, further research should be conducted in this regard.

5.4.9 Direct Shear Test Results

Results of direct shear tests are presented in two parts as shown in Figs. 5.51 and 5.52. Fig. 5.51 shows the horizontal displacement-shear stress relationship, while Fig. 5.52 shows the best fit using the Mohr-Coulomb envelope for the normal stress and maximum shear stress data. In the former part, the shape of the curves are shown to be for typical loose soils; the only exception is for the largest normal load, which is similar to those of dense soils. The Mohr-Coulomb envelope, shown Fig. 5.52, yielded an angle of internal friction (φ') of 36° and a cohesion intercept (c') of 50 kPa (i.e. 7 psi). Although the value of φ' is within those reported for sands (171), it is much more than those reported by Abu-Taleb and Egeli (65) for Eastern Saudi sabkhas (φ' = 0 to 22°), however, the methodology by which those values were determined was not reported. The values of c', nevertheless, was on the upper range of the values reported in Table 2.4.

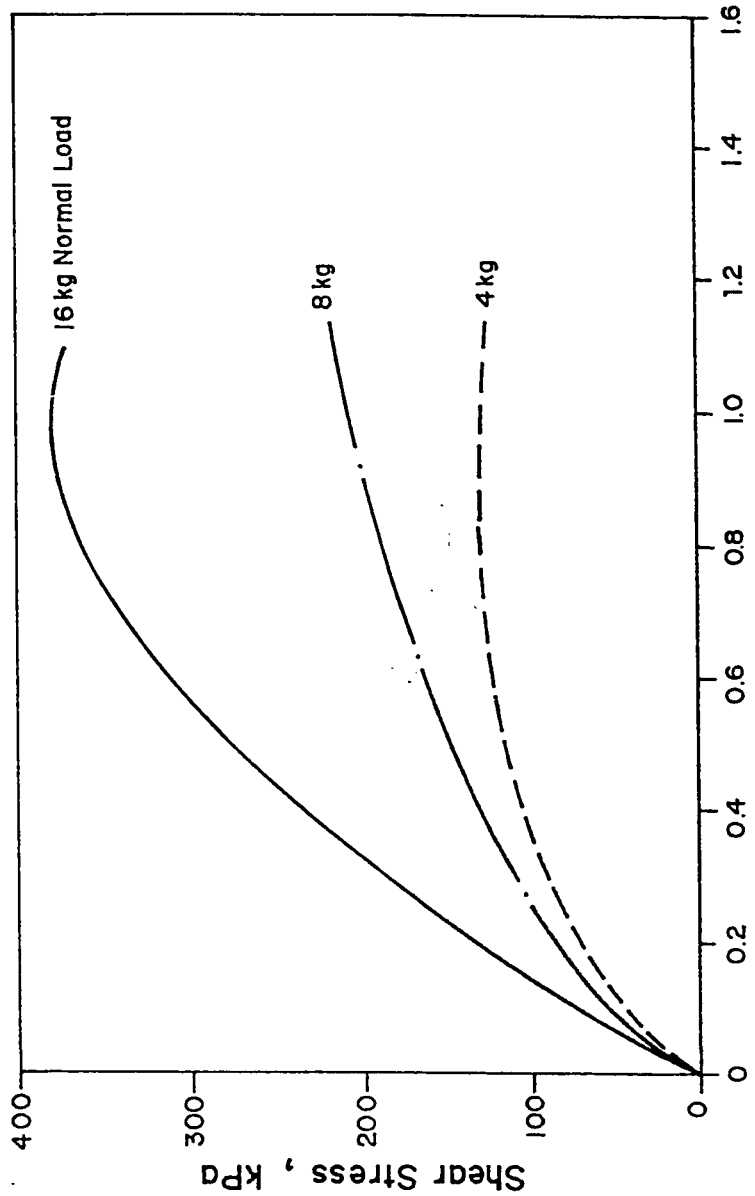

Fig. 5.51 : Shear Stress-Horizontal Displacement Data for the Direct Shear Test.

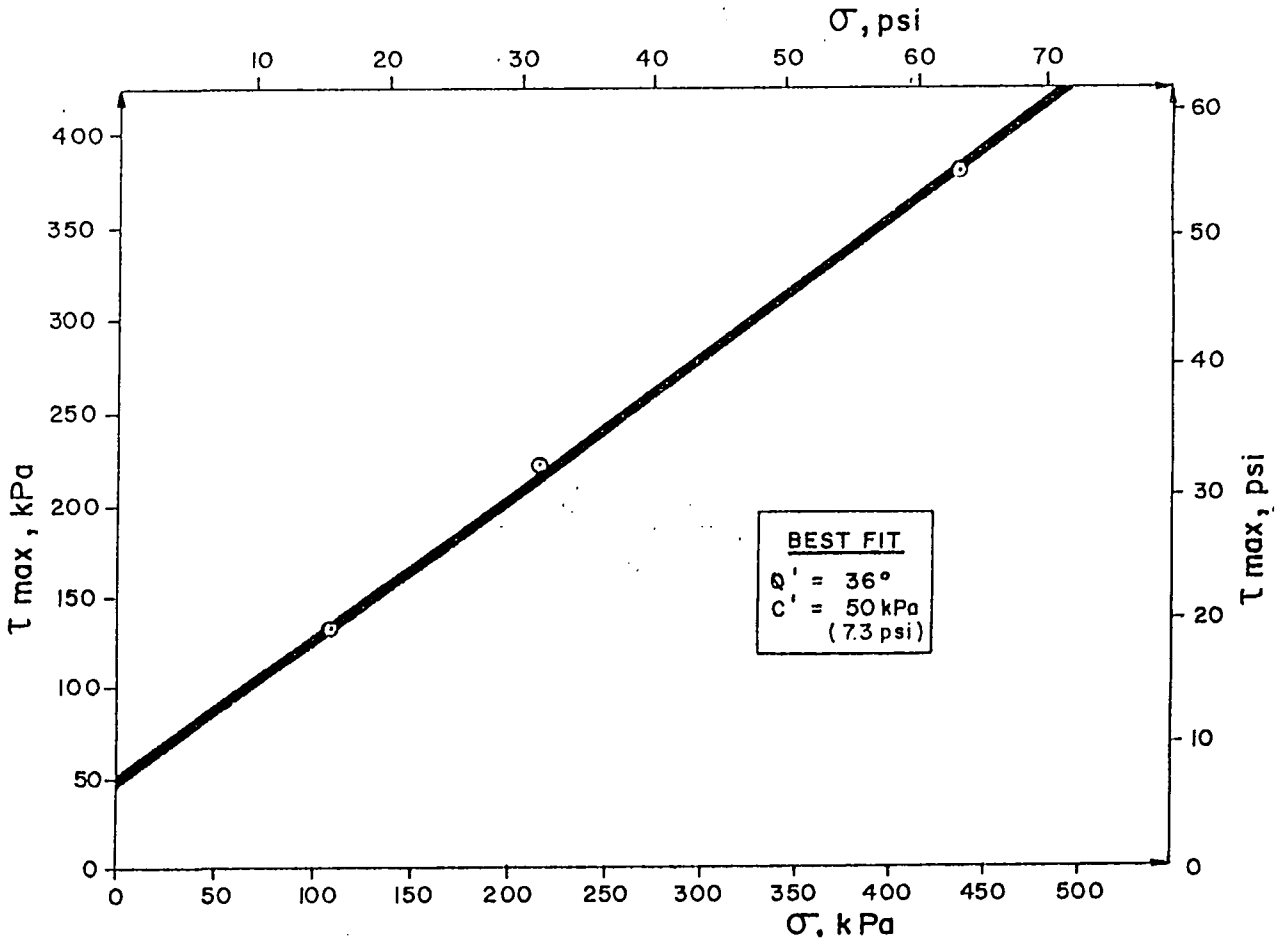

Fig. 5.52 : Mohr-Coulomb Failure Envelope for the Direct Shear Test.

5.4.10 Triaxial Test Results

Results of the consolidated-drained triaxial tests are shown in Figs. 5.53 and 5.54. Stress-strain data are shown in Fig. 5.53, where it is visible that some of the specimens did not respond very well. It is well-known that as the confining pressure increases the deviatoric stress should accordingly increase. The specimen that was subjected to 20 psi confining pressure showed almost the same deviatoric stress as the one subjected to 15 psi. This could be attributed to the variability of the sabkha soil; where the presence of diagenetic minerals could lead to significant reduction in strength. Plate 5.1 shows the presence of white material, probably gypsum, which was very soft. The Mohr-Coulomb failure envelope, therefore, could not pass tangentially through all the circles; nevertheless, the best fit seems to be quite representative to all specimens, as shown in Fig. 5.54.

In other triaxial tests, specimens were saturated with the minimum amount of either distilled water or sabkha brine, as stated previously in Sec. 4.3.11, in order to preserve the initial fabric of the specimens. Results of the CD triaxial tests in which the specimens were initially saturated with distilled water are shown in Figs. 5.55, 5.56 and 5.57, while those saturated with sabkha brine are shown in Figs. 5.58, 5.59 and 5.60. Similarly, results of the CU triaxial tests in which specimens were saturated with distilled water are shown in Figs. 5.61, 5.62 and 5.63, while those satu-

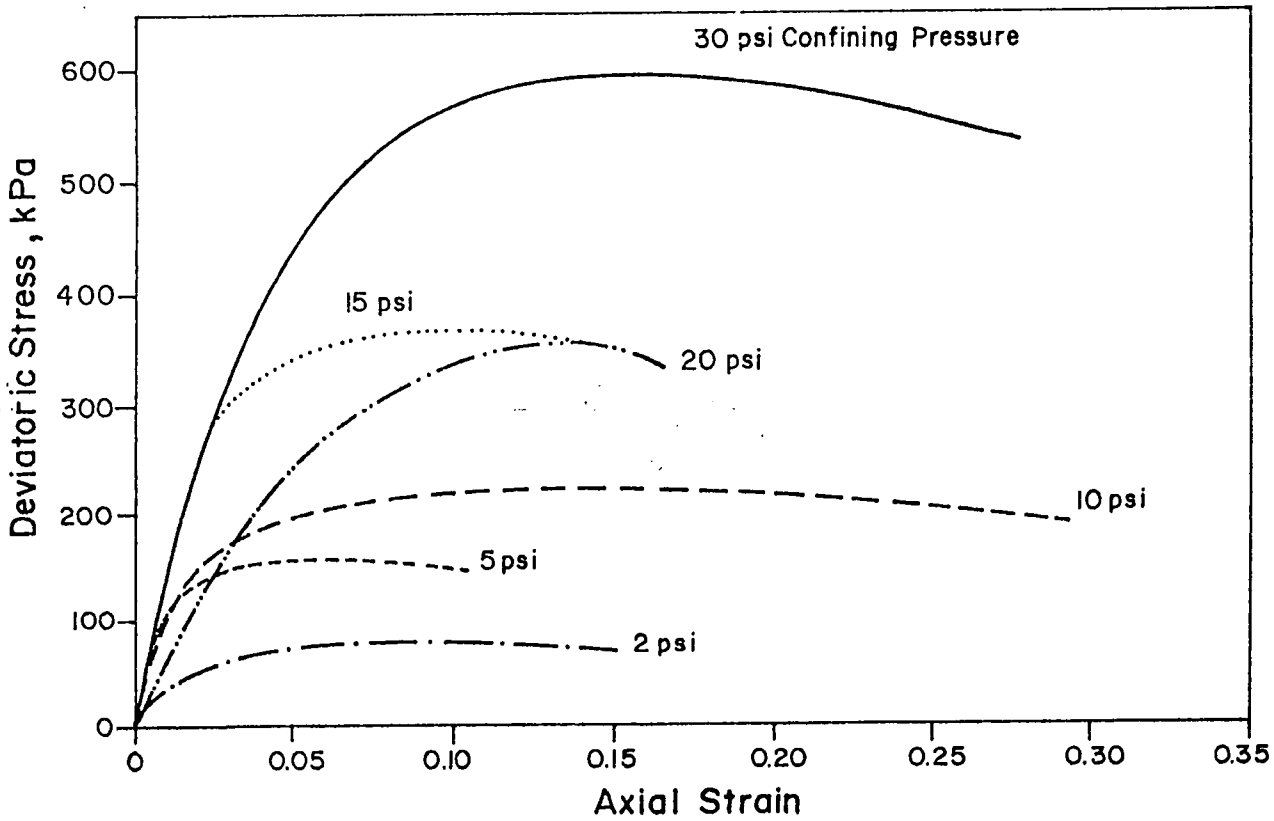

Fig. 5.53 : Stress-Strain Data for the CD Triaxial Test without Volume Change Measurements.

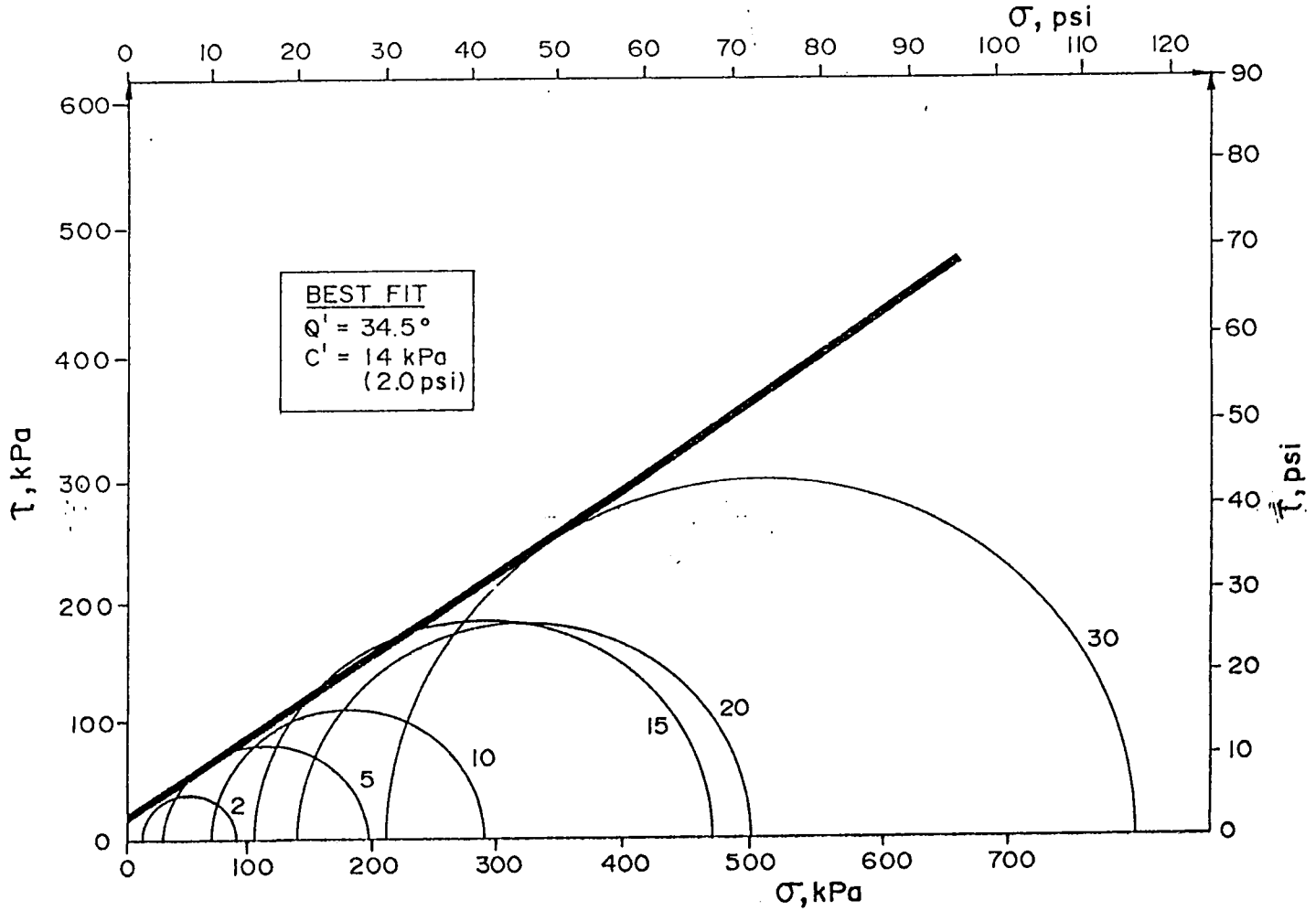

Fig. 5.54 : Mohr-Coulomb Failure Envelope for the CD Triaxial Test without Volume Change Measurements.

rated with sabkha brine are shown in Figs. 5.64, 5.65 and 5.66.

Since the ultimate findings of any triaxial test is to determine the effective and total angle of friction as well as the effective and total cohesion (φ', φ, c' and c, respectively), results of all triaxial tests conducted in this investigation are therefore summarized and presented in terms of these parameters, as shown in Table 5.15. These results reveal the following:

(i) All tests, with the exception of CD one in which the specimens were initially saturated with distilled water, have the same φ' (approximately 34°), while c' values varied from 0 to 34.5 kPa. Moreover, the φ value is also the same for all CU tests whether saturated with distilled water or sabkha brine (24° and 25°). Again, the value of c varied from 3 to 12 kPa.

(ii) Comparison of the three CD tests indicates that only the one in which the specimens were saturated with distilled water and for which volume change measurements were taken showed a reduced φ' compared with the other two CD tests (29° compared with 34° and 34.5°), despite the fact that the magnitude of volume change was negligibly small, as shown in Figs. 5.56 and 5.59 for both distilled water and sabkha brine, respectively. The variation in c' is again similar to

observation (i).

(iii) The reason behind the reduction in φ' due to saturation with distilled water and volume change measurement was primarily attributed to salt dissolution in spite of the small volume change that was allowed to take place. The small amount of distilled water expelled out during deviatoric loading was apparently sufficient to dissolve some salt which altered the initial cemented fabric of the sabkha and, consequently, led to 5° reduction in φ'. This hypothesis is supported by both results of either the CD tests in which no saturation took place or the CU tests in which the specimens were saturated with distilled water. For the latter, prevention of distilled water expulsion during deviatoric stress application did not cause any reduction in φ'.

(iv) The variation of both c' and c values is rather surprising in spite of the fact that φ' and φ showed high degree of consistency. This might be attributed to the initially heterogeneous fabric of these surficial sabkha samples. These samples were generally highly cemented and desiccated, as observed in Sec. 5.4.7, and these characteristics were more reflected by variation in the cohesion than in the angle of internal

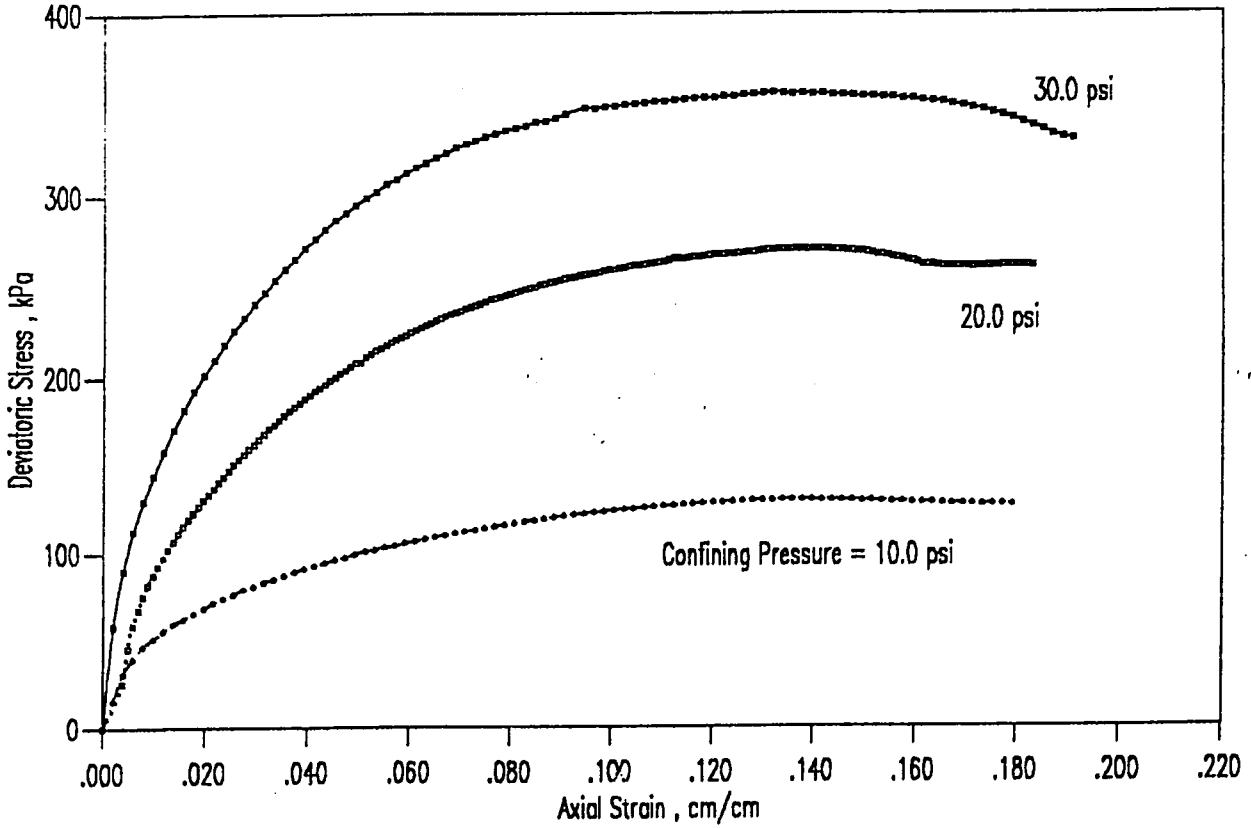

Fig. 5.55 : Stress–Strain Data for the CD Triaxial Test Saturated with Distilled Water

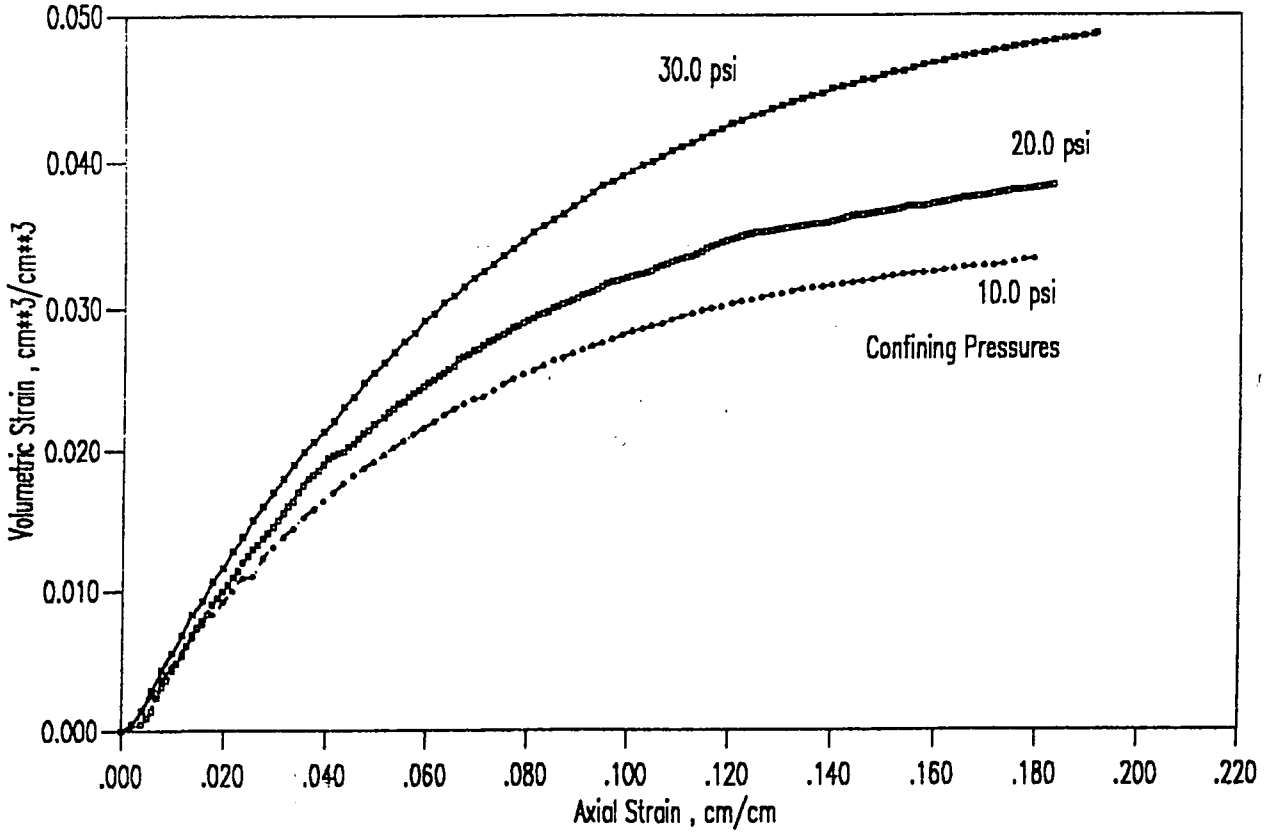

Fig. 5.56 : Volumetric Change Measurement for the CD Triaxial Test Saturated with Distilled Water

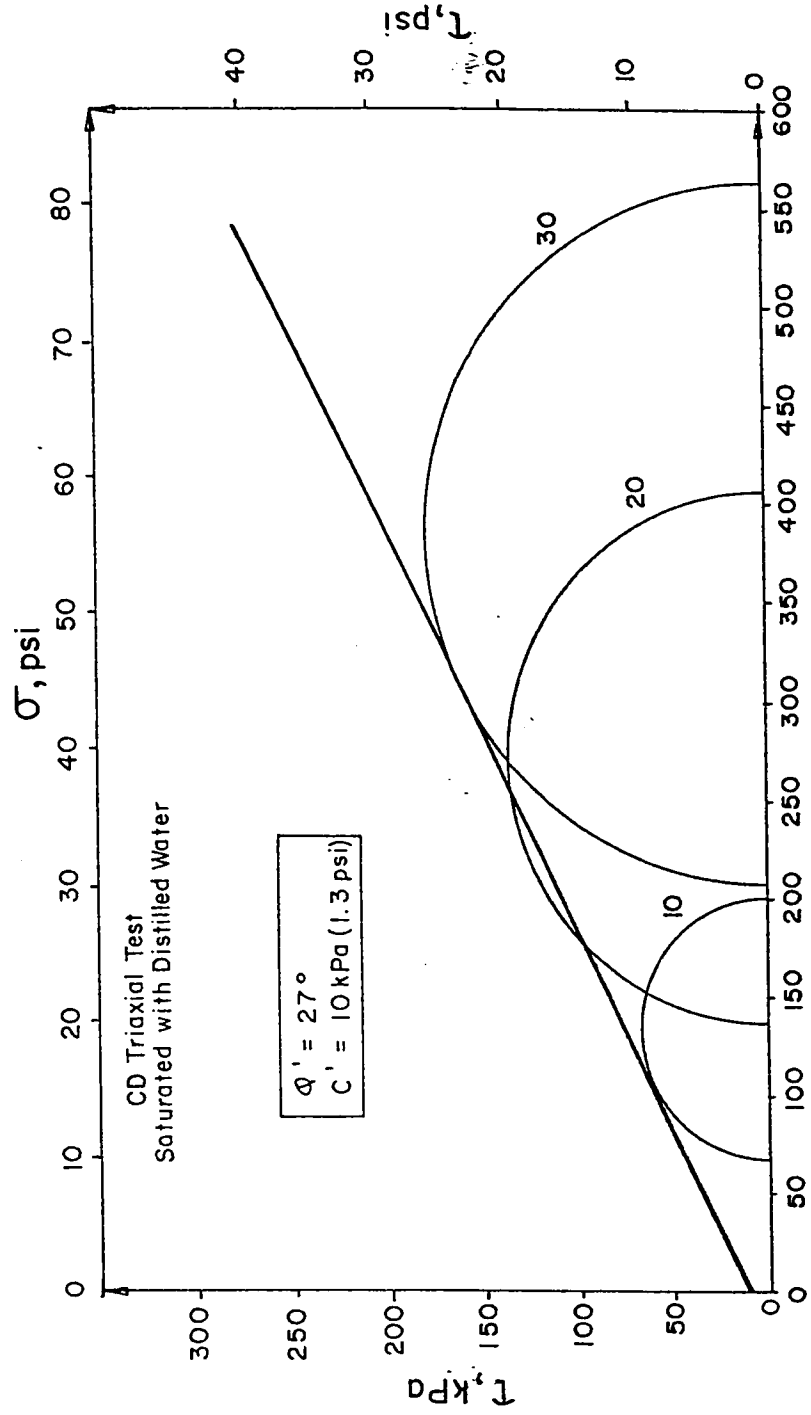

Fig. 5.57 : Mohr-Coloumb Failure Envelope for the CD Triaxial Test Saturated with Distilled Water.

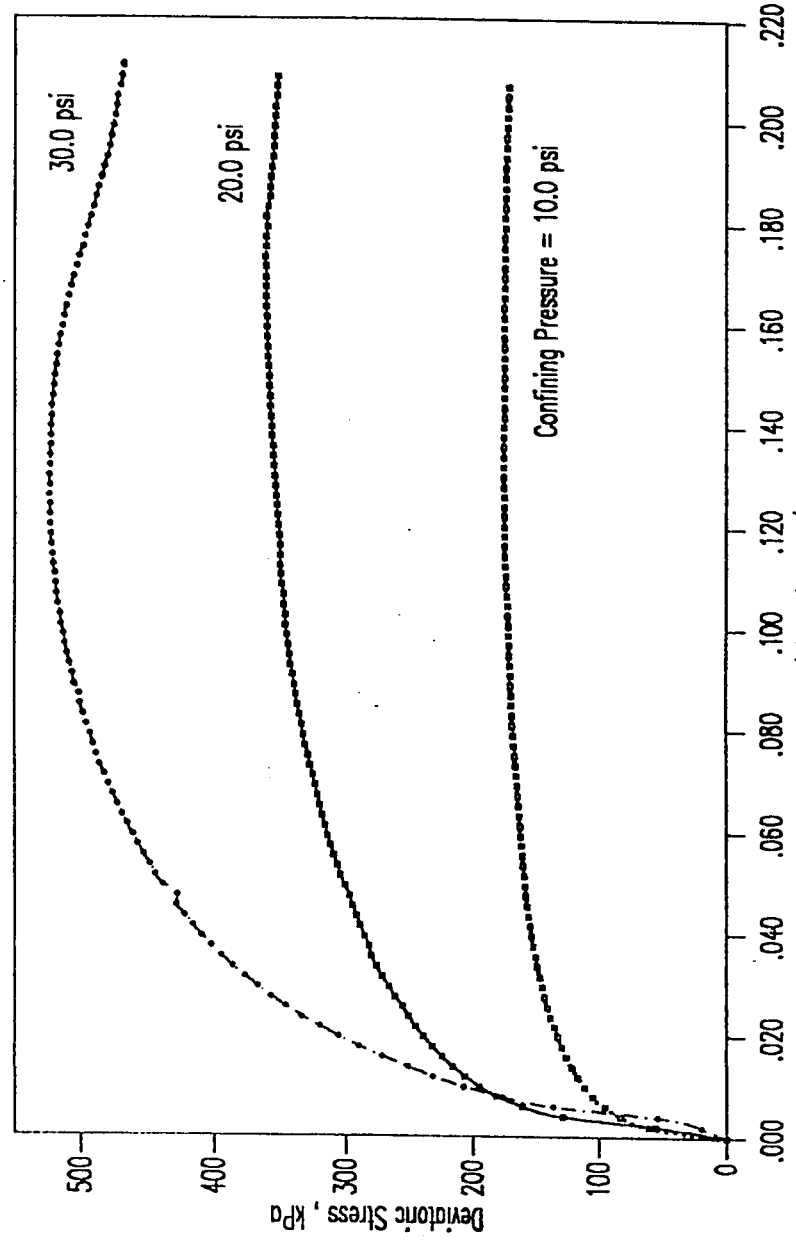

Fig. 5.58 : Stress–Strain Data for the CD Triaxial Test Saturated with Sabkha Brine

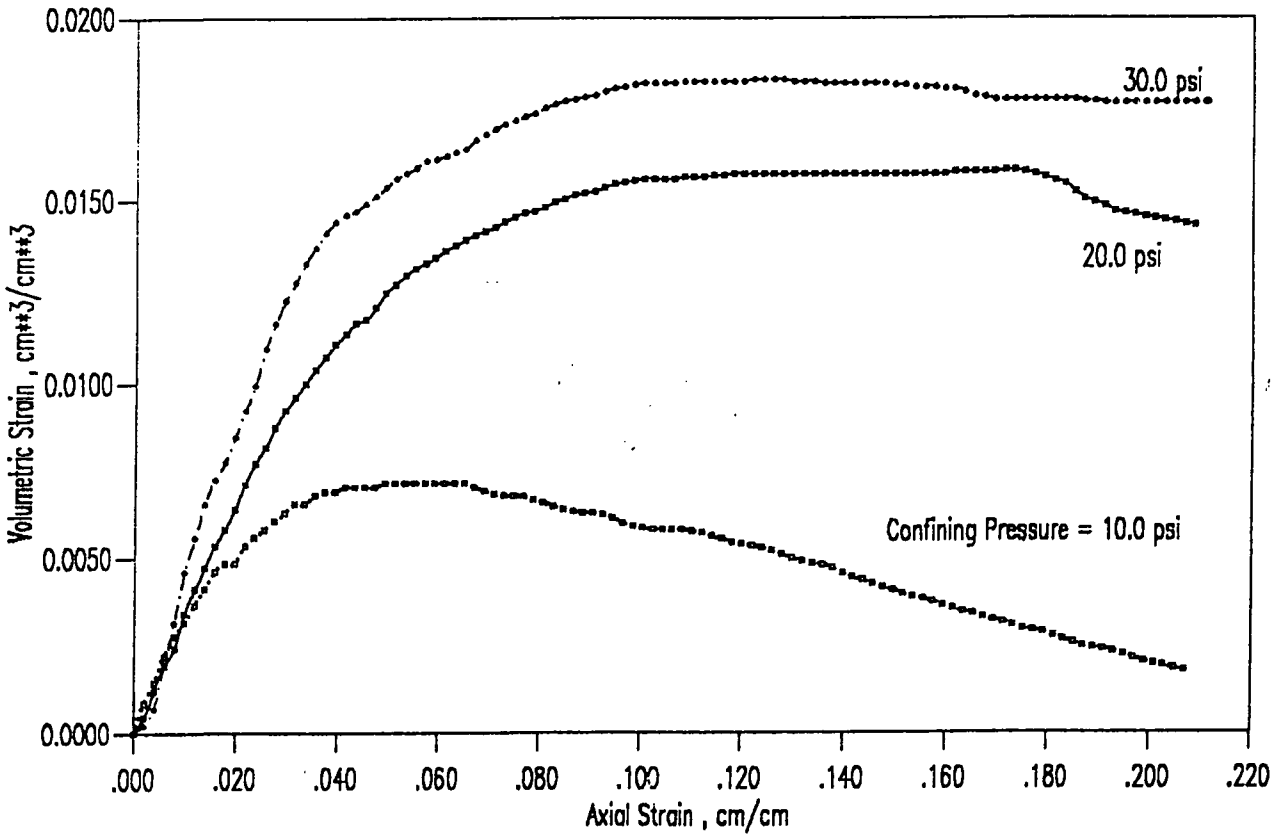

Fig. 5.59 : Volumetric Change Measurement for the CD Triaxial Test Saturated with Sabkha Brine

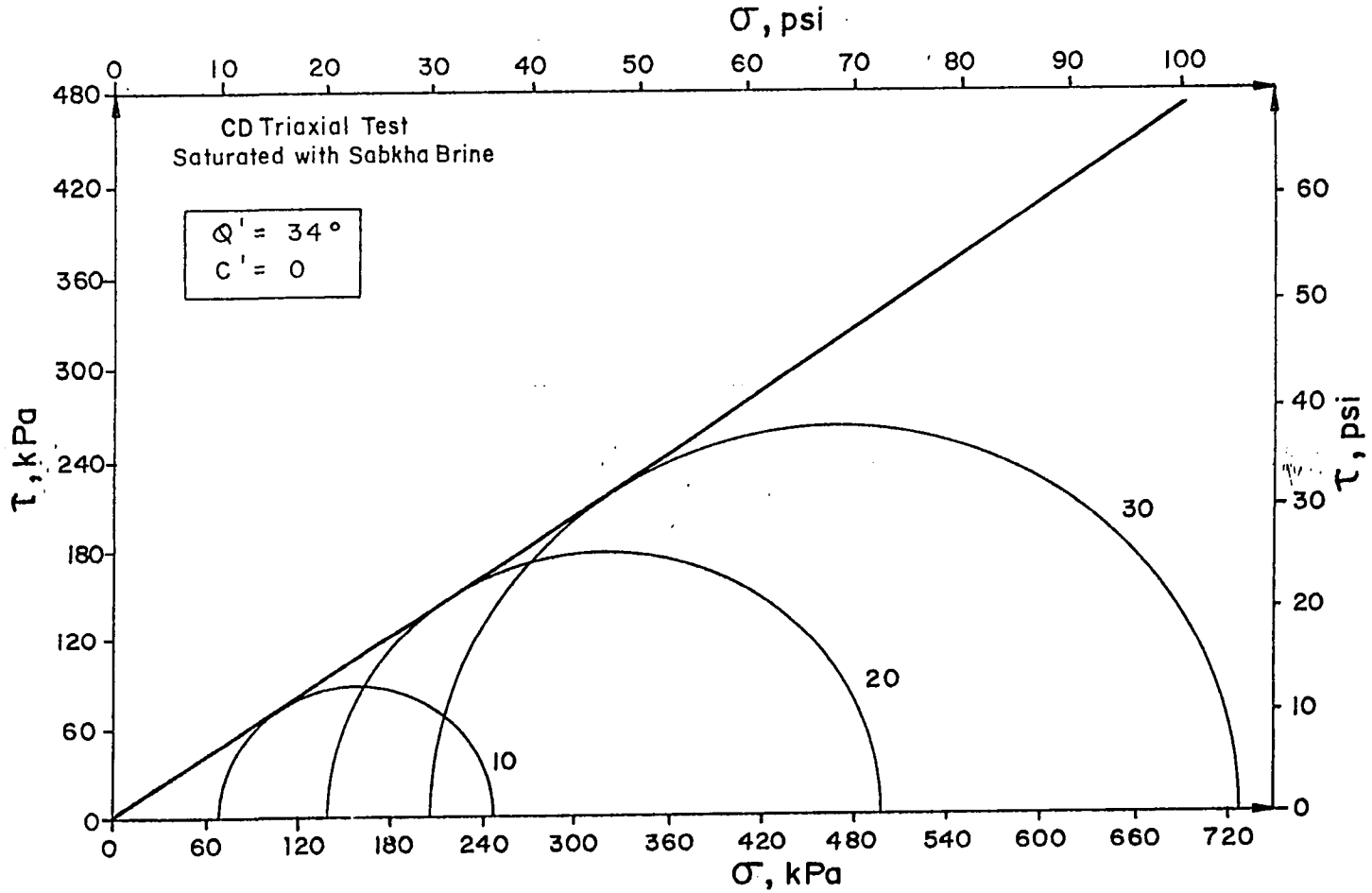

Fig. 5.60 : Mohr-Coloumb Failure Envelope for the CD Triaxial Test Saturated with Sabkha Brine.

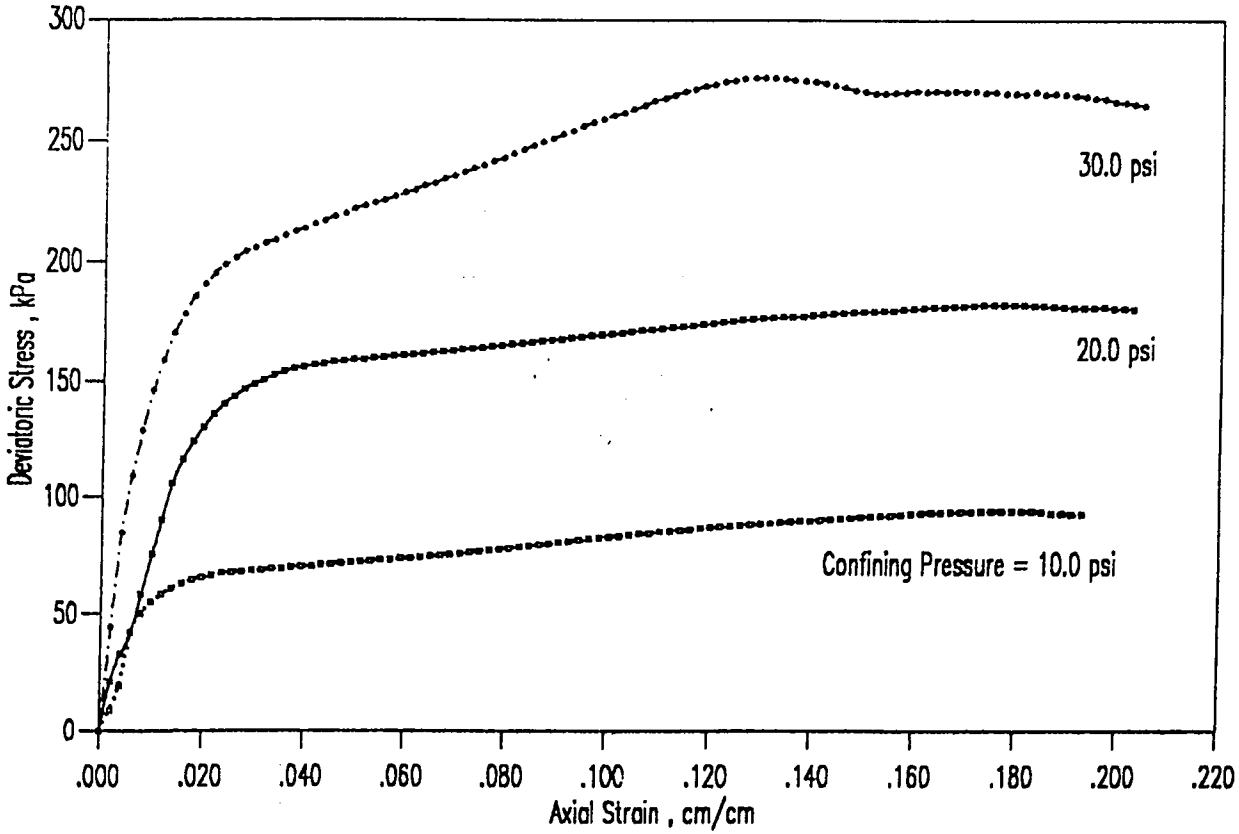

Fig. 5.61 : Stress–Strain Data for the CU Triaxial Test Saturated with Distilled Water

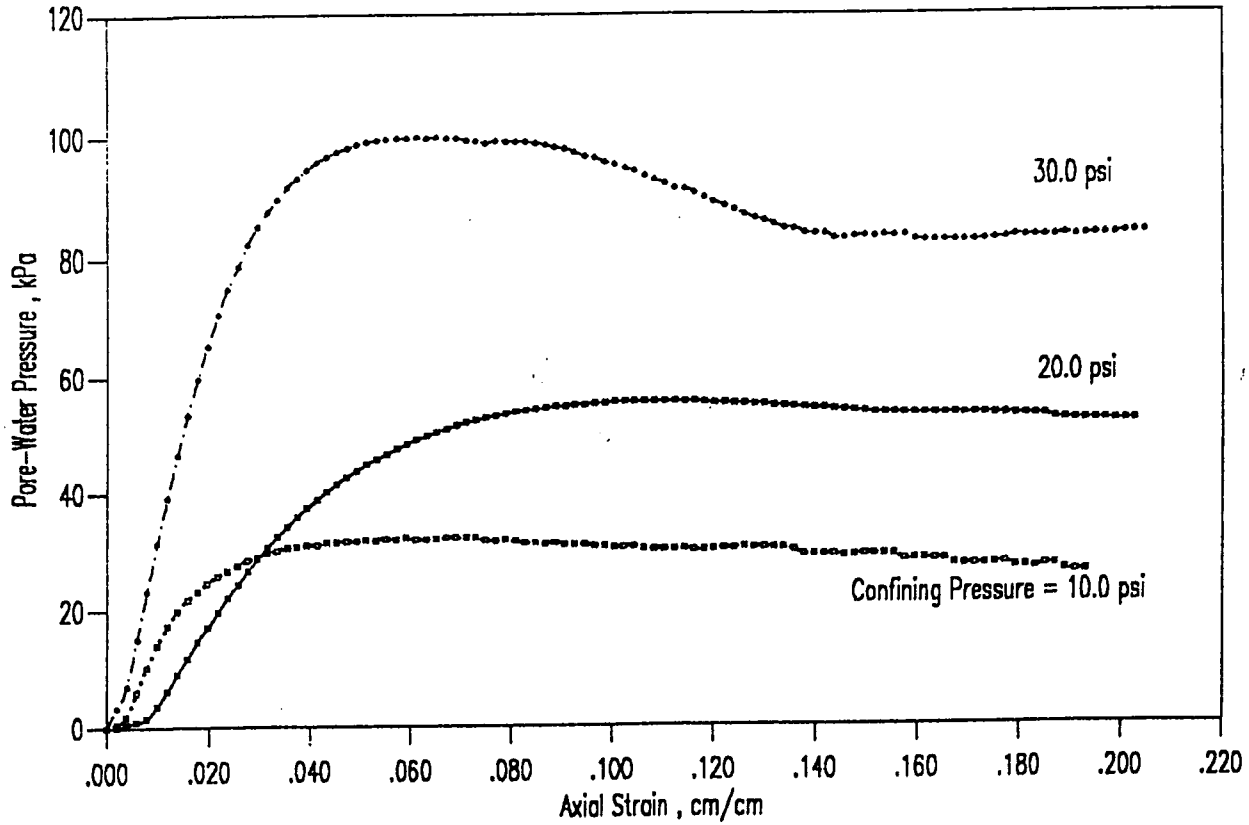

Fig. 5.62 : Pore-Water Pressure Measurement for the CU Triaxial Test Saturated with Distilled Water.

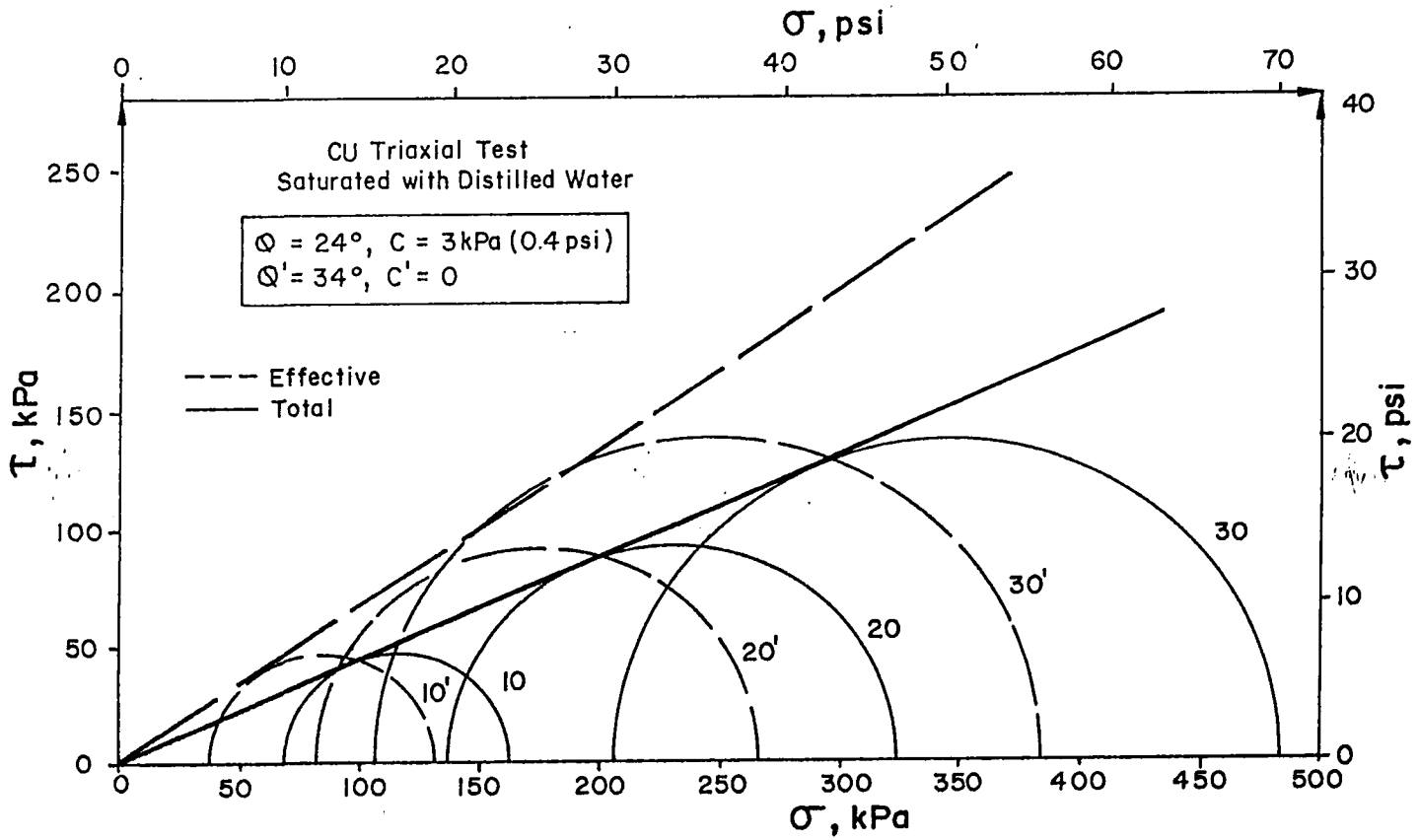

Fig. 5.63 : Mohr-Coloumb Failure Envelope for the CU Triaxial Test Saturated with Distilled Water.

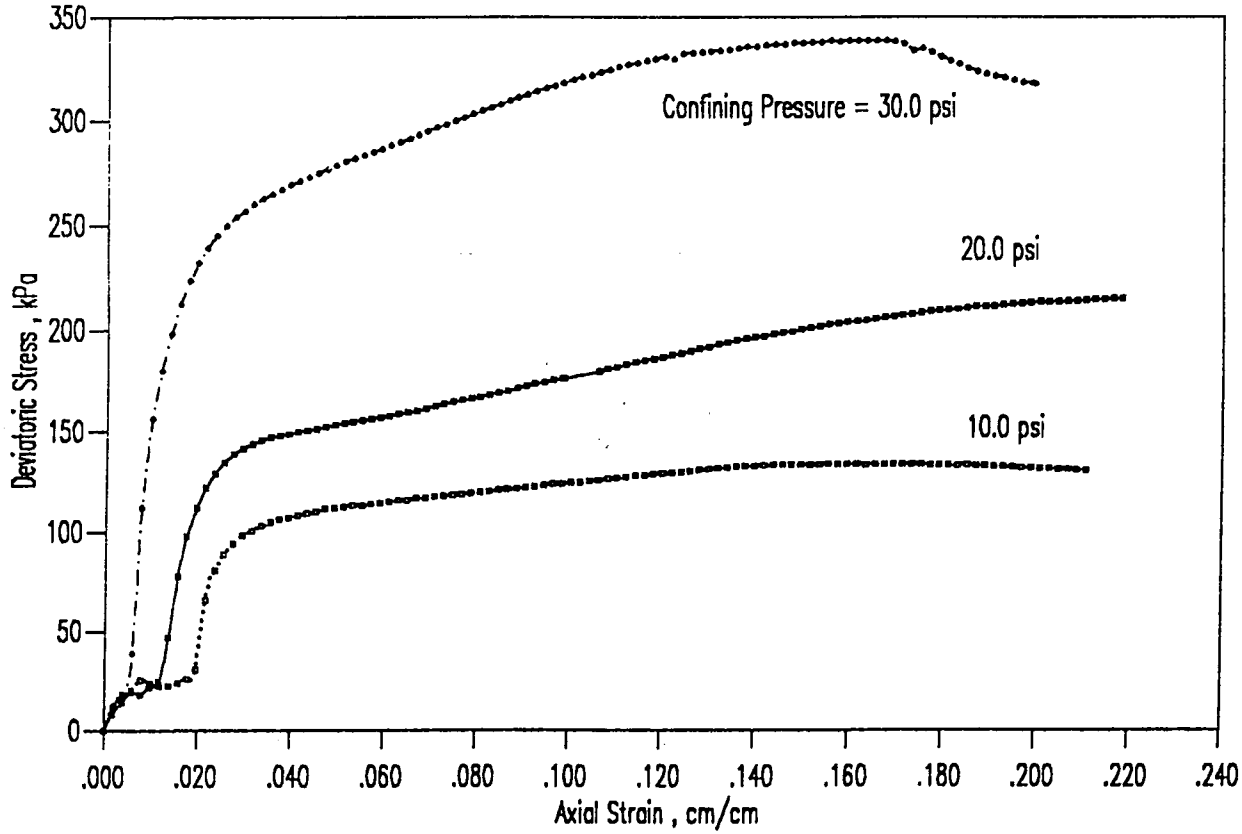

Fig. 5.64 : Stress–Strain Data for the CU Triaxial Test Saturated with Sabkha Brine

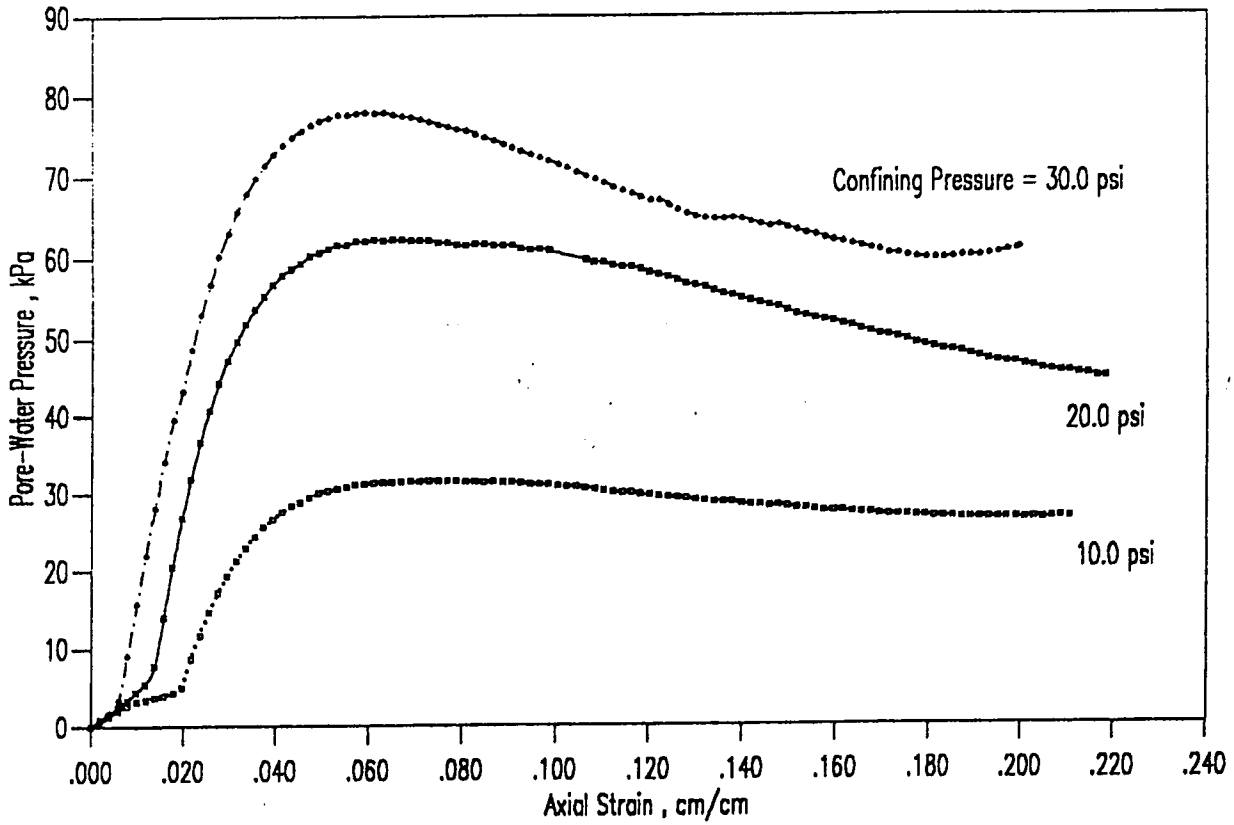

Fig. 5.65 : Pore-Water Pressure Measurement for the CU Triaxial Test Saturated with Sabkha Brine

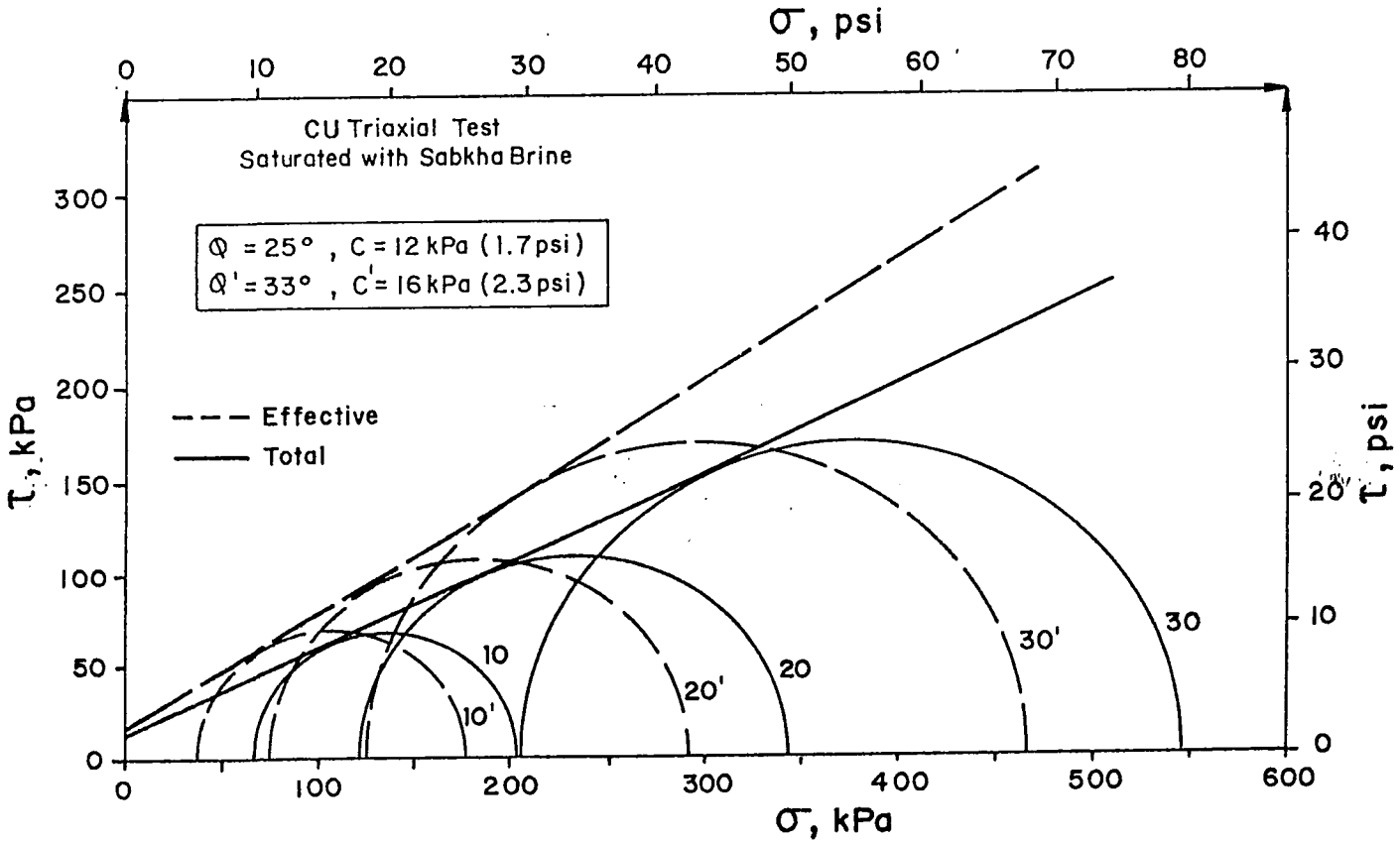

Fig. 5.66 : Mohr-Coloumb Failure Envelope for the CU Triaxial Test Saturated with Sabkha Brine.

Table 5.15 : Summary of Various Triaxial Test Results

Triaxial Test	Saturation with	Parameter Measured	Shear Strength Parameter			
			φ', deg.	c', kPa	φ, deg.	c, kPa
CD	No Saturation	No Volume Change Measurement	34.5	34.5	--	--
CD	Distilled Water	Volume Change	29	9	--	--
CD	Sabkha Brine	Volume Change	34	0	--	--
CU	Distilled Water	Pore-Water Pressure	34	0	24	3
CU	Sabkha Brine	Pore-Water Pressure	33	16	25	12

friction. It is worth mentioning that, with the exception of the CD tests for which saturation took place, the maximum difference in cohesion was only 16 kPa (2.3 psi), which is practically very small.

(v) Comparison of the CD tests in which neither saturation nor volume change measurements were taken, with the CD tests in which the specimens were initially saturated with sabkha brine or with both CU tests indicates that volume change measurement did not have any significant effect on the angle of internal friction. The increased c' value could be attributed to the less moisture content of these specimens compared to the others which were initially saturated.

(vi) Comparison of the shear strength parameters developed by the use of direct shear tests and the non-saturated CD triaxial tests (i.e., both had the same initial conditions) reveals the relatively higher effective angle of friction and cohesion as determined from the direct shear test than those determined from the triaxial test (i.e. $\varphi' = 36°$ and $c' = 50$ kPa compared with $\varphi' = 34.5°$ and $c' = 14$ kPa). This is attributed to the confining effect provided by the shear box. Das (204) reported that the angle of internal friction is slightly lower in the triaxial test

(from 0° to 3°) compared to the direct shear test. This agrees very well with the present results.

(vii) The last observation is the development of cohesion in spite of the cohesionless nature of this sabkha as reflected by the non-plastic characteristics. This small cohesion was the result of cementation that was developed by the presence of salt in sabkha.

5.4.11 Laboratory CBR Test Results

Data developed using California-bearing ratio (CBR) tests under natural and flooding conditions are shown in Figs. 5.67 and 5.68 and summarized in Table 5.7. Fig. 5.67 indicates the very low strength that surficial sabkha layers usually display. Naturally-existing sabkha have very low CBR values of only 3 to 4; whether the tests were conducted in the field or in the laboratory. These CBR values are rated as very poor (from 0 to 3) and poor to fair (from 3 to 7) according to the rate of performance by "The Asphalt Handbook" (205). Even these poor CBR values were reduced by as much as 50% when the sabkha soil was flooded with water as shown in Fig. 5.68 and Table 5.7. This indicates the high susceptibility of sabkha to collapse if they are inundated with water.

Comparison of CBR test results developed in the field

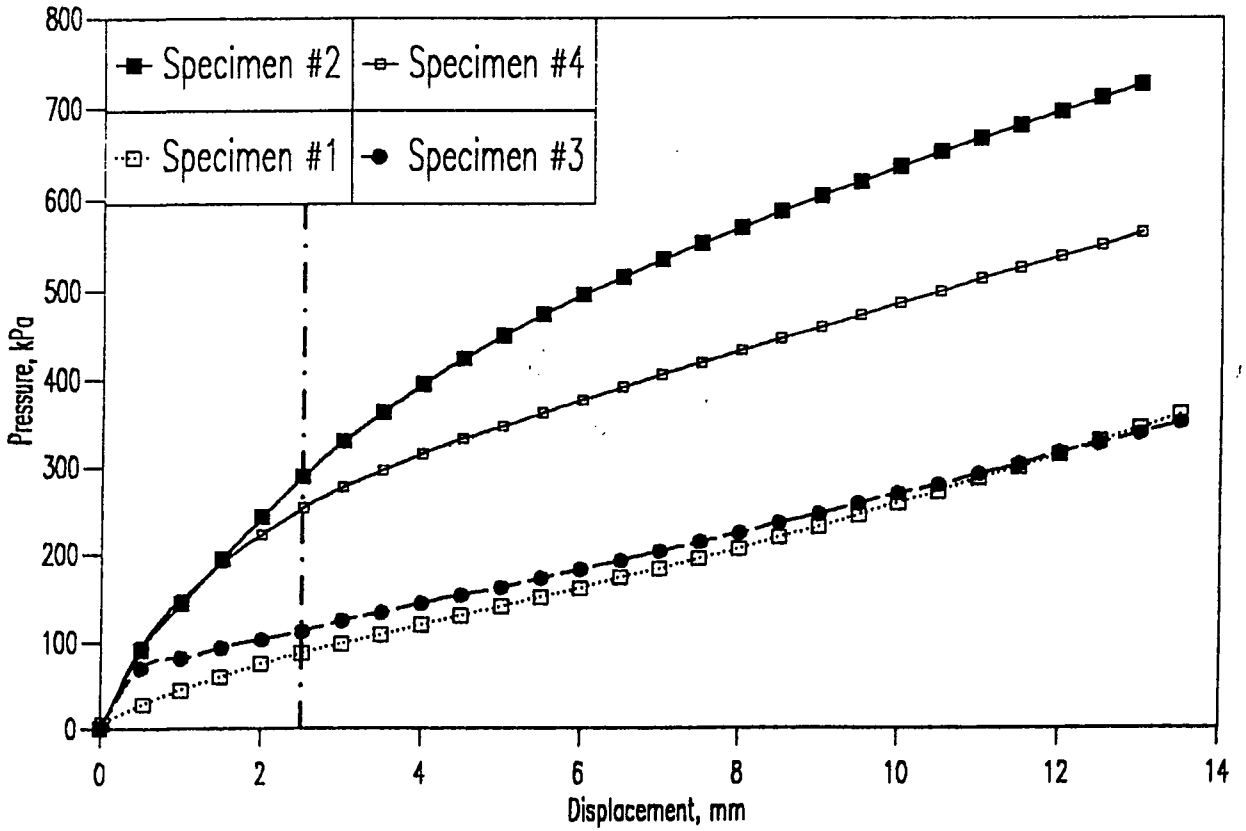

Fig. 5.67 : Laboratory CBR Test Results (Unsoaked Condition)

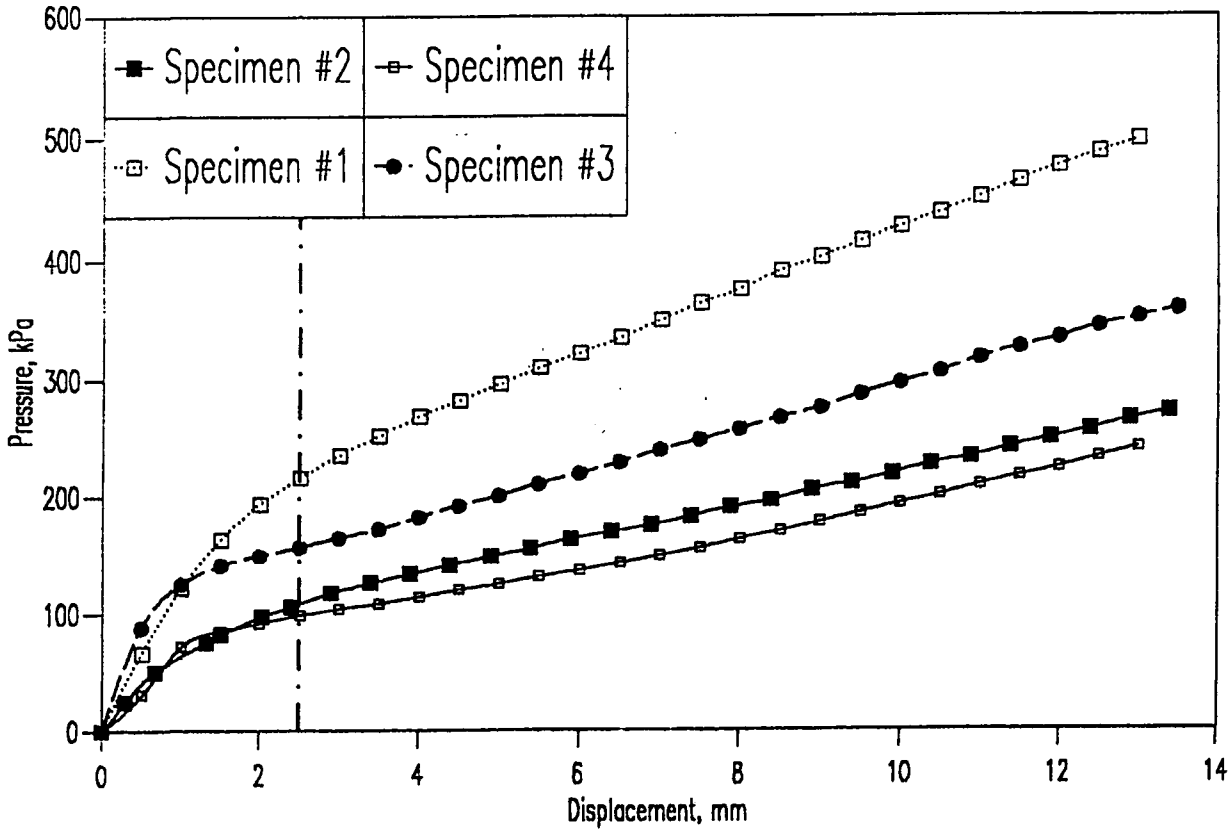

Fig. 5.68 : Laboratory CBR Test Results (Soaked Condition)

(Section 5.3.6) with those developed in laboratory shows similar results; nevertheless, slight variation did exist, particularly in the unsoaked (natural) conditions, which could be attributed to the heterogeneous nature of sabkha soils as well as sample disturbance.

Chapter 6

DURABILITY PERFORMANCE OF FOUNDATION MATERIALS IN SULFATE-CHLORIDE ENVIRONMENTS

The durability performance of foundation materials made with plain and blended cements in sulfate-chloride environments was evaluated in the laboratory by visual inspection and by measuring the degradation in compressive strength at periodic intervals. The mechanisms of sulfate attack in the $SO_4^{--}-Cl^-$ environments were elucidated using X-ray diffraction (XRD) and scanning electron microscopy equipped with energy dispersive X-ray analysis (SEM-EDXA) techniques. The corrosion of reinforcing steel in plain and blended cements was evaluated by determining the time to initiation of corrosion and measuring the corrosion current density. Pore solution analysis and expression technique was used to elucidate the mechanisms of reinforcement corrosion in pure chloride and chloride-sulfate environments. Field studies, in an exposure site at the selected Ras Al-Ghar sabkha, were used to further evaluate the strength reduction and reinforcement corrosion of plain and blended cements. The results of these extensive laboratory and field investigations are discussed this chapter.

6.1 PERFORMANCE OF PLAIN AND BLENDED CEMENT MORTARS IN SULFATE-CHLORIDE ENVIRONMENTS

6.1.1 Visual Inspection

Visual inspection of plain and blended cement mortar specimens immersed in the sulfate and sulfate-chloride solutions indicated different levels of deterioration. After about 720 days of exposure, maximum deterioration was observed in specimens exposed to the 2.1% pure sulfate solution. Signs of deterioration were noticed in silica fume cement specimens after about 50 days of immersion, whereas deterioration was observed in the blast furnace slag cement specimens after about 55 days of exposure. Signs of deterioration were observed in the fly ash blended cement specimens after about 80 days of immersion. Initiation of deterioration was observed in plain cement specimens after a relatively longer period of exposure to the sulfate solution compared to blended cements. Initiation of deterioration was indicated in Type I cement specimens after about 90 days of exposure. Type V cement specimens were observed to show signs of deterioration after about 110 days of exposure. The performance ratings, based on a six-point scale, to evaluate the degree of deterioration in the plain and blended cements, after one and two years of exposure, are shown in Table 6.1. The relationship between these performance ratings and the deterioration progress has already been discussed in Section 4.4.3.5. Deterioration was generally observed to occur at

the top edges of the specimens which progressed along the sides to the bottom edges. With an increase in the time of exposure, wider cracking at the edges and finally spalling off the surface skin at the sides was the predominant feature of failure. After prolonged exposure, the side surfaces spalled off the core leading to the weakening and delamination of the top and bottom surfaces as well. Eventually, the inner core of the specimen was exposed due to this all round delamination of the surface layers. This type of failure represents acidic and onion-peeling type of deterioration described in Section 3.2.2 and it characterizes the nature of failure in both plain and blended cements. The inner portion appeared to be strong and cohesive. This was especially observed in the silica fume blended cement specimens. Even when the original volume was reduced to about one-third, the inner core appeared to be strong enough to provide a sufficient residual strength. The five stages of deterioration leading to failure which were observed in both plain and blended cements are schematically presented in Fig. 6.1(a).

The deterioration ratings on the six-point scale for plain and blended cement specimens placed in the high sulfate-chloride solution (2.1% SO_4^{--} + 15.7% Cl^-) are shown in Table 6.2. These data indicate a similar general qualitative trend as indicated by the specimens exposed to the pure sulfate solution (Table 6.1). The degree of deterioration, however, was observed to be ameliorated

Table 6.1 : Durability Performance of Plain and Blended Cements in Pure Sulfate Solution

Cement Type	First Sign of Deterioration	Visual Deterioration Rating After		Deterioration Factor (%) After	
	Days	360 Days	720 Days	360 Days	720 Days
Type I	90	3	5	65	85
Type V	110	2	4	55	75
Fly Ash	80	3	5	77	85
Silica Fume	50	4	5	74	90
Blast Furnace Slag	55	4	5	67	95

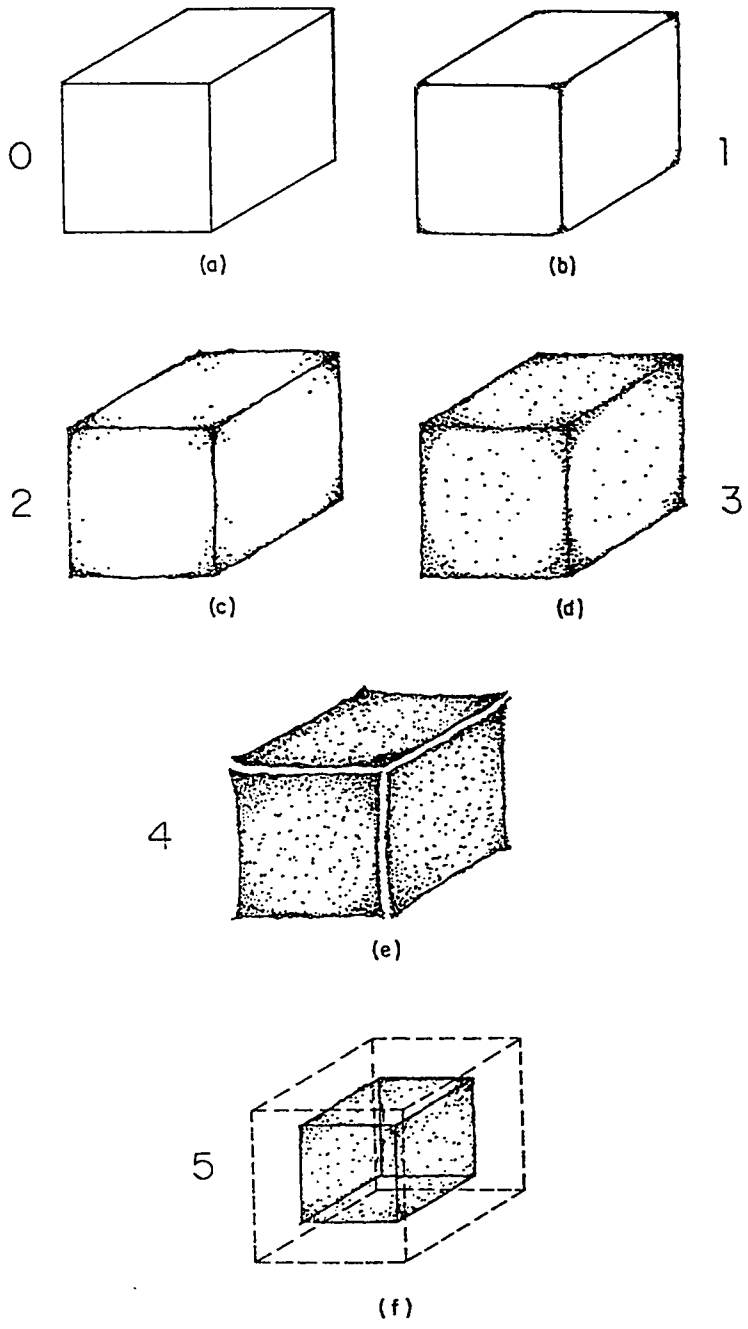

Fig. 6.1(a) : Schematic Representation of Deterioration Rating in Pure Sulfate and High Sulfate-Chloride Solutions.

Table 6.2 : Durability Performance of Plain and Blended Cements in High Sulfate-Chloride Solution

Cement Type	First Sign of Deterioration	Visual Deterioration Rating After		Deterioration Factor (%) After	
	Days	360 Days	720 Days	360 Days	720 Days
Type I	140	2	3	25	55
Type V	165	1	3	26	30
Fly Ash	120	2	3	20	46
Silica Fume	80	4	5	44	81
Blast Furnace Slag	90	3	5	58	84

and mitigated in specimens exposed to the sulfate-chloride interactive environment compared to specimens placed in pure sulfate solution. The first signs of deterioration were observed in silica fume and blast furnace slag cement specimens after about 80 and 90 days respectively. Fly ash, Type I and Type V cement specimens exhibited initiation of deterioration after 120, 140 and 165 days of exposure respectively. These data, indicating the mitigation of sulfate attack due to the addition of 15.7% chloride, also indicate that the ameliorative effect is not uniform in all cements. The effect of chlorides in reducing deterioration due to sulfate ions was observed to be more pronounced in the case of plain and fly ash blended cements compared to silica fume and blast furnace slag blended cements.

Visual inspection of specimens exposed to low sulfate-chloride solution (0.55% SO_4^{--} + 15.7% Cl^-) indicated no noticeable deterioration in any of the cements, although a crystalline salt growth was observed on all specimens. The salt growth was relatively more profuse on plain cement specimens compared to those made with silica fume, blast furnace slag and fly ash. The deterioration rating for the specimens made with plain and blended cements is shown in Table 6.3.

Results of the visual inspection carried out on specimens exposed to the pure chloride solution 15.7% (Cl^-) indicated no

deterioration after 720 days of exposure. However, crystalline salt growth was observed on all specimens made with plain and fly ash blended cements, although it was significantly less compared to the low sulfate-chloride solution, as shown in Fig. 6.1(b). The salt growth was observed in small isolated areas on the surface of the specimens. No salt deposit was observed on silica fume and blast furnace slag cement specimens. The deterioration rating for all specimens exposed to the pure chloride solution is shown in Table 6.4.

6.1.2 Characterization of Deterioration

In both pure sulfate and high sulfate-chloride environments, the progressive deterioration leading to failure was associated with increasing softening and disintegration of the hardened cement matrix, characterized by cohesionlessness and spalling of surfaces, rather than expansion and cracking. Some marginal expansion in volume did occur, but the binder decomposition feature completely overshadowed the expansion and cracking. This is clearly shown in Plates 6.1 through 6.4.

6.1.3 Reduction in Compressive Strength

In order to monitor the overall extent of deterioration which encompasses both softening and expansion-cracking types of sulfate attack, the deterioration was evaluated by strength loss than the traditional expansion measurements. To this end, the

Table 6.3 : Durability Performance of Plain and Blended Cements in Low Sulfate-Chloride Solution

Cement Type	First Sign of Deterioration	Visual Deterioration Rating After		Deterioration Factor (%) After	
	Days	360 Days	720 Days	360 Days	720 Days
Type I	-	0	1	16	23
Type V	-	0	1	15	20
Fly Ash	-	0	1	17	23
Silica Fume	-	0	0	15	22
Blast Furnace Slag	-	0	0	13	14

Table 6.4 : Durability Performance of Plain and Blended Cements in Pure Chloride Solution

Cement Type	First Sign of Deterioration	Visual Deterioration Rating After		Deterioration Factor (%) After	
	Days	360 Days	720 Days	360 Days	720 Days
Type I	-	0	0	12	9
Type V	-	0	0	23	28
Fly Ash	-	0	0	11	18
Silica Fume	-	0	0	22	25
Blast Furnace Slag	-	0	0	4	7

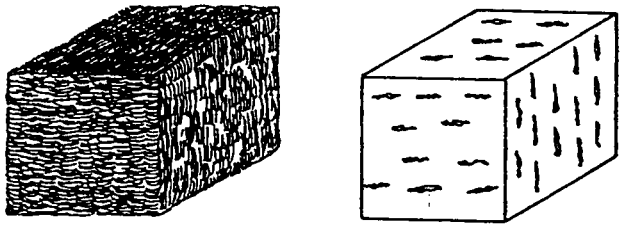

Low Sulfate-
Chloride Solution

Pure Chloride
Solution

Fig. 6.1(b) : Schematic Representation of Deterioration Rating in Low Sulfate-Chloride and Pure Chloride Solutions.

Plate 6.1 : Visual Documentation of the Different Cements in the Pure Sulfate Solution after 360 Days.

Plate 6.2 : Visual Documentation of the Different Cements in the High Sulfate-Chloride Solution after 360 Days.

Plate 6.3 : Visual Documentation of the Different Cements in the Pure Sulfate Solution after 720 Days.

Plate 6.4 : Visual Documentation of the Different Cements in the High Sulfate-Chloride Solution after 720 Days.

concept of a deterioration factor (DF), as defined by Rasheeduzzafar et al. (181), was used. This deterioration factor indicates the relative performance of cements tested in this investigation in the sulfate-chloride environments. The details of evaluating the deterioration factor (DF) have been discussed in Section 4.4.3.4.

The data on compressive strength development in plain and blended cement specimens placed in potable water are shown in Table 6.5 and plotted against the time of curing in Figs. 6.2 and 6.3. These data indicate that all plain and blended cements exhibit similar strengths after 14 days of water curing. After prolonged curing, for 180 days, maximum compressive strength was observed in silica fume blended cement specimens. After 720 days of curing, improvement in strength for all cements almost ceases to occur. Strength development in blast furnace slag cement was, however, relatively lower compared to other cements at all test ages.

The data on deterioration factors for plain and blended cements after 720 days of exposure to the four environments are shown in Figs. 6.4 through 6.8. Fig. 6.4 shows the deterioration factor (DF) for Type I cement. Sulfate deterioration for specimens exposed to high sulfate-chloride (2.1% SO_4^{--} + 15.7% Cl^-) environment was not appreciable up to an immersion period of 180 days as indicated by a DF value of 13% which remained constant for this

Table 6.5 : **Summary of Strength Devlopment in Plain and Blended Cement Mortar Specimens**

Curing Period Days	Compressive Strength (MPa)*				
	Type I	Type V	Fly Ash	Silica Fume	BFSC**
14	27.1	28.9	28.4	28.0	20.7
90	27.6	3.3	37.0	32.9	24.7
180	34.0	36.2	40.8	45.1	34.7
360	35.2	39.8	45.1	45.4	37.1
540	41.9	41.1	47.7	46.8	40.6
720	43.5	41.5	49.7	47.4	40.8

* Using 25 mm mortar cubes

** Blast furnace slag cement

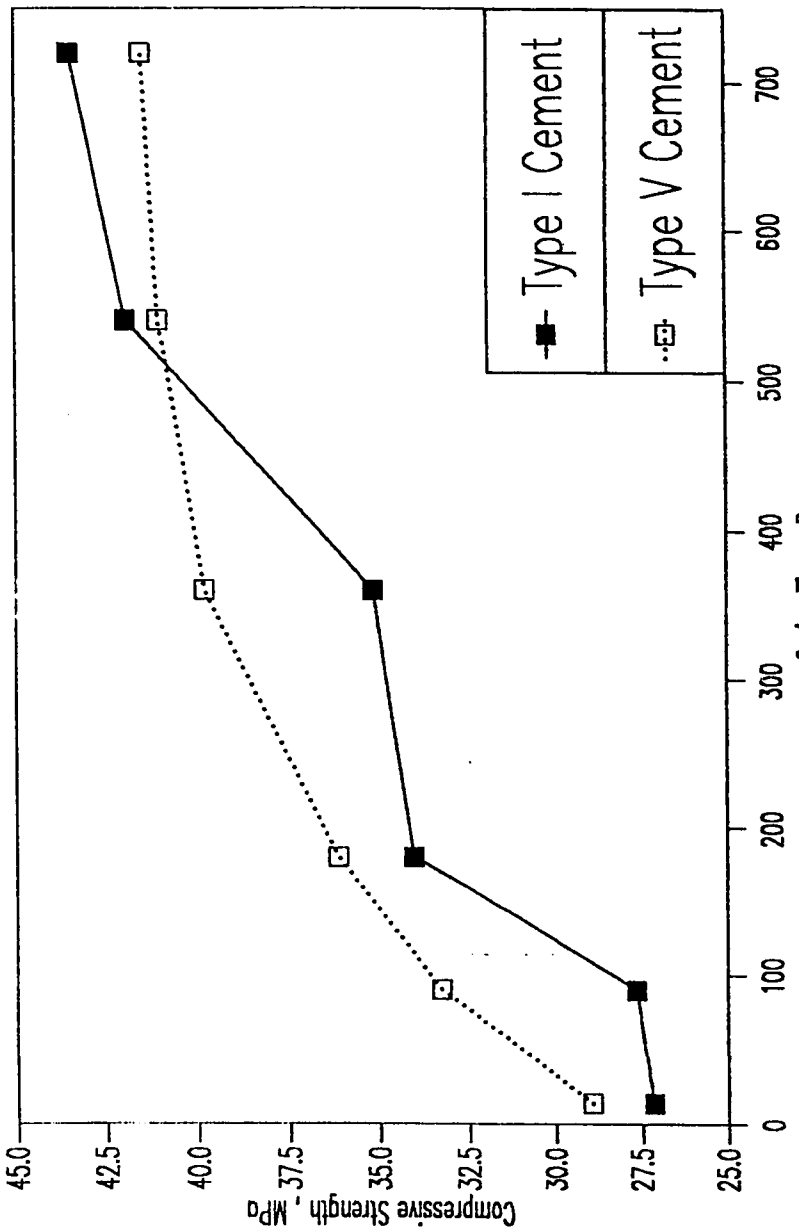

Fig. 6.2 : Strength Development in Plain Cement Mortar Specimens

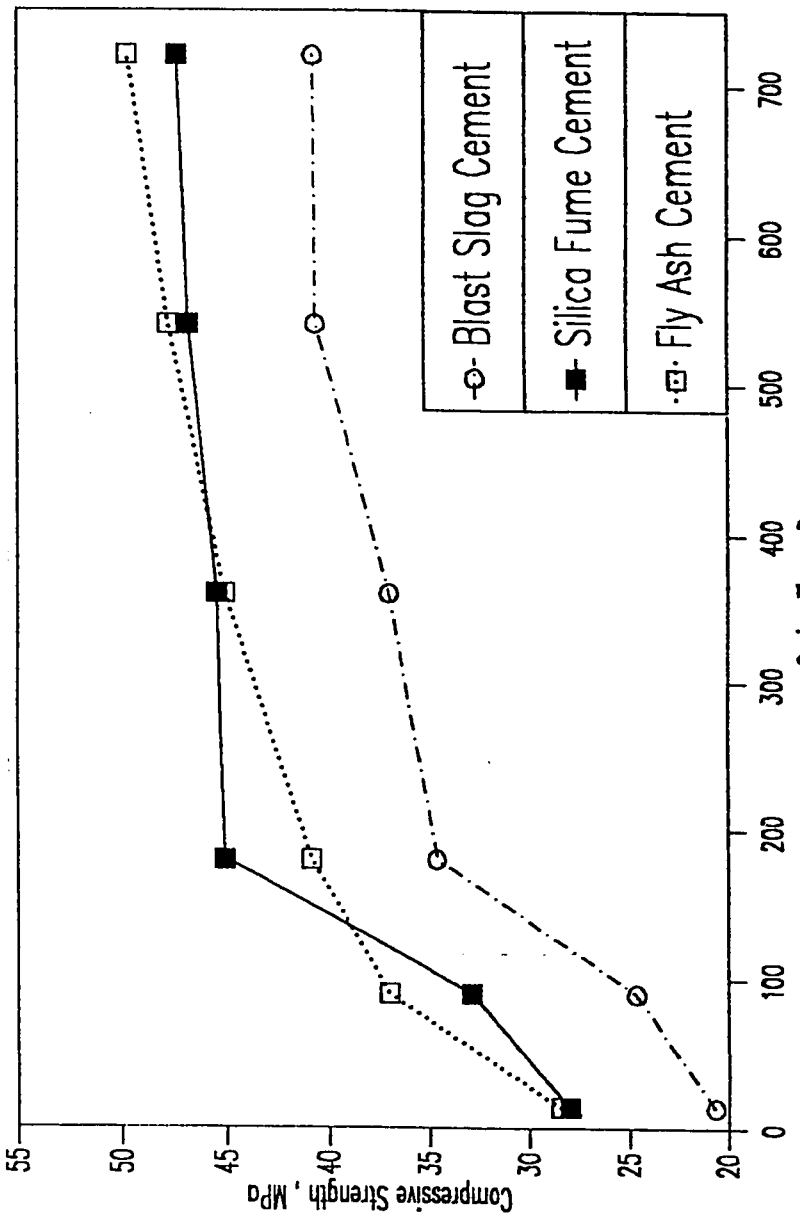

Fig. 6.3 : Strength Development in Blended Cement Mortar Specimens

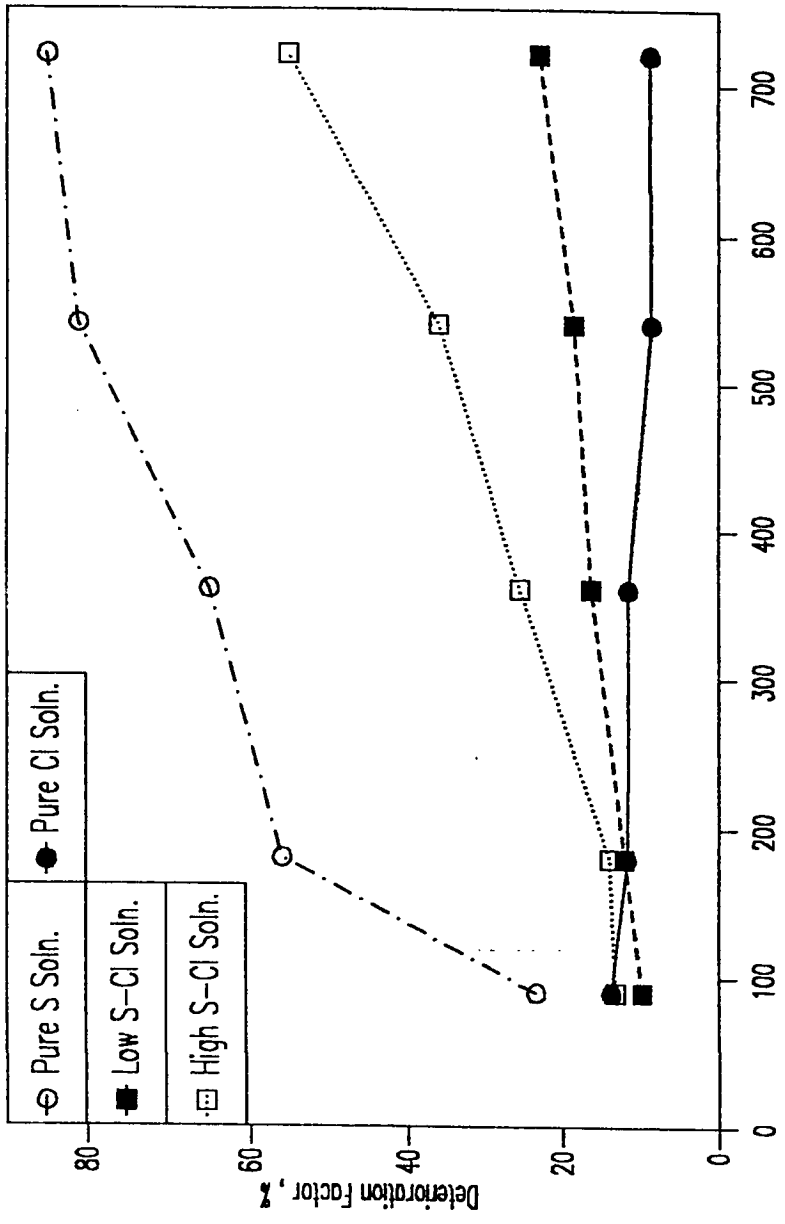

Fig. 6.4 : Reduction in Compressive Strength with Time (Type I Cement Mortar Specimens)

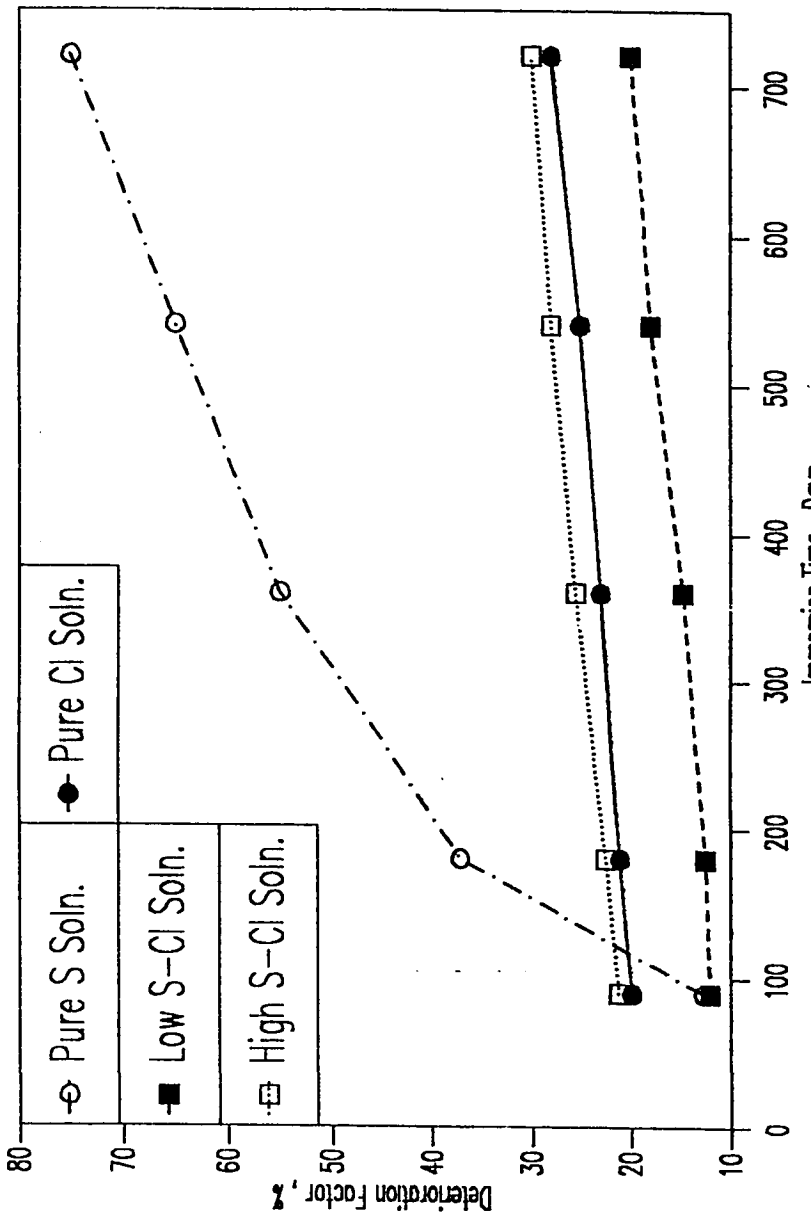

Fig. 6.5 : Reduction in Compressive Strength with Time (Type V Cement Mortar Specimens)

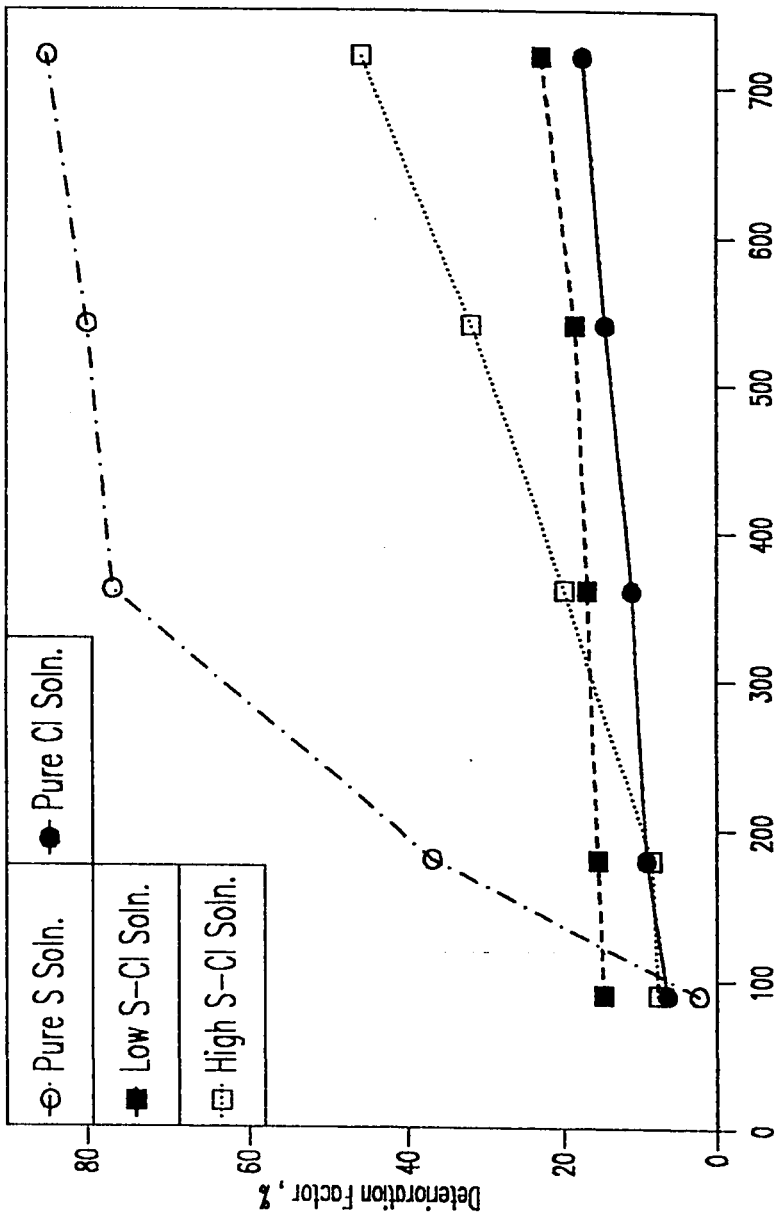

Fig 6.6 : Reduction in Compressive Strength with Time (Fly Ash Cement Mortar Specimens)

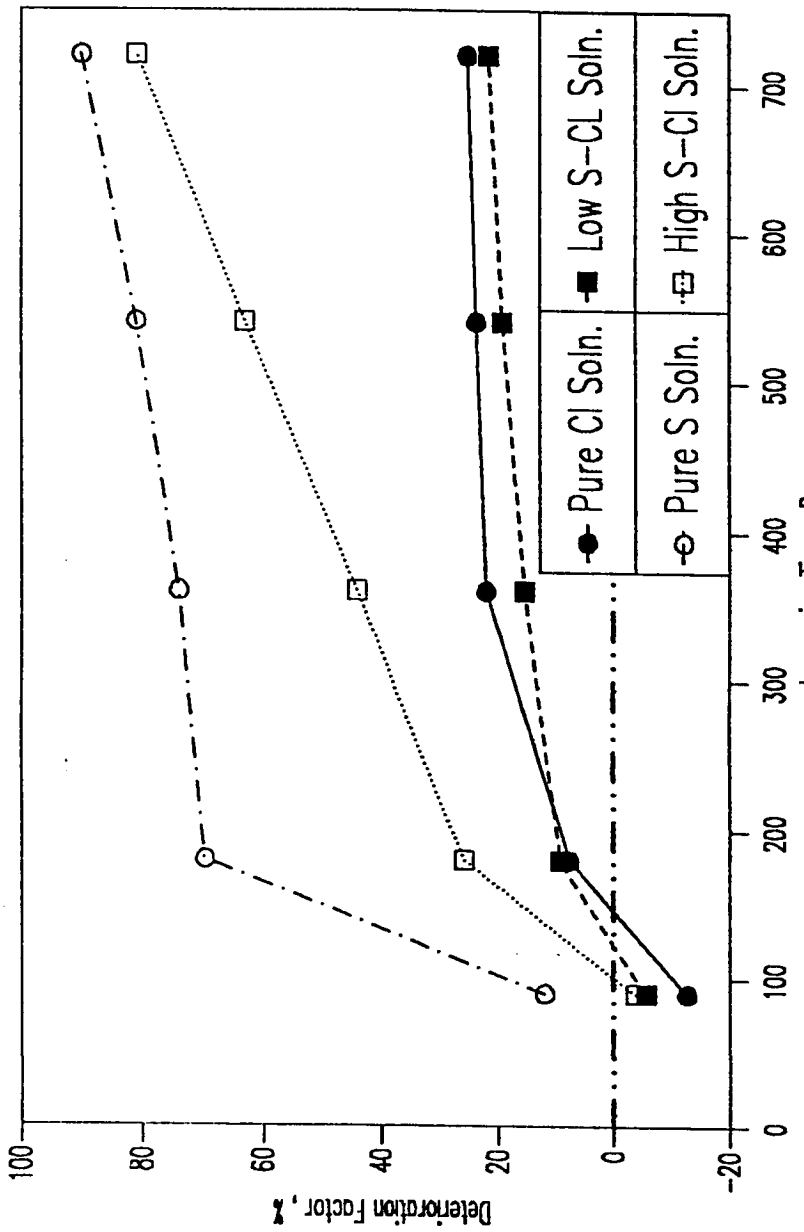

Fig 6.7 : Reduction in Compressive Strength with Time (Silica Fume Mortar Specimens)

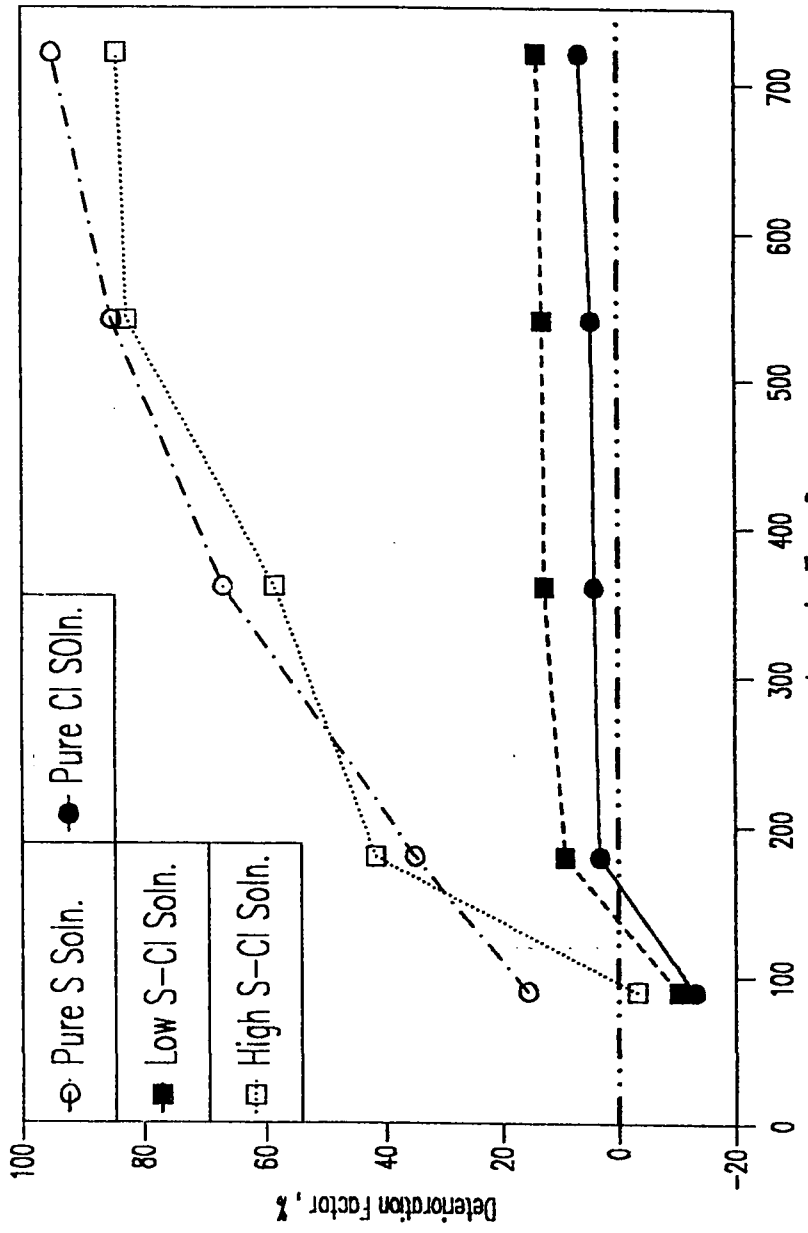

Fig. 6.8 : Reduction in Compressive Strength with Time (Blast Furnace Slag Cement Mortar Specimens)

period. For exposure periods in excess of 180 days, the DF increased linearly with time of exposure. The DF for specimens immersed in this solution was observed to increase to a value of 55% after 720 days of exposure. The deterioration factors for specimens immersed in pure chloride (15.7% Cl^-) and in low sulfate-chloride (0.55% SO_4^{--} + 15.7% Cl^-) solutions, after 720 days of immersion, were 8.7% and 23% respectively. The deterioration factor was observed to be maximum in specimens immersed in pure sulfate (2.1% SO_4^{--}) solution where the DF increased to a value of 85% after 720 days of exposure.

The data on sulfate deterioration in the case of Type V cement specimens (Fig. 6.5) indicates a qualitative trend similar to that observed in Type I cement specimens. The maximum deterioration factor was indicated for specimens placed in the pure sulfate solution. The deterioration factor in this solution after 720 days was of the order of 75%. Deterioration factors for specimens exposed to the high sulfate-chloride, low sulfate-chloride and pure chloride solutions were 30%, 20% and 28% respectively. Furthermore, the rate of increase of sulfate deterioration in specimens placed in these three solutions was observed to be insignificant. The deterioration factors with time of exposure are plotted in Fig. 6.6 for fly ash blended cement specimens. The deterioration factors with time of exposure for fly ash blended cement specimens

were observed to be similar to that observed in Type I cement specimens. Maximum deterioration was observed for specimens immersed in the pure sulfate solution. The DF after 720 days of immersion in this solution was approximately 85%. The deterioration factors for specimens exposed to the two sulfate-chloride solutions and pure chloride solution were approximately similar, up to an immersion period of about 180 days. The deterioration factors for specimens exposed to the high sulfate-chloride solution increased to a value of 46% with the increase in exposure time to 720 days in contrast to the deterioration factors for specimens immersed in the low sulfate-chloride and pure chloride solutions which remained more or less unchanged till about 720 days.

Data on deterioration factors for silica fume and blast furnace slag blended cements for 720 days of exposure to the four test solutions are shown in Figs. 6.7 and 6.8 respectively. The deterioration factors in specimens exposed to the two sulfate-chloride and pure chloride test solutions up to 90 days were observed to be negative. The negative deterioration factors at early ages in these specimens signify an increase in strength, which is attributable to the filling up of the pores by the reaction products of sulfate attack in the early periods of exposure thereby densifying the mortar matrix. Similar results have been reported by other investigators (206,207,etc.). The strength reduction factor for silica fume cement specimens after 180 days of immersion in the

pure sulfate solution was 74% which increased to 90% as the exposure period was prolonged to 720 days (Fig. 6.7). A similar trend was observed in the blast furnace slag cement specimens placed in the pure sulfate solution. The strength deterioration factor was found to be as high as 95% after an exposure period of 720 days. The performance of silica fume and blast furnace slag cements in the high sulfate-chloride solution is similar to their performance in the pure sulfate solution. Almost no deterioration in strength was observed up to 100 days in silica fume cement specimens placed in the high sulfate-chloride solution. However, the rate of deterioration increased almost linearly to a deterioration factor of as high as 81% after 720 days of exposure. The performance of blast furnace slag cement specimens in the pure sulfate and high sulfate-chloride solutions is almost identical (Fig. 6.8).

6.2 MINERALOGICAL COMPOSITION OF HYDRATED CEMENTS

A special feature included in this study was the mineralogical analysis of hydrated pastes of plain and blended cements specimens cured in water or those exposed to the various sulfate, chloride and sulfate-chloride environments after 720 days of immersion in these environments. X-ray diffraction (XRD) was employed for this purpose. Intensity of selected peaks from the X-ray diffractograms provides a semi-quantitative estimate of the various elements of interest.

The objective of the mineralogical analysis was to meticulously identify the effect of the specific exposure environments on the stability of the hydration products or the nature of their conversion into new phases which may affect the durability performance of these cements in the different exposure conditions studied.

6.2.1 Plain and Blended Cements in Potable Water

The X-ray diffractograms in Figs. 6.9 and 6.10, which are qualitatively very similar, show the products of hydration of Type I and Type V plain portland cements. A broad peak between 9° 2θ and 10° 2θ indicates the presence of primary sulfo-aluminate phase which may comprise **primary ettringite** ($C_6A\overline{S}_3H_{32}$), which has its major peak at 9.1° 2θ, **monosulfate** ($C_4A\overline{S}H_{12}$), which is generated from the partial conversion of ettringite, and a **"dynamic phase"**. This "dynamic phase" contains 12 to 32 moles of water and 1 to 3 moles of $C\overline{S}$, and it is termed dynamic in the sense that water molecules are decreasing from 32 to 12 and $C\overline{S}$ is dropping from 3 to 1 to become monosulfate. It, therefore, seems reasonable to assume that the broad band peaks between 9.1° 2θ and 9.9° 2θ in the X-ray diffractograms correspond to this "dynamic phase".

Both Type I and Type V cements show significant precipitation of portlandite (CH) through well-defined peaks at 17.9° 2θ and 34.5° 2θ. The C-S-H, being a poorly-crystallized or nearly

amorphous compound comprising of extremely finely divided particles of colloidal size, is indicated by the diffused band between 29.5 and 31.5° 2θ.

The X-ray diffractograms (Figs. 6.11 and 6.12) for the 20% fly ash and 10% silica fume blended cements show a similar primary sulfo-aluminate phase as indicated for plain Type I and Type V portland cements, by the presence of a diffused band between 9 and 10° 2θ.

The diffractograms in Figs. 6.11 and 6.12 when compared with the XRD of the parent Type I cement (Fig. 6.9) show significantly reduced portlandite (CH) due to the pozzolanic reaction between silica fume/fly ash and portlandite (CH), which effectively converts part of the original CH into secondary C-S-H. The C-S-H diffused band between 29.5 and 31.5° 2θ is present as in plain portland cements.

Fig. 6.13 shows the X-ray diffractogram developed for the hydration products of blast furnace slag cement in potable water. The primary ettringite-monosulfate phase, similar to that in plain, silica fume and fly ash blended cements, is also present in the blast furnace slag cement. However in the case of BFS cement, the peaks between 9.0 and 10.0° 2θ are noticeably better defined. Another primary ettringite peak is also present at 22.8° 2θ. This indicates the formation of more trisulfo-aluminate phase in BFS

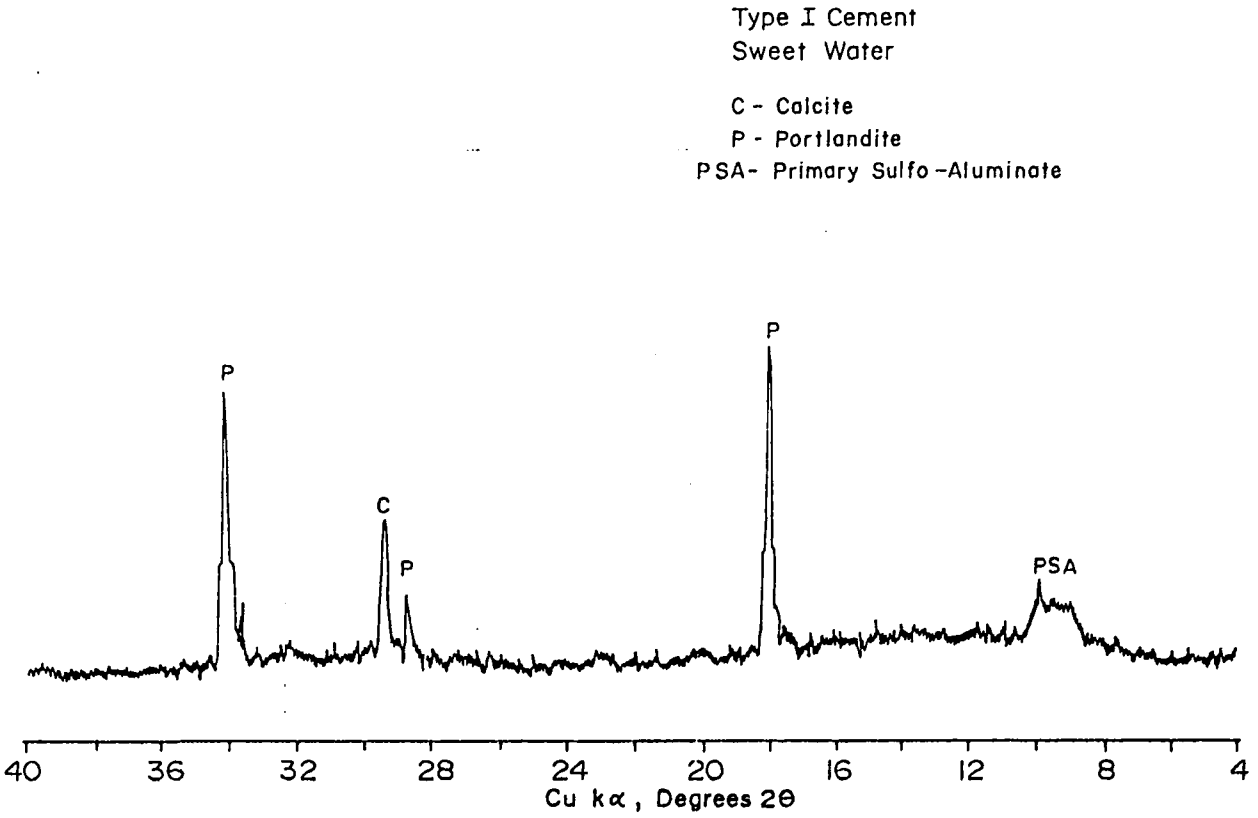

Fig. 6.9 : X-Ray Diffractogram for Type I Cement in Potable Water after 720 Days of Immersion.

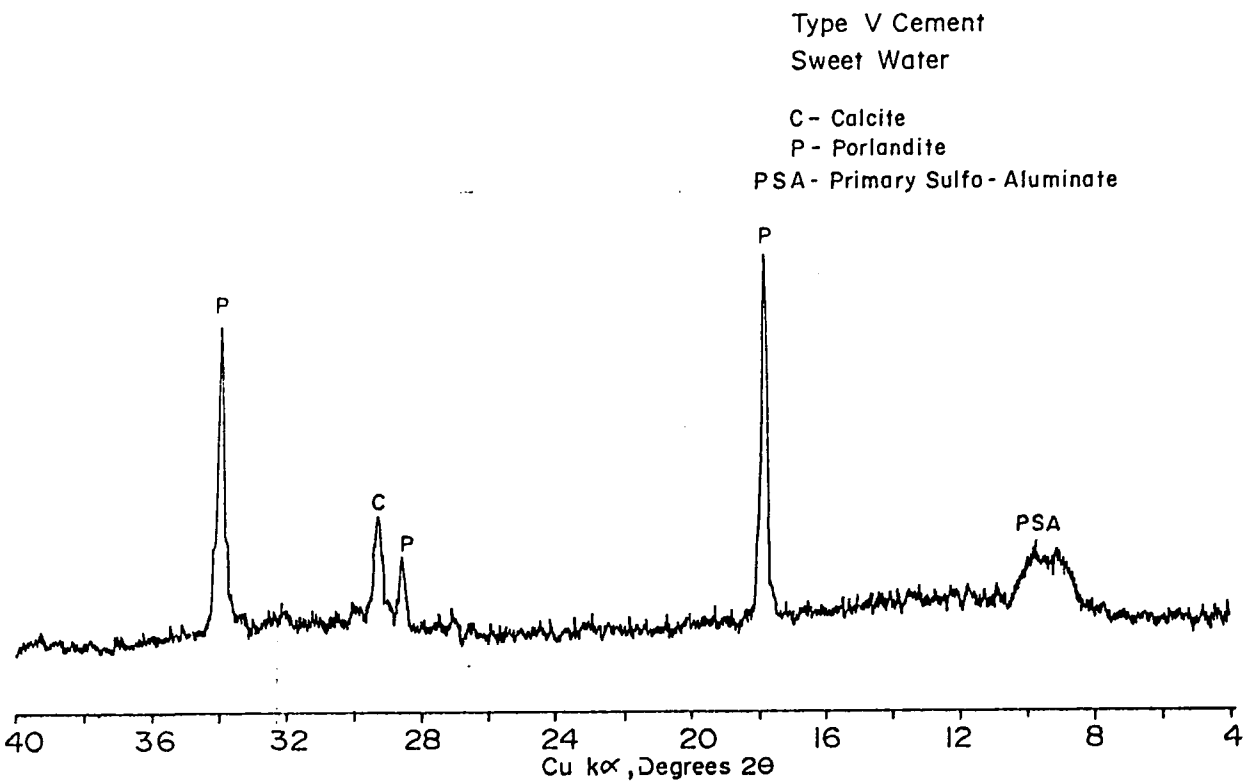

Fig. 6.10 : X-Ray Diffractogram for Type V Cement in Potable Water after 720 Days of Immersion.

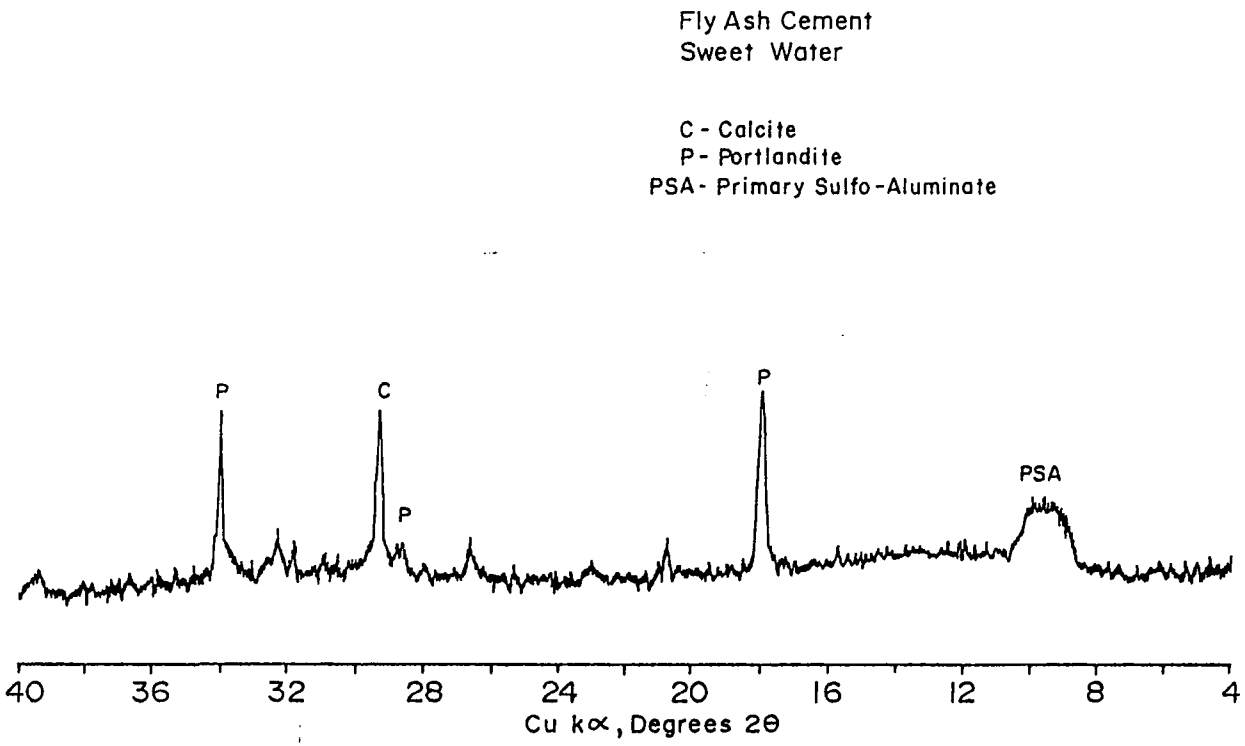

Fig. 6.11 : X-Ray Diffractogram for Fly Ash Cement in Potable Water after 720 days of immersion.

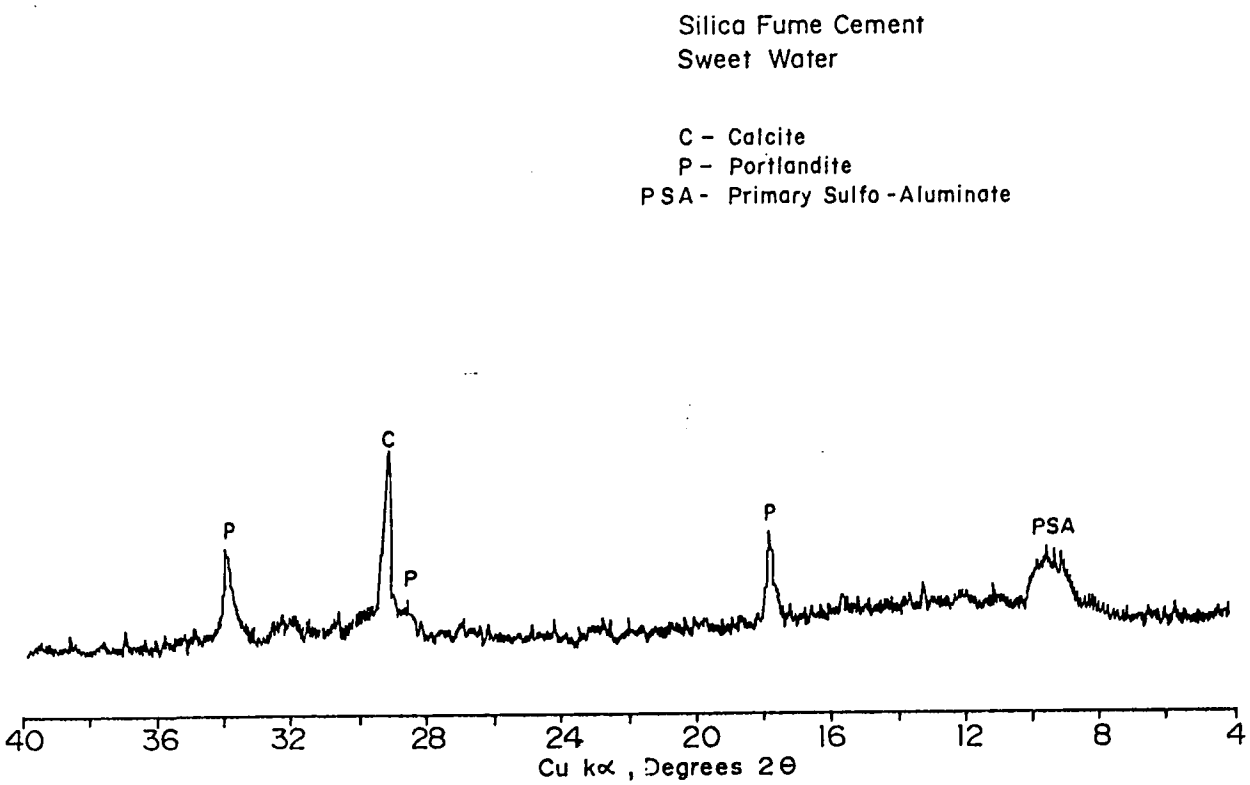

Fig. 6.12 : X-Ray Diffractogram for Silica Fume Cement in Potable Water after 720 Days of Immersion.

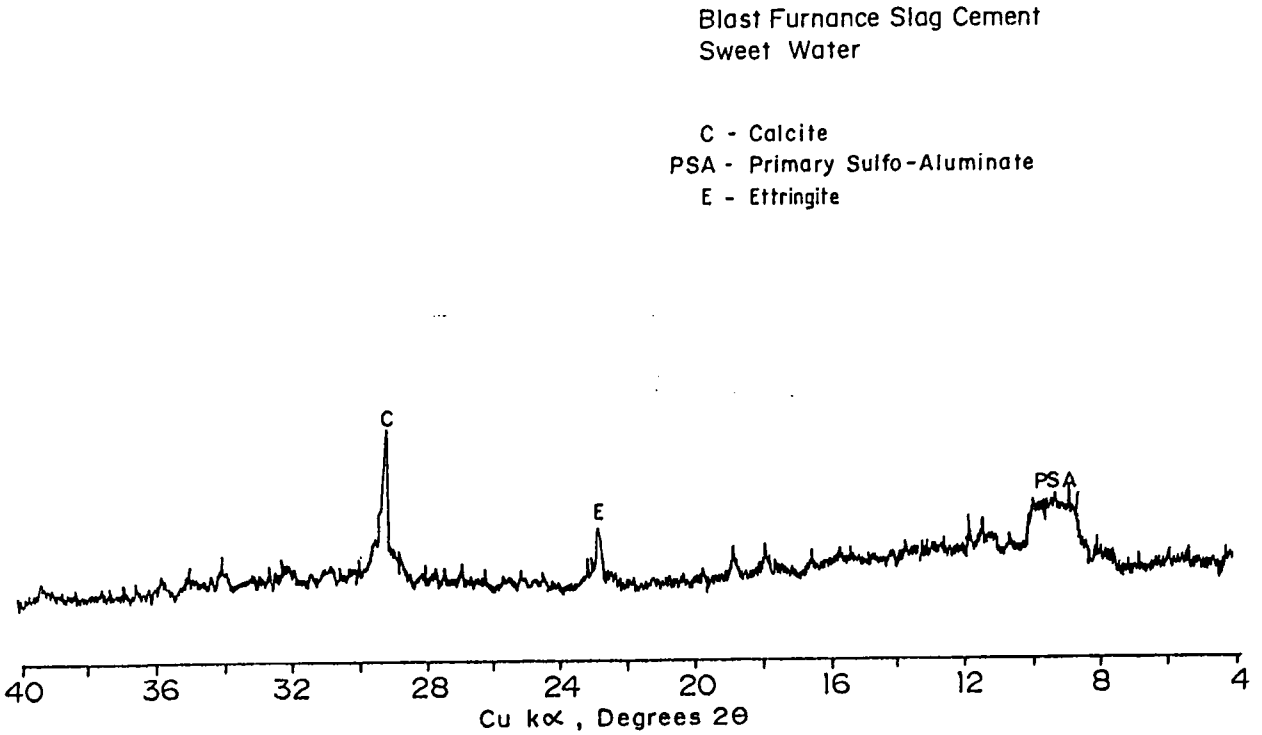

Fig. 6.13 : X-Ray Diffractogram for Blast Furnace Slag Cement in Potable Water after 720 Days of Immersion.

cement hydration than in the plain, silica fume and fly ash blended cements.

However, Fig. 6.13 shows an almost total disappearance of CH as a hydration product. This clearly indicates that in the case of blast furnace slag, CH produced by the hydration of the cement clinker, which precedes the hydration of slag, does not remain a product of hydration but acts as an alkaline slag activator and a reactant (208,209) during slag hydration, and is totally consumed in this process.

6.2.2 Plain and Blended Cements in Pure Sulfate Solution

The X-ray diffractograms for Type I and Type V cements (Figs. 6.14 and 6.15) exposed to magnesium-sodium sulfate environment show that portlandite has been reduced as a result of sulfate exposure and considerable amount of gypsum ($C\bar{S}H_2$) has been formed. The gypsum peaks at 11.7°, 20.7°, 28.9° 2θ are all well-defined. The XRD diagrams, however, show that the gypsum formed in Type V cement is significantly less than in Type I cement.

In addition to gypsum, ettringite peaks at 15.8° and 22.8° indicate the formation of secondary ettringite in Type I cement only. These peaks were absent for Type I cement in potable water. XRD for Type V cement (Fig. 6.15) does not show notice-

able secondary ettringite.

Peaks at 18.5°, 26.2° and 32.4° 2θ indicate the formation of brucite (MH) for both Type I and Type V cements. Primary ettringite-monosulfate phase between 9° and 10° 2θ is still present for both Type I and Type V cements.

Figs. 6.16 and 6.17 show the X-ray diffractograms for silica fume and fly ash blended cements in pure sulfate solution. It is seen that the portlandite (CH) is significantly reduced and large amount of gypsum is precipitated for both blended cements. Relatively, marginal quantity of ettringite and brucite is also formed. For silica fume blended cement, the primary sulfo-aluminate phase was not discernable.

Fig. 6.18 shows the diffractogram for BFS cement. It is seen that large amount of gypsum, which is significantly more than that in silica fume and fly ash blended cements, is precipitated in the exposed BFS cement. The primary sulfo-aluminate phase has disappeared and significant amount of secondary thaumasite is formed. Brucite and calcium aluminate hydrate (CAH) are also formed in relatively marginal quantities.

6.3 SULFATE ATTACK MECHANISMS

The deterioration factors in all plain and blended cements, which are in the range of 75% to 95% after 720 days of exposure,

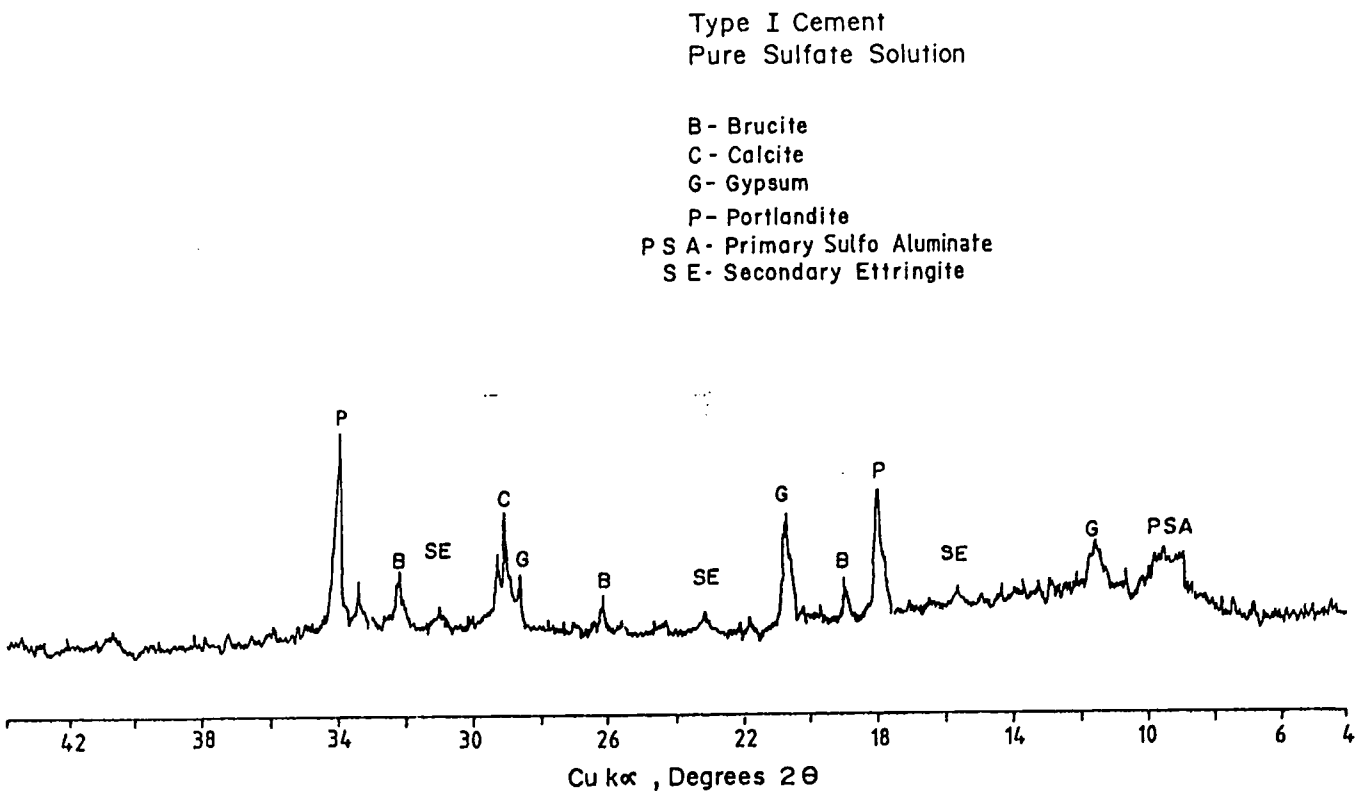

Fig. 6.14 : X-Ray Diffractogram for Type I Cement in Pure Sulfate Solution after 720 Days of Immersion.

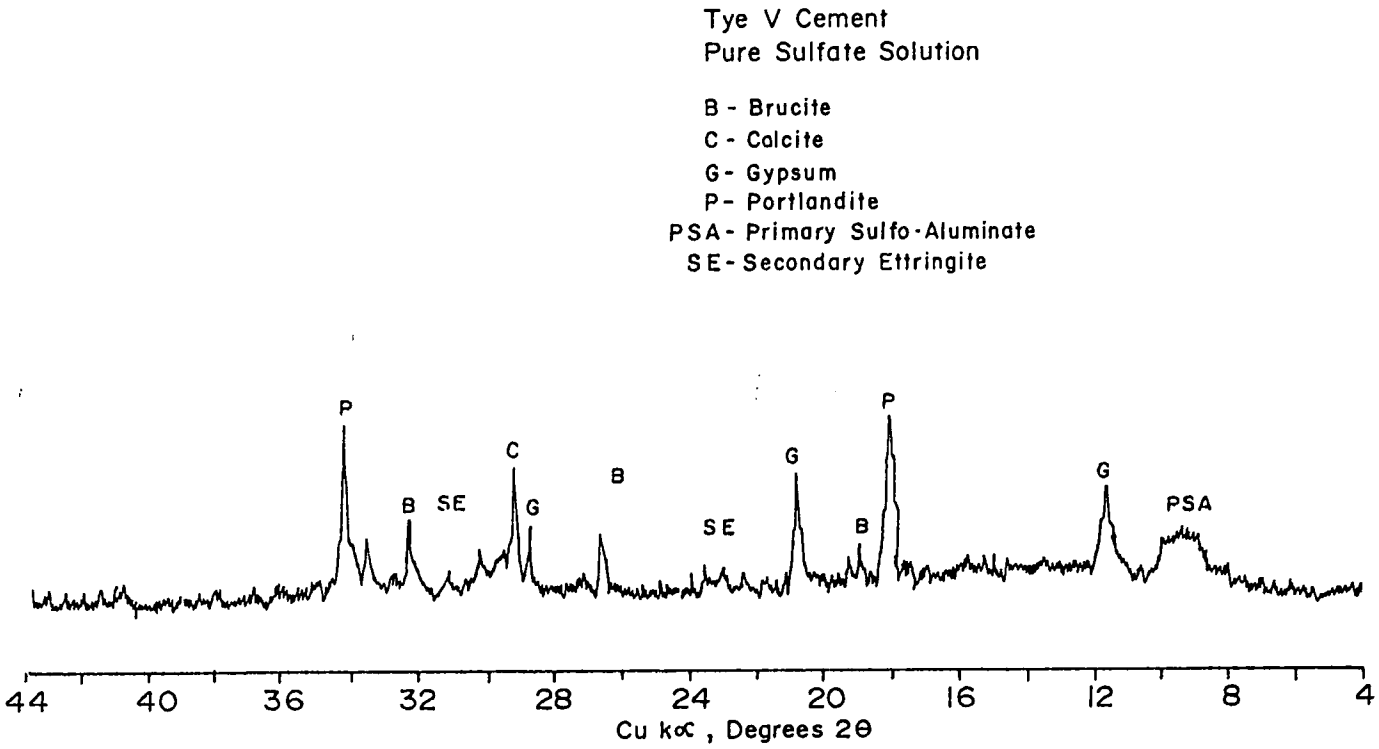

Fig. 6.15 : X-Ray diffractogram for Type V Cement in Pure Sulfate Solution after 720 Days of Immersion.

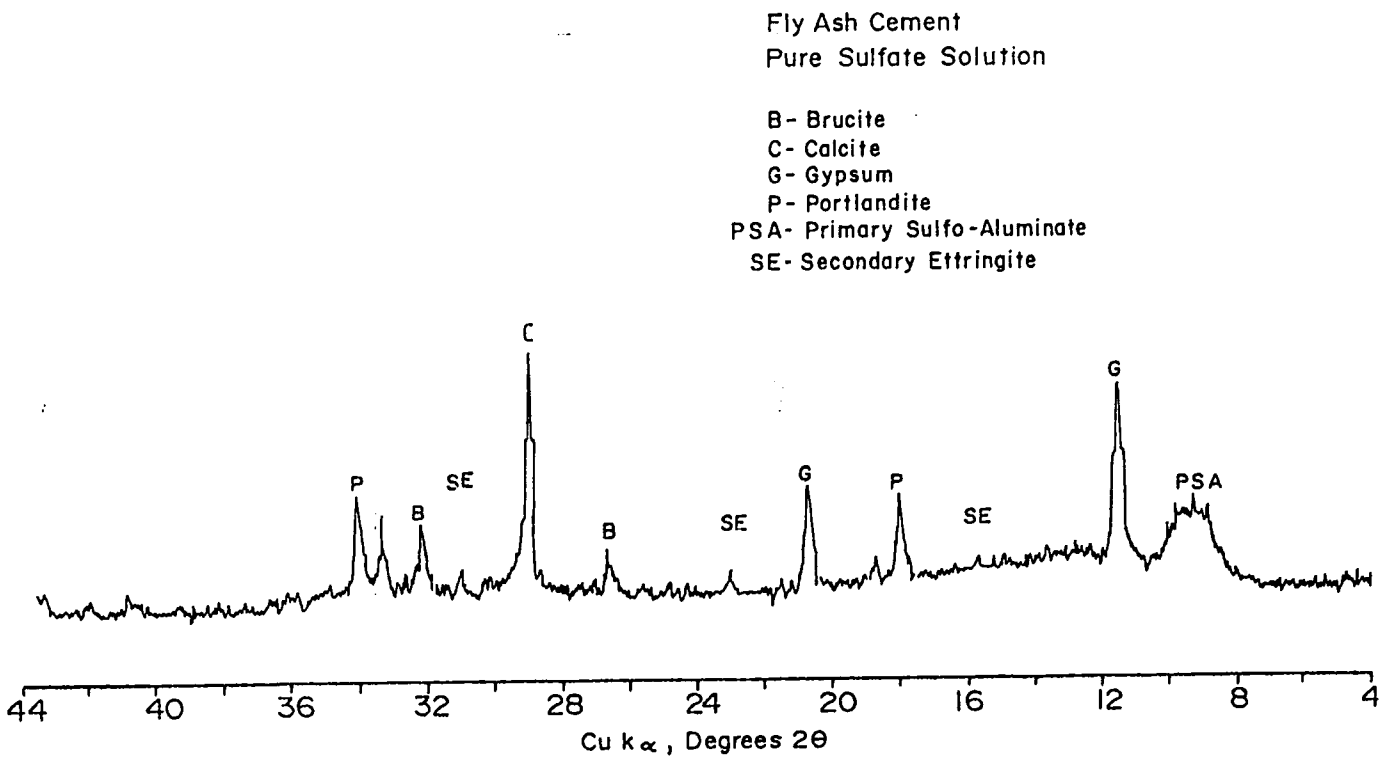

Fig. 6.16 : X-Ray Diffractogram for Fly ash Cement in Pure Sulfate Solution after 720 Days of Immersion.

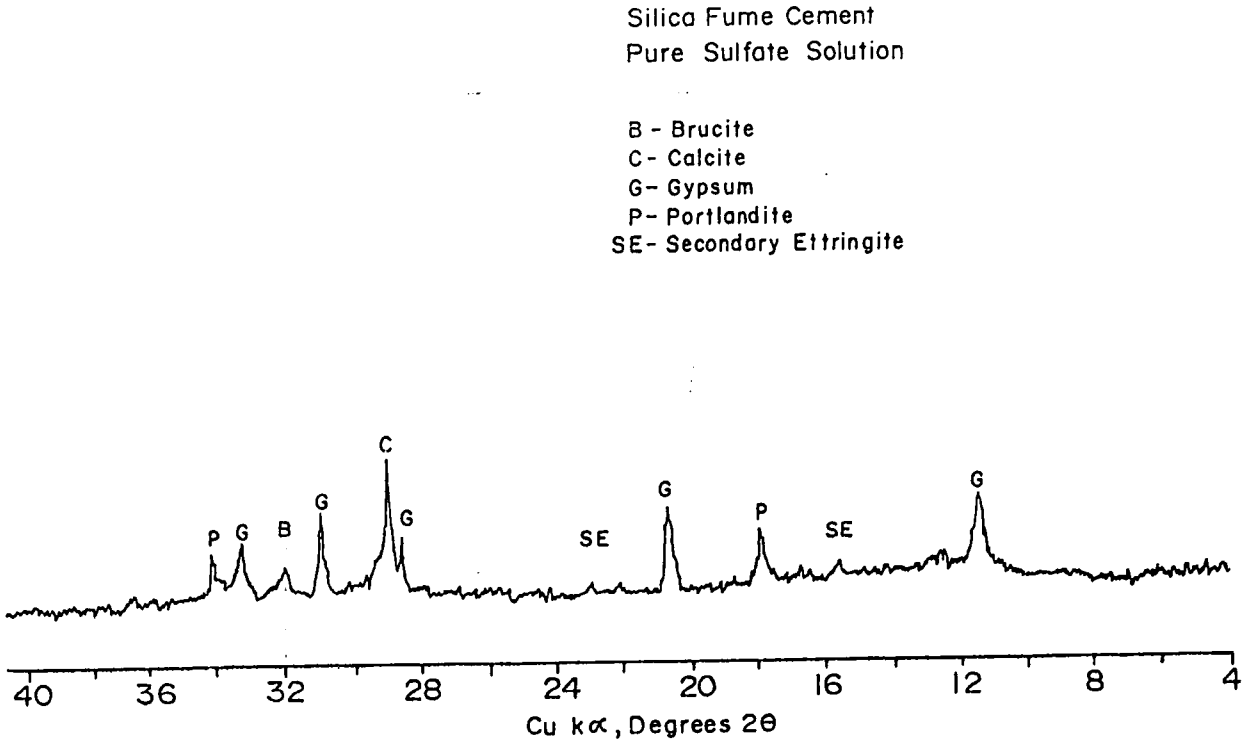

Fig. 6.17 : X-Ray Diffractogram for Silica Fume Cement in Pure Sulfate Solution after 720 Days of Immersion.

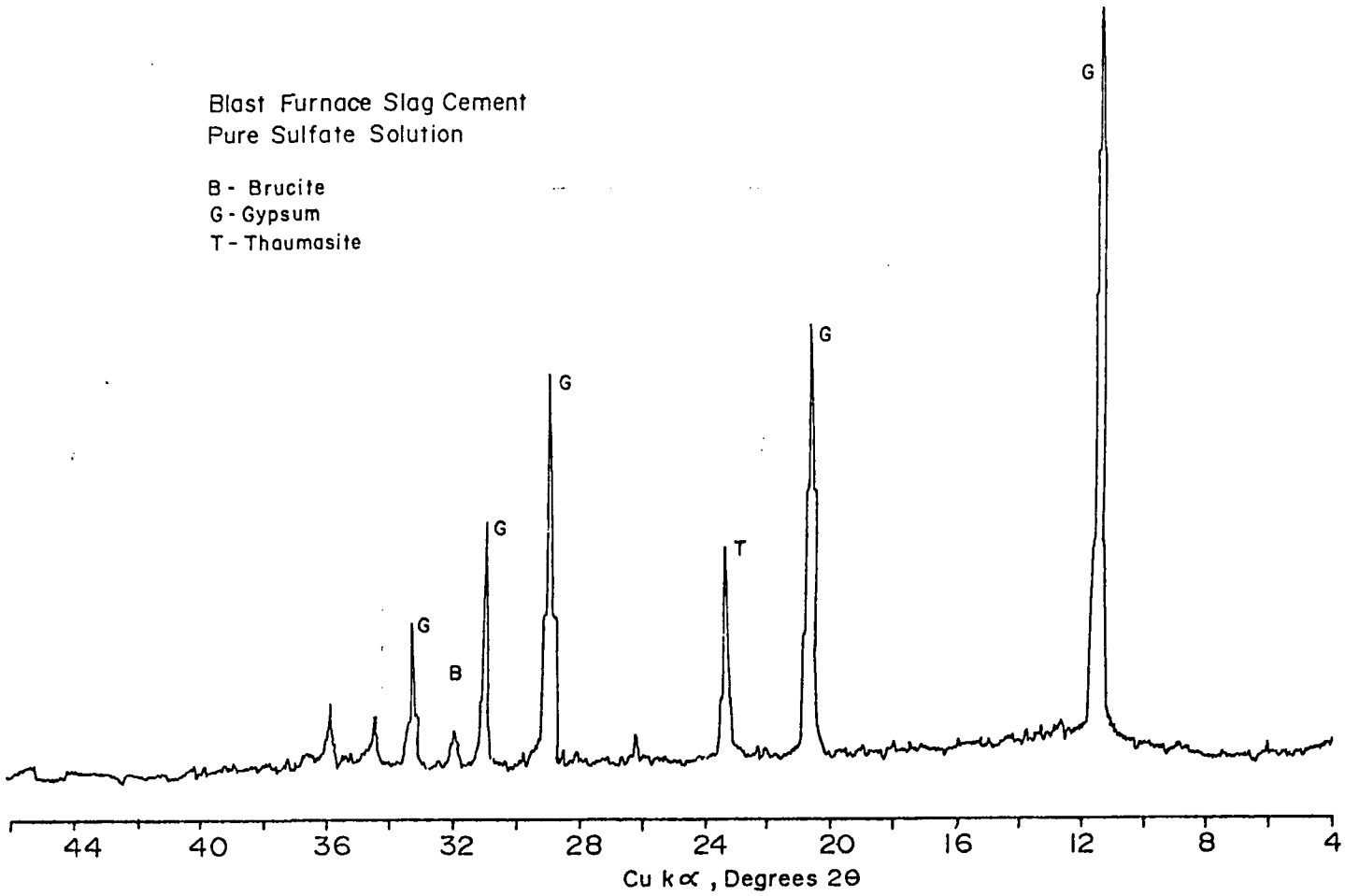

Fig. 6.18 : X-Ray Diffractogram for Blast Furnace Slag Cement in Pure Sulfate Solution after 720 Days of Immersion.

indicates a similar kind of degradation due to sulfate attack in all these cements. The attack on all plain and blended cements is primarily characterized by scaling, spalling and softening rather than expansion and cracking. In none of the specimens, the deep-seated swelling type of conventional sulfate reaction was noticeable. Invariably, the attack took the form of erosion of the cement paste, initially producing blistering and scaling of the surfaces and later causing delamination and loss of section.

The XRD patterns (Figs. 6.14 through 6.18) for all cements in the pure $M\bar{S}-N\bar{S}$ environment indicate either nil or only marginal presence of secondary trisulfate ($C_6A\,\bar{S}_3H_{32}$). The absence of ettringite from the highly deteriorated specimens is contrary to the conventional belief that sulfate attack is engendered by ettringite formation. The fact that expansive secondary ettringite is not a product of sulfate reaction in the cements listed in this study explains the absence of swelling and associated cracking. On the other hand, the X-ray diffractograms (Figs. 6.14 through 6.18) for the exposed cements exhibit sharp peaks of strong intensities at one, two or three spacings of 11.7, 20.7 and 28.9° 2θ, indicating massive precipitation of gypsum. Gypsum is formed by two mechanisms:

(i) as a result of reaction between $M\bar{S}$ and $N\bar{S}$ with CH liberated by the hydration of tricalcium and dicalcium

silicate phases of portland cement; and

(ii) as a result of the decompositional action of $M\bar{S}$ on calcium silicate hydrate (C-S-H).

The first mechanism based on the conversion of CH operates in accordance with the following reactions:

$$CH + N\bar{S} + 2H \rightarrow C\bar{S}H_2 + NH \qquad (6.1a)$$

$$CH + M\bar{S} + 2H \rightarrow C\bar{S}H_2 + MH \qquad (6.1b)$$

With the exception of BFS cement, the calcium hydroxide (CH) used in the above equations is liberated by the hydration of tricalcium and dicalcium silicates (C_3S and C_2S). This mode of gypsum formation is confirmed by the position that all exposed cements show in their XRD patterns formation of brucite (MH) as well as significant consumption of CH when the X-ray diffractograms (Figs. 6.14 through 6.18) of exposed cements are compared with those (Figs. 6.9 through 6.13) for the companion water-hydrated cements.

In the blast furnace slag blended cement, part or most of the CH generated by the hydration of the clinker acts as an alkaline activator of the slag (208,209) and is obviously consumed as a reactant. This is confirmed by the absence of CH peaks in the

XRD pattern for the hydrated BFS cement (Fig. 6.13). In the case of BFS cement, it is therefore hypothesized that the lime for gypsum formation is made available from the decomposition of hydrosilicates (C-S-H) which always occurs in $M\bar{S}$ solution (108,132,210).

Lea (132) has spelled out the mechanism of decomposition of C-S-H by $M\bar{S}$ leading to two consequences: (i) precipitation of gypsum, (ii) and the loss of strength of C-S-H binder. It is also pointed out that $M\bar{S}$ has a similar action to that of other sulfates in attacking calcium aluminate hydrate, but at later stages it induces a significantly different and more far-damaging effect because of its ability, as distinguished from other sulfates, to attack and decompose the calcium silicate hydrate.

Since Mg^{++} and Ca^{++} ions associate well with each other due to equal valence and similar ionic radii, $M\bar{S}$ reacts with C-S-H gel in the following manner (108,132,210):

$$C_xS_yH_z + xM\bar{S} + (3x + 0.5y - z)H \rightarrow xC\bar{S}H_2 + xMH + 0.5yS_2H \qquad (6.2)$$

The above reaction proceeds to completion because of the low solubility of MH (0.01 g/l compared to 1.37 g/l for CH). The

extremely low solubility of MH is accompanied by the fact that its saturated solution has a pH of about 10.5. This level of alkalinity is lower than the pH required to stabilize the hydrosilicates (C-S-H). The hydrosilicate then liberates lime to establish its equilibrium or stability pH. The liberated lime, however, instead of reestablishing the pH instantly, reacts with $M\bar{S}$ to form further MH and gypsum ($C\bar{S}H_2$) in accordance with reaction 6.1b. MH, being insoluble, separates from the solution, reducing the pH value to 10.5 again; more lime passes into solution by the decomposition of a further part of C-S-H to reestablish its stability pH. The reaction proceeds in this repetitive manner with more and more calcium sulfate ($C\bar{S}$) accumulating in solution until the environment becomes saturated whereby crystals of gypsum ($C\bar{S}H_2$) separate out. Gypsum produced from this reaction would react with calcium aluminates and monosulfate in high C_3A cements to produce more secondary expansive ettringite in accordance with the following reactions:

$$C_4AH_{13} + 3C\bar{S}H_2 + 14H \rightarrow C_6A\bar{S}_3H_{32} + CH \qquad (6.3)$$

$$C_4A\bar{S}H_{12} + 2C\bar{S}H_2 + 16H \rightarrow C_6A\bar{S}_3H_{32} \qquad (6.4)$$

$$C_3A + 3C\bar{S}H_2 + 26H \rightarrow C_6A\bar{S}_3H_{32} \qquad (6.5)$$

In relatively low C_3A cements, which is the situation in the Arabian Gulf region, as well as for the cements included in this study, massive precipitation of gypsum around C-S-H gel would facilitate the induction of sulfate ions into a C-S-H matrix leading to reduction of C-S-H binder strength.

MH, being the second product of reaction 6.2, has been found to react with the silicate hydrate (S_2H) which is also a product of C-S-H decomposition in reaction 6.2. MH and silicate hydrate (S_2H) reaction results in the formation of the non-cementitious magnesium silicate hydrate ($M_4SH_{8.5}$), in accordance with the following reaction:

$$4MH + SH_n \rightarrow M_4SH_{8.5} + (n-4.5)\ H \qquad (6.6)$$

The formation of non-cementitious M-S-H from the decomposition of cementitious C-S-H has been confirmed by several researchers. Cole (211) as well as Cole and Hueber (212) have reported a soft white material having the approximate composition $4MgO.SiO_2.8.5H_2O$ in a deteriorated concrete seawall. Regourd (213) has reported the presence of M-S-H in the polished sections of ordinary portland cement exposed to seawater for six months. In a recent study, using backscattered electron imaging (BEI) technique, Bonen and Cohen (214) have reported the presence of

M-S-H in a 10% silica fume blended cement exposed to $M\bar{S}$ solution.

6.3.1 Mechanism of Gypsum-Oriented Sulfate Attack

The relationship between C_3A content of cement and the ettringite-based swelling type of sulfate attack is now well-known. It is only the high C_3A cements which undergo ettringite-oriented sulfate attack. However, excessive gypsum precipitation around C-S-H gel engenders another kind of attack which, contrary to the ettringite-oriented swelling and expansion in high C_3A cements, occurs in low C_3A cements and is characterized by softening and loss of cohesion of the cement matrix. The mechanism of gypsum-oriented sulfate attack in low C_3A cement is based on the scenario that when continuous supply of sulfates progressively converts CH of the hydrated cement to gypsum, the initial (OH^-/CH)-dominated environment around C-S-H gel would be replaced by the (SO_4^{--}/$C\bar{S}H_2$)-dominated environment. This massive presence and concentration of sulfate ion around the hydrosilicates (C-S-H) facilitates the ingress of sulfate ions into the C-S-H gel matrix causing loss of strength and stiffness. A conceptual model of this change around the C-S-H environment due to massive gypsum formation is shown in Plate 6.5.

The entrance of sulfate ions in the C-S-H system is con-

firmed by several studies. A recent study (214) based on a backscattered electron imaging (BEI) technique clearly shows, in a BEI micrograph of 10% silica fume blended cement paste exposed to 4.2% $M\bar{S}$ solution (Plate 6.6), the gypsum crystals embedded within the reacted alite grain. Another research carried out by Jelenic et al. (215) related with the effect of gypsum on the hydration and strength development of commercial portland cements containing alkali sulfates, confirms that SO_3 is incorporated into $C-(S,\bar{S})-H$ gel and that the amount of SO_3 incorporated in $C-(S,\bar{S})-H$ phase increases with the increase in total SO_3 around C-S-H. They also confirm that this induction of SO_3 into C-S-H system gives a bad quality gel with lower compressive strength. In this study, scanning electron microscopy was used to study the microstructure of the hardened cement paste after exposure to sulfate solution. In almost all cements which had suffered severe sulfate deterioration, gypsum crystals had deeply intruded into C-S-H gel thereby creating a strong $SO_4^{--}/C\bar{S}H_2$ environment. A typical gypsum intrusion scenario is shown in a SEM micrograph (Plate 6.7). The left half of the micrograph shows the general field of intrusion of gypsum into C-S-H gel whereas the right half shows a magnification of box illustrating a cluster of gypsum crystals. The essential mechanism of gypsum-oriented sulfate attack is modelled in Plate 6.5.

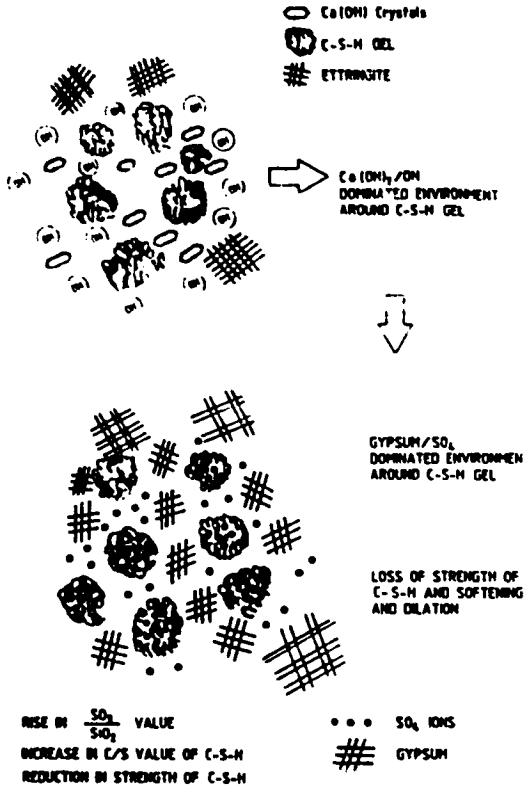

Plate 6.5 : **A Conceptual Model Showing the Essential Mechanism of Gypsum-Oriented Sulfate Attack.**

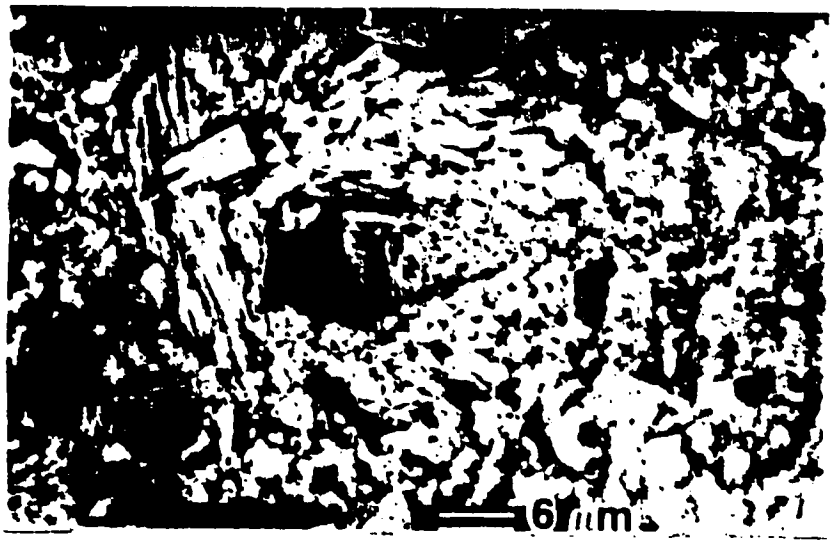

Plate 6.6 : Backscattered Electron Image (BEI) of 10% Silica Fume Paste Exposed to 4.2% Magnesium Sulfate Solution (Bonen and Cohen, 1992)

Plate 6.7 : SEM Micrograph Indicating Intrusion of Gypsum Crystals into CSH Gel.

The retrogression of strength of C-S-H in excessive gypsum environment is confirmed by the strength data developed by Mehta et al. (216) for alite cement mortars containing 0, 3, and 6% gypsum. The tests showed significant strength reduction in the presence of 6% gypsum. Bentur (217) has interpreted the effect of gypsum on the strength of pure C_3S pastes in terms of its effect on the quantity and quality of the C-S-H gel formed during hydration. An increase in the gypsum content, although increases the quantity of the C-S-H gel, reduces its quality and strength. An explanation for this reduction of C-S-H quality with increased presence of gypsum can be given in terms of an increase in the lime-to-silica (C/S) value of hydrosilicates (C-S-H). This increase is caused by the partial substitution of silica by sulfates in the C-S-H gel. Copeland and Kantro (218) were amongst the first to suggest the induction of sulfates into the C-S-H matrix. The ingress of sulfates results in the compositional changes in the C-S-H gel resulting in a rise in the SO_3-to-silica ($\overline{S}/S$) ratio. An increase in the $\overline{S}/S$ ratio in turn increases C/S value of the C-S-H gel (217). This increase reduces the intrinsic strength of the C-S-H gel, which is known to decrease linearly with an increase in its C/S mole ratio as shown in Figs. 6.19 and 6.20.

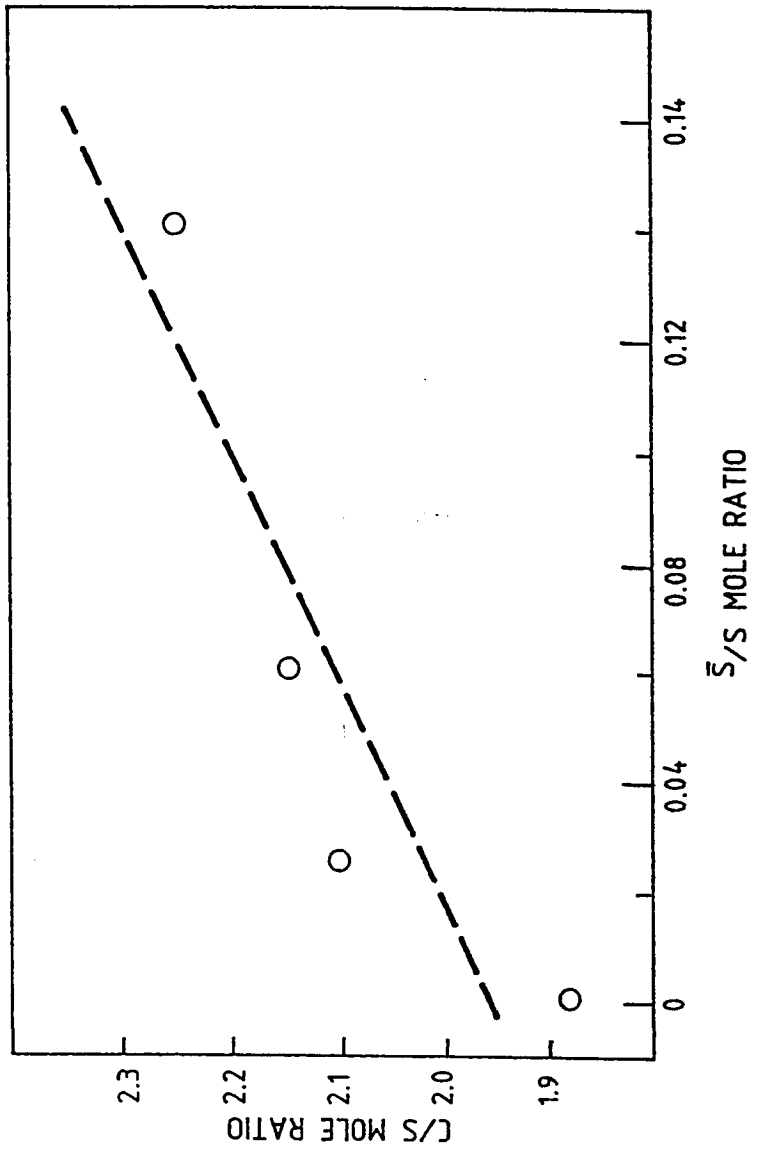

Fig. 6.19 : Effect of $\bar{S}$/S Ratio on C/S Ratio of C_3S Paste (Bentur, 1976).

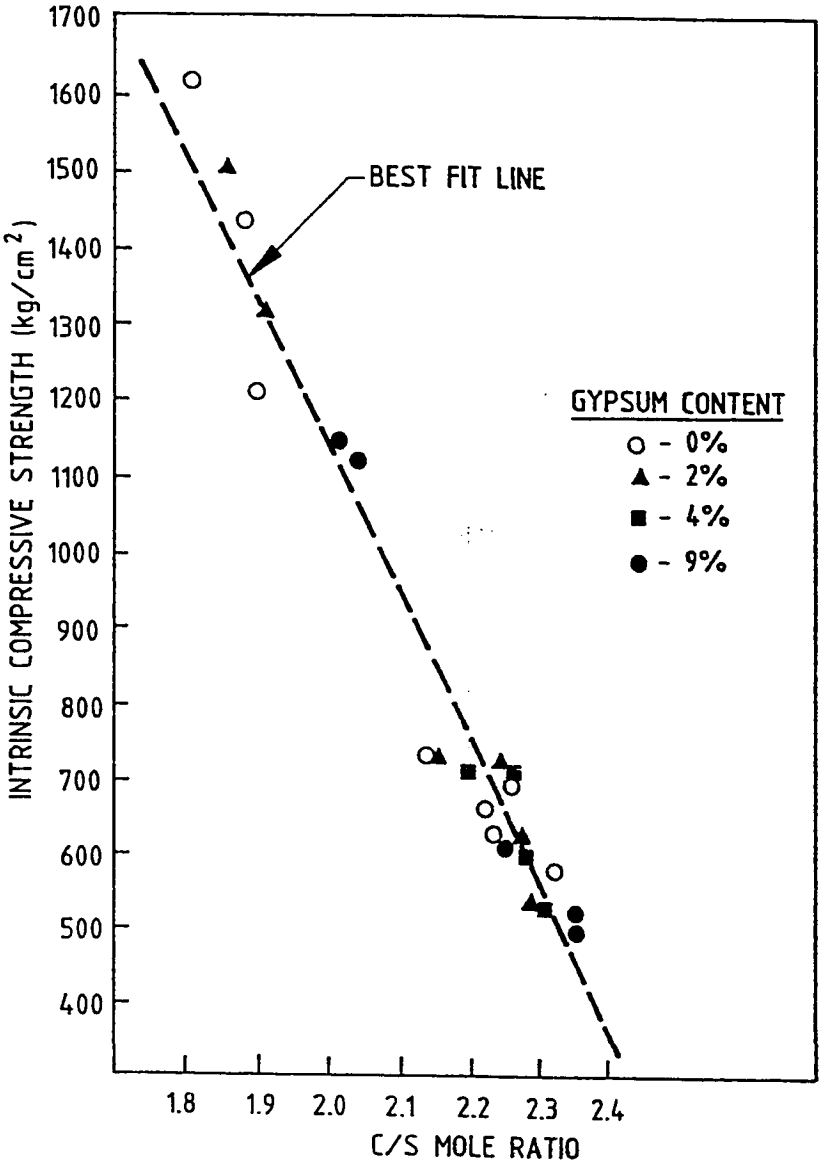

Fig. 6.20 : Effect of C/S Ratio on the Intrinsic Strength of C_3S Paste (Bentur, 1976).

6.3.1.1 *SEM Micrographs for Plain and Blended Cements in Potable Water*

A typical SEM micrograph for cements continuously hydrated in potable water is shown in Plate 6.8 for BFS cement. The micrograph in conjunction with the energy dispersive X-ray analysis (EDXA) for the general area (Fig. 6.21) shows a predominance of C-S-H gel and small quantities of primary sulfo-aluminate phase. A blow up of spot A (Plate 6.9) in conjunction with EDXA (Fig. 6.22) confirms the presence of mainly C-S-H and some primary sulfo-aluminate phase. Subsequent EDXA (Figs. 6.23 and 6.24) for spots B1 and B2 from the blow up micrograph (Plate 6.9) show mainly C-S-H phase.

The above position is typical for all cements tested in this program when they were continuously stored in water.

6.3.1.2 *SEM Micrographs for Plain and Blended Cements in Pure Magnesium-Sodium Sulfate Solution*

Plates 6.10 and 6.11 show SEM micrographs for Type V and Type I plain cements along with their EDXA outputs for the general area (Figs. 6.25 and 6.26) after 720 days of exposure to pure $M\bar{S}-N\bar{S}$ solution. For both plain cements, the SEM micrographs and the general area analysis show massive formation of gypsum along with significant presence of M-S-H. The C-S-H is noticeably reduced, indicating the decomposition of C-S-H to M-S-H

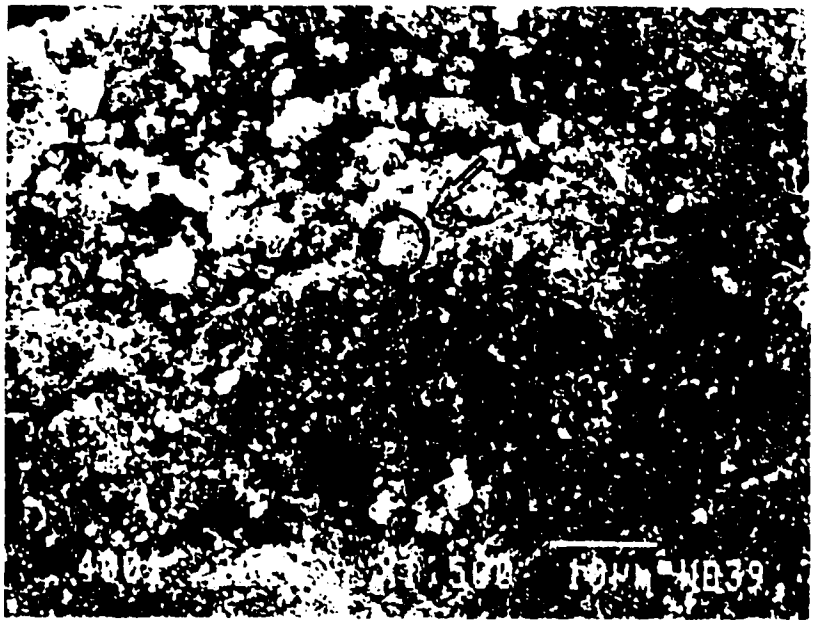

Plate 6.8 : SEM Micrograph for BFS Cement Cured in Potable Water.

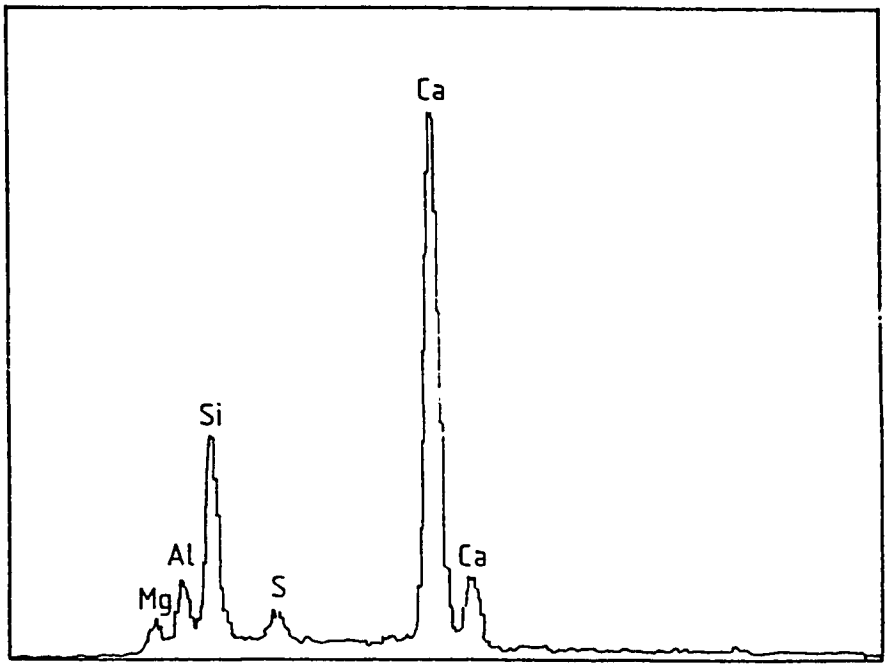

Fig. 6.21 : EDX Analysis for BFS Cement in Potable Water.

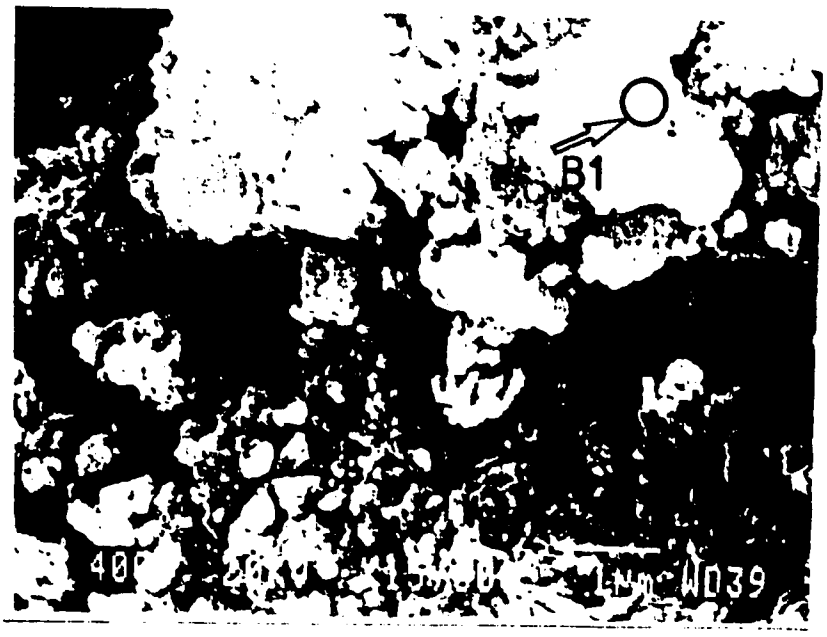

Plate 6.9 : A Blow up of Spot A in Plate 6.8.

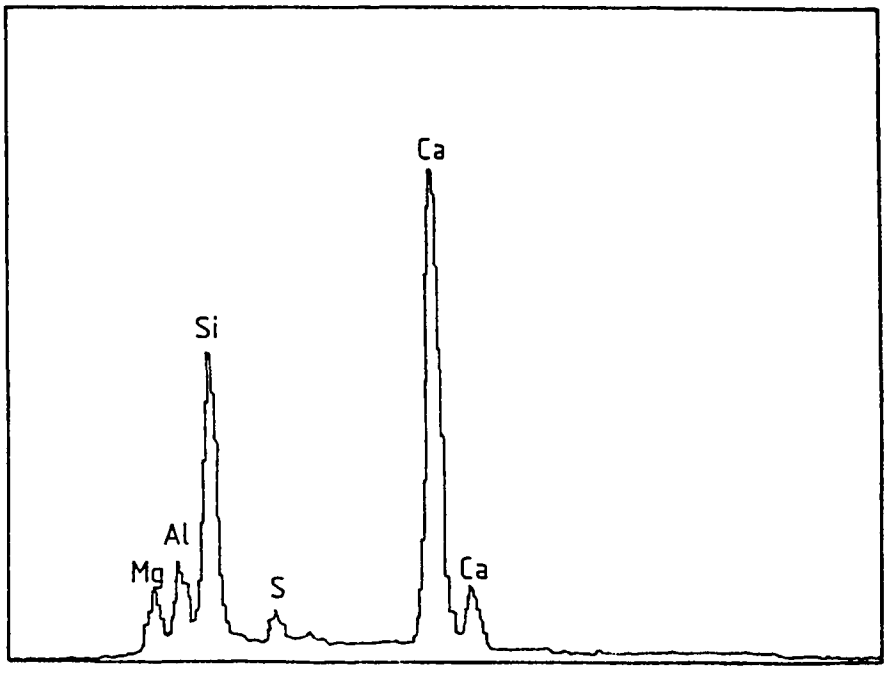

Fig. 6.22 : EDX Analysis for Spot A in Plate 6.8.

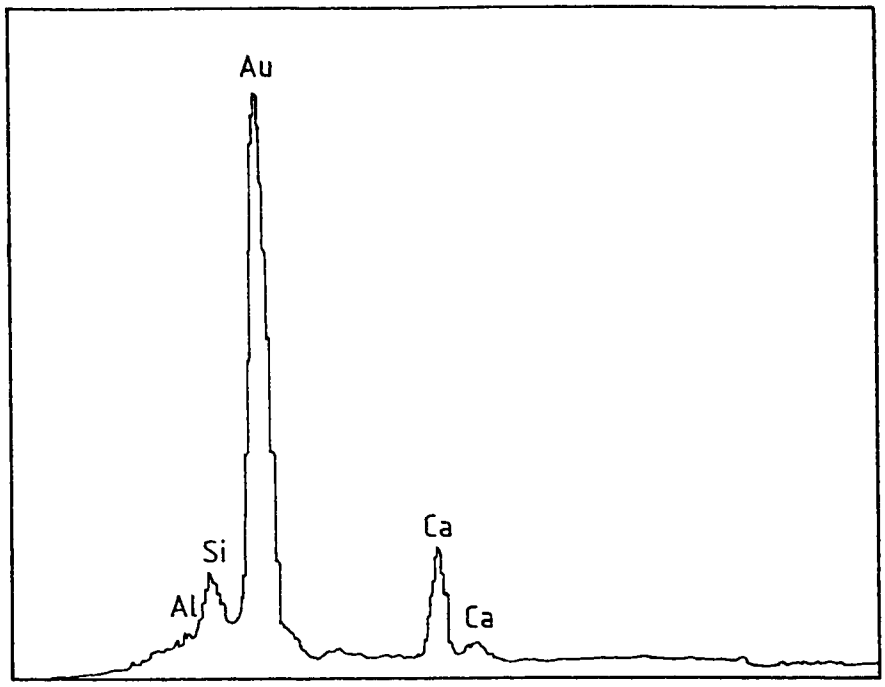

Fig. 6.23 : EDX Analysis for Spot B1 in Plate 6.9.

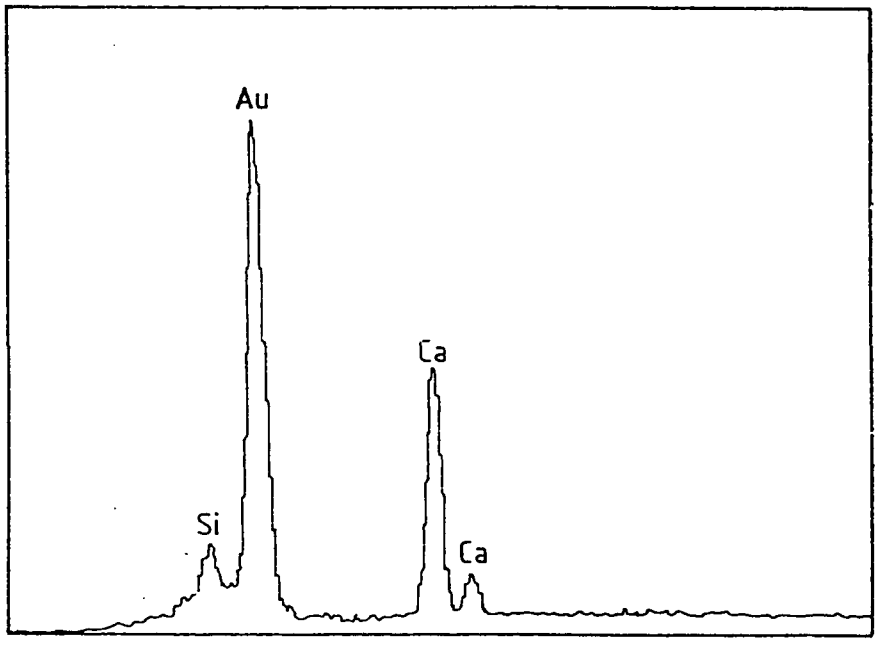

Fig. 6.24 : EDX Analysis for Spot B2 in Plate 6.8.

by the action of magnesium sulfate in accordance with equations 6.2 and 6.6. For Type V plain cement, a blow up of spot A (Plate 6.12) in conjunction with its EDXA output (Fig. 6.27) show predominant quantities of C-S-H and M-S-H overlying gypsum crystals. For the same cement, a blow up of spot B (Plate 6.13) in conjunction with its EDXA (Fig. 6.28) show massive gypsum with small quantities of C-S-H and M-S-H. For Type I plain cement, blow up of spot A (Plate 6.14) with EDXA (Fig. 6.29) shows predominantly C-S-H, whereas blow up of spot B (Plate 6.15) with EDXA (Fig. 6.30) show considerable amount of M-S-H intruded by gypsum. EDXA of spot C (Fig. 6.31) shows a location where only almost pure M-S-H is precipitated.

Plates 6.16 and 6.17 show the typical SEM micrographs of silica fume and blast furnace slag cements along with the EDXA outputs (Figs. 6.32 and 6.33) for the general area after 720 days of exposure to the pure $M\overline{S}-N\overline{S}$ solution. Micrographs for both blended cements placed in $M\overline{S}-N\overline{S}$ solution show massive gypsum in conjunction with significant quantities of M-S-H and C-S-H. A comparison of the micrographs and EDXA outputs for blast furnace slag in water and in pure sulfate solution (Plates 6.8 and 6.9 with Plate 6.17; and Figs. 6.21 through 6.24 with 6.33) clearly show that the predominantly present C-S-H has been significantly decomposed to M-S-H after exposure to pure $M\overline{S}-N\overline{S}$ solution.

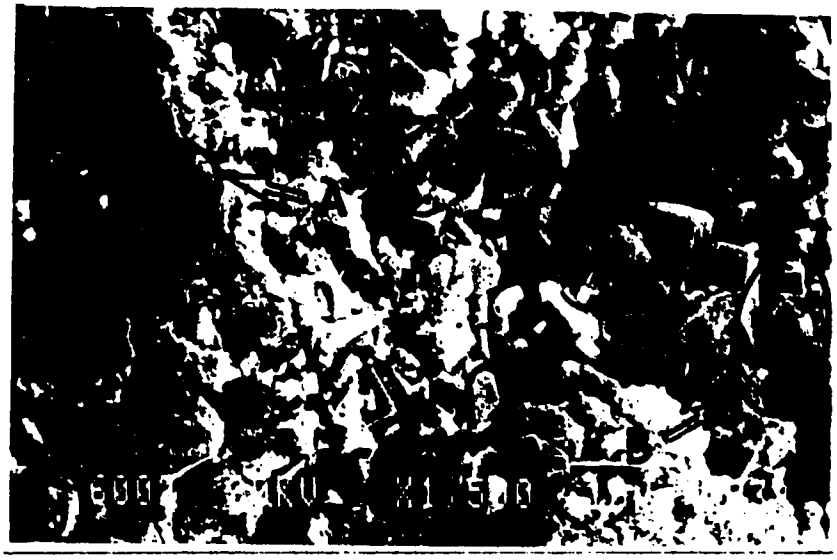

Plate 6.10 : SEM Micrograph for Type V Cement Exposed to Pure Sulfate Solution.

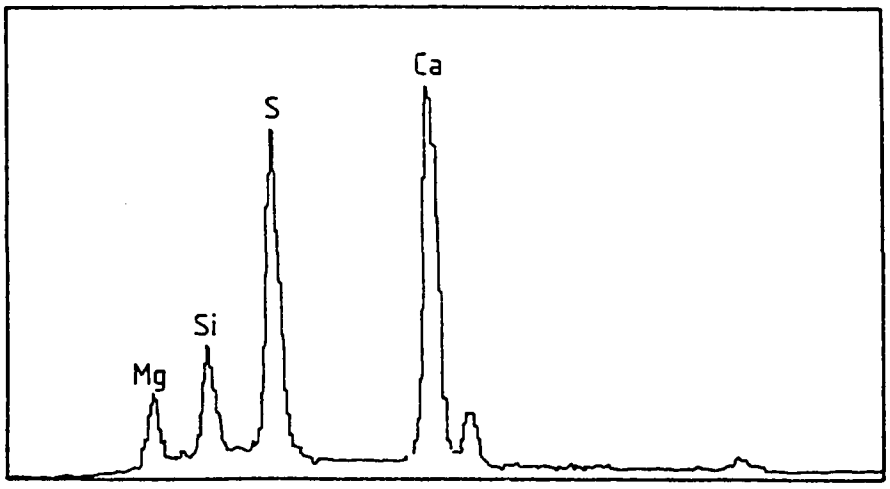

Fig. 6.25 : EDX Analysis for Type V Cement Exposed to Pure Sulfate Solution.

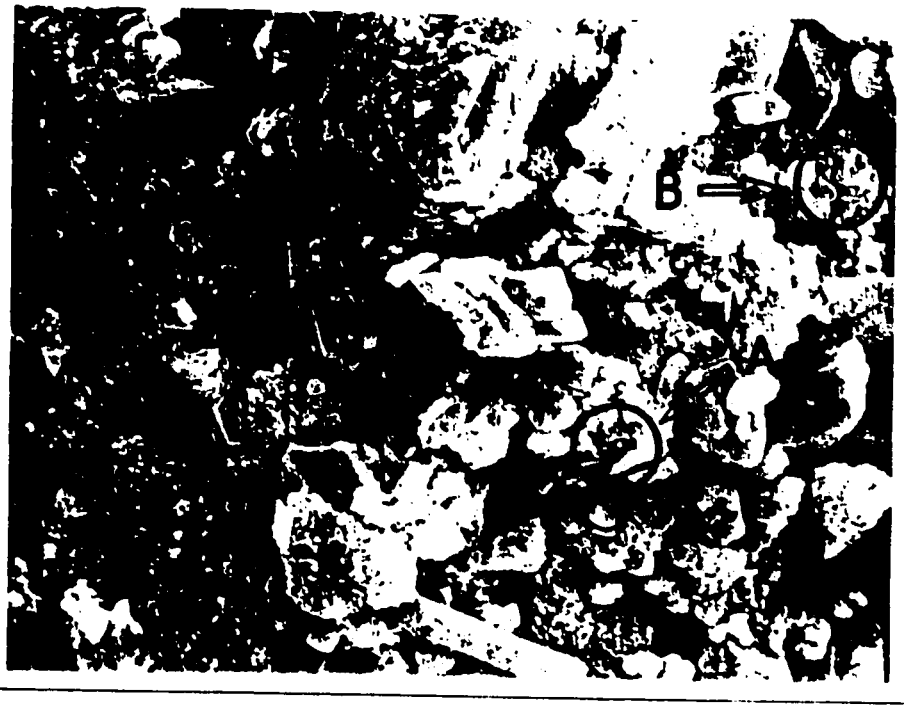

Plate 6.11 : SEM Micrograph for Type I Cement Exposed to Pure Sulfate Solution.

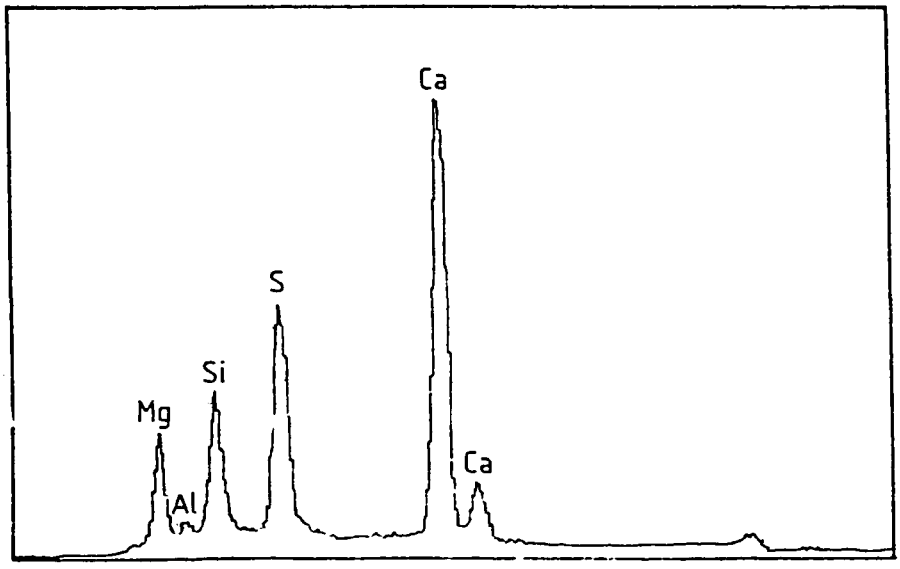

Fig. 6.26 : EDX Analysis for Type I Cement Exposed to Pure Sulfate Solution.

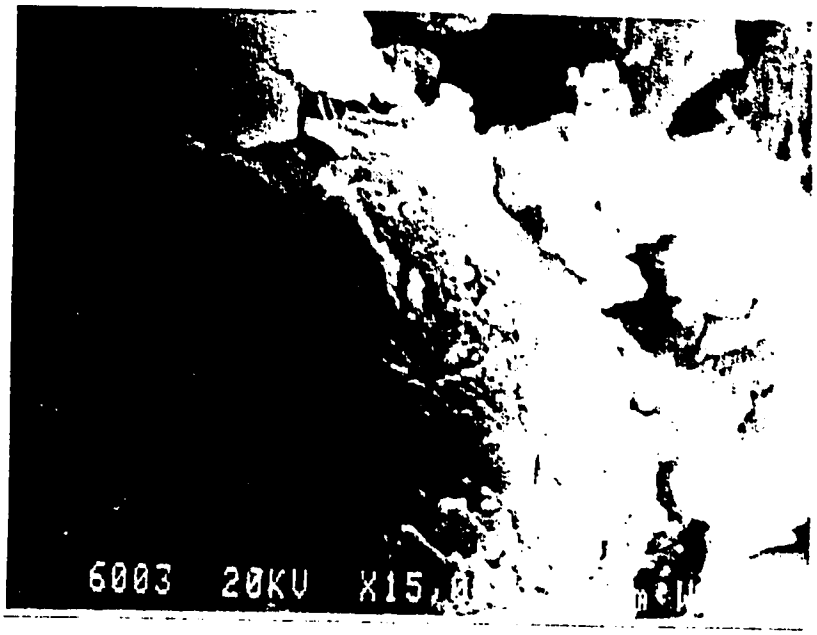

Plate 6.12 : A Blow up of Spot A in Plate 6.10.

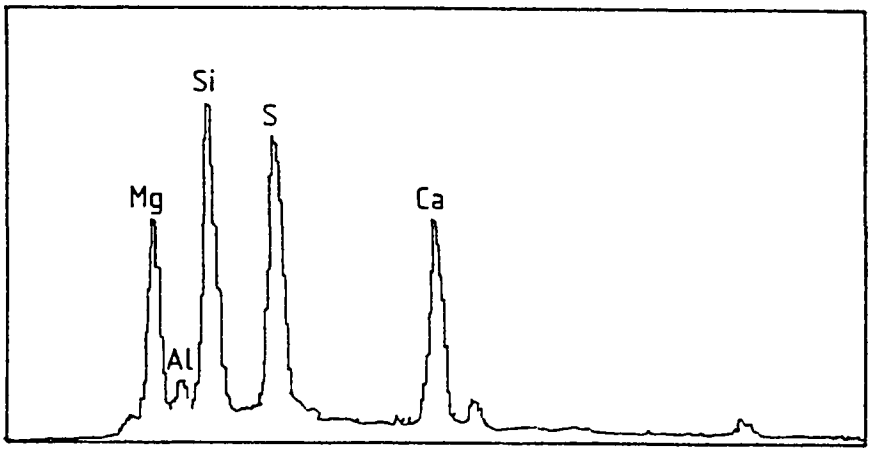

Fig. 6.27 : EDX Analysis for Spot A in Plate 6.10.

Plate 6.13 : A Blow up of Spot B in Plate 6.10.

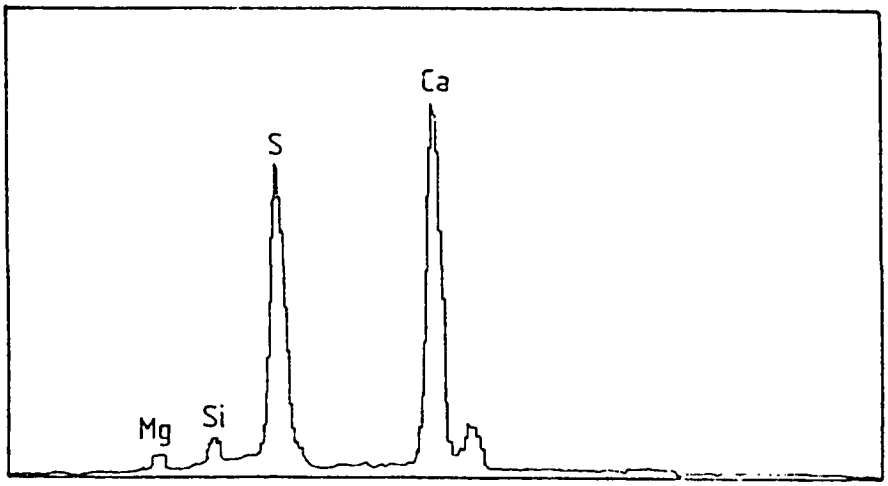

Fig. 6.28 : EDX Analysis for Spot B in Plate 6.10.

Plate 6.14 : A Blow up of Spot A in Plate 6.11.

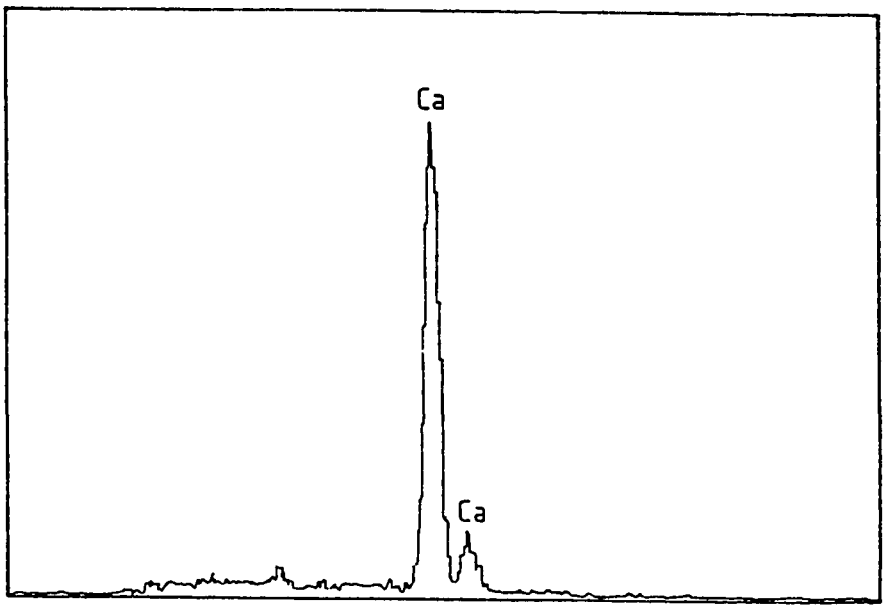

Fig. 6.29 : EDX Analysis for Spot A in Plate 6.11.

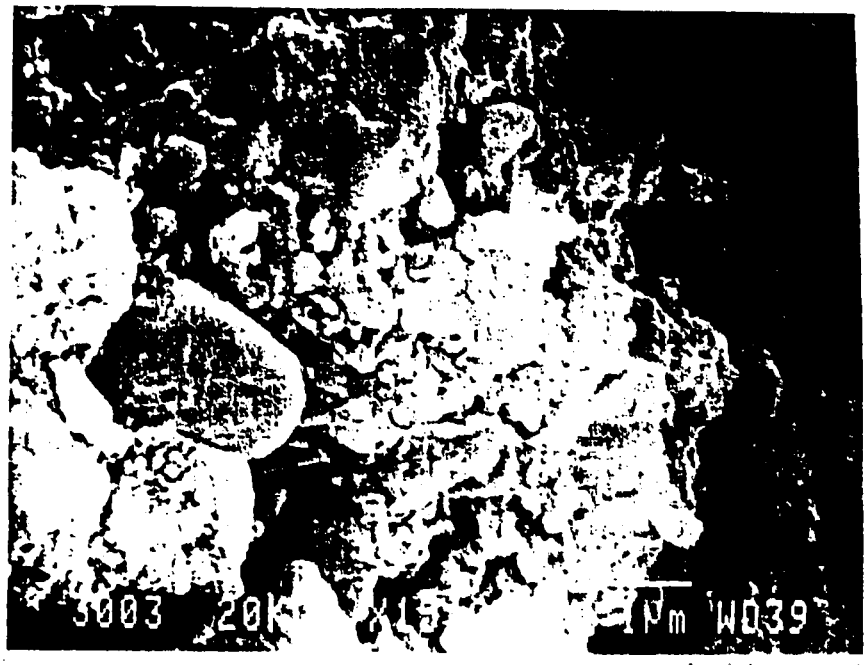

Plate 6.15 : A Blow up of Spot B in Plate 6.11.

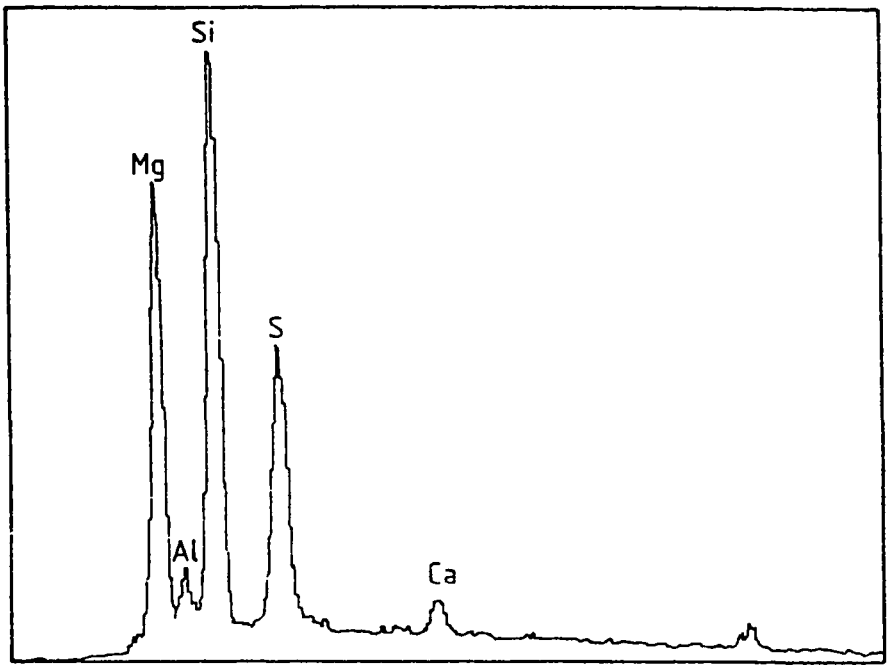

Fig. 6.30 : EDX Analysis for Spot B in Plate 6.11.

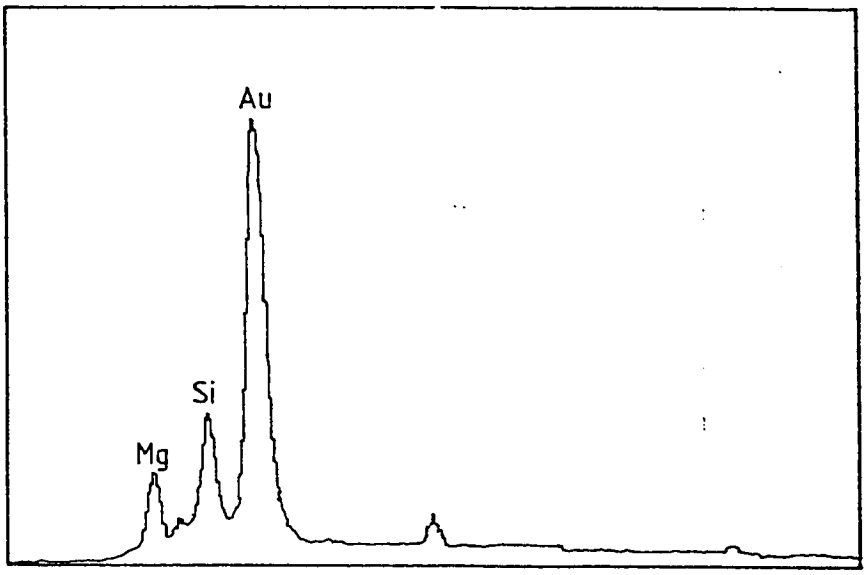

Fig. 6.31 : EDX Analysis for Spot C in Plate 6.11.

For blast furnace slag cement (Plate 6.17), the EDXA of the large amorphous area on the left (spot C, Fig. 6.34) indicates composition comprising predominantly M-S-H with sulfate intrusions. A blow up of spot B in Plate 6.17 (shown in Plate 6.18) in conjunction with its EDXA (Fig. 6.35) for spot B within the amorphous base indicates primarily M-S-H. Plate 6.18 clearly shows the fibrous and amorphous morphology of M-S-H. EDXA of spot A (Fig. 6.36) shows pure gypsum crystals.

For silica fume blended cement, the EDXA of the amorphous area (spot C, Plate 6.16) also shows predominantly M-S-H with intrusion of gypsum crystals, as confirmed by the EDXA analysis (Fig. 6.37). EDXA of spot B in the amorphous base (Fig. 6.38) shows the presence of only pure M-S-H. A blow up micrograph of this spot (Plate 6.19) clearly shows again the amorphous and fibrous morphology of M-S-H. EDXA of a typical crystal (Fig. 6.39) shows a pure gypsum crystal.

In conclusion, the SEM micrographs and their accompanying EDXA outputs for all plain and blended cements exposed to $M\overline{S}-N\overline{S}$ solution show the following salient common features:

(i) massive gypsum precipitation,

(ii) significant decomposition of cementitious C-S-H gel to non-cementitious M-S-H, and

(iii) amorphous and fibrous morphology of M-S-H.

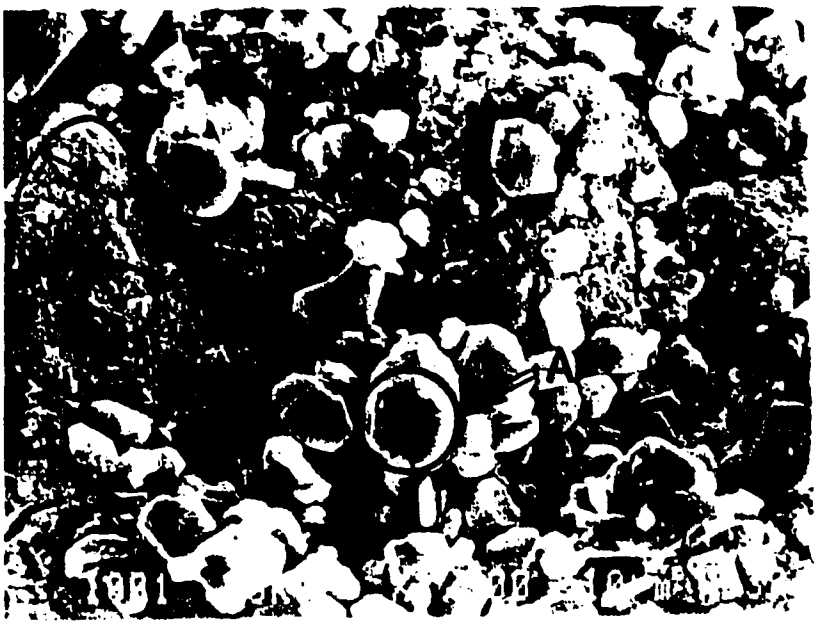

Plate 6.17 : SEM Micrograph for BFS Cement Exposed to Pure Sulfate Solution.

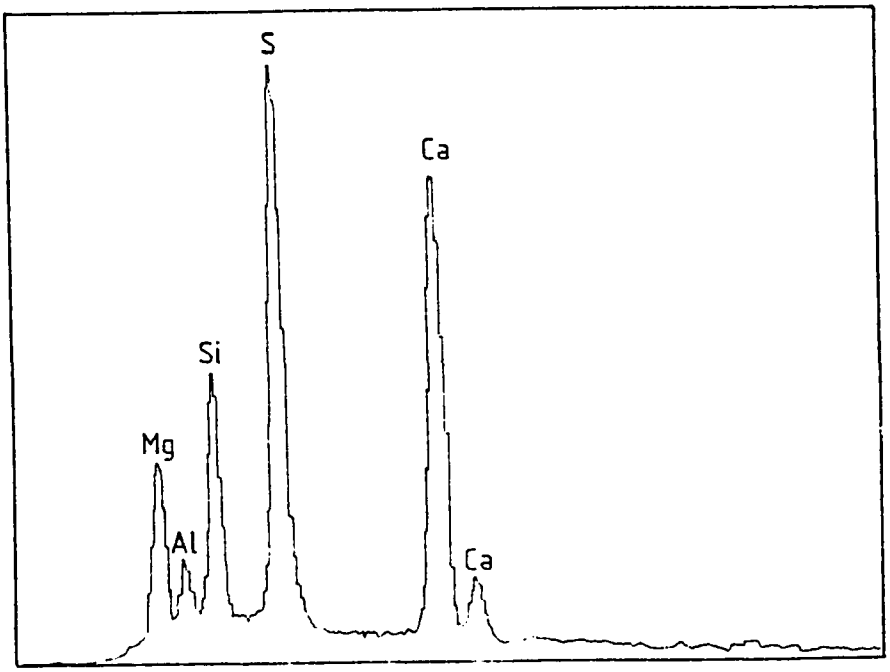

Fig. 6.33 : EDX Analysis for BFS Cement Exposed to Pure Sulfate Solution.

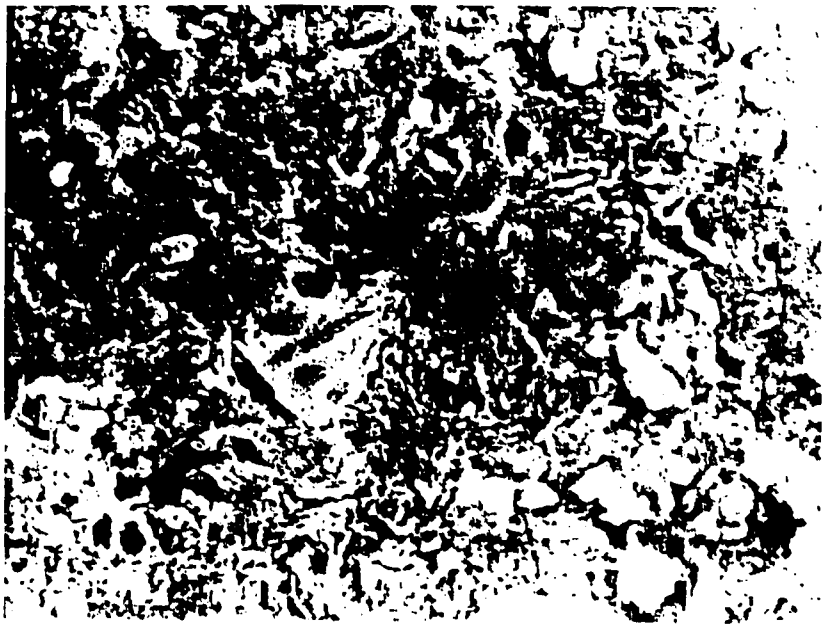

Plate 6.18 : A Blow up of Spot B in Plate 6.17.

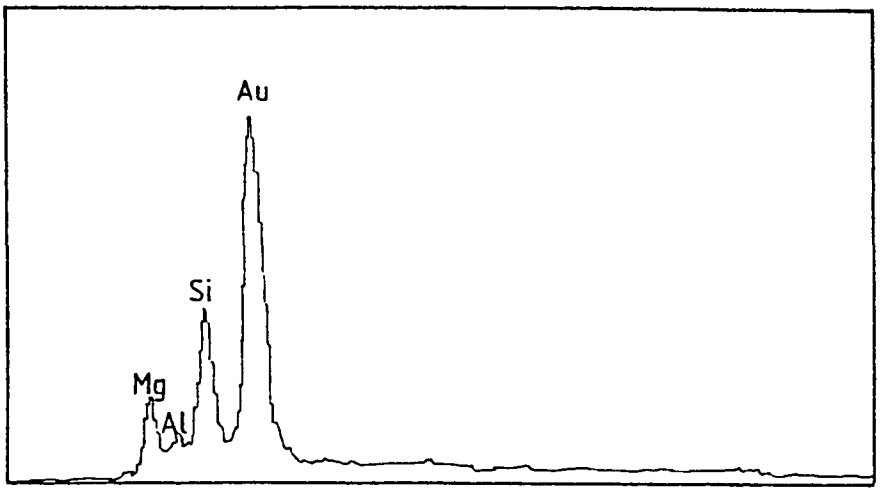

Fig. 6.35 : EDX Analysis for Spot B in Plate 6.17.

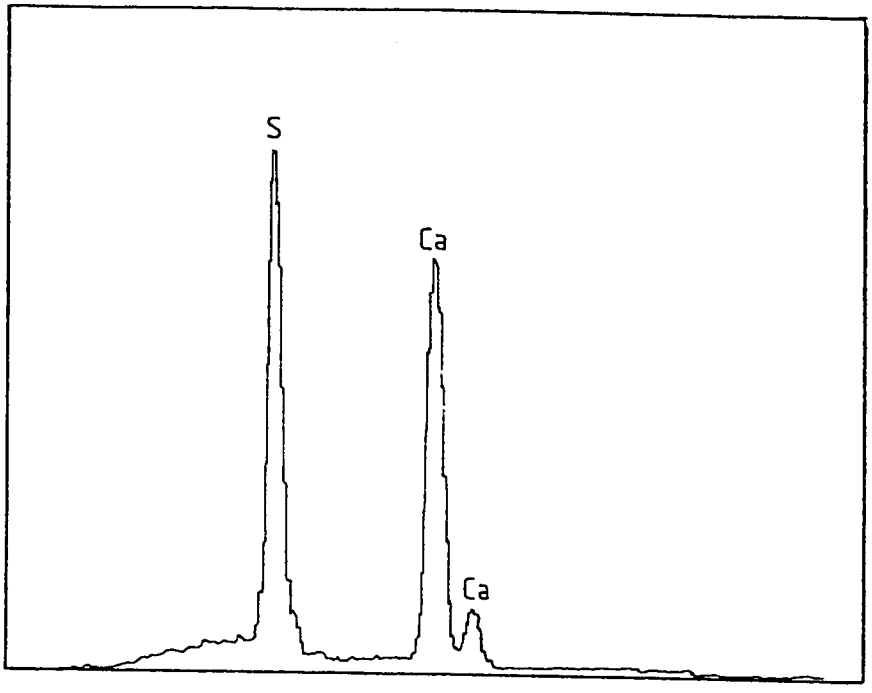

Fig. 6.36 : EDX Analysis for Spot A in Plate 6.17.

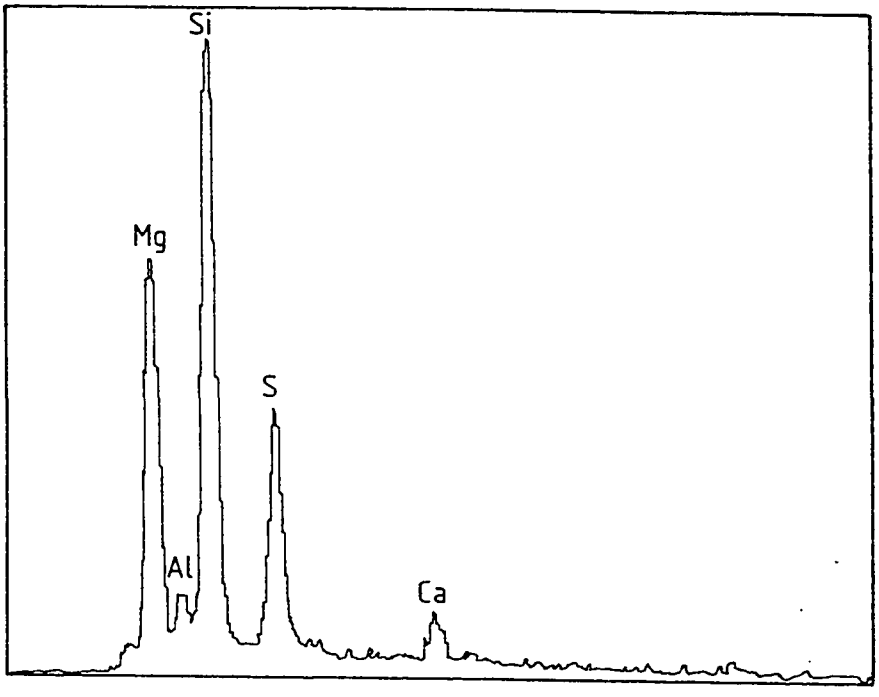

Fig. 6.37 : EDX Analysis for Spot C in Plate 6.16.

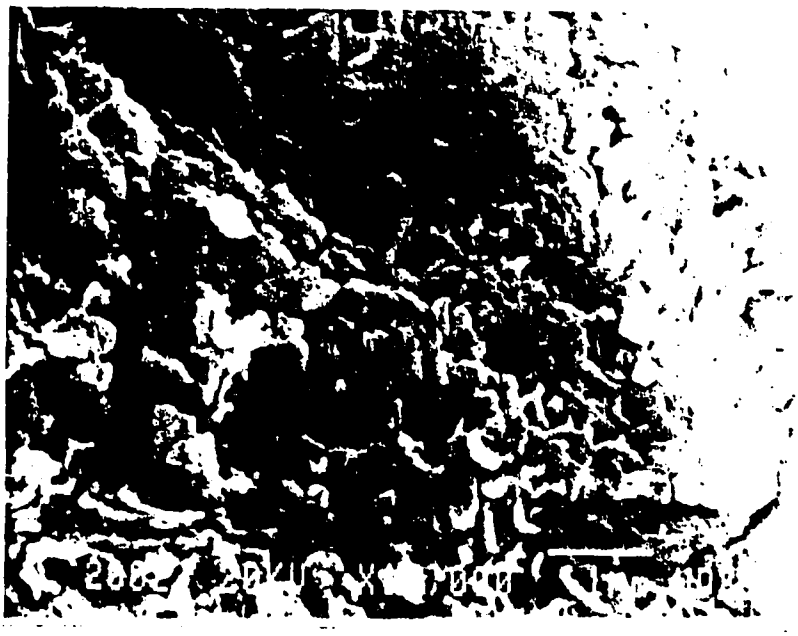

Plate 6.19 : A Blow up of Spot B in Plate 6.16.

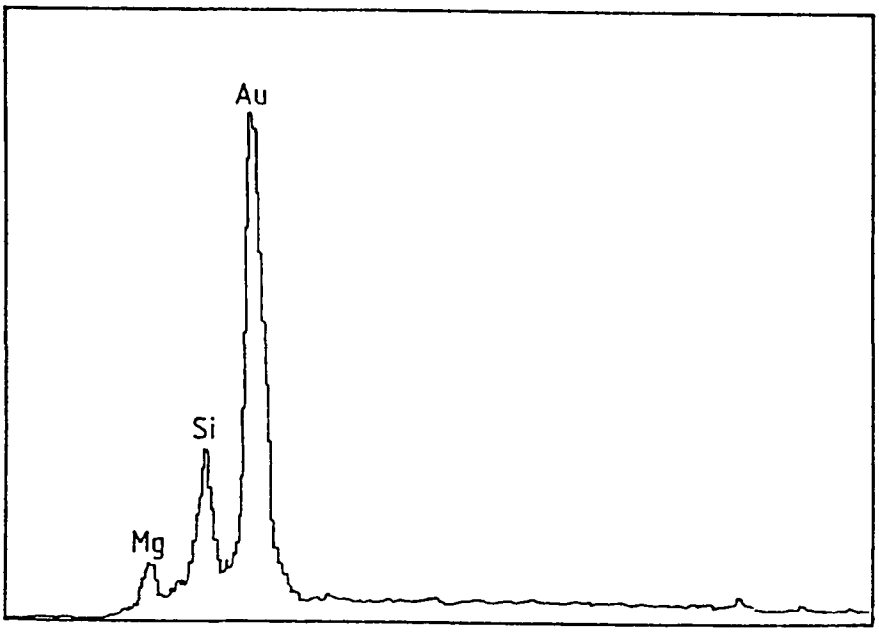

Fig. 6.38 : EDX Analysis for Spot B in Plate 6.16.

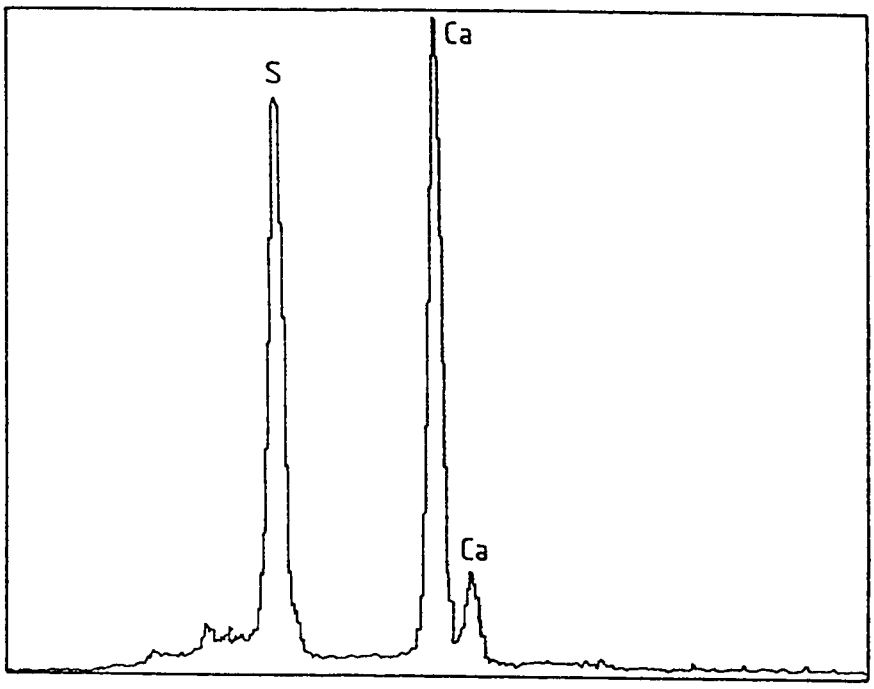

Fig. 6.39 : EDX Analysis for Gypsum Crystal Growth in Silica Fume Cement Exposed to Pure Sulfate Solution.

6.3.2 Magnesium-Gypsum Attack

In summary, as shown by X-ray diffractograms and SEM micrographs in previous sections, hydraulic cement systems exposed to pure $M\bar{S}-N\bar{S}$ environment would suffer degradation due to two concomitant effects:

(i) continuous decomposition of C-S-H to a non-cementitious M-S-H gel due to magnesium attack, whereupon the C-S-H binder progressively loses cohesion and strength, and

(ii) degradation of C-S-H binder due to sulfate induction into its matrix as a result of massive precipitation of gypsum around C-S-H.

The combined magnesium-gypsum-oriented sulfate attack would materialize only in exposure conditions where $M\bar{S}$ constitutes a noticeable proportion of the sulfate environment. However, the gypsum-oriented sulfate attack will occur in low C_3A cement construction in any sulfate environment and will be characterized by a state of cohesionlessness, spalling and softening (181). In contrast to the ettringite-oriented sulfate attack, which is characterized by expansion and cracking and is not observed in the Arabian Gulf region, the gypsum type of attack is highly prevalent in the Gulf construction due to the universal use of low C_3A sulfate

resistant Type V cements. Plates 6.20 and 6.21 show the typical mode of the gypsum-oriented sulfate attack in the Gulf region. Cement mortar blocks disintegrated and became cohesionless and granular due to the attack of sulfate salts contained in the groundwater drawn up by the capillary action. XRD pattern (Fig. 6.40) of the decomposed block material shows massive gypsum formation with almost no ettringite, in spite of the use of low C_3A Type V cement.

Even in relatively high C_3A cements, specially those containing high C_3S, which is the normal compositional position in the Gulf cements, if the sulfate concentration becomes excessive, and massive gypsum is precipitated due to the relatively large quantities of CH generated by the high C_3S cements, it is most likely that the gypsum-type of acidic attack would overshadow the ettringite-type swelling attack. This is shown in this study by the behavior of Type I (C_3A: 8.5%) cement when exposed to pure $M\bar{S}-N\bar{S}$ environment. It is seen that although some secondary ettringite is formed (Fig. 6.14), it fails to generate the ettringite-oriented expansion-cracking systems even after 720 days of exposure. This may be because, as Lea (132) explains, calcium sulfoaluminate is itself unstable in the presence of magnesium sulfate solution, and by the continued action of this salt, the sulfo-alumi-

Plate 6.20 : A Typical Mode of Gypsum-Oriented Sulfate Attack in the Arabian Gulf Region.

Plate 6.21 : Another Documentation of the Gypsum-Oriented Slfate Attack in the Arabian Gulf Region.

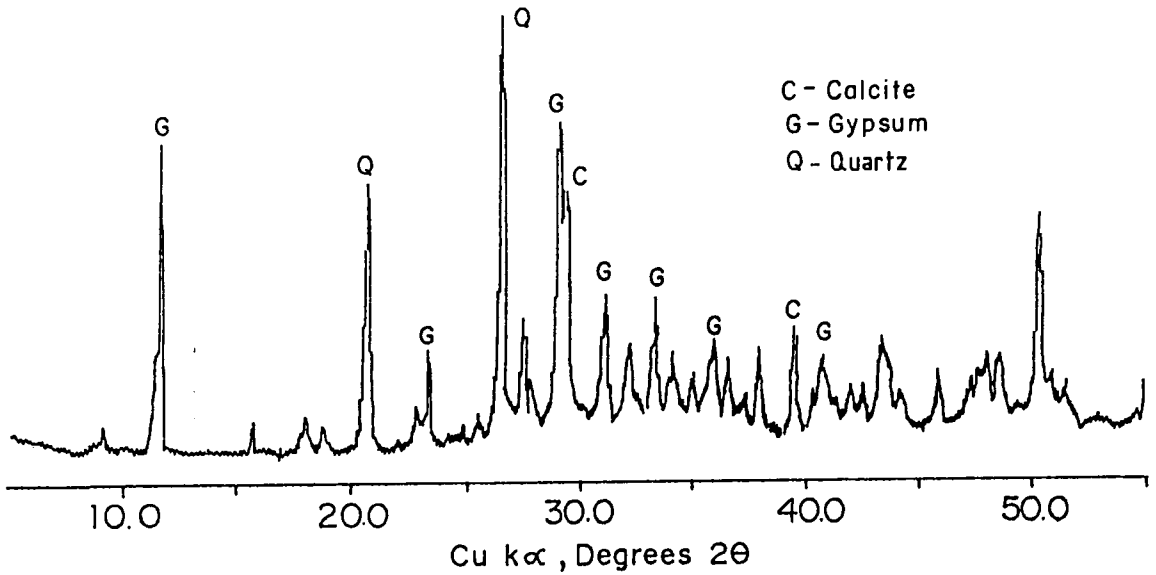

Fig. 6.40 : X-Ray Diffraction of the Deteriorated Block Material in Plate 6.5.4.1.

nate is ultimately decomposed again to form gypsum, hydrated alumina and magnesium hydroxide.

It would therefore seem that whereas in low C_3A cements the sulfate attack would always be gypsum-based, in relatively high C_3A cements, the nature of attack would be determined by the SO_4^{--} content. In relatively low SO_4^{--} exposure conditions and when gypsum is not precipitated massively, the attack will be engendered by ettringite and will be of a swelling-cracking type. As the SO_4^{--} concentration increases, the attack will transform to ettringite-gypsum type and with further increase in SO_4^{--} concentration, it would convert to pure gypsum-type, exhibiting cohesionlessness and softening.

The sulfate resistance performance of the five cements tested in this study after 360 and 720 days of exposure to the $M\bar{S}-N\bar{S}$ environment can be readily evaluated from Table 6.1 and Figs. 6.4 through 6.8. The visual ratings as well as the deterioration factors show that all cements are at about the same advanced level of disintegration and are well ahead of the 25% weight loss criterion which, according to Mehta (183), demarcates satisfactory from poor or very poor performance. All cements, in fact, are in a state which is well past the condition corresponding

to structural failure. Actually this is the situation even after 360 days of exposure where the deterioration factors range between 55% and 77% for various cements (Table 6.1). It is also interesting to observe that the performance of Type V (C_3A : 3.5%) cement in pure $M\bar{S}-N\bar{S}$ solution does not indicate marked advantage over Type I (C_3A : 8.5%) cement.

Also, the performance data show that cement blending by supplementary cementing materials, such as silica fume, fly ash and BFS, did not improve the sulfate resistance in pure $M\bar{S}-N\bar{S}$ exposure conditions over the performance of the parent cement. In fact, whereas fly ash blended cement had the same deterioration factor of 85% as the parent cement after 720 days of exposure, blending with silica fume and BFS cements enhanced the deterioration factors to 90% and 95% respectively compared to 85% for the parent cement. This shows a negative effect of silica fume and BFS blending on sulfate resistance of concrete if $M\bar{S}$ is a significant constituent of the sulfate environment. All five cements, including the three blended cements, showed the same type of blistering, spalling and softening type of deterioration which is the outcome of degradation and decomposition of the cementing material. It is quite obvious that in the pure $M\bar{S}-N\bar{S}$ exposure, these cements have suffered gypsum-magnesium-type of attack rather than the ettringite-type of swelling-cracking deterioration. This is

confirmed by X-ray diffractograms and SEM micrographs of Sections 6.2.2 and 6.3.1.2, which show massive gypsum formation for all cements and significant decomposition of cementitious C-S-H into non-cementitious M-S-H.

What is more interesting in these performance results is the fact that silica fume and BFS, the two high profile materials, which are well-known for enhancing the sulfate resistance in $N\overline{S}$ and $C\overline{S}$ environments, have aggravated the decomposition type of attack and deterioration in the pure $M\overline{S}-N\overline{S}$ exposure without enhancing the expansion-cracking mechanisms. The behavior of BFS is all the more unexpected as its high performance in marine structures is rather well-known.

The XRD patterns (Figs. 6.17 and 6.18) and SEM micrographs (Plates 6.16 through 6.19) for silica fume and BFS blended cements provide some indications of the possible mechanisms which aggravate the sulfate attack for these two blended cements in the $M\overline{S}-N\overline{S}$ environment.

The CH peaks in the XRD pattern for the silica fume cement specimens placed in water (Fig. 6.12), when compared with the CH peaks for the parent Type I cement (Fig. 6.9), indicate a reduction in CH content thereby confirming pozzolanic reaction. Further, a comparison of the CH peaks of silica fume blended

cement exposed to pure sulfate environment (Fig. 6.17) with the control (Fig. 6.14) shows again a second stage of CH consumption and appearance of gypsum peaks thereby confirming gypsum formation in accordance with equations 6.1a and 6.1b. However, the massive gypsum precipitation which is more than the gypsum formed in the parent Type I cement (Fig. 6.14) does not commensurate with the conversion of only CH to gypsum. It is quite clear that gypsum is being formed by a second mechanism of magnesium attack in accordance with equation 6.2 which may lead eventually to reaction 6.6. This is confirmed by the the SEM micrographs which show both excessive gypsum precipitation in conjunction with considerable M-S-H formation and also by the physical state of the specimens which progressively undergo decomposition of the binder phase (Plates 6.1 and 6.3), which is typical of the magnesium attack on cementitious materials.

It must also be noted that the magnesium attack on silica fume blended cements would also be enhanced due to the reduced CH in the pore solution. This reduction in CH results firstly from the pozzolanic reaction between reactive silica and CH, and secondly from the conversion of CH to gypsum by the reaction with sulfate ions, as shown in equations 6.1a and 6.1b. CH constitutes the first substance and line of reaction with magnesium and therefore acts as a buffer and a retarder of the magnesium attack on C-S-H. Its reduction in the pore solution would deflect the mag-

nesium attack to C-S-H more strongly thereby accelerating the decomposition of C-S-H in accordance with equations 6.2 and 6.6.

Another reason for the aggravated deterioration of silica fume blended cements may be a physical factor. Several investigators have greatly emphasized the protective role of the dense brucite layer formed on cement concrete surfaces (219). In a recent backscattered electron imaging (BEI) study, Bonen and Cohen (214) have confirmed the formation of a dense layer of brucite 40 to 120 μm thick. This layer is shown in Plate 6.22. It is argued that this layer of insoluble brucite effectively blocks the pores and prevents the penetration and ingress of further magnesium and sulfate ions into the hardened cement paste component of concrete. It is interesting to note that whereas brucite peaks exist in the case of exposed plain portland cements (Figs. 6.14 and 6.15), they are almost absent in the case of exposed silica fume blended cement (Fig. 6.17). It is possible that the absence of this pore blocking and segmenting layer makes the silica fume blended cement more vulnerable to the attack of magnesium and sulfate ions.

It is also interesting to note that the primary sulfo-aluminate phase formed during the hydration of silica fume blended cement disappears totally. This confirms that calcium sulfo-aluminates are unstable in magnesium sulfate environment and eventually decompose to form gypsum, hydrated alumina and brucite thereby further augmenting the gypsum content and its deleterious effects

ate 6.22 : Presence of Dense, Protective Brucite Layer on Surface of Silica Fume Specimen (Bonen and Cohen, 1992).

on the strength and stiffness of C-S-H. The nature of attack on BFS blended cement, which exhibits the highest 95% drop in strength (Fig. 6.8) further confirms the significant role of C-S-H decomposition mechanism in $M\bar{S}$ solutions. It is seen from the XRD pattern of the control specimens (Fig. 6.13) that CH is totally absent as a product of hydration. This is expected in view of the fact that CH, being the product of hydration of clinker which precedes the hydration of slag, acts as an alkaline activator and a as reactant in accordance with the following equation (208,209) and therefore gets consumed in this reaction:

$$C_5S_3A + 2CH + 14H \rightarrow C_4AH_{13} + 3C\text{-}S\text{-}H \qquad (6.7)$$

This absence of CH would deflect the magnesium attack to C-S-H and the actual massive precipitation of gypsum, as shown in the XRD pattern (Fig. 6.18) and the SEM micrograph (Plate 6.17) for BFS cement, is only possible when the magnesium-oriented C-S-H decomposition mechanism is very active. The C-S-H decomposition into non-cementitious M-S-H is confirmed by the SEM micrograph and EDXA output (Plate 6.17 and Fig. 6.33). This would imply an aggravated decomposition reaction, according to equation 6.2 and eventually reaction 6.6, explaining the excessive deterioration of the BFS blended cement.

It may also be noted that the significant mechanism of protective brucite surface deposition is also absent in BFS cement.

Further, the primary calcium sulfo-aluminate also disappears from the BFS cement matrix thereby increasing the gypsum content and its deleterious attack.

6.3.3 Performance of Plain and Blended Cements in Sodium Sulfate Environment Compared to Sodium-Magnesium Sulfate Environments

A separate series of durability tests were carried out at KFUPM (220) to evaluate the sulfate resistance performance of a large number of plain and blended cements in sodium sulfate ($N\bar{S}$) solution. Figs. 6.41 through 6.44 show the sulfate resistance performance of 20% fly ash, 10% microsilica and 60% and 70% BFS cements blended with 9% C_3A Type I cement in a 5% $N\bar{S}$ solution. It is seen that after 720 days, there is virtually no deterioration in the fly ash and microsilica blended cements. The 60% BFS cement, however, exhibits a 50% deterioration; whereas the 70% BFS cement shows excellent performance without any deterioration.

The above data clearly indicate that for all blended cements, the deterioration is significantly aggravated in $M\bar{S}-N\bar{S}$ compared to $N\bar{S}$ environments. Moreover, another study carried out at KFUPM (181) shows that for a 20% microsilica blended with 14% C_3A parent cement, XRD pattern (Fig. 6.45) for specimens exposed to 5% $N\bar{S}$ solution showed considerable amount of gypsum

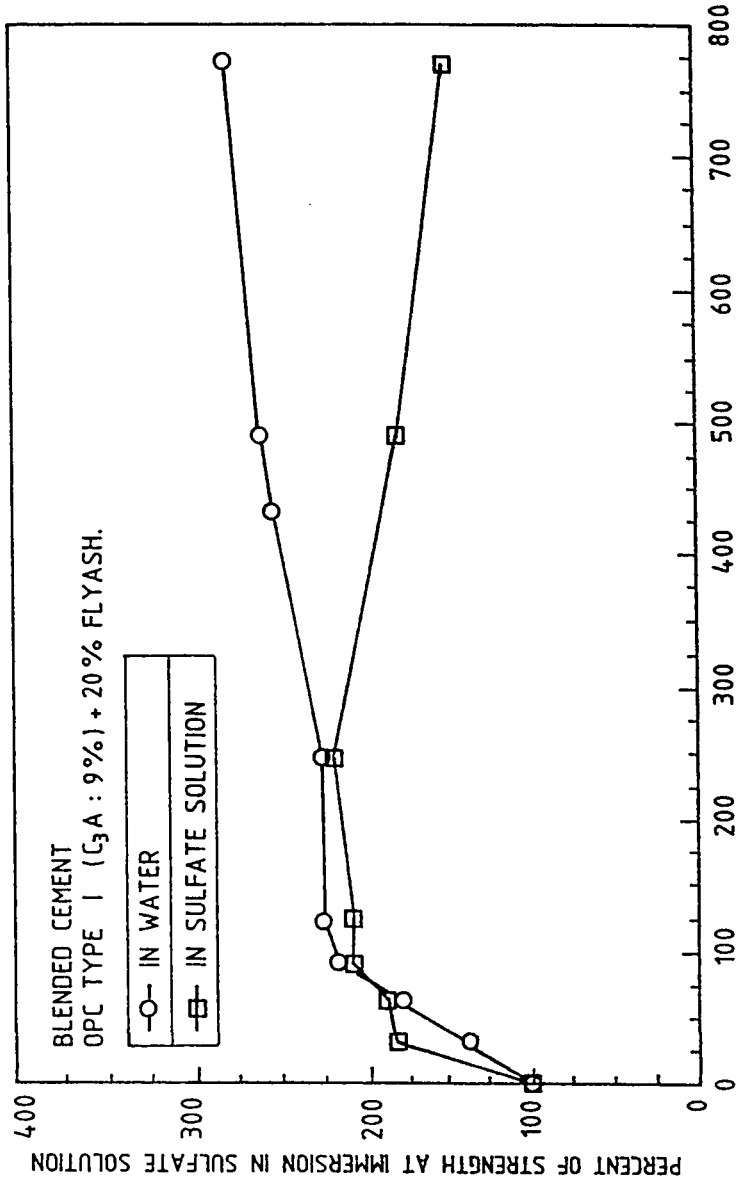

Fig. 6.41 : Performance of 20% Fly Ash Cement in 5% $N\bar{S}$ Solution (Rasheeduzzafar et al. 1992).

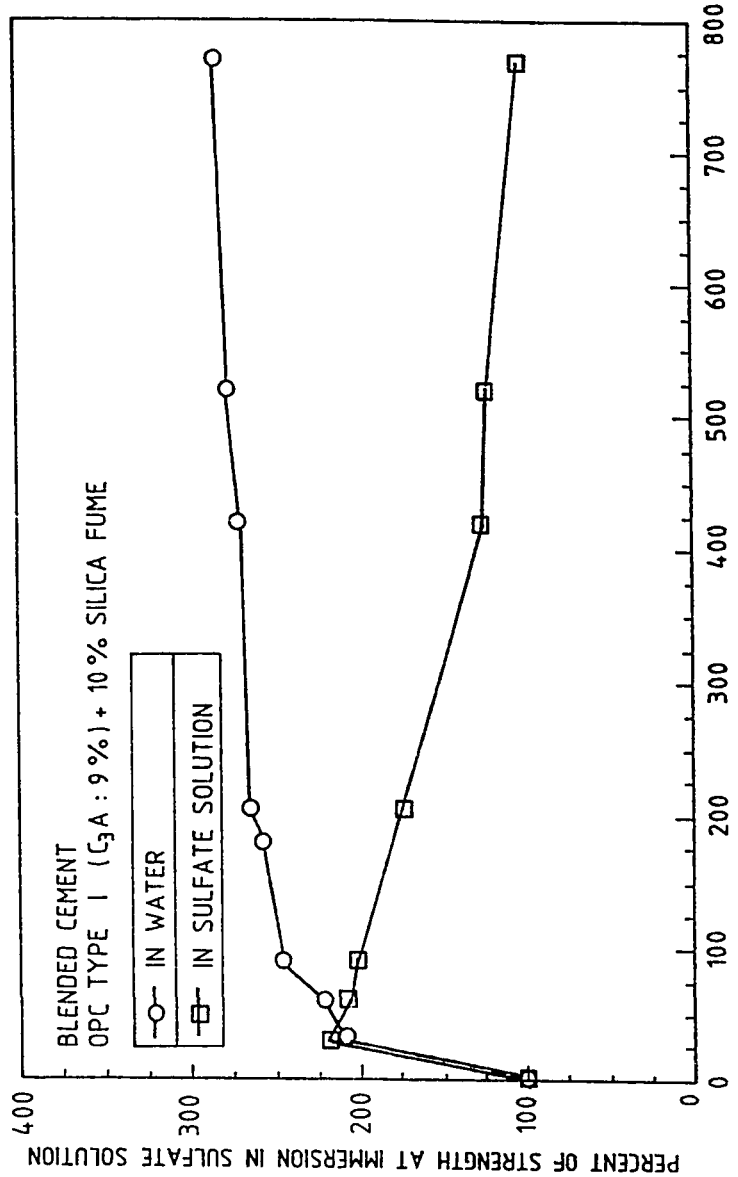

Fig. 6.42 : Performance of 10% Silica Fume Cement in 5% $N\bar{S}$ Solution (Rasheeduzzafar et al. 1992).

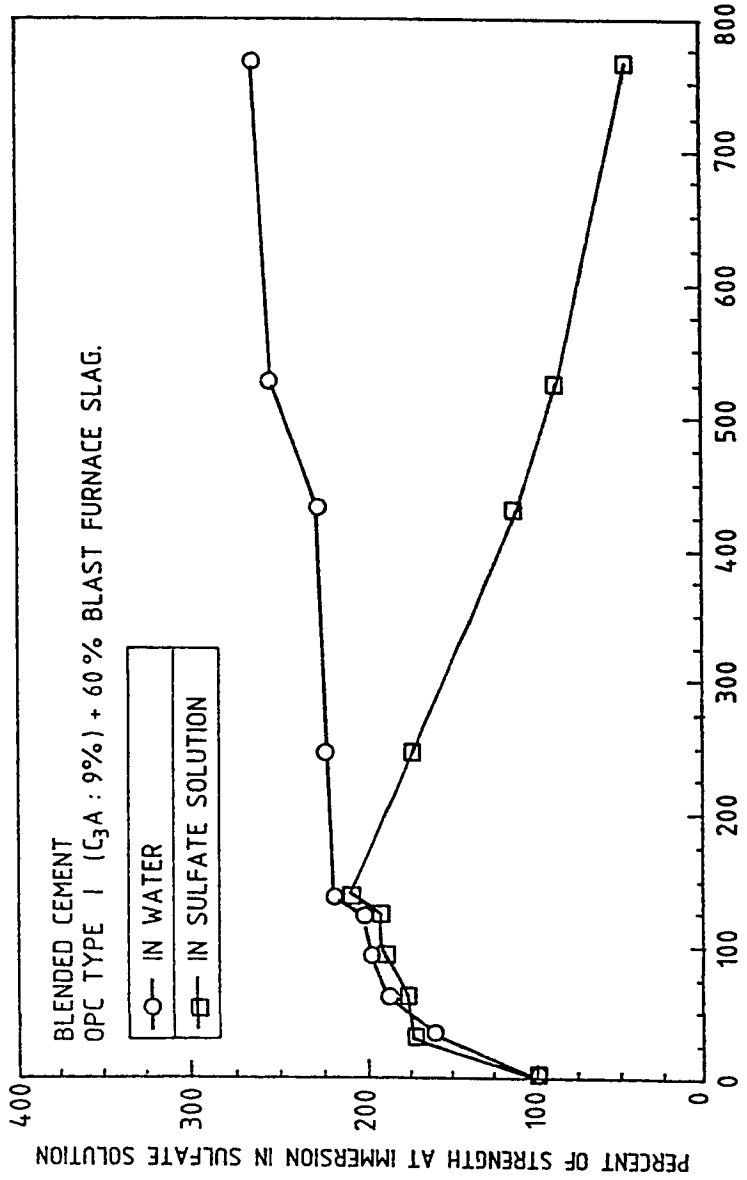

Fig. 6.43 : Performance of 60% BFS Cement in 5% $N\bar{S}$ Solution (Rasheeduzzafar et al. 1992).

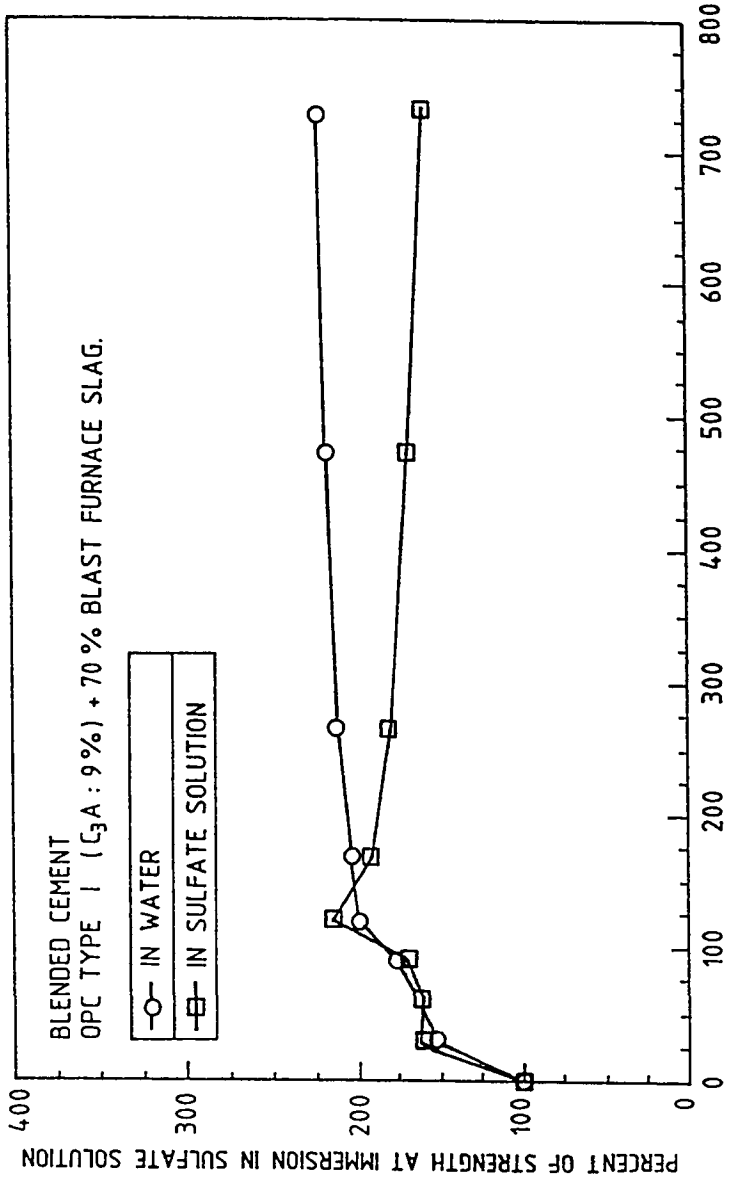

Fig. 6.44 : Performance of 70% BFS Cement in 5% $N\bar{S}$ Solution (Rasheeduzzafar et al., 1992).

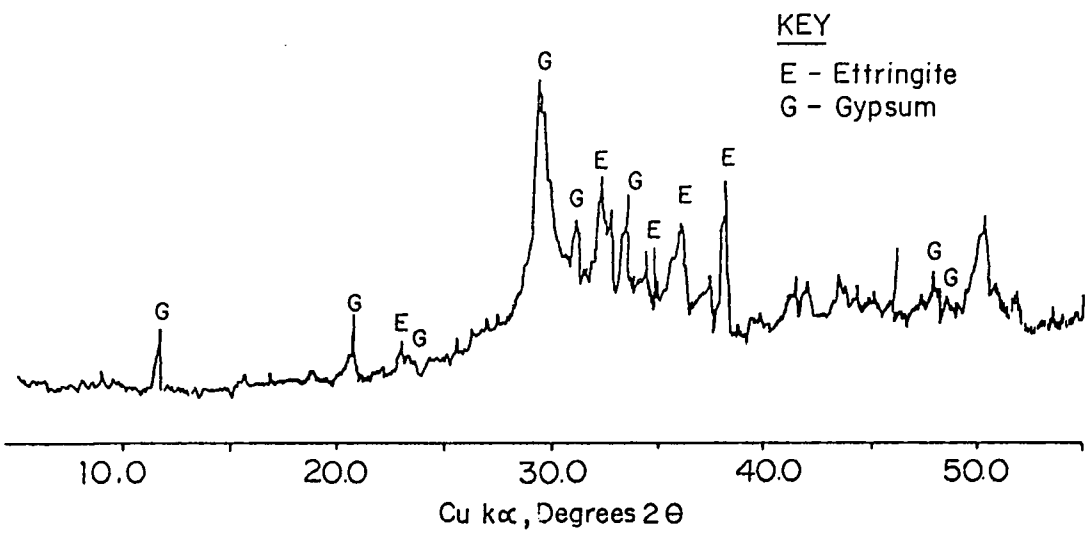

Fig. 6.45 : **X-Ray Pattern for the 20% Silica Fume Blended with Type I (C_3A = 14%) Exposed to 5% $N\overline{S}$ Solution (Rasheeduzzafar et al., 1990).**

and ettringite formation, but the specimens showed neither expansion nor softening and spalling type of deterioration. This indicates that microsilica blending in cements effectively suppresses the swelling type of mechanism but is extremely vulnerable to magnesium-oriented C-S-H decomposition mechanism.

The BFS blended cement performance data in the $N\bar{S}$ environment (Fig. 6.43) raises the question of optimizing the quantum of BFS blending. It is seen that whereas 60% slag cement shows considerable deterioration even in $N\bar{S}$ solution, a 70% slag cement shows no deterioration at all. The replacement level, therefore, appears to be a critical parameter and the indications are that the 60% cement replacement by BFS is not adequate for high performance. This may be, amongst other reasons discussed earlier, an additional factor for the excessive deterioration of the 60% BFS cement in pure $M\bar{S}-N\bar{S}$ environment. The replacement level, as an influential factor in sulfate durability performance, has also been emphasized by Bosch (221).

6.4 EFFECT OF CHLORIDES ON SULFATE ATTACK

The visual rating and deterioration factor data on the performance of plain and blended cements in high sulfate-chloride (2.1% SO_4^{--} + 15.7% Cl^-) environment are shown in Table 6.2 and Figs. 6.46 through 6.55. Observations after 360 and 720 days

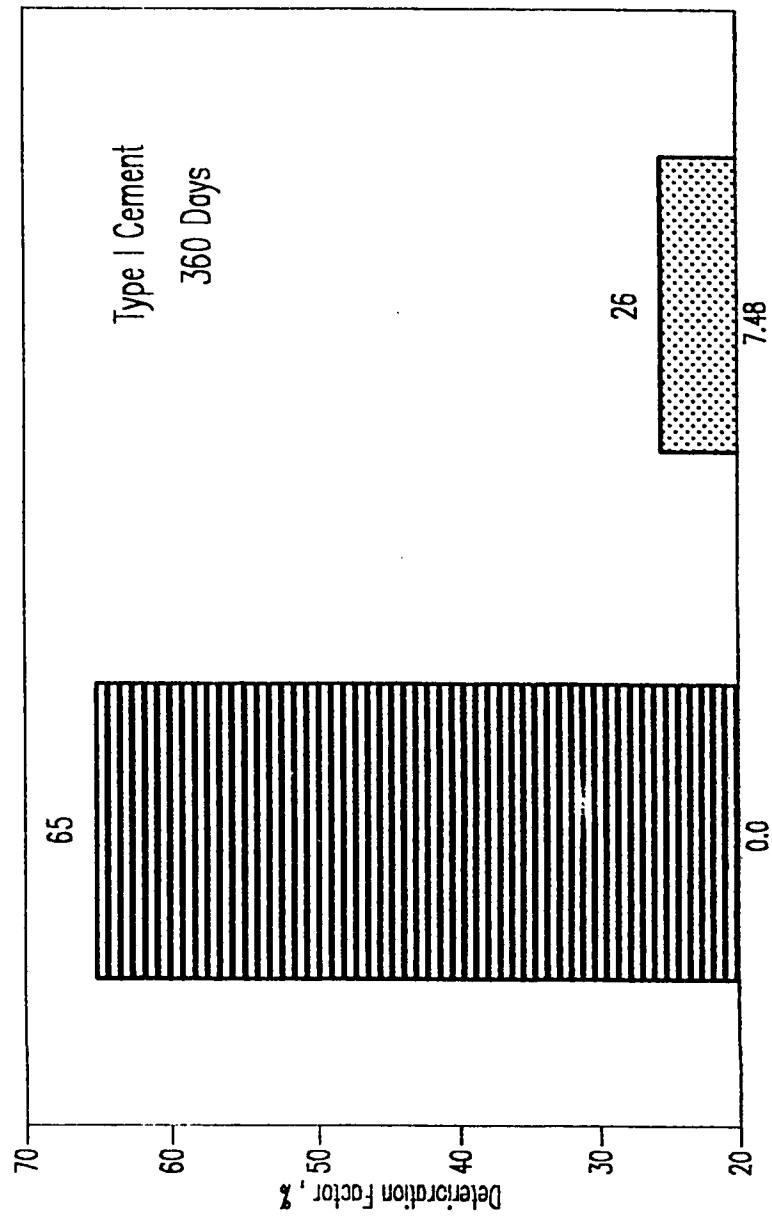

Fig. 6.46 : Effect of Chloride on Sulfate Attack in Type I Cement (360 Days)

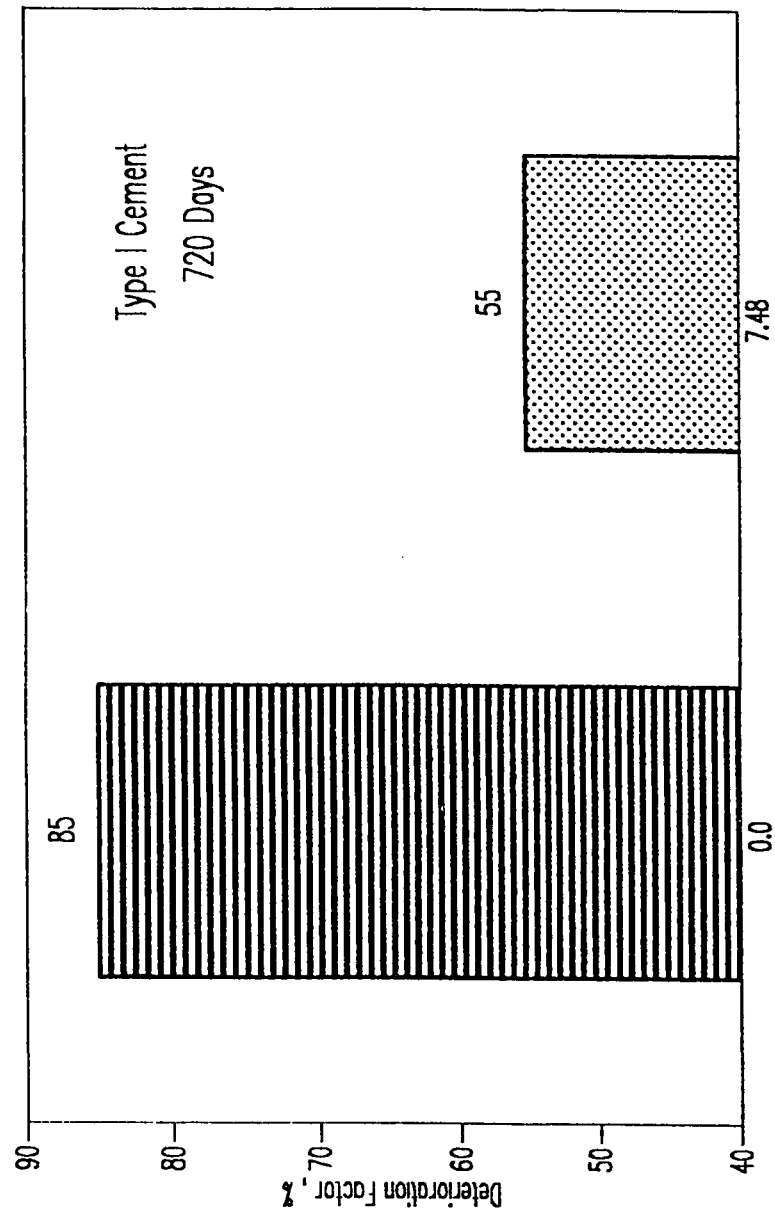

Fig. 6.47 : Effect of Chloride on Sulfate Attack in Type I Cement (720 Days)

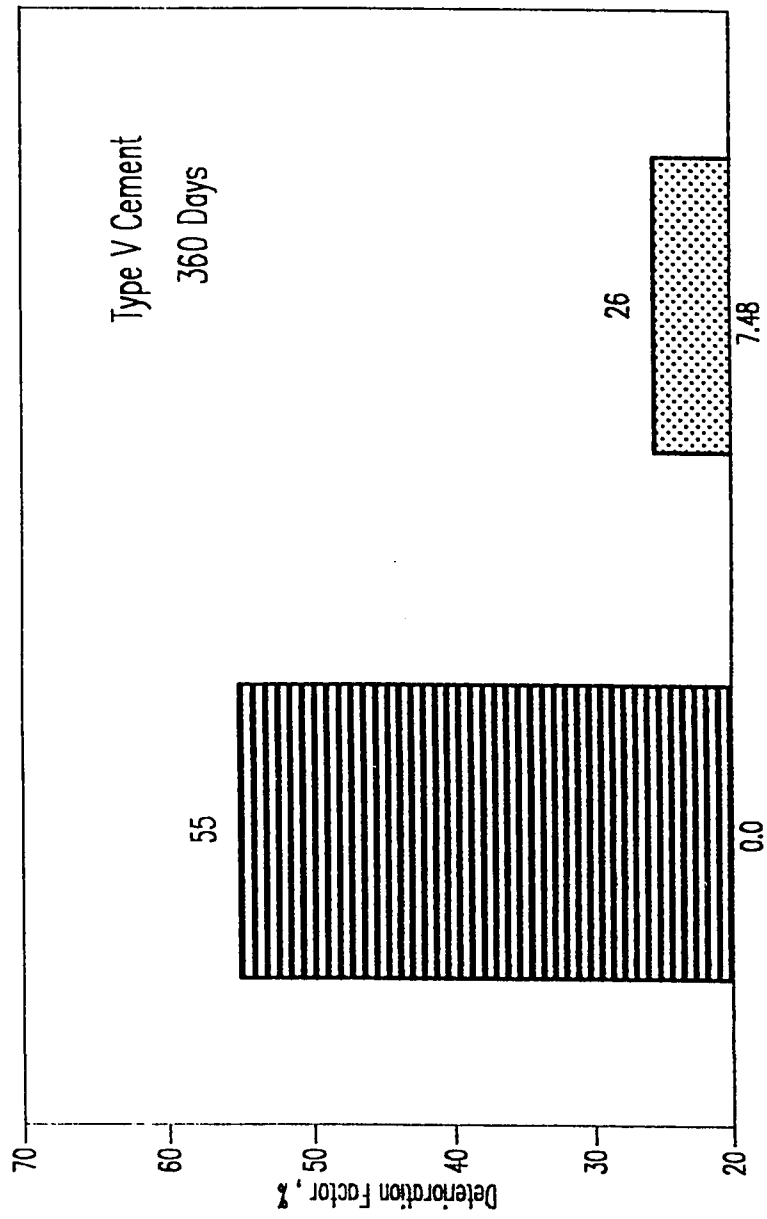

Fig. 6.48 : Effect of Chloride on Sulfate Attack in Type V Cement (360 Days)

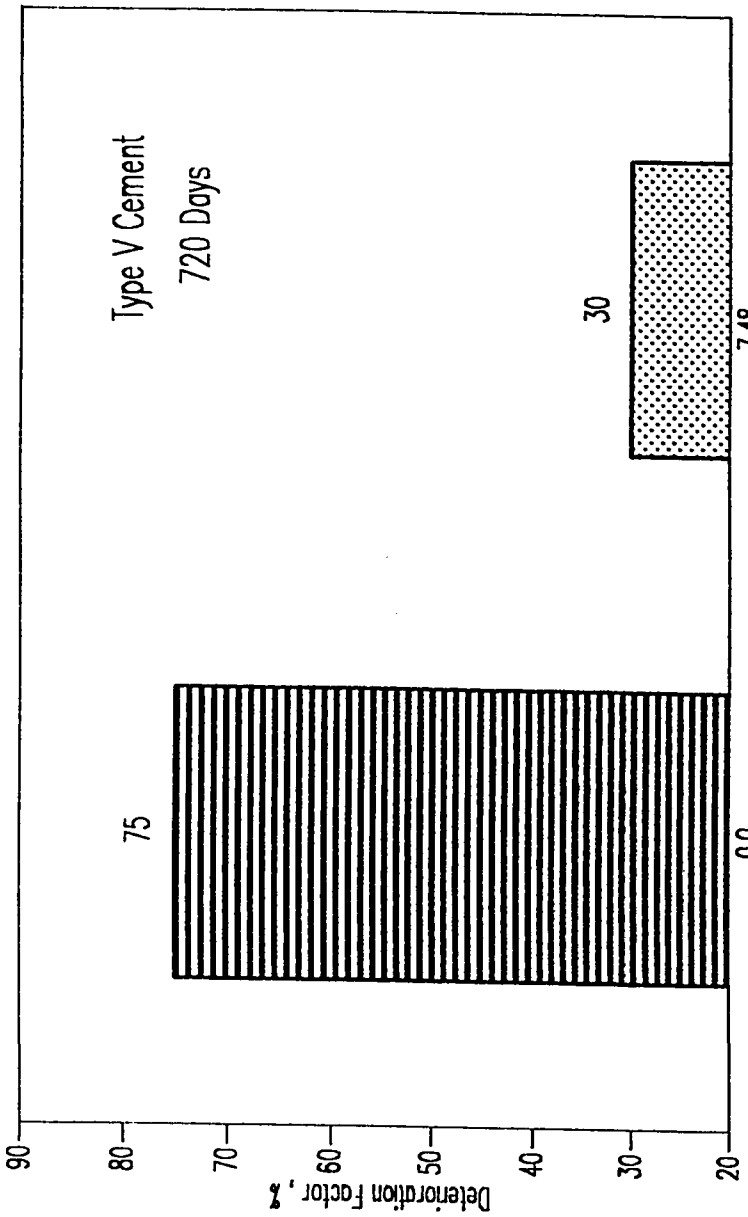

Fig. 6.49 : Effect of Chloride on Sulfate Attack in Type V Cement (720 Days)

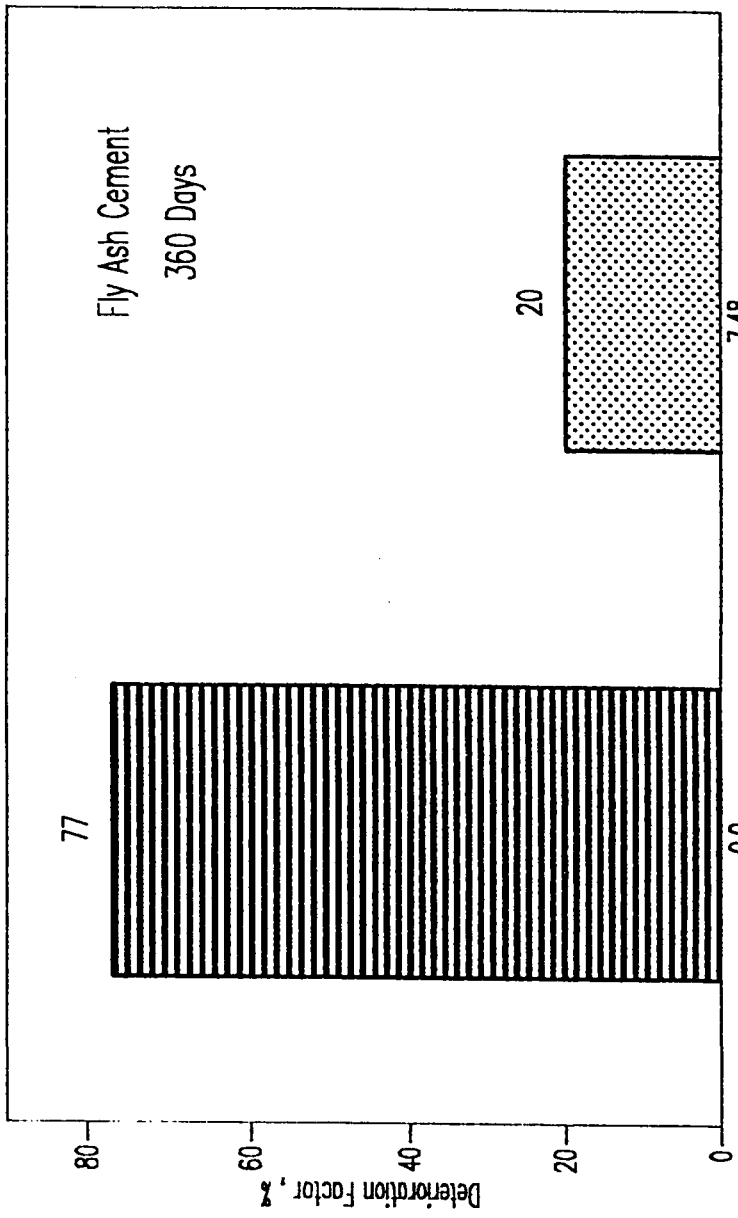

Fig. 6.50 : Effect of Chloride on Sulfate Attack in Fly Ash Cement (360 Days)

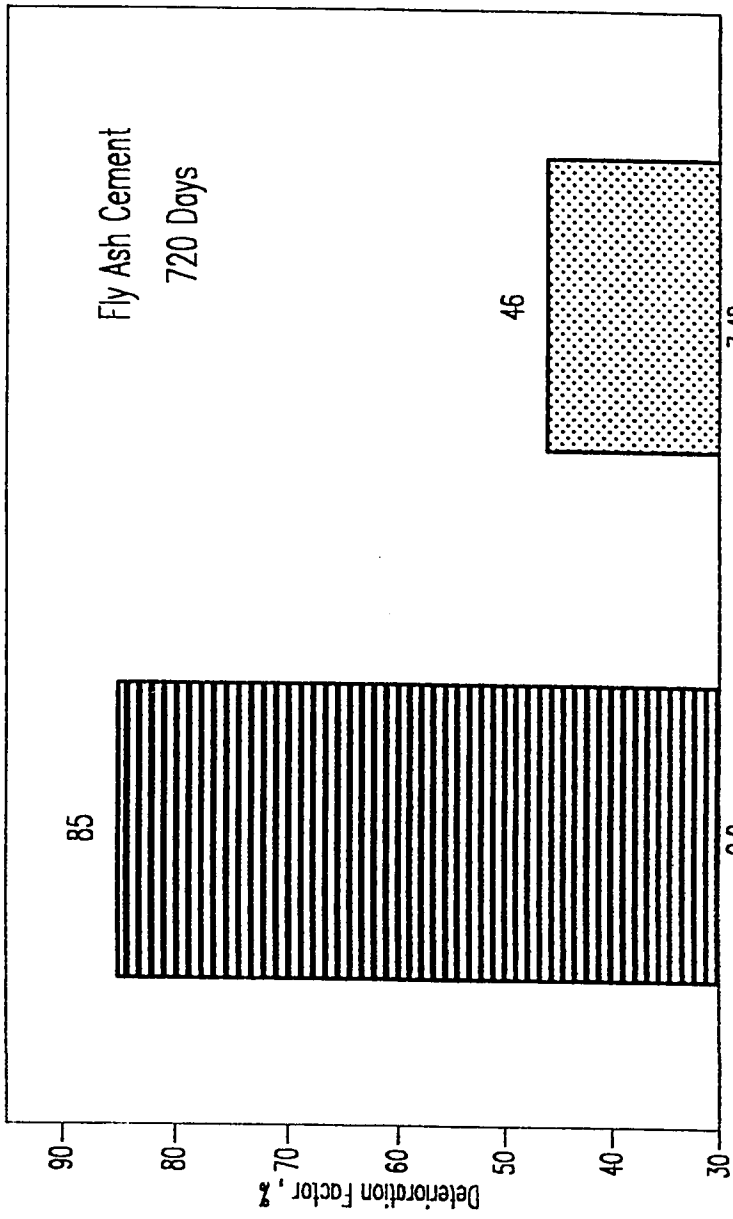

Fig. 6.51 : Effect of Chloride on Sulfate Attack in Fly Ash Cement (720 Days)

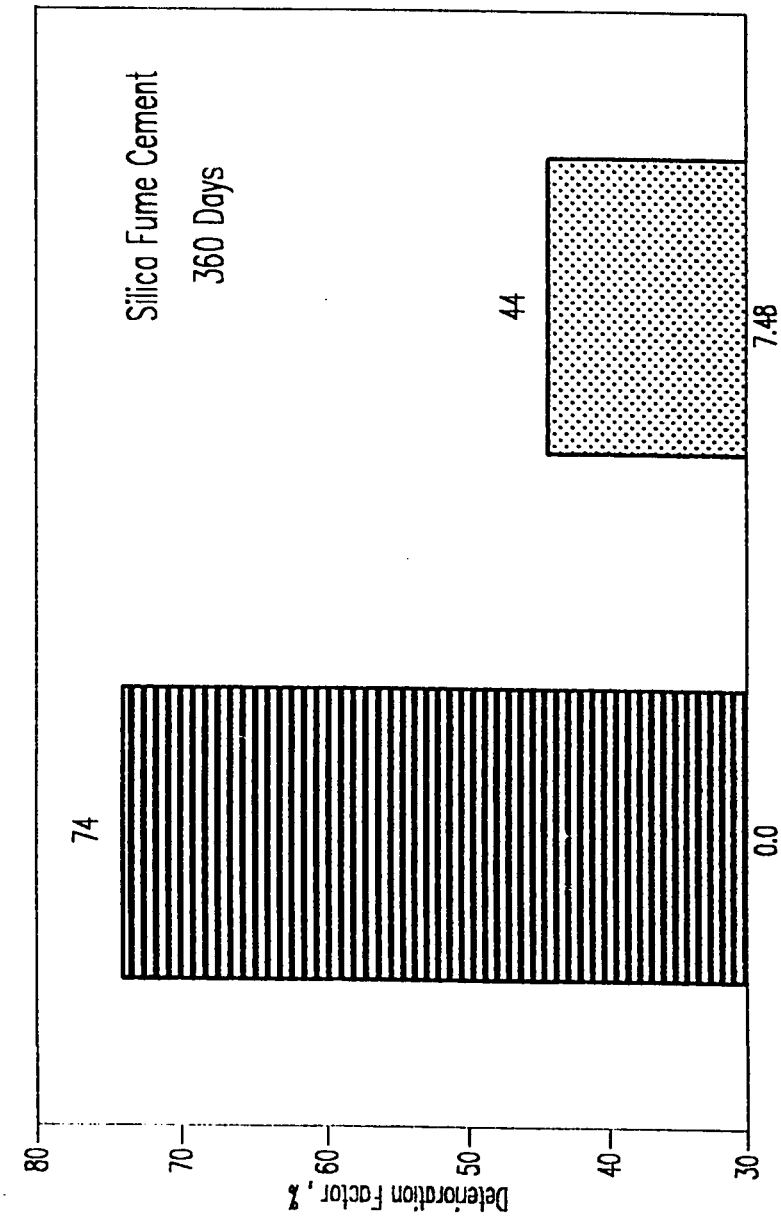

Fig. 6.52 : Effect of Chloride on Sulfate Attack in Silica Fume Cement (360 Days)

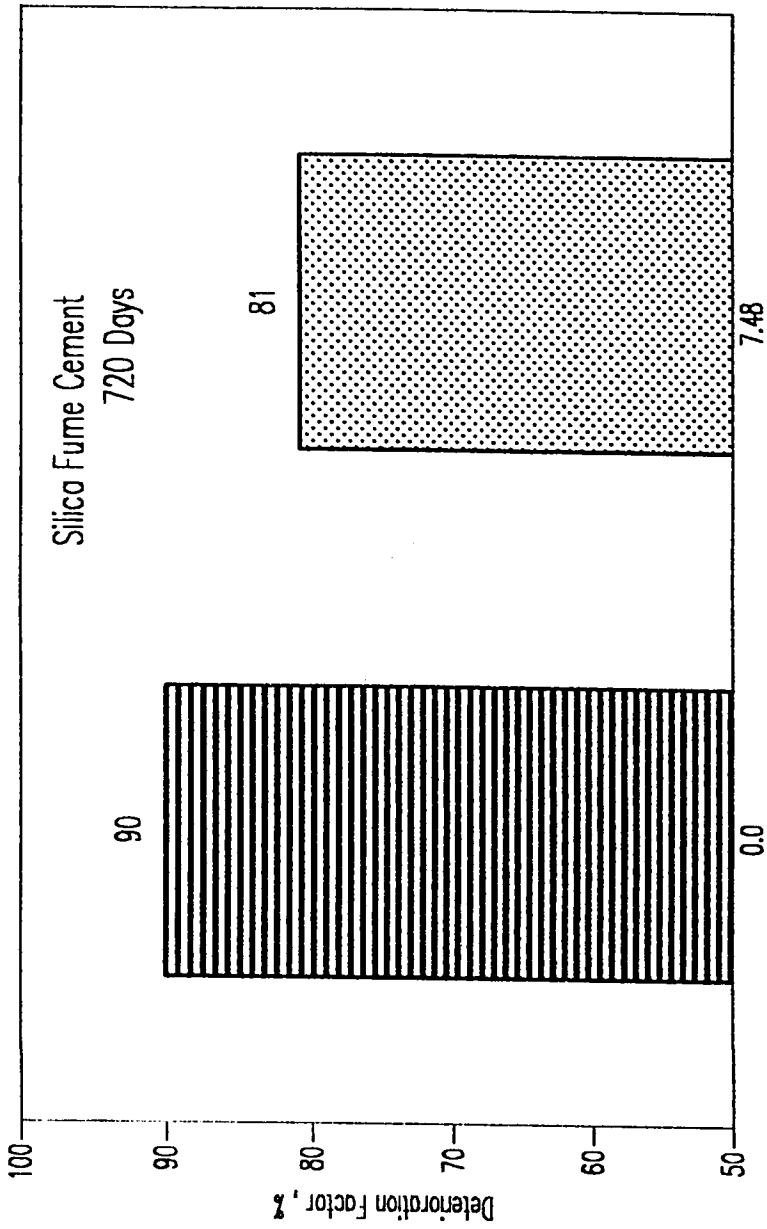

Fig. 6.53 : Effect of Chloride on Sulfate Attack in Silica Fume Cement (720 Days)

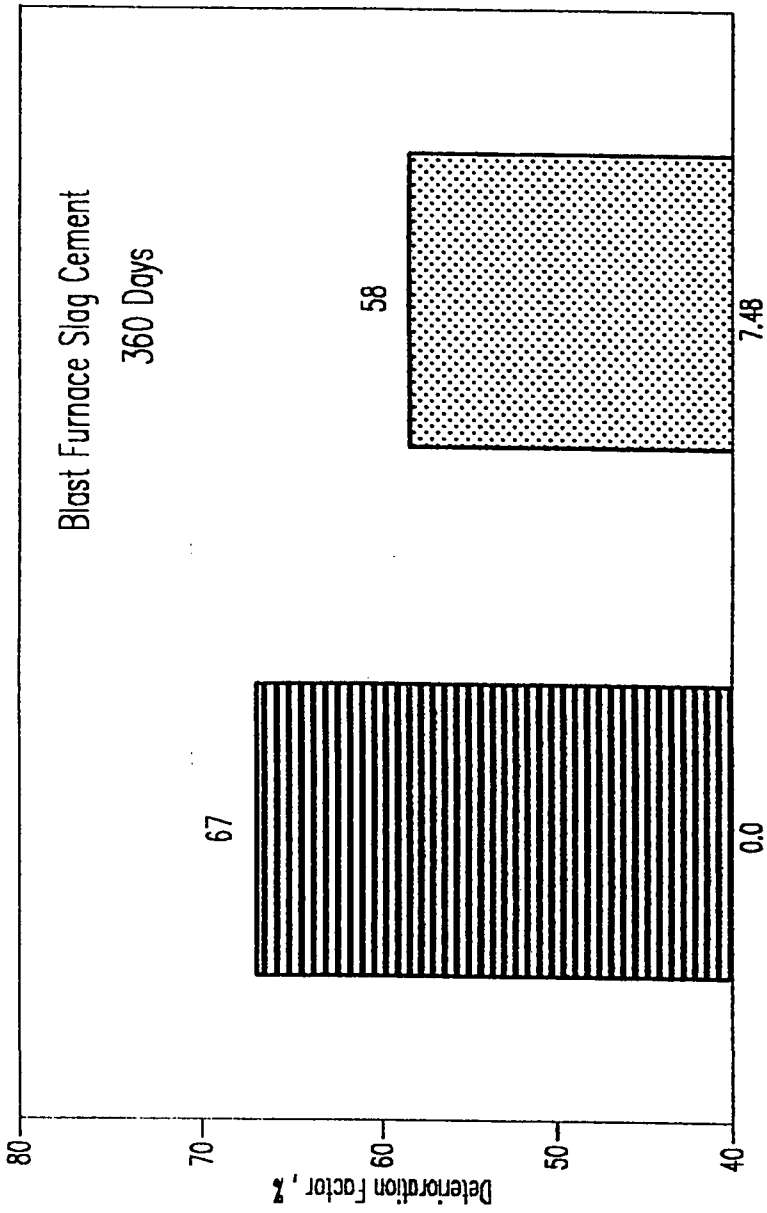

Fig. 6.54 : Effect of Chloride on Sulfate Attack in Blast Furnace Slag Cement (360 Days)

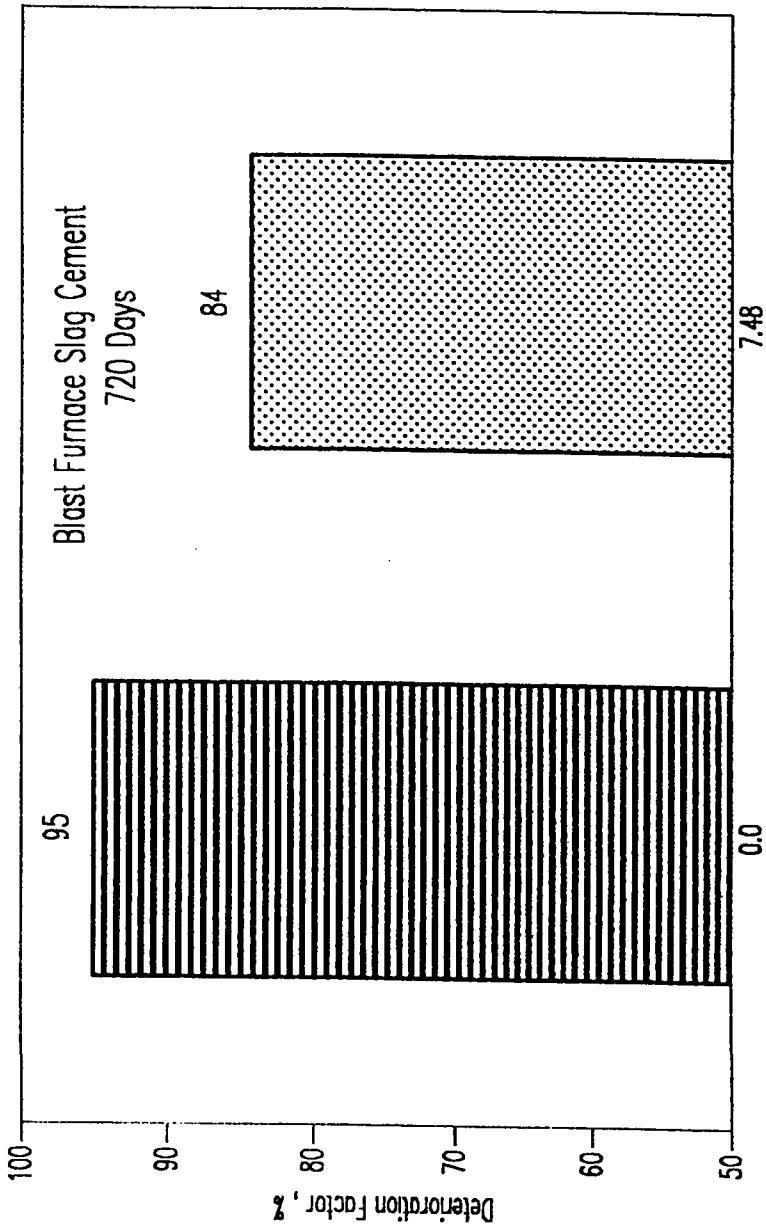

Fig. 6.55 : Effect of Chloride on Sulfate Attack in Blast Furnace Slag Cement (720 Days)

(Plates 6.2 and 6.4) indicate that the concomitant presence of chlorides with $M\overline{S}-N\overline{S}$ sulfate salts reduces deterioration and improve the sulfate resistance performance. However, the performance data in sulfate-chloride exposure (Figs. 6.4 to 6.8 and 6.46 to 6.55) also show that chloride beneficiation is not uniform for all cements. At 360 days, the beneficiation is maximum for fly ash blended cements where the deterioration factor is reduced from 77% in pure sulfate solution to 20% in sulfate-chloride solution, indicating a beneficiation of 57% which is solely attributable to the concomitant presence of chlorides with sulfate salts. For other cements, the chloride beneficiation after 360 days of exposure in descending order of magnitude are for Type I cement (65% to 25%), silica fume cement (74% to 44%), Type V cement (55% to 26%) and BFS cement (67% to 58%). The corresponding beneficiation after 720 days are not in the same order. After 720 days, the maximum beneficiation is for Type V cement (75% to 30%) and then in descending order for fly ash cement (85% to 46%), Type I cement (85% to 55%), BFS cement (95% to 84%) and silica fume cement (90% to 81%). A quantitative summary of the chloride beneficiation results after 720 days of exposure is presented in Table 6.6, which indicates that mitigation of sulfate deterioration due to the concomitant presence of chlorides could be considered significant only for plain and fly ash blended cements. Chloride beneficiation is almost insignificant for both BFS and silica fume blended cements.

Table 6.6 : Summary of Chloride Beneficiation in Plain and Blended Cements After 720 Days of Exposure

Cement Type	Deterioration Factor (%), in the Exposure:		Chloride Beneficiation (%)
	Pure Sulfate	High Sulfate-Chloride	
Type I	85	55	30
Type V	75	30	45
Fly Ash (20%) +Type I	85	46	39
Silica Fume 10%)	90	81	9
Blast Furnace Slag (60%) +Type I	95	84	11

Chloride beneficiation effect has been discussed in several reports with varying conclusions. Smith (128), Ben-Yair (131), Locher (121) and Al-Samarai and Raouf (124) state that chlorides enhance sulfate attack. Miller (117), Kind (110,127), Thorvaldson (119), Biczok (109), Lea (132) and more recently Harisson (118) find that chlorides mitigate sulfate attack. van Aardt (104), Dalq (123) and Yeginobali (122) state that the effect of the concomitant presence of chlorides on sulfate attack as insignificant. Kalousek and Benton (222) report moderate expansion due to the presence of chlorides due to the formation of calcium chloro-aluminate (Friedel's salt). Ftikos and Parissakis (223) report that the sulfate attack is of a different kind in the presence of chlorides. They report formation of a porous C-S-H gel due to the presence of calcium chloro-aluminate ($3CaO.Al_2O_3.\ CaCl_2.10H_2O$). Tests carried out by Locher (121) have shown that chlorides in sodium or magnesium solutions increase the sulfate attack in some cases. From a review of the literature, as discussed in Chapter 3, it is quite obvious that the effect of chlorides on sulfate attack is controversial and inconclusive. In view of the simultaneous presence of sulfates and chlorides in soils and groundwaters of the Arabian Gulf region, the sulfate-chloride interaction situation is of great significance from the standpoint of durability performance of foundations and substructures.

The X-ray patterns for all cements exposed to pure chloride solution (Figs. 6.56 through 6.60) show significant formation of calcium chloro-aluminate (Friedel's salt) with peaks at 11.2°, 22.8°, 30.9° and 38.8° 2θ. Also, in the low and high sulfate-chloride solutions, the calcium chloro-aluminate is present in all cements (Figs. 6.61 through 6.70).

Comparison of the XRD patterns for all plain and blended cements in pure sulfate environment (Figs. 6.14 through 6.18) with those in high sulfate-chloride environment (Figs. 6.66 through 6.70) indicated that the gypsum formation was either totally eliminated or significantly reduced due to the increased solubility of gypsum in chloride environment. The SEM technique was used to further elucidate the effect of chlorides on sulfate attack in sulfate-chloride environments.

Plate 6.23 shows a SEM micrograph for Type V cement in high $SO_4^{--} - Cl^-$ environment. The elemental area analysis (Fig. 6.71) indicates the total absence of gypsum and the presence of calcium chloro-aluminate (Friedel's salt), calcium silicate hydrate (C-S-H) and magnesium silicate hydrate (M-S-H). The results indicate that while gypsum was totally eliminated in the presence of chlorides, M-S-H is still present. Although the M-S-H may be envisaged as minimal, it is due to the presence of the gold-coating peak and the profuse formation of Friedel's salt. A blow up of

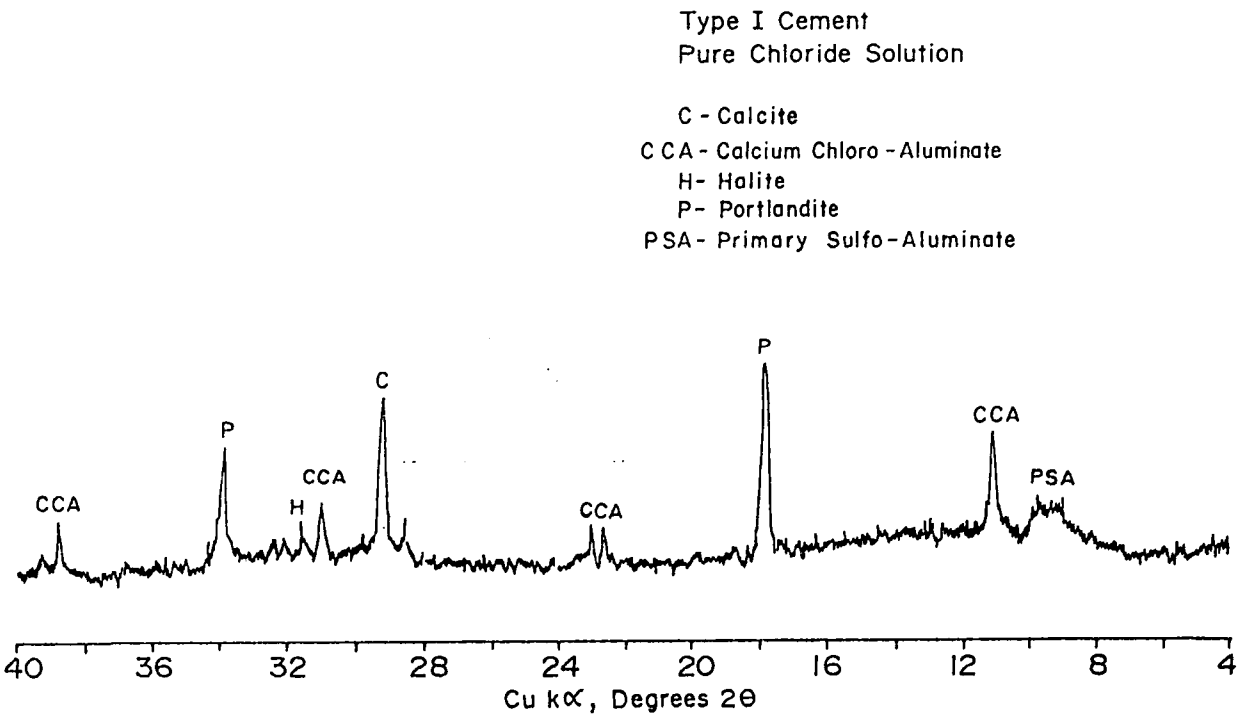

Fig. 6.56 : X-Ray Diffractogram for Type I Cement in Pure Chloride Solution after 720 Days.

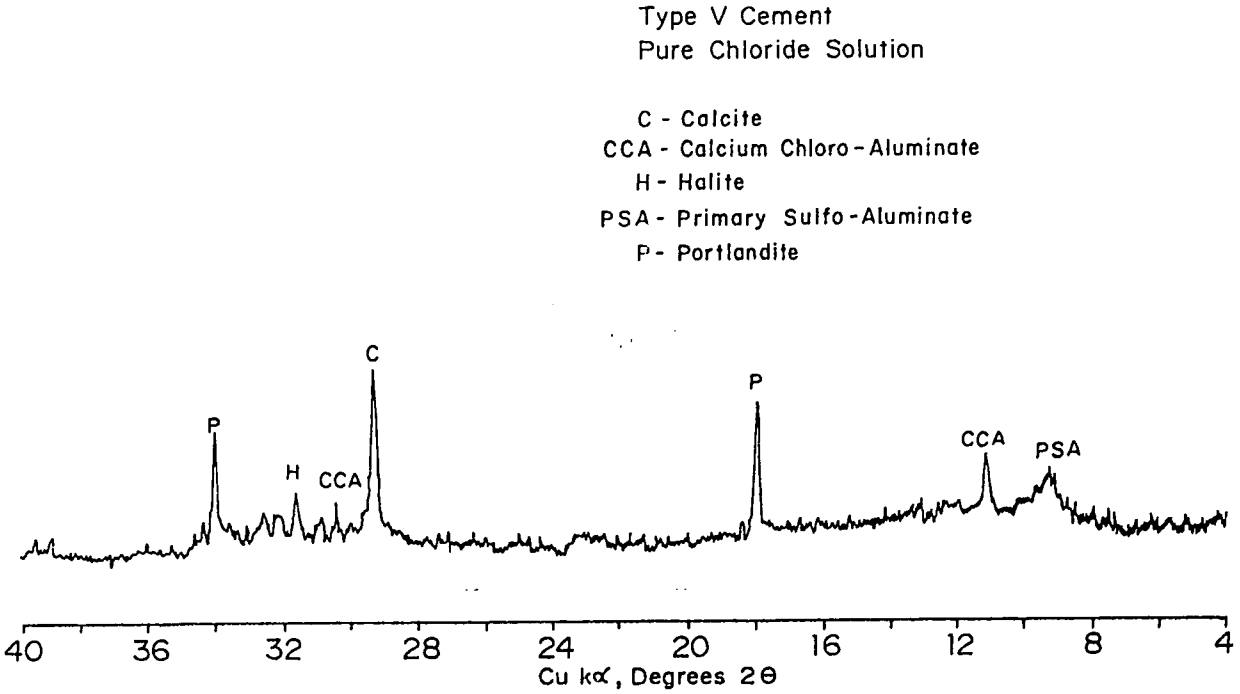

Fig. 6.57 : X-Ray Diffractogram for Type V Cement in Pure Chloride Solution after 720 Days.

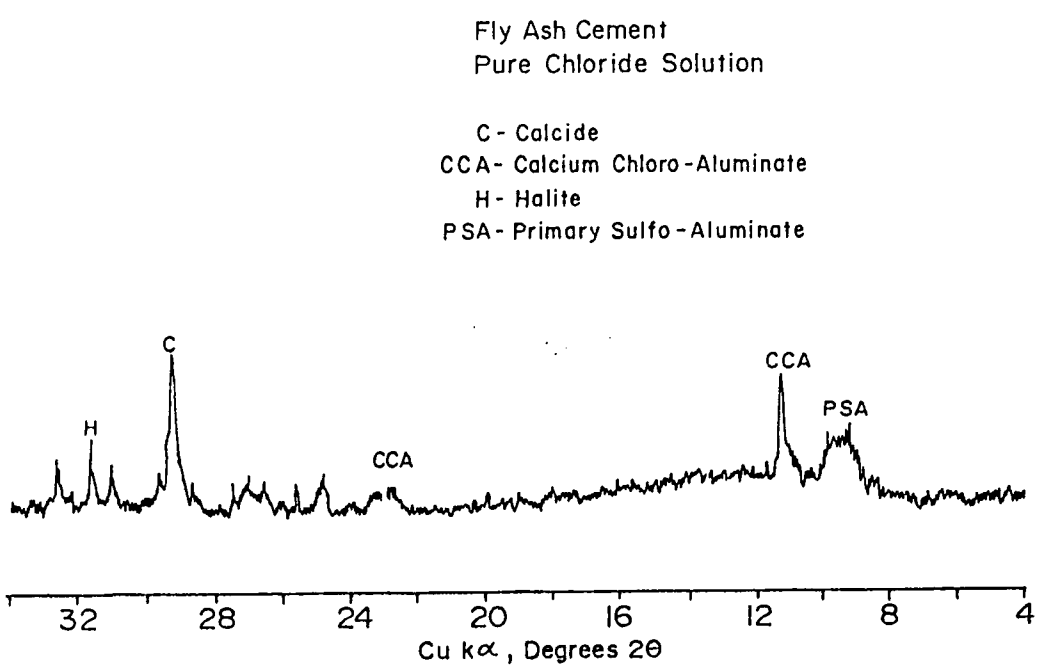

Fig. 6.58 : X-Ray Diffractogram for Fly Ash Cement in Pure Chloride Solution after 720 Days.

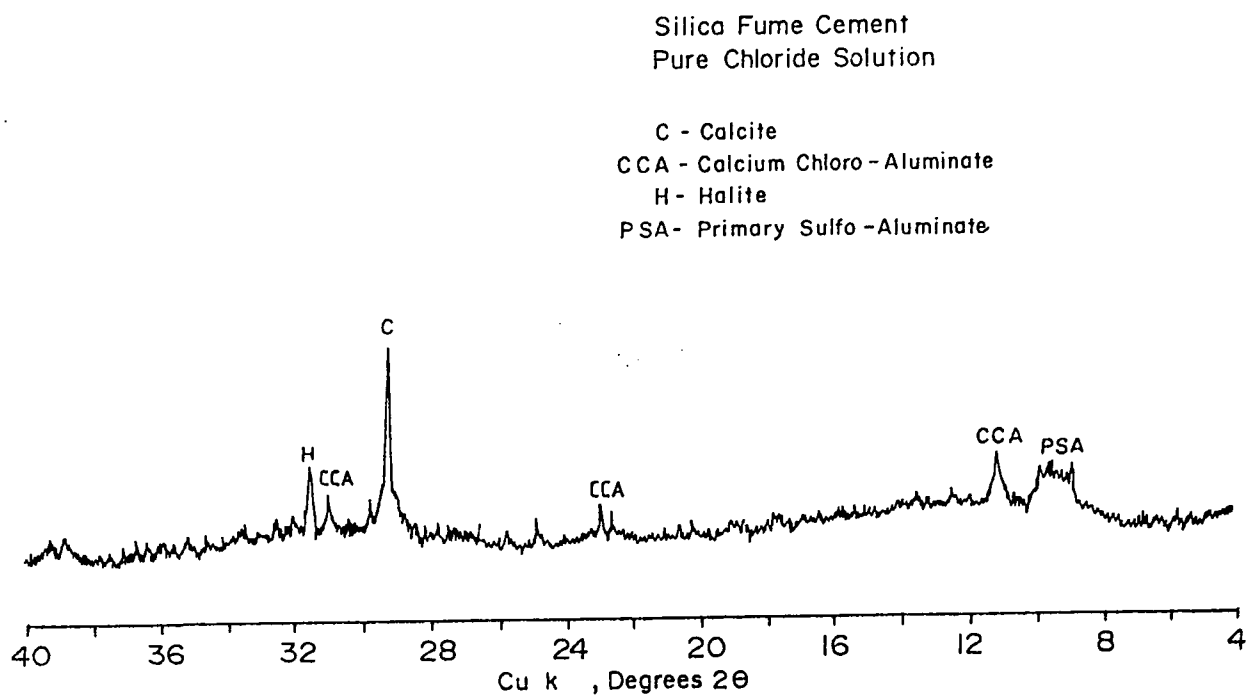

Fig. 6.59 : X-Ray Diffractogram for Silica Fume Cement in Pure Chloride Solution after 720 Days.

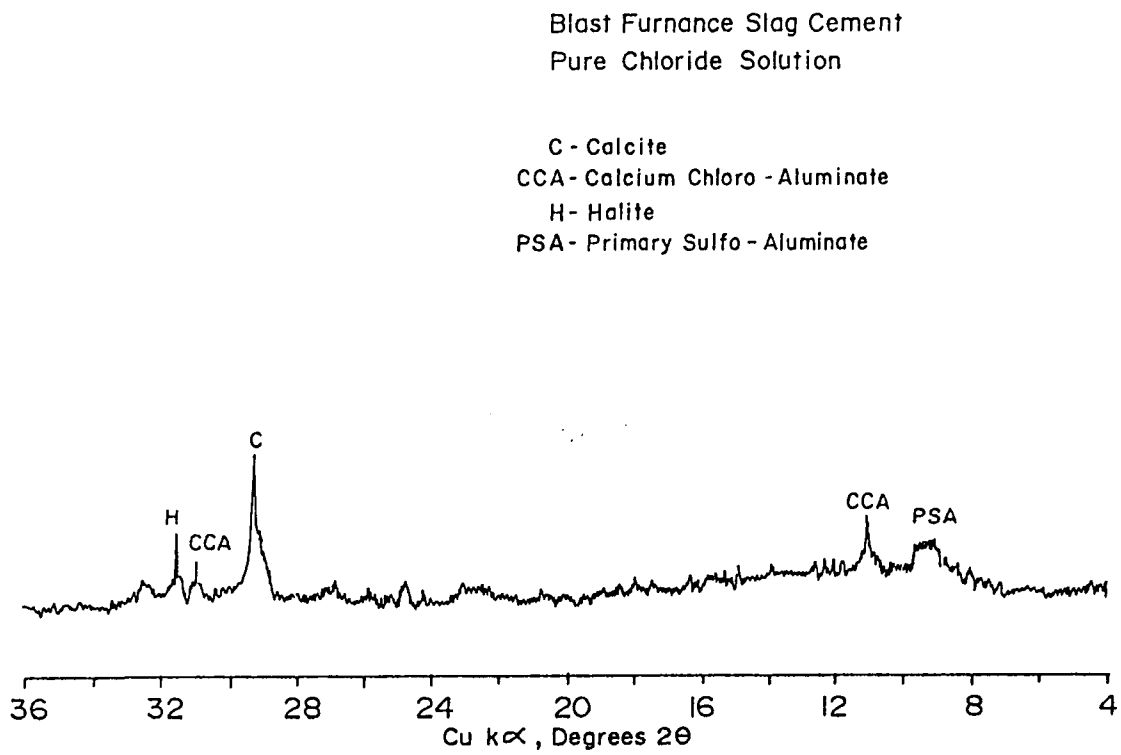

Fig. 6.60 : X-Ray Diffractogram for Blast Furnace Slag Cement in Pure Chloride Solution after 720 Days.

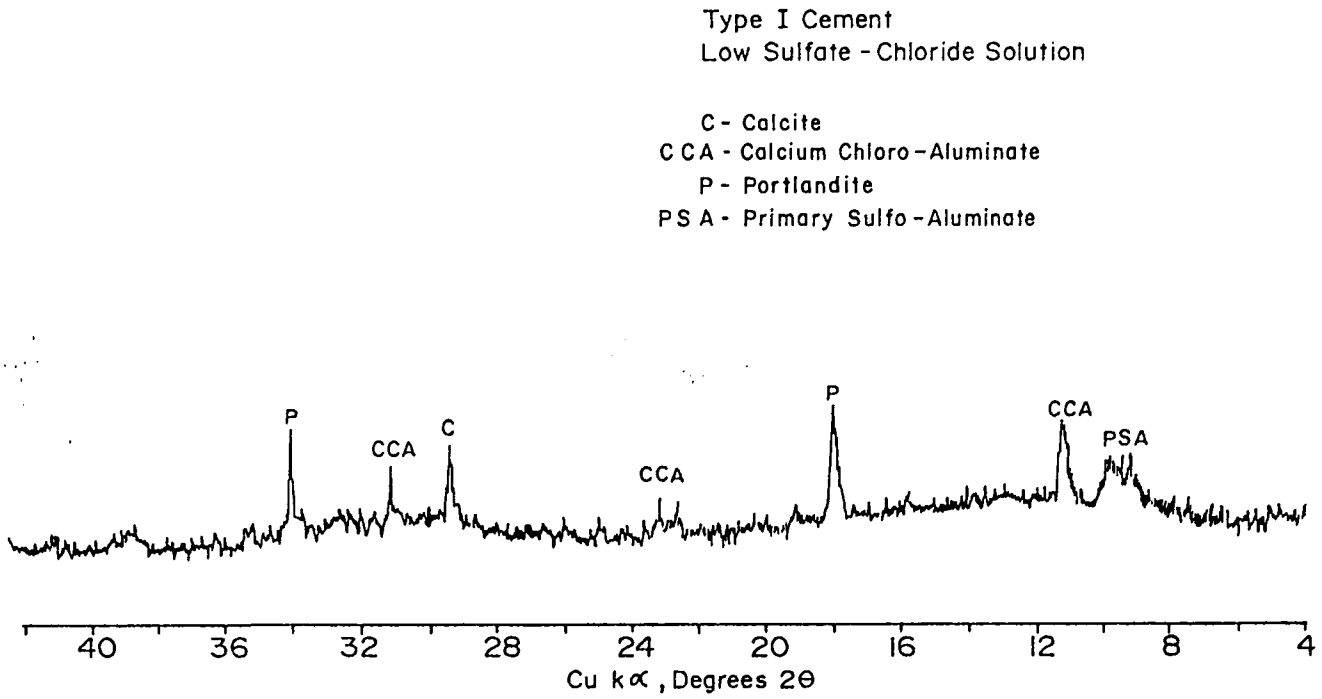

Fig. 6.61 : X-Ray Diffractogram for Type I Cement in Low Sulfate-Chloride Solution after 720 Days.

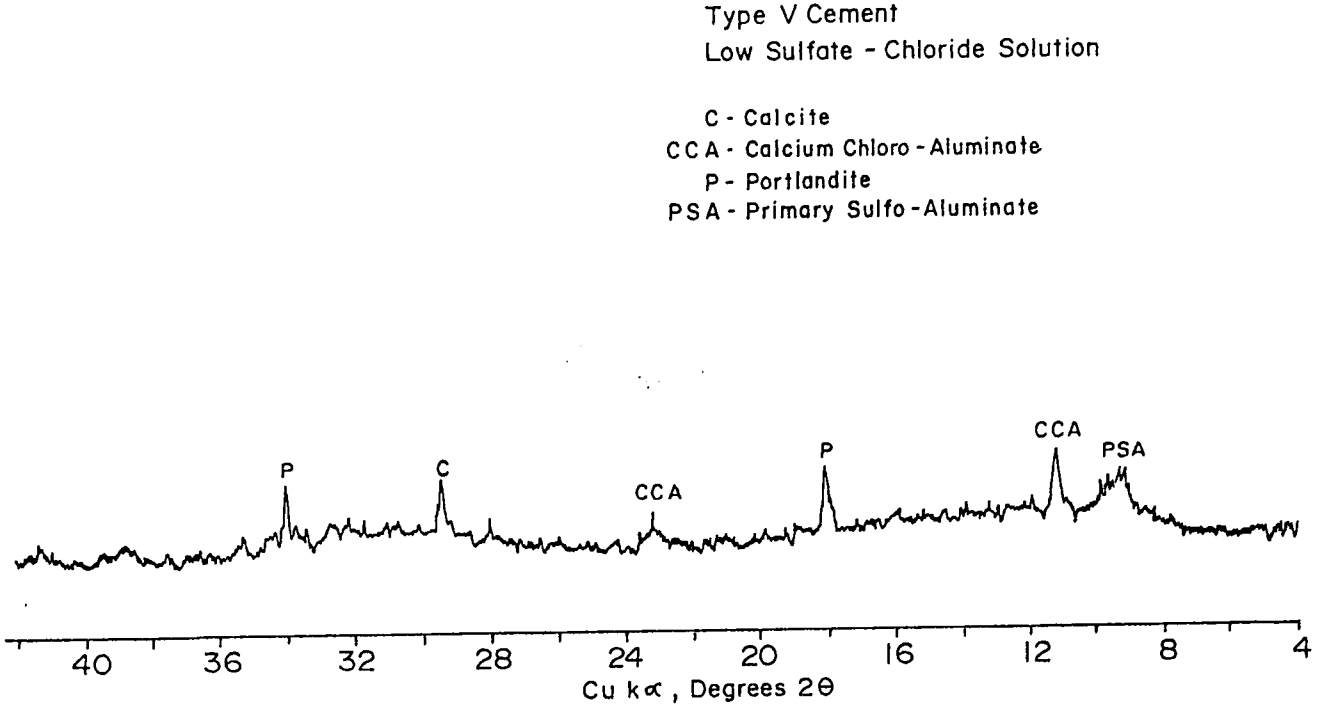

Fig. 6.62 : X-Ray Diffractogram for Type V Cement in Low Sulfate-Chloride Solution after 720 Days.

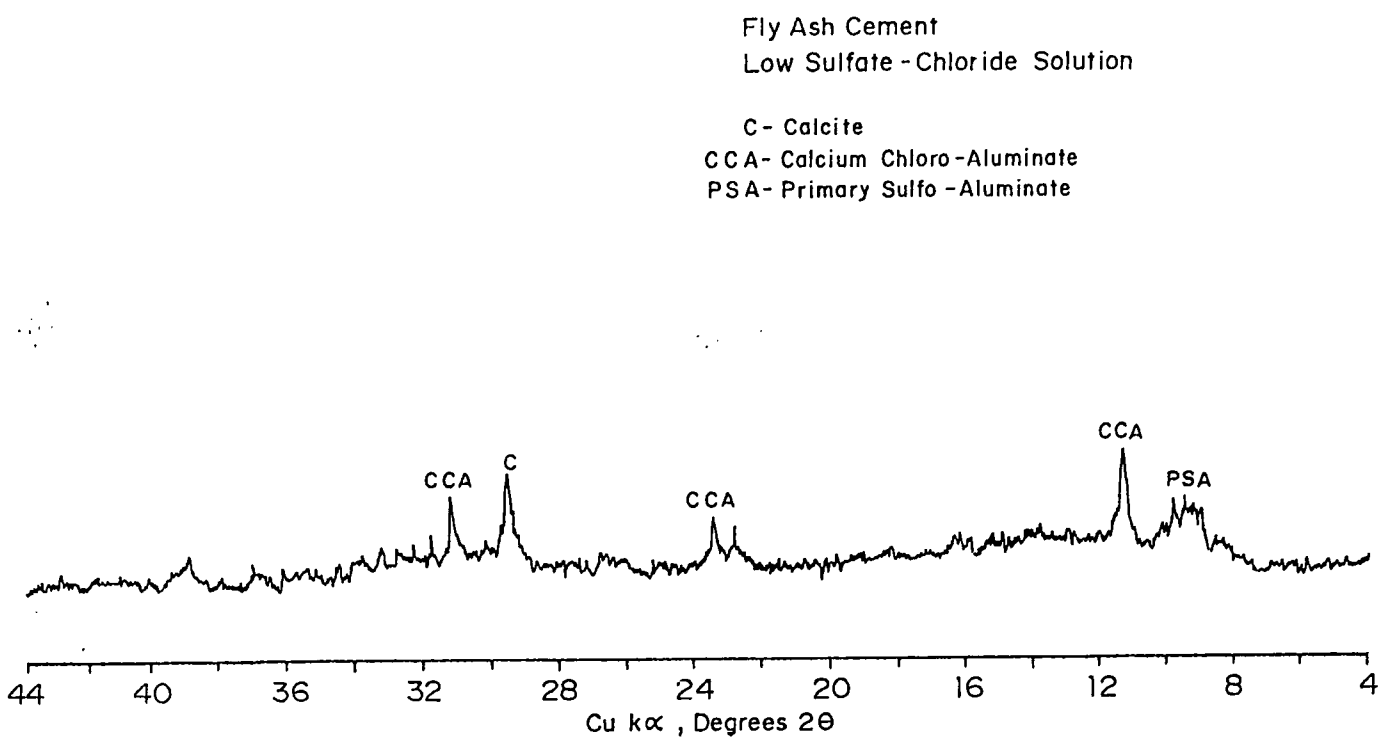

Fig. 6.63 : X-Ray Diffractogram for Fly Ash Cement in Low Sulfate-Chloride Solution after 720 Days.

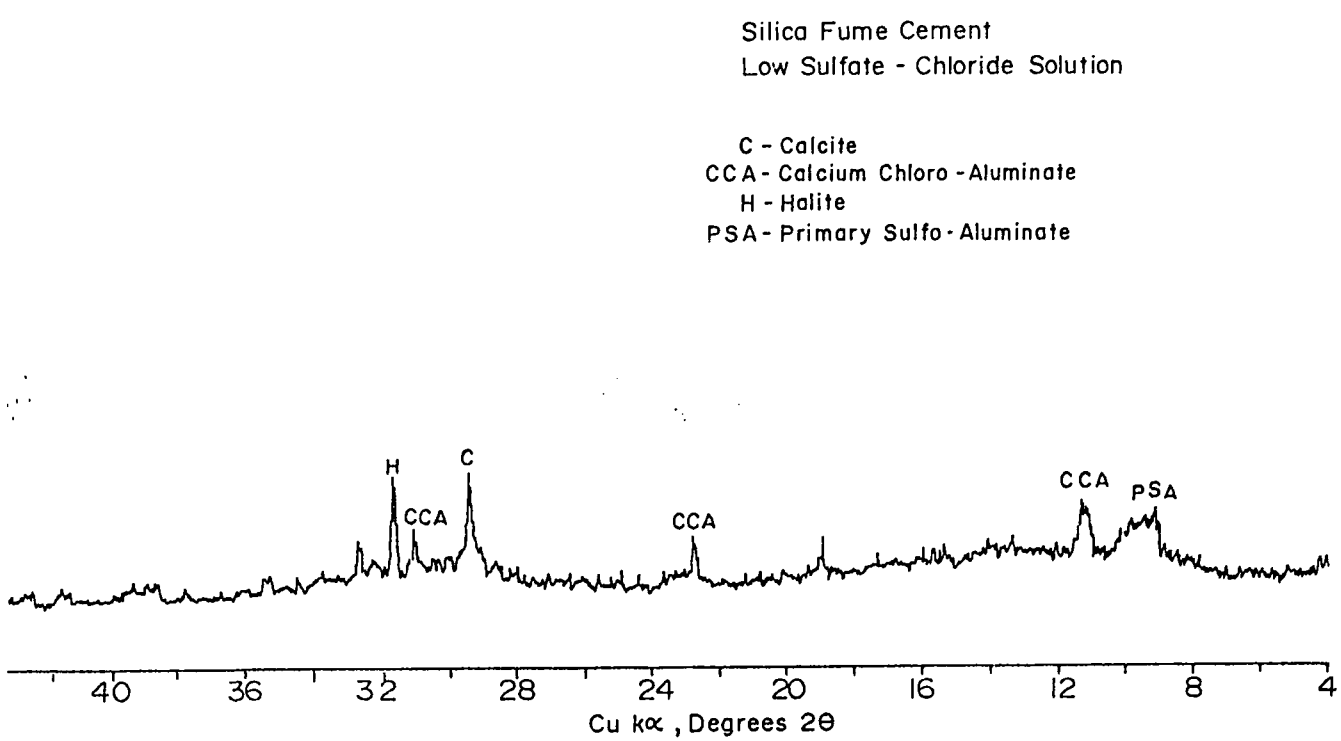

Fig. 6.64 : X-Ray Diffractogram for Silica Fume Cement in Low Sulfate-Chloride Solution after 720 Days.

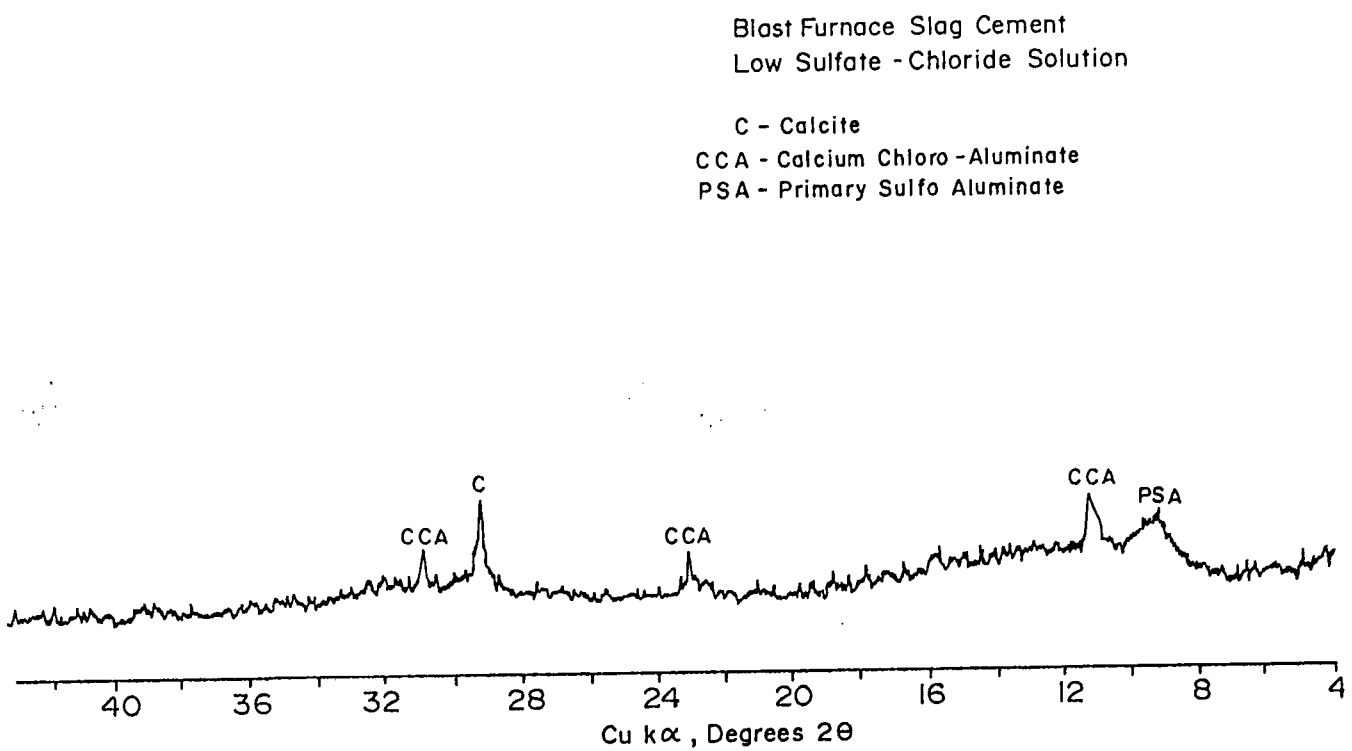

Fig. 6.65 : X-Ray Diffractogram for Blast Furnace Slag Cement in Low Sulfate-Chloride Solution after 720 Days.

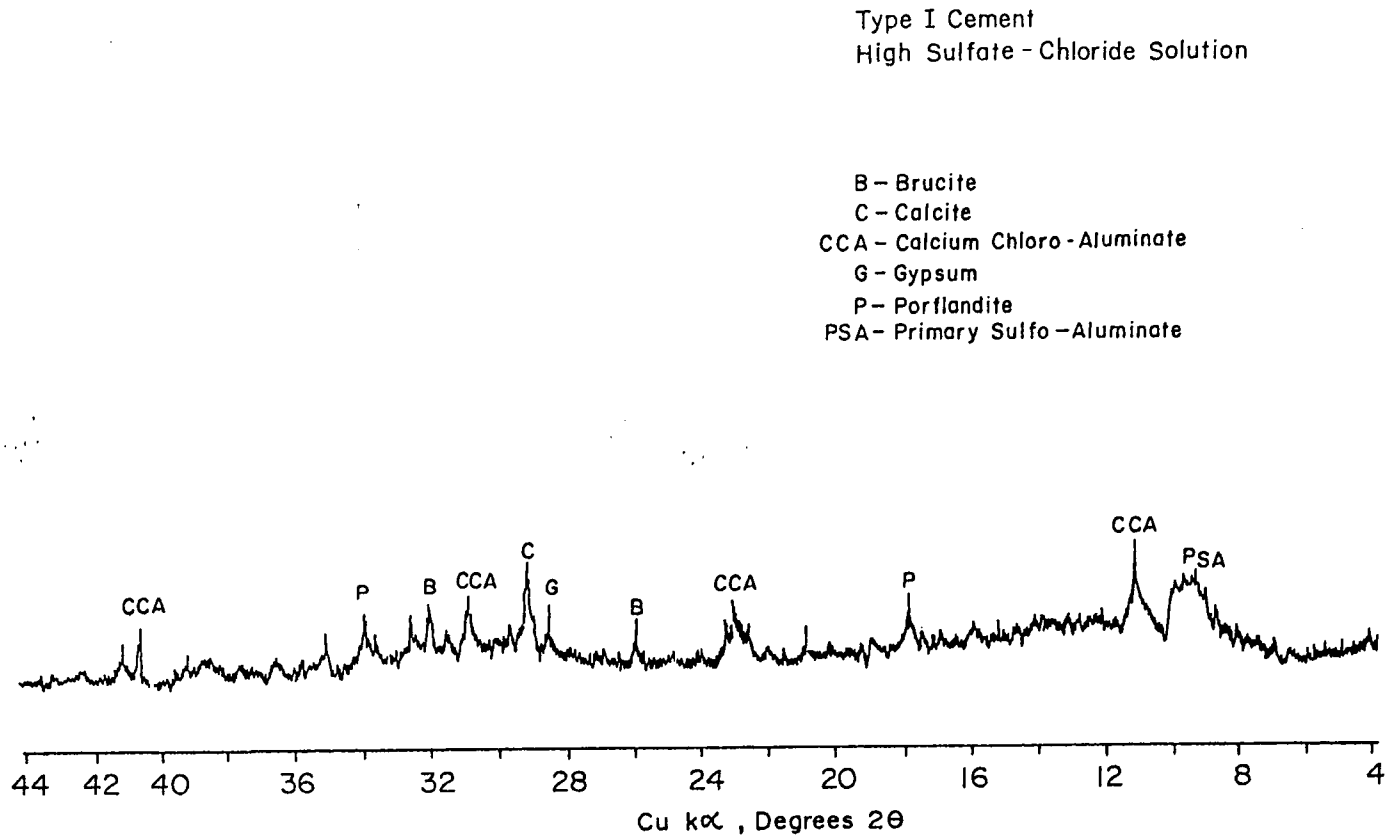

Fig. 6.66 : X-Ray Diffractogram for Type I Cement in High Sulfate-Chloride Solution after 720 Days.

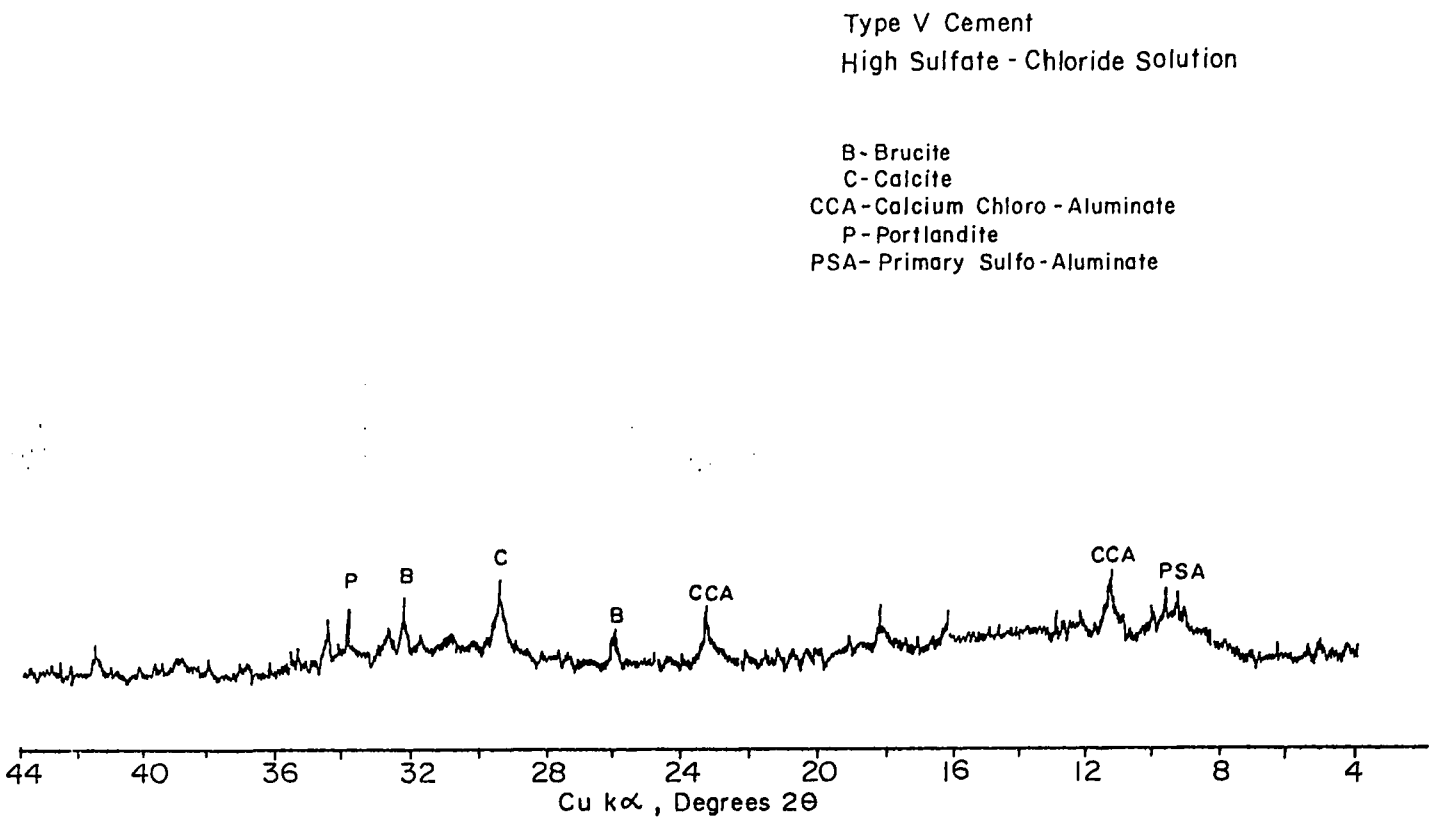

Fig. 6.67 : X-Ray Diffractogram for Type V Cement in High Sulfate-Chloride Solution after 720 Days.

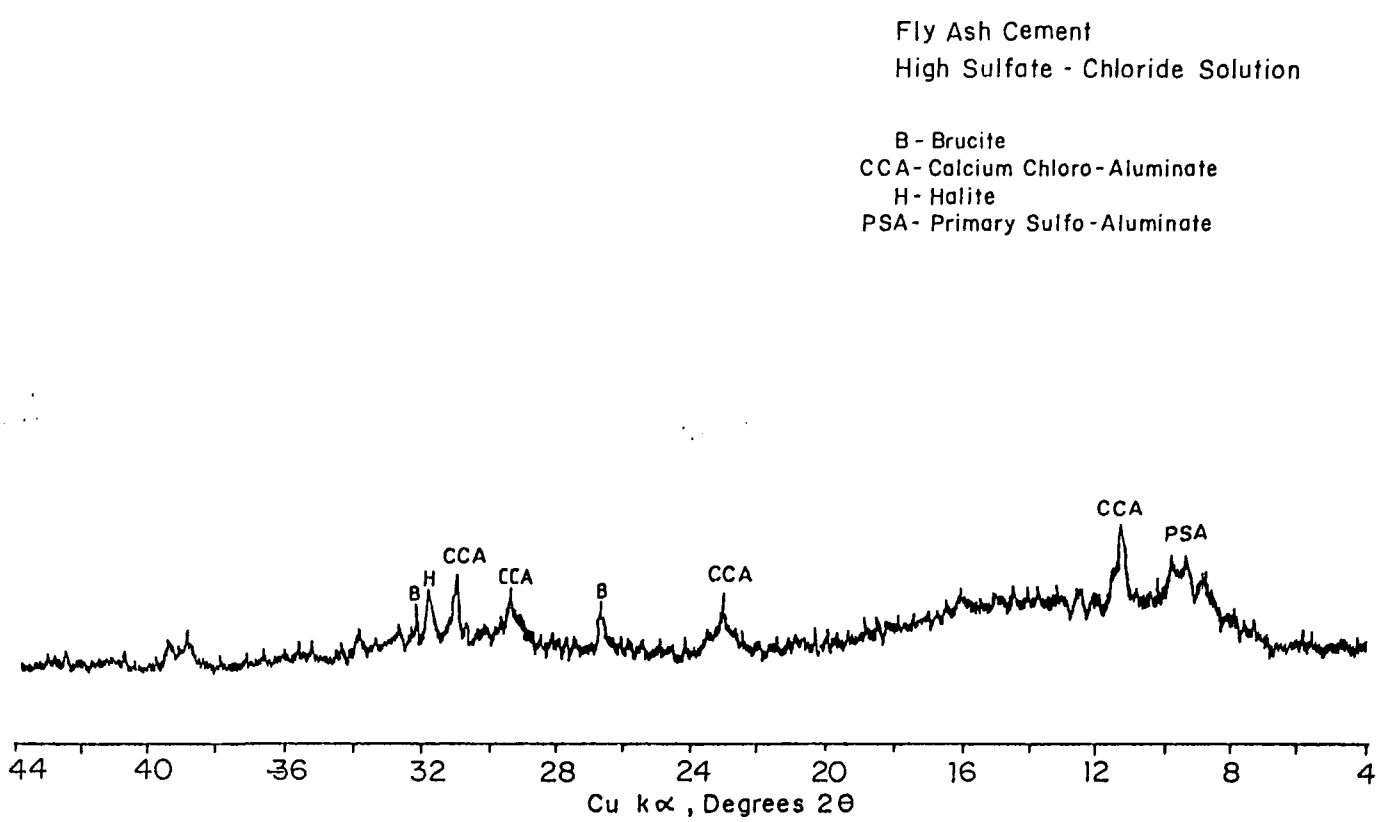

Fig. 6.68 : X-Ray Diffractogram for Fly Ash Cement in High Sulfate-Chloride Solution after 720 Days.

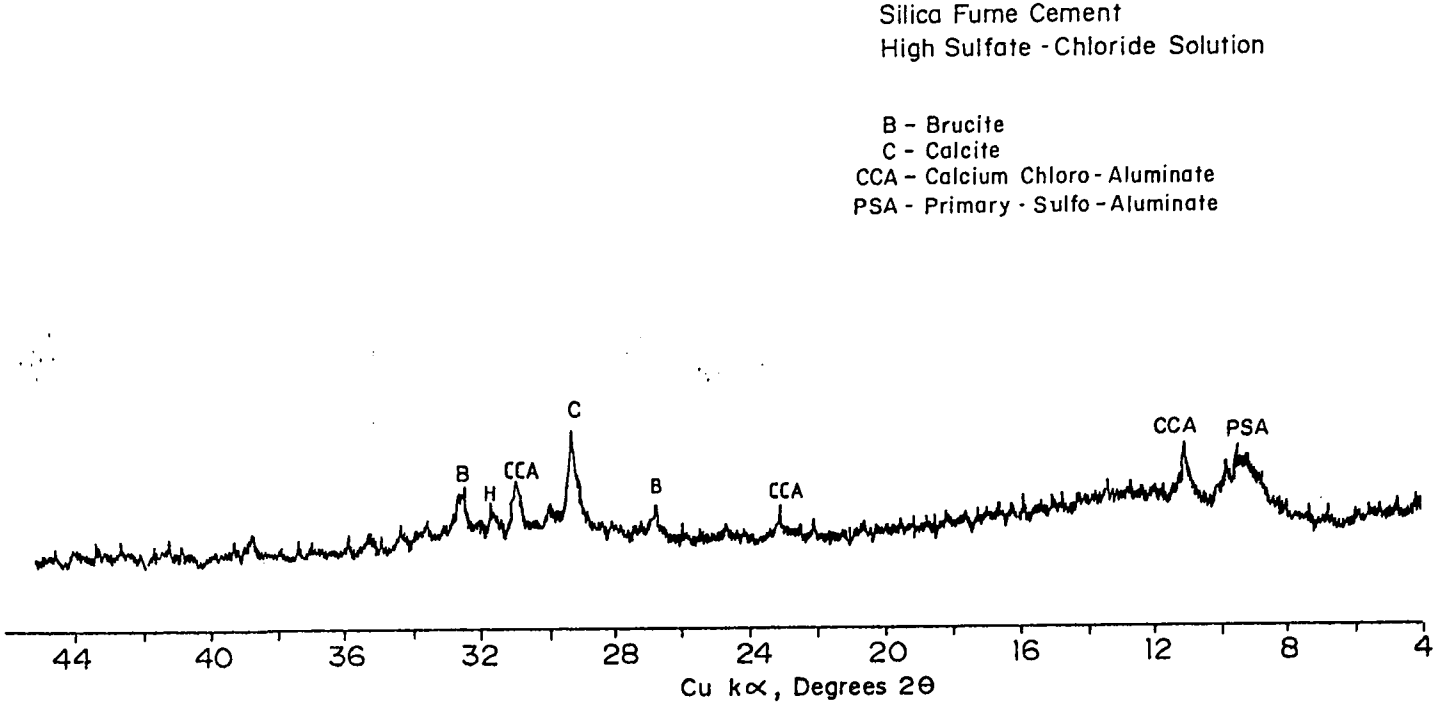

Fig. 6.69 : X-Ray Diffractogram for Silica Fume Cement in High Sulfate-Chloride Solution after 720 Days.

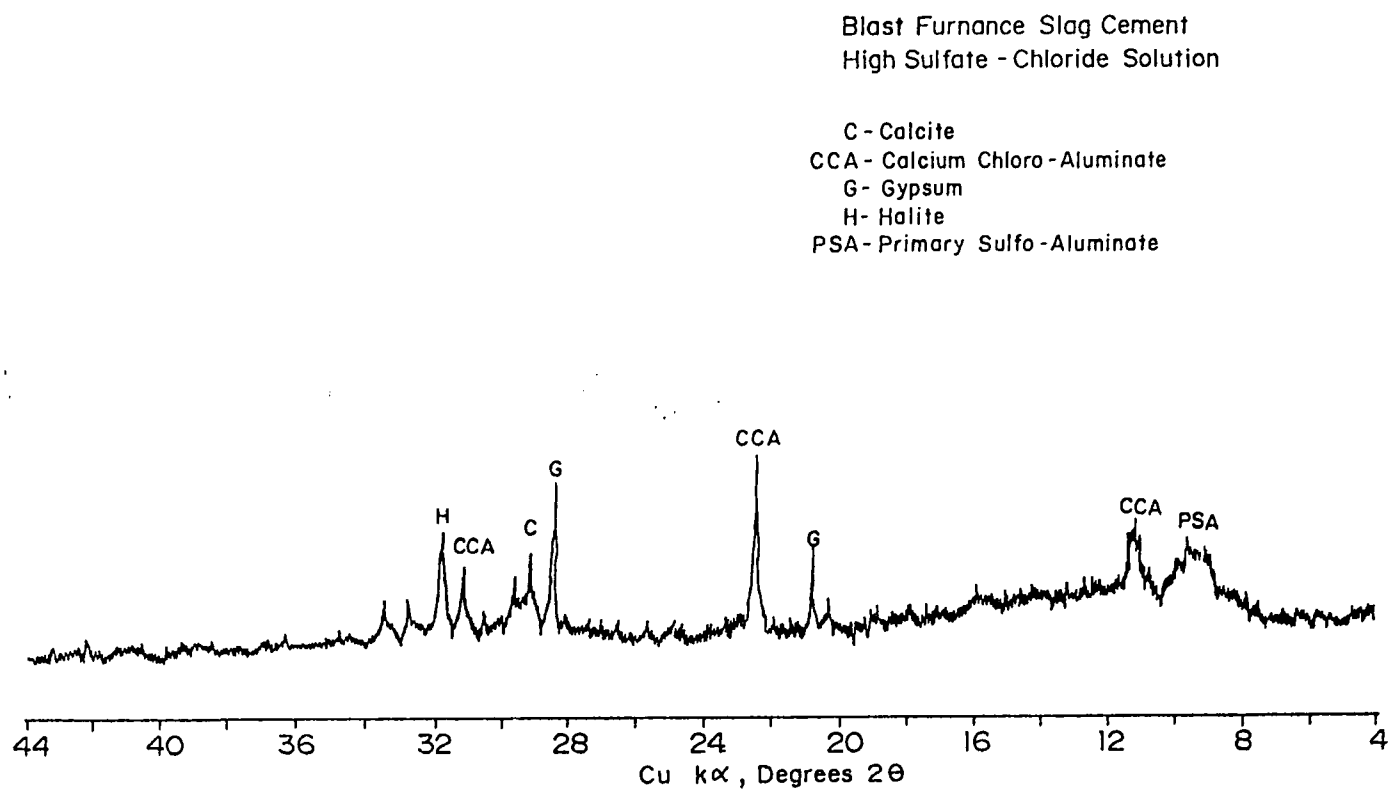

Fig. 6.70 : X-Ray Diffractogram for Blast Furnace Slag Cement in High Sulfate-Chloride Solution after 720 Days.

spot A shown in Plate 6.24 and its EDXA analysis shown in Fig. 6.72, indicate the presence of the same phases; namely calcium chloro-aluminate, M-S-H and C-S-H.

A SEM micrograph for silica fume blended cement exposed to the high sulfate-chloride environment is shown in Plate 6.25. The EDXA analysis (Fig. 6.73) indicates the presence of calcium chloro-aluminate, gypsum, M-S-H and C-S-H. Although here some gypsum is still present; its content is significantly reduced, as confirmed by the X-ray diffraction results. The M-S-H present in SF blended cement is observed to be more than in plain Type V cement.

Plate 6.26 shows a SEM micrograph for BFS blended cement. The elemental area analysis indicates the formation of Friedel's salt and M-S-H (Fig. 6.74). The EDXA analysis for spot A is shown in Fig. 6.75, which again indicates the presence of the same phases. Gypsum is almost totally eliminated. The M-S-H present in BFS blended cement is also observed to be more than in plain Type V cement.

These SEM micrographs confirm the significant reduction of gypsum formation in all cements and in particular in SF and BFS cements when they are placed in $SO_4^{--} - Cl^-$ environment in comparison to the massive gypsum formation when these cements are exposed to pure $M\bar{S} - N\bar{S}$ environment. Gypsum was observed to be

Plate 6.23 : SEM Micrograph for Type V Cement Exposed to High Sulfate-Chloride Solution.

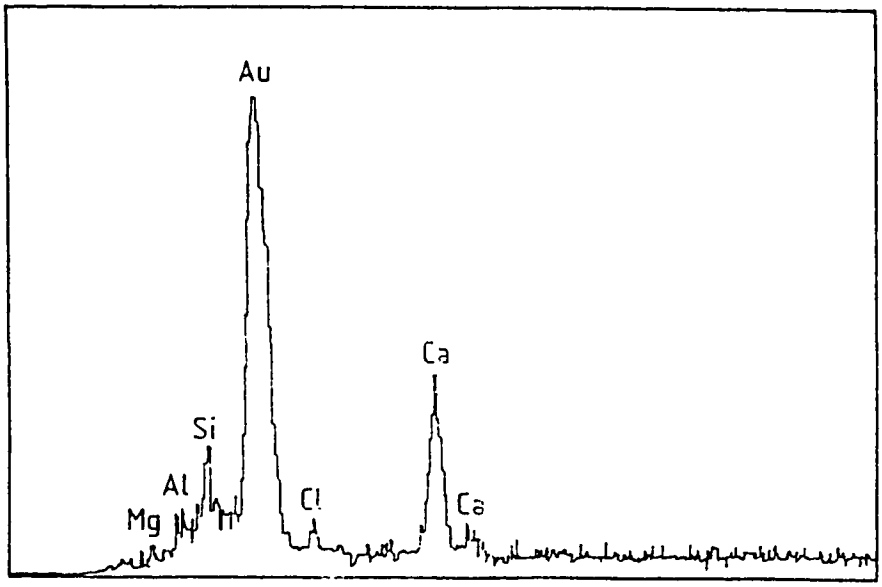

Fig. 6.71 : EDX analysis for Type V cement exposed to high sulfate-chloride solution.

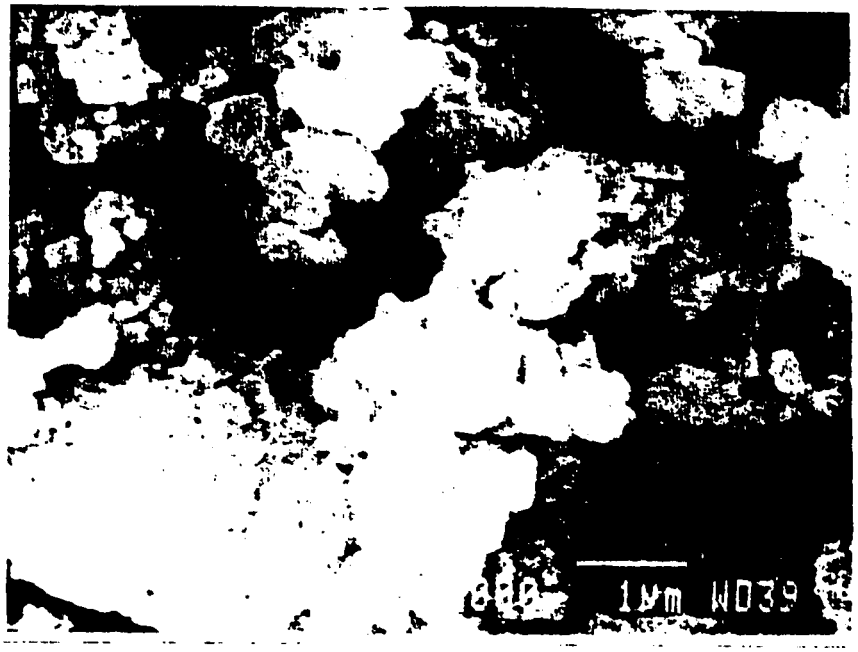

Plate 6.24 : SEM Micrograph for Spot A in Plate 6.23.

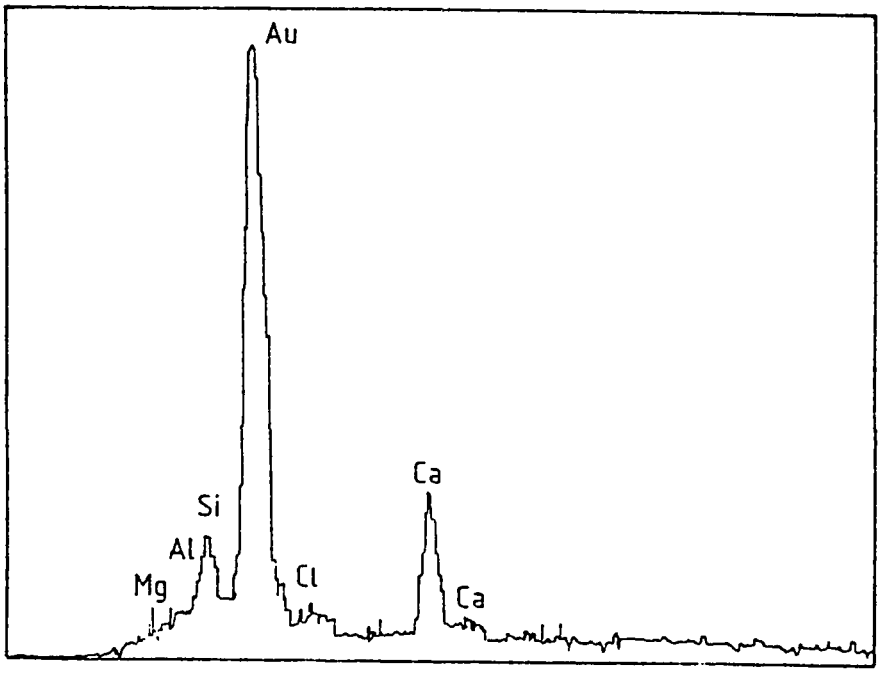

Fig. 6.72 : EDX analysis for spot A in Plate 6.23.

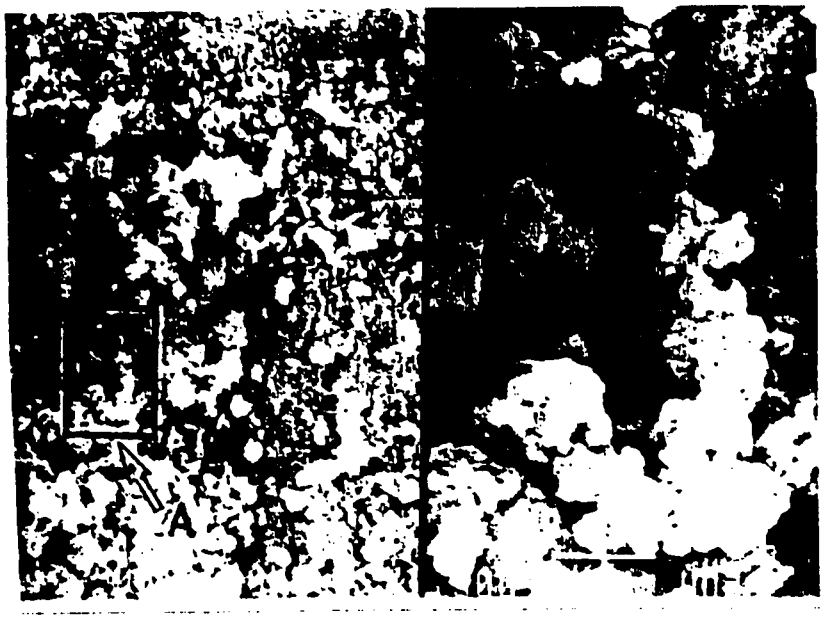

Plate 6.25 : SEM Micrograph for Silica Fume Cement Exposed to High Sulfate Chloride Solution.

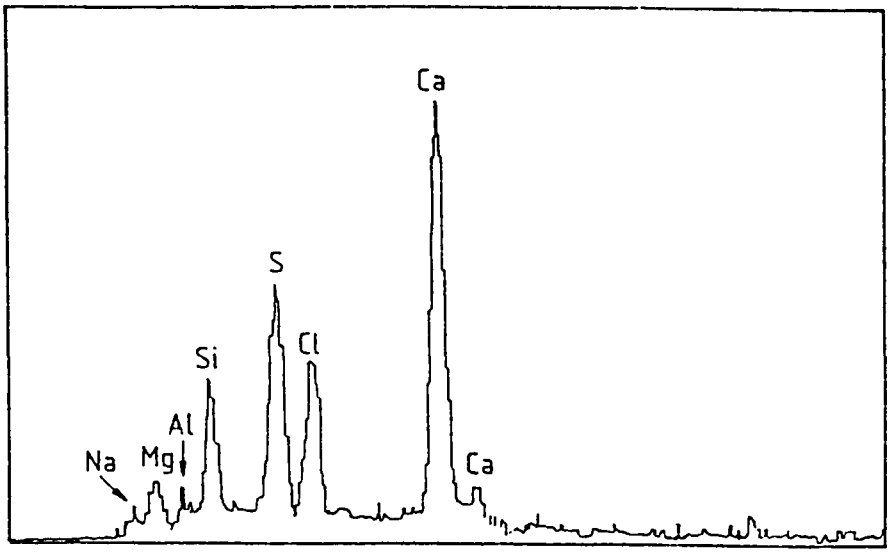

Fig. 6.73 : EDX analysis for silica fume cement exposed to high sulfate chloride solution.

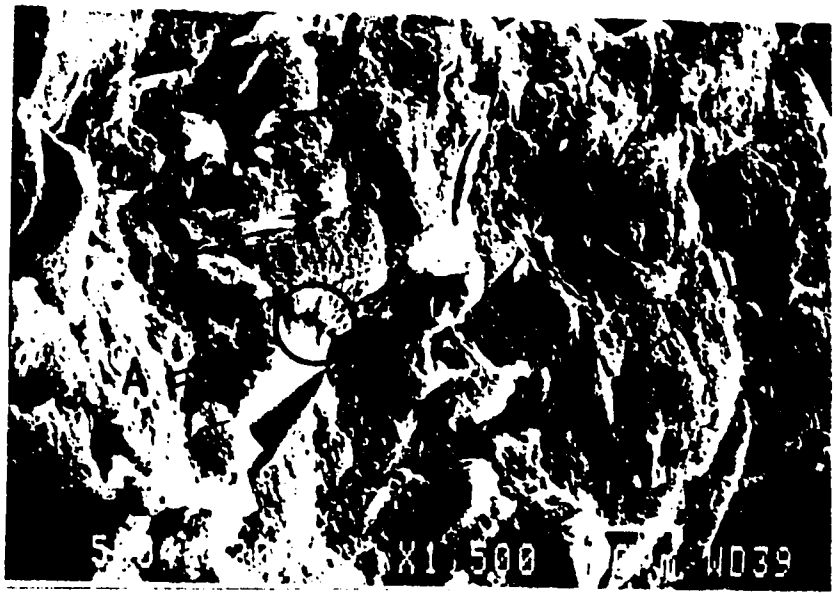

Plate 6.26 : SEM Micrograph for Blast Furnace Slag Cement Exposed to High Sulfate-Chloride Solution.

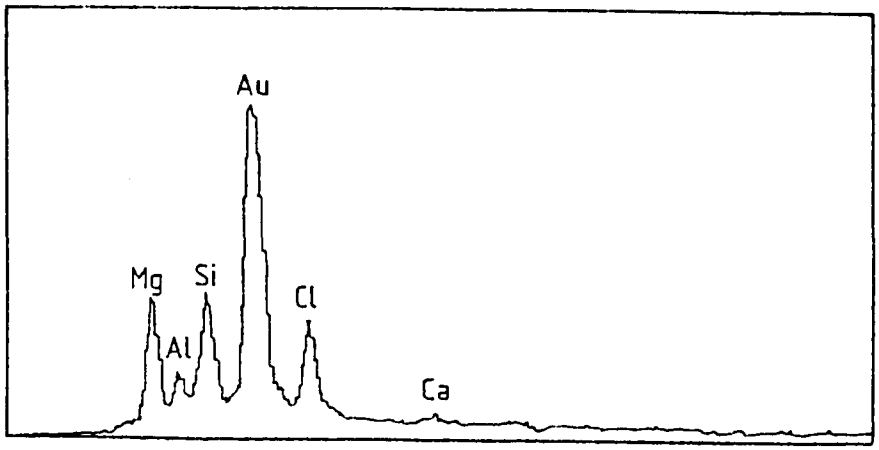

Fig. 6.74 : EDX analysis for BFS cement exposed to high sulfate-chloride solution.

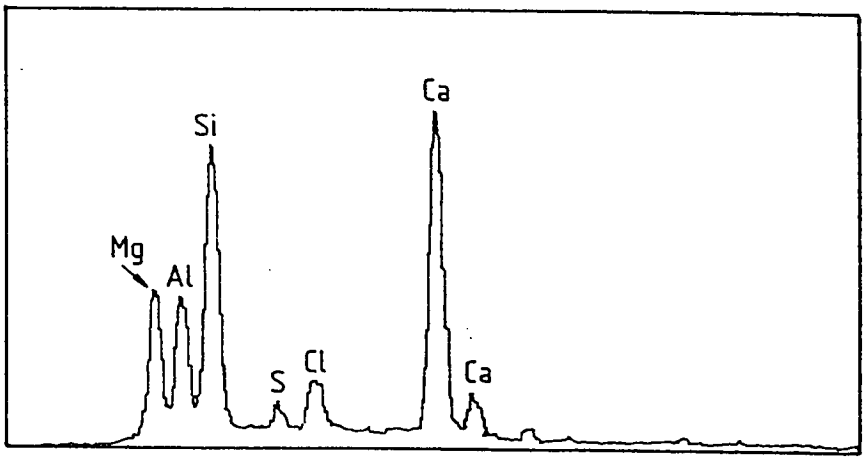

Fig. 6.75 : EDX analysis for spot A in Plate 6.26.

more in SF and BFS cements than in plain and fly ash blended cements. Further, M-S-H is present in all cements exposed to the chloride-sulfate environment; however, the quantity of M-S-H phase is observed to be significantly more in SF and BFS blended cements than in plain Type V cement.

However, it is important to note, from X-ray diffractograms (Figs. 6.66 through 6.70) and SEM micrographs (Plates 6.23 through 6.26) that in all cements, gypsum which was present in massive quantities after exposure to pure $M\bar{S}-N\bar{S}$ solution, is either entirely eliminated or reduced to insignificant levels when exposed to sulfate-chloride environments. It is seen that for plain Type I and Type V cements as well as for fly ash and silica fume blended cements, gypsum is almost completely eliminated (Figs. 6.66 through 6.69 and Plates 6.23 through 6.25), whereas for the BFS cements (Fig. 6.70), it is reduced to insignificant levels.

The usual mechanism advanced to explain the amelioration of sulfate attack by the concomitant presence of chlorides is based on the contention that in the presence of chlorides less trisulfate (ettringite) is formed. This reduction in trisulfate is attributed to the fact that the solubility of ettringite is increased by chloride ions and that a part of the aluminate (C_3A), which engenders ettringite formation, is combined as calcium chloro-aluminate (Friedel's salt), as reported by Lea (132) and Harrison (118). The

consequent assumption is to the effect that trisulfate crystallizes from the solution when chloride is present, because of the higher solubility of trisulfate in chloride-containing solutions and so it does not cause expansion. A similar explanation is provided by Kind (127) who thinks that because of its increased solubility in chloride solution, trisulfate crystallizes either in a small quantity or only in harmless formation in the pores of the hardened cement paste.

Tests carried out by Ogawa and Roy (224) confirm the mitigation of formation of expansive sulfo-aluminate phases in the presence of chlorides. It is shown that in sulfate-chloride environment, Friedel's salt was formed as a decomposition product of ettringite in the 20% NaCl solutions above 100°C. At lower temperatures, even if Friedel's salt is not formed, partial substitution of Cl^- in the ettringite structure may take place, producing a less expansive phase. Furthermore, the reaction of $C_4A_3\bar{S}H_{18}$ (monosulfo-aluminate) to form ettringite was retarded or depressed in a NaCl-containing solution. Cl^- enters the $C_4A_3\bar{S}H_{18}$ structure, replacing SO_4^{--}, and also modifying the morphology of the ettringite, forming thick, stubby and relatively non-expansive crystals instead of the usual elongated ones.

In the present study this explanation is not very viable as

the sulfate attack is not caused by trisulfate (ettringite) in the first place. The sulfate attack in these tests is due to gypsum formation and due to the magnesium decomposition of C-S-H gel. However, Lea (132) and Batta (225) have also reported the increased solubility of gypsum in chloride environments. This is confirmed by the XRD patterns and SEM micrographs which show the virtual elimination of massive gypsum formed in pure $M\bar{S}-N\bar{S}$ solution when the specimens are exposed to sulfate-chloride environment. It is therefore reasonable to assume that the concomitant presence of chlorides and sulfates would significantly mitigate that part of the sulfate attack which is caused by gypsum mechanism. However, chlorides do not ameliorate the magnesium decomposition of the C-S-H gel. This is amply clear from the SEM micrographs (Plates 6.23 through 6.26) which show that in all cements exposed to sulfate-chloride solutions, whereas gypsum was eliminated or substantially reduced, M-S-H was present almost in the same manner as in parallel cements exposed to the pure $M\bar{S}-N\bar{S}$ solution. Therefore, the attack based on magnesium mechanism will continue unhampered even when chlorides are present in the sulfate solution. This explains why the chloride beneficiation is only partial. Furthermore, since in the cases of silica fume and blast furnace slag blended cements, the magnesium decomposition of C-S-H gel is the predominant sulfate attack mechanism, chloride beneficiation is only marginal in the cases of these blended cements.

6.5 CORROSION OF REINFORCEMENT IN PLAIN AND BLENDED CEMENTS

This reinforcement corrosion study in the interactive sulfate-chloride exposure conditions has been carried out to include the two commonly occurring corrosion situations in foundation structures. The accelerated time to corrosion initiation and corrosion current density testing conditions simulate chloride corrosion situations where chlorides and sulfates permeate to the steel-concrete interface as secondary or external chlorides and sulfates through extraneous sources during the service life of concrete structures. Concrete substructures exposed to the sulfate-chloride bearing sabkha soils and groundwaters in the Middle East represent a typical situation of this category. On a global scale, concrete structures exposed to the marine environment, which is infected with both sulfates and chlorides, also fall in this category. However, in a second situation commonly prevalent in the Middle East, chlorides may initially be added to concrete through mix ingredients, such as from unwashed chloride-contaminated aggregates or usage of brackish mixing or curing water. This is a common construction practice in the Middle East where desalinated or potable water is relatively scarce. Pressure extrusion tests carried out in this study are related to this second situation where chlorides and sulfates are present as primary or internal chlorides and sulfates in the original concrete mix, as described in Sec. 4.4.3.3.

The performance of plain and blended cements in resisting reinforcement corrosion from external sulfates and chlorides was evaluated by measuring the corrosion potentials and corrosion current density using the linear polarization resistance technique. The corrosion potentials were measured against a saturated calomel electrode (SCE) using a high impedance voltmeter. The corrosion current density was measured using a microprocessor-based potentiostat/galvanostat. The details of the methodology used have been presented in Sections 4.4.3.6.1 and 4.4.3.6.2.

6.5.1 Time to Corrosion Initiation

The corrosion potentials of steel in concrete specimens made with plain and blended cements and exposed to the four test solutions are plotted against time of exposure in Figs. 6.76 through 6.79. Each point in these figures is an average of three readings taken on triplicate specimens representing similar concrete constituents and exposure conditions. The corrosion potential-time data were used to evaluate the time to initiation of corrosion based on the ASTM C 876 criterion of -350 mV CSE, i.e., -270 mV SCE. The corrosion initiation times based on the potential-time records for concrete specimens exposed to the four environments are summarized in Table 6.7. For the high sulfate-chloride exposure environment, potential measurements (Fig. 6.76) indicate initiation of corrosion of steel in Type I and Type V plain cement concrete specimens after 162 and 106 days respectively. Initiation of rein-

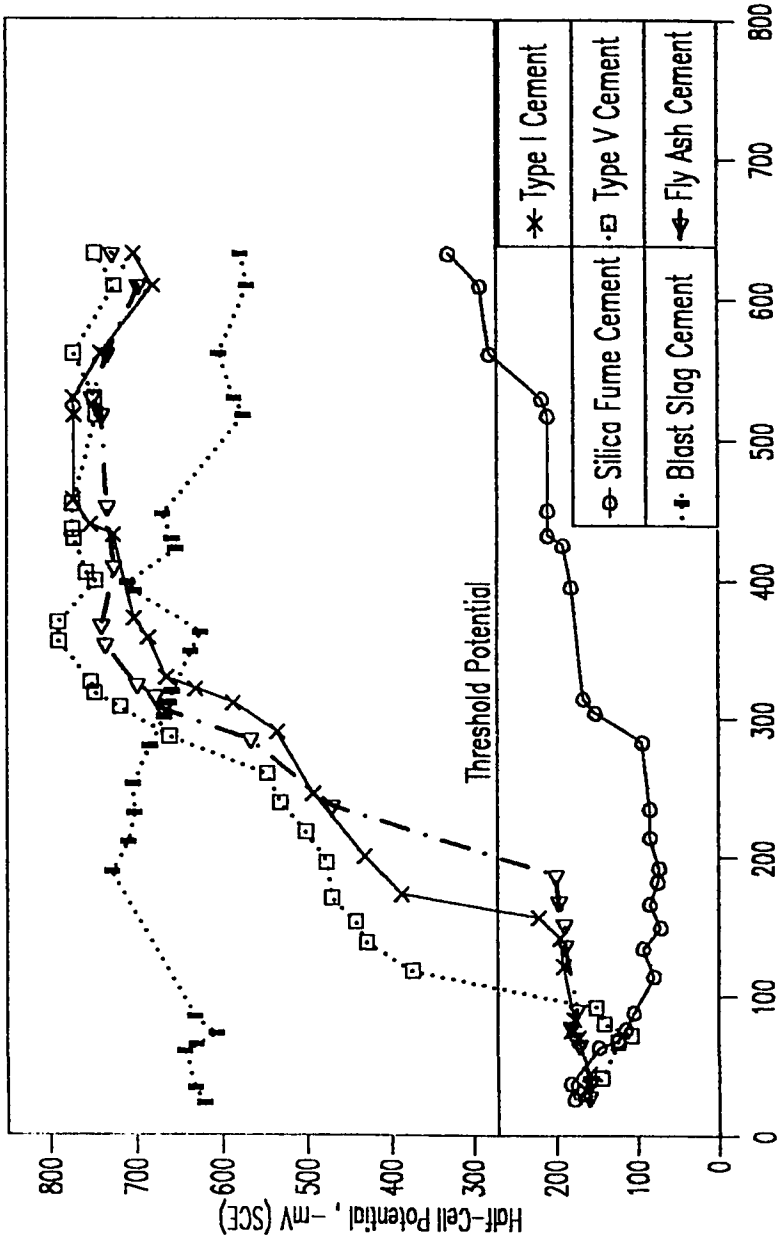

Fig. 6.76 : Half-Cell Potential-Time Record in High Sulfate-Chloride Solution

forcement corrosion in fly ash blended cement concrete specimens was indicated after 210 days of exposure. The corrosion potential-time curve for steel in silica fume blended cement concrete specimens crossed the -270 mV SCE threshold line after about 552 days of exposure. The corrosion potentials of steel in blast furnace slag cement concrete specimens were higher than -270 mV even before placement in the test environment, indicating that the ASTM C 876 criterion of -270 mV SCE is not applicable to evaluate the time to initiation of corrosion for steel in blast furnace slag cement concrete specimens (226). The higher potentials exhibited by steel in blast furnace slag cement concrete specimens are attributed to the greater amount of free water available compared to other cements made with the same water to cement ratio. The higher free water content may be attributed to a lower water requirement for the pozzolanic reaction of the slag than that for portland cement clinker hydration reaction. The free water in this cement is present in a much finer pore distribution than plain cements and, therefore, may impede the access of oxygen to the steel-concrete interface (227). Due to the limited access of oxygen, the passive film is not maintained, thereby giving the impression that the reinforcement is in active condition of corrosion. The corrosion rate, however, remains very low and the steel in BFS cement may be considered for all practical purposes to be in a non-corroding state. This situation is similar to the state of steel embedded in concrete structures located in the submerged zones of the marine

environment.

The time to initiation of reinforcement corrosion in plain Type I and Type V cement concretes exposed to the low sulfate-chloride environment was 109 and 80 days of exposure (Fig. 6.77). Times to initiation of corrosion of steel in fly ash and silica fume cement concrete specimens were 152 and 548 days respectively (Table 6.7). The steel in blast furnace slag cement concrete specimens again shows higher potentials than -270 mV SCE since the beginning of immersion.

The corrosion potential-time curves for specimens placed in the pure chloride environment are presented in Fig. 6.78. The initiation of reinforcement corrosion in plain Type I and Type V cement concrete specimens was indicated after after 175 and 107 days respectively, and that in fly ash and silica fume cement concretes after 220 and 631 days of exposure. The potential-time curve for steel in blast furnace slag cement concrete specimens shows a trend similar to that observed in the above sulfate-chloride environments.

The corrosion potential-time curves for specimens made with both plain and the three blended cements and placed in the pure sulfate environment indicate no rebar corrosion even after about two years of exposure (Fig. 6.79).

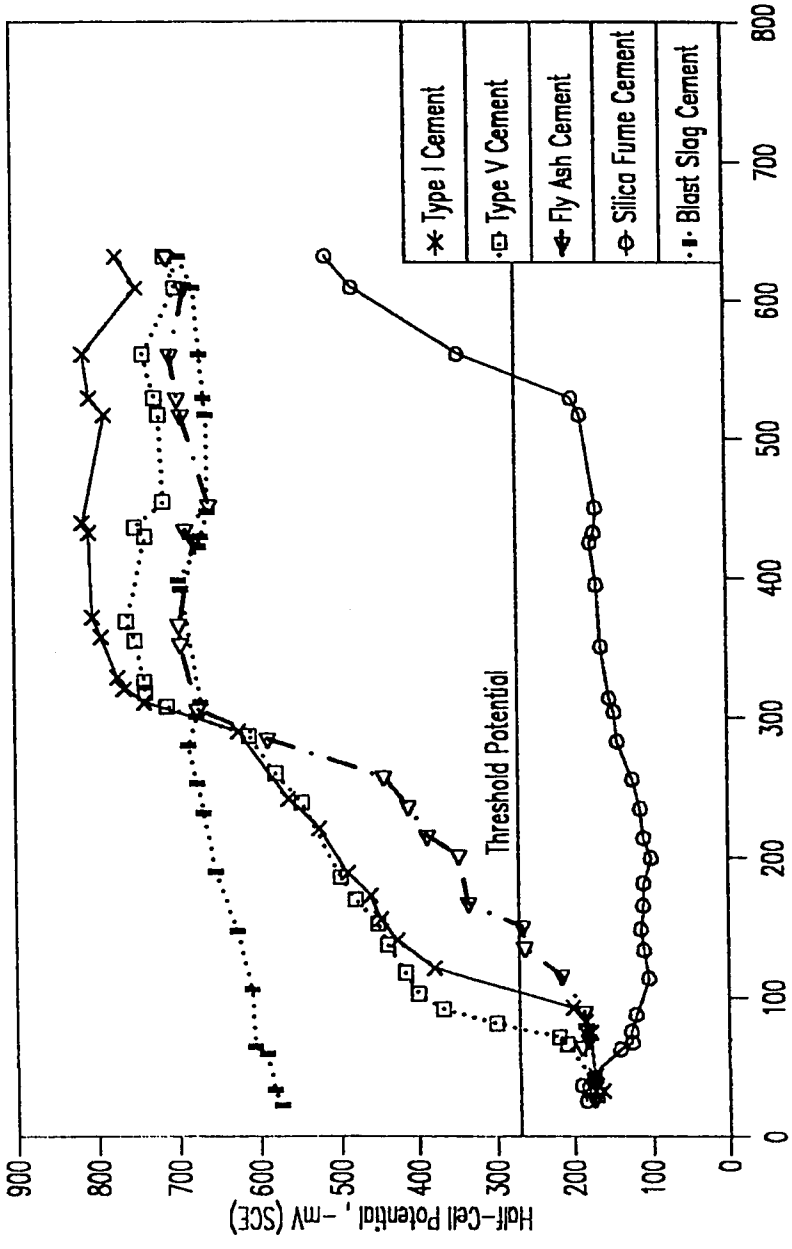

Fig. 6.77 : Half-Cell Potential-Time Record in Low Sulfate-Chloride Solution

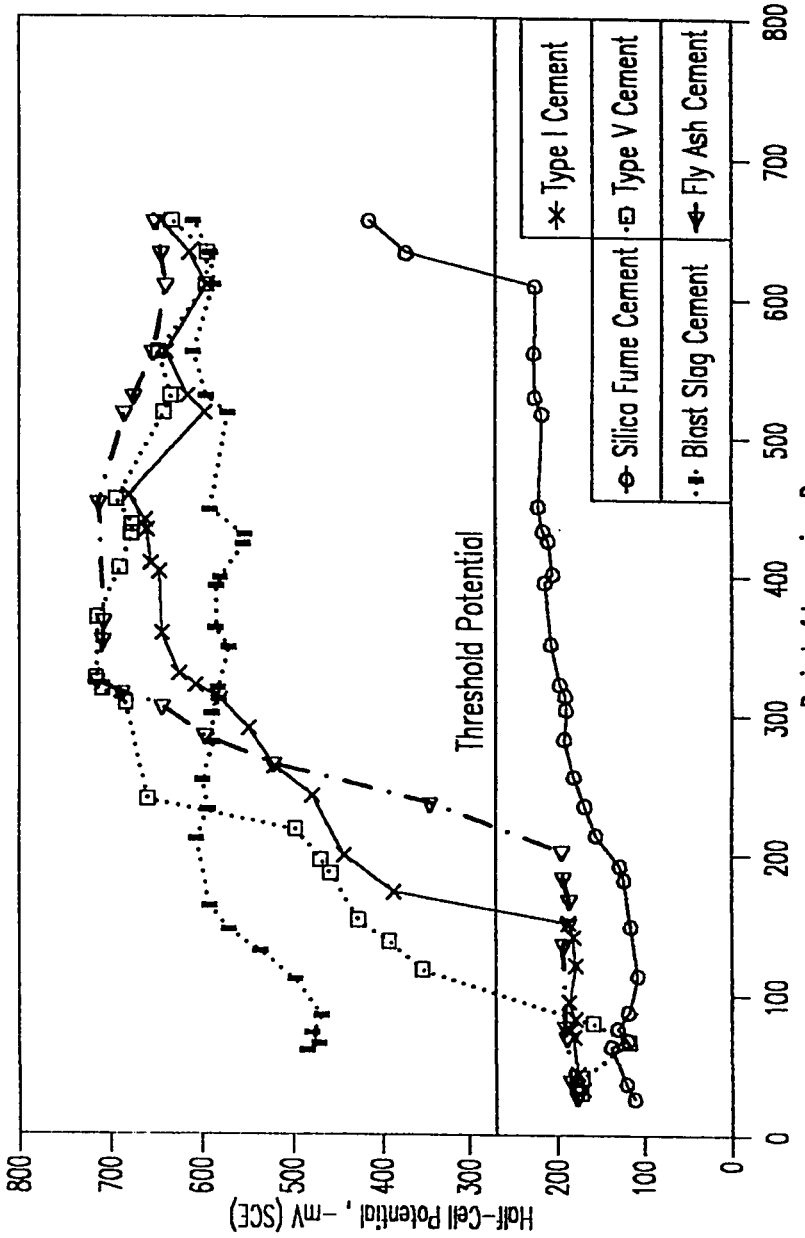

Fig. 6.78 : Half-Cell Potential-Time Record in Pure Chloride Solution

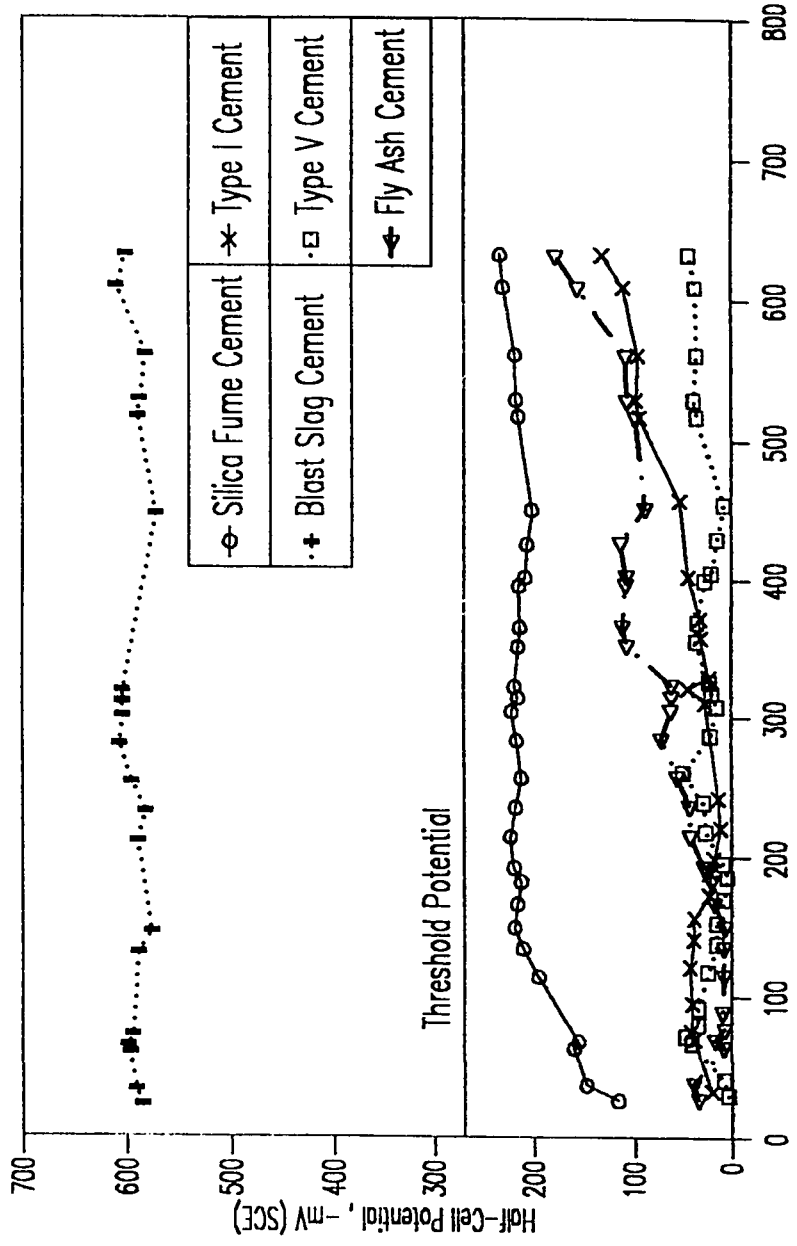

Figure 6.79 : Half-Cell Potential-Time Record in Pure Sulfate Solution

Table 6.7 : Summary of Time to Corrosion Initiation for Plain and Blended Cements Exposed to Various Environments

Cement	Time To Corrosion Initiation for Different Exposure Conditions (Days):			
	Pure Chloride	Low-Sulfate Chloride	High-Sulfate Chloride	Pure Sulfate
Type I	175	108	162	Passive
Type V	107	80	106	Passive
Fly Ash (20%) + Type I	220	152	210	Passive
Silica Fume (10%) + Type I	631	548	552	Passive

A summary of time to initiation of corrosion of steel in plain and blended cement concrete specimens placed in the four different chloride and/or sulfate environments is given in Table 6.7. These data indicate that the performance of silica fume cement, in terms of time to initiation of corrosion, was significantly superior to fly ash and plain cements. However, fly ash performs better than plain cements. In plain cements, Type I cement performs better than Type V cement in all chloride and chloride-sulfate environments. Further, these data also indicate that sulfate ions alone do not initiate reinforcement corrosion in plain and blended cement concrete specimens.

6.5.2 Corrosion Current Density

Quantitative information on reinforcement corrosion in plain and blended cement concrete specimens placed in the four test environments was developed by conducting linear polarization resistance technique. These tests were conducted after 425, 500 and 650 days of exposure to the four test environments, when it was expected that both sulfate and chloride ions would have reached the steel-concrete interface.

The data on corrosion current density, I_{corr}, on rebars embedded in Type I cement and placed in the four test environments are presented in Fig. 6.80. These data indicate absolutely minimal corrosion activity on steel in specimens placed in the pure

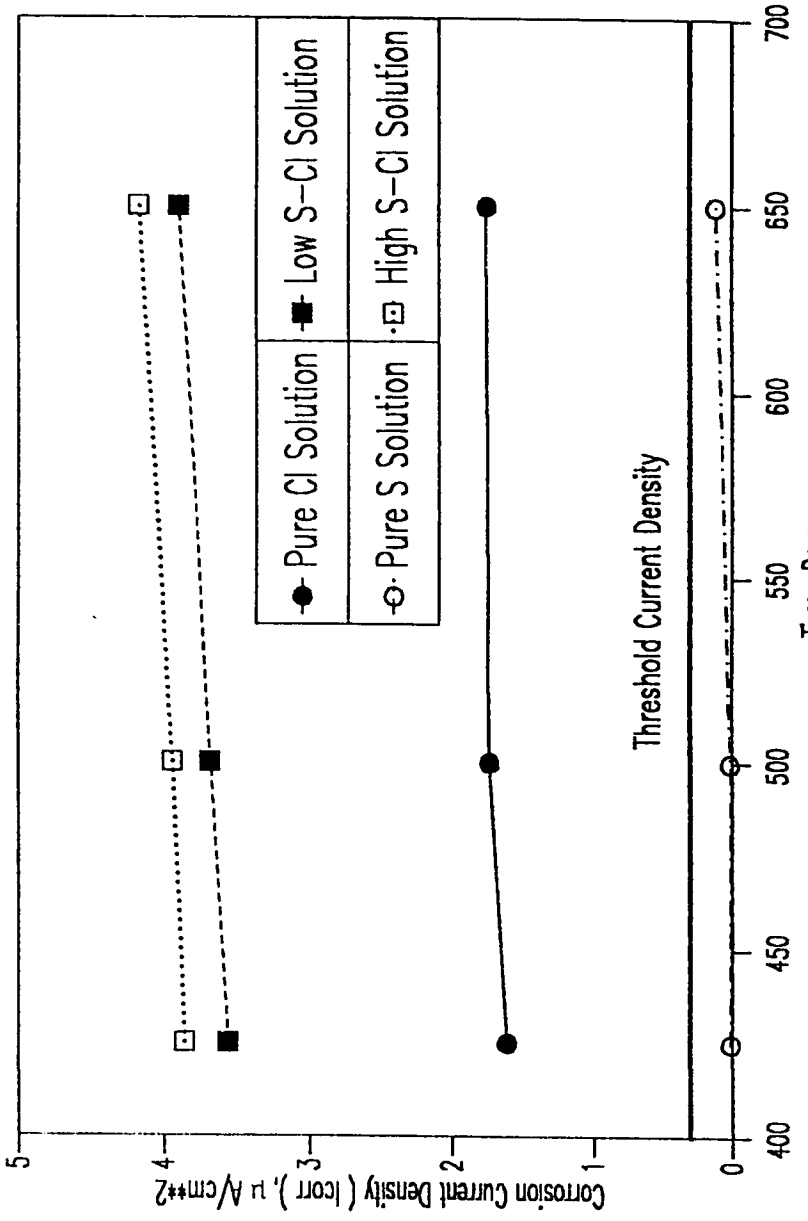

Fig. 6.80 : Corrosion Current Density on Steel in Type I Cement Concrete Specimens

sulfate environment thereby confirming the half-cell potential measurements. The corrosion current density on steel in specimens placed in the pure chloride solution was in the range of 1.61 to 1.75 $\mu A/cm^2$, whereas it was in the range of 3.86 to 4.16 $\mu A/cm^2$ for specimens placed in the high sulfate-chloride environment. The data on corrosion current density on steel in specimens placed in the low sulfate-chloride environment was in the range of 3.56 to 3.90 $\mu A/cm^2$.

The data on corrosion current density on steel in Type V cement concrete specimens are presented in Fig. 6.81. These data indicate maximum corrosion activity on steel placed in the high sulfate-chloride environment. The corrosion current density on steel in the specimens placed in this environment varied from 4.63 to 4.76 $\mu A/cm^2$ during the period from 425 to 650 days of immersion. The corrosion current density on steel in specimens placed in the low sulfate-chloride environment was in the range of 3.8 to 4.1 $\mu A/cm^2$. The corrosion current density on steel in specimens exposed to the pure chloride environment was in the range of 2.0 to 2.2 $\mu A/cm^2$. The corrosion current density on steel in specimens placed in the pure sulfate environment was in the range of 0.01 to 0.12 $\mu A/cm^2$.

The data on corrosion current density on steel in fly ash

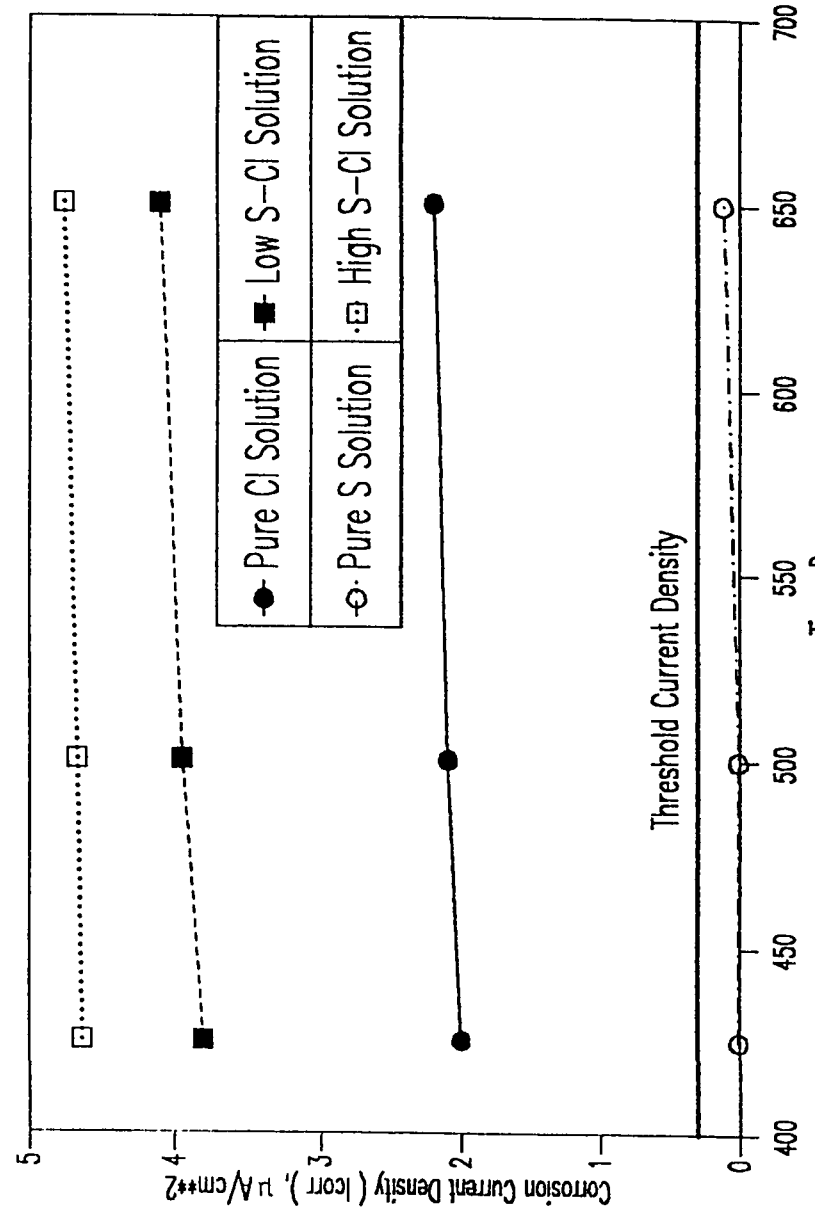

Fig. 6.81 : Corrosion Current Density on Steel in Type V Cement Concrete Specimens

blended cement concrete specimens are shown in Fig. 6.82. These data indicated a trend similar to that indicated by both Type I and Type V cement concrete specimens. The corrosion current density on steel in specimens exposed to the high sulfate-chloride environment was in the range of 1.18 to 1.72 $\mu A/cm^2$, whereas these values were in the range of 1.04 to 1.27 $\mu A/cm^2$ for specimens exposed to the low sulfate-chloride environment. The corrosion current density of steel in specimens exposed to the pure chloride solution was in the range of 0.48 to 0.99 $\mu A/cm^2$. The corrosion current density on steel in specimens exposed to the pure sulfate environment was again minimum, being 0.02 to 0.11 $\mu A/cm^2$.

The corrosion current density on steel in blast furnace slag cement concrete specimens exposed to the high sulfate-chloride environment was in the range of 0.30 to 0.50 $\mu A/cm^2$ (Fig. 6.84). The I_{corr} values were in the range of 0.27 to 0.44 $\mu A/cm^2$ in specimens exposed to the low sulfate-chloride environment. The corrosion current densities on steel in specimens exposed to the pure chloride and pure sulfate environments were in the range of 0.25 to 0.32 and 0.13 to 0.28 respectively. The I_{corr} values in specimens exposed to these environments, i.e., pure chloride and sulfate, are somewhat less than 0.3 $\mu A/cm^2$, which is the threshold value commonly used to denote corrosion initiation (187,188).

The data on corrosion current densities on steel in the silica fume cement concrete specimens exposed to the four test environments are presented in Fig. 6.83. The I_{corr} values in specimens exposed to the high sulfate-chloride environments were in the range of 0.06 to 0.29 $\mu A/cm^2$. The corrosion current density on bars in specimens exposed to the low sulfate-chloride environment was in the range of 0.03 to 0.24 $\mu A/cm^2$. The I_{corr} values in specimens exposed to the pure chloride and pure sulfate environment remained fairly unchanged at 0.02 to 0.06 and 0.01 to 0.05 $\mu A/cm^2$, respectively. It is to be noted that the I_{corr} values in the specimens made with silica fume cement exposed to the four test environments were less than 0.3 $\mu A/cm^2$, which is the normally considered as the threshold corrosion current density value for corrosion activation. According to Gonzalez et al. (187), if I_{corr} is greater than 0.3 $\mu A/cm^2$, then the reinforcing steel will be certainly in active state and if it is less than 0.1 $\mu A/cm^2$ then the reinforcing steel is certainly in passive state. If, however, the threshold I_{corr} value for corrosion initiation is assumed at 0.2 $\mu A/cm^2$, then corrosion initiation is indicated in steel embedded in silica fume concrete specimens exposed to the low sulfate-chloride and the high sulfate-chloride environments after 608 and 565 days of exposure. These values agree very well with the data on time

to initiation of corrosion for these specimens placed in these two environments using the half-cell measurement technique, according to which the time to initiation of corrosion is 548 and 552 days respectively.

A summary of the corrosion current density results is presented in Table 6.8. These data show the range of I_{corr} values for all cements in the various test environments during the period of 425 to 650 days of exposure. Table 6.9 summarizes the performance rating for plain and blended cements in resisting reinforcement corrosion in the chloride and sulfate-chloride environments after a period of 650 days. These ratings were developed using the performance of Type I cement as a reference. If the data on I_{corr} in specimens placed in the sulfate environment are excluded, as these values are very minimal, the corrosion current density on steel in silica fume blended concrete specimens is found to be 14 to 29 times less than that in Type I cement, as shown in Table 6.9. The corrosion current densities of steel in blast furnace slag and fly ash blended cement are approximately 5.5 to 8.9 and 1.8 to 3.1 times lower than in Type I cement concrete specimens. The performance of Type V cement is observed to be inferior to Type I cement; the I_{corr} rating of Type V cement varied from 0.80 to 0.95 compared to that in Type I cement (Table 6.9).

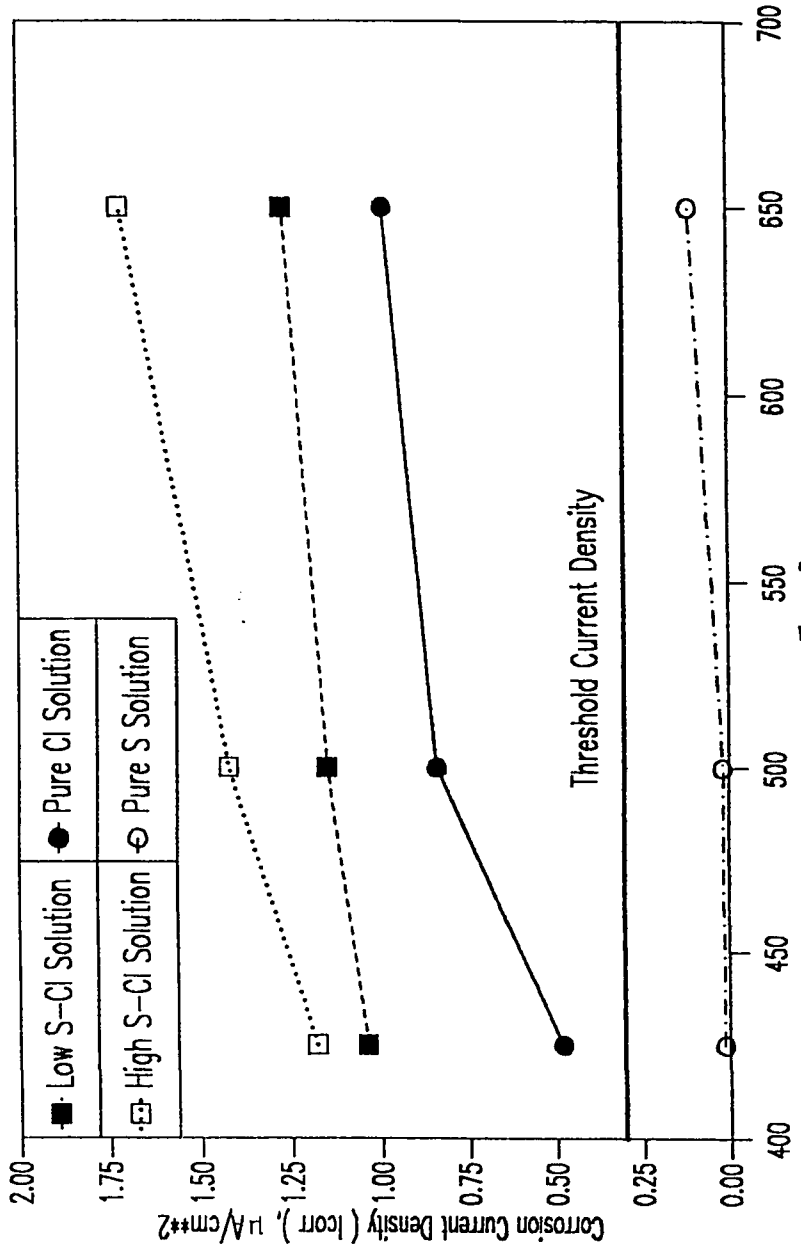

Fig. 6.82 : Corrosion Current Density on Steel in Fly Ash Cement Concrete Specimens

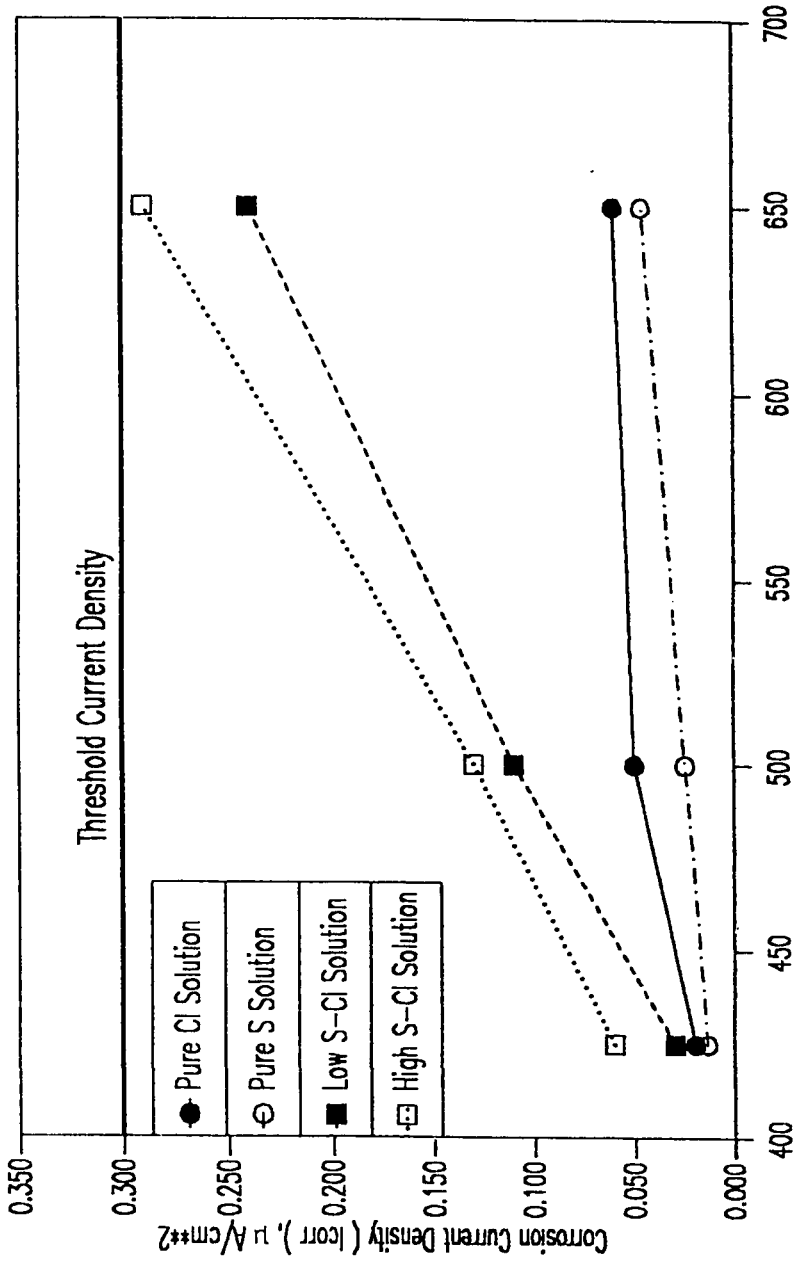

Fig. 6.83 : Corrosion Current Density on Steel in Silica Fume Cement Concrete Specimens

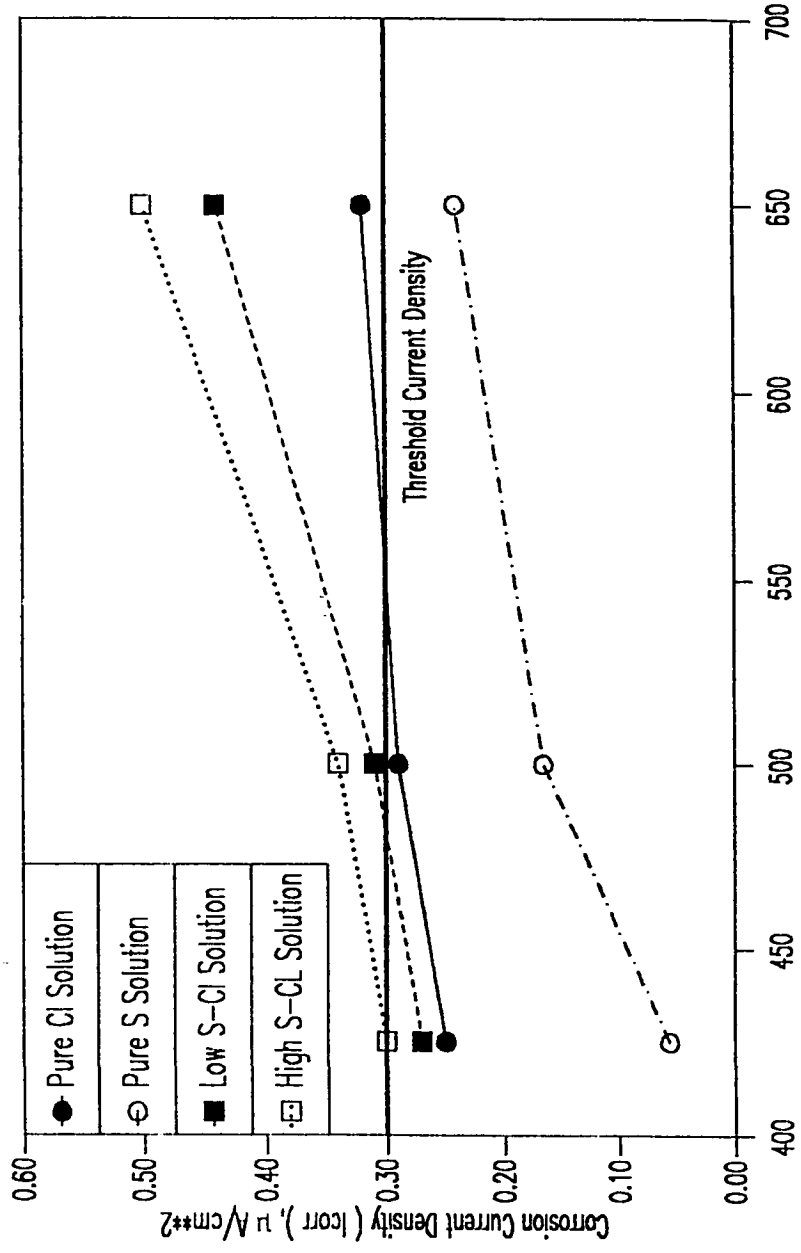

Fig. 6.84 : Corrosion Current Density on Steel in Blast Furnace Slag Cement Concrete Specimens

Table 6.8 : Summary of Corrosion Current Densities on Steel in Plain and Blended Cements Exposed to Various Environments

Cement	Corrosion Current Density for Different Exposure Conditions*, $\mu A/cm^2$			
	Pure Chloride	Low-Sulfate Chloride	High-Sulfate Chloride	Pure Sulfate
Type I	1.61-1.75	3.56-3.90	3.86-4.17	0.013-0.118
Type V	2.00-2.20	3.80-4.10	4.63-4.76	0.012-0.121
Fly Ash (20%) + Type I	0.48-0.99	1.04-1.27	1.18-1.72	0.016-0.113
Silica Fume (10%)+Type I	0.02-0.06	0.03-0.24	0.06-0.29	0.010-0.050
Blast Furnace Slag (60%) + Type I	0.25-0.32	0.27-0.44	0.30-0.50	0.13-0.28

* Exposure period varied from 425 days to 650 days.

Table 6.9 : Performance Rating of Plain and Blended Cements in Terms of Corrosion Current Density.

Cement	Performance Rating for Various Exposure Conditions*		
	Pure Chloride	Low-Sulfate Chloride	High-Sulfate Chloride
Type V	0.80	0.95	0.88
Fly Ash	1.77	3.07	2.42
Silica Fume	29.2	16.3	14.4
Blast Furnace Salg	5.47	8.86	8.34

* in terms of steel embeded in Type I cement after 650 days of exposure

6.5.3 Effect of Sulfate and Chloride Salts on Pore Solution Chemistry

In order to investigate the effect of sulfate and chloride ions on the pore solution chemistry, plain and blended cement paste specimens with chloride and chloride-sulfate contaminations were cast and the pore solution was extruded using the special pore solution expression devise. Thereafter, the pore solution was analyzed to determine the chloride and hydroxyl ion concentrations. These specimens were made with a chloride concentration of 0.6% by weight of cement, where only chlorides were present and with a chloride concentration of 0.6% and a total sulfate concentration of 6% (as SO_3) by weight of cement where both chlorides and sulfates were present conjointly. The concentration of chloride and sulfate ions in the pore solution of plain and blended cement paste specimens are shown in Table 6.10. This Table also shows the hydroxyl ion concentrations as well as the ratio of chloride to hydroxyl ion concentration (Cl^-/OH^-) in the pore solutions of plain and blended cements. The data in Table 6.10 on the Cl^- and OH^- ion concentrations show that for the plain as well as the three blended cements, the free chloride ion concentration increased sharply in the range from 4.77 to 18.25 times when the 6% SO_3 was added to the 0.6% chlorides in the cement paste. The minimum increase of 4.77 times was for the silica fume blended cement, and the maximum increase of 18.25 times was for the BFS cement, with

Table 6.10 : Summary of Pore Solution Results Expressed from Hardened Plain and Blended Cement Paste Specimens

Cement	Series #1 Only Primary Chlorides (Cl) added (0.6% by Weight of Cement)			Series #2 Chlorides and Sulfates added Concomitantly (0.6% Cl + 6% SO_3 by Weight of Cement)			Increase in Cl^-, OH^- and (Cl/OH) Ratio due to Sulfate Addition		
	Cl^-	OH^-	Cl^-/OH^-	Cl^-	OH^-	Cl^-/OH^-	Cl^-	OH^-	Cl^-/OH^-
Only Portland Cement Type I	71	339	0.209	942	1278	0.737	13.27	3.77	3.53
20% Fly Ash blended with OPC Type I	100	203	0.492	911	1013	0.899	9.11	4.99	1.83
60% BFS blended with OPC Type	55	272	0.202	1004	1214	0.827	18.25	4.46	4.09
10% Silica Fume blended with OPC Type I	173	78	2.218	826	308	2.680	4.77	3.95	1.21

13.26 and 9.11 times increase for the plain and fly ash blended cements respectively. However, with the addition of sodium sulfate, the OH^- ion concentration was found to increase by 3.99 to 4.99 folds.

Corrosion risk is measured not by the concentration of the free chlorides, but by the (Cl^-/OH^-) ratio. The (Cl^-/OH^-) ratio for silica fume cement, which is 4.5 to 11 times higher than for other cements, is shown to undergo only a minor change from 2.22 to 2.68 with the 6% SO_3 addition. However, the (Cl^-/OH^-) ratios for plain, fly ash and BFS cements undergo increases which vary from 1.83 times for the fly ash cement to 3.52 times for the OPC and 4.9 times for the BFS cement with the addition of the 6% sulfates.

6.6 MECHANISMS OF REINFORCEMENT CORROSION IN CHLORIDE-SULFATE ENVIRONMENTS

The interactive effect of sulfates and chlorides is hardly perceptible in the form of any systematic or methodical pattern for corrosion initiation time when corrosion is promoted by the conjoint action of external chlorides and sulfates. Corrosion initiation mechanism by mixed external solutions of sulfates and chlorides is logically and predominantly governed by: (i) the speed of diffusion of these ions in different concretes as well as (ii) the relative diffusivity of these ions in a particular concrete.

Taking the second factor first, there is considerable documented evidence which conclusively indicates that chlorides diffuse

manifold faster than sulfates into hardened cement paste (228,229). Rio and Turriziani (230) found in 15 months long Cl^- and SO_4^{--} penetration studies into plain and blended cements that the Cl^- penetration depth was about twice as much as that for SO_4^{--}. This is consistent with the diffusivity data of Barnes and Roy (231) who found in salt-containing mixtures (containing fly ash and/or slag) consistently lower diffusion rates by a factor of 2 to 5 times for SO_4^{--} than Na^+ and others (135) who found the chloride anion diffusion is considerably faster than SO_4^{--} and other cations. Based on an extensive literature review, Oberholster (232) reported that the diffusion coefficient of chloride ion into hardened cement pastes increases when the chloride ions are associated with divalent ions compared to monovalent ions. It was further reported (232) that the **diffusion of chlorides is generally 10 to 100 times faster than that of sulfates.** The greater penetration of chlorides compared with sulfates was also observed by Stratful (133) who found that concrete retained fourteen times more chlorides by weight than sulfates.

These data suggest that when Cl^- and SO_4^{--} ions in mixed chloride-sulfate solutions diffuse through concrete, chlorides would penetrate significantly faster than sulfate ions to the steel-concrete interface and would therefore influence the corrosion mechanism

related to corrosion initiation almost independent of sulfates. This is clearly shown by the time to corrosion initiation data where the sulfates have almost no significant or systematic effect on corrosion initiation time.

The first factor, related to the diffusivity of chloride ions in concretes of different impermeability, has a predominant influence in determining the corrosion initiation time for the various types of plain and blended cements used in this investigation. It is seen that the silica fume blended cement concrete offers 5.2 to 6.9 times better corrosion protection performance than plain Type I cement concrete (Table 6.7). This is clearly explained by the fact that silica fume addition renders concrete significantly more impermeable compared to plain concrete. Manmohan and Mehta (233) and Nyame and Illston (234) have shown that in concrete, it is the pore size distribution rather than the total porosity which governs the penetration of aggressive ions into concrete. Tests carried out at the King Fahd University of Petroleum and Minerals (178) show that the average pore radius is reduced from 285Å to 181Å with 10% silica fume blending. Similar results were obtained by Kumar et al. (235) for a paste made with 0.4 water to solid silica fume ratio, the medium pore size was reduced from 15 nm to 7.5 nm and the coefficient of chloride diffusion for 10% silica fume was reduced from 227×10^{-13} m^2/sec to 15.6×10^{-13} m^2/sec. Page and Havdahl (236) have also reported a reduction in the chlo-

ride diffusion coefficient from 160×10^{-9} m^2/sec to 22×10^{-9} m^2/sec for 10% silica fume blended cement paste. Likewise, chloride diffusion from sea water has been studied by Fisher et al., as reported by Sellevold and Nilsen (237). Their results indicate that a concrete with 8% condensed silica fume addition has a chloride diffusion of 1.1×10^{-8} m^2/sec whereas an equivalent concrete without silica fume has a coefficient of 1.5×10^{-7} m^2/sec .

A very similar explanation is applicable to BFS cement where it has been shown by several investigators (238,239) that slag blending increases very significantly the impermeability of BFS cements. Bakker (135) has presented a hydration mechanism model to explain the development of an impermeable microstructure for BFS cement. The two-fold superior corrosion protection performance in terms of corrosion initiation time of fly ash cement concrete also reflects a denser microstructure due to the segmentation and blocking of the pores by the secondary C-S-H products as a result of the pozzolanic reaction between fly ash and calcium hydroxide.

The data on time to initiation of corrosion and corrosion current density also show a superior performance of Type I cement over Type V cement. This is ascribable to the greater chloride binding by C_3A for Type I cement compared to Type V cement (145). Also Holden et al (134) have shown a 2.5 times greater

diffusivity of Cl^- ions in Type V cement compared to Type I cement. This may also be attributable to the complexing of chlorides with C_3A during the process of permeation.

Whereas corrosion initiation time is not affected by the concomitant presence of sulfate and chloride ions, however, once the sulfate ions reach the steel level and sufficient concentrations of both chlorides and sulfates are together available at the steel-concrete interface, the corrosion process is conjointly affected by these two ions, and sulfates are seen to increase the corrosion current density for all cements. In order to visualize the role of sulfate ions on the chloride-induced corrosion, the data on corrosion current density on steel embedded in plain cements are presented in Figs. 6.85 through 6.87 for immersion periods of 425, 500 and 650 days respectively. The I_{corr} data were plotted as a function of sulfate/chloride ratio where SO_4^{--}/Cl^- ratios of 0, 0.035 and 0.134 represent the pure chloride, low sulfate-chloride and high sulfate-chloride test environments, respectively. In all of these environments, the chloride concentration remained invariant at 15.7%. Similarly, Figs. 6.88 through 6.90 show the I_{corr} data on steel embedded in fly ash, silica fume and blast furnace slag blended cements in the same environments. These data, for both plain and blended cements, indicate that as the sulfate concentration increases, the corrosion current density increases, irrespec-

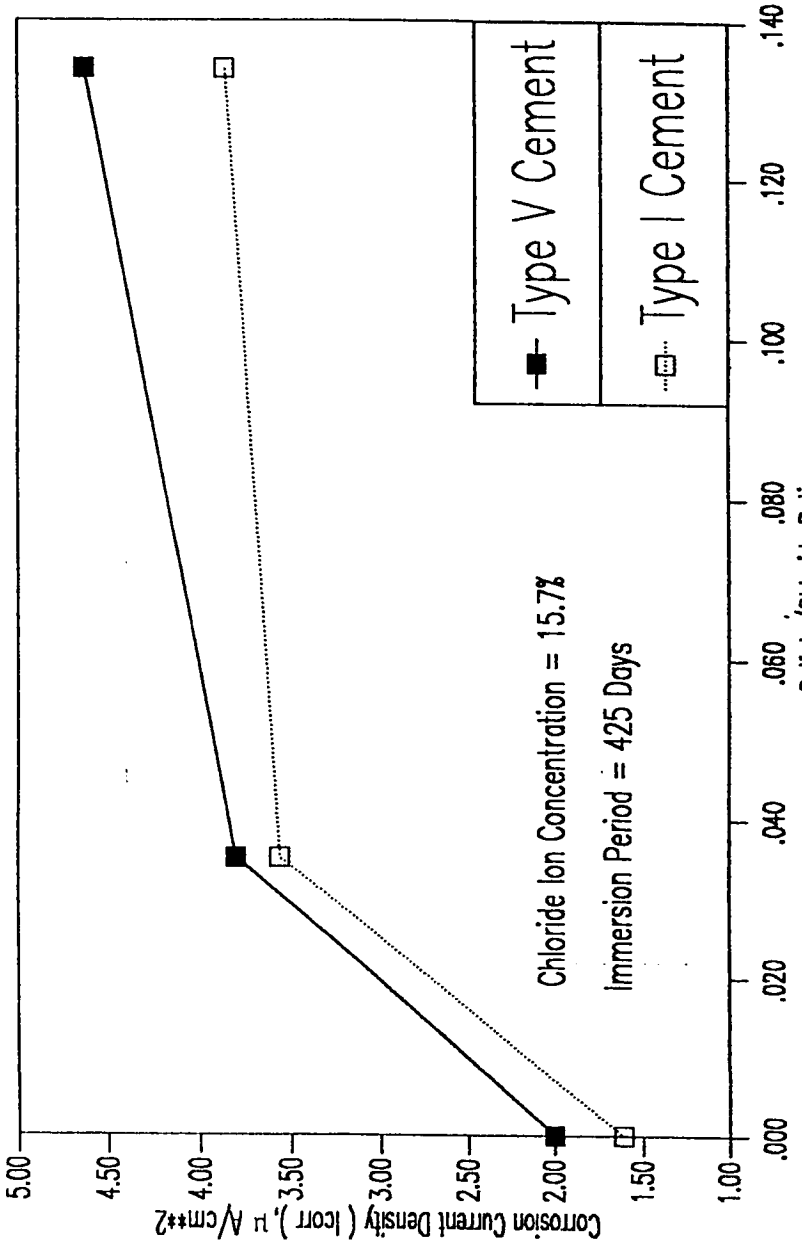

Fig. 6.85 : Effect of Sulfate Ions on Chloride–Induced Corrosion Rates in Plain Cements (425 Days)

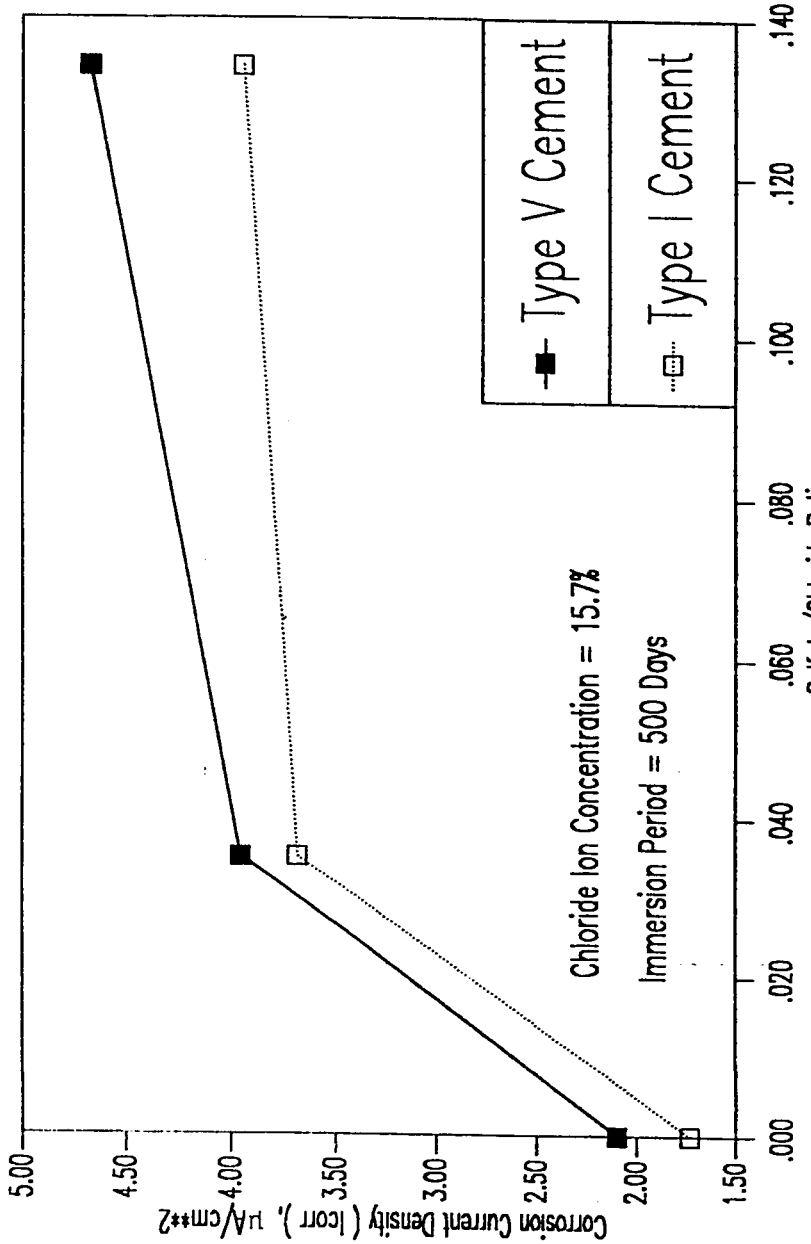

Fig. 6.86 : Effect of Sulfate Ions on Chloride–Induced Corrosion Rates in Plain Cements (500 Days)

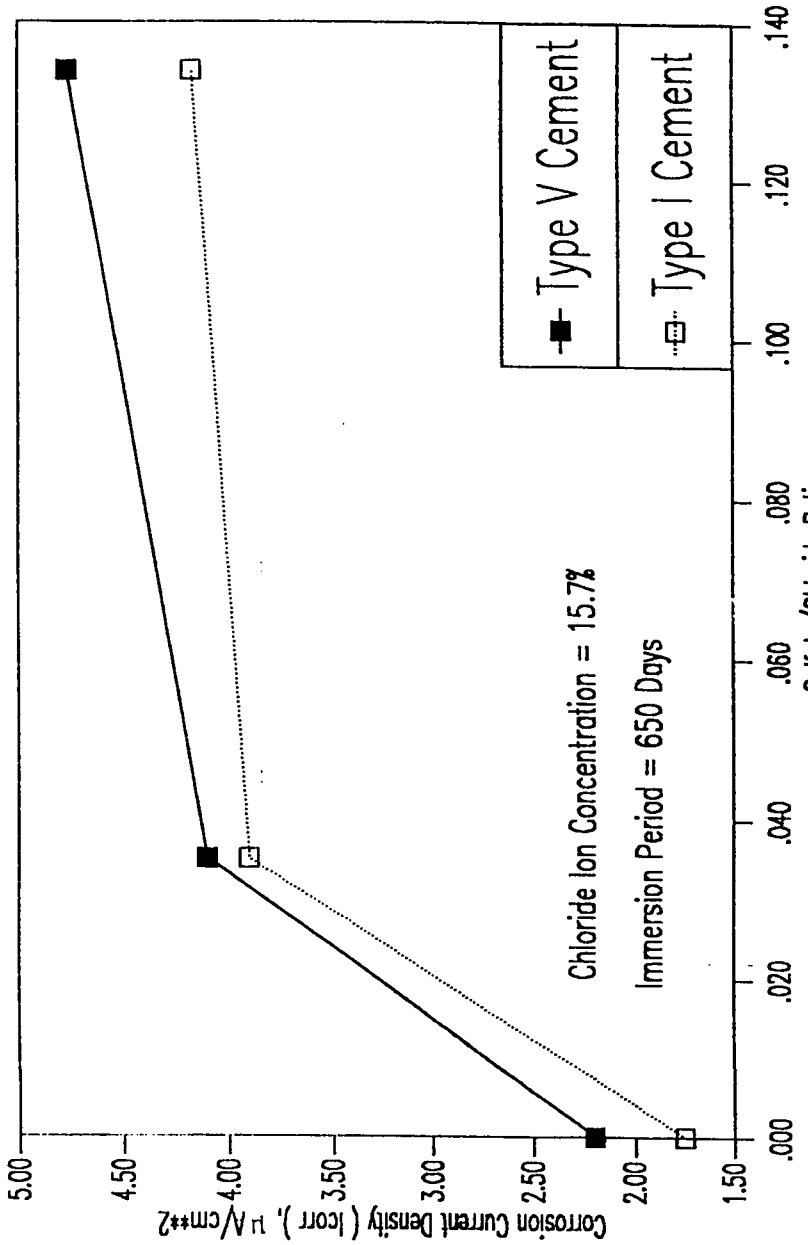

Fig. 6.87 : Effect of Sulfate Ions on Chloride–Induced Corrosion Rates in Plain Cements (650 Days)

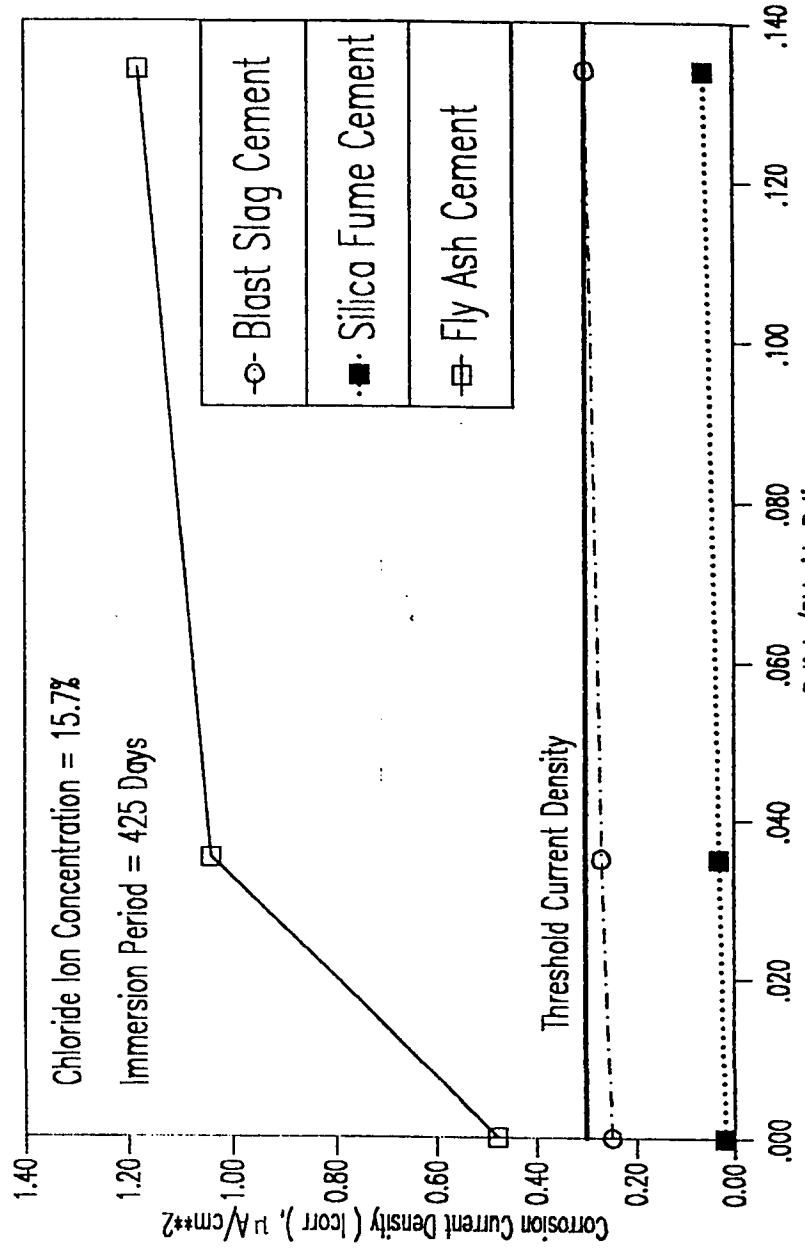

Fig. 6.88 : Effect of Sulfate Ion on Chloride–Induced Corrosion Rates in Blended Cements (425 Days)

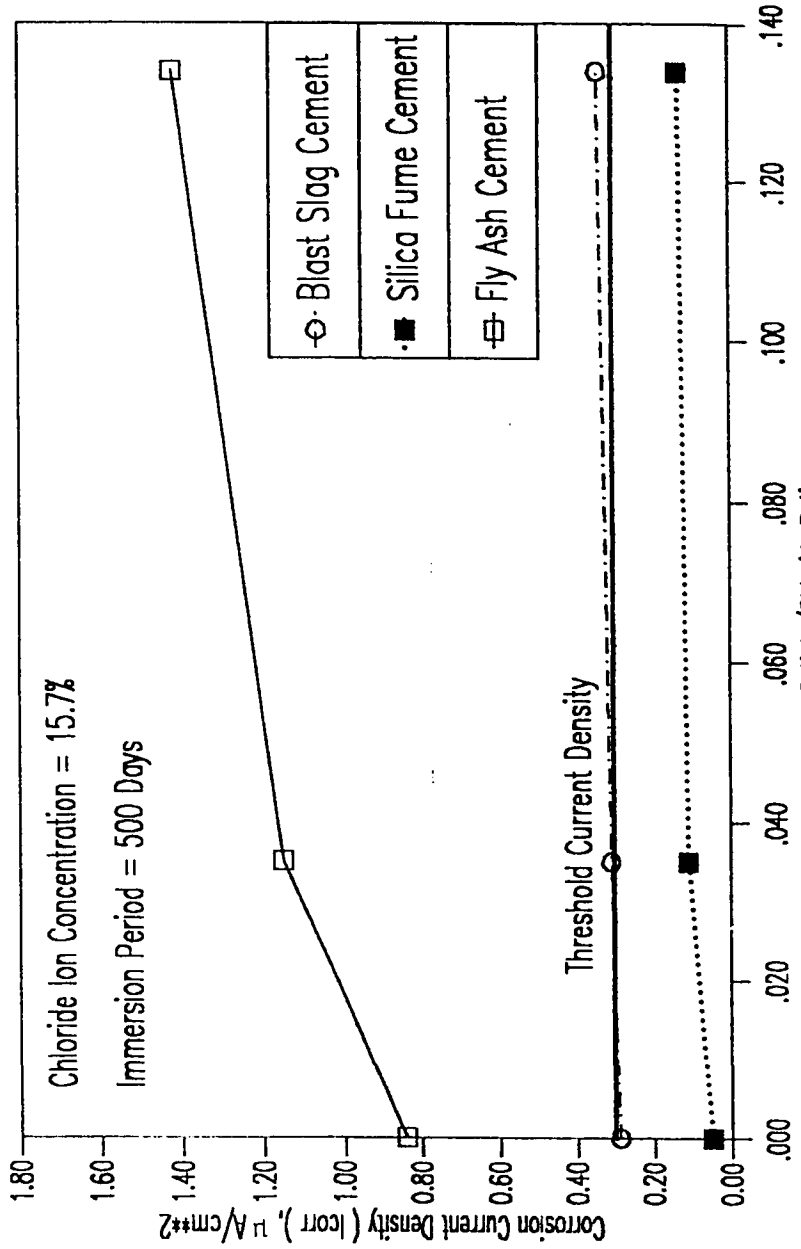

Fig. 6.89 : Effect of Sulfate Ions on Cholride–Induced Corrosion in Blended Cements (500 Days)

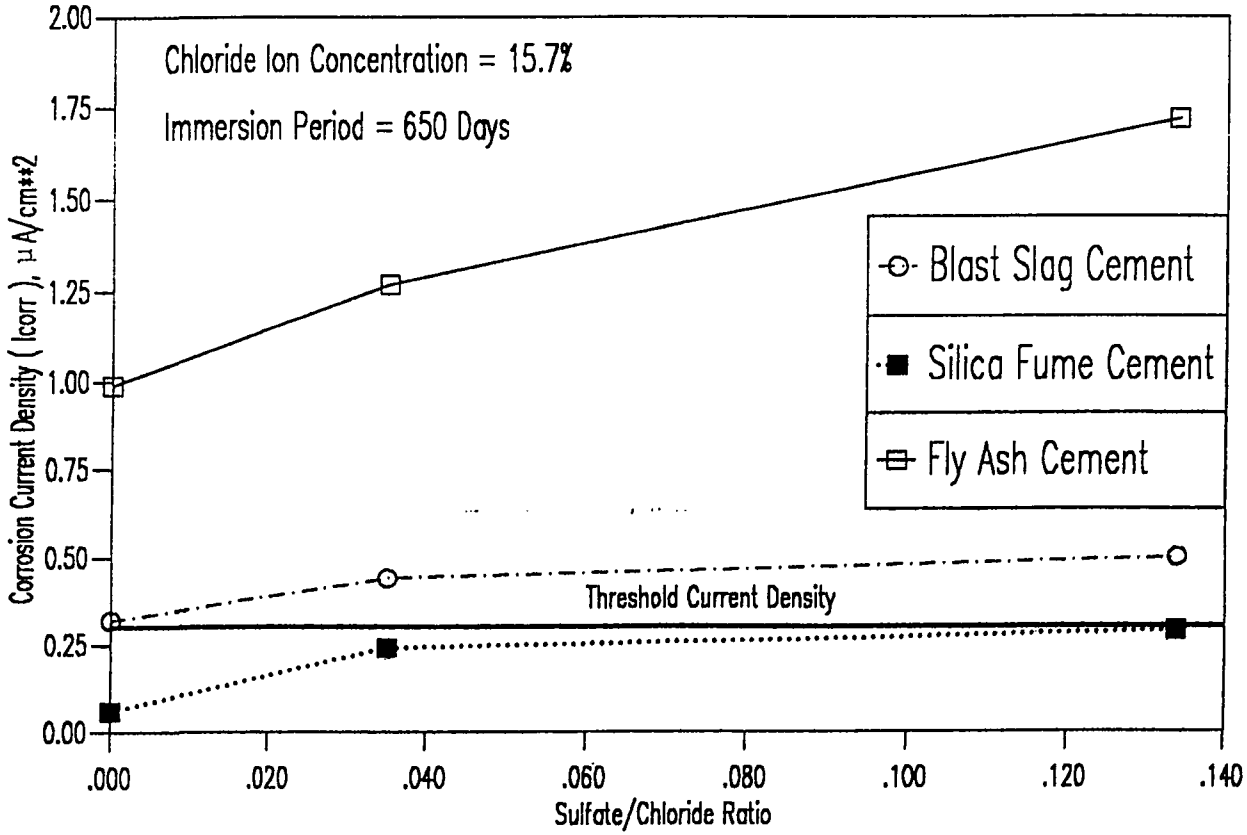

Fig. 6.90 : Effect of Sulfate Ions on Chloride-Induced Corrosion Rates in Blended Cements (650 Days)

tive of the cement type.

The pore solution chemistry of these cements, as elaborated by the pore solution expression analysis results for chloride and hydroxyl ion concentrations as well as the (Cl^-/OH^-) ratios, also clearly shows the increased aggressivity of the internal environment of concrete when sulfates are conjointly present with chlorides. It is also seen that for all cements the chloride concentrations in the pore solution are increased manifold by the concomitant presence of sulfate and chloride ions. Further, except for silica fume cement, where the increase in the (Cl^-/OH^-) ratio is 21%, the (Cl^-/OH^-) ratios for all other cements are increased in the range from 1.83 to 4.09 times. This increase in the aggressivity of the internal environment due to the concomitant presence of sulfates and chlorides is ascribable to the significantly increased concentration of chlorides in the pore solution caused by the presence of sulfates. This increase in chloride concentration is ascribable to two factors:

i) part of the C_3A, which binds the chlorides into calcium chloro-aluminate, preferentially combines with sulfates leaving less C_3A to complex with chlorides. This significantly reduces the removal of free chlorides from the pore solution, and

ii) sulfates, added as sodium sulfate, increase the alkalinity

of the pore solution about four times, as shown in Table 6.10, which inhibits chloride binding.

It is also interesting to note that although (Cl^-/OH^-) ratio for silica fume concrete is manifold higher than the (Cl^-/OH^-) ratio for other cements, steel in silica fume blended cements and exposed to the various test environments show the least corrosion activity which is less than the threshold corrosion current density in all exposure environments. This clearly indicates that the mechanism of reinforcement corrosion is not only a simple function of the chemical aggressivity of the pore solution of the internal environment of cement paste and concrete. In actual practice, corrosion of reinforcement is governed by an interplay of several factors which include, amongst other, the microstructure of the cement paste. The densification of the microstructure determines the diffusion of oxygen to the steel-concrete interface for cathodic depolarization as well as the electrical resistivity of concrete (240). Corrosion being an electrochemical process, the manifold increase in the electrical resistivity of silica fume blended cement concrete significantly mitigates the corrosion process by impeding the flow of corrosion current.

6.7 STRENGTH REDUCTION AND REINFORCEMENT CORROSION IN SPECIMENS BURIED IN THE ACTUAL SABKHA ENVIRONMENT

6.7.1 Strength Reduction

The effect of the high salinity of both sabkha soil and its groundwater on the performance of plain and blended cements was evaluated by measuring the compressive strength after exposure periods of 3, 6, 12 and 18 months. The compressive strength after these exposure periods was compared with the compressive strength prior to placing the specimens in the exposure site. In normal situation, concrete strength generally increases with the period of curing. Any reduction in strength with increasing period of curing is indicative of deterioration of the bond between cement and aggregate which could be caused by surface softening and/or expansion resulting from the reaction between sulfate salts in the sabkha and cement hydrates. The compressive strength reduction in plain cement mortar specimens is shown in Fig. 6.91. These data indicate that the compressive strength in mortar specimens made with Type I and Type V cement continued to be higher than the 14-day value even after an exposure period of about 540 days. The strength reduction in cement mortar specimens blended with fly ash (20% replacement of cement), silica fume (10% cement replacement) and blast furnace slag cement (60% granulated blast furnace slag and 40% Type I cement) specimens is shown in Fig. 6.92. These data indicate an increase in the compressive strength

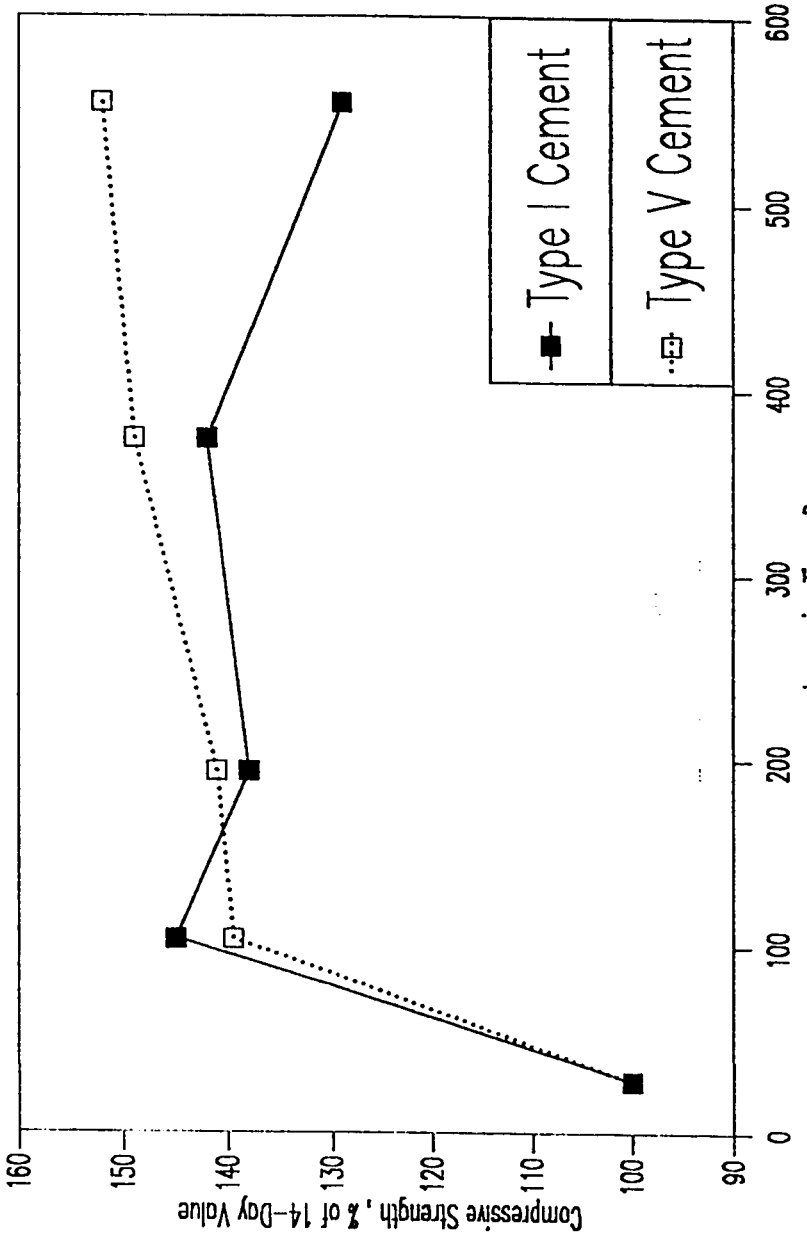

Fig. 6.91 : Compressive Strength Reduction in Field Mortar Specimens (Plain Cements)

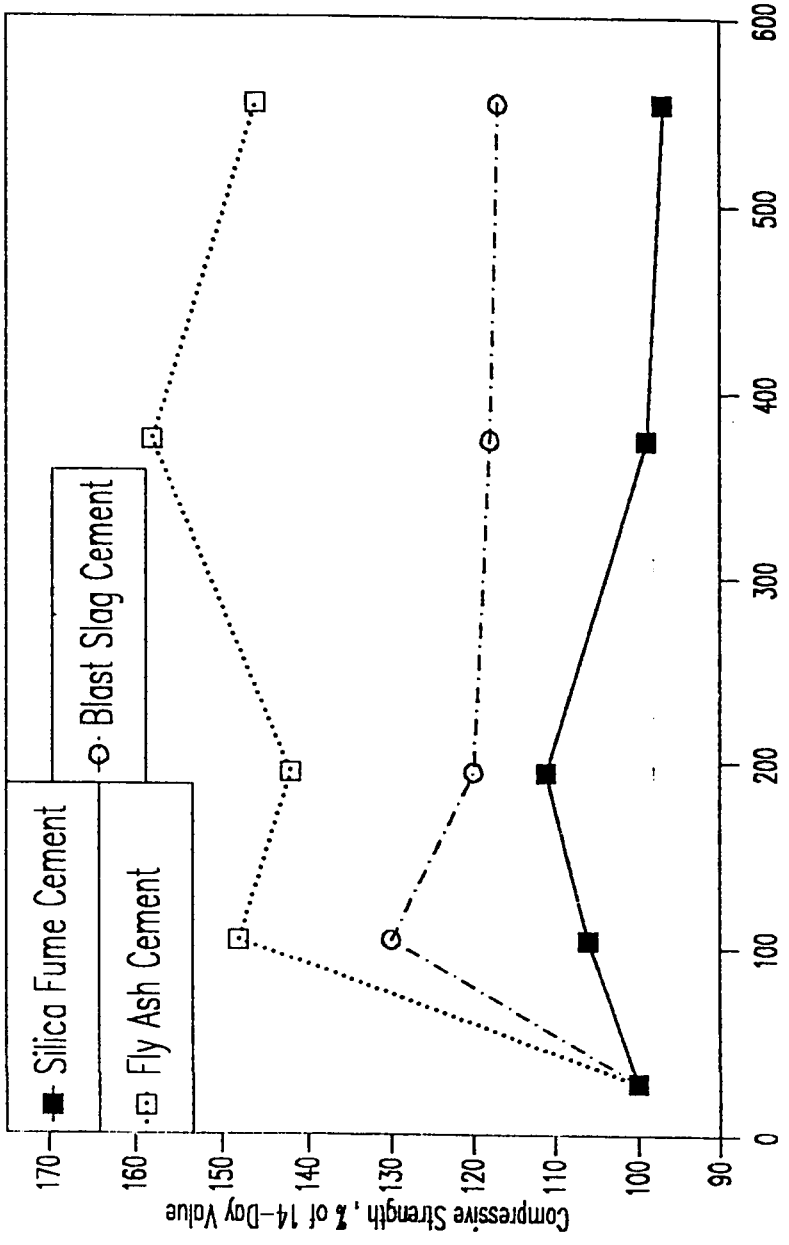

Fig. 6.92 : Compressive Strength Reduction in Field Mortar Specimens (Blended Cements)

with period of immersion for mortar specimens made with fly ash and blast furnace slag cement. The strength development with increasing period of immersion was found to be higher in fly ash cement mortar specimens compared to blast furnace slag cement mortar specimens. In the silica fume mortar specimens, compressive strength reduction was indicated after an exposure period of about 200 days.

6.7.2 Chlorides and Hydroxyl Ion Concentrations

The data on hydroxyl and chloride ion concentration are presented in Table 6.11. The OH^- ion concentration in plain cements was in the range of 1.75 to 1.80% by weight of cement. The OH^- ion concentrations in mortar specimens made by blending Type I cement with silica fume, fly ash and blast furnace slag cement mortar were 1.02, 1.14 and 0.48% by weight of cement respectively. The water-soluble chloride content was 3.17% and 3.32% by weight of cement in Type I and Type V cement mortar specimens respectively. This indicates that the effect of cement type is not very significant on the water-soluble chloride concentration in specimens exposed to the highly aggressive sabkha environment. The water-soluble chloride concentrations were 2.84, 3.12 and 3.32% in specimens made with Type I cement blended with fly ash, blast furnace slag and silica fume respectively. The water-soluble chloride concentration in all specimens is much higher than the allowable value of 0.15% suggested by ACI Committee 318

(189). The (Cl^-/OH^-) ratio in plain cements was 1.8, while it was 2.5, 3.3 and 6.5 respectively in Type I cement blended with fly ash, silica fume and blast furnace slag.

6.7.3 Reinforcement Corrosion

After retrieving the steel from the mortar specimens, the reinforcing steel was visually inspected to determine the corroded percent area. Results of this inspection after 180, 360 and 540 days of burial at the Ras Al-Ghar sabkha site are shown in Table 6.12. These data indicate that the percentage of corroded surface area increased with the period of exposure. After 18 months of exposure, the corroded area was 50 and 60% respectively in Type I and Type V cement mortar specimens. Although the corroded area seemed to be widely spread, the corrosion product was not observed to be deep enough; only three to five very shallow pits were observed in these specimens. The corroded area in the fly ash, blast furnace slag and silica fume cement mortar specimens was approximately 25, 25 and 20% respectively after 18 months of exposure. The loss in weight of the steel bars, after cleaning with the Clarke's solution, is shown in Table 6.13. The weight loss in plain cement was 0.65%. The weight loss due to corrosion of steel bars embedded in fly ash, silica fume and blast furnace slag blended cement mortar specimens was 0.39, 0.02 and 0.03% respectively.

Table 6.11 : Summary of Chemical Analysis Results of Filed Mortar Specimens after 540 Days of Exposure

Cement	Cl^-, % (by weight of cement)	OH^-, % (by weight of cement)	(Cl^-/OH^-) Ratio
Type I	3.17	1.75	1.81
Type V	3.32	1.80	1.84
Fly Ash	2.84	1.14	2.47
Silica Fume	3.32	1.02	3.25
Blast Furnace Slag	3.12	0.48	6.49

Table 6.12 : Corroded Surfce Area of Reinforcing Steel in Field Mortar Specimens

Cement	Corroded Area of Reinforcing Steel (%) after:		
	180 Days	360 Days	540 Days
Type I	10	40	50
Type V	25	50	60
Fly Ash	5	15	25
Silica Fume	3	8	20
Blast Furnace Slag	8	15	25

Table 6.13 : Loss in Weight in Reinforcing Steel and Performance Rating in Field Mortar Specimens after 540 Days of Exposure

Cement	Metal Weight Loss (%)	Performance Rating*
Type I	0.64	1
Type V	0.63	1.0
Fly Ash	0.39	1.6
Silica Fume	0.02	32
Blast Furnace Slag	0.03	21

* in terms of Type I cement

6.7.4 Discussion of the Field Results

The performance of plain and blended cements in sabkha soils was evaluated by determining strength reduction, measuring chloride and hydroxyl ion concentrations, and evaluating reinforcement corrosion. The compressive strength data indicate no significant reduction in the compressive strength with period of exposure in plain cement mortar specimens. On the contrary, the strength of almost all cements was observed to be higher than the 14-day strength, even after an exposure period of 550 days. The effect of cement type, based on C_3A variation, on strength reduction was not significant. The compressive strength data for blended cements indicated an increase in strength in fly ash and blast furnace slag cement mortar specimens over the 14-day strength value. The strength development was, however, found to be higher in fly ash cement mortar compared to blast furnace slag cement specimens. Mortar specimens made with silica fume blended cements, however, indicated a marginal reduction in strength, over the initial strength values after about 300 days of exposure.

The concentration of free chloride ions (i.e., water-soluble chlorides) was considerably more than the value of 0.15% (by weight of cement) recommended by the ACI 318 (189) for concrete structures exposed to chloride-bearing waters to avoid the risk of corrosion. According to Hausmann (241), the risk of corrosion is greater when the (Cl^-/OH^-) ratio is above 0.6. The (Cl^-/OH^-)

ratio in all plain and blended cements is again more than this value. This indicates that the chances of corrosion are higher in reinforced concrete structures placed in the aggressive environment of the sabkha. However, very low corrosion was observed on steel placed in silica fume and blast furnace slag cement mortar specimens even though the (Cl^-/OH^-) ratio in these cements was much higher than that in plain cements. The low corrosion rate may be attributed to the high electrical resistivity provided by these cements. The dense and impermeable structure of the blast furnace and silica fume cements, impedes the flow of electrical current from anodic to the cathodic sites (242,243). The other factor which helps the progress of corrosion is the availability of oxygen. The rate of oxygen diffusion is significantly affected by the extent to which the concrete is saturated with water. Since the availability of oxygen is very limited in structures placed below the ground level, reinforcement corrosion is therefore assumed to proceed at a slower pace, even in the presence of high chloride concentrations. However, at the soil-air interface, where abundant oxygen is available, corrosion proceeds at a rapid rate. This phenomenon appears to be of importance in structures which are submerged deep into the ground and only a small portion is exposed above the ground. If these structures are placed in highly contaminated soils, reinforcement corrosion is initiated at the soil-air interface, while the buried portion remains free of corrosion due to the scarcity of oxygen. The small anode (at the soil-air interface)

compared to a large cathode (submerged portion) leads to localized corrosion at the anodic sites. Reduction in the diameter of reinforcing steel, in deep foundations placed in sabkha soils, to the extent of more than 50% has been observed (148).

The reinforcement corrosion data indicate superior performance by blended cements in resisting reinforcement corrosion compared to plain cements. The corrosion rates of steel in fly ash, blast furnace slag and silica fume concretes were 2, 21, and 32 times lower than in plain cement concrete, as shown in Table 6.13. This indicates that the reduction in the compressive strength in the silica fume blended cement specimens did not accelerate the reinforcement corrosion process thereby confirming the accelerated laboratory test results which showed superior corrosion resistance for silica fume blended cement in spite of the deterioration in the high sulfate-chloride environment. Consequently, it should be realized that the magnitude of deterioration observed in the mortar specimens is probably exaggerated by the small size of these specimens. It is possible that the reduction in strength due to sulfate ions in actual concrete structures may not be as high as that observed in the small laboratory specimens. Further, the surface deterioration can be mitigated by applying a water-resistant epoxy-based coating.

Chapter 7

CONCLUSIONS

1. The field tests had revealed the stratigraphy of the Ras Al-Ghar sabkha which typically consists of the followings:

   - A top salt-encrusted layer characterized by profuse cementation.

   - A loose sandy layer with soft diagenetic minerals intercalated with crystals of salt.

   - A pure salt layer with a thickness of 4.5 meters.

   - A loose to dense deep stratum characterized by the presence of various types of sands and shell fragments. The denseness of this layer increases with depth.

2. Plate-load tests indicated that flooding the sabkha terrains with sabkha brine resulted in insignificant compressibility and minor reduction in the modulus of subgrade reaction compared with the natural condition.

3. The standard sieving techniques were inappropriate for both grain-size analysis and sabkha soil classification. The use of both methylene chloride and sabkha brine were more appropriate.

4. The coefficient of permeability decreased with test repetitions when sabkha brine was used as the seeping liquid, and increased when distilled water was used. Permeability to distilled water was about 10 times more than the permeability to sabkha brine, both in constant and variable head permeability tests.

5. All consolidated-drained (CD) and consolidated-undrained (CU) triaxial tests conducted on Ras Al-Ghar sabkha indicated consistent results. An exception was observed by the CD triaxial tests in which the specimens were initially saturated with distilled water and volume change measurements were subsequently taken place. These CD tests indicated reduced angle of internal friction (φ') due the dissolution of salts from the sabkha matrix.

6. Both field and laboratory CBR tests confirmed the fact that the Ras Al-Ghar sabkha possessed low strength. This low strength was further reduced by 50% upon flooding the sabkha with water.

7. The conventional oedometer that is normally used in consolidation tests was incapable of detecting the collapse potential of the sabkha. Further, the compression and swelling indices did not vary with the type of flooding liquid.

8. The collapse potential of sabkha, as determined by the

modified oedometer, could be classified as "very severe trouble". This was attributed to an interplay of salt dissolution, leaching of calcium ions and soil grain adjustment.

9. The compression and swelling indices confirmed the fact that the Ras Al-Ghar sabkha had low to medium compressibility. This indicates the chances of collapse, rather than the compressibility, should be of prime concern for the geotechnical engineers.

10. The sulfate deterioration is controlled by magnesium-gypsum attack on CSH binder rather than ettringite-oriented expansion and cracking. This is clear from the fact that the sulfate deterioration in all plain and blended cements was primarily characterized by scaling, spalling and softening rather than expansion and cracking. In none of the specimens the deep-seated swelling type ettringite-oriented conventional sulfate reaction was noticeable.

11. For all cements exposed to pure $M\bar{S}$–$N\bar{S}$ solution, either nil or only marginal secondary trisulfate ($C_6A\bar{S}_3H_{32}$) was discernible. On the other hand, XRD patterns as well as SEM-EDXA micrographs showed massive gypsum formation in all cements exposed to the pure sulfate solution.

12. Magnesium decomposition of the hydrosilicate binder by a

mechanism of lowering the alkalinity and causing a de-stabilization of CSH and the eventual conversion of CSH binder to non-cementitious magnesium silicate hydrate (MSH) on $M\bar{S}-N\bar{S}$ exposure was confirmed by the presence of significant MSH in SEM-EDXA micrographs in plain as well as in blended cements. This mechanism is therefore, very effectively operative in engendering loss of cohesion and spalling type of deterioration.

13. The mechanism of gypsum-oriented sulfate attack is based on the transformation of a $Ca(OH)_2/OH^-$ dominated environment around CSH to a $C\bar{S}H_2/SO_4^{--}$ dominated environment. In this environment, CSH binder loses strength progressively and becomes soft thereby encouraging the growth of gypsum crystals which cause further disintegration and spalling.

14. The combined magnesium-gypsum oriented sulfate attack would materialize only in exposure conditions where $M\bar{S}$ constitutes a noticeable proportion of the sulfate environment. However, gypsum-oriented sulfate attack will occur in low C_3A cement constructions in any sulfate environment and will be characterized by cohesionless, spalling and softening.

15. The ettringite-oriented sulfate attack characterized by

expansion and engendered in high C_3A cements and cracking is not observed in the Arabian Gulf region. However, the gypsum type of attack is highly prevalent due to the common use of high C_3S Type V cements.

16. All the five plain and blended cements deteriorated excessively, reaching well ahead of the failure stage after 720 days of accelerated exposure to $M\overline{S}-N\overline{S}$ exposure environment.

17. Sulfate resistant Type V plain cement did not indicate any marked advantage over Type I cement in $M\overline{S}-N\overline{S}$ exposure conditions. Both cement types deteriorated almost equally.

18. All the three blended cements namely, silica fume, fly ash and BFS, showed equally or even somewhat higher deterioration than plain cements in the $M\overline{S}-N\overline{S}$ sulfate environment.

19. All cements suffered magnesium-gypsum type of sulfate attack rather than ettringite type of swelling-cracking deterioration. Silica fume and BFS, the two high profile materials, which have proven capacity to enhance sulfate resistance in $N\overline{S}$ and $C\overline{S}$ environments have suffered aggravated magnesium-gypsum decomposition type of attack and deterioration in $M\overline{S}-N\overline{S}$ exposure.

20. Evidence provided by XRD patterns and SEM-EDXA micrographs indicated that excessive sulfate attack on silica fume in $M\overline{S}-N\overline{S}$ environment is engendered by an excessive magnesium decomposition due to the lower CH content as well as due to the absence of pore blocking and segmenting protective mechanism generated by brucite formation.

21. BFS cement generates massive gypsum which is manifold the quantity of gypsum generated by other cements. In the absence of significant CH as a product of hydration, this massive gypsum formation in BFS cement is attributable to an enhanced and aggravated magnesium-based decomposition of the calcium hydrosilicates (CSH) thereby explaining the maximum deterioration suffered by BFS cement.

22. Chloride beneficiation for sulfate deterioration in a sulfate-chloride environment is only significant in the case of plain and fly ash blended cements. For silica fume and BFS blended cements, the beneficial effect of chlorides is only marginal.

23. Chloride beneficiation is attributable to the virtual elimination of massive gypsum formed in the pure $M\overline{S}-N\overline{S}$ solution when the cements are exposed to the sulfate-chloride environment. Concomitant presence of chlorides therefore significantly mitigates that part of the sulfate attack which is caused by the

gypsum mechanism. However, chlorides do not ameliorate the magnesium decomposition of CSH binder. This explains the partial nature of chloride beneficiation and since chloride beneficiation is only marginal for silica fume and BFS cements, it also indirectly confirms the magnesium decomposition of CSH binder as the predominant mechanism of attack in SF and BFS cements.

24. Corrosion initiation in the secondary or the external chloride, low sulfate-chloride and high-sulfate chloride environments is governed by the permeability of the cement matrix which controls the mobility and diffusion of the chlorides ion to the steel-concrete interface. Silica fume blended cement performs 5 fold better than plain cements. Fly ash cements show about 1.5 times better performance. Type I cement performs better than Type V cement due to the more chloride binding by C_3A.

25. When secondary or external chlorides and sulfates reach the steel-concrete interface in sufficient quantities, the concomitant presence of sulfates generally increases the corrosion current densities for both plain and blended cements. These data indicate an adverse conjoint effect of sulfates in terms of the chloride-induced corrosion of reinforcement in sulfate-chloride environments.

26. Rebars in all cements showed passivity in the pure sulfate environment.

27. The concomitant presence of chlorides and sulfates, present as primary salts at the time of mixing concrete, results in drastic changes in the pore solution chemistry of all plain and blended cements. The concentration of free chlorides in the pore solutions as well as the (Cl^-/OH^-) ratio are increased very significantly thereby enhancing the aggressivity of the internal environment of cement paste matrix in terms of corrosion. These data further confirm the adverse or negative effect on rebar corrosion when sulfates are conjointly present with chlorides. This effect is ascribable to the preferential binding of C_3A by sulfates as well as to the inhibiting effect of increased alkalinity caused by the presence of sodium sulfate on the chloride binding.

28. Despite the very aggressive internal chemical environment for the silica fume blended cement, characterized by a three to ten fold higher (Cl^-/OH^-) value, the corrosion current density is the lowest and generally below the threshold corrosion current density. This effect is ascribable to an interplay of several corrosion mitigating factors operative in silica concrete, specially its dense structure, low oxygen diffusion and high electrical resistivity.

29. The water-soluble chloride concentration in all cement mortar specimens placed in the sabkha was more than the normally accepted threshold value of 0.15% by weight of cement. Similarly, the (chloride/hydroxyl) ion ratio was more than 0.6 in all cement mixtures investigated. This indicates that the chances of corrosion in all cements placed in sabkha environments are greatly increased.

30. The data on reinforcement corrosion in plain and blended cements developed by degree of reinforcement corrosion, as evaluated by metal weight loss, indicate that the corrosion activity was lower in blended cement mortars compared to plain cements. The corrosion rate of steel in fly ash, blast furnace slag and silica fume blended cements was 2, 21 and 32 times lower than in plain cements.

31. Data developed in this investigation indicate that blending of cement with silica fume protects the reinforcing steel from chloride-induced corrosion. However, protective measures like coating the exterior surface with a water-resistant epoxy-based coating will be necessary to protect concrete from deterioration due to the magnesium-based sulfate attack.

Chapter 8

REFERENCES

1) Fookes, P.G., French, W.J. and Rice, S.M.M., Reply to Discussion of "The Influence of Ground and Groundwater Geochemistry on Construction in the Middle East," **Quarterly Journal of Engineering Geology,** London, Vol. 19, 1986, pp. 214.

2) Johnson, H., Kamal, M.R., Pierson, G.O. and Ramsay, J.B., "Sabkhahs of Eastern Saudi Arabia," In: Al-Sayyari, S. S. and Zotl, J. G. (Ed.), **Quarternary Period in Saudi Arabia,** Springer-Verlag, Austria, 1978, pp. 84-93.

3) El-Naggar, Z.R., "Foundation Problems in Sabkhah Deposits," In: Abdul-Jauwad, S. (Coordinator), **Short Course on Foundation Engineering for Practicing Engineer,** KFUPM, Dhahran, April 9-13, 1988, pp. SD1-SD54.

4) Kinsman, D.J.J., "Modes of Formation, Sedimentary Associations, and Diagnostic Features of Shallow-Water and Supratidal Evaporites," **The American Association of Petroleum Geologists Bulletin (AAPG),** Vol. 53, No. 4, 1969, pp. 830-840.

5) Renfro, A.R., "Genesis of Evaporite-Associated Stratiform Metalliferous Deposits - A Sabkha Process," **Economic**

Geology, Vol. 69, No. I, 1974, pp. 33-45.

6) Kinsman, D.J.J. and Park, R.K., "Studies in Recent Sedimentology and Early Diagenesis, Trucial Coast, Arabian Gulf," Proc., **Second AIME Regional Symposium,** March, 1968, pp. 279-293.

7) Butler, G.P., "Modern Evaporite Deposition and Geochemistry of Coexisting Brines, The Sabkha, Trucial Coast, Arabian Gulf," **Journal of Sedimentary Petrology,** Vol. 39, No. 1, 1969, pp. 70-89.

8) Evans, G., Schmidt, V., Bush, P. and Nelson, H., "Stratigraphy and Geologic History of the Sabkha, Abu-Dhabi, Persian Gulf," **Sedimentology,** Vol. 12, 1969, pp. 145-159.

9) Shearman, D.J., "Origin of Marine Evaporites by Diagenesis," **Transactions of Institution of Mining and Metallurgy,** Vol. 75, No. 717, 1966, pp. B208-B215.

10) Ellis, G.I., Arabian Salt-Bearing Soil (Sabkha) As An Engineering Material, **TRRL Report LR 523,** Crowthorne, Berkshire, 1973, p. 21.

11) Butler, G.P., "Recent Gypsum and Anhydrite of the Abu Dhabi Sabkha, Trucial Coasts: An Alternative Explanation of Origin," **Third Symposium on Salt: Northern Ohio Geol. Soc.,** Cleveland, Vol. 1, 1970, pp. 120-152 (cited in Ref.

3).

12) Friedman, G.M., "Significance of Red Sea in Problem of Evaporites and Basinal Limestone," **A.A.P.G. Bulletin,** Vol. 56, No. 6, 1972, pp. 1072-1086 (cited in Ref. 3)

13) Illing, L.V., Wells, A.J. and Taylor, J.C.M., "Penecontemporary Dolomite in the Persian Gulf," In: **Dolomitization and Limestone Diagenesis,** SEPM Spec. Pub. 13, 1965, pp. 38-111 (cited in Ref. 4).

14) Illing, L.V., and Taylor, J.C.M., Discussion: London, **Inst. Mining and Metallurgy Trans.,** Sec. B., Vol. 76, 1967, pp. 883-884.

15) Fookes, P.G., French, W.J. and Rice, S.M.M., "The Influence of Ground and Groundwater Geochemistry on Construction in the Middle East," **Quarterly Jour. Eng. Geol.,** Vol. 18, 1985, pp. 101-128.

16) Smith, C.L., **Brines of Wadi As Sirhan - Kingdom of Saudi Arabia,** U.S. Department of the Interior, Geologic Survey, Saudi Arabian Mission, No. TR1, 1980, p. 26.

17) Holm, D.A., "Desert Geomorphology in the Arabian Peninsula," **Science,** Vol. 132, No. 3437, 1960, pp. 1369-1379.

18) Al-Messairiei, H. and Feroz, S., "Geotechnical Aspect in

Developing Madinat Al-Jubail Al-Sinaiyah," Proc. **Second Saudi Eng. Conference,** Dhahran, paper # 202, 1985, pp. 2383-2412.

19) Fookes, P.G., "Road Geotechnics in Hot Deserts," **Journal of the Institution of Highway Engineers,** Vol. XXIII, No. 10, 1976, pp. 11-23.

20) Fookes, P.G. and Collis, L., "Problems in the Middle East," **Concrete,** Vol. 9, No. 7, 1975, pp. 12-17.

21) Ali, K.M. and Hossain, D., "Geotechnical and Geochemical Characteristics of Obhor Sub-Soil," **Journal of King Abdulaziz University: Earth Science,** Vol. 1, 1988, pp. 205-225.

22) Hossain, D. and Ali, K.M., "Shear Strength and Consolidation Characteristics of Obhor Sabkhas, Saudi Arabia," **Quarterly Journal of Engineering Geology,** London, Vol. 21, 1988, pp. 347-359.

23) Abou Al-Heija. M.K. and Shehata, W.M., "Engineering Properties of Al-Lith Sabkha, Saudi Arabia," **5th International IAEG Congress,** Buenes Aires, 1986, pp. 935-941.

24) Stipho, A.S., "Some Engineering Properties of Stabilized Soils," **Engineering Geology,** Vol. 26, 1989, pp. 181-197.

25) Erol, A.O., "Engineering Geological Considerations in a Salt

Dome Region Surrounded by Sabkha Sediments, Saudi Arabia," **Engineering Geology,** Vol. 26, 1989, pp. 215-232.

26) Hodgson, I.F., Caronna, S. and Abu-Taleb, M.G., "Geotechnical Aspects of a Development Project for the Coastal Town of Jizan," **Second Symposium on Geotechnical Problems in Saudi Arabia,** Riyadh, May, 1989, pp. 164-179.

27) Fookes, P.G. and Higginbottom, I.E., "Some Problems of Construction Aggregates in Desert Areas, with Reference to the Arabian Peninsula-1: Occurrence and Special Characteristics," Proc. **Institution of Civil Engineers,** Vol. 68, Part 1, 1980, pp. 39-67.

28) Al-Amoudi, O.S.B., "Sabkhas Around the Arabian Gulf - Literature Review," **A Term Paper submitted for the Course: Arab Gulf Sedimentation (GEOL 516),** (Course Instructor: Dr. El-Naggar, Z.), May, 1987, p. 59.

29) Newbery, J. and Subramaniam, A.S., "Middle East - Sewerage Projects for Coastal Towns of the Libyan Arab Republic," **Quarterly Journal of Engineering Geology,** Vol. 11, 1978, pp. 101-112.

30) Khan, I.H. and Hasnain, S.I., "Engineering Properties of Sabkhas in the Benghazi Plain and Construction Problems," **Engineering Geology,** Vol. 17, 1981, pp. 175-183.

31) Dregne, H.E., "Soils of Arid Regions," **Developments in Soil Science,** Amsterdam, Vol. 6, 1976 (cited in Ref. 3).

32) Wood, G.V. and Wolfe, M.J., "Sabkha Cycles in the Arab/ Darb Formation off the Trucial Coast of Arabia," **Sedimentology,** Vol. 12, 1969, pp. 165-191.

33) Purser, B.H., (Ed.), **The Persian Gulf,** Springer-Verlag, 1973, p. 471.

34) Bathurst, R.G.C., "Carbonate Sediments and Their Diagenesis," **Developments in Sedimentology,** Second Enlarged Edition, Elsevier, 1975, p. 658.

35) Felber, H., Hotzl, H., Maurin, V., Moser, H., Ravert, W. and Zotl, J.G., "Sea Level Fluctuations During the Quarternary Period," in Al-Sayyari and Zotl (Editors): **Quarternary Period in Saudi Arabia,** Springer-Verlag, Austria, 1978, pp. 50-58 (cited in Ref. 3).

36) Fairbridge, R.W., "Eustatic Changes in Sea Level," In: **Physics and Chemistry of the Earth,** Vol. 4, Pergamon Press, 1961 (cited in Ref. 33).

37) Millman, J.D. and Emery, K.O., "Sea Levels During the Past 35000 Years," **Science,** Vol. 162, 1968, pp. 1121-1123 (cited in Ref. 3).

38) Evans, G., Kendall, C. and Skipwith, P., "Origin of the Coastal Flats, the Sabkhas of the Trucial Coast, the Persian Gulf," **Nature,** Vol. 202, 1964, pp. 385-386.

39) Kinsman, D.J.J., "The Recent Carbonate Sediments near Halat El Bahrani, Trucial Coast, Persian Gulf," in: van Straaten, L.M.J.U. (Editor), **Deltaic and Shallow Marine Deposits,** Sed., Vol. 1, Elsevier Pub. Co., 1964, pp. 185-192.

40) Bush, P., "Some Aspects of the Diagenetic History of the Sabkha in Abu Dhabi," Persian Gulf," in Purser, B. H. (Ed.), **The Persian Gulf,** Springer-Verlag, Austria, 1973, pp. 395-407.

41) Jergman, K., "Salts in Soil and Water within the Arid Climatic Zone Effects on Engineering Geology - with Examples from Saudi Arabia," **Swedish Council for Building Research,** Stockholm, D6-1984, p. 187 (cited in Ref. 3).

42) Glennie, K.W., "Desert Sedimentary Environments," **Developments in Sedimentology,** Vol. 14, Elsevier, Amsterdam, 1970, p. 222 (cited in Ref. 3).

43) Fookes, P.G., "Middle East - Inherent Ground Problems," **Quarterly Journal of Engineering Geology,** Vol. 11, 1978, pp. 33-49.

44) Patterson, R.J. and Kinsman, D.J.J., "Hydrologic Framework of a Sabkha along Arabian Gulf," **A.A.P.G. Bulletin,** Vol. 65, No. 8, August, 1981, pp. 1457-1475.

45) Privett, D., "Monthly Charts of Evaporation from the Northern Indian Ocean (including the Red Sea and the Persian Gulf," **Q.J.R. Met. Soc.,** Vol. 85, 1959, pp. 424-428 (cited in Ref. 3).

46) Kinsman, D.J.J., "Evaporite: Relative Humidity Control of Primary Mineral Facies," **Jour. of Sed. Petrology,** Vol. 46, 1976, pp. 273-279.

47) Kinsman, D. J. J., "Gypsum and Anhydrite of Recent Age, Trucial Coast, Persian Gulf," in: **Second Symposium on Salt: Northern Ohio Geol. Soc.,** Cleveland, Vol. 1, 1966, pp. 302-326.

48) Ellis, C.I. and Russell, R.B.C., "The Use of Salt-Laden Soils (Sabkha) for Low Cost Roads," **TRRL Report PA 78/74,** Crowthorne, Berkshire, 1974 (presented at a conference on Low Cost Roads, Kuwait, November, 1974).

49) Taylor, J.C.M. and Illing, L.V., "Holocene Intertidal Calcium Carbonate Cementation, Qatar, Persian Gulf," **Sedimentology,** Vol. 12, 1969, pp. 69-107.

50) Kamal, M.R, Johnson, D.H., Pierson, G.O. and Ramsay,

J.B., "Preliminary Geochemical and Geologic Studies of Sabkhat Al-Riyas, Saudi Arabia," paper to be presented at the **Second Arab Conference for Mineral Resources,** Riyadh, Saudi Arabia, 2-8 November, 1974.

51) Obika, B., Freer-Hewish, R. J. and Fookes, P. G., "Soluble Salt Damage to Thin Bituminous Road and Runway Surfaces," **Quarterly Journal of Engineering Geology,** Vol. 22, 1989, pp. 59-73.

52) Loberg, B., **Geologi,** Stockholm, 1980 (cited in Ref. 3).

53) Borchert, H. and Muir, R.O., "Salt Deposits: The Origin, Metamorphism and Deformation of Evaporates," **(Princeton, N.J., and London: D. Van Nostrand, 1964),** p. 300 (cited in Ref. 9).

54) De Groot, K., "The Chemistry of Submarine Cement Formation at Dohat Hussain in the Persian Gulf," **Sedimentology,** Vol. 12, 1969, pp. 63-68.

55) Shinn, E.A., "Submarine Lithification of Holocene Carbonate Sediments in the Persian Gulf," **Sedimentology,** Vol. 12, 1969, pp. 109-144.

56) Evans, G. and Shearman, D.J., "Celestite from the Sediments of the Trucial Coast of the Persian Gulf," **Nature,** Vol. 202, 1964, pp. 759-761.

57) Levy, Y., "The Origin and Evolution of Brine in Coastal Sabkhas, Northern Sinai," **Journal of Sedimentary Petrology,** Vol. 47, No. 1, 1977, pp. 451-462.

58) Levy, Y., "Description and Mode of Formation of the Supratidal Evaporite Facies in Northern Sinai Coastal Plain," **Journal of Sedimentary Petrology,** Vol. 47, No. 1, 1977, pp. 462-474.

59) James, A.N. and Little, A.L., Discussion on the paper "The Influence of Ground and Groundwater Geochemistry on Construction in the Middle East," **Quarterly Journal of Engineering Geology,** Vol. 19, 1986, pp. 209-214.

60) Akili, W. and Torrance, J.K., "The Development and Geotechnical Problems of Sabkha, with Preliminary Experiments on the Static Penetration Resistance of Cemented Sands," **Quarterly Journal of Engineering Geology,** Vol. 14, 1981, pp. 59-73.

61) Hsu, K.J. and Schneider, J., "Progress Report on Dolomitization-Hydrology of Abu Dhabi Sabkha, Arabian Gulf," In: Purser, B. H. (Editor), **The Persian Gulf,** Springer-Verlag, 1973, pp. 409-422.

62) Akili, W. "On Sabkha Sands of Eastern Saudi Arabia," Proceedings, **Symposium on Geotechnical Problems in Saudi Ara-**

bia, Riyadh, Vol. II, 1981, pp. 775-791.

63) Russell, R.B.C., "Chemical and Physical Properties of Sabkha-type Materials," **TRRL Supplementary Report 79UC,** Crowthorne, Berkshire, 1974.

64) Epps, R.J., "Geotechnical Practices and Ground Conditions in Coastal Regions of the United Arab Emirates," **Ground Engineering,** Vol. 13, No. 5, July, 1980, pp. 19-25.

65) Abu-Taleb, M.G. and Egeli, I., "Some Geotechnical Problems in Eastern Province of Saudi Arabia," Proceedings, **Symposium on Geotechnical Problems in Saudi Arabia,** Riyadh, 1981, pp. 799-811.

66) Tomlinson, M.J., "Middle East - Highway and Airfield Pavements," **Quarterly Journal of Engineering Geology,** Vol. 11, 1978, pp. 65-73.

67) Tobin, M.B., "Factors Influencing Road Design, Construction and Maintenance in the United Arab Emirates," Proc. **Institution of Civil Engineers,** Part 1, Vol. 68, 1980, pp. 27-38.

68) Akili, W. and Fletcher, E.H., "Ground Conditions for Housing Foundations in Dhahran Region, Eastern Province, Saudi Arabia," Proceedings, **First International Conference on Housing Problems in Developing Countries,** Dhahran, Vol. 2, 1978, pp. 533-546.

69) Akili, W. and Ahmed, N., "The Sabkhas of Eastern Saudi Arabia: Geotechnical Considerations," Proc. **First Saudi Eng. Conf.,** Jeddah, Vol. II, May, 1983, pp. 300-322.

70) Owais, Issa and Bowman, J., "Geotechnical Considerations for Construction in Saudi Arabia," **Journal of the Geotechnical Engineering Division, ASCE.,** Vol. 107, GT3, 1981, pp. 319-338.

71) Al-Amoudi, O.S.B., Abduljauwad, S.N., El-Naggar, Z.R., Safar, M.M., "Geotechnical Considerations on Field and Laboratory Testing of Sabkhas," Symposium on **Recent Advances in Geotechnical Engineering III,** Singapore, 1991, pp. 1-6.

72) Fookes, P.G. and French, W J., "Soluble Salt Damage to Surfaced Roads in the Middle East," **Highway Engineer,** Vol. 24, No. 12, December 1977, pp. 10-20.

73) Blight, G.E., "Migration of Subgrade Salt Damages Thin Pavements," Proceedings of **the American Society of Civil Engineers,** Vol.192, 1976, pp. 779-791.

74) Ghazali, F.M., Fatani, M.N.Y., and Khan, A.M., "Geotechnical Properties of Sabkha Soils of Jeddah and Jizan, Saudi Arabia," Proceedings, **2nd Saudi Engineering Conference,** KFUPM, Dhahran, Vol. 1, 1985, pp. 286-307.

75) Juillie, Y. and Sherwood, D.E., "Improvement of Sabkha Soil

of the Arabian Gulf Coast," Proceedings, **8th European Conference on Soil Mech. and Found. Eng.,** Helsinki, Vol. 2, Session 7-21, 1983, pp. 781-788.

76) Menard, L. and Bruise, Y., "Theoretical and Practical Aspects of Dynamic Consolidation," **Geotechnique,** Vol. 15, No. 1, 1975, pp. 3-18.

77) Al-Amoudi, O.S.B. and Asi, I.M., "An Investigation on Improvement of Sabkha Properties," Symposium on **Recent Advances in Geotechnical Engineering III,** Singapore, 1991, pp. 7-12.

78) Stipho, A.S., "On the Engineering Properties of Salina Soil," **Quarterly Journal of Engineering Geology,** Vol. 18, 1985, pp. 129-137.

79) French, W.J. and Poole, A.B., "Alkali Aggressive Aggregates in the Middle East," **Concrete,** Vol. 10, No. 1, 1976 (cited in Ref. 3).

80) Mindness, S. and Young, J.F., **Concrete,** Prentice-Hall, Inc., New York, 1981.

81) Rasheeduzzafar, Dakhil, F.H., Al-Gahtani, A.S., "The Deterioration of Concrete Structures in the Environment of Eastern Saudi Arabia," the **Arabian Journal for Science and Engineering,** Vol. 3, No. 3, 1982, pp. 191-209.

82) Al-Kurdi, S.M.A., **Durability Assessment Criterion for Concrete and Reinforcement Exposed to Simulated Environmental Conditions for Saudi Arabia,** M.S. Thesis, Department of Civil Engineering, KFUPM, Dhahran, 1984.

83) Mahamud, M.M., **Durability and Thermal Incompatibility of Concrete Constituents Made from Local Materials in the Arabian Gulf Countries,** M.S. Thesis, Department of Civil Engineering, KFUPM, Dhahran, 1988.

84) Rasheeduzzafar, "Durability Requirements of Concrete Construction in the Gulf Region with an Appraisal of the ACI Code," Keynote Lecture, **1st Regional Conference in Civil Engineering,** Bahrain, 1989, p. 59.

85) Maslehuddin, M., Rasheeduzzafar, and Al-Mana, A.I., "The Effect of Aggregate Grading and Admixtures on Concrete Durability," Proceedings, **3rd Saudi Engineering Conference,** King Saud University, Riyadh, Vol. 1, 1991, pp. 103-109.

86) Rasheeduzzafar, Dakhil, F.H., Bader, M.A., "Toward Solving the Concrete Deterioration Problem in the Gulf Region," the **Arabian Journal for Science and Engineering,** Vol. 11, No. 2, 1984, pp. 129-146.

87) Maslehuddin, M., **Optimization of Concrete Mix Design for**

Durability in the Eastern Province of Saudi Arabia, M.S. Thesis, Department of Civil Engineering, KFUPM, Dhahran, 1981.

88) Al-Gahtani, A.S., **An Investigation of Corrosion of Steel Reinforcement in Concrete in Eastern Saudi Arabia,** M.S. Thesis, Department of Civil Engineering, KFUPM, Dhahran, 1981.

89) Hanif M., **Performance of Pozzolan Cement Concrete in a High Chloride-Sulfate Environment,** M.S. Thesis, Department of Civil Engineering, KFUPM, Dhahran, 1982.

90) Al-Amoudi, O.S.B., **Studies on the Evaluation of Permeability and Corrosion Resisting Characteristics of Portland Pozzoaln Concrete,** M.S. Thesis, Department of Civil Engineering, KFUPM, Dhahran, 1985.

91) Neville, A., "Corrosion of Reinforcement," **Concrete,** Vol. 7, No. 6, June 1983, pp. 48-50.

92) Verberk, G.J., "Mechanisms of Corrosion of in Concrete," **ACI SP-49,** American Concrete Institute, Detroit, 1975, pp. 21-38.

93) Rasheeduzzafar, Dakhil, F.H., Ahmad, F.A., "Corrosion Deterioration of Reinforcement in Concrete Structures," **Symposium of Building Structures-Diagnosis and Therapy,**

Venice, 1983, pp. 147-157.

94) Pourbiax, M., **Atlas of Electrochemical Equilibrium in Aqueous Solutions,** Pergamon Press Limited, London, 1976.

95) Clear, K.C., "Permenant Bridge Deck Repair," **Public Roads,** Vol. 39, No. 2, 1975, pp. 53-62

96) Clear, K.C. and Hay, R.E., **Time-to-Corrosion of Reinforcing Steel in Concrete Slab, V.1:Effect of Mix Design and Construction Parameters,** Public Roads, Interim Report No. FHWA-RD-73-32, Federal Highway Administration, April 1973.

97) Lewis, D.A., "Some Aspects of the Corrosion of Steel in Concrete," Proceedings, **1st International Congress on Metallic Corrosion,** London, 1962, pp. 547-555.

98) Page, C.L. and Treadaway, K.W.J., "Aspects of Electrochemistry of Steeel in Concrete," **Nature,** No. 297, May 11982, pp. 109-115.

99) Figg, J.W., "Chemical Attack on Hardened Concrete, Effect of Sulphates and Chlorides," **Bulletin of the Institution of Corrosion Science and Technology,** No. 75, July 1979, pp. 12-23.

100) Bernston, L. and Chandra, S., "Damage of COncrete Sleepers by Calcium Chloride," **Cement and Concrete Research,**

Vol. 12, No. 1, 1982, pp. 87-92.

101) Neville, A.M., "Behavior of Concrete in Saturated and Weak Solution of Magnesium Sulphate or Calcium Chloride," **Journal of Materials, ASTM,** Vol. 4, No. 4, Dec. 1969, pp. 781-816.

102) Chatterji, S., "Mechanisms of $CaCl_2$ Attack on Portland Cement Concrete," **Cement and Concrete Research,** Vol. 8, No. 4, 1978, pp. 461-468.

103) Lawrence M. and Vivian, H.E., "The Action of concentrated and Weak Calcium Chloride on Mortar and Concrete," **Australian Journal of Applied Science,** Vol. II, No. 4, 1960, pp. 490-498.

104) van Aardt, J.H.P., "Deterioration of Cement Products in Aggressive Media," Proceedings, **4th International Symposium on the Chemistry of Cement,** Washington, D.C., Paper VI-S1, Vol. 2, 1960, pp. 835-853.

105) Lerch, W., Ashton, F.W. and Bogue, " The Sulphoaluminates of Calcium," **National Bureau of Standards, Journal of Research,** Vol. 2, No. 4, 1929, pp. 715-731.

106) Aroni, S., Polivka, M., Bressler, B., **Expansive Cements and Expanding Concrete,** Report No. 66-7, Department of Civil Eng., University of California, Berkeley, 1966, p. 74.

107) Mehta, P.K., "Mechanisms of Expansion Associated with Ettringite Formation," **Cement and Concrete Research,** Vol. 3, No. 1, 1973, pp. 1-6.

108) Mather, M., "Field and Laboratory Studies of the Sulphate Resistance of Concrete," **Performance of Concrete,** Swenson, E.G. (Editor), University of Toronto Press, 1968, pp. 66-76.

109) Biczok, I., **Concrete Corrosion, Concrete Protection,** 8th Edition, Akademiai Kiado, Budapest, 1980.

110) Kind, V.V., "Effect of Chlorides on the Speed of Sulfate Corrosion of Portland Cement," **Tsement, BRE,** No. 346, Vol. 22, Part 1, 1956, pp. 3-6.

111) Mehta, P.K., "Durability of Concrete in Marine Environment-A Review, **ACI SP-65,** American Concrete Institute, Detroit, 1980, pp. 1-20.

112) Woods, H., **Durability of Concrete Construction,** ACI Monograph No. 4, ACI/Iowa State University Press, Detroit, 1968.

113) Eglinton, M.S., **Concrete and Its Chemical Behavior,** Thomas Telford Ltd., London, 1987.

114) Schwiete, H.E., Ludwig, U. and Albeck, J., **Zement-Kalk-Gips,** Vol. 58, No. 9, 1969, pp. 225-234 (cited in Ref. 129).

115) Mehta, P.K., "Effect of Cement Composition on Corrosion of Reinforcing Steel in Concrete," **ASTM STP 629** Philadelphia, ASTM, 1977, pp. 12-19.

116) Verberk, G.J., "Field and Laboratory Studies of the Sulphate Resistance of Concrete," **Performance of Concrete,** Swenson, E.G. (Editor), University of Toronto Press, 1968, pp. 113-124.

117) Miller, D.G., "Laboratory Investigation of the Influence of Curing Conditions and Various Admixtures on the Life of Concrete Stored in Sulphate Solutions as Indicated by Physical Changes," **Proceedings, ASTM,** Vol. 2, Part 2, 1924, pp. 847-863.

118) Harrison, W.H., "Effect of Chloride in Mix Ingredients on Sulphate Resistance of Concrete," **Magazine of Concrete Research,** Vol. 42, No. 152, Sept. 1990, pp. 113-126.

119) Thorvaldson, T., "Chemical Aspects of the Durability of Cement Products," Proceedings, **3rd International Symposium on the Chemistry of Cement,** London, 1952, pp. 436-466.

120) Brown, A.W, **Contribution to Discussion on Ref. (121),** p. 335.

121) Locher, F.W., "Influence of Chloride and Hydrocarbonate on Sulphate Attack," Proceedings, **5th International Symp. on**

the Chemistry of Cement, Tokyo, Supplementary paper III-124, Vol. 3, 1968, pp. 328-335.

122) Yeginobali, A., "Sulphate Resistance of Mortars Mixed with Sea Waters," Proceedings, **3rd International Conference on Durability of Building Materials and Components,** Espoo, Finland, Vol. 3, 1984, pp. 55-65.

123) Dalq, P., "Influence of Calcium Chloride on Concrete Resistance to Sulphated Waters," Proceedings, **Symposium on Durability of Concrete,** Prague, RILEM, Paris, Final Report, Part II, 1969, pp. C63-C71.

124) Al-Samarai, M.A., and Raouf, Z.A., "Deterioration of Concrete Due to Sulphate Attack in Iraq," Proceedings, **2nd International Conference on Deterioration and Repair of Reinforced Concrete in the Arabian Gulf,"** Bahrain, Vol. 1, 1987, pp. 555-566.

125) Cook, H.K., **Contribution to Discussion on Ref. (119),** pp. 481-482.

126) Batta, G. and Baiverlin, J., **Contribution to Discussion on Ref. (119),** pp. 476-481.

127) Kind, V.V., "Some Questions and Problems in the Field of Corrosion of Concrete Used in Hydrotechnical Structures," Proceedings, **Conference on Corrosion of Concrete,** Moscow,

1953. English Translation: I.P.S.T., Jerusalem, 1962, pp. 31-38.

128) Smith, F.L., **Effect of Calcium Chloride Additions on Sulfate Resistance of Concrete Placed and Initially Cured at 40° and 70°F Temperatures,** Concrete Laboratory Report No. C-900, Division of Engineering Laboratories, Bureau of Reclamation, July 7, 1959.

129) Hjorth, L., "Cement Specifications for Concrete Exposed to Chlorides and Sulfates," Proceedings, **CEB-RILEM International Workshop on Durability of Concrete Structures,** Copenhagen, May 1983, pp. 229-235.

130) Heller, L. and Ben-Yair, M., "Effect of Sulphate Solutions on Normal and Sulphate-Resisting Portland Cements," **Journal of Applied Chemistry,** Vol. 14, January 1964, pp. 20-30.

131) Ben-Yair, M., "The Effect of Chlorides on Concrete in Hot and Arid Regions," **Cement and Concrete Research,** Vol. 4, No. 3, 1974, pp. 405-416.

132) Lea, F.M., **The Chemistry of Cement and Concrete,** 3rd Edition, Edward Arnold Ltd., London, 1970.

133) Stratful, R.F., "Effect on Reinforced Concrete in Sodium Chloride and Sodium Sulfate Environments," **Materials Protection,** Vol. 3, No. 12, December 1964, pp. 74-80.

134) Holden, W.R., Page, C.L. and Short, N.R., "The Influence of Chlorides and Sulfates on Concrete Durability", **Corrosion of Reinforcement in Concrete Construction,** Crane, A.P. (Editor), Society of Chemical Industry, London, 1983, pp. 143-149.

135) Bakker, R.F.M., "Permeability of Blended Cement Concretes", **ACI SP-79,** American Concrete Institute, Detroit, 1983, pp. 589-605.

136) Page, C.L., Short, N.R. and El Tarras, A., "Diffusion of Chloride Ions in Hardened Cement Pastes," **Cement and Concrete Research,** Vol. 11, 1981, pp. 395-406.

137) Mehta, P.K., "Pozzolanic and Cementitious By-Products as Mineral Admixtures for Concrete - A Critical Review," **ACI SP-79,** American Concrete Institute, Detroit,Vol. 1, 1987, pp. 1-46.

138) Maslehuddin, M., Saricimen, H. and Al-Mana, A.I., "Effect of Fly Ash Addition on the Corrosion Resisting Characteristics of Concrete," **ACI Materials Journal,** Vol. 84, No. 1, Jan.-Feb. 1987, pp. 42-52.

139) Mehta, P.K., "Durability of Concrete - Fifty Years of Progress?," **ACI SP-126,** American Concrete Institute, Detroit, Vol. 1, 1991, pp. 1-31.

140) Mehta, P.K., **Concrete: Structure, Properties, and Materials,** Prentice-Hall, Inc., New Jersey, 1986.

141) Al-Amoudi, O.S.B., Rasheeduzzafar, and Maslehuddin, M., "Carbonation and Corrosion of Rebars in Salt Contaminated OPC/PFA Concretes, **Cement and Concrete Research,** Vol. 21, No. 1, 1991, pp. 38-50.

142) Tsukayama, R., Abe, H. and Nagataki, S., "Long-Term Experiments on the Neutralisation of Concrete Mixed with Fly Ash and the Corrosion of Reinforcement,"Proceedings, **7th International Congress on the Chemistry of Cement,** Paris, Editions Septima, Vol. 3, 1980, pp. IV30-IV35.

143) Haque, M.N. and Kayyali, O., Contribution to Discussion on Ref. (141), **Cement and Concrete Research,** Vol. 21, No. 5, 1991, pp. 953-955.

144) Al-Amoudi, O.S.B., Abduljauwad, S.N., Rasheeduzzafar and Maslehuddin, M., " Effect of Chloride and Sulfate Contamination in Soils on Corrosion of Steel and Concrete," **Transportation Research Record,** accepted for publication.

145) Rasheeduzzafar, Al-Saadoun, S.S.,Al-Gahtani, A.S., and Dahkil, F.H., "Effect of Tricalcium Aluminate Content on Corrosion of Reinforcing Steel in Concrete," **Cement and Concrete Research,** Vol. 20, No. 5, 1990, pp. 723-738.

146) **"Rehabilitation and Protection of Electrical Manholes/Handholes and Substations at Madinat Al-Jubail Al-Sinaiyah, Saudi Arabia,"** Engineering and Design Services Department, SCECO-East, Dammam. DWO #47/06, October 1990.

147) Bashenini, M.S., Bhandari, B.M. and Davis, K.G., "Corrosion Control Procedures for Reinforced-Concrete Power Manholes, **Materials Performance,** October1989, pp. 17-24.

148) Maslehuddin, M., Saricimen, H., Al-Mana, A.I., and Shamim, M., "Performance of Concrete in a High Chloride-Sulfate Environment", **ACI SP-122,** American Concrete Institute, Detroit, 1990, pp. 419-494.

149) Saricimen, H., Al-Tayyib, A.J., Maslehuddin, M. and Shamim, M. "Concrete Deterioration in High Chloride and Sulfate Environment and Repair Strategies," **ACI SP-128,** American Concrete Institute, Detroit, 1991, pp. 19-32.

150) Bowles, J.E., **Foundation Analysis and Design,** 3rd edition, McGraw-Hill Book Company, 1982.

151) Hvorslev, M.J., **Subsurface Exploration and Sampling of Soils for Civil Engineering Purposes,** U.S. Army Waterways Experiment Station, Vicksburg, Mississippi, 1949, p. 521.

152) Robertson, P.K., Campanella, R.G. and Wightman, A., "SPT-CPT Correlations," **ASCE, Journal of Geotechnical**

Engineering, Vol. 109, No. 11, 1983, pp. 1449-1459.

153) **European Symposium on Penetration Testing,** Proceedings, ESOPT I, Stockholm, National Swedish Building Research, 1974.

154) Schmertmann, J.H., **Predicting the q_c/N Ratio,** Final Report D-636, Engineering and Industrial Experiment Station, Dept. of Civil Engg., University of Florida, Gainesville, 1976.

155) **Symposium on Cone Penetration Testing and Experience,** Proceedings, Geotechnical Engineering Division, ASCE, 1981.

156) Briaud, J.L., Tucker, R. and Olsen, R.S., **Cone Penetration and Foundation Design,** Vol. II, Texas A & M University, 1985.

157) Mitchell, J.K. and Gardner, W.S., "In Situ Measurement of Volume Change Characteristics," **Speciality Conference on In Situ Measurement of Soil Properties,** Geotechnical Engineering Division, ASCE, Vol. II, 1975, pp. 279-345.

158) Briaud, J.L. and Gambin, M., "Suggested Practice for Drilling Boreholes for Pressuremeter Testing," **Geotechnical Testing Journal, ASTM,** Vol. 7, No. 1, March 1984, pp. 36-40.

159) **The OYO Elastmeter 100, Model-4149: Operation Manual,** OYO Corporation, Tokyo, Japan, March 1984.

160) Briaud, J. L., Tucker, L. and Olsen, R.S., **Pressuremeter and Foundation Design,** Vol. 1, Texas A & M University, 1985.

161) Terzaghi, K. and Peck, R.B., **Soil Mechanics in Engineering Practice,** 2nd edition, A Wiley International Edition, John Wiley and Sons, Inc., New York, 1967.

162) Sonnenfeld, P., **Brines and Evaporites,** Academic Press, Inc., Florida, 1984.

163) Wray, W.K., **Measuring Engineering Properties of Soil,** Prentice-Hall, Inc., New Jersey, 1986.

164) Lambe, T.W., **Soil Testing for Engineers,** John Wiley & Sons, Inc., New York, 1951.

165) AASHTO, **Standard Specifications for Transportation Materials and Methods of Sampling and Testing,** 12th edition, Washington, D.C., Part I: Specifications, Part II: Tests, 1978.

166) Casagrande, A., "Classification and Identification of Soils," **Transactions, ASCE,** Vol. 113, 1948, pp. 901-930.

167) Holtz, R.D. and Kovacs, W.D., **An Introduction to Geotechnical Engineering,** Prentice-Hall, Inc., New Jersey, 1981.

168) Shehata, W.M., Al-Saafin, A.K., Harari, Z.Y., and Bader, T.A., "Potential Sabkha Hazards in Saudi Arabia," **6th**

International IAEG Congress, Price, D.G. (Editor), Amsterdam, 1990, pp. 2003-2010.

169) Taylor, D.W., **Fundamentals of Soil Mechanics,** John Wiley & Sons, Inc., New York, 1948.

170) Swan, L.H., "Evaluating Settlements of Compacted Fill in Saudi Arabia," **2nd Symposium on Geotechnical Problems in Saudi Arabia,** King Saud University, Riyadh, 1989, pp. 149-163.

171) Bowles, J.E., **Physical and Geotechnical Properties of Soils,** McGraw-Hill, Inc., New York, 1979.

172) **Standard Test Method for Length Change of Hydraulic-Cement Mortars Exposed to a Mixed Sodium and Magnesium Sulfate Solution,** American Society for Testing and Materials, Philadelphia, ASTM, C 1012-84, Vol. 4, No. 1, 1986, pp. 617-621.

173) Patzias, T., "The Development of ASTM Method C 1012 with Recommended Acceptance Limits for Sulfate Resistance of Hydraulic Cements," **Cement, Concrete, and Aggregates,** Vol. 13, No. 1, Summer 1991, pp. 50-57.

174) Brown, G. (Editor), **The X-Ray Identification and Crystal Structures of Clay Materials,** The Mineralogical Society of London, London, 1961.

175) Grim, R.E., **Clay Mineralogy,** 2nd edition, McGraw-Hill, New York, 1968.

176) Mitchell, J.K., **Fundamentals of Soil Behavior,** John Wiley and Sons, Inc., New York, 1976.

177) **Guide to Compounds of Interest in Cement and Concrete Research,** Special Report 127, Highway Research Board, Washington, D. C., 1972, p. 53.

178) Hussain, S.E., **Mechanisms of High Durability Performance of Plain and Blended Cements,** Ph.D. Dissertation, Department of Civil Engineering, KFUPM, Dhahran, August 1991.

179) Clear, K.C. and Harrigan, E.T., **Sampling and Testing for Chloride Ion in Concrete,** Report No. FHWA-RD-77-85, Federal Highway Administration, Washington, D.C., 1979 (cited in Ref. 178).

180) Mehta, P.K. and Gjorv, O.E.,"A New Test for Sulfate Resistance of Cements," **Journal of Testing and Evaluation,** Vol. 2, No. 6, Nov. 1974, pp. 510-514.

181) Rasheeduzzafar, Dakhil, F.H., Al-Gahtani, A.S., Al-Saadoun, S.S., and Bader, M.A., "Influence of Cement Composition on the Corrosion of Reinforcement and Sulfate Resistance of Concrete," **ACI Materials Journal,** Vol. 87, No. 2, March-April 1990, pp. 114-122.

182) Price, G.C., "Investigation of Concrete Materials for the South Saskatchewan River Dam," **Proceedings, ASTM,** Vol. 61, 1961, pp. 1155-1179.

183) Mehta, P.K., "Studies on Chemical Resistance of Low Water to Cement Ratio Concretes," **Cement and Concrete Research,** Vol. 15, No. 6, 1985, pp. 969-978.

184 Dhir, R.K., Jones, M.R. and McCarthy, M.J., "Measurement of Reinforcement Corrosion in Concrete Structures," **Concrete,** January 1991, pp. 15-19.

185) Maslehuddin, M. and Al-Amoudi, O.S.B., "Corrosion of Reinforcing Steel in Concrete: Its Monitoring and Prevention," Proceedings, **Symposium on Corrosion and Its Control,** King Saud University, Riyadh, 1992, pp. 100-115.

186) Stern, M. and Geary, A.L., "Electrochemical Polarization: I. A Theoretical Analysis of the Shape of Polarization Curves," **Jour. of Electrochemical Society,** No. 104, 1957, pp. 56-63.

187) Gonzalez, J.A., Algaba, S. and Andrade, C., "Corrosion of Reinforcing Bars in Carbonated Concrete" **British Corrosion Journal,** Vol. 15, No. 3, 1980, pp. 135-139.

188) Andrade, C., Castelo, V., Alonso, C., and Gonzalez, J.A., "The Determination of the Corrosion Rate of Steel Embedded in Concrete by the Polarization Resistance and AC Impedance

Methods," **ASTM STP 906,** American Society for Materials and Testing, Philadelphia, 1986, pp. 43-63

189) American Concrete Institute, **Building Code Requirements for Reinforced Concrete,** ACI 318-85, 1985.

190) Stagg, K.G. and Zienkiewicz, O.C. (Editors), **Rock Mechanics in Engineering Practice,** John Wiley and Sons, Inc., New York, 1968.

191) Gavish, E., "Recent Sabkhas Marginal to the Southern Coasts of Sinai, Red Sea," Hypersaline Brine and Evaporitic Environments, **Developments in Sedimentology,** Vol. 28, 1980, pp. 233-251.

192) Al-Sanad, H. and Al-Bader, B., "Laboratory Study on Leaching of Calcareous Soil from Kuwait," **ASCE, Journal of Geotechnical Engineering,** Vol. 116, No. 12, 1990, pp. 1797-1809.

193) Sabtan, A.A. and Shehata, W.M. "Potential Geotechnical Problems Along the Mid-Western Coastal Plains of Saudi Arabia," Proceedings, **IV Congress International Association of Engineering Geology,** New Delhi, India, Vol. 1, Theme 1, 1982, pp. I-309-I.319.

194) Leonards, G.A., "Estimating Consolidation Settlements of Shallow Foundations on Overconsolidated Clays," **TRB Special**

Report 163, 1976, pp. 13-16.

195) Saeedy, H.S. and Mollah, M.A., "Geotechnical Study of the North and Northwestern Coast of the Arabian Gulf," **Engineering Geology,** Vol. 28, 1990, pp. 27-40.

196) Dhowian, A.W., "Secondary Compression of Sabkha 'Salina' Soils," **Engineering Geology,** Vol. 30, 1991, pp. 155-169.

197) Knight, K., "The Origin and Occurrence of Collapsing Soils," Proceedings, **3rd Regional Conference for Africa on Soil Mechanics and Foundation Engineering,** Vol. 3, 1963, pp. 127-130 (cited in Ref. 25).

198) Jennings, J.E. and Knight, K., "A Guide to Construction on or with Materials Exhibiting Additional Settlement due to Collapse of Grain Structure," Proceedings, **6th Regional Conference on Soil Mechanics and Foundation Engineering,** 1975, pp. 99-105.

199) Kezdi, A., **Handbook of Soil Mechanics, Soil Physics,** Vol. 1, Elsevier, Amsterdam, The Netherlands, 1974 (cited in Ref. 200).

200) Lutenegger, A.J. and Saber, R. T., "Determination of Collapse Potential of Soils," **Geotechnical Testing Journal, ASTM,** Vol. III, No. 2, 1988, pp. 173-178.

201) Lambe, T.W., and Whitman, R.V., **Soil Mechanics,** John Wiley & Sons, New York, 1969.

202) Barden, L., McGown, A. and Collins, K., "The Collapse Mechanism in Partly Saturated Soil," **Engineering Geology,** Vol. 20, 1973, pp. 49-60 (cited in Ref. 203).

203) Koerner, R.M., **Construction and Geotechnical Methods in Foundation Engineering,** McGraw-Hill, Inc., New York, 1984.

204) Das, B.M., **Advanced Soil Mechanics,** Hemisphere Publishing Corporation, New York, 1983.

205) Bowles, J.E., **Engineering Properties of Soils and Their Measurement,** 2nd edition, McGraw-Hill Book Company, New York, 1978.

206) Brown, P.W., "An Evaluation of the Sulfate Resistance of Cements in a Controlled Environment," **Cement and Concrete Research,** Vol. 11, 1981, pp. 719-727.

207) Irassar, F. and Batic, F., "Effect of Low Calcium Fly Ash on Sulfate Resistance of OPC Cement," **Cement and Concrete Research,** Vol.19, No. 2, 1989, pp. 194-202.

208) Regourd, M., "Structure and Behavior of Slag Portland Cement Hydrates," Proceedings, **7th International Congress on the Chemistry of Cement,** Paris, Editions Septima, Part

III-2, Vol. IV, 1980, pp. 10-26.

209) Daimon, M., "Mechanism and Kinetics of Slag Cement Hydration," Proceedings, **7th International Congress on the Chemistry of Cement,** Paris, Editions Septima, Part III-2, Vol. IV, 1980, pp. 2-9.

210) Calleja, J., "Durability," Proceedings, **7th International Congress on the Chemistry of Cement,** Paris, Editions Septima, Vol. 1, 1980, pp. 2/1-2/48.

211) Cole, W.F., "A Crystalline Hydrated Magnesium Silicate Formed in the Breakdown of a Concrete Sea-Wall," **Nature,** Vol. 171, No. 4347, 1953, pp. 354-355.

212) Cole, W.F. and Hueber, H.V., "Hydrated Magnesium Silicates and Aluminates Formed Synthetically and by the Action of Sea Water on Concrete," **Silicate Industriels (Mons),** Vol. 22, No. 2, 1957, pp. 75-85 (cited in Ref. 132).

213) Regourd, M., "Physico-Chemical Studies of Cement Pastes, Mortars, and Concretes Exposed to Sea Water," **ACI SP-65,** American Concrete Institute, Detroit, 1980, pp. 63-82.

214) Bonen, D. and Cohen, M.D., "Magnesium Sulfate Attack on Portland Cement Paste - I. Microstructural Analysis," **Cement and Concrete Research,** Vol. 22, No. 1, 1992, pp. 169-180.

215) Jelenic, I., Panovic, A., Halle, R., and Gacesa, T., "Effect of Gypsum on the Hydration and Strength Development of Commercial Portland Cements Containing Alkali Sulfates," **Cement and Concrete Research,** Vol. 7, No. 3, 1977, pp. 239-246.

216) Mehta, P.K., Pirtz, D., Polivka, M., "Properties of Alite Cements," **Cement and Concrete Research,** Vol. 9, No. 4, 1979, pp. 439-450.

217) Bentur, A., "Effect of Gypsum on the Hydration and Strength of C_3S Pastes," **Journal of the American Ceramic Society,** Vol. 59, No. 5-6, 1976, pp. 210-213.

218) Copeland, L.E., and Kantro, D.L., "Hydration of Portland Cement," Proceedings, **5th International Symposium on the Chemistry of Cement,** Cement Association of Japan, Tokyo, Vol. 2, 1969, pp. 387-421.

219) Cohen, M.D., and Bentur, A., "Durability of Portland Cement-Silica Fume Pastes in Magnesium Sulfate and Sodium Sulfate Solutions," **ACI Materials Journal,** Vol. 85, No. 3, May-June 1988, pp. 148-157.

220) Rasheeduzzafar, Dakhil, F.H., Bader, M.A., Al-Gahtani, A.S., and Al-Saadoun, S.S., "New Cement Specifications for Durable Concretes in Saudi Arabia," **Project No. AR-6-138,**

King Abdul Aziz City for Science and Technology (KACST), Riyadh, in progress.

221) Bosch, V.D., "Performance of Mortars Specimens in Chemical and Accelerated Marine Exposure," **ACI SP-65,** American Concrete Institute, Detroit, 1980, pp. 427-507.

222) Kalousek, G.L., and Benton, E.J., "Mechanism of Seawater Attack on Cement Pastes," **ACI Journal,** Vol. 67, February, 1970, pp. 187-192.

223) Ftikos, C., and Parissakis, G., "A Study on the Effect of Some Ions Contained in Sea Water on Hydrated Cement Compounds," **ACI SP-100,** American Concrete Institute, Detroit, 1987, pp. 1651-1664.

224) Ogawa, K. and Roy, D. M., " $C_4A_3\overline{S}$ Hydration, Ettringite Formation, and Its Expansion Mechanism: III. Effect of CaO, NaOH and NaCl; Conclusions," **Cement and Concrete Research,** Vol. 12, No. 2, 1982, pp. 247-256.

225) Batta, G., **Annals Trav. Publ. Belg.,** August 1948 (cited in Ref. 132).

226) Maslehuddin, M., Al-Mana, A.I., Saricimen, H. and Shamim, M., "Corrosion of Reinforcing Steel in Concrete Containing

Slag or Pozzolan", **Cement, Concrete and Aggregates,** Vol. 12, No. 1, 1990, pp. 24-31.

227) Arup, H., "The Mechanism of the Protection of Steel by Concrete", **Corrosion of Reinforcement in Concrete Structures,** Crane, A.P. (Editor), Ellis Horwood, London, 1985, pp. 151-157.

228) Roy, D.M., "Mechanism of Cement Paste Degradation Due to Chemical and Physical Factors," Proceedings, **8th International Congress on the Chemistry of Cement,** Rio de Janeiro (Brazil), 1986, pp. 362-380.

229) Tuutti, K., "Service Life of Structures with Regard to Corrosion of Embedded Steel", **ACI SP-65,** American Concrete Institute, Detroit, 1980, pp. 223-236.

230) Rio, A., and Turriziani, R., **Il Cemento,** Vol, 80, No. 1, 1983, pp. 37-48 (cited in Ref. 227).

231) Barnes, M., and Roy, D.M., **"Leaching of Saltstones Containing Fly Ash and Slag,"** Internal Report, 1985 (cited in Ref. 227).

232) Oberholster, R.E., "Pore Structure, Permeability and Diffusivity of Hardened Cement Paste and Concrete in Relation to Durability: Status and Prospects," Proceedings, **8th International Congress on the Chemistry of Cement,** Rio de

Janeiro (Brazil), Sub-Theme 4.1, Sept. 1986, pp. 323-335.

233) Manmohan, D. and Mehta, P. K., "Influence of Pozzolanic, Slag and Chemical Admixtures on Pore Size Distribution and Permeability of Hardened Cement Pastes", **Cement, Concrete and Aggregates,** Vol. 3, No. 1, 1981, pp. 63-67.

234) Nyame, B. K. and Illuston, J. M., "Capillary Pore Structure and the Permeability of Hardened Cement Paste", Proceedings, **7th International Congress on the Chemistry of Cement,** Paris, Vol. 13, 1980, pp. VI181-VI186.

235) Kumar, A., Komarneni, S., and Roy, D.M., "Diffusion of Cs^+ and Cl^- Through Sealing Materials," **Cement and Concrete Research,** Vol. 17, No. 1, 1987, pp. 153-160.

236) Page, C.L. and Havdahl, J., "Electrochemical Monitoring of Corrosion of Steel in Microsilica Cement Pastes," **Materials and Structures, RILEM,** Vol. 18, No. 103, Jan.-Feb. 1985, pp. 41-47.

237) Sellevold, E.J. and Nilsen, T., "Condensed Silica Fume in concrete: A World Review," Chapter 3, **Supplementary Cementing Materials for Concrete,** Malhotra, V.M. (Editor), Canadian Government Publishing Centre, Ottawa, 1987, pp. 165-243.

238) Hooton, R.D., "Permeability and Pore Structure of Cement Pastes Containing Fly Ash, Slag, and Silica Fume," **ASTM STP 897,** ASTM, Philadelphia, 1986, pp. 128-143.

239) Douglas, E., "Blast Furnace Slag Cement Mortar and Concrete: Durability Aspects," Chapter 6, **Supplementary Cementing Materials for Concrete,** Malhotra, V.M. (Editor), Canadian Government Publishing Centre, Ottawa, 1987, pp. 335-369.

240) Gjorv, O. E., "Durability of Concrete Containing Condensed Silica Fume", **ACI SP-79,** American Concrete Institute, Detroit, Vol. 2, 1983, pp. 695-708.

241) Hausmann, D.A., "Steel Corrosion in Concrete, How Does It Occur?", **Materials Protection,** Vol. 6, no. 11, 1967, pp. 19-23.

242) Abdul Hadi, S.S., **Electrical Resistivity of Concrete in Relation to Corrosion of Reinforcement,** M.S. Thesis, Department of Civil Engineering, KFUPM, Dhahran, 1982.

243) Beaton, J.L., Spellman, D.L., and Stratful, R.F., "Corrosion of Steel in Continuously Submerged Reinforced Concrete Piling," **Highway Research Record,** No. 204, 1967, pp. 11-21.

APPENDIX

Raw Data for the Pressuremeter Test

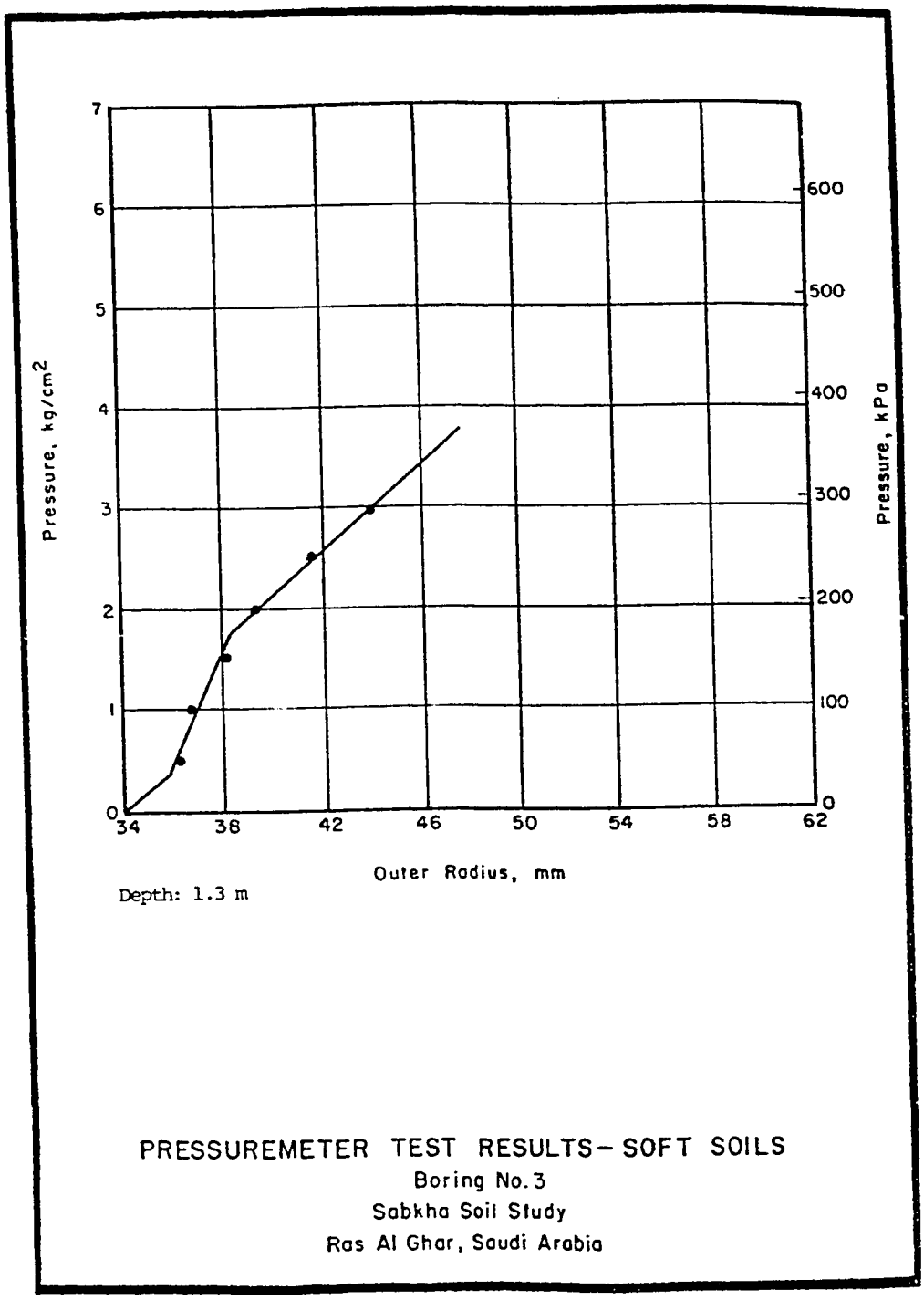

Fig. A1: Pressuremeter Test Data Conducted at a Depth of 1.3 m

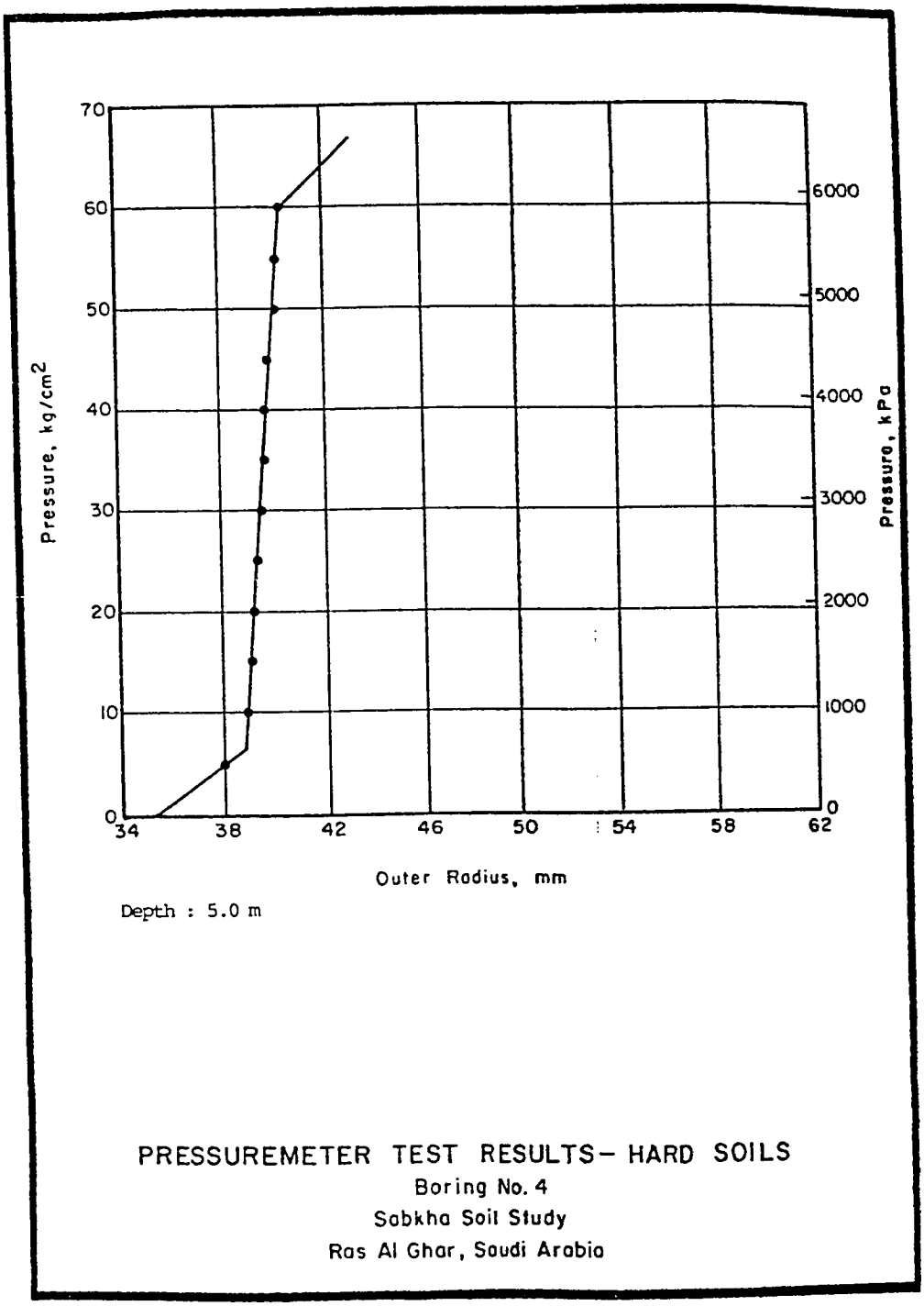

Fig. A2: Pressuremeter Test Data Conducted at a Depth of 5.0 m

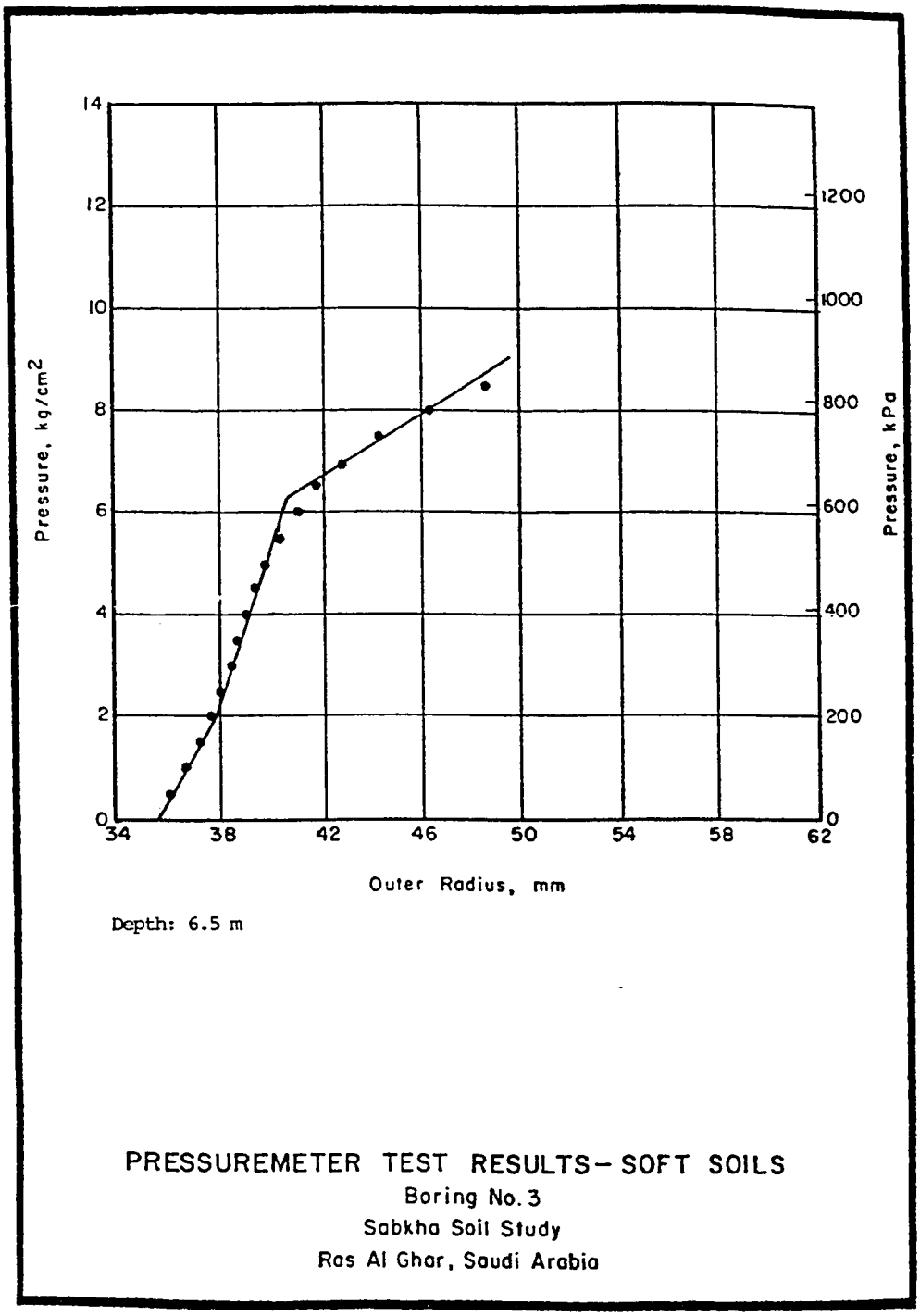

Fig. A3: Pressuremeter Test Data Conducted at a Depth of 6.5 m

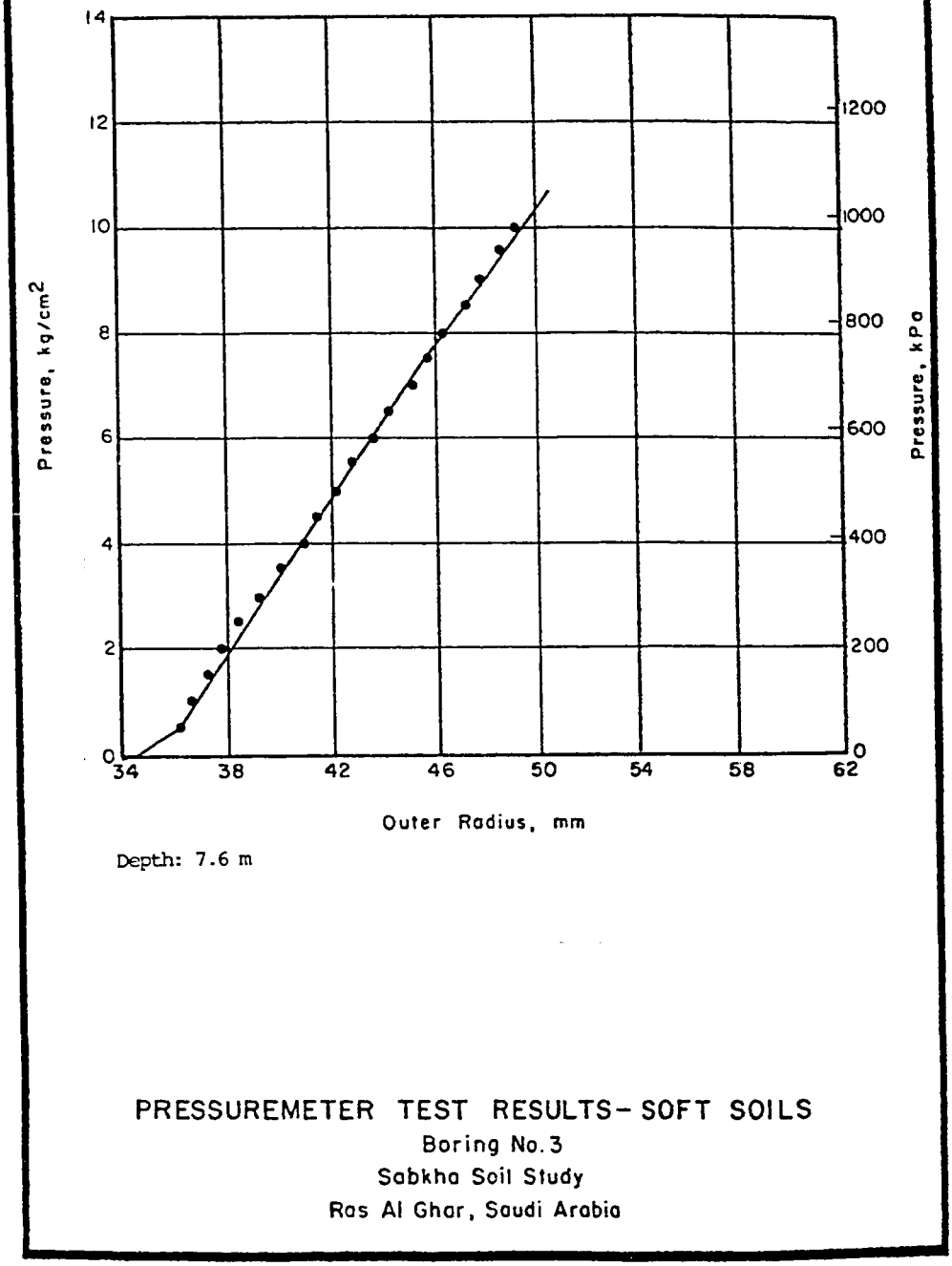

Fig. A4: Pressuremeter Test Data Conducted at a Depth of 7.6 m

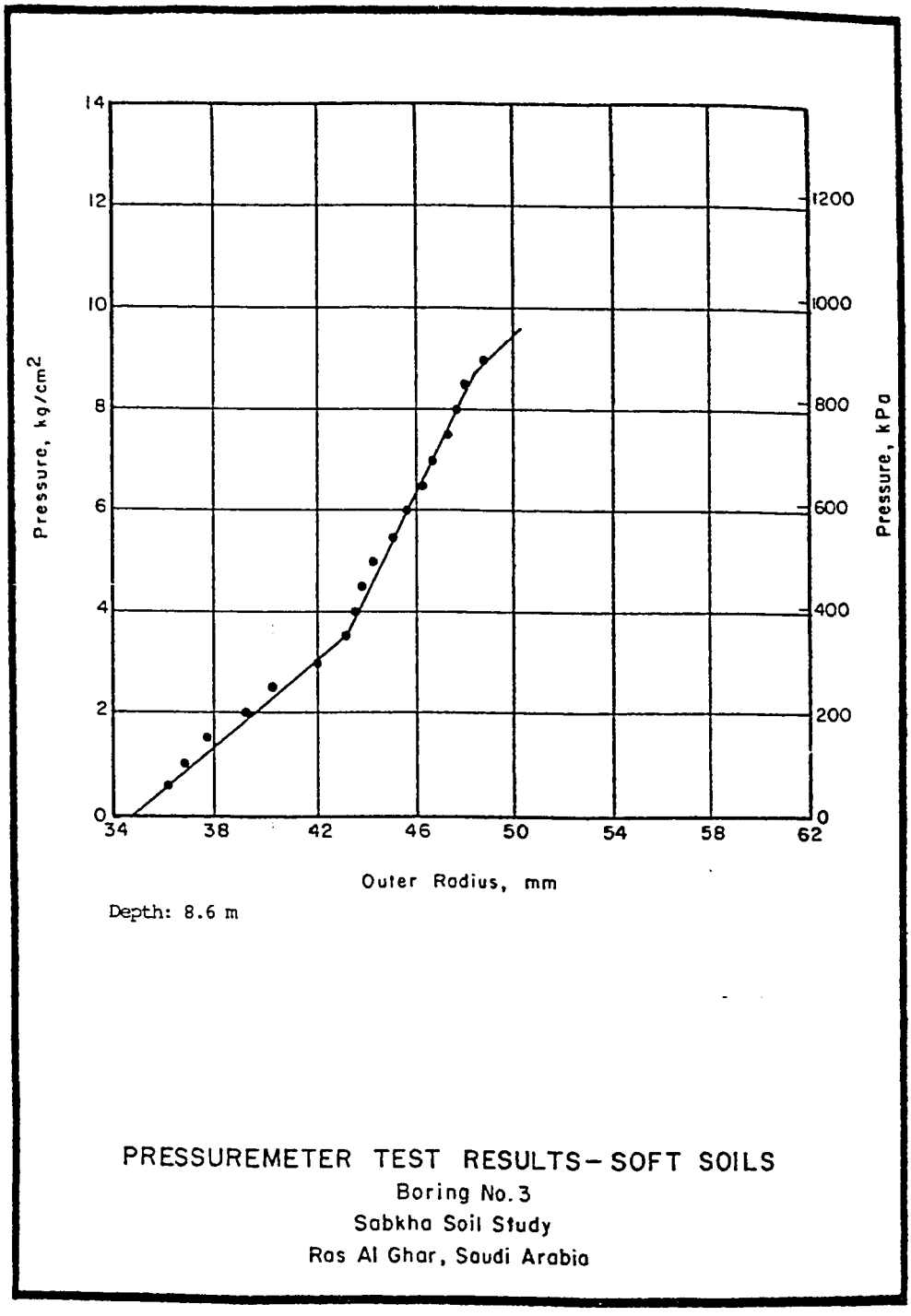

Fig. A5: Pressuremeter Test Data Conducted at a Depth of 8.6 m

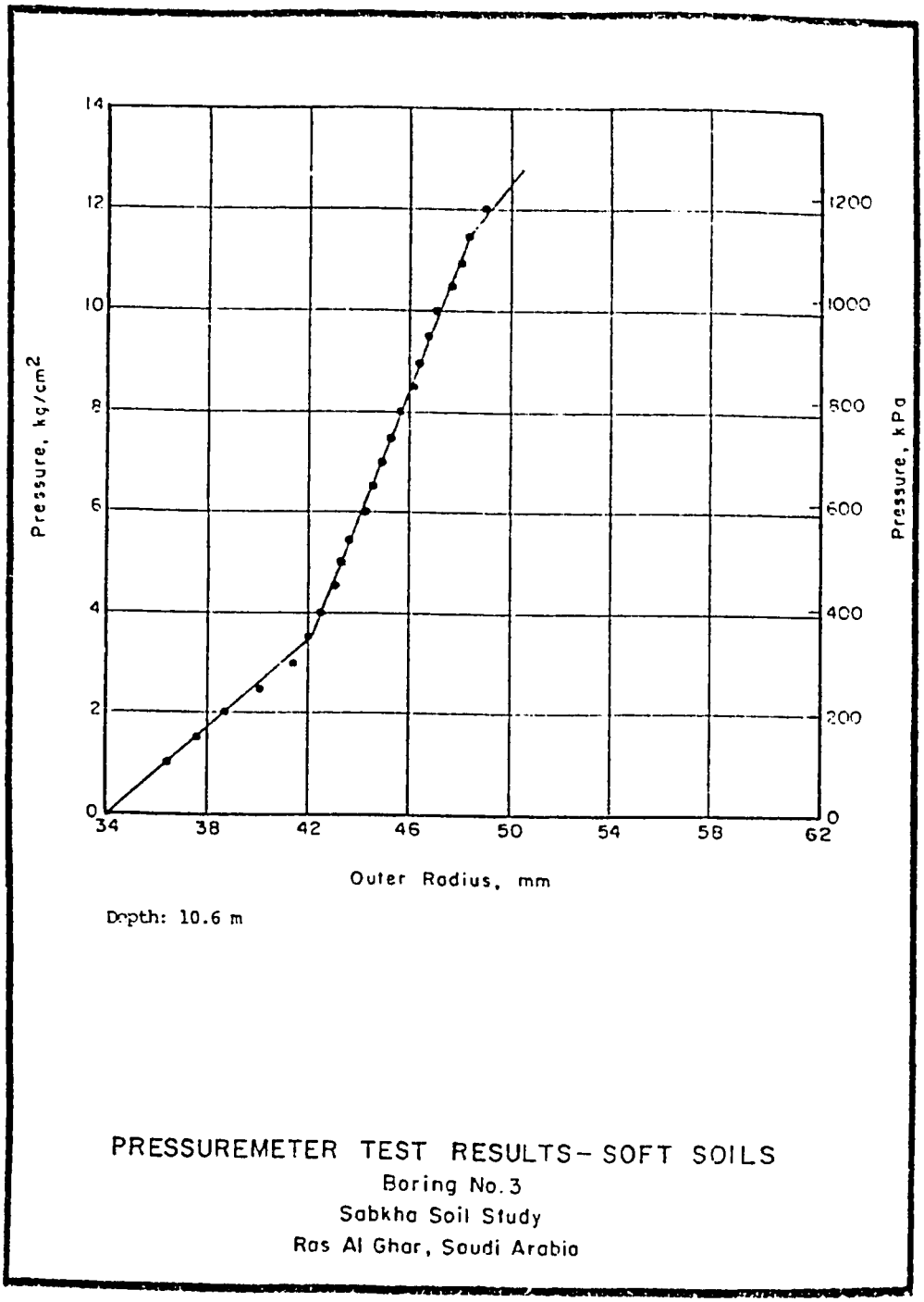

Fig. A6: Pressuremeter Test Data Conducted at a Depth of 10.6 m

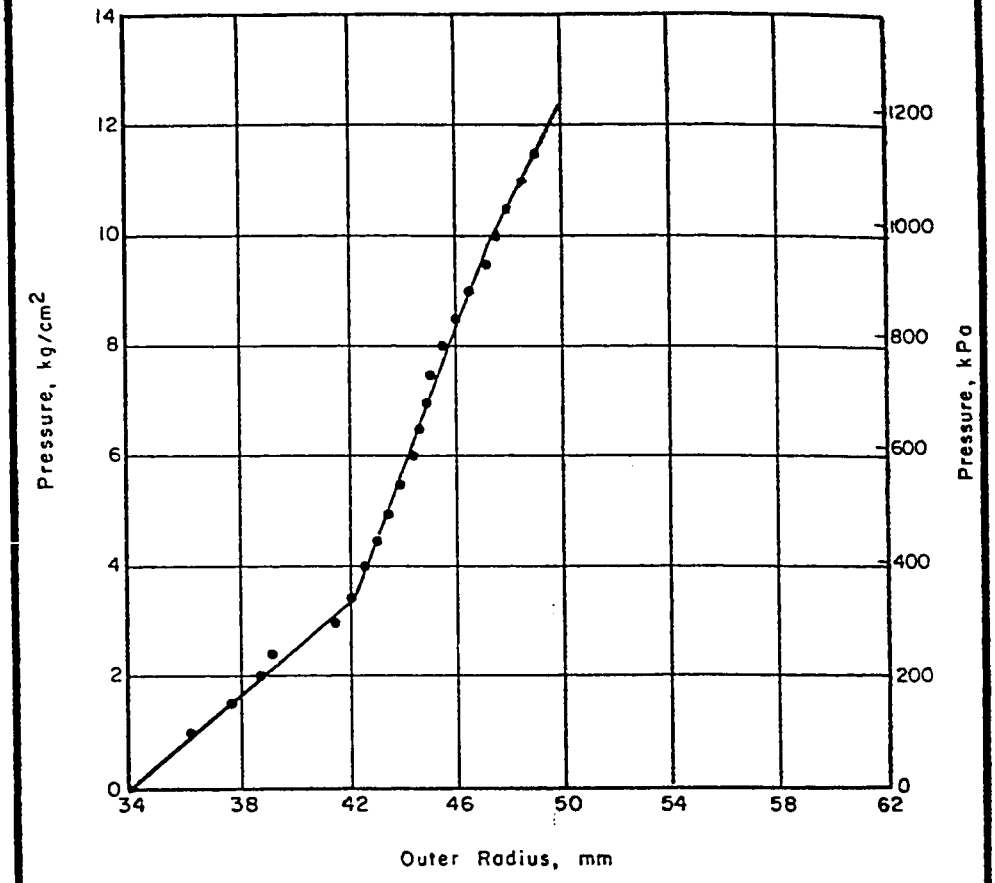

Fig. A7: Pressuremeter Test Data Conducted at a Depth of 11.6 m

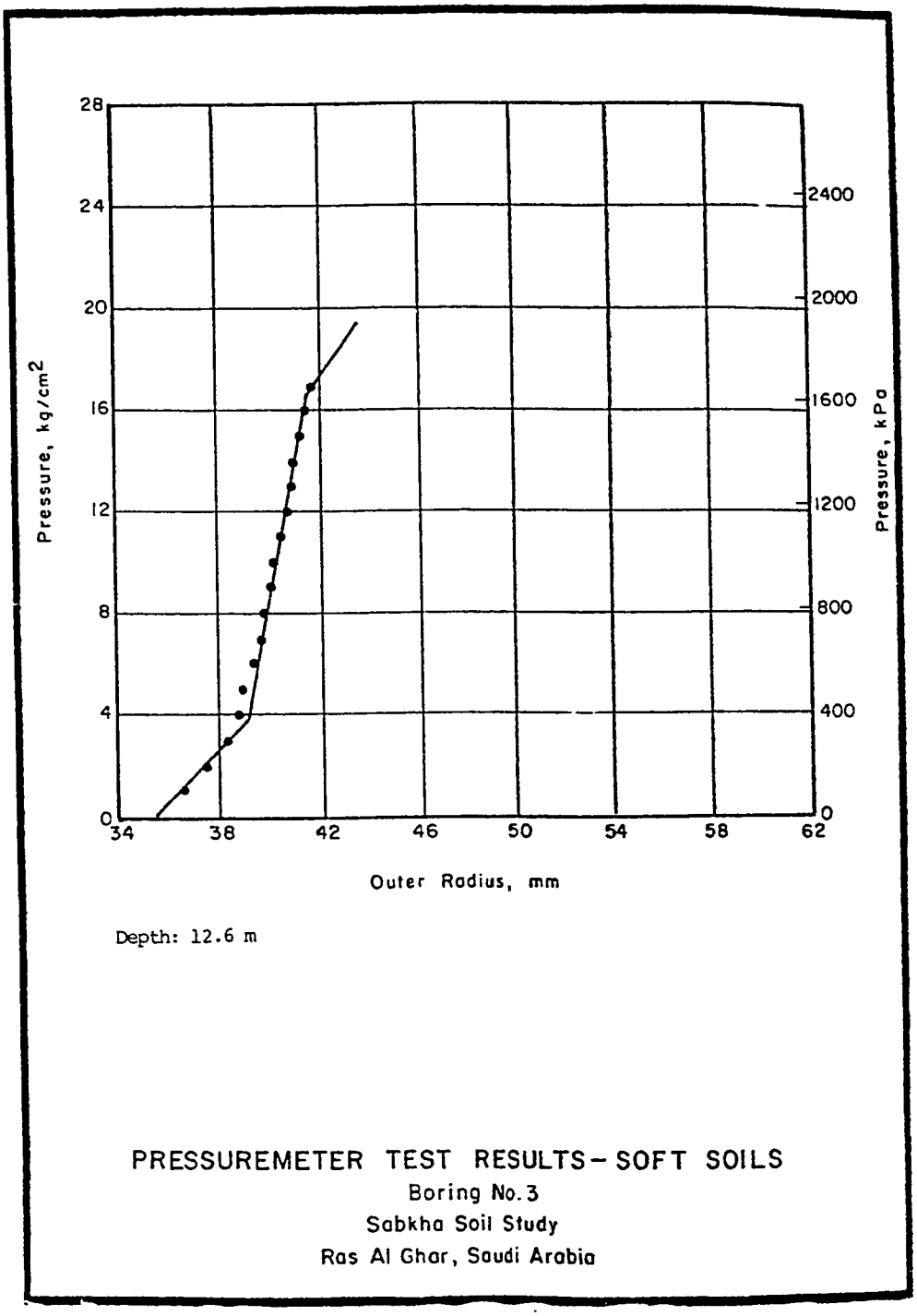

Fig. A8: Pressuremeter Test Data Conducted at a Depth of 12.6 m